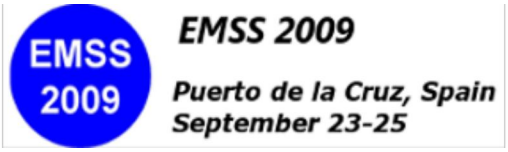

Contents

WELCOME TO EMSS 2009

This 21th EMSS edition asserts the importance of maintaining a high quality International forum for the Simulation Community in which different modeling approaches can be discussed in a friendly but also rigorous ambient. The inherent complexity of present industrial, business, biological, medicine and health care system, together with the changing mentality in the management of those systems under new sustainable rules, provoke the necessity for a better understanding of the internal system's dynamic.

Sometimes, there is a well accepted misunderstanding regarding the term "system complexity" due to a real lack of knowledge on system behavior that appears as emergent dynamics fostered by subsystem interactions. Non justified delays, congestions and idleness are not any longer tolerated by efficient and competitive production and supply chain systems. Present industrial crisis pushed a cross-roads moment in which efficiency should be the driver and the goal of most re-engineering processes. Thus, new design process oriented tools will be essential to tackle efficiency from the strategic and operational point of view in order to address the long term production problems considering also short term aspects. It is widely acknowledged that simulation is a powerful computer-based tool that enables decision-makers in business and industry to improve operational and organizational efficiency; therefore today M&S (Modeling and Simulation) is becoming even more important considering the necessity to introduce new economic, environmental and social sustainability issues.

We are sure that EMSS2009 forum will foster deeper academic and technical discussions on promoting simulation techniques as a basis for new generation decision support tools.

This year, and for the sixth time, the European Modeling and Simulation Symposium (EMSS2009) has been organized in the International Mediterranean Modeling Multiconference (I3M), born in 2004, as a cooperation among a very wide simulation community that is composed by historical simulation Institutions such as McLeod Institute of Simulation Science (MISS, www.simulationscience.org) as well as by new born dynamic organizations such as the Simulation Council of the SCS International: International Mediterranean and Latin America Council of Simulation (I_M_CS, www.i-m-cs.org).

The very high quality level achieved by this conference, it is confirmed by the fact that also in 2009, two special issues in International Journals have been arranged for publication based on their best papers:

- Industry and Supply Chain: Technical, Economic and Environmental Sustainability.
  Guest Editor: Francesco Longo
- Modeling & Applied Simulation: Advanced Methodologies and Techniques.
  Guest Editors: Agostino Bruzzone, and Iván Castilla.

We wish you a fruitful conference and a pleasant stay in Puerto de la Cruz, Tenerife.

EMSS Proceedings Editors,

Rosa M. Aguilar, ISAATC, Universidad de La Laguna, Spain
Agostino G. Bruzzone, MISS-DIPTEM, University of Genoa, Italy
Claudia Frydman, LSIS, Domaine Universitaire de Saint-JeromeLSIS, France

Francesco Longo, MSC-LES, University of Calabria, Italy
Khalid Mekouar, Higher School of Engineering in Applied Sciences - ESISA
Miquel Angel Piera, MISS - Spanish Center, Univ. Autònoma de Barcelona, Spain

I3M Organizers

Academic Sponsors

Sponsors

DECISION TAKING ON THE PRODUCTION STRATEGY OF A MANUFACTURING FACILITY. AN INTEGRATED METHODOLOGY

Juan Ignacio Latorre [(a)], Emilio Jiménez[(b)], Mercedes Pérez [(c)]

(a) Department of Mechanical Engineering, Energetics and Materials. Public University of Navarre. 31500 Tudela, Spain.
(b) Department of Electrical Engineering. University of La Rioja. 26004 Logroño, Spain.
(c) Department of Mechanical Engineering . University of La Rioja. 26004 Logroño, Spain.

[(a)] juanignacio.latorre@unavarra.es, [(b)] emilio.jimenez@unirioja.es, [(c)] mercedes.perez@unirioja.es

ABSTRACT
With a benchmark as background, the optimisation problem that arises in the decision taking process of determining uncertain parameters related to the production strategy in a manufacturing system, the Alternatives Aggregation Petri nets are presented. It is an aim of this paper explain how is it possible to simplify a multiobjective disjunctive optimisation problem into a single one which can be solved in a single stage once the AAPN has been built.

Keywords: Alternative Aggregation Petri net, manufacturing strategy, optimisation, decision problem

1. INTRODUCTION

Nowadays, the manufacturing companies develop their activities in a complex, changing and global environment, where the operations management should be able to adapt the manufacturing strategy to the characteristics of every new situation (market, technology, human resources, etc) (Heizer 2008).

On the other hand, a large number of manufacturing facilities can be considered as discrete event systems (DEVS) (Jiménez 2005). That means that their state evolve by the occurrence of discrete synchronized events.

In a facitity considered as a DEVS, the manufacturing strategy can affect in a decisive way the structure of a manufacturing system (Jiménez 2002). The concept of structure includes the layout, the flexibility of the different subsystems, the coordination between them (synchronisation and concurrence), etc. Therefore, in the design process of a manufacturing facility, it has to be taken into consideration the manufacturing strategy that will be applied in the future operation.

2. MANUFACTURING STRATEGY

There are two manufacturing strategies that can be considered to plan the production of a facility: the *push* and *pull* strategies (Kusiak 2000).

The *push* principle is a simple and classical strategy, which had a good reputation when the production was oriented to the maximal use of the production resources. Each manufacturing stage *push* the next one to produce with the items provided, regardless of the next stage requirements. The push strategy might lead to overproduction in case that the market is not able to acquire all the finished production.

On the other hand, the *pull* strategy leads to the concept of lean production. Production at each manufacturing stage is only afforded if there is a request from the following stage. As the last link in the supply chain, there is an order from the customer which determines what product is manufactured, in which quantity and what should be its characteristics.

In brief, an interesting advantage from the *pull* strategy is the reduction in over production, work in process (WIP), etc.(Heizer 2008).

Nevertheless, the *pull* system is a more complex system to be implemented and requires high flexibility from the manufacturing facility. On the other hand, the system utilization of the and the production rate tend to decrease comparing to the *push* principle (Kussiak 2000).

A mixed *push-pull* strategy can also lead to good results. It is common to assign a push principle to the bottlenecks in the manufacturing facility. The subsystems around the bottleneck are operated under pull principles.

3. CASE STUDY: BENCHMARK

In order to illustrate the described concepts it has been chosen a classical benchmark (Zhou 1999) where it is necessary to take a decision among different manufacturing strategies. This benchmark describes a flexible manufacturing

system composed by four work-cells (WC_i) and an assembly shop (***AS***). Each WC_i consists of a machining cell (MC_i), an assembly cell (AC_i) and a robot (R_i). Automatic Guided Vehicles (AGVs) are present in the system to transport items (parts and subassemblies). See Figure 1.

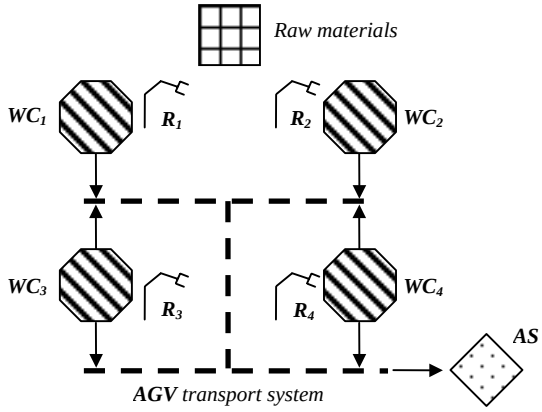

Figure. 1. Layout of the manufacturing

The manufacturing system can produce two different types of products:

- PR_1 is produced by assembling in ***AS*** a certain combination of parts that have been machined previously in some MC_i as it is described in Figure 2. The system works as flexible manufacturing system (FMS).

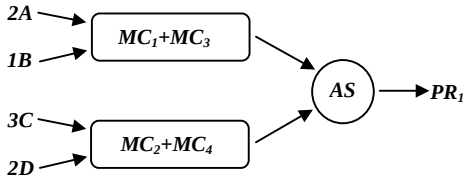

Figure 2. Manufactur. sequence for PR_1.

- PR_2 is produced by assembling in ***AS*** parts, previously assembled in AC_i in the same quantity as in the FMS process. In this case the system works as flexible assembly system (FAS).

In fact, the only difference between FMS and FAS is the processing time that a part should be processed in each WC_i.

The application of *push* and *pull* manufacturing strategies can be performed by considering a precedence relation among the different machines. With the *push* paradigm a machine starts producing when it is idle and has resources enough. On the other hand, with the *pull* strategy, a machine produces when the following machine (in the manufacturing sequence) demands more parts (Zhou 1999).

4. THREE LEVELS OF THE PROBLEM DEFINITION

The purpose of the original work on this benchmark is to choose between a manufacturing strategy among both paradigms *push* and *pull* based on a performance evaluation of the different possibilities. In fact, some other parameters should be adjusted, as the number and the routes of the AGV to perform the movement of parts between the WC_i and ***AS***.

The primary objectives are to minimize the work process inventory (WIP) and maximize the system utilization and production rate. It is necessary to take an appropriate decision about which manufacturing strategy to choose: *push*, *pull*, or a combination of both.

4.1. Decision problem based on a DEVS

The DEVS of the case study has some undefined characteristics. A ***decision problem*** based on this manufacturing system is a choice among several alternatives, in response to a question posed on any of the undefined characteristics of *D* or its dynamics.

In other words, our purpose is to answer the following question:

Which alternatives for each one of the undefined characteristics of the system, described in *table 1*, are the best to achieve the objectives?

Table 1. Undefined characteristics of the system.

Undefined characteristic of the system	Alternatives
Manufacturing strategy	{*Push*, *pull*, combination}
Different routes for AGVs	{1 zone, 2 zones, 3 zones}
Number of AGVs per route	{1,2}
Production lot sizes	{2A+1B+3C+2D, 1A+1B+1C+1D}

The multiple objective, as described before, is to obtain the minimal WIP and the maximal system utilization and production rate.

All those decisions can be considered operation decisions and not design decisions, because they do not belong to the design process of the system and can be modified during the operation of the facility.

4.2. The paradigm of the PN

With the aim of solving the decision problem based on a DEVS it is a necessary step to obtain a model of the system which describes, by means of an appropriate formalism, the restrictions to the behaviour of the original system. The manufacturing system of the case study can be described as DEVS and it shows a behaviour characterised by concurrence (work orders, machines and robots), parallelism (WC_i), synchronisation and resource sharing (buffers and robots).

Petri nets (PN) are a paradigm that can cope with such a description in a double way: a graphical and intuitive one and an algebraic one which is suitable to perform a structural analysis and to be processed by automatic calculation in a computer (Jiménez 2006).

A broad description of the theory of PN and their properties can be found in the references (Silva 1993 and David 2005).

In order to model the benchmark an abbreviation of the ordinary Petri nets, the generalized Petri nets, will be considered.

4.3. The PN model of the benchmark

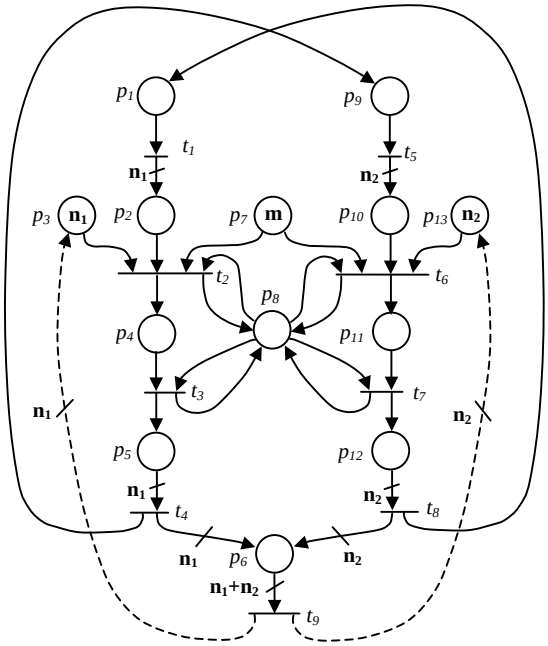

Figure 3. PN model of any

The processing time of the different parts in the $\mathbf{WC_i}$ is the difference between FMS and FAS. This time will be associated to certain transitions in the PN model.

The PN model of any of the work cells ($\boldsymbol{WC_i}$), under the push strategy, is described in Figure 3.

4.3.1. The PN model of the undefined characteristics of the system.

In the PN model represented in Figure 3, $\mathbf{n_1}$ and $\mathbf{n_2}$ represent the number of parts of a certain type (*A*, *B*, *C* or *D*) to be produced in $\boldsymbol{WC_i}$, in a continuous sequence. The weight of the arcs of value $\mathbf{n_1}$ or $\mathbf{n_2}$ and the initial marking of p_3 and p_{13} are the way to model the production lot sizes.

On the other hand, the manufacturing strategy of $\boldsymbol{WC_i}$ is modeled by means of the arcs represented by dashed lines. When the origin of the arc is in the transition t_9 of the same $\boldsymbol{WC_i}$, then the manufacturing order is given when the machine is unloaded. In this case the manufacturing strategy is *push*. The production is performed whenever $\boldsymbol{WC_i}$ becomes idle, regardless the downstream demand.

In order to implement a *pull* strategy, the origin of the arc can begin in the t_9 transition of the downstream $\boldsymbol{WC_j}$, that is, the destination work cell of the parts manufactured by $\boldsymbol{WC_i}$. This idea can be seen in Figure 4.

4.3.2. The PN model of AGVs.

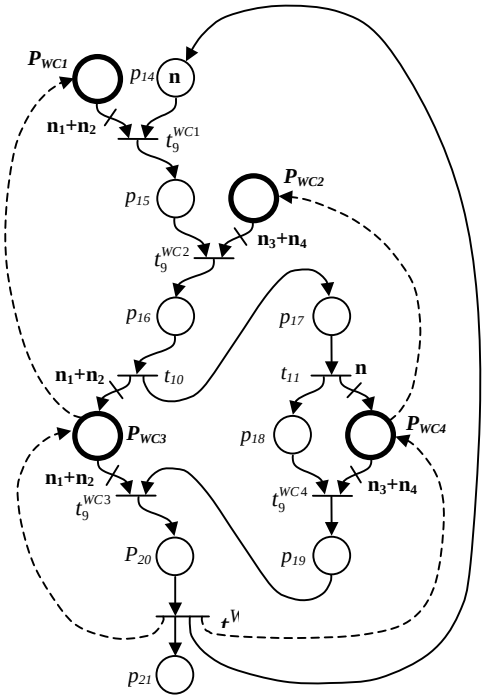

Figure 4. PN model of the AGV (1 route) and the manufacturing strategy pull.

In Figure 4 the complete PN model of the manufacturing system is described. Places p_{14} to p_{20} correspond to the **n** AGV which transport parts between the subsystems. All the AGVs perform the same route.

The other alternatives for the decision problem (2 and 3 routes) imply the modification of the arcs of the Petri net, hence, generating a different PN model. The case of 2 routes can be seen in Figure 5: {p_{14}, p_{15}, p_{16}, p_{17}} and {p_{18}, p_{19}, p_{20}}.

The alternative of 3 routes can be implemented with three groups of AGVs ($\mathbf{n_a}$, $\mathbf{n_b}$ and $\mathbf{n_c}$) which transport parts between {$\boldsymbol{WC_1}$, $\boldsymbol{WC_3}$}, {$\boldsymbol{WC_2}$, $\boldsymbol{WC_4}$} and {$\boldsymbol{WC_3}$, $\boldsymbol{WC_4}$, $\boldsymbol{AS}$} respectively.

In the models, p_{21} is a place which has the purpose of counting the final products. Finally, each $\boldsymbol{P_{WCi}}$ is a macroplace into which each workcell is reduced.

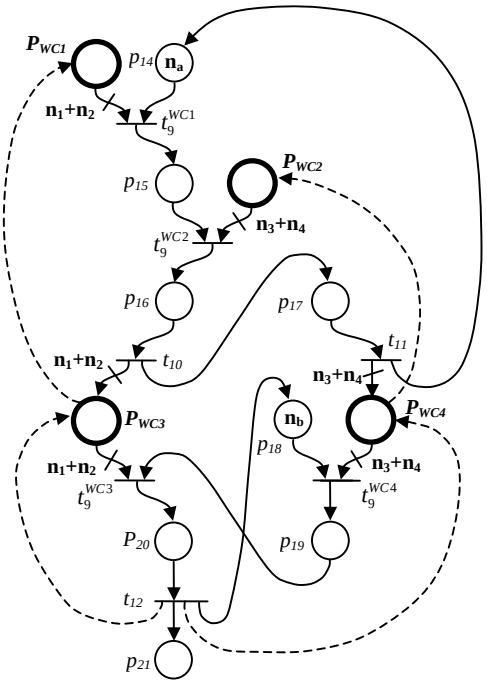

Figure 5. PN model of the AGV (2 routes) and the manufacturing strategy pull.

The WIP can be evaluated from the marking of the Petri net at the end of the manufacturing period analysed. The system utilisation can be known by adding the time each machine is working and comparing it to the total time. Finally, the production rate can be obtained by dividing the final marking of p_{21}.

4.4. Decision problem based on n Petri nets

Let us consider the following set S_R of alternative Petri nets:

$S_R = \{R_{ij} \mid i=1,\ldots,4,\ j=1,2,3\ \}$, where

R_{1k} = Pull manufacturing strategy

R_{2k} = Push strategy

R_{3k} = Combined pull $\{\boldsymbol{WC_1}, \boldsymbol{WC_2}\}$ and push $\{\boldsymbol{WC_3}, \boldsymbol{WC_4}\}$

R_{4k} = Combined pull $\{\boldsymbol{WC_3}, \boldsymbol{WC_4}\}$ and push $\{\boldsymbol{WC_1}, \boldsymbol{WC_2}\}$

R_{j1} = 1 AGVs route

R_{j2} = 2 AGVs routes

R_{j3} = 3 AGVs routes

A decision problem based on S_R is posed as the choice of one alternative for each undefined characteristic of the manufacturing system to achieve the multiple objective. In this problem the undefined characteristics are represented by S_R. It must be taken into account that the initial marking of any R_{ij} also contains some undefined parameters: $\boldsymbol{n_1}$, $\boldsymbol{n_2}$, $\boldsymbol{n_3}$, $\boldsymbol{n_4}$ (production lot size) and $\boldsymbol{n}$ (or $\boldsymbol{n_a}$, $\boldsymbol{n_b}$ and $\boldsymbol{n_c}$ for the number of AGVs in each route).

4.5. Optimisation problem based on n Petri nets

As it has been seen, this problem is a multiobjective disjunctive optimisation one, where there are parameters to maximize (production rate and system utilization) and others to minimize (WIP) simultaneously. The problem can be posed in several ways. A unique objective function is going to be considered in order to simplify the problem. The objective function is a weighted sum of the original goals:

$f(x) = \alpha_1 \cdot f_1(x) + \alpha_2 \cdot f_2(x) + \alpha_3 \cdot f_3(x)$, where

$f(x) \in \mathrm{P}$ and

$\alpha_1 > 0$, while $\alpha_2, \alpha_3 < 0$

and $|\alpha_i|$, $i \in \{1,2,3\}$ is the weight of each individual goal or the relative importance given to each one of them in the specific problem.

On the other hand, the structure of a solution is as described bellow:

$x=\{x_1, x_2, x_3\}$, where:

- x_1 stands for the chosen R_{jk} as solution for the manufacturing strategy, and number of AGVs routes. Hence $x_1 \in \{1,\ldots, 12\}$, as the number of alternative Petri nets is 12.
- x_2 is the vector $\{\boldsymbol{n_a}, \boldsymbol{n_b}, \boldsymbol{n_c}\}$ of AGVs per route. Of course, if the number of routes is one, then $\boldsymbol{n_a}=\boldsymbol{n}$ and $\boldsymbol{n_b}=\boldsymbol{n_c}=0$.
- x_3 is the production lot size. In the original benchmark only two possibilities were taken into account. $x_3 = \{\boldsymbol{n_1}, \boldsymbol{n_2}, \boldsymbol{n_3}, \boldsymbol{n_4}\} \in \{(2,1,3,2), (1,1,1,1)\}$. In the present case study it is very easy to increase the number of possibilities.

The **optimisation problem based on *12* alternative Petri net models** S_R is defined in the following way:

minimize $f(x)$ where

- $f(x) = \alpha_1 \cdot f_1(x) + \alpha_2 \cdot f_2(x) + \alpha_3 \cdot f_3(x)$, $f(x) \in \mathrm{P}$, $\alpha_1 > 0$, $\alpha_2, \alpha_3 < 0$
- $x=\{x_1, x_2, x_3\} \in \Omega = (\bigcup_{i=1}^{12} \Omega_i)$
- $\Omega_i = \{\ x \in \mathrm{P}^n \mid\ m \in \mathrm{M}(R_{jk})\ \}$, where $i \ni x_1=i$ then R_{jk} is chosen. $\mathrm{M}(R_{jk})$ is the set of markings of R_{jk} reachable from marking m_{0jk}, and m represents every marking of R_{jk} used in the construction of x, where $R_{jk} \in S_R$.
- Boundary conditions:

  $m_0(p_7) = m \leq k$, that implies an initial limitation of raw materials.

  $m_f(p_{21}) = 17$, that imposes the condition of a final production of 17 products.

5. SOLUTION STRATEGIES

This problem of disjunctive optimisation can be solved in several ways. The most usual methodology consists of using the strategy of "divide and conquer", which is applied posing twelve optimisation/simulation problems, one

for any of the alternative Petri nets. The second phase is the choice of the best solution. (Guash 2002 and Latorre 2006)

A new methodology to solve this problem is presented in this paper. The methodology is applied in only one phase and to a single problem and it is based on the Alternatives Aggregation Petri nets (AAPN).

6. THE AAPN (ALTERNATIVES AGGREGATION PETRI NETS)

An AAPN is a single PN model constructed from S_R (set of alternative Petri nets). The purpose of the AAPN is to provide with an efficient methodology to solve disjunctive optimisation problems in one step process.

In this benchmark, all the decisions to be taken are operation decisions, not design decisions, because they can be changed during the operation of the facility. Nevertheless, as it has been seen, those operation decisions affect to the structure of the PN model (arcs, places or transitions) (Latorre 2007).

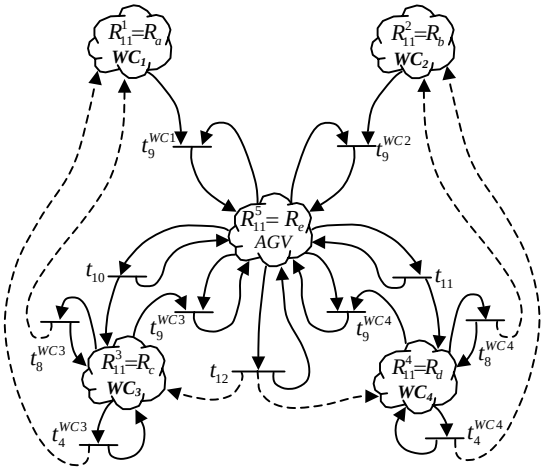

Figure 6. Subnets of R11 (pull stratr.+1 route)

In order to construct R^*, an AAPN, from S_R, it is necessary to consider all the alternative PN from S_R and divide them into subnets, trying to find as much shared subnets as possible (see 6.1. definitions).

In the Figure 6 it can be seen the division into subnets of $R_{11} = \{R_{11}^1, R_{11}^2, R_{11}^3, R_{11}^4, R_{11}^5\}$, where they also have received a generic name R_a, R_b, R_c, R_d and R_e since they are shared subnets with other alternative Petri nets. On the other hand, it is possible to identify the specific structure of the *pull* strategy by means of the dashed arcs. For the sake of the simplicity the weight of the arcs is omitted in the picture.

In the Figure 7 it is possible to see the alternative PN which corresponds to a *push* strategy and 1 route for the AGVs. The differences with the previous case (R_{11} in Figure 6) are the dashed arcs which model the manufacturing strategy.

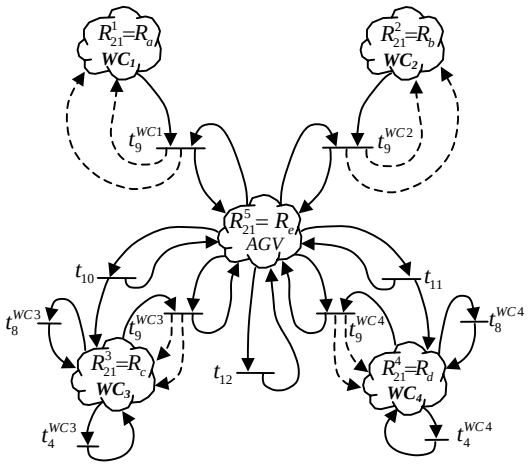

Figure 7. Subnets of R21 (push stratr.+1 route)

It is easy to see how the other combination of manufacturing strategies will be modelled. The only modification needed is to combine the dashed arcs in Figures *6* and *7*.

If the set of alternative PN which correspond to the case of 2 AGV routes is analysed, it will be seen that it is possible to define the same structure of subnets, with R_a, R_b, R_c, R_d and a new $R_f = R_{12}^5$ which refers to the two AGV routes model. In Figure *5* it is possible to see that the link transitions between $\boldsymbol{WC_i}$ and AGV are the same than in the case of a 1 AGV route. On the other hand the models for the manufacturing strategies are the same, since the subnets of the workcells do not change.

6.1. Definitions and examples

i) R_i^k is said to be a ***shared subnet*** in S_R if $\exists\, j \in \mathbb{N}$, $1 \le j \le n, j \ne i \ni R_i^k$ is a subnet of $R_j \in S_R$.
In this example $R_{jk}^1 = R_a$, where $j \in \{1,\ldots,4\}$ and $k \in \{1,2,3\}$ are the same *shared subnet* in all R_{jk}. Moreover $R_{j1}^5 = R_e$, where $j \in \{1,\ldots,4\}$ are *shared subnets* and also are $R_{j2}^5 = R_f$ and $R_{j3}^5 = R_g$.

ii) $p \in P_i^k$ is an ***input border place*** of R_i^k if $\exists\, p' \in R_i \ni p' \notin R_i^k \wedge p' \in {}^\circ t$ where $t \in {}^\circ p$.

iii) $p \in P_i^k$ is an ***optput border place*** of R_i^k if $\exists\, p' \in R_i \ni p' \notin R_i^k \wedge p' \in t^\circ$ where $t \in p^\circ$.
In this case study p_6 is an *output border place* of R_a, R_b, R_c and R_d while p_{15} is an *input border place* of R_e.

iv) $p_6^{WC1} \in P_a$ is a ***choice place*** of R_a because $t_9^{WC1}(R_{11})$, $t_9^{WC1}(R_{12}) \in p_6{}^\circ \wedge p_{15}(R_e) \in t_9^{WC1}(R_{11})^\circ$, $p_{15}(R_f) \in t_9^{WC1}(R_{12})^\circ$.

A set of choice variables is defined as

$A=\{A_1, \ldots, A_{12}\}$, where A_i, $i=1,\ldots,12$ are boolean variables.

From these previous steps, it is possible to construct an AAPN as a tool to solve an optimisation problem based in 12 alternative PN models. The construction algorithm which will be presented comprises four steps.

6.2. Algorithm: construction of R^*, an AAPN from S_R

Step 1: Divide every $R_i \in S_R$ into R^j_i , $j=1,\ldots,n_i$, subnets of R_i.

Step 2: Determine the sets of input and output border places for every R^j_i , $i=1,\ldots,n$; $j=1,\ldots,n_i$

Step 3: Define an appropriate designation for every subnet, place and transition, in a way that the shared subnets include unique names.

Step 4: Aggregate all the subnets in a single R^*:

- ***Step 4.1***: $i=1$, $j=1$, $R^*=\varnothing$
- ***Step 4.2***: if $R^j_i \not\subset R^*$ then $R^*= R^j_i \cup R^*$
- ***Step 4.3***: link R^j_i to R^* with the original transitions in R_i
- ***Step 4.4***: if a link transition $t \in p^\circ$ and p is a choice place $\Rightarrow$ associate the choice variable A_i to t.
- ***Step 4.5***: $j=j+1$; if $j \le n_i$ then go to ***4.2***
- ***Step 4.5***: $j=1$; $i=i+1$; if $i \le n$ then go to ***4.2***.

Figure 8 shows a schema of an AAPN R^* as it can be constructed from the original set of alternative Petri nets S_R, the set of choice variables $A = \{A_i \mid i=1,\ldots,12\}$, and the shared subnets R_a, R_b, R_c, R_d, R_e, R_f, R_g.

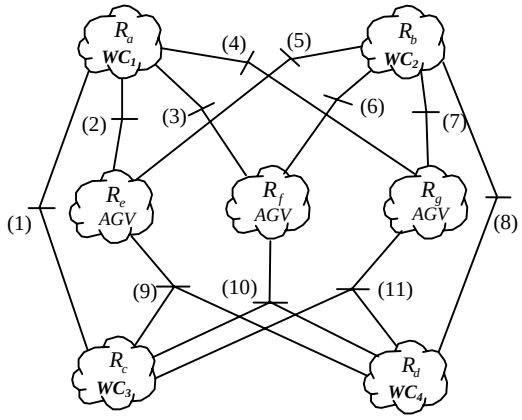

Fig. 8. Schema of the AAPN R^*.

In order to provide with a simple representation of the AAPN R^* in the Figure 8 the following simplifications have been used.

a) The set of arcs from/to a subnet to/from a link transition have been simplified into a segment.

b) The link transitions have been grouped and numerated. For example:
(2) = { t_9^{WC1} , A_1, A_2, A_3, A_4} = this set of transitions which in the alternative PN have the name t_9^{WC1} will be active in the AAPN R^* when any of the referred A_i are active.

With this AAPN, the original disjunctive optimisation problem can be transformed into a single optimisation problem which can be solved by any well-known method like heuristics or artificial intelligence algorithms.

7. CONCLUSIONS

It has been seen how to construct an AAPN from a benchmark, where a performance analysis had been developed in order to take some decisions on certain parameters of the system. The AAPN has allowed to transform 12 different optimisation or simulation problems into a single one. The AAPN profit from several facts: the first one is the similarities in the different alternative PN, which are considered in R^* as shared subnets. The second fact is that its construction can be performed in an autonomous way by a computer and all the optimisation procedure finished in a fast and efficient way. On the other hand, once the AAPN has been constructed it is easy to add small structural variations and to perform sensitivity analysis with AAPN: what is the impact in the performance of a production system of the lot size, setup time and variability of processing time.

For all those reasons the AAPN constitute a promising way to help in the decision taking process that are related to structural decisions in DEVS.

8. REFERENCES

David, R.,Alla, H. 2005 *Discrete, Continuous and Hybrid Petri Nets*. Springer.

Guash, A., Piera, M.À., Casanovas, J., Figueras, J. 2002. *Modelado y simulación. Aplicación a procesos Logisticos, de fabricación y servicios*. Barcelona.Ed. UPC.

Heizer, J., Render, B. 2008. *Operations Management.* Prentice Hall.

Jiménez, E. 2002. *Técnicas de automatización avanzada en procesos industriales*. *PhD Thesis*. Logroño. Ed. Univ. de La Rioja

Jiménez, E., Pérez, M, Latorre, I. 2006 Industrial applications of Petri nets: system modelling and simulation. *Proceedings of European Modelling Simulation Symposium*. 159-164. Barcelona.

Jiménez, E., Pérez, M., Latorre, J.I. 2005 ,On deterministic modelling and simulation of manufacturing systems with Petri nets,. *Proceedings of European Modelling Simulation Symposium*, 129-136. Marseille.

Kusiak, A 2000. *Computational Intelligence in Design and Manufacturing*. Wiley-Interscience.

Latorre, J.I., Jiménez, E., Pérez, M. 2006 Comparison of optimization techniques applied to a flexible manufacturing system. *Proceedings of European Modelling Simulation Symposium*, 141-146. Barcelona.

Latorre, J.I., Jiménez, E., Pérez, M. 2007 Macro-Reachability Tree Exploration for D.E.S. Design Optimization. *Proceedings of the 6th EUROSIM Congress on Modelling and Simulation*. Ljubljana (Slovenia).

Silva, M. 1993. Introducing Petri nets, *In Practice of Petri Nets in Manufacturing* 1-62. Ed. Chapman&hall

Zhou, M. Venkatesh, K. 1999 *Modelling, Simulation and Control of Flexible Manufacturing Systems. A Petri Net Approach*, WS World Scientific.

AUTHORS BIOGRAPHY

Juan Ignacio Latorre is Industrial Engineer. He has developed his professional career in the industry and in educative institutions. Currently he is preparing his PhD Thesis in DEVS optimisation based on PN. Nowadays he is a teacher at the Public University of Navarra. His research areas include factory automation, modeling and simulation, and industrial processes. His main works are developed with the automatic group of the University of La Rioja.

Emilio Jiménez Macías studied Industrial Engineering (with Computer Science, Electronics and Automation specialty) by the University of Zaragoza. After working several years in the industrial private sector (Researching and Developing Department head position), returned to the university, as an Assistant Professor to the University of La Rioja, in 1997, where he works presently in the Electrical Engineering Department (Coordinator of the System Engineering and Automation Group). In 2001 he presented his PhD thesis about Industrial Automation. His research areas include factory automation, modeling and simulation, and industrial processes. His main works are developed with the automatic group of the University of Zaragoza.

Mercedes Pérez de la Parte received the BS degree in Telecommunications Engineering from the University of Seville in 1997. She has held research and teaching positions at the University of Los Andes, Venezuela, in 2000, and research position at the University of Seville since 1997 until present. She has attended all the PhD courses and is presently preparing her PhD dissertation. She is Assistant Proffesor at the Departamento de Ingeniería de Sistemas y Automática of the University of Seville, Spain, since 2000.

DYNAMIC STAND ASSIGNMENT TO IMPROVE AIRPORT GATES OCCUPANCY

Miquel Angel Piera [(a)], Mercedes Narciso [(b)] , Juan Jose Ramos [(c)] ,Toni Laserna [(d)]
Autonomous University of Barcelona, Department of Telecommunications and Systems Engineering.
Barcelona, Spain.

[(a)]MiquelAngel.Piera@uab.es, [(b)]Mercedes.Narciso@uab.es,[(c)]juanjose.ramos@uab.es, [(d)]tlaserna@dlm-solutions.com

ABSTRACT
The Gate Assignment Problem (GAP) is an easily-understood but difficult to solve problem when trying to optimize a certain cost function such as the distance a passenger is required to walk inside the terminal to reach his or her departure gate. The assignment of aircraft arriving out of schedule to available gates is a major issue easy to solve when stands are placed in the same module but very difficult to solve when stands are placed in different modules due to passenger movement through the terminal. To preserve quality factor services to passengers while protecting turn-around aircraft times, most airports have modified the infrastructure by increasing the number of contact points. In this paper a challenging approach to evaluate the minimum number of stands to cope with a time window perturbation for a certain arrival traffic is presented. Emergent dynamics are analyzed when the number of gates is increased and a model to evaluate different gate assignment policies to mitigate undesirable consequences is introduced.

Keywords: Timed Coloured Petri Nets, State Space, Airports, Gate Assignment Problem.

1. INTRODUCTION

The growth in air travel is outstripping the capacity of the airport and air traffic control (ATC) system, resulting in increasing congestion and delays. However, a misunderstanding of the poor utilization of the available infrastructure usually leads to greater investments in additional gates, runways and extensive pavements for taxiways and aprons. In order to avoid this expensive approach, it is important to remove non-productive operations due to poor scheduling approaches.

Different kind of perturbations such as: weather, traffic congestion in some air traffic sectors, and late departures at the origin airport, leads to a typical time window predictibility around [+15 .. -15] minutes with respect to the expected arrival time for more than 40% of the landing operation along the day.

Unexpected changes in the flight schedules may disrupt the initial aircraft-gate assignment, and result in congestions and delays in getting aircraft onto gates. Thus a small delay caused by a reassignment to a remote point will introduce an extra deadline on the disembarking process which will be propagated through passenger actions (ie. transfer operations) and also on the boarding process.

A single delay in a certain operation can be easily propagated through all the airport subsystems. It can be noticed that in order to avoid idleness in handling resources, handling operations usually are scheduled to saturate workers and resources while providing a timely service. In this context, a similar event propagation appears due to a delay in the start of the fuel truck positioning operation which can cause a delay in the freedom of the truck, which can generate a delay in attending to the next fueling operation.

Figure 1 illustrates some of the resources that should be properly coordinated in a turn-around operation.

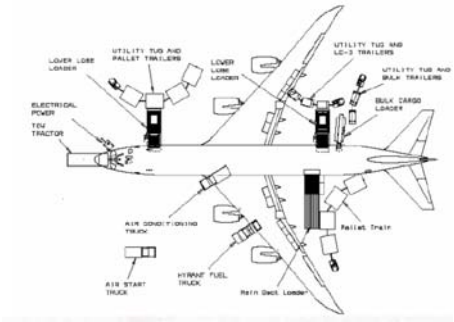

Figure 1: Resources to be Schedulled in a Turn-around Operation

Figure 2 shows the optimal sequence of activities that should be coordinated during the turn-around operation. As it can be easy observed, a small delay in the start of a certain operation can be easily propagated to other sequential operations to be performed in the same aircraft but also to the starting time of the operation in other aircrafts when handling systems are running short of resources to optimize costs.

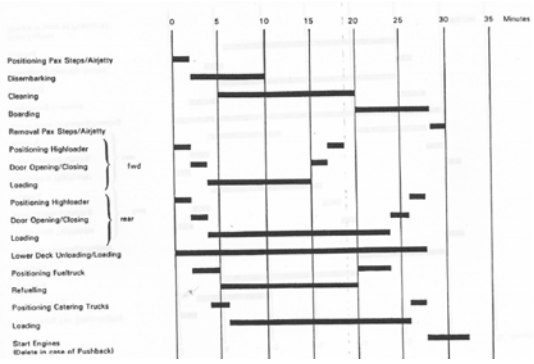

Figure 2: Turn-around Gantt Diagram

An important source of perturbations that affects drastically handling resources availability and handling operational costs (and sometimes turns around times) is last-moment gate reassignments. In fact, each time a flight is reassigned to a remote point, it generates an extra workload to its handling company (buses and stairs together with other resources are required). To minimize last minute gate reassignments to remote points, some airports have increased the number of terminals and contact points to tackle poor arrival predictability.

To tackle uncertainty by increasing the number of resources deals with a considerable economic investment, but deals also with undesirable emergent dynamics caused mainly by longer distances between terminals. Figure 3 shows the PMI airport layout in which it is easy to check that longer distance between gates forces lower handling resources productivity due to displacements.

In this context, it is important to view the operations from the airport side perspective. For the airport, the flight has three phases: an Inbound Phase, a Ground Phase and an Outbound Phase. A delayed inbound flight has an impact on the Ground Phase, but also on the Outbound Phase of the flight with the same air-frame, on the crew and on the flights carrying connecting passengers.

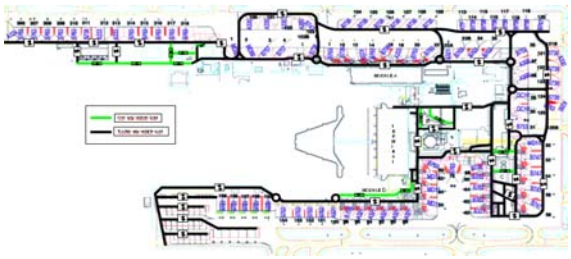

Figure 3: PMI Airport

To avoid delay propagation, a deep knowledge about all the events that take place and their interactions in each phase is important. Thus, by considering the Ground Phase, the turn-around, landing, take-off and taxiing operations can be formalized as a set of interrelated events which, properly coordinated, will satisfy the aircraft operative needs under certain service quality factors (SQF). With a proper model specification considering its interactions with Inbound and Outbound phases, it will be possible to optimize operation efficiency through the proper management of airport re-sources (e.g. airport slots, stands and gates, check-in desks and baggage belts), considering the dynamics and costs of the passenger and aircraft operations.

In the particular case of turn-around operations, it is easy to understand the system dynamics from a discrete event system approach, in which each operation has a certain number of preconditions, duration time estimation, and a set of post-conditions (changes in the state of airport information).

A Colored Petri Net model describing the gate assignment problem has been developed to improve gate occupancy from a logistic point of view.

2. SYSTEM DESCRIPTION

There are several research works that can be found in the literature (Cheng 1998; Dinga 2005; Haghani and Chen 1998; Hon 1999; Yan 2002) optimizing gate assignments according to several QoS passenger parameters, such as minimizing the walking distance between terminals for transfer operations. Most of the proposed algorithms focus either on the strategic aspects or in the operational aspects.

Airport infrastructure over sizing is often a consequence of underestimating the influence of operational issues at the design stage.

The gate over-sizing approach usually deals with hard to solve drawbacks in both areas:

- Strategic:
  - The increment of contact points, usually leads to more complex airport layouts.
  - Due to an unnecessary increment of gates, longer distances must be properly managed by employees and passengers.

- Operational:
  - Airlines Constraints: Some airlines prefer to allocate their flight in the same area to reduce passenger handling costs.
  - Passenger Constraints: Transfer connectivity is highly dependent of the distances between terminals when flights are late on the arrival.
  - Handling Constraints: Most handling companies prefer to concentrate in a narrow area all the operations to be served in the same time horizon to the different flights.
  - ATC Constraints: Complex layouts increase the number of taxiways to be properly managed to support a safety movement of aircrafts.

Thus, strategic design decisions affect the performance of most airport operations: handling, taxiing, transfers, etc. Furthermore, gate occupancy usually is quite low regarding the number of aircrafts that are assigned to remote points due to discordances between the ETA (Estimated time of Arrival) and the arrival time, and also between the departure time and the ETD (Estimated time of Departure).

A proper analysis of the cause-effect relationship between the main perturbation factor that decreases the contact point occupancy and increases the remote point occupancy should contribute to improve quantitatively and qualitatively the airport operations and consequently reduce the cost of airport taxes, handling and airlines.

Figure 4 illustrate the result of a typical gate assignment process in which ETA's and ETD's are used in the gate occupancy optimization.

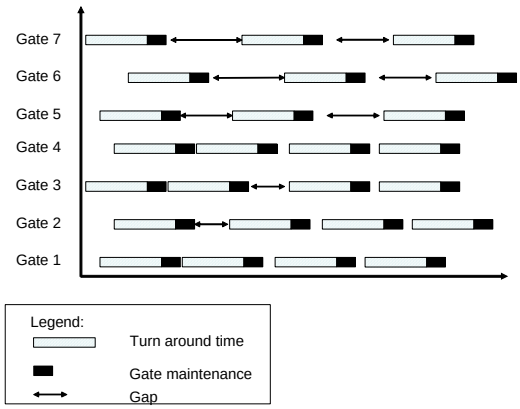

Figure 4: Gate Planning

Despite the assignment proposed to gates nº 1 and nº 3 should provide a better gate occupancy, at the end of the day, the occupancy of both usually is lower than gates with an initial poor occupancy assignment such as gates nº 6 and nº 7.

Figure 5 illustrates the time events that affect the state of gate nº 4 according to the planned flights arrival and departures.

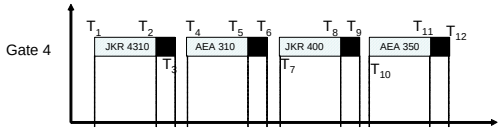

Figure 5: Estimated Events on Gate nº 4

Analyzing the main causes of poor gate occupancy of an optimal gate assignment, there are 3 different causes that affects drastically to contact point occupancies:

1. Late Arrival: Due to constant ATFM perturbations, a considerable amount of flights have a delay on the arrival around 15 minutes. When gate assignments have been planned according to a high occupancy value, a late arrival could overlap two aircrafts in the same gate for a short period of time.

   To avoid this situation, usually late flights are re-scheduled to remote points. Figure 6 (top part) illustrates a late arrival perturbation of aircraft AEA310 (with ETA in T_4 and landing at $T_{4'}$, $T_4<T_{4'}$) together with the result of the re-scheduling (bottom part).

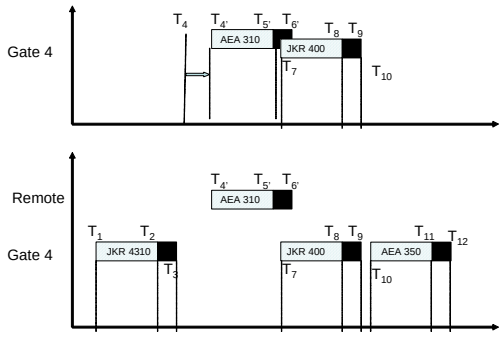

Figure 6: Late Arrival Perturbation

2. Early Arrival: Due to poor predictability, a considerable amount of aircraft gets the destination airport earlier than the ETA. An earlier arrival could overlap two aircraft on the same gate. Figure 7 (top part) illustrates an earlier arrival perturbation of aircraft AEA310 (with ETA in T_4 and landing at $T_{4'}$, , $T_4>T_{4'}$), together with the result of the re-scheduling (bottom part).

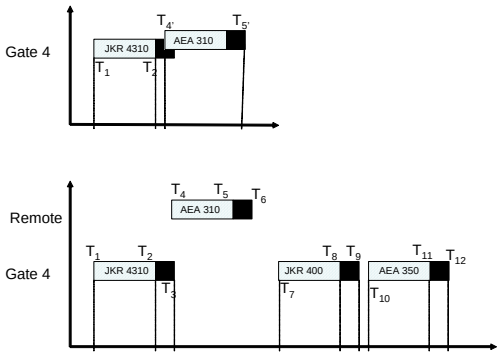

Figure 7: Earlier Arrival Perturbation

3. Late Departure: Finally, due to last moment problems such as technical problems with the aircrafts, late clearance due to taxi-out saturation, or a delay in the embarkement, sometimes the gate is not released at the ETD and the next flight can be re-scheduled to a remote point. Figure 8 (top part) illustrates a departure delay perturbation of aircraft AEA310 (with ETD in T_5 and departure at $T_{5'}$, $T_5 < T_{5'}$) , together with the result of the re-scheduling (bottom part).

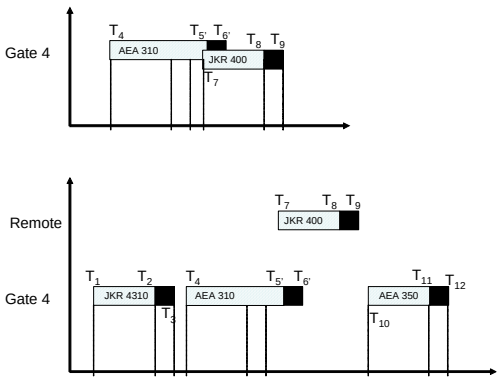

Figure 8: Late Departure Perturbation

As it can be seen in the bottom part of figures 7,8 and 9, there is a high correlation between ETA and ETD perturbations and a low gate occupancy factor when the original planning strategy tries to maximize the gate occupancy factor.

3. COLORED PETRI NET FORMALISM

Colored Petri Net formalism are well known by the OR and Simulation community for their capability in simulating and analyzing discrete event system (Jenssen 1997). In this section, the CPN model developed to determine the consequences of a ETA and ETD perturbations on different gate configurations is illustrated.

CPN has been chosen as the modeling formalism due to its ability to describe the complete structure of a system together with its behavior and the information about the system state (Piera, Narciso, Guasch and Riera 2004) through the use of a functional programming language. A Petri Net can be defined as a bipartite directed graph describing the structure of a discrete event system, while the dynamics of the system is described by the execution of the PN. A PN is coloured if the tokens are distinguishable. The main CPN components are: state vectors, arc expressions and guards, color sets, places and transitions. See (Jensen 1997; Piera, Narciso, Guasch and Riera 2004) for the description of these terms and tutorial on CPN.

Mathematically, a CPN can be defined as a tuple of 9 elements, CPN = (∑, P, T, A, N, C, G, E, I). The meaning of each tuple is described below:

- ∑ = on nc indicates the color definition: Finite set and not empty. This allows the specification of attributes that must be defined for every entity type that needs to be modeled. is the color (attribute) of the entity type i.
- P = Indicates place nodes: Finite set of place nodes that permits the system's state specification. It contains the number of tokens and the colors of each token.
- T = Represents transitions: Finite set of transition nodes.
- A = Represents the arcs: Finite set of arcs.
- N: Node Function, allows the association of each arc with its node terminals (the origin and destination nodes). The nodes must be of different types; i.e. if a node is a transition, the connecting node must be a place and vice versa.
- C: Set of color functions, allows the specification of the entity type that can be stored in every place node:
- G: Guard function associated with transition node , enables or disables an event associated with the transition in function of the value of the entity attributes to be processed.
- E: Arc expression , indicates which type of tokens can be used to fire a transition.
- I: Initialization function, specifies color values of the initial tokens stored in each place. This is referred to as the initial state of the CPN.

4. CPN GATE ASSIGNMENT MODEL

To model the gate assignment problem as a discrete event system, it is necessary to define the events that are relevant to the gate occupancy factor. CPN allows the representation of a system in a compact structure with few places and transitions. Table 1 summarizes the meaning of the events modeled

Table 1: Transition Definitions

Transition	Meaning
T1	A new gate is generated each time an arrival is programmed and there are no free gates for the demanded slot
T2	Match a gate with a programmed arrival
T3	A new gate is generated due to perturbations on the programmed time that leads an aircraft without a gate.
T4	Releases a gate once the aircraft start the taxi-out operation.
T5	It generates a ETA perturbation according to the predictability parameter.

The relevant information to determine the evolution of the different states of the gates according to estimated time arrivals and estimated time departures together with delay perturbations is supported by the places described in table 2 and colours described in table 3.

Table 2:Place Node Descriptions

Place	Colour	Meaning
P1	A	Programmed flights.
P2	C	Available Airport Gates
P3	A	Gates pending to be released
P4	A	Aircrafts landed
P5	D	Flow Control Information

Table 3: Colour Descriptions

Colour	Definition	Meaning
A	Product a_id*t_ar*t_r	Aircraft

		Information
A_id	integer	Aircraft identifier
T_ar	integer	Estimated Time of Arrival
T_r	integer	Round time
C	Product g_id*gt_id*gt_i*gt_f*ge	Gate Information
G_id	integer	Gate identifier
Gt_id	integer	Terminal identifier
gT_i	Integer	Initial time for gate occupancy
Gt_f	Integer	Final time of gate occupancy
ge	integer	State of the gate
D	Product ng*nfg	Global information
Ng	Integer	Number total of gates
nfg	integer	Number of free gates at a certain time instant

Figure 9 illustrates the gate assignment problem specified under the colored petri net formalism. The proposed model computes the number of gates required to attend the handling operations on a certain airport with aircrafts arriving with a programmed slot every 2 minutes. The model doesn't consider remote points, thus the results generated correspond to the ideal scenario in which all passenger will embark/disembark through a contact point. A predictability of ±15 minutes is considered, and all gates are allocated at the ETA and released at ETD, thus when a perturbation affects an arrival or a departure a free gate is assigned to the aircraft and the original programmed gate remains busy.

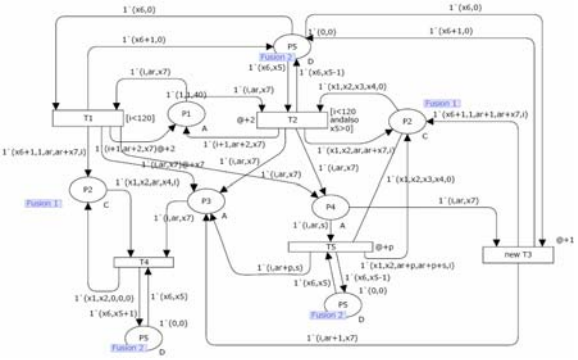

Figure 9: Gate Assignment Model

The minimum number of gates required to attend the slot demand is 22 gates when there are no perturbations affecting the ETA's neither the ETD's. Figure 10 summarizes the results obtained under a non-preemptive policy for different predictability contexts (from no arrival time perturbations until ±15 minutes delays).

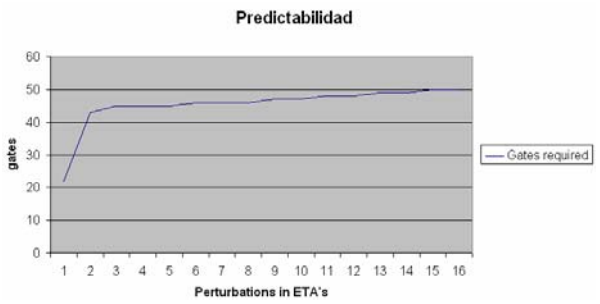

Figure 10: Gates required in a non preemptive policy

To avoid over sizing contact point infrastructure, some terminals are designed to support passenger movements between gates when in the same terminal area it is possible to swap between gates with practical no distance increments to passengers. Figure 11 illustrates terminal configurations in which gate re-scheduling is fully supported by the layout configuration.

Figure 11: Gate Sharing Configuration

Figure 12 summarizes the results obtained under a preemptive policy for different predictability contexts (from 0 perturbations until ±15 minutes) in which gates of the same terminal can be re-scheduled without affecting passenger QoS.

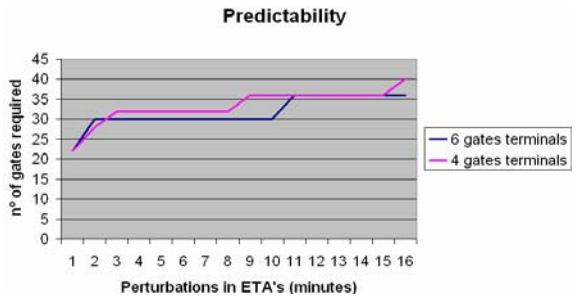

Figure 12: Gates Required in a Preemptive Policy

It can be noticed that the possibility of last moment gate re-scheduling between gates placed in the same terminal (in a narrow area) can reduce considerably the

infrastructure investments while preserving passenger QoS.

Figure 13 shows the CPN model with the new constraints to support gates rescheduling under a preemptive policy.

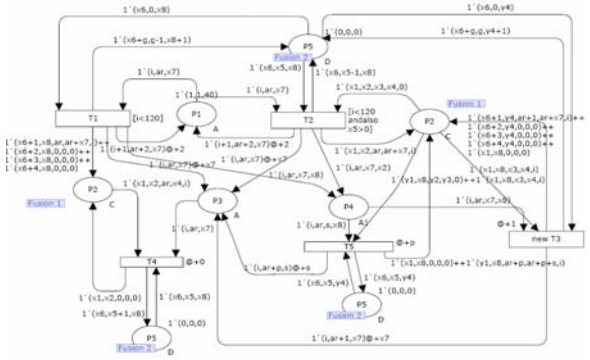

Figure 13: Gate assignment model with a preemptive policy

5. CONCLUSION

This paper provided an overview of the Stand Allocation System from an strategical and operational point of view. Right now, most European flights have predictability around ±15 minutes on arrivals and departures. The future SESAR project seeks predictability around ±1 minute in the arrivals.

The results obtained show that reducing uncertainty in the arrivals, its is possible to minimize infrastructure investments. Furthermore, layout design should be very sensitive to ATFM predictability to avoid gate saturation or idleness.

ACKNOWLEDGMENTS

This work is partly funded by the Science and Innovation Ministry of the Spanish Government "Discrete Event Simulation Platform to improve the flexible coordination of land/air side operations in the Terminal Maneuvering Area (TMA) at a commercial airport" CICYT Spanish program TRA2008-05266/TAIR, and the ATLANTIDA project: "New technologies applied to UAV's for research and ATM development" (CEN20072008)*.

REFERENCES

Cheng, Y. 1998. Rule-based reactive model for the simulation of aircraft on airport gates. *Knowledge-Based Systems* 10. 225-236.

Dinga,H. 2005. The over-constrained airport gate assignment problem. *Computers & Operations Research* , 32, 1867-1880.

Jensen K., 1997. Colored Petri Nets: Basics concepts, analysis methods and practical use. *Springer*, Vol. 1, 2, 3.

Haghani A., Chen M. 1998. Optimizing Gate Assignments at Airport Terminals. *Transportation Research* .-A, 32, 437-454.

Hon Wai Chun et al., 1999. HKIA SAS: A Constraint-Based Airport Stand Allocation System Developed with Software Components. *IAAI-99 Proceedings.*

Piera, M.A.; Narciso, M.; Guasch, T. and Riera, 2004. Optimization of Logistic and Manufacturing Systems through Simulation: A Colored Petri Net-Based Methodology. *SIMULATION: Transactions of The Society for Modeling and Simulation International*, 80, 121-130.

Yan S., et al.,2002. A simulation framework for evaluating airport gate assignments". *Transportation Research* .Part A, 36, 885-898.

MODELLING AND SIMULATION WITH DISCRETE AND CONTINUOUS PN: SEMANTICS AND DELAYS

Emilio Jiménez[(a)], Mercedes Pérez [(b)], Juan Ignacio Latorre [(c)]

(a) Department of Electrical Engineering. University of La Rioja. 26004 Logroño, Spain.
(b) Department of Mechanical Engineering . University of La Rioja. 26004 Logroño, Spain.
(c) Department of Mechanical Engineering, Energetics and Materials. Public University of Navarre. 31500 Tudela, Spain.

[(a)] emilio.jimenez@unirioja.es, [(b)] mercedes.perez@unirioja.es, [(c)] juanignacio.latorre@unavarra.es

ABSTRACT

Petri Nets (PN) constitute a paradigm for the modeling, simulation, analysis, synthesis and implementation of discrete systems, and can be interpreted as an underlying global structure common to a family of formalisms with different levels of abstraction and interpretations. Based on previous works, this paper complements the analysis of the use of PN for modeling and simulation, and the choice of the appropriate PN formalism, depending on the level of abstraction of the formalism and on the interpretative extensions they are provided with. In this work the analysis is complemented with a study of the meaning of the semantics or interpretation of timed transitions, where timing is modeled as a delay. The paper analyses the relationships between the semantics in the discrete case and in the continuized model, as well as the comparison with the continuous models of system dynamics.

KEYWORDS

Petri nets, modeling & simulation, system dynamics.

1 INTRODUCTION

Petri Nets (PN) constitute a paradigm for the modeling, simulation, analysis, synthesis and implementation of discrete systems, and can be interpreted as an underlying global structure common to a family of formalisms with different levels of abstraction and interpretations.

They have been widely used in automated manufacturing systems, in practically all the levels of decision-making and detail, due to their efficiency to cope with concurrence, parallel evolutions and synchronism.

Based on previous works, this paper complements the analysis of the use of PN for modeling and simulation, and the choice of the appropriate PN formalism, depending on the level of abstraction of the formalism and to the interpretative extensions they are provided with.

In this work the analysis is complemented with a study of the meaning of the semantics or interpretation of timed transitions, from the point of view of system dynamics, where timing is modeled as a delay, modeled in an especial way.

Moreover, even when dealing with DES, the intrinsic nature of the parts of the model (discrete, continuous or hybrid) must be considered. Continuous PNs, was originally devised like an approach to deal with discrete systems efficiently when the well-known problem of state explosion occurs; but they can also be used as a formalism to model continuous concepts of the production systems (as usual with Forrester Diagrams in system dynamics).

The paper analyses the relationships between the semantics in the discrete case and in the continuized model, as well as the comparison with the continuous models of system dynamics.

2 INTRODUCTION TO PN

Petri nets (PN) constitute a well-known formal paradigm for the modelling, simulation, analysis, synthesis and implementation of systems that "can be seen" as discrete. We assume the reader is familiar with modelling and simulation with PN (see for instance Silva (1993), DiCesare et al. (1993), Banks et al. (2001), David and Alla (2005) for an introduction of the basic concepts and notations).

We will just remark that a system is an structure N= <P,T,Pre,Post> (Pre and Post represent the static structure of the model, from which the token flow matrix C= Post-Pre can be deduced) provided with an initial marking over P, m_0. A Petri net structure can also be represented as a bipartite directed graph, in which places are usually represented as circles and transitions as bars. In a PN, the marking defines the state of the system, and it is changed by the firing of transitions, thanks to the occurrence of their associated events. Starting from a PN system, a state (or fundamental) equation can be written: $\mathbf{m} = \mathbf{m_0} + \mathbf{C} \cdot \boldsymbol{\sigma}$, where $\boldsymbol{\sigma} \in N^{|T|}$ and $\mathbf{m} \in N^{|P|}$

The places of a PN system could be seen as the state variables, and the marking vector as the state vector (however, it must be taken into account that there may exist redundancies).

Under this previous general description, PN constitute a family of related formalisms, with different

abstraction levels (elementary, place/transition, coloured, predicate/transition, etc.) and different interpretations (autonomous, timed (deterministic, stochastic…), etc.) providing a rich modelling paradigm for discrete event dynamic systems (DEDS).

3 SEMANTICS

Apart from the abstraction level, the interpretative extensions also define the PN formalism and its behavior, as for instance, timed PN, in their various forms: deterministic, stochastic, … Timed PN can work in very diverse ways. PNs can be timed on the places or on the transitions –both are equivalent and therefore convertible one into another–; but even in the deterministic systems with constant delays, it is necessary to endow the timing with a meaning or semantics, apart from defining the conflict resolution way. Special care should be taken over the models when the enabling degree can be higher than one, since the behavior can vary totally according to the semantics (or interpretation) in those cases; this is one of the most frequent errors made in the modeling of deterministic timed systems (Jiménez and Pérez 2004, Jiménez et al. 2005).

3.1 On the servers

Let us suppose a process involving:

– a robot that transports parts from a place to another one, spending a certain amount of time;

– a conveyor belt –where only a few parts can fit in at the same time– that moves the parts in a certain time;

– another conveyor belt where many more parts than the ones actually arriving can fit in.

These three subprocesses that introduce delay can be mo-deled by the structure in the left top corner in Figure 1. All of them are correctly represented by that model, but then the timed transition of each sub process has to be endowed with different semantics: Single Server Sema-ntics (SSS), Finite Servers Semantics (FSS), and Infini-te Servers Semantics (ISS), respectively. If the maxim-um enabling degree is 1, the behavior of all those syst-ems is equivalent; otherwise they differ from each other.

Therefore, it is necessary to establish the semantics to build a model. Let us consider that the semantics represents the number of servers that reach a timed transition –for instance, the number of robots that make the transport, whose duration determines the delay–. We can model the above-mentioned behaviors –Single Server (SS), Finite Server (FS) and Infinite Server (IS)– by using the ISS and FSS, as is shown in Figure 1. It can be seen that ISS is more general, since a behavior of IS cannot be modeled with SSS. Anyway, if the system is bounded, they have equal modeling capability.

Let us note that part of the structure of the PN have been repeated in order to model each one of the servers with FSS (Figure 1, SSS-FS, where just 2 servers have been modeled). This repetition in the structure can be avoided by using colored PNs; then just one of the repeated structures must be included, with so many marks (instead of only one) as the number of servers. More services would have been modeled with more tokens, instead of with structure repetition.

3.2 On the service of the servers

Apart from the number of servers, the number of services of each server can also be considered. Let us now assume that, as soon as a part reaches a certain position, an elevator is called –it takes some time to arrive– and, when it arrives, it can transport up to three parts. This is a case of a Single Server with Multiple Service (SSMS). The extension to several servers (more elevators) or to infinite service (more capacity than the number of parts that can ever be) is straightforward. Figure 2 show the temporal evolution of the four behaviors that have been presented, when two tokens arrive simultaneously to the "input" place.

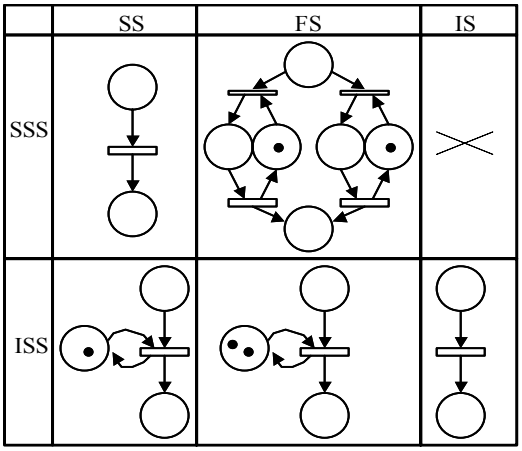

Figure 1: SS, FS (2S) and IS Behaviors Modeled with SSS and ISS Petri Nets respectively.

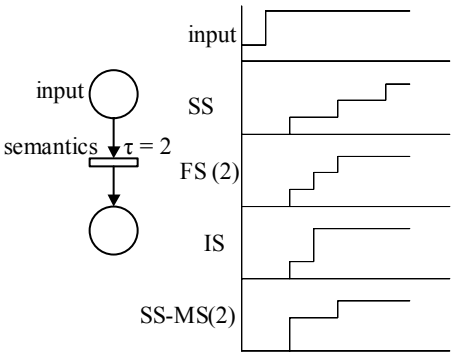

Figure 2: Different Behaviors of a Deterministic Timed Transition depending on the Semantics: SS, FS (2 Servers), IS, SSMS (2 Services per Server)

Figure 3 illustrates the models of a system of SSMS, developed with SSS and ISS respectively. The ISS model just includes a self-loop in order to fire the timed transition sequentially; nevertheless in these examples the importance of the choice of the appropriate semantics is illustrated even in immediate

transitions (without delay): when 2 parts are lifted by the elevator, the SSS model says that one part is lifted before the other one; although the state where only one part has been lifted is ephemeral, in the real system both parts go simultaneously. Evidently, another model can be deve-loped with SSS that modifies and corrects that behavior.

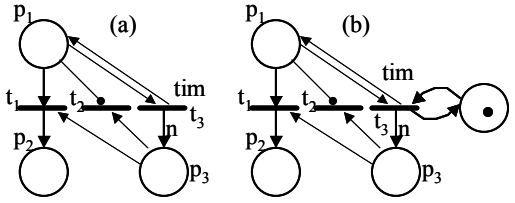

Figure 3: SSMS (*n* Services per Server), Modeled with SSS (a) and ISS (b) Respectively.

Note that Infinite Servers does not limit the possibility of multiple service. Let us analyze the PN in figure 4, with ISS, and its behavior in figure 5 depending on the service *n*. The time in transition 2 is also n, in order to present the same throughput for any n. Figure 5 shows that the permanent is similar, but the transient is different for any different service.

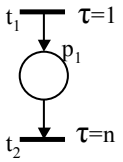

Figure 4: ISMS (*n* Services per Server), with constant throughput.

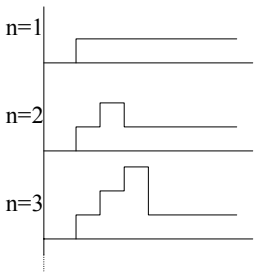

Figure 5: Different behavior of PN in Figure 4 depending on the service n.

3.3 On the conflict resolution

The importance of the conflict resolution with the models can be shown in the models in Figure 6. Let us suppose that they model the same behavior of the models in figure 3, that is, SSMS behavior modeled with SSS and ISS respectively. Their behavior is the correct one if, with the used formalism and its rules, a marking enables all the transitions involved in a conflict, and the token is not reserved for any transition in particular. If tokens are reserved, those models are not correct;

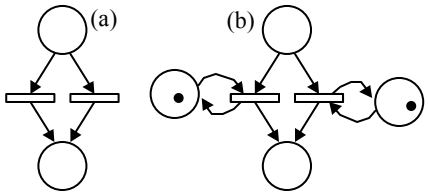

Figure 6: SSMS (2 services per server) modeled with SSS and ISS respectively, sensitive to Tokens' Reservation

Figure 7 shows the evolution of models in figure 4 with tokens' reservation and without it. In this case both are different, and the corresponding to a SSMS behavior is only the last one. Usually, when omitted, a tokens' reservation is assumed in conflicts, although it is better to explicitly indicate it.

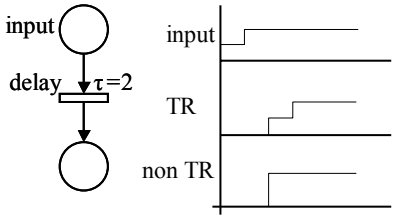

Figure 7: evolution of models in figure 4 with tokens' reservation and without it.

Note that again two servers have been modeled by two similar structures, and again the use of colored PNs would have reduced the model size. More services would have been modeled with more tokens, instead of with structure repetition.

3.4 On the memory of the servers

The semantics that have been mentioned in the previous section are only some of the possible ones - the most usual. As an example of all the possibilities, we can consider all of them (any number of servers, of service, and reservation or not) with memory of the waited time of every server.

The memory would affect only to transitions involved in a choice or conflict, because a token can enable a transition, which start the temporization, but before finishing it the token can disappears by the firing of other transition of the conflict.

If the passed time of the timed transitions is wanted to be kept, a "continuous" memory is needed to memorize the passed time. If the semantic that is being used do not includes memory for the servers, but we needs to model it, a continuous PN subsystem can be added to de PN, as it will be shown in the next section.

4 DELAYS IN CONTINUOUS AND CONTINUIZED SYSTEMS

4.1 Continuous models. System dynamics and forrester diagrams

Forrester diagrams (FD) (Forrester 1961) constitute a graphic representation of (eventually non positive and non linear) ODES (Farina and Rinaldi 2000, Silva and Recalde 2003), and they are mainly used to simulate the evolution of continuous dynamic systems.

Let be a general case of unforced linear ODES, $\dot{\mathbf{x}}(t) = \boldsymbol{A}\ \mathbf{x}(t)$, with dimension 2. Its solution is $e^{\mathbf{A}t} \cdot \mathbf{x}(0)$. Certain particular cases that exemplify the types of behaviour of this system are shown in Table 1. Exponential (positive and negative), linear, oscillating, hyperbolic and even sine growing behaviours can been seen.

Table 1: Examples of behaviour that can be modelled with ODES with dimension 2.

A	eig(A)	e^{At}
$\begin{bmatrix} \pm a_1 & 0 \\ 0 & \pm a_2 \end{bmatrix}$	$\pm a_1, \pm a_2$	$\begin{bmatrix} e^{\pm a1\cdot t} & 0 \\ 0 & e^{\pm a2\cdot t} \end{bmatrix}$
$\begin{bmatrix} 0 & 0 \\ a & 0 \end{bmatrix}$	a, 0	$\begin{bmatrix} 1 & 0 \\ a\cdot t & 1 \end{bmatrix}$
$\begin{bmatrix} 0 & a \\ 1/a & 0 \end{bmatrix}$	1, –1	$\begin{bmatrix} \text{hcos } t & a\cdot\text{hsin } t \\ (\text{hsin } t)/a & \text{hcos } t \end{bmatrix}$
$\begin{bmatrix} 0 & a \\ -1/a & 0 \end{bmatrix}$	i, –i	$\begin{bmatrix} \cos t & a\cdot\sin t \\ (-\sin t)/a & \cos t \end{bmatrix}$
$\begin{bmatrix} 0 & a \\ -1/a & 1 \end{bmatrix}$	$\frac{1}{2}+\frac{\sqrt{3}}{2}\text{i}, \frac{1}{2}-\frac{\sqrt{3}}{2}\text{i}$	$\frac{e^{t/2}}{\sqrt{3}}\begin{bmatrix} -\sin\frac{\sqrt{3}\cdot t}{2}+\sqrt{3}\cos\frac{\sqrt{3}\cdot t}{2} & \ldots \\ -\frac{1}{a}\sin\frac{\sqrt{3}\cdot t}{2} & \ldots \end{bmatrix}$

4.2 Types of delays in system dynamics

Models with material and information delays are frequently used in FD. In both cases delays are modelled either as one first order system, or as several ones in series (usually three), but no additional modelling elements are used. Table 2 shows both types of delays. Note that the dynamics (the differential equation) is similar in both delays (a first order system), but material delay is applied to a flow (material channels) while information delay is applied to the information of a state variable (information channels from a level) (Jiménez et al. 2001, Jiménez et al. 2004).

Table 2. Sketch, differential equation, and FD in material and information delays.

Material Delay	Information Delay
x_1 → Delay → x_2	x_1 ⇢ Delay ⇢ x_2
$\dot{x}_2 = \frac{1}{T_a}(x_2 - x_1)$ (T_a is the delay time)	
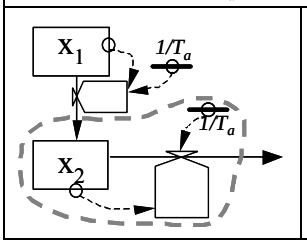	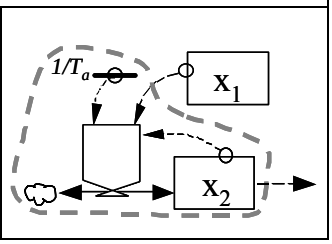

Figure 8 shows the FD of the thirsd order delay system and the corresponding ODES.

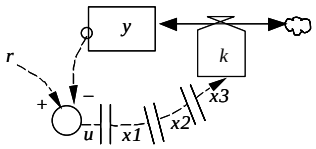

$dx_1/dt = 3a\cdot(r - y - x_1)$
$dx_2/dt = 3a\cdot(x_1 - x_2)$
$dx_3/dt = 3a\cdot(x_2 - x_3)$
$dy/dt = x_3$

Figure 8. DF modelling a system of storage with information delay, and its equivalent ODES.

4.3 Continuized models. Continuous PN.

The discrete models must be continuized due to the well-known "state explosion problem", which means that the group of reachable states of a discrete PN system can become extremely large when the number of elements increases. The continuization simplifies the model and permits the use of different mathematical tools (linear programming techniques, differential equations, etc.) (Silva and Recalde 2002).

In continuous PN any non-negative real marking is allowed (in a discrete PN the marking is restricted to be integer). The firing of a transition is similar: *t* is *enabled* at **m** iff $\forall\ p \in {}^\bullet t$, $\mathbf{m}[p] > 0$. The *enabling degree* is defined as $\text{enab}(t,\mathbf{m}) = \min_{p \in {}^\bullet t} \{\mathbf{m}[p]/\mathbf{Pre}[p,t]\}$, and the firing of *t* in a certain quantity $\alpha \le \text{enab}(t,\mathbf{m})$ leads to a new marking $\mathbf{m}' = \mathbf{m} + \alpha \cdot \mathbf{C}[p,t]$. Independently of the temporary interpretation of the PN (deterministic, Markovian stochastic, etc.), the interpretation of the transition firing will be deterministic in the approximated continuous model. Not all discrete nets can be appropriately continuized, and the properties can differ surprisingly between the discrete model and its continuous approximation (then, care must be taken when continuizing a model).

4.4 Semantics in continuous PN

The state equation $\mathbf{m} = \mathbf{m_0} + \mathbf{C} \cdot \boldsymbol{\sigma}$ summarizes the marking evolution, and as it varies in a continuous way, it can be derived with respect to time: $\dot{m} = \mathbf{C} \cdot \dot{\sigma}$ (Recalde and Silva 2001). The value $\dot{\sigma}$ represents the

flow through the transitions, and it is usually denoted by **f**. On the whole it depends locally on the marking and, therefore, on time. If $\mathbf{f}(\tau)$ is defined with the usual semantics in discrete nets, by an interpretive extension, the temporary evolution of the Continuous PN can be obtained:

- *Infinite Server Semantics* The enabling degree of t_i is $\mathbf{e}(\tau)[t_i]= \min_{p\in\bullet ti} \{\mathbf{m}[p]/\mathbf{Pre}[p,t_i]\}$ and represents the number of active servers in the transition at instant τ. The rate associated to t_i is $\boldsymbol{\lambda}[t_i]$ and transitions fire with $\mathbf{f}(\tau)[t_i]=\boldsymbol{\lambda}[t_i]\cdot\mathbf{e}(\tau)[t_i]$.
- *Finite Server Semantics*. The firing speed $\mathbf{f}(\tau)[t_i]$ is upper bounded by $K[t_i]$ times the speed of one server $\mathbf{F}[t_i]$, and then the transitions are fired with $\mathbf{f}(\tau)[t_i]\leq K[t_i]\cdot\mathbf{F}[t_i]$. Obiously $\mathbf{f}(\tau)[t_i]=K[t_i]\cdot\mathbf{F}[t_i]$ if $\mathbf{e}(\tau)[t_i] \geq K[t_i]$
- Multiple service. The rate associated to t_i ,$\boldsymbol{\lambda}[t_i]$, must by multiply by the service $n[t_i]$.

4.5 Delays in continuous PN

In PN material delays are often used, similar to material delays in FD, but similar delays can also be modelled with the information. Table 3 shows both types of delays in ISSCPN. The dynamics (the differential equation) is again similar in both delays (a first order system), but material delay is applied to the flow (arcs) while information delay is applied to the information of a state variable (control arcs with the information of a place).

Table 3. Sketch, differential equation, FD and ISSCPNs in material and information delays.

Material Delay	Information Delay
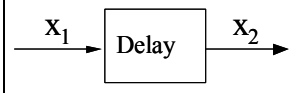	
$\dot{x}_2 = \frac{1}{T_a}(x_2 - x_1)$ (T_a is the delay time)	
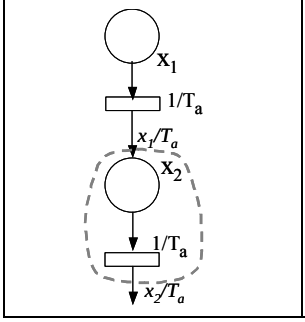	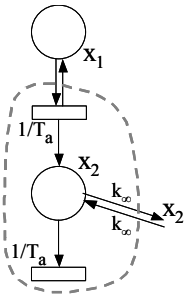

But there exist another important difference between the delays y continuous systems and in continuized systems. With the ISSCPN formalism we can model the delays used in SD, but with the ISSCPN formalism and the PN methodology a delay is just a transition. The difference between both methodologies arises from the fact that in FD a delay of something (material or information) is modelled, while in PN a delay of every part (of the material, usually) is modelled.

REFERENCES

Banks, J., Carson, J. S., Nelson, B. L. and Nicol, D. M., 2001. *Discrete event system simulation*. Ed. Prentice-Hall Inc, Upper Saddle River, USA.

David, R. and Alla, H., 2005. *Discrete continuous and hybrid petri nets*. Ed. Springer-Verlag, Berlin.

DiCesare, F., Harhalakis, G., Proth, J. M., Silva, M. and Vernadat, F. B., 1993. *Practice of Petri nets in manufacturing*. Ed. Chapman & Hall, London, UK.

Farina and Rinaldi, 2000. Positive Linear Systems. Theory and Applications. Pure and Applied Mathematics, John Wiley and Sons, New Cork.

Forrester, J. W., 1961. Industrial Dynamics. MIT Press, Mass, Cambridge.

Jiménez, E. and Pérez, M., 2004. "Simulation and optimization of logistic and production systems using discrete and continuos PN". *Simulation: Transactions of the Society for Modeling and Simulation International*, 80, (3), 131-142.

Jiménez, E., Pérez, M. and Latorre, J. I., 2005. "On deterministic modelling and simulation of manufacturing systems with Petri nets". *Proceedings of European Modeling Simulation Symposium (EMSS05),* pp. 129-136.

Jiménez, E., Recalde, L. and Silva, M., 2001. "Forrester Diagrams and Continuous Petri Nets: a Comparative View". *Proceedings of the 8th IEEE Internstional. Conference on Emerging Technologies and Factory Automation*, (2) 85-94.

Jiménez, E., Recalde, L., Julvez, J. and Silva, M., 2004. "Continuous Views of Discrete Event Systems: considerations on Forrester Diagrams and Petri Nets". *Proceedings of IEEE International Conference on Systems, Man & Cybernetics (SMCC'04).*

Recalde, L. and Silva, M., 2001. "PN fluidification revisited: Semantics and steady state", APII-JESA, 35(4):435-449.

Silva, M. and Recalde, L., 2002. "Petri nets and integrality relaxations: A view of continuous Petri nets", IEEE Trans. On Systems, Man, and Cybernetics, 32(4):314-327.

Silva, M. and Recalde, L., 2003. "Unforced Continuous Petri Nets and Positive Systems. Positive Systems", Proc. First Multidisciplinary International Symposium on Positive Systems: Theory and Applications (POSTA 2003), 294, pp55-62.

Silva, M., 1993. Introducing Petri Nets. In *Practice of Petri Nets in Manufacturing*, 1-62. Chapman&Hall.

AUTHORS BIOGRAPHY

Emilio Jiménez Macías studied Industrial Engineering (with Computer Science, Electronics and Automation specialty) by the University of Zaragoza. After working several years in the industrial private sector (Researching and Developing Department head position), returned to the university, as an Assistant Professor to the University of La Rioja, in 1997, where he works presently in the Electrical Engineering Department (Coordinator of the System Engineering and Automation Group). In 2001 he presented his PhD thesis about Industrial Automation. His research areas include factory automation, modeling and simulation, and industrial processes. His main works are developed with the automatic group of the University of Zaragoza.

Mercedes Pérez de la Parte received the BS degree in Telecommunications Engineering from the University of Seville in 1997. She has held research and teaching positions at the University of Los Andes, Venezuela, in 2000, and research position at the University of Seville since 1997 until present. She has attended all the PhD courses and is presently preparing her PhD dissertation. She is Assistant Proffesor at the Departamento de Ingeniería de Sistemas y Automática of the University of Seville, Spain, since 2000.

Juan Ignacio Latorre is Industrial Engineer. He has developed his professional career in the industry and in educative institutions. Currently he is preparing his PhD Thesis in DEVS optimisation based on PN. Nowadays he is a teacher at the Public University of Navarra. His research areas include factory automation, modeling and simulation, and industrial processes. His main works are developed with the automatic group of the University of La Rioja.

PERFORMANCE OPTIMIZATION OF A CNC MACHINE THROUGH EXPLORATION OF TIMED STATE SPACE

Miguel A. Mujica[a], Miquel Angel Piera[b]

[a,b]Autonomous University of Barcelona,
Department of Telecommunications and Systems Engineering,
Barcelona, Spain

[a]MiguelAntonio.Mujica@uab.es, [b]MiquelAngel.Piera@uab.cat

ABSTRACT
Flexible production units provide very efficient mechanisms to adapt the type and production rate according to fluctuations in the demand. The optimal sequence of the different manufacturing tasks in each machine is a challenging problem that can deal with important productivity benefits. In this paper a Coloured Petri Net model of an eyeglass flexible production machine to support the evaluation of different task sequences for a given production mix, is presented. The problem of finding an optimal sequence for this machine is faced with an approach which uses the state space of the model as a search space. Due to the state space explosion, the model has been developed to support some heuristics in order to avoid the analysis of non-optimal scenarios.

Keywords: timed coloured Petri nets, state space, time, manufacture, production systems, optimization

1. INTRODUCTION

A manufacturing process can be understood as a sequence of different activities that transform raw materials into goods. According to each particular industry, different transformation tasks (each one with a particular set of constraints) must be properly sequenced. The coordination of production resources through production steps must be carried out under the time restrictions inherent to the dynamic of the system (scheduling).

Due to the inherent difficulties to deal with a sequence that could minimize non-productive time operations and maximize a cost function preserving all the production constraints, it is necessary to develop decision support tools that help the scheduler or decision maker to give an acceptable schedule or solution which fulfils all the requirements.

Industrial systems can be modelled in detail using available simulation tools (Arena, PROMODEL, etc), which result very useful to evaluate the performance of different scenarios. Unfortunately, simulation techniques as a decision support tool has the drawback that it only covers a small set of the whole possible scenarios of the system which does not guarantee that the obtained production sequence is the best one.

In order to ensure optimality all the possible scenarios of a system must be analyzed, but this process can not be performed using now a days commercial simulation tools. Coloured Petri Nets (CPN) is a modelling formalism which has been widely used to model and verify discrete event systems. The timed state space of CPN (TSS) is an analysis tool which allows storing the different states of the model along with their time characteristics. State Space analysis has been used traditionally to verify properties such as liveness, boundedness and reachability among others (Jensen and Christensen 2009). The TSS can also be explored in order to find sequences of nodes in the state space (paths) that go from an initial node (initial state of the model) to an objective one. The problem that arises with state space approaches is the state explosion (Valmari 1996) which sometimes forces a partial exploration of the TSS or the implementation of reduction techniques (Christensen and Mailund 2002, Jensen and Kristensen 2009) which can not be applied in all types of models.

In (Narciso et al. 2005) an approach to explore the most promising branches of the TSS of a system specified under the CPN formalism is presented, which evaluates the time stamp values of each node to determine if a branch must be explored or not. In (Mujica and Piera 2007, Mujica and Piera 2008) the original algorithm has been redesigned to separate the generation of the TSS from the analysis of repeated nodes supporting specific heuristics for both phases (two-step algorithm) which produces a better overall performance.

Analyzing the TSS under this perspective does not ensure optimality yet, but the performance is improved yielding results close to optimal configurations or even obtaining sometimes the optimal solutions after the second phase. The two-step algorithm has been implemented to give a solution for the model of an eyeglass production machine.

The number of nodes in the TSS of the developed model varies according to the workload to be

sequenced. The normal workload for this kind of machines ranges from 20 to 25 eyeglasses per hour.

The rest of this paper is organized as follows. In the following section the modelling formalism and the analysis tool is introduced. In section 3 the CPN model of the CNC machine is presented. In section 4 the CNC model is analyzed using the two-step algorithm with different workloads. The results and comparison tables are presented in section 5. Finally, conclusion and future work are given in section 6.

2. COLOURED PETRI NET FORMALISM

A Coloured Petri Net can be defined as the tuple (Jensen 1997):

$$CPN = (\sum, P, T, A, N, C, G, E, I)$$

Where

$\sum = \{ C_1, C_2, \ldots, C_{cn}\}$ represents the finite and not-empty set of colours. They allow the attribute specification of each modelled entity.

$P = \{ P_1, P_2, \ldots, P_{np}\}$ represents the finite set of place nodes.

$T = \{ T_1, T_2, \ldots, T_{tn}\}$ represents the set of transition nodes which normally are associated to activities in the real system.

$A = \{ A_1, A_2, \ldots, A_{an}\}$ represents the directed arc set, which relates transitions and place nodes.

N = is the node function $N(A_i)$, which is associated with the input and output arcs. If one is a place node then the other must be a transition node and vice versa.

C = is the colour set function, $C(P_i)$, which specifies the combination of colours for each place node.

$$C(P_i) = C_j \qquad P_i \in P, C_j \in \sum$$

G = is a guard function, it is associated to transition nodes, $G(T_i)$, and normally used to inhibit the event associated with the transition based on the attribute values of the processed entities. If the processed entities satisfy the arc expression but not the guard, the transition will not be enabled.

E = Is the function for the arc expressions $E(A_i)$. For the input arcs it specifies the quantity and type of entities that can be selected among the ones present in the place node in order to enable the transition. When it deals with an output place, it specifies the values of the output tokens for the state generated when transition fires.

I = Initialization function $I(P_i)$, it allows the value specification for the initial entities in the place nodes at the beginning of the simulation. It is the initial state for a particular scenario.

The number of tokens and the token colours in each individual place represent the state or *marking* of the model.

2.1. The Timed State Space

The state space of CPN models is the set of all possible states that can be reached from an initial state; therefore it is also called the *reachability tree* (RT). Traditionally the RT has been used to evaluate CPN properties such as *reachability*, *boundedness*, *liveness* among others (Christensen and Mailund 2002, Jensen 1997) which determine the behaviour of the model.

The RT is a directed graph in which the nodes represent the states of the CPN model that are connected with their successor nodes through directed arcs. The characteristics of the reachability tree are:

- The root node represents the initial marking of the system.
- There must be generated as many successor nodes as enabled transitions a particular state has.
- The successor nodes correspond to the new states once the firings have taken place.
- The connecting arcs represent transition firings and also contain the information of the elements that caused the firings.
- If it is detected that a successor state has been previously generated, it will be labelled as *Old* and it will not be evaluated again.
- If a state does not have any enabled transition, this state will be called a *Dead Marking.*
- If a node is neither a dead marking nor a repeated one, it is a new state (which denotes a state never reached before).

In order to evaluate the system performance, it is more useful to develop timed CPN models. They differ from the ordinary CPN in the way that the tokens have time stamps and each state has a global clock (Jensen 1997). However in most cases the timed reachability tree (TRT) is bigger that the one for the underlying untimed CPN model because it is typical that the model reaches states whose underlying untimed states are the same of others differing only in the time stamps values.

2.2. The Improved Two-Step Algorithm

A two-step algorithm (Mujica and Piera 2008) has been developed based on the previous work of Narciso and Piera (2005), which analyzes the sub trees of the repeated untimed states to avoid the generation of branches that only differ from each other by their time values.

In the first step, the algorithm generates the different states that can be reached by the model using a depth-first traversal algorithm (DFS) until the complete RT is generated or the final conditions are satisfied (Mujica and Piera 2008). During this phase when a state is generated whose underlying untimed state is exactly the same as a previously generated one but differs only by its time values the repeated state is not evaluated and the original state (old node) is stored in a data structure along with the time elements of the repeated state. This procedure is carried out for all the repeated states

consequently reducing the computational effort through the avoidance of branch exploration in the RT.

In the first step, the state-generation algorithm searches for the objective states. Once the states are found, it stores the path that leads from the initial state to the objective one. Figure 1 illustrates the elements of the two-step algorithm. On the left hand side there is the RT structure and one feasible path, on the right hand side the old-node structure, altogether generated during the first step. In this first step some questions about the model properties can be answered as well (e.g. deadlocks, reachability, etc).

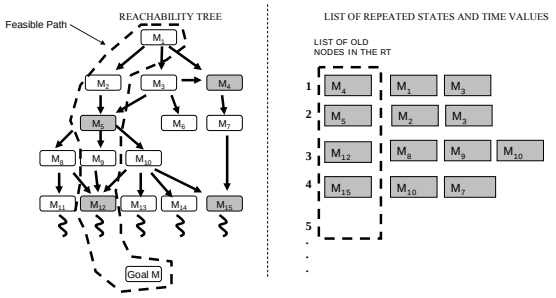

Figure 1: A feasible path and the old-node list

The second step of the algorithm (Mujica and Piera 2007, Mujica and Piera 2008) evaluates the old nodes through the analysis of the time elements of the repeated states stored in the old-node structure (right hand side of the figure) in order to optimize the feasible paths. It analyses the repeated nodes to determine which time stamp combination is the best for the optimization objectives (reduction of makespan). The old nodes are evaluated under the decision rule presented in (Narciso et al. 2005); those which lead to an objective state with poor time values are not analyzed. For the repeated nodes which give an unclear result, an exploration to the objective state is done, allowing evaluating the final state and taking a decision. A time updating is done in the feasible path for those states for which better values can be surely produced in the objective state.

Let us take the M_4 old node as an example; the analysis of the repeated states time stamps deals with a node with better time values (let us consider M_3), then nodes in the feasible path will be updated with new time stamps information till the objective state.

When the main objective is the optimization of the makespan, it is possible to improve the performance analysis of the two-step algorithm through heuristics in the first step. The idea behind the heuristics is to lead the DFS algorithm through the implementation of a cost function that assigns a value to each node in the successor nodes. The function analyzes the time stamp values of a state and assigns a value to each state to differentiate which one will increase less the global clock in the subsequent evaluation. The DFS algorithm selects the states that reduce the most the global clock advance.

3. SYSTEM DESCRIPTION

The presented case study is about the scheduling of an automated machine which has to verify and correct eyeglasses. Figure 2 illustrates the elements of the automated machine.

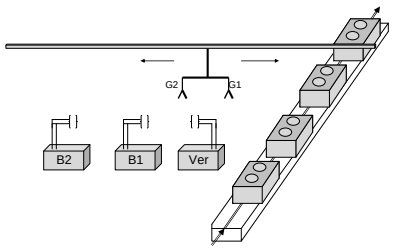

Figure 2: The automated CNC machine

The machine has three work stations. One is for verification purposes (**Ver**), it checks whether the lenses have the correct dimension specification. The second and third work stations make some labour on the lenses so they can fit in the correspondent chassis model (**Bevelling: B1 and B2**). One crane with two holders (**G1** and **G2**) is used for the transportation of the lenses from the buckets with lenses to the work stations. Each eyeglass is composed by two lenses (right and left lenses). The glasses must follow a sequence through the whole process. First they must be verified and then they must be bevelled. It is not mandatory that once one eyeglass has undergone one operation it must follow the remaining operations immediately. It is possible that the machine takes one lens for an operation, and thereafter takes a different one for another operation. The lenses can be selected for their operations without any particular order, but the operation sequence of each eyeglass must follow a specific order: a verifying operation followed by a bevelling operation.

The latter must be done for each pair of lenses so if three glasses are to be processed, then six lenses must follow the operations in the work stations.

The problem consist to determine the best sequence of operations (considering also the crane movements) to serve a certain lens bevelling mix. Note that there are three different bevel operations according to the glass support characteristics, each bevel operation require a different time, which complicates considerably the scheduling policy to avoid idleness stats in the crane and in the verification machine.

3.1. Colour Definition

The production system was modelled with the Timed-CPN formalism. Information about processing times for the bevelling operations as well as the values of the operation sequences have been coded in the colours of each token. Table 1 shows the colours used to encode the information in the model. Column one defines the variable used for the colour, column two defines the

domain values of the correspondent variables, and column three gives a brief description of the information stored in the colours.

Table 1: Colour definition for the CPN Model

COLOUR	DEFINITION	DESCRIPTION
I	{0,1}	This colour is used to allow only one lens movement through the guard in place G
Idc	Integer	This colour is used only as identifier
lid	Integer	This colour is used as the lens identifier in the VER place.
lidl	Integer	This colour is used for the identifier of the left lens in the glass
lidr	Integer	This colour is used for the identifier of the right lens in the glass
ell	Integer	This colour identifies the number of operation already taken in the left lens
elr	Integer	This colour identifies the number of operation already taken in the right lens
tvisll	Integer	This colour specifies the time spent when the left lens is being beveled
tvislr	Integer	This colour specifies the time spent when the right lens is being beveled
posc	Integer	This colour is used as an identifier of the number of lenses of the same type
posg	Integer	This colour is used to specify the physical position of the creane that move the lenses

The place nodes in the CPN model use multisets composed with the colours previously defined, Table 2 shows the colour sets used for the different place nodes in the CPN model.

Table 2: Colour set definition for the place nodes

PLACE	COLOUR SET	DESCRIPTION
Buckets	C=product idc*posc*lidl*lidr*ell*elr*tvisll*tvislr	The tokens in this place hold the information of each pair of glasses, defined by the values of the colours.
Crane	G= product lidl*lidr*posg	The tokens in this place model the information of the crane that moves the lenses through the different stations in the process.
G	I	This place is used only to limit the movement of the crane with the corresponent guards in the transitions that model the movement of the crane
Ver	V= lidl	The tokens in this place represent the verifying machine, since there is only one verifying station it only has one token.
Bevelin g	V=lidl	The tokens of this place model the bevelling machines, in this case the system has two machines therefore the model will have two tokens.

3.2. The CPN transitions

The model has been developed in group of transitions; two of those groups are for the bevelling and verifying operations, and the rest for modelling the transport of the lenses through the different stations in the system.

3.2.1. Operation Transitions

The verifying operation is a group of four transitions, two for the left lenses, and another two for the right lenses. These transitions model the activities undergone by the lenses during the operation processes. The common input places to these transitions are **Ver**, **Crane**, **Buckets** and **G**. Figure 3 illustrates one of the transitions of this second group. Transition T9 will be enabled if some conditions are satisfied:

- There are buckets which have already been verified once (**ell=2**)
- The crane is in position number three (**posg=3**), i.e. one token of type 1'(g1,g2,3)
- One of the holders of the crane is available (**g1=0 orelse g2=0**)
- The verifying machine is available (**c3<1000**)
- The G place doesn't constraints the firing of this transition but it helps to activate a crane movement.

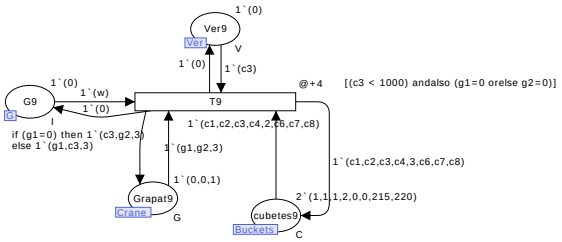

Figure 3: Example of verifying transitions

The bevelling operations are a group of four transitions, two for the right lenses and another two for the left lenses. These transitions also have four input places: **Bevelling**, **Crane**, **Buckets** and **G**. In order to fire the bevelling operation, the following conditions must be satisfied:

- The crane must have available holders (**g1=0 orelse g2=0**)
- The previous operations (verifying1, veryfing2) have been already performed. This is verified with the identifiers **ell** or **elr**.
- The sequence of the bevelling operations is the correct one (**lidr** or **lidr** identifiers)
- The crane is in the correct position for the bevelling operations (**posg = 4**)

Each time one of these transitions fires, the colour of the token in place G is turned into 0, allowing another movement of the crane.

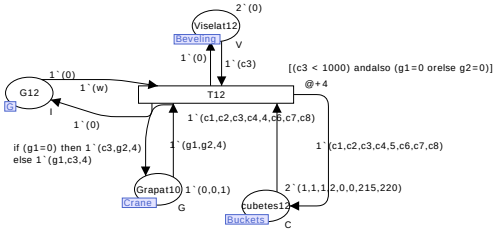

Figure 4: Example of bevelling transitions

3.2.2. Movement Transitions

The modelling of the pick up and delivery of lenses by the crane is modelled with four transitions, two transitions for the left lenses and another two for the right lenses. Figure 5 presents one transition

corresponding to the left lenses. The transition models the pick up of the left lenses from the buckets.

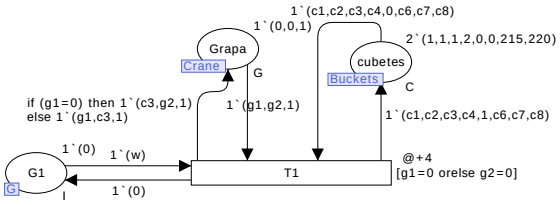

Figure 5: The pick up transitions

In order to pick up any lens, the following conditions must be satisfied:

- The crane must be in the correct position (**posg=1**)
- The lenses to be picked up must be ready for the initial operation (**ell=0**)
- Any of the two holders of the crane must be empty (**g1=0 orelse g2=0**)
- In the case of releasing the lenses, the correspondent transition is equivalent, and can be easily constructed. The conditions that must hold for that transition are:
- The crane must be in the delivery position for the correspondent operation
- The operation taken in the left lens must be the correspondent to the operation, expressed by the **ell** colour
- The crane must carry the correspondent lens

The movement of the crane is modelled by a group of four transitions. Figure 6 exemplifies one transition of the movement group.

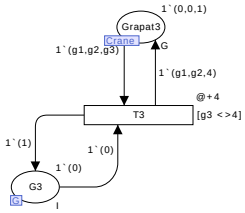

Figure 6: Crane movement

The crane movement is modelled by the token in the place node **Crane**, the **posg** colour models the current position of the crane. Two conditions must be fulfilled in order to allow the movement:

- The correspondent position is not already occupied by the crane (**g3<> 4**)
- Last operation was not a crane movement., i.e. the token in the G place is 1'(0)

The transitions presented in this section are examples of the group transitions. The complete model can be constructed in a straightforward way following the examples given.

4. IMPLEMENTED SCENARIOS

The eyeglasses types are differentiated by the identifiers and by the amount of work that must be done in the bevelling operation. Based on this information, three types of glasses are defined for the CPN model which corresponds to tokens in the **Buckets** place node:

Type A glass: 1'(1,1,1,2,0,0,215,220)
Type B glass: 1'(2,1,3,4,0,0,120,120)
Type C glass: 1'(3,1,5,6,0,0,540,540)

In order to analyze the system, some workloads were evaluated. Table 3 shows the workload information. The first column shows the size and type of glasses to be processed, and the second presents their correspondent initial state of the timed CPN model.

Table 3: Workload scenarios

WorkLoad	Initial Marking
2 Glasses, 2 type A	Crane: 1'(0,0,1)@0 Buckets: 2'(1,1,1,2,0,0,215,220)@[0,0] G: 1'(0)@0 Ver: 1'(0)@0 Beveling: 2'(0)@[0,0]
3 Glasses, 3 type A	Crane: 1'(0,0,1)@0 Buckets: 3'(1,1,1,2,0,0,215,220)@[0,0,0] G: 1'(0)@0 Ver: 1'(0)@0 Beveling: 2'(0)@[0,0]
3 Glasses, 2 type A, 1 type B	Crane: 1'(0,0,1)@0 Buckets: 2'(1,1,1,2,0,0,215,220)@[0,0]+1'(2,1,3,4,0,0,120,120)@0 G: 1'(0)@0 Ver: 1'(0)@0 Beveling: 2'(0)@[0,0]
4 Glasses, 2 type A, 1 type B, 1 type C	Crane: 1'(0,0,1)@0 Buckets: 2'(1,1,1,2,0,0,215,220)@[0,0] +1'(2,1,3,4,0,0,120,120)@0 +1'(3,1,5,6,0,0,540,540)@0 G: 1'(0)@0 Ver: 1'(0)@0 Beveling: 2'(0)@[0,0]
22 Lenses (Normal Workload): 7 type A, 13 type B, 2 type C	Crane: 1'(0,0,1)@0 Buckets: 7'(1,1,1,2,0,0,215,220)[0,0,0,0,0,0,0] +13'(2,1,3,4,0,0,120,120)@[0,0,0,0,0,0,0,0,0,0,0,0,0] +2'(3,1,5,6,0,0,540,540)@[0,0] G: 1'(0)@[0] Ver: 1'(0)@[0] Beveling: 2'(0)@[0,0]

The analysis of the RT started with small workloads for the same type of eyeglasses (i.e. 2 and 3 eyeglasses of type A). The model was then tested increasing the variety in the workload. The model was finally tested using a real-size workload (22 lenses).

The primary target of these tests was to evaluate the size of the TSS and the final objective was to obtain an optimal scheduling for real-size workloads.

5. RESULTS

The two-step algorithm was applied to the workloads and the resulting makespan for the different configurations is presented in Table 4. The first column shows the final state of the system along with its time stamp values, the second column shows the makespan of the final state expressed in seconds, the third column shows if the RT was explored completely and the fourth column shows information about the generated tree.

Table 4: Scenario Solution

Final Marking	Makespan	No. of Different analyzed Nodes	Structural Information of the TRT
Crane: 1'(0,0,1)@616 Buckets: 2'(1,1,1,2,6,6,215,220) @[599,616] G: 1'(0)@591 Ver:1'(0)@376 Beveling:2'(0)@[599,616]	616 seg.	Complete RT	No. Nodes: 19,232 No. Arcs:59,610 No. OLD Nodes:15,431 Levels: 53
Crane: 1'(0,0,1)@1632 Buckets: 3'(1,1,1,2,6,6,215,220) @[1109,1385,1628] G: 1'(0)@1632 Ver: 1'(0)@1393 Beveling: 2'(0)@[1377,1620]	1,228 seg	Complete RT	No. Nodes: 172,242 No. Arcs:765,177 No. OLD Nodes:145,911 Levels: 84
Crane: 1'(0,0,1)@0 Buckets: 2'(1,1,1,2,6,6,215,220) @[0,0] +1'(2,1,3,4,6,6,120,120)@0 G: 1'(0)@0 Ver: 1'(0)@0 Beveling: 2'(0)@[0,0]	1,183 seg	Complete RT	No. Nodes: 562,799 No. Arcs:1,800,951 No. OLD Nodes:471,939 Levels: 81
Crane: 1'(0,0,1)@1898 Buckets: 2'(1,1,1,2,6,6,215,220) @[1483,1874] +1'(2,1,3,4,6,6,120,120)@1878 +1'(3,1,5,6,6,6,540,540)@1894 G: 1'(0)@1898 Ver: 1'(0)@1639 Beveling: 2'(0)@[1866,1886]	1,906 1,898	500,000 nodes 800,000 nodes	--- ---
Crane: 1'(0,0,1)@10421 Buckets: 7'(1,1,1,2,6,6,215,220) @[8253,8512,8771,9030,9314,9598,9849] +13'(2,1,3,4,6,6,120,120) @[6062,6226,6390,6554,6718,6882,7046, 7210,7362,7452,7641,7830,7994] +2'(3,1,5,6,6,6,540,540)@[5898,10417] G: 1'(0)@[10421] Ver: 1'(0)@[9857] Beveling: 2'(0)@[9841,10409]	10,421 seg	800,000 nodes	---

The results of the first three scenarios were obtained exploring the complete RT for those workloads. It can be seen that when the workload comprises more than three eye glasses, the analyzed RT is bigger than 800,000 nodes. Therefore the biggest workload for these machines was solved with a partial analysis, giving a makespan of 10,421 sec.

The RT for this workload was not completely explored because it shown memory overloading problems. When the RT is partially explored, it is not possible to know how close to the optimal the solution is. In order to compare the two-step algorithm approach with another one, the same model has been coded in CPN Tools whose SS tool generates the complete RT without any simplification. Table 5 presents a SS comparison between these two approaches.

Table 5: Comparison with the CPN SS algorithm

Workload	CPN Tools Timed Model	Two-Step Algorithm
2 Glasses, 2 type A	Nodes: 389,884 Arcs: 457,992 Secs: 8558 Status: Full	No. Nodes: 19,232 No. Arcs:59,610 No. OLD Nodes:15,431 Levels: 53
3 Glasses, 3 type A	Unable to Generate the SS	No. Nodes: 172,242 No. Arcs:765,177 No. OLD Nodes:145,911 Levels: 84
3 Glasses, 2 type A, 1 type B	Unable to Generate the SS	No. Nodes: 562,799 No. Arcs:1,800,951 No. OLD Nodes:471,939 Levels: 81

This table allows appreciating the amount of computational efforts avoided with the two-step algorithm. It can be seen that the size of the RT using an exhaustive search for timed models is considerable bigger than the one generated by the two-step algorithm. The saved information by the two-step algorithm allows exploring in the second step the branches that give better results in the objective state. It can also be appreciated that for big workloads the algorithm in CPN Tools fails generating the whole SS due to computer resource limitations.

6. CONCLUSIONS AND FUTURE WORK

A case study of an eyeglasses CNC machine has been presented. It can process a variety of eyeglasses with different type of lenses. Some operations must be carried out on the lenses, and they must follow a specified sequence in order to be completed. The problem of sequencing the operations in an optimal way is a difficult task and must be solved in a smart way due to the combinatorial nature of the problem. The scheduling problem was solved for five workloads, but the complete RT could be explored only in the first three cases which appear to have a relative small RT.

The biggest workload problem could not be solved exploring the complete RT due to computer resource limitations, but the advantage of using a DFS algorithm is that it allowed generating a feasible path. Due to that the DFS algorithm selects the nodes to be analyzed based on a heuristic which has given good results in other applications (Mujica and Piera 2008) it can be trusted that the given solution is not too far from the optimal. The optimal scheduling of the normal workload is left as an opened unsolved problem. Based on the size of the state space it can be used as a benchmarking for optimization algorithms.

REFERENCES

Christensen, S., Mailund, T., 2002, "A Generalized Sweep-Line Method for Safety Properties", in FME, Springer – Verlag, Berlin-Heidelberg.

Jensen, K 1997. "Coloured Petri Nets: Basic Concepts, Analysis Methods and Practical Use". Vol. 1 Springer-Verlag. Berlin.

Jensen, K, 1997, "Coloured Petri Nets: Basic Concepts, Analysis Methods and Practical Use", Vol 2, Springer-Verlag. Berlin

Jensen K, Kristensen L.M.; 2009, "Coloured Petri Nets: Modeling and Validation of Concurrent Systems", Springer-Verlag.

Mujica, M., Piera, M.A., 2007,"Improvements for a Coloured Petri Net Simulator", in *Proceedings of the 6th EUROSIM Congress on Modeling and Simulation*, September 9-13, Ljubljana, Slovenia

Mujica, M., Piera, M.A., 2008,"Optimizing Time Performance in Reachability Tree-Based Simulation", in *Proceedings of the International Mediterranean Modeling Multiconference*, September 17-19, Campora Sant Giovanni, Italy.

Narciso, M., Piera, M.A., y Figueras J., 2005, "Optimización de Sistemas Logísticos Mediante Simulación: Una Metodología Basada en Redes de Petri Coloreadas", Revista Iberoamericana de Automática e Informática Industrial, vol 2(4), p.p. 54-65IAII, Valencia, España.

Valmari A.,1996, "The State Explosion Problem", in *Lecture Notes in Computer Science*, vol 1491, Springer-Verlag, London

http://wiki.daimi.au.dk/cpntools/_home.wiki

AUTHORS BIOGRAPHY

Miguel A. Mújica Mota was born in Mexico City. He studied chemical engineering at Autonomous Metropolitan University of Mexico, an MSc in Operations Research in the National Autonomous University of México. He also received a Master's in Industrial Informatics from the Autonomous University of Barcelona. Actually he is a PhD Student at Autonomous University of Barcelona. He also has professional experience in manufacture and production planning in the cosmetic industry. His research interest focuses on optimization techniques using the Coloured Petri Nets formalism aiming to solve industrial problems.

Miquel Àngel Piera received his MSc (Control Engineering) from the University of Manchester Institute of Technology in 1990 and his PhD degree from the Autonomous University of Barcelona (Spain) in 1994. He participates in industrial research projects in the logistics and manufacturing field and at present he is Co-director of LogiSim, a Modelling and Simulation Institution sponsored and founded by the local government of Catalonia. Recently, he has published a modelling and simulation book that is being used for teaching in many Spanish universities.

PETRI NET BASED SCHEDULING APPROACH COMBINING DISPATCHING RULES AND LOCAL SEARCH

Gašper Mušič[(a)]

[(a)]University of Ljubljana
Faculty of Electrical Engineering
Tržaška 25, Ljubljana, Slovenia

[(a)]gasper.music@fe.uni-lj.si

ABSTRACT

The paper deals with Petri net based scheduling approach, where constructive heuristics in the form of dispatching rules is combined with a meta-heuristic embedded within the local search optimization algorithm. The approach is tested on some standard job shop benchmark problems.

Keywords: Petri nets, simulation, optimization, scheduling

1. INTRODUCTION

Optimization of planning and scheduling problems has been a subject of intensive research efforts within the production control community for several decades. Recently, the research interest in the scheduling area is increased due to the developments in other related technological fields, such as parallel processing in multi-core processors or cooperating action of autonomous mobile systems.

Among modelling formalisms suitable for description of systems with highly parallel and cooperating activities, Petri nets are perhaps the most widely used one. With Petri nets, production systems' specific properties, such as conflicts, deadlocks, limited buffer sizes, and finite resource constraints can be easily represented in the model (Tuncel and Bayhan 2007). This motivated the investigation of Petri net based optimization of planning and scheduling problems.

In our previous work a simulation based optimization approach applying Petri nets was intensively studied, as well as other, more classical approaches, such as dispatching rules and reachability tree based heuristic search (Gradišar and Mušič 2007, Löscher, Mušič and Breitenecker 2007, Mušič, Löscher and Breitenecker 2008, Mušič 2008).

In the reported works, Petri nets based scheduling methods were compared and a certain level of experience was gained about the behaviour of the methods in relation to different scales of problems. Among others, reachability tree based heuristic search methods were of particular interest, since the rich structural analysis framework of Petri nets seemed a promising way to derive a suitable heuristic function that would significantly improve the efficiency of the search and obtained results.

The obtained results meet the expectations for small or moderate size problems. Unfortunately, the results for complex problems, such as standard job-shop benchmark problems (Taillard 1993), are not satisfactorily, even with the advanced heuristic functions, such as proposed in (Yu, Reyes, Cang and Lloyd 2003).

Dispatching rules, on the other hand, are not among the best strategies for small size problems, since in general only a suboptimal solution can be obtained. Their performance, however, is not decreased for larger problems. The obtained solutions are still suboptimal but are obtained in computational time that is significantly shorter compared to other methods.

This motivated the investigations on combination of dispatching rules with other methods. In particular, a combination of dispatching rules and local search is tested in this paper.

2. JOB-SHOP SCHEDULING AND DISPATCHING RULES

A job-shop scheduling problem is a well known problem in the field of operations research. It is defined as the determination of the order in which a set of jobs (tasks)$\{J_i|i = 1,\ldots,n\}$ is to be processed through a set of machines (resources) $\{M_k|k = 1,\ldots,m\}$.

Job i is specified by a set of operations $\{o_j|j = 1,\ldots,m_j\}$ representing the processing requirements on various machines. Processing times are assigned to individual operations. Job shop problem assumes that all jobs have to be processed on all machines while the operations processing order (routing) is determined but not identical for individual jobs. The objective of a job shop scheduling problem is most often to determine a job sequence schedule for every machine, which will minimize the total makespan time.

This objective can be reached with various strategies including heuristic based dispatching rules. Application of dispatching rules in scheduling systems has been intensively investigated over the last decades. They are also used in commercially available production scheduling systems (Haupt 1989). Extensive overview of various rules and comments about their performance can be found in

Table 1: A subset of elementary dispatching rules

Rule	Meaning
SPT	Shortest Processing Time
LPT	Longest Processing Time
SR	Shortest Remaining processing time
LR	Longest Remaining processing time
RND	Random
FCFS	First Come First Served
EDD	Earliest Due Date

(Blackstone, Phillips and Hogg 1982, Haupt 1989, Panwalkar and Iskander 1977).

Dispatching rules belong to a set of constructive heuristic methods. The schedule is built step by step, making a rule-based decision whenever a conflict occurs, i.e. a machine is free and there are a number of candidate jobs that can be assigned to the machine.

Dispatching rules are useful for finding a reasonably good schedule with regards to a single objective such as the makespan (Pinedo 1995). Despite several reports on evaluation of various scheduling rules, it is impossible to identify any single rule as the best in all circumstances (Blackstone, Phillips and Hogg 1982). Some commonly used elementary dispatching rules are listed in Table 1.

3. LOCAL SEARCH

Local search is an iterative procedure which moves from one solution in the search space S to another as long as necessary. In order to systematically search through S, the possible moves from a solution s to the next solution should be restricted in some way. To describe such restrictions a neighbourhood structure $N : S \rightarrow 2^S$ is introduced on S. For each $s \in S$, $N(s)$ describes the subset of solutions which can be reached in one step by moving from s. The set $N(s)$ is called the neighbourhood of s. Usually it is not possible to calculate the neighbourhood structure $N(s)$ beforehand because S has an exponential size. To overcome this difficulty, a set AM of allowed modifications $F : S \rightarrow S$ is introduced. For a given solution s, the neighbourhood of s can be defined by $N(s) = \{F(s) \,|\, F \in AM\}$.

A general local search method may be described as follows. Each iteration starts with a solution $s \in S$ and then a solution $s' \in N(s)$ or a modification $F \in AM$ which provides $s' = F(s)$ is chosen. Based on the values of the objective function $f : S \rightarrow \mathbb{R}$, $f(s)$ and $f(s')$, the new solution is adopted or discarded. The next iteration starts with either the old or the new solution. Different methods of choice of the starting solution for the next iteration lead to different local search techniques (Brucker 2001).

3.1. Simulated Annealing

Local search algorithms are simple to implement and fast in execution, but they have the main disadvantage that they can terminate in the first local minimum, which might give an objective function that deviates substantially from the global minimum. The useful algorithms should be able to leave the local minimum by sometimes accepting transitions leading to an increase in the objective function. Simulated Annealing is an example of such an approach where cost-increasing transitions are accepted with a non-zero probability which decreases gradually as the algorithm continues its execution (Vidal 1993).

The pseudo-code of the Simulated Annealing local search algorithm is shown in Algorithm 1.

Algorithm 1 Simulated Annealing

```
generate initial solution s ∈ S;
i := 0;
repeat
  generate neighbour solution s' ∈ N(s);
  if f(s') ≤ f(s) then
    s := s';
  else if min(1, exp((f(s)−f(s'))/c_i)) > rnd([0,1]) then
    s := s';
  end if
  c_{i+1} := g(c_i);
  i := i + 1;
until termination criterion
```

During the Simulated Annealing based optimization run:

- s' is chosen randomly from $N(s)$
- in the $i-th$ step s' is accepted with probability

$$min(1, exp(\frac{f(s) - f(s')}{c_i}))$$

where (c_i) is a sequence of positive control parameters with $\lim_{i\rightarrow\infty} c_i = 0$.

This way, a local minimum can be left, but the probability for doing so will be low after a large number of steps. In the shown algorithm $rnd[0, 1]$ denotes a random function returning uniformly distributed random values between 0 and 1. Furthermore, the sequence (c_i) is created by a function g, i.e. $c_{i+1} = g(c_i)\ \forall\, i$ (Brucker 2001).

4. PETRI NETS AND A COMBINED METHOD

The previously described scheduling methods can be used in combination with various modelling formalisms. As mentioned in the introduction, a Petri net framework will be used here.

4.1. Petri nets

In the paper, Petri nets (Murata 1989, Cassandras and Lafortune 1999) are represented as Place/Transition (P/T) nets in a form of a five-tuple (P, T, I, O, M_0), where

- $P = \{p_1, p_2, \ldots, p_m\}, m > 0$ is a finite set of places.
- $T = \{t_1, t_2, \ldots, t_n\}, n > 0$ is a finite set of transitions (with $P \cup T \neq \emptyset$ and $P \cap T = \emptyset$).
- $I : (P \times T) \rightarrow \mathbb{N}$ is the input arc function. If there exists an arc with weight k connecting p_i to t_j, then $I(p_i, t_j) = k$, otherwise $I(p_i, t_j) = 0$.

– $O : (P \times T) \rightarrow \mathbb{N}$ is the output arc function. If there exists an arc with weight k connecting t_j to p_i, then $O(p_i, t_j) = k$, otherwise $O(p_i, t_j) = 0$.
– $M : P \rightarrow \mathbb{N}$ is the marking, M_0 is the initial marking.

Let ${}^\bullet t_j \subseteq P$ denote the set of places which are inputs to transition $t_j \in T$, i.e., there exists an arc from every $p_i \in {}^\bullet t_j$ to t_j. Transition t_j is enabled by a given marking if, and only if, $M(p_i) \geqslant I(p_i, t_j), \forall p_i \in {}^\bullet t_j$. An enabled transition can fire, and as a result removes tokens from input places and creates tokens in output places. If transition t fires, then the new marking is given by $M'(p_i) = M(p_i) + O(p_i, t_j) - I(p_i, t_j), \forall p_i \in P$.

The structure of the Petri net can also be given in a matrix representation (Murata 1989, Zhou and Venkatesh 1999). A $m \times n$ input matrix $\mathbf{I}$ is defined, whose (i, j) entry is $I(p_i, t_j)$. Similarly, an output matrix $\mathbf{O}$ of the same size is defined, whose elements are defined with $O(p_i, t_j)$. Matrices $\mathbf{I}$ and $\mathbf{O}$ precisely describe the structure of the Petri net and enable to explore the structure by linear algebraic techniques. Furthermore, the marking vector $\mathbf{M}$ where $M_i = M(p_i)$, and a firing vector $\mathbf{v}$ where every nonzero entry $v_j = c_j$ indicates that a transition t_j is fired c_j-times, are defined. Using these matrices a state equation

$$\mathbf{M}_k = \mathbf{M}_{k-1} + (\mathbf{O} - \mathbf{I}) \cdot \mathbf{v}_k \qquad (1)$$

can be written. The subscript k denotes a k-th firing in some firing sequence. It is important to note that a parallel firing of several transitions as well as multiple firings of a transition can be described with the state equation (1).

In order to enable a timed analysis of the modelled system behaviour, a P/T Petri net has to be extended with time information. A holding-duration principle (Bowden 2000) is used in the paper, meaning that a created token is considered unavailable for the time assigned to transition that created the token. The unavailable token can not enable a transition and therefore causes a delay in the subsequent transition firings. This principle is graphically represented in Figure 1, where the available tokens are schematized with the corresponding number of undistinguishable (black) tokens and the unavailable tokens are indicated by empty circles. The time duration of each transition is given beside the transition, e.g., $f(t_1) = d_1$. When the time duration is 0 this denotation is omitted. In Figure 1, τ denotes a model time represented by a global clock and τ_f denotes the firing time of a transition.

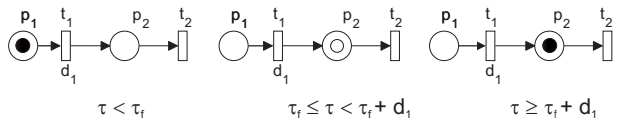

Figure 1: Timed Petri net with holding durations

It is natural to use holding durations when modelling most scheduling processes as transitions represent starting of operations, and generally once an operation starts it does not stop to allow another operation to start in between.

By using holding durations the formal representation of the timed Petri net is extended with the information of time, represented by the multiple $TPN = (P, T, I, O, M_0^t, d)$, where:

- P, T, I, O are the same as above,
- M_0^t is the initial state of a timed Petri net.
- $d : T \rightarrow \mathbb{R}_0^+$ is the function that assigns a non-negative deterministic time-delay to every $t_j \in T$.

The state of a timed Petri net is a combination of three functions $M^t = (m, n, r)$, where,

- $m : P \rightarrow \mathbb{N}$ is a marking function of available tokens.
- $n : P \rightarrow \mathbb{N}$ is a marking function of unavailable tokens.
- r is a remaining-holding-time function that assigns values to a number of local clocks that measure the remaining time for each unavailable token (if any) in a place.

A transition t_j is enabled by a given marking if, and only if, $m(p_i) \geqslant I(p_i, t_j)$, $\forall p_i \in \bullet t_j$. The firing of transitions is considered to be instantaneous. A new local clock is created for every newly created token and the initial value of the clock is determined by the delay of the transition that created the token. When no transition is enabled, the time of the global clock is incremented by the value of the smallest local clock. An unavailable token in a place where a local clock becomes available and the clock is destroyed. The enabling condition is then checked again.

The state equation (1) holds also for a timed Petri net with the difference that the marking vector components should be interpreted as $M_i = m(p_i) + n(p_i)$.

4.2. Petri net modelling of scheduling problems

An important concept in PNs is that of conflict. Two transition firings are in conflict if either one of them can occur, but not both of them. Conflict occurs between transitions that are enabled by the same marking, where the firing of one transition disables the other transition.

The conflicts and the related conflict resolution strategy play a central role when modelling scheduling problems. This may be illustrated by a simple example, shown in Figure 2. The example involves two machines $M = \{M_1, M_2\}$, which should process two jobs $J = \{J_1, J_2\}$, and where $J_1 = \{o_1(M_1) \prec o_2(M_2)\}$ and $J_2 = \{o_3(M_1)\}$. Job J_1 therefore consist of two operations, the first one using machine M_1 and the second one machine M_2, while job J_2 involves a single operation using machine M_1. Obviously, the two jobs compete for machine M_1. This is modelled as a conflict between transitions starting corresponding operations.

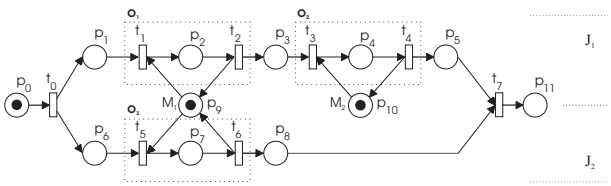

Figure 2: A PN model of a simple scheduling problem

Place p_9 is a resource place. It models the machine M_1 and is linked to t_1 and t_5, which start two distinct operations. Clearly, the conflict between t_1 and t_5 models a decision, whether machine M_1 should be allocated to job J_1 or J_2 first.

Similarly, other decisions are modelled as conflicts linked to resource places. The solution of the scheduling problem therefore maps to a conflict resolution in the given Petri net model.

4.3. Derivation of optimal or sub-optimal schedules

A derived Petri-net model can be simulated by an appropriate simulation algorithm. During the simulation, the occurring conflicts are resolved 'on the fly', e.g. by randomly choosing a transition in conflict that should fire. Instead, **heuristic dispatching rules**, (Panwalkar and Iskander 1977, Blackstone, Phillips and Hogg 1982), such as Shortest Processing Time (SPT) or Longest Processing Time (LPT), can be introduced when solving the conflicting situations. By introducing different heuristic dispatching rules (priority rules) decisions can be made easily. In this way, only one path from the reachability graph is calculated, which means that the algorithm does not require a lot of computational effort. The schedule of process operations can be determined by observing the marking evolution of the net. Depending on the given scheduling problem a convenient rule should be chosen. Usually, different rules are needed to improve different predefined production objectives (makespan, throughput, production rates, and other temporal quantities).

A more extensive exploration of the reachability tree is possible by **PN-based heuristic search method** proposed by Lee and DiCesare (1994). It is based on generating parts of the Petri net reachability tree, where the branches are weighted by the time of the corresponding operations. Sum of the weights on the path from the initial to a terminal node gives a required processing time by the chosen transition firing sequence. Such a sequence corresponds to a schedule, and by evaluating a number of sequences a (sub)optimal schedule can be determined. The method is further investigated in Yu et al. (2003), where a modified heuristic function is proposed and tested on a number of benchmark tests.

4.4. A combined method

Recent reports in scheduling literature show an increased interest in the use of meta-heuristics, such as genetic algorithms (GA), simulated annealing (SA), and tabu search (TS). Meta-heuristics have also been combined with Petri net modelling framework to solve complex scheduling problems (Tuncel and Bayhan 2007). With such an approach, the modelling power of Petri nets can be employed, and relatively good solutions of scheduling problems can be found with a reasonable computational effort. Compared to reachability tree based search methods, meta-heuristics require less memory.

On the other hand, systems based on dispatching rules are easily adapted to Petri net models, and provide solutions in short-time, which makes them applicable even for on-line scheduling. They can also been used for scheduling of complex systems, which makes them interesting for practice.

In order to combine good properties of dispatching rules with the potential of meta-heuristics, an approach is proposed here where dispatching rule based construction of scheduling solutions is embedded within the iterative procedure of the meta-heuristic based local search. More precisely, when generating a neighbouring solution to the current solution, the new solution is constructed in a rule based manner.

The simulated annealing approach is used for its simplicity, while the procedure could be easily adapted also to other methods. A solution $s \in S$ is represented by a sequence of firing vectors $s = \mathbf{v}_1\mathbf{v}_2 \dots \mathbf{v}_i \dots \mathbf{v}_f, \mathbf{v}_i \in \mathbb{N}^n$ that brings the initial marking M_0^t of a timed Petri net $TPN = (P, T, I, O, M_0^t, d)$ to the desired final marking M_f^t. A general concurrency assumption is considered, placing no restriction on the transition firings that may occur at the same time and their multiplicity. Thus in general, $\mathbf{v}_i$ contains more than one non-zero component and the corresponding values can be greater than one.

The initial solution is generated in a constructive manner, starting at initial marking and firing as many enabled transitions as possible at every step. Eventual conflicts are resolved by the chosen dispatching rule, e.g., if the SPT rule is chosen, the conflicting transition with the smallest time delay is chosen for firing. In case more than one conflicting transition is equally optimal with regard to the chosen rule, random choice is used among them. In case of several conflicts also the conflict resolution order is determined by the same rule, e.g., in case of SPT rule, the conflict involving the transition with the smallest time delay is resolved first. In case of several equal conflicts, a random choice is applied here as well.

Once a solution s is determined the neighbourhood $N(s)$ is defined as a set of all firing vector sequences that are derived in the following way:

- a firing vector $\mathbf{v}_i \in s$ is chosen,
- the initial part of s up to $\mathbf{v}_i$ is retained,
- the remainder of firing vector sequence is constructed anew in the same manner as at the previous solution, with the exception that the first conflict is resolved randomly.

During the iterative procedure, a new solution is constructed in the described way at every iteration. The resulting makespan is compared to the makespan of the previous solution and then the choice of the active solution for the next iteration is made in the same way as with the standard Simulated Annealing algorithm. The proposed approach is summarized by the Algorithm 2.

In the implementation of the algorithm, a small portion of the reachability tree is kept in memory for every active solution s. This portion of the reachability tree includes a sequence of markings determined by $\mathbf{v}_i \in s$. Both the marking vectors related to available and unavailable tokens must be kept, as well as the states of eventual active local clocks. This way the choice of an alternative firing

Algorithm 2 Simulated Annealing with Dispatching Rules

construct the initial solution $s \in S$ by a dispatching rule;
$i := 0$;
repeat
  randomly choose a firing vector $\mathbf{v}_i$ in s;
  copy s up to $\mathbf{v}_i$ to s';
  continue with the s' construction until a conflict is detected;
  resolve the conflict randomly;
  construct the remainder of s' by the dispatching rule;
  if $f(s') \leq f(s)$ **then**
    $s := s'$;
  else if $min(1, exp(\frac{f(s)-f(s')}{c_i})) > rnd([0,1])$ **then**
    $s := s'$;
  end if
  $c_{i+1} := g(c_i)$;
  $i := i + 1$;
until termination criterion

vector in a sequence is translated to a choice of a marking at a certain level of the tree, and then a modification of the firing vector that is used for the generation of the next marking. Only the marking sequences corresponding to the solutions s and s' are kept, so the memory requirements of the algorithm are low.

5. BENCHMARK TESTS

The performance of the algorithm was tested on a series of standard benchmark tests proposed by Taillard (1993), which are also available at *http://mistic.heig-vd.ch/taillard/*.

The job shop problem instances were considered, which are determined by the number of jobs and machines, predefined job routings and a set of randomly generated durations of job operations on specific machines.

To illustrate the problem instances a PN model of a simple non-standard problem instance (based on a test example from Taillard (1993)) is shown in Figure 3. The problem consists of four jobs and four machines. The job routings can be seen from the model while the operation durations are shown in Table 2.

Comparison of the minimum makespan for the problem calculated by the proposed algorithm and some other standard algorithms is shown in Table 3, where SA-SPT

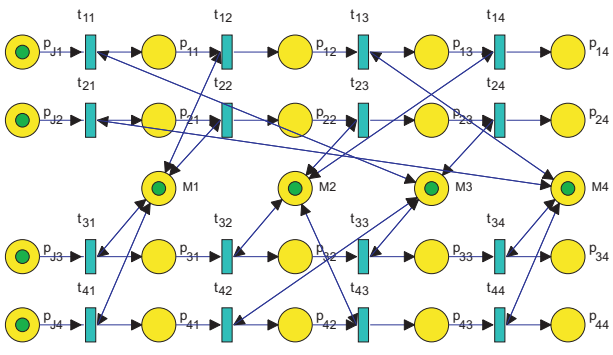

Figure 3: A simple job shop problem

Table 2: Operation durations for a simple job shop problem

Operation\Job	J_1	J_2	J_3	J_4
o_1	54	9	38	95
o_2	34	15	19	34
o_3	61	89	28	7
o_4	2	70	87	29

Table 3: Calculated makespan for a simple job shop problem

Algorithm	Makespan
SPT	286
LPT	341
SA-SPT	286
RT-search	272

denotes the proposed combined algorithm with the Simulated Annealing and the SPT rule, and RT-search stands for a reachability tree based heuristic search (Lee and DiCesare 1994, Yu et al. 2003). Here the heuristic function was chosen as proposed in Yu et al. (2003): $h(m) = -w' \cdot \overline{O} \cdot depth(M)$, where $\overline{O}$ is the average processing time of an operation, $depth(M)$ is the number of transition firings needed to reach M from M_0 and w' is a parameter set to $1/(2/3 \cdot n_{resources})$.

Clearly, the reachability tree based search outperforms other algorithms with regard to the result. It must be noted, however, that the computational effort in this case is much higher.

This drawback is much more obvious with complex problems. Table 4 shows the results for the standard job shop benchmarks with 15 jobs and 15 machines (Taillard 1993). For reference also the optimal values are listed (source: *http://mistic.heig-vd.ch/taillard/*). The reachability tree based search has to be limited to predefined maximum tree size in order to complete in a reasonable time. In addition to that, the heuristic function used within the search has to be chosen such that the search is directed more into the depth of the tree (increased w'), which makes the obtained solution very sensitive to decisions taken at initial levels of the tree and in many cases the quality of the obtained solutions is rather low. In contrast to that the SPT rule performs reasonably well with very low computational effort while the proposed SA-SPT algorithm enables to further improve the SPT solutions with a moderate effort.

Table 4: Calculated makespan for a set of 15 jobs/15 machines problems

Algorithm	Makespan				
	ta01	ta02	ta03	ta04	ta05
SPT*	1462	1429	1452	1668	1618
LPT*	1701	1674	1655	1751	1828
SA-SPT	1359	1358	1352	1362	1352
RT-search	1592	1465	1637	1590	1568
optimum	1231	1244	1218	1175	1224

* min out of 100 runs

To fully evaluate the potential of the proposed combination, a more exhaustive set of problem instances should be considered and the obtained results should be compared to other approaches.

6. CONCLUSIONS

The presented results indicate that the proposed combination of dispatching rules and local search performs relatively well with a moderate computational effort. The approach may be interesting for practice, in particular because of easy adaptation to various rules and also to different types of problem. In general, any scheduling problem that can be represented by a timed Petri net can be optimized in the the proposed way.

REFERENCES

Blackstone, J. H., Phillips, D. T. and Hogg, G. L., 1982. A state-of-the-art survey of dispatching rules for manufacturing job shop operations, *International Journal of Production Research*, 20 (1), 27–45.

Bowden, F. D. J., 2000. A brief survey and synthesis of the roles of time in petri nets, *Mathematical & Computer Modelling*, 31, 55–68.

Brucker, P., 2001. *Scheduling Algorithms*, Springer-Verlag Berlin Heidelberg.

Cassandras, C. G. and Lafortune, S., 1999. *Introduction to Discrete Event Systems*, Kluwer Academic Publishers, Dordrecht.

Gradišar, D. and Mušič, G., 2007. Production-process modelling based on production-management data: a Petri-net approach, *International Journal of Computer Integrated Manufacturing*, 20 (8), 794–810.

Haupt, R., 1989. A survey of priority rule-based scheduling, *OR Spectrum*, 11 (1), 3–16.

Lee, D. Y. and DiCesare, F., 1994. Scheduling flexible manufacturing systems using Petri nets and heuristic search, *IEEE Transactions on robotics and automation*, 10 (2), 123–132.

Löscher, T., Mušič, G. and Breitenecker, F., 2007. Optimisation of scheduling problems based on timed petri nets, *Proc. EUROSIM 2007*, Vol. II, Ljubljana, Slovenia.

Murata, T., 1989. Petri nets: Properties, analysis and applications, *Proc. IEEE*, 77, 541–580.

Mušič, G., 2008. Timed Petri net simulation and related scheduling methods: a brief comparison, *The 20th European Modeling & Simulation Symposium*, Campora S. Giovanni (Amantea, CS), Italy, pp. 380–385.

Mušič, G., Löscher, T. and Breitenecker, F., 2008. Simulation based scheduling applying Petri nets with sequences and priorities, *UKSIM 10th International Conference on Computer Modelling and Simulation*, Cambridge, UK, pp. 455–460.

Panwalkar, S. S. and Iskander, W., 1977. A survey of scheduling rules, *Operations Research*, 25 (1), 45–61.

Pinedo, M., 1995. *Scheduling: theory, algorithms, and systems*, Prentice-Hall, Inc., Englewood Cliffs, New Jersey.

Taillard, E., 1993. Benchmarks for basic scheduling problems, *European Journal of Operational Research*, 64, 278–285.

Tuncel, G. and Bayhan, G. M., 2007. Applications of Petri nets in production scheduling: a review, *International Journal of Advanced Manufacturing Technology*, 34, 762–773.

Vidal, R. V. V. (ed.), 1993. *Applied Simulated Annealing*, Springer-Verlag Berlin Heidelberg.

Yu, H., Reyes, A., Cang, S. and Lloyd, S., 2003. Combined Petri net modelling and AI based heuristic hybrid search for flexible manufacturing systems-part II: Heuristic hybrid search, *Computers and Industrial Engineering*, 44 (4), 545–566.

Zhou, M. and Venkatesh, K., 1999. *Modeling, Simulation, and Control of Flexible Manufacturing Systems: A Petri Net Approach*, World Scientific.

AUTHOR BIOGRAPHY

GAŠPER MUŠIČ received B.Sc., M.Sc. and Ph.D. degrees in electrical engineering from the University of Ljubljana, Slovenia in 1992, 1995, and 1998, respectively. He is Associate Professor at the Faculty of Electrical Engineering, University of Ljubljana. His research interests are in discrete event and hybrid dynamical systems, supervisory control, planning, scheduling, and industrial production control. His Web page can be found at `http://msc.fe.uni-lj.si/Staff.asp`.

THE DESIGN OF A MANUFACTURING FACILITY. AN EFFICIENT APPROACH BASED ON ALTERNATIVES AGGREGATION PETRI NETS.

Juan Ignacio Latorre [(a)], Emilio Jiménez[(b)], Mercedes Pérez [(c)], Eduardo Martínez [(d)]

(a) Department of Mechanical Engineering, Energetics and Materials. Public University of Navarre. 31500 Tudela, Spain.
(b) Department of Electrical Engineering. University of La Rioja. 26004 Logroño, Spain.
(c and d) Department of Mechanical Engineering . University of La Rioja. 26004 Logroño, Spain.

[(a)] juanignacio.latorre@unavarra.es, [(b)] emilio.jimenez@unirioja.es, [(c)] mercedes.perez@unirioja.es, [(d)] eduardo.martinezc@unirioja.es

ABSTRACT
The design of a manufacturing facility is a process that has important consequences during the whole lifespan of the system. In this paper, a case study shows a new methodology to solve design decision problems in discrete event systems (DEVS). This technique is based in the Alternatives Aggregation Petri nets (AAPN). This new type of Petri net allows to develop a unique model to cope with a disjunctive optimisation problem. This problem arises from the alternative systems accepted as feasible solutions for the layout and composition of the system. A comparison with a traditional approach shows that the new method can deal with a complex design problem in less time and with similar accuracy in the solution.

Keywords: Alternatives Aggregation Petri nets, optimisation, discrete event systems, decision problem

1. INTRODUCTION

A manufacturing facility is a system from where a high performance is usually requested (Heizer 2008). This performance implies that the right decisions should be taken in an appropriate moment. When the system is in operation the decisions to be taken differ from the decisions to be taken in the design process of the facility (referred to the capacity, equipment characteristics and location, etc) (Kusiak 2000 and Latorre 2007).

A large number of logistic and industrial systems of both academical and economical interest can be described as Discrete Event Systems (DEVS) (Jiménez 2002, Jiménez 2005). That means that their state evolve by the occurrence of discrete synchronized events.

2. THE CASE STUDY

A manufacturing system in process of being designed is taken into consideration. Some of its characteristics are undetermined. Therefore, it is an interesting objective to develop a tool capable to help in the task of taking the appropriate decisions.

The manufacturing system is organized in three stages: raw materials feeding system, flexible manufacturing system and assembling, and packing system. A layout can be seen on Figure 1.

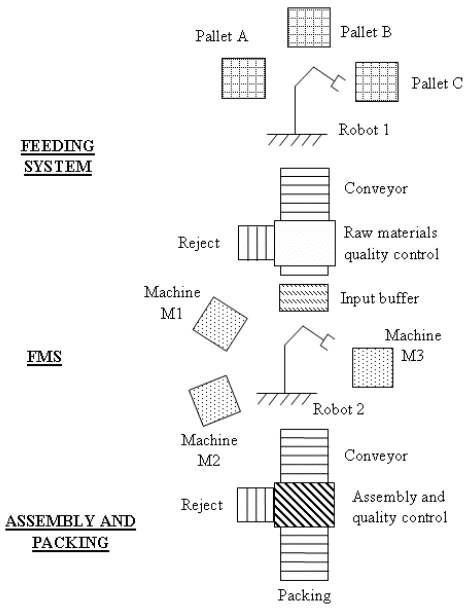

Figure 1 : Layout of the first alternative for the system.

The facility feeding system handles three types of raw materials, which are provided in pallets.

A robot picks up the raw materials, one by one, and puts them onto a conveyor that drives them to a quality control. The raw materials suitable for the production are led to the flexible manufacturing system (FMS).

A raw material buffer can be installed at this place, according to an appropriate decision.

The flexible manufacturing system is composed by three machines and a robot.

The processed parts are moved by the robot to an output system. An output buffer of undetermined capacity can also been installed.

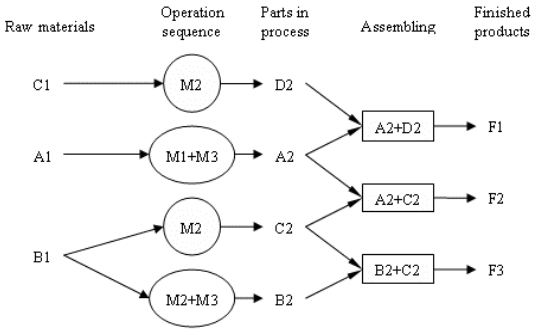

Figure 2 : Flow materials, parts and products.

The last stage in the production process is the assembly and packing. All the possibilities of machining and assembly can be seen on Figure 2.

Two suppliers propose different solutions for the assembly and packing system: a dedicated system and a FMS. Both alternatives are presented respectively on Figures 1 and 3.

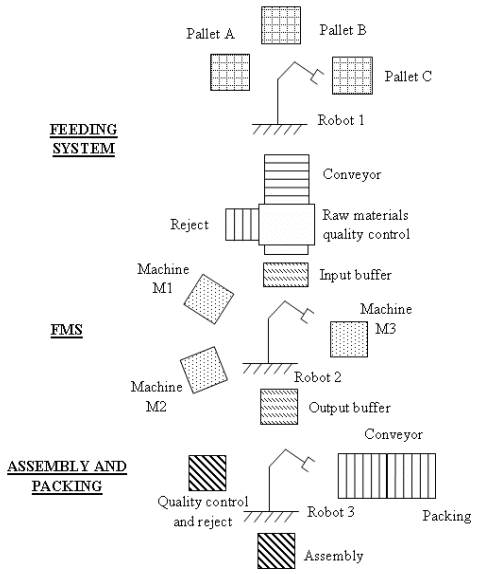

Figure 3 : Layout of the second alternative for the system.

3. DECISION AND OPTIMISATION PROBLEMS

3.1. Decision problem based on a DEVS

A **decision problem** based on a DEVS *D* is a choice, among several alternatives, in response to a question posed on any of the undefined characteristics of *D* or its dynamics.

Considering the manufacturing system of the described case study as the DEVS *D*, the following undefined characteristics can be identified:

C1) Capacity of the raw material pallets.
C2) Number of robots in the manufacturing feeding system.
C3) Presence or not of a raw materials input buffer for the FMS and its size.
C4) Number of robots in the FMS
C5) Layout of the FMS.
C6) Assembling and packing system.
C7) In case of the second alternative is chosen for this last manufacturing subsystem, its characteristics.
C8) Manufacturing strategy (scheduling).

The solution to this problem consists in the choice of a solution to specify the undefined parameters of *D*: C1 to C7 are design parameters and C8 is an operation parameter.

3.2. The paradigm of the Petri nets

In order to solve the decision problem based on a DEVS it is a necessary step to obtain a model of the system which describes, by means of an appropriate formalism, the restrictions to the behaviour of the original system. The manufacturing system of the case study can be described as DEVS and it shows a behaviour characterised by concurrence (robot 2 and machines in FMS), parallelism (feeding system and FMS), synchronisation and resource sharing (buffers and robots).

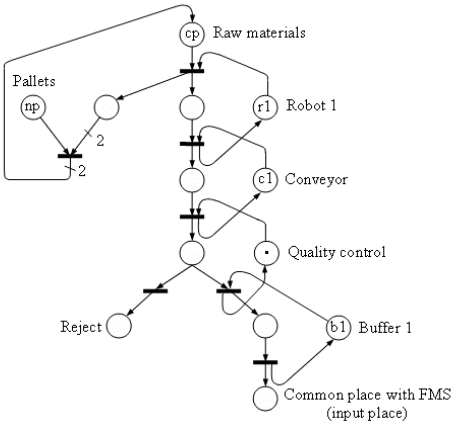

Figure 4 : Petri net of the feeding system.

Petri nets (PN) are a paradigm that can cope with such a description in a double way: a graphical and intuitive one and an algebraic one which is suitable to perform a structural analysis and to be processed by automatic calculation in a computer (Jiménez 2006).

A broad description of the theory of PN and their properties can be found in the references (Silva 1993 and David 2005).

In this paper the following notation for generalized Petri nets is used:

R marked Petri net.
m_o initial marking of *R*.
m reachable marking of *R*.

$^\circ t$ = set of input places of t.
t° = set of output places of t.
$^\circ p$ = set of input transitions of p.
p° = set of output transitions of p.
R^k_i subnet k of the Petri net R_i.

A further step to solve the problem of obtaining the best performance from the manufacturing system D can be to formulate the problem under formal mathematical approach. For this purpose the formalism of the Petri nets is used.

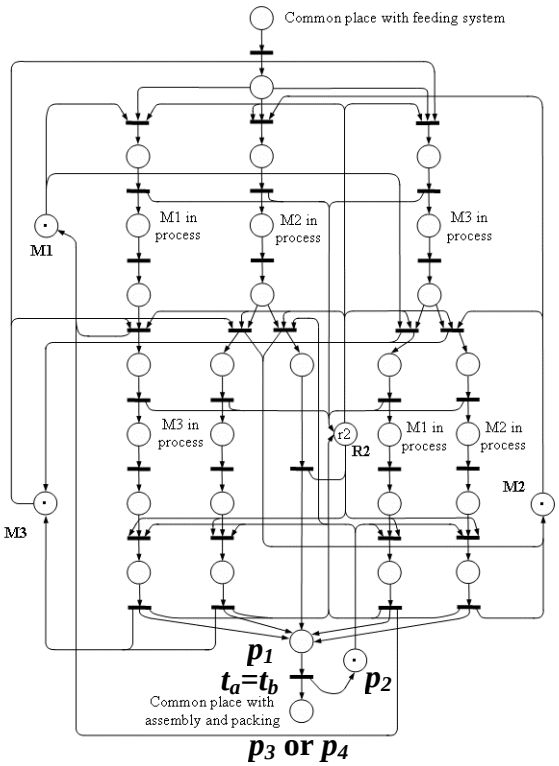

Figure 5 : Petri net of the flexible manufacturing system.

One of the undefined characteristics of the DEVS D is the subsystem of assembling and packing. Two different alternatives have been considered which can be modelled easily with generalized Petri nets by means of a bottom-up strategy.

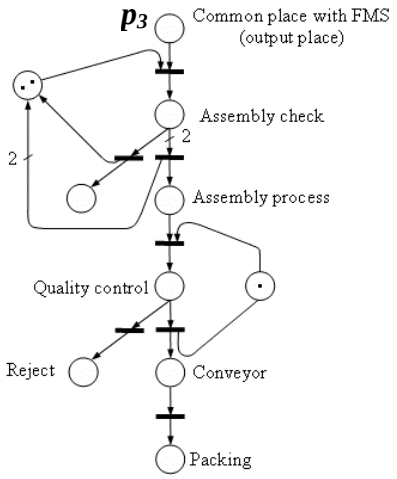

Figure 6 : Petri net of the first alternative for the assempling stage.

The subnets of this case study have been linked by means of common places. The first two models, represented in Figures 4 and 5, correspond to the feeding system and the flexible manufacturing system.

For the assembly and packing subsystem, the two alternatives are modelled with the PN presented in Figures 6 and 7.

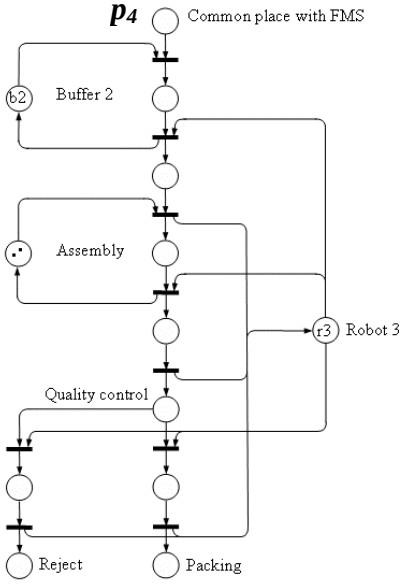

Figure 7 : Petri net of the second alternative for the assembling stage.

The complete alternative Petri net set S_R = $\{R_1, R_2\}$, were R_1 (Figures 1, 2 and 3) and R_2 (Figures 1, 2 and 4) are obtained linking the appropriate subsystems by means of the common places.

3.3. Decision problem based on 2 PN models

A **decision problem** based on S_R is a choice in response to a question posed on any of the undefined characteristics of D, where both the

DEVS and its undefined characteristics are represented by S_Q, m_0 and the dynamics of the Petri net. $S_Q = \{Q_1, Q_2\}$, and Q_i is the unmarked PN R_i.

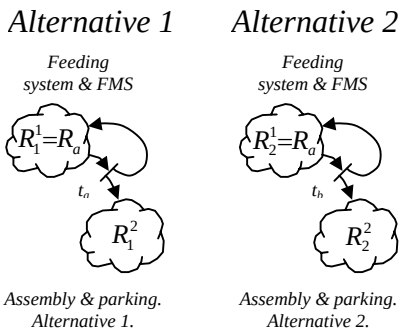

Figure 8. Alternative PN for D

The operation and design decisions of the original problem are translated into decisions on the marking (m) or the structural characteristics of the PN (α, β, P or T). These last parameters should be chosen among the different possibilities defined by S_Q.

The undefined characteristics C1 to C6 and C8 can be translated into decisions on the marking of specific places. C7 is the only parameter that must be represented by structural characteristics.

Figure *8* presents the alternative Petri nets of S_R as feasible solutions of the decision problem. The PN are represented by common (R_a is a shared subnet) and different subnets.

3.4. Optimisation problem based on 2 PN models

The decision taking on the characteristics of the partially undefined PN model of *D* or on its dynamics can be associated to an optimisation problem as it is described in the following definition:

An important step is to define the structure of a solution of the problem. It has to be taken into consideration that a solution has to integrate all the information needed to solve the uncertain characteristics of *D*, posed in the original decision problem.

In this example the structure chosen for a solution is shown in Figure *9* in the form $x=\{x_1, x_2, \ldots, x_9\}$, where x_1=cp, x_2=r1, x_3=b1, x_4=r2, x_5=pm, x_6=pn3, x_7=b2, x_8=r3, x_9=sod.

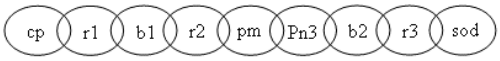

Abrev.	Parameter to be optimised	Boundaries
cp	Pallets capacity	[1,20]
r1	Number of feeding robots	[1,3]
b1	Capacity of FMS input buffer	[1,10]
r2	Number of FMS robots	[1,3]
pm	FMS layout	[1,6]
Pn3	Assembly and packing layout	[1,2]
b2	Capacity of FMS output buffer	[1,10]
r3	Number of assembly robots	[1,3]
sod	Sequence of manufacturing decisions	[1,3]

Figure 9. Structure of a solution.

A second step consists of defining the objective function:

$f(x) = f_1(m_f) - f_2(x_2,x_3,x_4,x_6,x_7,x_8) - f_3(m_f) - f_4(m_f)$

In this case study the following addends have been taken into consideration:

$f_1(mf)$ = benefit obtained by selling the finished products, where *mf* is the final marking in the simulated evolution of the manufacturing system.

$f_2(x_2,x_3,x_4,x_6,x_7,x_8)$ = investment in fixed assets.

$f_3(m_f)$ = cost of the rejected material.

$f_4(m_f)$ = investment in work in process (WIP).

The **optimisation problem based on *2* alternative Petri net models** $S_R = \{R_1, R_2\}$ is defined in the following way:

maximize $f(x)$, where

- $x \in \Omega = \Omega_1 \cup \Omega_2$
- $\Omega_i = \{ x \in P^n \mid i=1,2 \wedge m_j \in M(R_i) \}$, $M(R_i)$ is the set of markings of R_i reachable from marking m_{0i}, and m_j represents every marking of R_i used in the construction of *x*.
- Boundary condition: $\phi(m_0) \leq k$, that describes the initial limitation of place for pallets in the raw material storage.

This problem of disjunctive optimisation can be solved in several ways. The most usual methodology consists of using the strategy of "divide and conquer", which is applied posing two optimisation problems, one for any of the alternative Petri nets. The second phase is the choice of the best solution.

A new methodology to solve this problem is presented in this paper. The methodology is applied in only one phase and to a single problem and it is based on the Alternatives Aggregation Petri nets (AAPN).

4. ALTERNATIVES AGGREGATION PETRI NETS

One of the main advantages of the AAPN is that they can profit from similarities in the alternative PN models.

For that reason, the existence of only one solution space of reduced size to be explored, and not two different non-reduced ones, can lead to fast searches and to the need of limited computer resources.

In the example $S_R = \{R_1, R_2\}$. As it is shown in Figure *8*, R_1 can be divided in two subnets R^1_1 and R^2_1. On the other hand R_2 can be split into another pair of subnets R^1_2 and R^2_2. The criterion considered in the choice of the subnets has been the same original manufacturing systems that have lead to the bottom-up modelling of the PN (Latorre 2007).

4.1. Definitions

i) R^k_i is said to be a ***shared subnet*** in S_R if $\exists\, j \in \mathbb{N}$, $1 \le j \le n, j \ne i \ni R^k_i$ is a subnet of $R_j \in S_R$.
In this example $R^2_1 = R^2_2 = R_a$ are the same *shared subnet* in R_1 and R_2.
ii) $p \in P^k_i$ is an ***input border place*** of R^k_i if $\exists\, p' \in R_i \ni p' \notin R^k_i \wedge p' \in {}^\circ t$ where $t \in {}^\circ p$.
iii) $p \in P^k_i$ is an ***optput border place*** of R^k_i if $\exists\, p' \in R_i \ni p' \notin R^k_i \wedge p' \in t^\circ$ where $t \in p^\circ$.
In this example p_1 is an *output border place* of R_a, while p_2 is its only *input border place*.
On the other hand p_3 and p_4 are input border places of R^2_1 and R^2_2 respectively. These subnets haven't any *output border places*.
iv) $p_1 \in P_a$ is a ***choice place*** of R_a because $t_a, t_b \in p_1{}^\circ \wedge p_3 \in t_a{}^\circ$, $p_4 \in t_b{}^\circ$, where $p_3 \in R^2_1$, $p_4 \in R^2_2$.
A set of choice variables is defined as $A=\{A_1, A_2\}$, where A_1 and A_2 are boolean variables.
From these definitions, it will be explained how to construct an AAPN as a tool to solve an optimisation problem based in 2 alternative PN models. The construction algorithm which will be presented comprises four steps.

4.2. Algorithm: construction of R^*, an AAPN from S_R

Step 1: Divide every $R_i \in S_R$ into R^j_i, $j=1,\ldots,n_i$, subnets of R_i.
Step 2: Determine the sets of input and output border places for every R^j_i, $i=1,\ldots,n$; $j=1,\ldots,n_i$
Step 3: Define an appropriate designation for every subnet, place and transition, in a way that the shared subnets include unique names.
Step 4: Aggregate all the subnets in a single R^*:

- ***Step 4.1***: $i=1$, $j=1$, $R^* = \varnothing$
- ***Step 4.2***: if $R^j_i \not\subset R^*$ then $R^* = R^j_i \cup R^*$
- ***Step 4.3***: link R^j_i to R^* with the original transitions in R_i
- ***Step 4.4***: if a link transition $t \in p^\circ$ and p is a choice place $\Rightarrow$ associate the choice variable A_i to t.
- ***Step 4.5***: $j=j+1$; if $j \le n_i$ then go to ***4.2***
- ***Step 4.5***: $j=1$; $i=i+1$; if $i \le n$ then go to ***4.2***.

Figure *10* shows an AAPN R^* as it has been constructed from the original set of alternative Petri nets of Figure *8*, the set of choice variables $A = \{A_1, A_2\}$, and the shared subnet R_a.

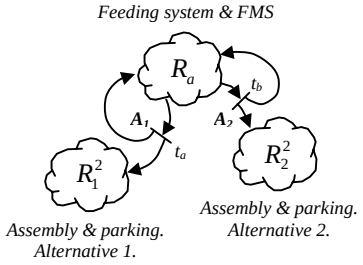

Figure 10. AAPN R^* for D

4.3. Reduction rate of (R*, SR)

$q^* = 69$ is the number of places of R^* and q_i is the number of places of $R_i \in S_R$, hence $q_1 = 56$, $q_2 = 59$.

$$r_r\left(R^*, S_R\right) = \frac{q^*}{\sum_{i=1}^{n} q_i} = 0.6 \qquad (1)$$

The reduction rate or r_r is a parameter which describes the size of P^* compared to that of $P_1 \cup P_2$. A reduction in the size of the Petri net will lead in most of the cases to a reduction in the size of the state space. This statement will be true if the shared Petri net R_a leads to common states for the evolution of R_1 and for R_2. In that case these common states will be explored only one time in the R^* optimisation and two times in the "divide and conquer" strategy.

If we consider a situation with a large number of alternative PN and a lot of shared subnets, the comparison would be even more favourable to R^*.

For this reason r_r might be regarded as a qualitative indicator of the efficiency of R* optimisation compared to other methods.

5. THE OPTIMISATION PROBLEM BASED ON THE AAPN R^*

It is similar to the optimisation problem based on 2 Petri net models described in (**3.4**),with the following modification:

$x \in \Omega$, where $\Omega = \{ x \in \mathrm{P}^n \mid m_j \in \mathrm{M}(R^*)\}$, where m_j represents every marking of R^* used in the construction of x and R^*.

6. THE METHOD TO SOLVE THE PROBLEM: GENETIC ALGORITHMS

The method to solve the optimization problem based on R^* can be chosen among all the classical possibilities developed for the non-disjunctive optimisation problems based on a Petri net model. Those methods include exhaustive search, heuristics, artificial intelligence and simulation among other well-know techniques.

In this work a genetic algorithm has been developed as a method specially suitable and

easy to implement in the optimisation problem based on an AAPN R^*.

6.1. Application of GA and solution of the optimisation problem

A genetic algorithm is based on the definition of feasible solution which may be called individual or chromosome. The solution defined in (**3.4**) is appropriate for this technique. The particularity of a problem based on an AAPN consists in the fact that a certain solution should explore only an allowed region of the state space. This free region is characterized by a set $A=\{A_1, A_2\}$ where only one of the choice variables remains true. The solution structure that has been defined in (**3.4**) contains x_6=pn3 $\in \{1,2\}$ which can be associated to A: if $x_6=1 \Rightarrow A_1$=true $\wedge$ A_2=false but if $x_6=2 \Rightarrow A_1$=false $\wedge$ A_2=true

6.2. The decisions taken: solution of the decision problem

After adjusting the parameters of the algorithm, the objective function and the time durations in the associated T-timed PN, a certain solution x has been obtained: $x=\{3,1,8,1,4,1,20,1,sod\}$, where *sod* is a sequence of decisions to solve the actual conflicts in the evolution of the PN.
In this solution the alternative manufacturing system that has been chosen is the FMS.

7. COMPARISON TO OTHER METHOD

In order to evaluate the efficiency of the AAPN-based methodology a comparison of its performance versus the one of "divide and conquer" strategy has been made. This last method consists of two optimisation processes (for R_1 and R_2) and the choice of the best solution among both results.

The same genetic algorithm has been applied to both approaches and some parameters of the search in the state space have been compared. The reference of the comparison has been the AAPN optimisation parameters. The genetic algorithm has reached 15 generations of solutions, considered as stop criterion of the optimisation procedure.

7.1. Computer time

Table 1. Comparison of computer working time

	1 hour	2 h	4 h	6 h
R^*	0	0	0	0
R_1	5.11%	3.04%	2.86%	5.28%
R_2	-0.11%	-2.41%	-2.3%	-0.29%

This table represents the percentage of computer working time each specific optimisation algorithm needs in relation to the AAPN algorithm. This time is represented for different values of the manufacturing simulated time (1h to 6h).

As it can be seen the AAPN algorithm requires a similar time than the other algorithms. Therefore a complete optimisation of R^* will need half the time than the "divide and conquer" strategy.

7.2. Quality of the solution

Table 2. Comparison of the objective function

	1 hour	2 h	4 h	6 h
R^*	0	0	0	0
R_1	-1.89%	-0.91%	3.7%	1.38%
R_2	-4.19%	-8.62%	2.85%	-5.89%

In this case the comparison has been performed among the value of the objective function takes on the solutions obtained with the different algorithms.

It can be seen that the value, and therefore the quality of the solution, is similar with the three methods.

7.3. Conclusions of the comparison

As it has been seen in the previous comparison, in this case study the AAPN-based algorithm outperforms largely the classical methodology in computer time. Nevertheless, this good result does not imply a loss of quality in the solution.

8. CONCLUSIONS

In this paper a case study shows a new methodology to solve design decision problems in DEVS. This methodology is based in the Alternatives Aggregation Petri nets.

The results obtained compared to a classical approach of "divide and conquer" improve largely the computer time without a loss in the quality of the solution.

A further reseach step in the field of the AAPN will be to put them to the test in a variety of decision problems and compare their performance and results with other techniques when they are applicable.

9. REFERENCES

David, R.,Alla, H. 2005 *Discrete, Continuous and Hybrid Petri Nets*. Springer.

Guash, A., Piera, M.À., Casanovas, J., Figueras, J. 2002. *Modelado y simulación. Aplicación a procesos Logisticos, de fabricación y servicios*. Barcelona.Ed. UPC.

Heizer, J., Render, B. 2008. *Operations Management.* Prentice Hall.

Jiménez, E. 2002. *Técnicas de automatización avanzada en procesos industriales*. *PhD Thesis*. Logroño. Ed. Univ. de La Rioja

Jiménez, E., Pérez, M, Latorre, I. 2006 Industrial applications of Petri nets: system modelling and simulation. *Proceedings of European Modelling Simulation Symposium*. 159-164. Barcelona.

Jiménez, E., Pérez, M., Latorre, J.I. 2005 ,On deterministic modelling and simulation of manufacturing systems with Petri nets,. *Proceedings of European Modelling Simulation Symposium*, 129-136. Marseille.

Kusiak, A 2000. *Computational Intelligence in Design and Manufacturing*. Wiley-Interscience.

Latorre, J.I., Jiménez, E., Pérez, M. 2006 Comparison of optimization techniques applied to a flexible manufacturing system. *Proceedings of European Modelling Simulation Symposium*, 141-146. Barcelona.

Latorre, J.I., Jiménez, E., Pérez, M. 2007 Macro-Reachability Tree Exploration for D.E.S. Design Optimization. *Proceedings of the 6th EUROSIM Congress on Modelling and Simulation*. Ljubljana (Slovenia).

Lee, D.Y., DiCesare, F., 1992. FMS scheduling using Petri nets and heuristic search. *Robotics and Automation. Proceedings*, Volume 2, 1057 – 1062

Silva, M. 1993. Introducing Petri nets, *In Practice of Petri Nets in Manufacturing* 1-62. Ed. Chapman&hall

Zhou, M. Venkatesh, K. 1999 *Modelling, Simulation and Control of Flexible Manufacturing Systems. A Petri Net Approach*, WS World Scientific

AUTHORS BIOGRAPHY

Juan Ignacio Latorre Biel is Industrial Engineer. He has developed his professional career in the industry and in educative institutions. Currently he is preparing his PhD Thesis in DEVS optimisation based on PN. Nowadays he is a teacher at the Public University of Navarra. His research areas include factory automation, modeling and simulation, and industrial processes. His main works are developed with the automatic group of the University of La Rioja.

Emilio Jiménez Macías studied Industrial Engineering (with Computer Science, Electronics and Automation specialty) by the University of Zaragoza. After working several years in the industrial private sector (Researching and Developing Department head position), returned to the university, as an Assistant Professor to the University of La Rioja, in 1997, where he works presently in the Electrical Engineering Department (Coordinator of the System Engineering and Automation Group). In 2001 he presented his PhD thesis about Industrial Automation. His research areas include factory automation, modeling and simulation, and industrial processes. His main works are developed with the automatic group of the University of Zaragoza.

Mercedes Pérez de la Parte received the BS degree in Telecommunications Engineering from the University of Seville in 1997. She has held research and teaching positions at the University of Los Andes, Venezuela, in 2000, and research position at the University of Seville since 1997 until present. She has attended all the PhD courses and is presently preparing her PhD dissertation. She is Assistant Proffesor at the Departamento de Ingeniería de Sistemas y Automática of the University of Seville, Spain, since 2000.

Eduardo Martínez Cámara studied Industrial Engineering by the University of La Rioja. He works presently at the private industry sector, and he is Assistant Teacher in the Mechanical Engineering Department of the University of La Rioja. His research areas include factory automation, modeling and simulation, and industrial processes. His main works are developed with the automatic group of the University of La Rioja.

THE PROBLEM OF DESIGNING DISCRETE EVENTS SYSTEMS. A NEW METHODOLOGICAL APPROACH.

Juan Ignacio Latorre [(a)], Emilio Jiménez[(b)], Mercedes Pérez [(c)], Julio Blanco [(d)]

(a) Department of Mechanical Engineering, Energetics and Materials. Public University of Navarre. 31500 Tudela, Spain.
(b) Department of Electrical Engineering. University of La Rioja. 26004 Logroño, Spain.
(c and d) Department of Mechanical Engineering. University of La Rioja. 26004 Logroño, Spain.

[(a)] juanignacio.latorre@unavarra.es, [(b)] emilio.jimenez@unirioja.es, [(c)] mercedes.perez@unirioja.es, [(d)] julio.blanco@unirioja.es

ABSTRACT

The need to obtain a high performance from a given manufacturing or logistic system, that can be modelled as a discrete event system (DEVS), leads to a decision problem. In this paper, several definitions are presented to formalize the evolution of a problem from a decision one to a disjunctive optimisation problem based on several alternative Petri net models. This last definition copes with the general problem of the design and operation of a DEVS. A new type of Petri net is presented: the Alternatives Aggregation Petri nets (AAPN), as a promising tool to solve this general problem in an efficient way. An AAPN is constructed by aggregating the alternative Petri net models, which are feasible solutions to the DEVS design. As a result, the optimisation problem can be solved by means of classical methods like exhaustive or heuristic search in a single phase.

Keywords: Alternatives Aggregation Petri nets, optimisation, discrete event systems, decision problem

1. INTRODUCTION

A large number of logistic and industrial systems of both academical and economical interest can be described as Discrete Event Systems (DEVS) (Jiménez 2002, Jiménez 2005). That means that their state evolve by the occurrence of discrete synchronized events.

In the design and operation of a DEVS it is a logic and usual objective to try to get the best performance from it (Heizer 2008). In order to reach this objective it is necesary to choose the appropriate characteristics for the undefined system and its dynamics. As a consecuence it can be seen that the original problem of obtaining the best performance can be changed into the problem of taking the appropriate decisions in the design and the operation of the system. Such a problem can be defined in the following way:

Definition 1. Decision problem based on a discrete event system.

Let *D* be a partially undefined discrete event system.

A **decision problem** based on *D* is a choice, among several alternatives, in response to a question posed on any of the undefined characteristics of *D* or its dynamics.

If we consider a manufacturing facility, some undefined characteristics that can be taken into account could be the capacity of a storage buffer, the size of the pallets of raw materials, the assignment of tasks to the different machines in a certain period of time or the number of items a robot should pick up at a time. This definition also includes, as possible undefined characteristics, deeper uncertainties as the specific machinery that can be acquired and set up to perform a certain task in the operation of the facility, among all the alternatives that could be found in the market.

In the previous set of examples, two types of uncertainties have been mentioned: the ones related to the operation of the system and the ones related to its design. (Latorre 2007)

As an example of design decision problem for a manufacturing system Figure 1 is presented. Three alternative layouts and production equipment are considered. The best option should be chosen to make up the manufacturing system.

The procedure to obtain a solution to a decision problem is a subject of the operational reseach, which has provided with several techniques since the birth of this discipline, more than 60 years ago. (Ríos 2002 and Heizer 2008))

According to the characteristics and complexity of the optimisation problem, a diversity of methodologies can be used to solve it: linear or integer programming, search in the space of solutions, or simulation are some examples of usual techniques.

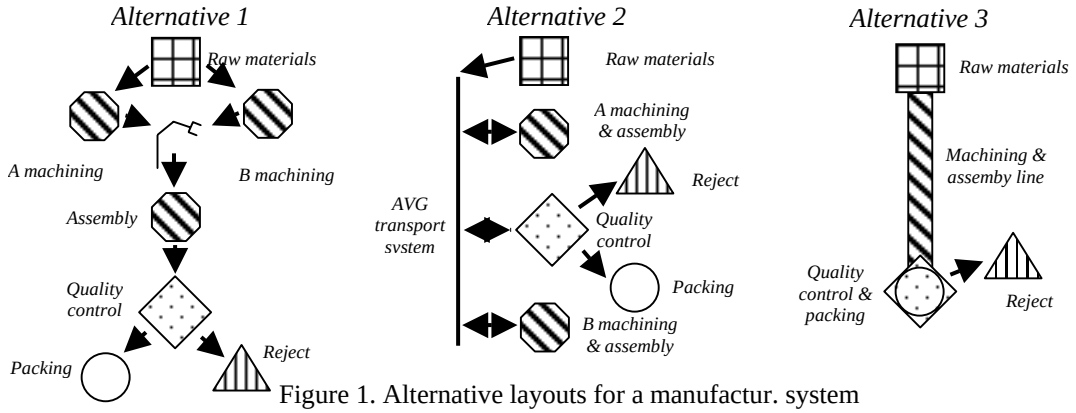

Figure 1. Alternative layouts for a manufactur. system

Among them, simulation is the only one that can cope with any system (that can be modelled with enough accuracy). The inconveniences of simulation are well known and include that it is not an optimisation technique; the results depend on the initial data, the incertitude in the generalisation of the conclusions because only specific areas of the space of solutions are explored and the absence of a general procedure to choose the simulations to be performed. This last characteristic implies that it is necessary an uncertain amount of simulations to reach a satisfactory result (Guash 2002).

The other methodologies have the handicap of not being suitable for all types of problems. Some problems are so complex that they even do not allow to find with certitude the best solution with a reasonable use of computational resources. For those problems heuristic and artificial intelligence techniques have been developed and applied with different degrees of success (Latorre 2006).

2. DESIGNING AND OPERATING A DEVS

The problem of taking decisions in the operation of a DEVS has been broadly studied (for example many techniques have been developed to solve scheduling problems (Lee 1992 and Rodríguez 2004). Nevertheless an optimal solution for some of those problems has not been found yet.

On the other hand, the problem of taking decisions in the design process of a DEVS has not received so much attention, despite the fact that a mistake in this stage will influence the performance of the system during its entire lifespan (Kusiak 2000). Several methods which can be taken into consideration in the design process of a DEVS are: imitating the know-how or tradition, the trial and error method combined with simulation or the choice among a reduced set of alternatives, optimisation of each one of them and comparison of the results (Zhou 1999). The design problem will be the one on which the present document is focused.

In order to solve the decision problem based on a DEVS it is a necessary step to obtain a model of the system which describes, by means of an appropriate formalism, the restrictions to the behaviour of the original system. The logistic and manufacturing systems described as DEVS usually show a behaviour characterised by concurrence, parallelism, synchronisation and resource sharing. Petri nets (PN) are a paradigm that can cope with such a description in a double way: a graphical and intuitive one and an algebraic one which is suitable to perform a structural analysis and to be processed by automatic calculation in a computer (Jiménez 2006).

3. THE PARADIGM OF PETRI NETS

A broad description of the theory of PN and their properties can be found in the references (Silva 1993 and David 2005).

In this paper the following notation for generalized Petri nets is used:

P = finite, not empty, set of places.

T = finite, not empty, set of transitions.

α: $P \times T \rightarrow \mathrm{N}_0$ input incidence application.

β: $T \times P \rightarrow \mathrm{N}_0$ output incidence application.

$Q = < P, T, \alpha, \beta >$ unmarked Petri net.

m_o is the initial marking associated to Q.

$R = <Q , m_o>$, marked Petri net.

$m : P \rightarrow \mathrm{N}_0$ reachable marking of R.

${}^\circ t = \{p \in P \mid \alpha(p,t) >0 \}$ set of input places of t.

$t^\circ = \{p \in P \mid \beta(t,p) >0 \}$ set of output places of t.

${}^\circ p = \{t \in T \mid \beta(p,t) >0 \}$ set of input transitions of p.

$p^\circ = \{t \in T \mid \alpha(t,p) >0 \}$ set of output transitions of p.

R_i^k subnet k of the Petri net R_i.

A further step to solve the problem of obtaining the best performance from a logistic or manufacturing system can be to formulate the problem under formal mathematical approach. For this purpose the formalism of the Petri nets is used.

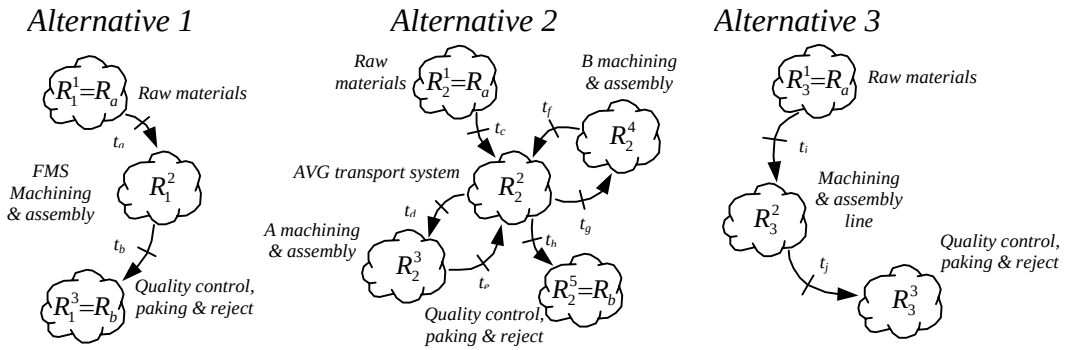

Figure 2. Alternative Petri nets for a manufactur. system

Definition 2. Decision problem based on n alternative Petri net models.
Let D be a partially undefined DEVS.
Let $S_Q=\{Q_i \mid i=1,\ldots,n\}$ be a set of unmarked Petri nets, where any of those PN has been developed as an alternative model for D.
Let m_{0i} be the initial marking vector associated to Q_i, where the initial marking of some of the places may be undefined and represented by means of variables $m_i(p_j)=m_{ij}$.
Let $m_0 = \{ m_{01}, m_{02}, \ldots, m_{0n} \}$
Let the *ith* marked PN be $R_i = \langle Q_i, m_{0i} \rangle$, and therefore let $S_R=\{ R_i \mid i=1,\ldots,n \}$ be the set of marked PN.

A **decision problem** based on S_R is a choice in response to a question posed on any of the undefined characteristics of D, where both the DEVS and its undefined characteristics are represented by S_Q, m_0 and the dynamics of the Petri net.

The operation and design decisions of the original problem are translated into decisions on the marking (m) or the structural characteristics of the PN (α, β, P or T). These last parameters should be chosen among the different possibilities defined by S_Q.

In Figure 2 the PN models of the three alternatives presented in Figure 1 are shown. They are represented by means of subnets. Some of them appear in different alternative PN because they model the same subsystems. They are called shared subnets (R_a and R_b in the figures).

4. OPTIMISATION PROBLEM

The decision taking on the characteristics of the partially undefined PN model of a DEVS or on its dynamics can be associated to an optimisation problem as it is described in the following definition:

Definition 3. Optimisation problem based on *n* alternative Petri net models.
Let us consider a certain decision problem based on a set of alternative PN models $S_R = \{ R_i \mid R_i = \langle Q_i, m_{0i} \rangle, i=1,\ldots,n \}$, where Q_i is an unmarked Petri net and m_{0i} is the initial marking associated to Q_i. Notice that the initial marking of some places may be undefined and expressed by means of variables x_i.
Let $x \in \Omega$, where Ω is the solution space. x is every feasible or candidate solution and can be written in the form: $x=\{x_1, x_2, \ldots, x_n\}$. It should contain all the information needed to take the decisions aimed for (see ***definition 1***).
Let $f(x)$:$\mathrm{P}^n \rightarrow \mathrm{P}^m$ be the objective function.

An **optimisation problem based on *n* alternative Petri net models** S_R is defined as:
max or min $f(x)$

where $x \in \Omega$, $\Omega = (\bigcup_{i=1}^{n} \Omega_i) \cap \Omega_{n+1}$, and

i) $\Omega_i = \{ x \in \mathrm{P}^n \mid m_j \in \mathrm{M}(R_i) \}$, where $\mathrm{M}(R_i)$ is the set of markings of R_i reachable from marking m_{0i}, and m_j represents every marking of R_i used in the construction of x and $R_i \in S_R$.

ii) $\Omega_{n+1} = \{ x \in \mathrm{P}^n \mid g_j(x) \le 0, j=1,\ldots,p \}$, where g_j: $\Omega_{n+1} \rightarrow \mathrm{P}^k$.

iii) $\phi_j(x(m_0),m_0,x(m_f),m_f) \le 0, j=1,\ldots,r$

4.1. Constraints i)

Any feasible solution must satisfy that the markings m_j considered in a direct or indirect way in the construction of the solution x, are reachable markings of at least one marked PN $R_i \in S_R$. In other words, the feasible solutions should comply with the evolution rules defined for one of the alternative PN model of the system R_i.

4.2. Constraints ii)

They can be non linear. An example of these constraints is a limit imposed on the maximal cost of the work in process inventory (WIP) at any time in a manufacturing facility.

4.3. Constraints iii) or boundary conditions

They can specify the constraints that the solution x must satisfy in the initial and final states of the PN evolution. For example, they

may state respectively a maximal amount of raw materials at disposal of the manufacturing process or a minimal amount of production for a certain set of products.

Once the decision problem on a partially defined DEVS is transformed into an optimisation problem based on a set of alternative PN, a strategy to obtain a solution can be presented.

5. DRAWBACKS OF UP-TO-DATE TECHNIQUES APPLIED TO THE DESIGN PROCESS OF A DEVS

A usual method to solve the optimisation problem based on *n* alternative Petri net models is oriented to the "divide and conquer" paradigm. Under this point of view, the original optimisation problem is divided into n problems, each one of them is constrainted by only one alternative Petri net model $R_i = \langle Q_i, m_{0i} \rangle$. Each *ith* problem is obtained by reducing the solution space of the original problem to $\Omega = \Omega_i \cap \Omega_{n+1}$, where

$\Omega_i = \{ x \in \mathrm{N}^n \mid m_j \in M(R_i) \}$. That is to say, the feasible solutions should comply with the evolution rules defined by R_i, the alternative PN model of the system.

Each one of the simple problems can be solved by searching for the optimum in the solution space of the problem. After solving the *n* optimisations of every simple problem, a second stage consists of performing an additional search of the best solution among the *n* results.

This "divide and conquer" technique implies a double stage optimisation process, where the first one implies to solve n different optimisation problems. When n is a large number, the complete process may be intractable. This problem might be afforded by a prior reduction in the set of alternative systems. In this case the choice of the alternative models to be optimised can jeopardise the generalisation of the results to S_R.

The second phase in the optimisation consists of a comparison between all the solutions obtained from the first stage. As those processes can be approximate ones and with a partially random nature, the comparison might be more reasonable if the complete optimisation process could be performed in a single step.

6. ALTERNATIVES AGGREGATION PETRI NETS (AAPN)

The methodology proposed in this paper is based on a new type of Petri Nets which has been called Alternatives Aggregation Petri Net (AAPN). It provides with the possibility to solve the optimisation problem based on n Petri net models with a one problem and one stage approach (Latorre 2007).

One of the main advantages of the AAPN is that they can profit from similarities in the alternative PN models. It is very common, in DEVS design problems, that the alternative PN models have common subnets in their structure.

On the other hand, the existence of only one solution space and not n different ones to be explored can lead to fast searches and the use of limited computer resources even when n is a large number. In order to explain how an AAPN is constructed it is necessary to define some conceps previously.

Let $S_R = \{ R_i \mid R_i = \langle Q_i, m_{i0} \rangle, i = 1,...,n \}$ be a set of alternative PN models for a certain partially undefined DEVS *D*.

Let $R^k_i = <Q^k_i , m^k_{io}>$ be a subnet of $R_i. \in S_R$ where $Q^k_i = <P^k_i, T^k_i, \alpha^k_i, \beta^k_i>$

Definition 4. Shared subnet

R^k_i is said to be a shared subnet in S_R if $\exists\, j \in \mathrm{N}$, $1 \le j \le n, j \ne i \ni R^k_i$ is a subnet of $R_j \in S_R$.

This concept is defined to profit from the common subnets in the alternative PN when the optimisation technique is performed.

In *Fig. 2*, R_a is a shared subnet by R_1, R_2 and R_3, while R_b is shared by R_1 and R_2.

Definition 5. Border place

i) $p \in P^k_i$ is an ***input border place*** of R^k_i if
$\exists\, p' \in R_i \ni p' \notin R^k_i \wedge p' \in {}^\circ t$ where $t \in {}^\circ p$

ii) $p \in P^k_i$ is an ***optput border place*** of R^k_i if
$\exists\, p' \in R_i \ni p' \notin R^k_i \wedge p' \in t^\circ$ where $t \in p^\circ$

Definition 6: Output subnet set

$R^k_i{}^\circ = \{ R^j_i$ subnet of $R_i \mid \exists\, p \in P^k_i, p' \in P^j_i, t \in T_i \ni p \in {}^\circ t \wedge p' \in t^\circ \}$ is the output subnet set of R^k_i.

Definition 6b. Choice place

$p \in P^k_i$ is a *choice place* of R^k_i if
$\exists\, S_{R2}, S_{R3} \subseteq S_R \wedge S_{R2} \cap S_{R3} \ne \varnothing \ni$
i) $\exists\, R^{k2}_i \in R^k_i{}^\circ \subseteq S_{R2} = \{ R_{j2} = <Q_{j2}, m_{0j2}> \mid j_2 = 1,\ldots,n_2 \}$
ii) $\exists\, R^{k3}_i \in R^k_i{}^\circ \subseteq S_{R3} = \{ R_{j3} = <Q_{j3}, m_{0j3}> \mid j_3 = 1,\ldots,n_3 \}$
iii) $\exists\, t_1, t_2 \in p^\circ \wedge$
iv) $\exists\, p_1 \in t_1{}^\circ \ni p_1 \in P^{k2}_i$
v) $\exists\, p_2 \in t_2{}^\circ \ni p_2 \in P^{k3}_i$.

In other words, the output set of R^k_i contains subnets in different alternative Petri nets (R_i and R_j).

Definition 7. Choice variable

A set of choice variables is $A = \{A_i \mid i = 1,\ldots,n\}$, where each A_i is a Boolean variable.

From these definitions, it will be explained how to construct an AAPN as a tool to solve an optimisation problem based in n alternative PN models. The construction algorithm which will be presented comprises four steps.

Algorithm 1: construction of R^*, an AAPN from S_R

Step 1: Divide every $R_i \in S_R$ into R^j_i , $j=1,\ldots,n_i$, subnets of R_i.

Step 2: Determine the sets of input and output border places for every R^j_i , $i=1,\ldots,n$; $j=1,\ldots,n_i$

Step 3: Define an appropriate designation for every subnet, place and transition, in a way that the shared subnets include unique names.

Step 4: Aggregate all the subnets in a single R^*:

Step 4.1: $i=1$, $j=1$, $R^*=\varnothing$

Step 4.2: if $R^j_i \not\subset R^*$ then $R^*= R^j_i \cup R^*$

Step 4.3: link R^j_i to R^* with the original transitions in R_i

Step 4.4: if a link transition $t \in p^\circ$ and p is a choice place $\Rightarrow$ associate the choice variable A_i to t.

Step 4.5: $j=j+1$; if $j \le n_i$ then go to ***step 4.2***

Step 4.5: $j=1$; $i=i+1$; if $i \le n$ then go to ***step 4.2***.

Fig. 3 shows an AAPN R^* as it has been constructed from the original set of alternative Petri nets of *Fig. 2* and the set of choice variables $A = \{A_1, A_2, A_3\}$. See also the shared subnets R_a and R_b.

Definition 8: Reduction rate of (R^*, S_R)

$$r_r\left(R^*, S_R\right) = \frac{q^*}{\sum_{i=1}^{n} q_i} \qquad (1)$$

where q^* is the number of places of R^* and q_i is the number of places of $R_i \in S_R$, $i=1,\ldots,n$.

This rate is a measure of the size of R^* compared to the size of the set of alternative PN. The smaller the reduction rate is, the larger the amount of shared subnets is.

Some properties of the AAPN are:

Given $S_R = \{\ R_i \ | R_i = \langle Q_i, m_{0i} \rangle, i = 1,\ldots, n\ \}$

Proposition 1: R^* always exists.

Proposition 2: R^* is not unique.

It is convenient to choose the best AAPN R^* to solve efficiently a given optimisation problem.

Proposition 3: $M(R_i) \subseteq M(R^*)$

All the markings reachable for any of the alternative PN are also reachable for R^*.

Proposition 4: $M(R^*) \subseteq \bigcup_{i=1}^{n} M(R_i)$

The reachable markings of R^* are also reachable of at least one alternative Petri net $R_i \in S_R$.

Definition 9: optimisation problem based on the AAPN R^*

It is similar to ***definition 3***,with the following modifications:

$x \in \Omega$, $\Omega = \Omega_1 \cap \Omega_2$

ii) $\Omega_1 = \{\ x \in \mathrm{P}^n \mid\ m_j \in \mathrm{M}(R^*)\}$, where m_j represents every marking of R^* used in the construction of x and R^* is an AAPN obtained from S_R.

iii) Ω_2 substitutes Ω_{n+1}.

Theorem: x is a solution of an optimisation problem based on $S_R \Leftrightarrow x$ is a solution of an optimisation problem based on R^*

It has been seen that it is possible to solve a ***decision problem based on a DEVS*** by using ***Alternatives Aggregation Petri Net***, including both, design and operation decisions.

When the value of the ***reduction rate*** is small, it is expected that the performance of AAPN will be better or at least similar to other Petri net-based techniques. In the cases when the ***reduction rate*** is not favourable it is also expected a good performance of the AAPN compared to other techniques.

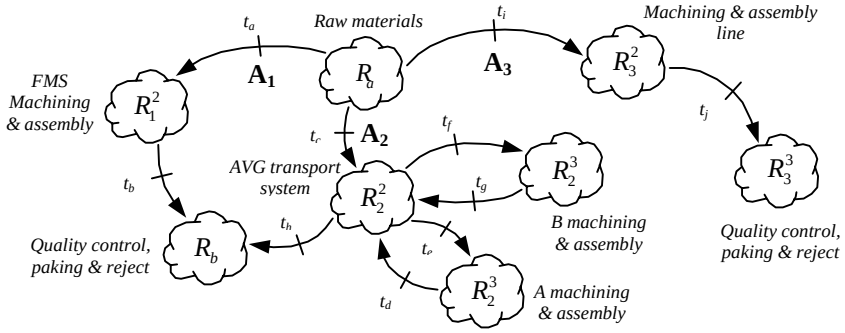

Figure 3. Alternatives aggregation PN for a manufacturing system

7. CONCLUSIONS

In this paper several definitions of decision and optimisation problems have been stated.

Moreover, a new type of PN, the AAPN has been presented and some of their properties have been enunciated.

The AAPN-based method allows to cope, in a compact and efficient way, with decision problems where there are a large amount of alternatives in the design of a DEVS. This statement is also true when the alternatives are unknown and they should verify a set of specifications.

A further reseach step in the field of the AAPN will be to put them to the test in a variety of decision problems and compare their performance and results with other techniques when they are applicable. The results that have been obtained so far are promising. (Latorre 2007)

8. REFERENCES

David, R.,Alla, H. 2005 *Discrete, Continuous and Hybrid Petri Nets*. Springer.

Guash, A., Piera, M.À., Casanovas, J., Figueras, J. 2002. *Modelado y simulación. Aplicación a procesos Logisticos, de fabricación y servicios*. Barcelona.Ed. UPC.

Heizer, J., Render, B. 2008. *Operations Management.* Prentice Hall.

Jiménez, E. 2002. *Técnicas de automatización avanzada en procesos industriales. PhD Thesis*. Logroño. Ed. Univ. de La Rioja

Jiménez, E., Pérez, M, Latorre, I. 2006 Industrial applications of Petri nets: system modelling and simulation. *Proceedings of European Modelling Simulation Symposium*. 159-164. Barcelona.

Jiménez, E., Pérez, M., Latorre, J.I. 2005 ,On deterministic modelling and simulation of manufacturing systems with Petri nets,. *Proceedings of European Modelling Simulation Symposium*, 129-136. Marseille.

Kusiak, A 2000. *Computational Intelligence in Design and Manufacturing*. Wiley-Interscience.

Latorre, J.I., Jiménez, E., Pérez, M. 2006 Comparison of optimization techniques applied to a flexible manufacturing system. *Proceedings of European Modelling Simulation Symposium*, 141-146. Barcelona.

Latorre, J.I., Jiménez, E., Pérez, M. 2007 Macro-Reachability Tree Exploration for D.E.S. Design Optimization. *Proceedings of the 6th EUROSIM Congress on Modelling and Simulation*. Ljubljana (Slovenia).

Lee, D.Y., DiCesare, F., 1992. FMS scheduling using Petri nets and heuristic search. *Robotics and Automation. Proceedings*, Volume 2, 1057 – 1062

Ríos, S., Bielza, C., Mateos, A. 2002. *Fundamentos de los sistemas de ayuda a la decisión* Madrid. Ed. RA-MA.

Rodríguez, D., Zimmermann, A, Silva, M. 2004. Two Heuristics for the Improvement of a Two-Phase Optimization Method for Manufacturing Systems. *Proc. of the IEEE Systems, Man & Cybernetics Conference.*

Silva, M. 1993. Introducing Petri nets, *In Practice of Petri Nets in Manufacturing* 1-62. Ed. Chapman&hall

Zhou, M. Venkatesh, K. 1999 *Modelling, Simulation and Control of Flexible Manufacturing Systems. A Petri Net Approach*, WS World Scientific

AUTHORS BIOGRAPHY

Juan Ignacio Latorre Biel is Industrial Engineer. He has developed his professional career in the industry and in educative institutions. Currently he is preparing his PhD Thesis in DEVS optimisation based on PN. Nowadays he is a teacher at the Public University of Navarra. His research areas include factory automation, modeling and simulation, and industrial processes. His main works are developed with the automatic group of the University of La Rioja.

Emilio Jiménez Macías studied Industrial Engineering (with Computer Science, Electronics and Automation specialty) by the University of Zaragoza. After working several years in the industrial private sector (Researching and Developing Department head position), returned to the university, as an Assistant Professor to the University of La Rioja, in 1997, where he works presently in the Electrical Engineering Department (Coordinator of the System Engineering and Automation Group). In 2001 he presented his PhD thesis about Industrial Automation. His research areas include factory automation, modeling and simulation, and industrial processes. His main works are developed with the automatic group of the University of Zaragoza.

Mercedes Pérez de la Parte received the BS degree in Telecommunications Engineering from the University of Seville in 1997. She has held research and teaching positions at the University of Los Andes, Venezuela, in 2000, and research position at the University of Seville since 1997 until present. She has attended all the PhD courses and is presently preparing her PhD dissertation. She is Assistant Proffesor at the Departamento de Ingeniería de Sistemas y Automática of the University of Seville, Spain, since 2000.

Julio Blanco Fernandez studied Industrial Engineering by the University of the Basque Country. He works presently in the Mechanical Engineering Department (Coordinator of the Fabrication Processes Engineering Group) of the University of La Rioja. His research areas include factory automation, modeling and simulation, and industrial processes. His main works are developed with the automatic group of the University of La Rioja.

TOWARDS COSIMULATING SYSTEMC AND COLOURED PETRI NET MODELS FOR SOC FUNCTIONAL AND PERFORMANCE EVALUATION

M. Westergaard[(a)], L.M. Kristensen[(b)], M. Kuusela[(c)]

[(a)] Department of Computer Science, Aarhus University, Aarhus, Denmark.
[(b)] Department of Computer Engineering, Bergen University College, Bergen, Norway.
[(c)] OMAP Platforms Business Unit, Texas Instruments France, Villeneuve-Loubet, France.

[(a)]mw@cs.au.dk, [(b)]lmkr@hib.no, [(c)]m-kuusela@ti.com

ABSTRACT

Semiconductor technology miniaturization allows packing more transistors onto a single chip. The resulting System on Chip (SoC) designs are predominant for embedded systems such as mobile devices. Such complex chips are composed of several subsystems called Intellectual Property blocks (IPs) which can be developed by independent partners. Functional verification of large SoC platforms is an increasingly demanding task. A common approach is to use SystemC-based simulation to verify functionality and evaluate the performance using executable models. The downside of this approach is that developing SystemC models can be very time consuming, so we propose to use a coloured Petri net model to describe how IPs are interconnected and use SystemC to describe the IPs themselves. Our approach focuses on fast simulation and a natural way for the user to interconnect the two kinds of models. We demonstrate our approach using a prototype, showing that the cosimulation indeed shows promise.

Keywords: SystemC, coloured Petri nets, cosimulation, System on Chip

1. INTRODUCTION

Modern chip design for embedded devices is often centered around the concept of *System on Chip* (SoC) as devices such as cell phones benefit from the progress of the semiconductor process technology. In these platforms, complex systems including components such as general-purpose CPUs, DSPs (digital sound processors), audio and video accelerators, DMA (direct memory access) engines, graphics accelerators and a vast choice of peripherals, are integrated on a single chip. In Fig. 1, we see an example of an SoC, namely Texas Instruments' OMAP44x architecture (Texas Instruments 2009), which is intended for, e.g., mobile phones. Each of the components, called *Intellectual Property blocks* (IPs), can be contributed by separate companies or different parts of a single company, but must still be able to work together. The IPs are designed to be low-power and low-cost parts and often have intricate timing requirements, making the functional verification of such systems increasingly difficult. Therefore the IPs are modeled using an executable modeling language and simulation based validation is performed to ensure that, e.g., the multimedia decoder can operate fast enough to decode an incoming stream before it is sent to the digital-to-analog converter for playback.

When an IP is purchased for inclusion in an SoC, one often obtains a model of the component for inclusion in a whole-system simulation. Such a model is often created using SystemC (IEEE-1666), an industry-standard for creating models based on an extension of C++. SystemC supports simulation based analysis and is well-suited for making models that deal with intricate details of systems, such as electronic signals. SystemC has a couple of weaknesses as well, as it has no formal semantics and therefore is not well-suited for performing formal verification. Furthermore, SystemC is not very well-suited for modeling in a top-down approach where implementation details are deferred until they are needed, and SystemC is inherently textual, making it difficult to get and idea of, e.g., which parts of the chip are currently working or idle, unless a lot of post-processing of simulation results is performed. All of these traits make it tedious and time consuming to create models in SystemC, which postpones the moment where the modeling effort actually pays off by revealing problems in the design.

The coloured Petri nets formalism (CP-nets or CPNs) (Jensen and Kristensen 2009) is a graphical formalism for constructing models of concurrent systems. CP-nets has a formal semantics and can be analyzed using, e.g., state-space analysis (also known as state enumeration, reachability analysis, and model-checking) or invariant analysis. CPN models provide a high level of abstraction and a built-in graphical representation that makes it easy to see which parts of the model that currently process data. The draw-back of CP-nets is that it is not very well-suited for low-level processing as it has to be done either as graphical notation or directly as programming. Also, since many IP modules obtainable are modeled using SystemC, double effort has to be put into making models of the obtained IPs or translating the CPN model to SystemC for simulation along with the purchased models.

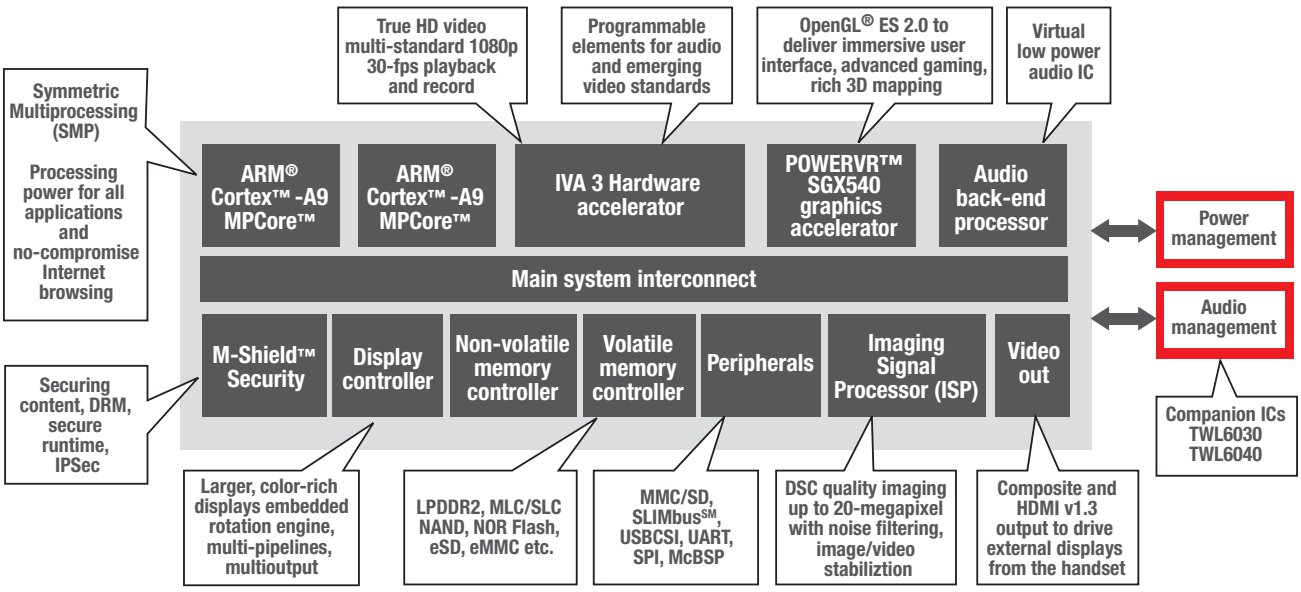

Figure 1: Block diagram of Texas Instruments' OMAP44x platform.

During development of the next generation SoC, some IPs were modeled using coloured Petri nets instead of SystemC. Due to the next generation being work in progress, we cannot go into further details about the specifics of the model nor the modeled architecture, but we can sum up some the experiences with using CPN models for SoC modeling and verification. Firstly, a CPN model has been made faster than a corresponding SystemC model, making it possible to catch errors earlier in the process and increase confidence in the new architecture. The model made it possible to catch a functionality error, and subsequent performance simulation provided input to making reasonable trade-offs between implementation of some sub-blocks in hardware or software. All in all, the model did provide interesting insights for a real-life example. Unfortunately, the model also had limitations. The biggest limitation is that the performance of the connection between the modeled block and the memory subsystem could not be evaluated even though a cycle accurate model of the memory system was available in SystemC.

We see that CPN models and SystemC models complement each other very well; one language's weaknesses are the other language's strengths. It would therefore be nice to be able to use the IP models in SystemC with a more high-level model created using CP-nets. In this way it is possible to have the SystemC models specify the low levels of the model and graphically compose the IPs using CP-nets, allowing us to have a high-level view of which IPs are processing during the simulation. In this paper we describe an architecture for doing this by running a number of CPN simulation kernels in parallel with a number of SystemC simulation kernels, what we call a *cosimulation*.

The reason for introducing our own kind of cosimulation instead of relying on, e.g., the High-Level Architecture (HLA) (IEEE-1516), is mainly due to speed of development and speed of execution; please refer to Sect. 3 for a more detailed discussion.

The rest of this paper is structured as follows: First, we briefly introduce SystemC and CP-nets using a simple example, in Sect. 3 we present the algorithm used to cosimulate models, and in Sect. 4 we describe a prototype of the cosimulation algorithm, our experiences from the prototype, and propose an architecture of a real implementation. Finally, in Sect. 5, we sum up our conclusions and provide directions for future work.

2. BACKGROUND

In this section we introduce the formalisms SystemC and coloured Petri nets using an example of a simple stop-and-wait communication protocol over an unreliable network. It is not crucial to understand the details of the languages nor the example, but just to give an impression of models and their communication primitives.

2.1. Coloured Petri Nets

At the top level (Fig. 2) the model consists of three modules, a Sender, a Receiver, and a Network. Before we explain the top level, let us look at the implementation of the receiver as a CPN model (Fig. 3). The Receiver consists of four *places* (named B, C, NextRec, and Received) with *types* written below them (INTxDATA for B, INT for C and NextRec, and DATA for Received) and one *transition* (named Receive Packet). Places can contain *tokens* written in rectangles above the places (in this example, NextRec contains one token with the value 2 and Received contains one token with the value "CP-"). C contains no tokens and B contains two tokens with the more complex values (1, "CP-") and (2, "net"). Tokens can have *time stamps* written after the @-sign to the right of the value of the token (in this example, the token (1, "CP-") on B has the time stamp 69, 2 on NextRec has time stamp 113, and "CP-" on Received

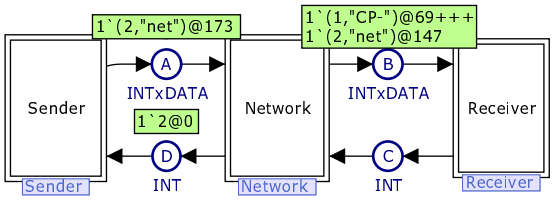

Figure 2: Top level of network protocol.

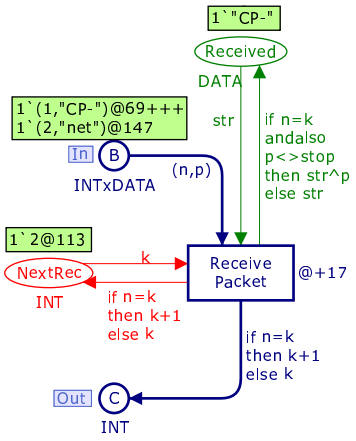

Figure 3: Receiver of network protocol.

has no time stamp). There are *arcs* between places and transitions. An arc from a place to a transition indicates that in order for the transition to be *enabled* tokens with the appropriate values must be available on the place(s) (called *input places* of the transition). When a transition is enabled, it can *occur*, and the result is that tokens are removed from its input places and tokens are produced on the places connected via arcs from the transition (the *output places*). Arcs contain expressions that describe which tokens can be moved, but we will not go into detail about that here. A CPN model has a global clock that governs when tokens are available; they are available if their time stamp is less than or equal to the value of the global clock. Transitions can have inscriptions after the @+-sign next to the transition that describe how long they take to occur (here Receive Packet takes 17 time units to occur). This influences the time stamp of produced tokens.

The gist of the receiver is that a packet (a pair of a packet number and some data) arrives on B, NextRec contains an internal counter that keeps track of which packet we expect, and Received contains the data we have received until now. In this case, Receive Packet is enabled. When it occurs, it consumes the packet from B. The serial number of the received packet (n) is compared with the number of the next expected packet (k). If the packet is the expected one, we append the data to Received, increment NextRec, and transmit an acknowledgement for the next packet onto C. If we receive another packet, we drop the packet, keep the value of the NextRec counter, and send an acknowledgement for the expected packet.

The top level of the protocol is shown in Fig. 2. It consists of four places and three *substitution transitions*, Sender, Network, and Receiver, drawn using a double outline. The idea is that a substitution transition represents a module. Here, the Receiver substitution transition represents the receiver module from Fig. 3. Communication between the top level and the module uses *port places*; in Fig. 3 we have two port places, B and C. We can distinguish port places from normal places by the inscription saying either In (on B) or Out (on C), which specifies that information flows into or out of the module. When a token is produced on the B place in Fig. 2, it appears on the B port place in Fig. 3; in the example, we see that both B places indeed have the same marking.

We will not go into details about the implementation of the Network module, but merely say that it implements a bidirectional network link that can drop and delay packets.

2.2. SystemC

We wish to model the Sender module using SystemC. SystemC models consist of modules that are organized in a hierarchy. Modules have interfaces consisting of ports that can be connected to other ports using channels. In Listing 1, we see a very simplistic SystemC version of the sender. We define a module Sender (l. 4) and give it two ports, p_in and p_out (ll. 5–6). The sender has some local data, a variable nextPacket (l. 39) for keeping track of which packet to send next, and an array of all packets we intend to send, allMes (l. 40). These are set up in the constructor (ll. 9–12), where we also indicate (ll.14–15) that our module has two threads, SendPacket, responsible for transmitting packets, and ReceiveAck, responsible for receiving and processing acknowledgements. We indicate that we are interested in being notified when data arrives on p_in (l. 16). The SendPacket thread (ll. 19–26) loops through all packets, writing them to p_out and delaying for sendDelay time units between transmitting each packet. The ReceiveAck thread (ll. 28–37) receives acknowledgements from p_in and updates nextPacket, so the next packet is transmitted. We see that the model basically is C++ code and despite its simplicity still comprises over 40 lines of code. We would normally split the code up in interface and implementation parts, but have neglected to do so here in order to keep the code simple.

We need to set up a complete system in order to run our sender. In Listing 2, we see how such a setup could look like. We basically have a module Top (l. 6) which is a simplified version of the top level in the CPN model (Fig. 2). The top module sets up two channels (ll. 7–8), D and A (using the same names as in Fig. 2). The constructor initializes the sender and receiver test bench (l. 13) and connects the ports via channels (ll.14–17). The main method initializes the top level (l. 22) and starts the simulation (l. 23).

Now, our goal is to use the code in Listing 1 as the sender module in the CPN top level (Fig. 2) with the CPN implementation of the network (not shown) and the CPN version of the receiver (Fig. 3) in a single simulation run.

3. ALGORITHM

As our primary goal is to be able to simulate real-life System-on-Chip (SoC) systems, which are typically modeled on the nanosecond scale, we need to be able to perform very fast simulation, and it is not feasible to tightly synchronize the CPN and SystemC parts of the model if we wish to simulate several seconds of activity. Instead, we try to only synchronize models when needed, i.e., when one part has done everything it can do at one time stamp and needs to increment its clock, or whenever information is exchanged. In the following we will refer to CPN and SystemC simulation kernels as *components* in cosimulations.

Aside from requiring loose coupling between the components, we prefer a truly distributed algorithm in order to avoid having to rely on a coordinator. As a goal of the project is to find out whether CPN/SystemC cosimulation is possible, feasible, and can actually benefit modeling, we also want to do relatively fast prototyping. For these reasons, we decided to make our own implementation of cosimulation instead of using an off-the-shelf technology such as HLA. HLA enforces a stricter synchronization than we need, so by making our own implementation, we believe we can achieve better performance. Furthermore, implementing a generic HLA interface for CPN models is a non-trivial task, and does not satisfy our requirement of fast development. Finally, HLA relies on coordinators which conflicts with our desire for a distributed algorithm.

Listing 1: Sender.h

```
1  #include "systemc.h"
2  #include "INTxDATA.h"

4  SC_MODULE (Sender) {
5    sc_port<sc_fifo_out_if<INTxDATA> > p_out;
6    sc_port<sc_fifo_in_if<int> >  p_in;

8    SC_CTOR(Sender) {
9      nextPacket = 1;
10     for (int i = 0; i < 2; i++)
11       allMes[i].no = i + 1;
12     allMes[0].mes = "CP-"; allMes[1].mes = "net";

14     SC_THREAD(SendPacket);
15     SC_THREAD(ReceiveAck);
16     sensitive << p_in;
17   }

19   void SendPacket(void) {
20     sc_time sendDelay = sc_time(9,SC_NS);

22     while (nextPacket < 3){
23       wait(sendDelay);
24       p_out->write(allMes[nextPacket-1]);
25     }
26   }

28   void ReceiveAck(void) {
29     sc_time ackDelay = sc_time(7,SC_NS);
30     int newNo;

32     while (true){
33       newNo = p_in->read();
34       wait(ackDelay);
35       nextPacket = newNo;
36     }
37   }
38 private:
39   int nextPacket;
40   INTxDATA allMes[2];
41 };
```

Listing 2: sc_main.cpp

```
1  #include <systemc.h>
2  #include "Sender.h"
3  #include "ReceiverTestBench.h"
4  #include "INTxDATA.h"

6  SC_MODULE (Top) {
7    sc_fifo<int> D;
8    sc_fifo<INTxDATA> A;

10   Sender S;
11   ReceiverTestBench RTB;

13   SC_CTOR(Top): S("S"), RTB("RTB") {
14     S.p_out(A);
15     S.p_in(D);
16     RTB.p_in(A);
17     RTB.p_out(D);
18   }
19 };

21 int sc_main(int argc, char* argv[]) {
22   Top SenderReceiver("SenderReceiver");
23   sc_start();
24   return 0;
25 }
```

Our algorithm is shown as Algorithm 1. Basically, it runs two nested loops (ll. 2–6 and 3–5). The inner loop executes steps locally as long as possible at the current time. A step is an atomic operation dependent on the modeling formalism; for CPN models a step is executing a transition and for SystemC a step can be thought of as executing a line of code (though the real rule is more complex). The inner loop also sends outgoing information to other components and receives information from other components (here we have shown a single-threaded implementation that exchanges information after every step, but we can of course make a multi-threaded version or only exchange information when it is no longer possible to make local steps). When we can make no more steps locally, we find the allowed time increase by calculating the global minimum of requested time increases from all components.

Algorithm 1 The Cosimulation Algorithm

```
1: Time ← 0
2: while true do
3:   while LocalStepIsPossibleAt( Time ) do
4:     executeOneStepLocally()
5:     sendAndReceive()
6:   Time ← distributedGlobalMin(
                              desiredIncrease() )
```

We note that exchange of information takes place without global synchronization. Participants simply communicate directly and if incoming information causes components to be able to execute more local steps they just do so, and reevaluate how much they want to increment time. This means that our synchronization algorithm does not have to deal with information exchange.

4. EVALUATION

Naturally, Algorithm 1 needs to be implemented for each kind of simulation kernel we wish to be able to use for cosimulation. Our primary goal is to make implementations of CP-nets and SystemC models, but the algorithm is general and can in principle be implemented for any timed executable formalism. In order to evaluate Algorithm 1 and whether CPN/SystemC cosimulation is feasible, we have developed a prototype to show that is is possible to integrate the two languages but also to show that it is possible to make the integration without (or with very few) changes to the SystemC kernel, as there are multiple vendors with different implementations.

Algorithm 1 does not specify how we calculate the global minimum required for synchronization. It is possible to do this without imposing any restrictions on the network structure, e.g., by using flooding, but making assumptions allows a much easier and faster implementation. As both CP-nets and SystemC models are naturally structured hierarchically with components containing nested components, optionally in several layers, making the assumption that components are structured in a tree is no real restriction.

The architecture of our prototype can be seen in Fig. 4. We first look at the static architecture from the top of Fig. 4. The prototype consists of three kinds of processes: a SystemC simulation kernel (left), an extended version of the of the ASCoVeCo State-space Analysis Platform (ASAP) (Westergaard, Evangelista, and Kristensen 2009), which contains a library called ACCESS/CPN (Westergaard and Kristensen 2009), making it easy to interact programmatically with the CPN simulator of CPN Tools (Ratzer, Wells, Lassen, Laursen, Qvortrup, Stissing, Westergaard, Christensen, and Jensen 2003) (right). The yellow/light gray boxes are already part of a standard SystemC simulation kernel, ASAP, or CPN Tools' simulator process and therefore does not have to be built from scratch. We have added a Cosimulation layer on top of the SystemC model. The cosimulation layer basically provides stubs for modules that are external (such as a CPN model or another SystemC model). Like with Remote Procedure Call (RPC) (Srinivasan 1995) systems, the stub module looks like any other module to the rest of the system and takes care of communicating with the other components. In the example in Sect. 2, the stub would consist of an implementation of ReceiverTestBench referred to Listing 2 and the cosimulation layer would consist of code like Listing 2 along with a communication library. Currently, we need to write such stubs manually, but we are confident that stubs can be generated automatically. The stub communicates using ONC-RPC (Srinivasan 1995) (formerly known as Sun RPC and available on all major platforms) with a SystemC cosimulation job in the middle ASAP process. For easy prototyping, we have selected to do most of the implementation in Java (ASAP is written in Java) rather than directly in SystemC (extension of C++) and CPN (written in Standard ML). The

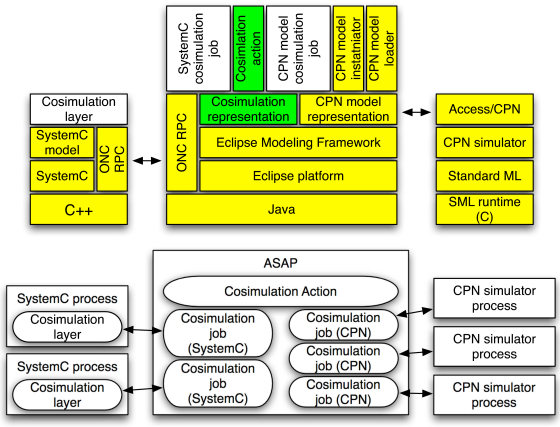

Figure 4: The conceptual architecture (top) and run-time architecture (bottom) of the prototype

SystemC cosimulation job and CPN cosimulation job from the ASAP process contain most of the implementation of Algorithm 1 specific for SystemC and CPN models. Between those, we have a Cosimulation action, which takes care of starting and connecting the correct components based on a Cosimulation representation which describes which components to use and how to compose them. We believe that the cosimulation action and cosimulation representation (marked in green, dark gray) can later be reused in a subsequent real implementation. Access/CPN abstracts away the communication between the ASAP and CPN simulator process, so we do not have to make changes to the CPN simulator.

At run-time, a cosimulation looks like Fig. 4 (bottom). Each rectangle is a running process, and each rounded rectangle is a task running within the process, corresponding to the blocks from the static architecture. We see that all simulators are external and can run on separate machines. We have implemented Algorithm 1 within the ASAP process (this in particular means that the distributed algorithm runs within one process). We have implemented the algorithm in full generality using channel communication only, but as we were not concerned with speed in our prototype, decided against setting up a truly distributed environment in the prototype.

The only non-trivial part is how to do the minimum calculation in line 6 of Algorithm 1. Our algorithm uses that the components are organized in a tree, and we will use normal tree terminology (root, parent, and children). Naturally, each node knows how many children it has and its parent. The idea is that each node requests a time increase from its parent. The parent then returns the allotted time increase. When a node wants to increase time, it waits for all its children to request a time increase. It takes the minimum of all of these votes (including its own) and requests this time increase from its parent. When it receives a response from the parent, it announces this increase to all children. The root just announces to all children without propagating to its (non-existing) parent. The algorithm can be improved in various ways. For

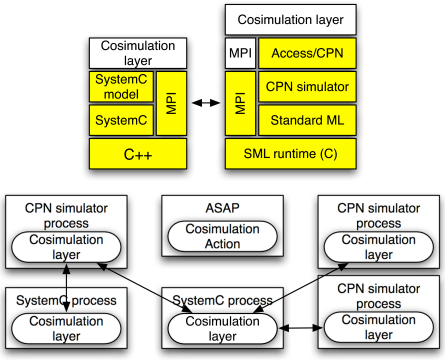

Figure 5: The conceptual architecture (top) and run-time architecture (bottom) of real implementation

example, as soon as a node realizes that only the minimum time increase can be granted (0 or 1 depending on whether we allow requesting a zero time increase), it can just announce the result to all children and continue propagating up in the tree. Also, a parent node need not actually announce the lowest time increase. It can announce the time increase requested by the node that has the second lowest request minus one, and sub-trees can then autonomously proceed (knowing that other sub-trees will not be able to proceed as they cannot receive data since information flows only up and down the tree).

For a real implementation we propose the much simpler architecture from Fig. 5. In this architecture, we have removed the centralized process and instead made real implementations of the Cosimulation layer for both SystemC and CPN. We have also replaced ONC-RPC with Message Passing Interface (MPI) (Message Passing Interface Forum 1997) which is an industry standard for very fast communication between distributed components. In order to use MPI, we will have to embed a standard MPI implementation into the SML run-time and add code to interface with that from SML code. The run-time behaviour is as one would expect. Instead of having the communication being mediated by ASAP, ASAP now just sets up a cosimulation, and the components communicate directly with each other, and ASAP can process the results after simulation.

One of our design goals was that we did not want to change the SystemC kernel. Instead, we have created a cosimulation layer as a regular SystemC process, so our prototype shows that this is feasible. For efficient implementation we probably need to augment the CPN simulator, but that is less of a problem, since we have control over it. Our implementation shows that the algorithm has the potential to provide efficient cosimulation and that it is possible to get meaningful results from the components of the model (currently we just extract log files, but it should be easy to map these back to the models, mostly for the CPN models to get graphical feedback). As a bonus, our prototype shows that it is possible to do reasonable distributed simulation of CPN models.

5. CONCLUSION AND FUTURE WORK

In this paper we have described an algorithm for cosimulation of CPN and SystemC models for verification of SoC platforms. The algorithm allows loose coupling between different simulation kernels, which we believe provide faster simulation. We believe that the prototype looks interesting and is worth pursuing further. The prototype has even provided some unforeseen benefits, such as distributed simulation of CPN models.

We have already mentioned that the High Level Architecture (HLA) provides similar features. HLA, however, has some problems that we wish to avoid. The main reason for not using HLA for the prototype was that it is too complex to get working code up and running fast. We also believe that the relatively tight coupling between the components of HLA is undesirable for performance reasons. Finally, our proposed system is completely distributed, whereas HLA has centralized components. Our distributed approach allows more decoupling, improves scalability, and provides a simpler implementation.

Future work includes making a real implementation as proposed in the previous section. We have not currently implemented all of the optimizations to the distributed minimum calculation described in the previous section, and these should be implemented and evaluated. It would be interesting to take compare a real implementation with an implementation using HLA for cosimulation of CPN and SystemC models, which would require making an implementation of HLA for CPN models. Finally, we have until now only dealt with simulation of composite models. It would be interesting to also look at verification, e.g., by means of state-spaces, which seems quite promising as modular approaches for CP-nets perform very well when systems are loosely synchronized, which is indeed the case here.

ACKNOWLEDGEMENTS

This work is in part supported by the Danish Research Council for Technology and Production.

REFERENCES

IEEE-1516, Modeling and Simulation High Level Architecture.

IEEE-1666, IEEE Standard System C Language Reference Manual.

Jensen, K. and Kristensen, L.M., 2009, *Coloured Petri Nets – Modelling and Validation of Concurrent Systems*, Heidelberg: Springer-Verlag.

Message Passing Interface Forum, 1997, *MPI-2: Extensions to the Message-Passing Interface*, http://www.mcs.anl.gov/research/projects/mpi/mpi-standard/mpi-report-2.0/mpi2-report.htm [Accessed 8 June 2009]

Ratzer, A.V., Wells, L., Lassen, H.M., Laursen, M., Qvortrup, J.F., Stissing, M., Westergaard, M., Christensen, S., and Jensen, K., 2003, CPN Tools for Editing, Simulating, and Analysing Coloured Petri Nets, *Proceedings of the Petri Net Conference*,

pp. 450–462, June, Eindhoven, The Netherlands.
Srinivasan, R., 1995, *RPC: Remote Procedure CAll Protocol Specification Version 2*, RFC 1831.
Texas Instruments, 2009, *OMAP™ Applications Processors: OMAP™ 4 Platform*, http://www.ti.com/omap4 [Accessed 8 June 2009]
Westergaard, M., Evangelista, S., Kristensen, L., 2009, ASAP: An Extensible Platform for State Space Analysis, *Proceedings of the Petri Net Conference*, pp. 303-312, June, Paris, France.
Westergaard, M., Kristensen, L., 2009, The Access/CPN Framework: A Tool for Interacting With the CPN Tools Simulator, *Proceedings of the Petri Net Conference*, pp. 313-322, June, Paris, France.

AUTHORS BIOGRAPHY

Michael Westergaard is a PostDoc at Aarhus University, Denmark, where he obtained his PhD in Computer Science in 2007. He is working with modeling and analysis of concurrent systems using coloured Petri nets, and in particular analysis by means of state space exploration. He is involved in development of tools as well as algorithms to facilitate state space exploration for real-life systems, in particular CPN Tools and the ASAP model checking platform, and the ComBack state space method.

Lars Michael Kristensen is Professor in Computer Engineering at Bergen University College. He has more than 10 years of research experience in development and application of formal methods to concurrent systems. A main focus has been the theoretical foundation of state space methods and their implementation in computer tools, in particular in the context of Coloured Petri Nets. Important research contributions have been the development of the sweep-line state space space method, the development of two variants of the stubborn set partial-order method, and the development of the ComBack method. A strong focus has also been on evaluating the research results in industrial cooperation projects. He acted as researcher in the development of the state space tools of Design/CPN and CPN Tools, and he is the scientific leader of the ASCoVeCO project in the context of which the ASAP model checking platform is being developed. He has recently co-authored a new textbook on Coloured Petri Nets published by Springer-Verlag. In 2007 he received the Danish Independent Research Councils' Young Researcher's Award.

Maija Kuusela received her M.Sc. degree in Information Technology from Helsinki University of Technology, Finland in 1981 and her PhD degree in Mathematics from Duke University, North Carolina in 1986. During her professional carrier she has held positions at Nokia Research Center in Helsinki, Finland and at Texas Instruments France. Her current post as systems architect at OMAP Platforms Business Unit at Texas Instruments France includes modeling and performance evaluation of multiprocessor platforms and multimedia accelerator architectures.

A DYNAMIC PROCESS MODELING OF WAREHOUSE OPERATIONS

Raid Al-Aomar[(a)], Amer Momani[(b)]

[(a)]Industrial Engineering & Management, University of Sharjah, UAE
[(b)]Industrial Engineering, Jordan University of Science & Technology, JORADN

[(a)]ralaomar@sharjah.ac.ae, [(b)] ammomani@just.edu.jo

ABSTRACT
This paper presents an approach for dynamic process modeling of warehouse operations. Modeled warehouse operations include receiving raw materials, feeding materials to production, and shipping finished items. Such operations have substantial impact on the performance of inventory system, production system, delivery reliability, and the overall supply chain. The proposed approach utilizes discrete event simulation to transform a static process map into a dynamic process flow. The approach is a combination of Process Mapping, Process Measurement, and Process Simulation. It aims at defining, visualizing, measuring, and improving (streamlining) warehouse operations to better support the supply, production, and distribution operations. Used measures of performance include number of completed transactions, labor utilization, and operation cost. An example of warehouse is used to illustrate the development and application of the proposed dynamic process modeling approach.

Keywords: process mapping, simulation, warehouse operations, process improvement

1. INTRODUCTION

Process modeling involves the application of modeling tools (analytical and graphical) to acquire process knowledge and represent process structure and operation. Commonly used process models provide a graphical description of the process elements, activities, resources, and relationships using a process diagram (i.e., a process map or flowchart). As discussed in Greasley (2006), the objective of process modeling is to better understand the process and to provide a mean for process design and improvement.

Due to the dynamic, stochastic, and complex nature of today's business processes, however, simulation modeling is commonly used in process management and engineering. The graphical representation of the process in a process map or flowchart is only one requirement of process simulation. As noted by Gagliardi, *et al.* (2007), simulation modeling in general and Discrete Event Simulation (DES) in particular has an increasingly growing role in process improvement, design, and problem-solving. This can be mainly attributed to the tremendous improvement in simulation software and the integration to statistical and optimization methods. DES models the system as it evolves over time by a representation in which system variables change at discrete points in time. It is widely used in modeling a variety of real-world production and service systems. Details and applications of DES can be found Law (2006), Nelson *et al.* (2006), and Banks (1998).

Simulation has traditionally been used to study, design, and improve warehouse operations. As a key element in the supply chain, warehouses and distribution centers have been playing an important role in modern logistics systems. As discussed by Lambert (1998), improving warehouse operations improves the performance of the whole logistics system due to its impact on key business functions (e.g. manufacturing, transportation, and retailing). Thus, simulation is used to model warehouse operations and provide warehouse managers and supervisors with a flexible mean validate the performance of warehouse designs and to study the impact of changes made to warehouse layout, staffing level, or equipment before investing any capital. Examples of work in this regard include Burnett and LeBaron (2001), Zhou, et al. (2005), and Kosfeld (1998).

As an alternative to building complex simulation models, however, many practitioners still rely on static process mapping and flowcharting in their improvement studies. This is mainly due to modeling difficulties, the duration and requirements of the full-blown simulation, and the cost of specialized simulation software.

This paper presents a Dynamic Process Modeling (DPM) approach based on process mapping, measurement, and simulation. It is aimed at modeling warehouse operations and addressing several challenging decisions are very difficult to make using analytical models. Simulation is utilized in the same modeling environment to translate the static process map into a dynamic and stochastic representation of the underlying process (warehouse operations). It expands the process diagram by incorporating process cycle time, costs, resources, and inherent variability. Section 2 sheds more light on warehouse operations, section 3 presents the DPM approach, section 4 discusses the application of DPM to an application example, section 5 summarizes the results, and section 6 concludes.

2. WAREHOUSE OPERATIONS

Key warehouse operations often involve receiving inbound materials, feeding material to other business functions, and shipping outbound items. This also includes other activities such as material handling, sorting, storing, packaging, labeling, wrapping, pricing, docking, racking, and picking. Whether connected to a plant or as a stand alone facility, the warehouse may also handle final assembly, re-working, kitting, pricing, and other value-added actvities. A detailed description of warehouse operations can be found in Mulcahy (1993).

As discussed in Baker and Canessa (2009) and Jinxiang *et al.* (2007), common problems in warehouse design often include maintaining high service level with a reduced workforce, coping with the limitation of physical layout and structure, and managing a highly variable workload and demand rates. It is, therefore, essential to assess the ability of the company's warehouse facilities and operations to support other business functions. This includes checking if the warehouse's physical layout and staffing level are adequate to support production and meet the current volumes of inbound/outbound items at a reasonable cost. The objective is to organize and properly staff the warehouse to avoid late shipments to customers, production outages, and inventory errors due to inadequate work force levels.

Having the right metrics for the performance of warehouse operations is key to being able to assess current performance and justify improvement actions. These metrics are set to track several aspects of operation including service level, costs, productivity, and capacity/resource utilization.

Several methods are often adopted to assess warehouse operations in terms of a defined set of performance metrics. These methods which vary in complexity and focus include process mapping, mathematical modeling, benchmarking warehouse operations and costs, auditing labor productivity, establishing and maintaining operation standards, and simulating warehouse operations.

Another key advantage of dynamic process modeling is to facilitate the development of *lean warehouses*. Main warehouse relevant lean principles include waste reduction in material, effort, inventory, time, and delay. Dynamic modeling of warehouse operations helps bringing lean into the warehouse. In a lean context, value stream mapping is a material and information flow map that provides a good way to gain an understanding of how a warehouse operates and clues to what should be improved.

3. DPM APPROACH

As shown in Figure 1, the proposed Dynamic Process Modeling (DPM) approach consists of three main steps; Process Mapping, Process Measurement, and Process Simulation. In process mapping, we conceptualize and characterize the underlying process in terms of content and logic. A process flow chart or block diagram is used to map the process. In process measurement, we collect pertinent data and measure the process in terms of time, labor, and cost. The process map (structure) and measurements (data) are then used to develop a process simulation model. The approach is focused on gaining process knowledge and improving warehouse operations.

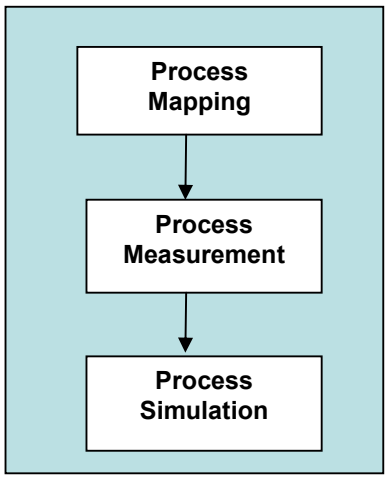

Figure 1: DPM Approach

3.1. Process Mapping

This step involves the flowcharting process structure and flow based on warehouse layout and material handling activities. The developed diagram visually depicts the sequence of events in warehouse operations. It often includes additional information such as capacity, inventory, and equipment information. It breaks the process down into individual events or activities showing the logical relationships between them. Constructing flowcharts promotes better understanding of processes, and better understanding of processes is a pre-requisite for improvement.

3.2. Process Measurement

At this step, pertinent data to each process step in each warehouse operation is collected to be fed into the model. This includes estimating demand rates, determining shift pattern and labor distribution, and measuring cycle times, driving times, material handling times, loading/unloading times, and times of other applicable activities such as sorting, labeling, picking, etc.

3.3. Process Simulation

This step focuses on developing and validating a dynamic simulation model that measures process performance under warehouse resource allocation, variable activity times, and operating conditions. Building a good simulation model for warehousing operations is not trivial. It involves modeling human activities, complex procedures, and varying operating patterns. Simulation runs are then set to measure process performance and used for process improvement.

4. APPLICATION EXAMPLE

The raw materials warehouse example consists of three main parallel operations (Receiving, Feeding, and Shipping). Each operation is controlled using estimations of item demand rate, cycle times, labor resources, and costs. The three main warehouse operations are described as follows:

1. Receiving: unloading raw materials from the containers to the warehouse through two gates (details will be shown later), and arranging the raw material within the warehouse and attics.
2. Feeding the machines in the factory with the needed raw materials, and this job has the priority among any other jobs.
3. Shipping: loading items from the warehouse to containers to be exported to other countries.

A block diagram of the three warehouse operations is shown in Figure 2.

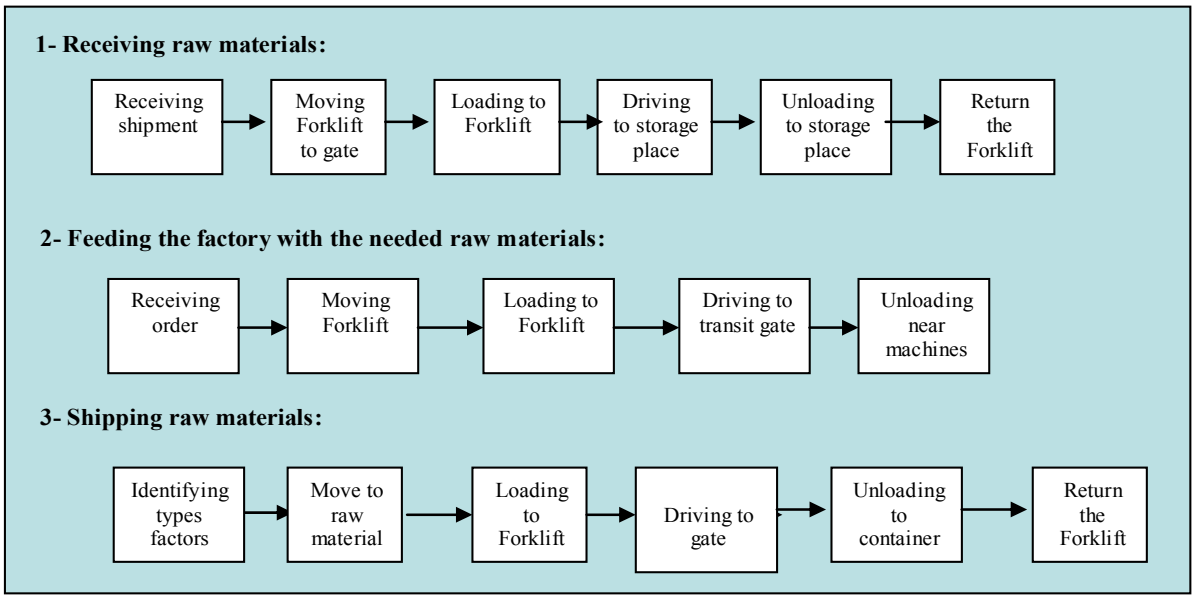

Figure 2: Process Map of Warehouse Operations

4.1. Warehouse Layout

As shown in Figure 3, the raw material warehouse has a rectangular shape of 114 meter length and 35.5 widths, with two main gates; the front gate, and the back gate. It is divided into two parts; the first part is also divided into five storage sections. The other section is utilized as a head office, stationary storage, transit stations, and also storage sections.

4.2. Process Measurement

The following process measurements were taken: demand rates, loading/unloading times, driving times, and warehouse operating pattern including labor distribution. The warehouse receives on average 2-3 trucks/day which translates into receiving 80 forklift-load/day. The warehouse feeds on average 11-17 forklift-load/shift to the plant which is on average 40 forklift-load/day (3 shifts). The warehouse is expected to perform a total of about 300 transactions (forklift-load) per day. Finally, the warehouse ships on average 2-8 trucks/day which translates into shipping about 160 forklift-load/day. Times for unloading raw material (receiving) and loading raw materials (shipping) are summarized in Table 1. Table 2 shows the times for feeding the factory with needed materials including driving times.

Table 1: Shipping/receiving times (min)

Driving to material	Loading forklift	Driving to gate	Unloading forklift
1'05"	22"	1'27"	36"
1'19"	26"	1'35"	45"
1'01"	20"	1'24"	30"
1'10"	24"	1'32"	39"
1'22")	28"	1'37"	44"
41"	25"	59"	26"
30"	19"	42"	20"
32"	20"	44"	24"
34"	20"	46"	25"
31"	20"	44"	21"

Table 2: Feeding the plant times (min)

Transit	Moving forklift	Loading Forklift	Driving to factory	Unloading near machines	Frequency per day
T1	22"	20"	2'40"	1'09"	3-4
	20"	19"	2'42"	55"	3-4
T3	20"	15"	74"	21"	7-10
	16"	15"	33"	14"	7-10
	45"	23"	4'25"	59"	2-3
	41"	20"	4'14"	50"	2-3

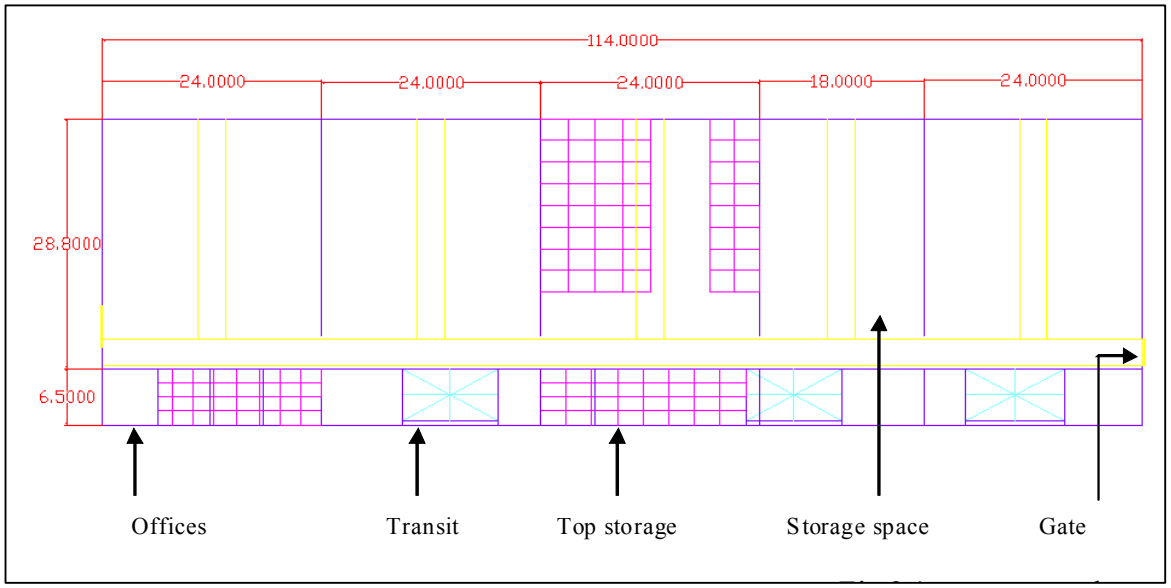

Figure 3: Layout of Raw Material Warehouse

The developed model also incorporates labor resources. Workers work in the receiving area to unload the trucks and store items and in the outbound area to pick, stage, and package products and to load the out-bound trucks. The distribution and operating pattern of warehouse labor is shown in Table 3.

Table 3: Warehouse operating pattern

shift	duration	No. of workers	details
A	7 am-3:30 pm	9	3 forklift drivers 2 operators 2 store keepers 1 inventory manager 1 assistant manager
B	3 pm-11:30 pm	6	1 forklift driver 2 operators 1 store keeper 1 inventory manager 1 assistant manager
C	11 pm-7:30 am	4	1 forklift driver 1 store keeper 2 operators

4.3. Process Model

In the developed process model, we abstracted the set of activities related to the move, control, and storage of finished products and identified the patterns that can be used to characterize the key process elements. Particularly we focused on the three type of flows: inbound (or receiving) process, outbound (i.e. part of order cycle process), and feeding production. Each process contains a sequence of activities performed at a number of locations using a set of dedicated or shared resources. The logic is defined to control the flow of materials through these activities.

The model is implemented using iGrafx™ process modeling and simulation software (iGrafx™, 2009). The mapping, modeling, and simulation features of iGrafx™ allow for drawing a process diagram, creating a process model, defining one or more simulation scenarios, simulating the process, and then reviewing the process results in a simulation report. It provides an excellent environment to model process details (cycle times, resources, operating pattern, and costs) and run dynamic simulations of the process flow. A number of test runs were undertaken to verify the model. A warehouse supervisor has also checked the model to ensure validity. Model results are defined in a customized report that highlights utilization, cost, and productivity. The developed process simulation model is shown in Figure 4.

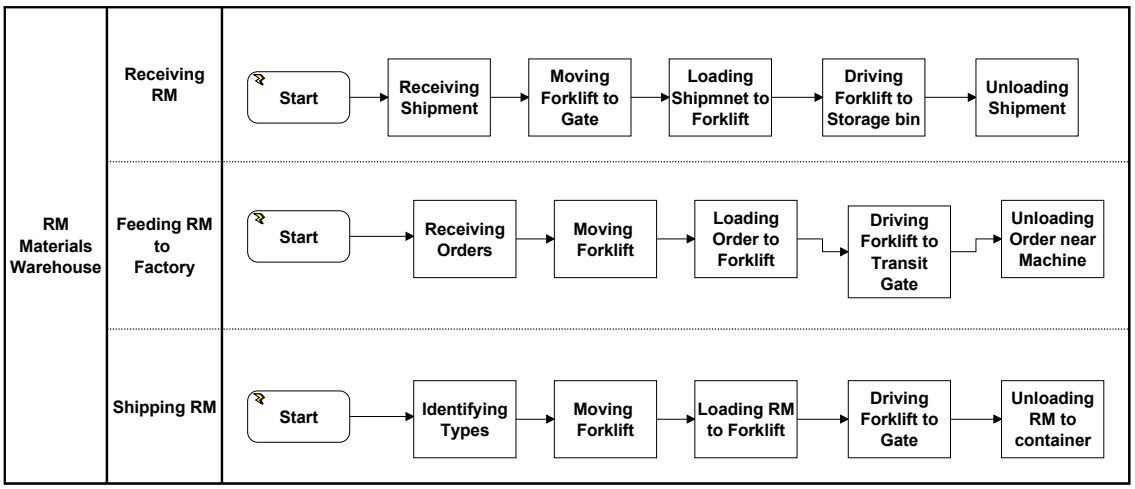

Figure 4: The process simulation model of warehouse operations

5. RESULTS

Output measures generated by the simulation are specified in three aspects: productivity (completed transactions), utilization (drivers and workers), and cost of warehousing operations. Completed transactions include receiving, feeding, and shipping operations. Cost includes labor wages ($5/hr for workers and $7.5/hr for drivers) and other direct and indirect (overhead) costs at the three operations.

Process current state involves 5 drivers and 5 workers to perform the three warehouse operations. Running the dynamic process model for 40 hrs (one week) of operations generates the results shown in Figure 5.

As shown in Figure 5, drivers and workers are low utilized and the processed transactions exceed the demand rates. Cost of warehouse operations per week is relatively high especially for shipping transactions. Such performance issues cannot be identified without the dynamic modeling of the process. To explore the potential of process improvement, the process model is rerun using only one driver and one worker. Results are shown in Figure 5.

It is clear from Figure 6, that one driver is not enough due to high utilization. The single worker has acceptable utilization. Compared to the results in Figure 5, the total cost of warehouse operations is almost 50% less.

Completed transactions cannot meet the warehouse demand rates. It is, therefore, necessary to seek a tradeoff process setup. To this end and to further demonstrate the benefit of dynamic process mapping, a full factorial experimental design is developed by changing levels of workers and drivers. Simulation results of run experiments are summarized in Table 4.

Resource Count

Driver	5
Worker	5

Average Resource Utilization

Driver	52.86
Worker	35.76

Transactions Count

RM Materials Warehouse/Feeding RM to Factory	53
RM Materials Warehouse/Receiving RM	95
RM Materials Warehouse/Shipping RM	210

Total Cost

RM Materials Warehouse/Feeding RM to Factory	$2145.29
RM Materials Warehouse/Receiving RM	$4902.98
RM Materials Warehouse/Shipping RM	$9072.88

Figure 5: Results of current state process simulation

Resource Count

Driver	1
Worker	1

Average Resource Utilization

Driver	96.98
Worker	65.82

Transactions Count

RM Materials Warehouse/Feeding RM to Factory	20
RM Materials Warehouse/Receiving RM	17
RM Materials Warehouse/Shipping RM	89

Total Cost

RM Materials Warehouse/Feeding RM to Factory	$1270.96
RM Materials Warehouse/Receiving RM	$1769.59
RM Materials Warehouse/Shipping RM	$5560.46

Figure 6: Simulation results (reduced resources)

Table 4: Results of simulation experiments

Exp#	Worker	Driver	TransCount	Cost
1	1	1	126	5321
2	1	2	170	7194
3	1	3	175	7399
4	1	4	176	7446
5	1	5	177	7485
6	2	1	132	5544
7	2	2	224	9672
8	2	3	237	10009
9	2	4	247	10382
10	2	5	272	11592
11	3	1	131	5581
12	3	2	226	9721
13	***3***	***3***	***296***	***12816***
14	3	4	350	15265
15	3	5	359	15697
16	4	1	130	5516
17	4	2	222	9565
18	4	3	295	12849
19	4	4	362	15780
20	4	5	353	15404
21	5	1	129	5502
22	5	2	228	9822
23	5	3	295	12868
24	5	4	355	15466
25	5	5	349	15220

Based on the results of Table 4, 3 drivers and 3 workers will be sufficient to meet the demand rate of about 300 transactions at acceptable cost and utilization. Details of this process setup are shown in Figure 7.

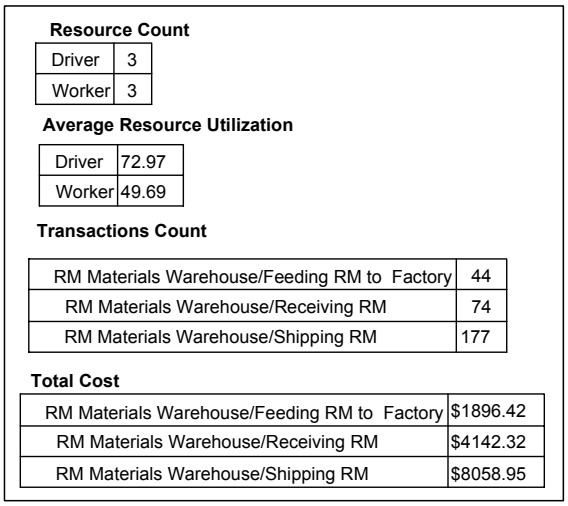

Figure 7: Simulation results (selected process setup)

6. CONCLUSION

The paper presented a practical approach for dynamic process modeling of three warehouse operations (material receiving, feeding plant, and product shipping).The approach consists of process mapping, measurement, and simulation. The approach is demonstrated through an application example of typical warehouse operations. The process is modeled, diagnosed, and configured based on three measures of performance; transactions completed, resource utilization, and total cost. The dynamic process model served as a flexible platform for measuring process performance and improving warehouse operations. The power of the approach stemmed from utilizing the platform for process excellence where the dynamic process modeling is found to be an effective approach for designing new warehouse operations or improving the performance of existing ones.

REFERENCES

Baker, P., Canessa, M., 2009. Warehouse Design: A Structured Approach, European Journal of Operational Research, Vol. 193, pp. 425-436.

Banks, J. (editor)., 1998. Handbook of Simulation, Principles, Methodology, Advances, Applications, and Practice. John Wiley & Sons, Inc. New York.

Burnett, D., LeBaron, T., 2001. Efficiently Modeling Warehouse Systems. *Proceedings of the 2001 Winter Simulation Conference*. pp. 1001-1006.

Gagliardi, J.P., Renaud, J., Ruiz, A., 2007. A Simulation Model to improve Warehouse Operations**.** *Proceedings of the 2007 Winter Simulation Conference.* pp. 2012-2018.

Greasley, A., 2006. Using Process Mapping and Business Process Simulation to Support a Process-Based Approach to change in a Public Sector Organization, Technovation, Vol. 26, pp. 95-103.

iGrafx process for Six Sigma, 2009. Corel Corporation.

Jinxiang, G., Goetschalckx, M., and McGinnis L.F., 2007. Research on warehouse operation: A comprehensive review, European Journal of Operational Research, Vol. 177, pp. 1-12.

Kosfeld, M., 1998. Warehouse Design through Dynamic Simulation. *Proceedings of the 1998 Winter Simulation Conference.* pp. 1049-1053.

Lambert, D.M., J.R. Stock and L.M. Ellam., 1998. *Fundamentals of logistics management*. Irwin/McGraw-Hill.

Law, A., 2006. *Simulation Modeling and Analysis (4th e*), McGraw-Hill College.

Mulcahy*,* D.E., 1993. *Warehouse Distribution and Operations Handbook.* McGraw-Hill Professional Publishing.

Nelson, B.L., Banks, J., Carson, J.S., and Nicol, D.M., 2006. *Discrete-Event System Simulation (3rd e)*, Prentice Hal.

Zhou, M., Setavoraphan, k., Chen, Z., 2005. Conceptual Simulation Modeling of Warehouse operations**.** *Proceedings of the 2005 Winter Simulation Conference*. pp. 1621-1626.

AUTOMATIC WAREHOUSE MODELING AND SIMULATION

A. Guasch[(a)], M.A. Piera[(b)], J. Figueras[(c)]

[(a)]LogiSim, Universitat Politècnica de Catalunya
[(b)]LogiSim, Universitat Autònoma de Barcelona
[(c)]LogiSim, Universitat Politècnica de Catalunya

[(a)]toni.guasch@upc.edu, [(b)]miquelAngel.Piera@uab.es, [(c)]jaume.figueras@upc.edu

ABSTRACT
In this paper we analyze the impact of using a second transelevator in the performance of a printing plant automatic warehouse. A direct previous attempt to use the second transelevator was not successful since both transelevators were competing for the same physical space, therefore, a simulation study was proposed as a non intrusive way to study and propose a better working configuration.

Keywords: warehouse simulation

1. INTRODUCTION

The target printing plant is located in Spain. It has 6 presses with a printing capacity of 37500 newspapers per hour. When the project started at the beginning of 2008, the main plant bottleneck was feeding the presses with paper reels, especially in the night shift, where most of the production is scheduled.

The goal of this work is the analysis of the process and the proposal of improvements using a simulation model. The core of the model is the intermediate warehouse which feeds the presses with paper reels according to a predefined schedule.

The simulation project has been developed in three main phases. The first phase consists in the modeling and simulation of the automatic warehouse as it is. The results of this phase have been used for verification, validation and gaining the credibility of the plant managers. In the second phase the proposed improvements have been added to the model and the impact on the final performance has been analyzed. In the third phase, the impact of the failures has been measured.

The main components of the simulation model are the dynamics of the transelevator; the physical intermediate warehouse and its storing policy; and the input/output reel flow to/from the intermediate warehouse.

2. DESCRIPTION OF THE SYSTEM

Next figure shows the structure of the printing plant as well as the normal flow of paper reels within the plant.

The focus of this work is the processes that take place within the intermediate warehouse.

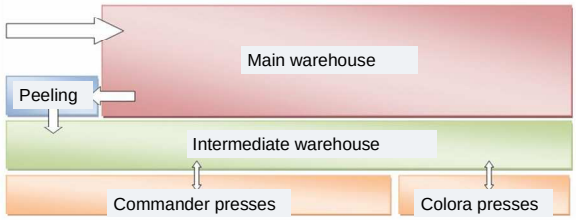

Figure 1: Printing Plant Diagram

2.1. Intermediate warehouse

Figure 2 shows a synoptic of the intermediate warehouse. In the upper left side the input from the peeling zone is shown. The lower side shows the six groups of reel carriers that feed the presses.

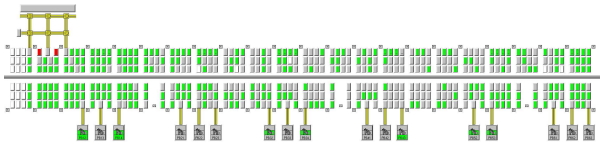

Figure 2: Intermediate Warehouse

In the initial configuration, one transelevator moves along the central rail and is the responsible for all reel moving operations. A second transelevator is available and also moves along the central rail but it is not used in the initial configuration. It is only used in case of failures in the first transelevator. The warehouse has there storage levels at both sides of the central rail.

Measures of the transfer time (loading and unloading) and measures of the vertical and horizontal movement time have been experimentally taken in the plant. Vertical and horizontal movements are performed in parallel. Therefore, the used movement time is the highest of both, the vertical and the horizontal times.

2.2. Movement orders

The control system handles 7 different movement orders in the intermediate warehouse (Table 1).

Table 1: Movement Orders

Tranport type	Description
ENTB	Entrance through the peeling zone
EBPB	Exit to the presses

RBPB	Entrance from the presses (half used reels)
RAPB	Entrance of reel adapters from the presses
EAPB	Exit of adapters to the presses
TALM	Internal transport
PREP	Exit to the peeling zone

These orders have an initial position, a final position and details about the reel or adapted to transport.

2.3. Types of reels

The plant works with to types of reels, in accordance with the two types of presses that have the plant: COMMANDER and COLORA. The main difference between both is the width of the reel.

2.4. Failures

A complete list of failures of year 2007 has been used to model the failures. The busy-time approach has been used to model them (Law 2007).

2.5. Recorded data

All the orders executed by the intermediate warehouse have been recorded along two different weeks, for each order, the following information has been recorded:

- time of the order,
- the time that the order is being processed. Is the time that the transelevator starts movement for processing the order,
- the time when the order is completed.

For each week, the initial status of the warehouse has been also recorded. This data has been used for two different tasks:

1. the arrival time of the orders, the type of the orders and its origin and destination is feed into the simulator as input data. Therefore, it is not needed to model or emulate the scheduling module,
2. this data has also been used for verification and validation. Since we feed the simulation with the real orders we should expect that the values of the simulation statistics will be very similar to the real plant statistics.

3. SIMULATION MODEL, VERIFICATION AND VALIDATION

3.1. Phase 1. Initial system

The first phase consists in the modeling and simulation of the automatic warehouse as it was before the conclusions of the project were adopted. Thus, only one transelevator is used. Moreover, the failures are not taken into account.

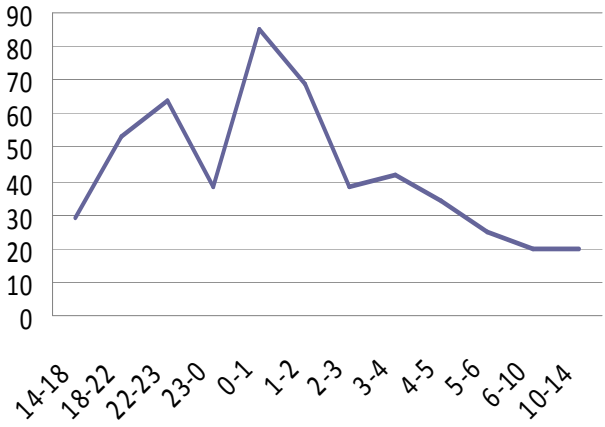

Figure 3: Transelevator expected utilization degree

Figure 3 shows the expected utilization degree of the transelevator obtained by the simulation with data of the first week. The peak hour is between 0:00 and 1:00 a.m. GMT with a utilization value between 70% and 80%. The real value is slightly higher since in phase 1 failures are not included. Moreover, since this is the average utilization for the complete week, there are days with higher utilization. This high utilization values may cause significant delay in completing the orders. This causes significant perturbations in the logistic transportation process from the plant to the final customers,

3.1.1. Validation of the initial model

The order waiting time and the movement time statistics for a week period have been used for model validation. Figure 4 and 5 show the real and the fitted (continuous line) distributions of the real and simulated data. The mean waiting time of the real data is 14 seconds higher than the simulated data since it is affected by the failures that are not included in this simulation phase.

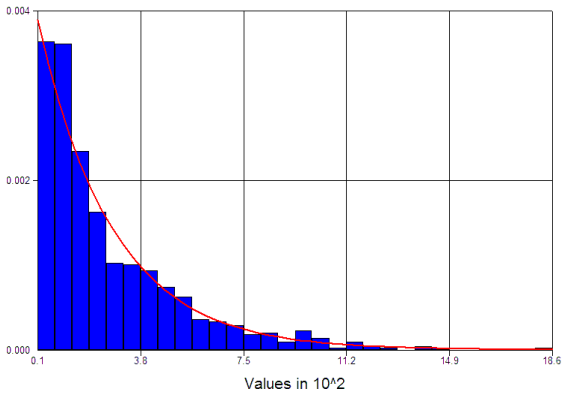

Figure 4: Waiting times (real data). Expo(267) s.

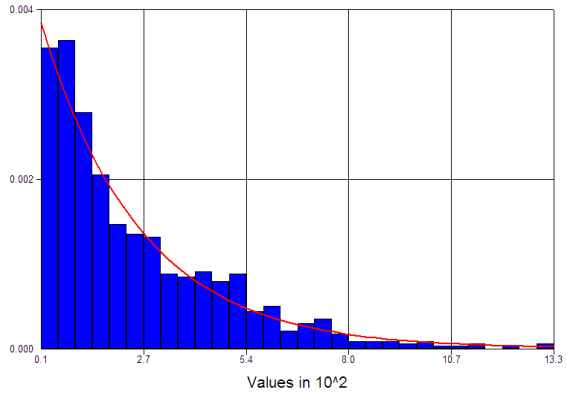

Figure 5: Waiting times (simulated data). Expo(253) s.

The real movement time sample have been filtered in order to remove a small data subset with moving values abnormally high caused by failures in the process.

The mean of the real movement time is 93 seconds and the mean of the simulation movement time is 94.5 seconds. The movement of reels within the intermediate warehouse is a deterministic process; therefore, the simulation data matches quite well the real data since the simulation model uses the same set of orders.

3.2. Phase 2. System with two transelevators

A direct previous attempt to use the second transelevator was not successful since both transelevators were competing for the same physical space. Thought the COLORA and COMMANDER presses use separate areas, the COLORA reels are stored along the whole intermediate warehouse (Figure 6), therefore, one transelevator forced the other one to retire in order to execute most of the orders. This conflict situation resulted in a decrease of performance with respect to the use of a single transelevator.

Thus, plant manager's improvement suggestions were related to changes in the scheduling system, in the intermediate warehouse management or in the workers procedures. Since most of the proposes changes were complex or expensive to implement, we suggested to try again to use both transelevators splitting the intermediate warehouse in two different zones plus and exchanging area that is used to pass reels between transelevators.

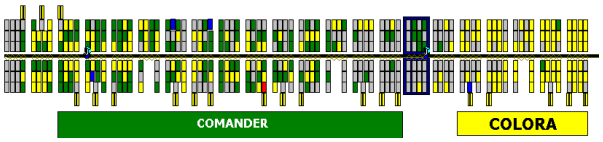

Figure 6: Intermediate Warehouse

The questions that we wanted to answer were:

- What is the position of the exchange area that best balances the load between both transelevators?
- What performance has the system with this new configuration?

The exchange area has been selected as a zone of 4 columns in the warehouse (24 storing positions). This is an exclusion area since only one transelevator can work in this area at a give time.

Four different positions of the exchange area have been tested, positions 61, 53, 46 and 38. The position 61 shown in Figure 6 is the rectangle that appears between the COLORA and COMMANDER zones. Position 1 corresponds to the first left column in the warehouse.

3.3. Phase 3. Two transelevators and failures

The objective of this phase is to analyze the impact of the failures in the system performance.

The busy-time approach has been used to model the failures. Since the only available information was the mean time between failures (MTBF) and the mean time to repair (MTTR) we have used Gamma distributions as proposed by Law (2007). The busy distribution is,

$$\alpha_B = 0.7$$
$$\beta_B = \frac{e \cdot \mu_D}{0.7(1-e)} \quad (1)$$

and the downtime distribution is,

$$\alpha_D = 1.3$$
$$\beta_D = \frac{\mu_D}{1.3} \quad (2)$$

where,

$$e = \frac{\mu_B}{\mu_B + \mu_D} \quad (3)$$

The mean of the busy time has been obtained from the MTBF taking into account that the transelevator was busy the 37,2% of the total time. The derived distributions that have been used in the model are:

- Busy uptime: Gamma(0.7, 13296) seconds
- Downtime: Gamma(1.3, 685) seconds

4. RESULTS

In this section the results of the three different phases are presented. The statistics that are used for the analysis are the lead time of the orders and the utilization of the transelevator/s.

4.1. Phase 1. Initial system

The comparison of Figure 7 and 8 shows a correlation between the utilization and the lead time. When the utilization is higher the lead time reaches the top value of 400 seconds. Remember that those are average values using the processed orders of a typical week. Moreover, the failures are not included.

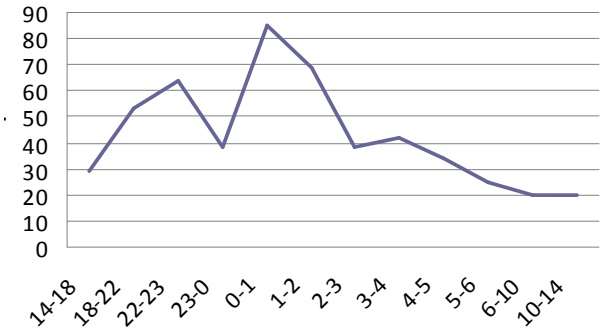

Figure 7: Transelevator utilization

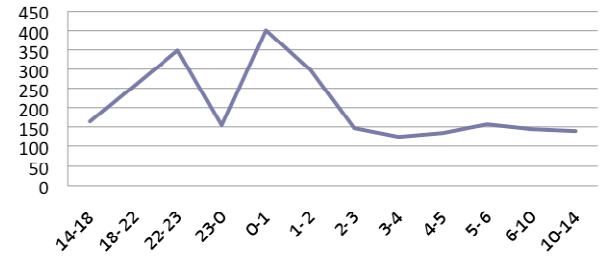

Figure 8: Order's lead time (seconds)

4.2. Phase 2. System with two transelevators

Using two transelevators the average hourly lead time remains almost constant along the busiest hours of the day. These statistics are also independent of the position of the exchanging zone. This is because most of the orders do not wait in the processing queue. Thus, the lead time is the transportation time.

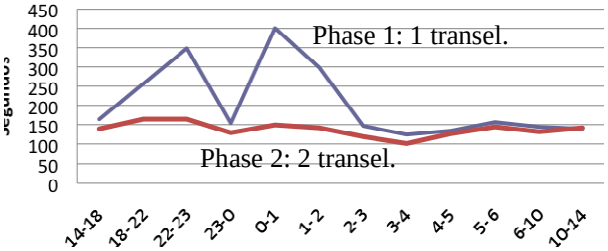

Figure 9: Order's lead time using one or two transelevators

It seams from the previous figure that the system has enough capacity for processing the orders without delay. The utilization statistics confirms this conclusion.

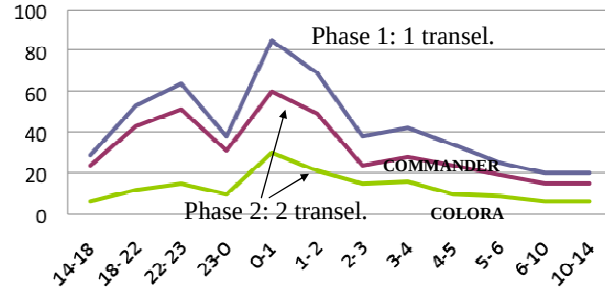

Figure 10: Transelevators utilization (pos. 61)

Figure 10 shows the utilization degree of left (COMMANDER area) and right (COLORA area) transelevators in the configuration of phase 2 against the utilization of the single working transelevator in phase 1. The maximum utilization in the phase 2 configuration is of 60%. Much lower than the 85% utilization in the single transelevator configuration. These results correspond to the exchange position number 61. In this case, the workload for the transelevators is unbalanced. Figure 11 shows the results for exchange position number 46. The workload at peach hours is balanced. The left transelevator has more loads from 14:00 to 23:00 due that this period is used to feed the intermediate warehouse from reels coming from the main warehouse through the peeling area.

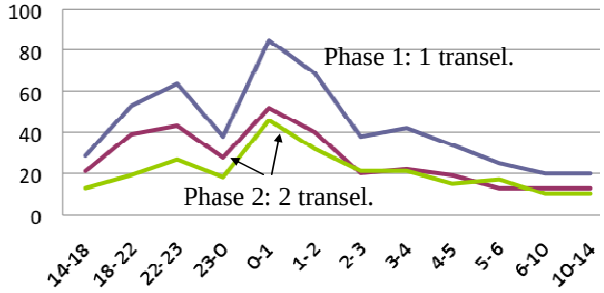

Figure 11: Transelevators utilization (pos. 46)

4.3. Phase 3. Two transelevators and failures

As is shown in Figure 12, the impact of the failures on the orders lead time is much higher with the one transelevator configuration since it has fewer margins for recovering (reducing the queue of orders) after the failure.

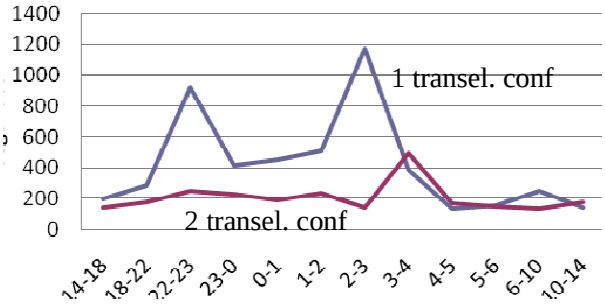

Figure 12: Order's lead time using one or two transelevators with failures in the model

To reduce the impact of the failures in the two transelevators configuration, if the repair time is expected to be high, plant operators should be able to switch to the one transelevator configuration. So that all the presses can be feed with paper reels.

5. CONCLUSIONS

This paper describes a modeling and simulation project developed for a printing plant and it shows the potential of simulation for analyzing several warehouse configurations.

The developed model shows that and increase of performance of 30% can be achieved dividing the warehouse in two zones and placing the exchange zone in the right position. The changes required in the PLC's for the control of the two transelevators are made by the plant maintenance department.

Further improvements might be attained by improving the scheduling system or the intermediate warehouse management system. However, the required changes are more complex and more expensive since the scheduling and management software has been developed by third party providers.

ACKNOWLEDGMENTS

We shall acknowledge the excellent work of the Computer Science Engineer Carlos Carmona during the development of this project.

REFERENCES

Law, A.M. 2007. *Simulation Modeling and Analysis*. McGraw-Hill, 687-694.

AUTHORS BIOGRAPHY

Born in 1958, Dr. Antoni Guasch is a research engineer focusing on modelling, simulation and optimization of dynamic systems, especially continuous and discrete-event simulation of industrial processes. He received his Ph.D. from the UPC in 1987. After a postdoctoral period at the State University of California (USA), he becomes a Professor of the UPC (www.upc.edu). He is now Professor in the department of "Ingeniería de Sistemas, Automática e Informática Industrial" in the UPC. Since 1990, Prof Guasch has lead 35 industrial projects related with modelling, simulation and optimization of nuclear, textile, transportation, car manufacturing and steel industrial processes. Prof. Guasch has also been the Scientific Co-ordinator and researcher in 7 scientific projects. He has also been involved in the organization of local and international simulation conferences. For example, he was the Conference Chairman of the European Simulation Multiconference that was held in Barcelona in 1994. Prof. Guasch has recently published a modelling and simulation book that is being used for teaching in many Spanish universities. Prof. Guasch currently research projected sponsored by SIEMENS is related to the development of power management optimization algorithms for the Barcelona new L9 subway network. L9 will be the first metro line without driver of Spain and one of the largest (45 km) and modern automatic line without driver of the World. Prof. Guasch is also contributing to the development of toopath (www.toopath.com), a web server system for the free tracking of mobile devices.

Jaume Figueras, born in 1974, had his degree in Computer Science in 1998. He research in Automatic Control and Computer Simulation an Optimization. He has designed and developed CORAL, an optimal control system for sewer networks, applied at Barcelona (Spain); PLIO, an optimal control system and planner for drinking water production and distribution, applied at Santiago de Chile (Chile) and Murcia (Spain). Nowadays He participates in different industrial projects, like the power consumption optimization of tramway lines in Barcelona with TRAM and SIEMENS and the development of tooPath (http://www.toopath.com) a free web tracking system of mobile devices. He is also the local representative of OSM (http://www.openstreetmap.org) in Catalonia and participates in different FOSS projects.

METHODS FOR ANALYSIS OF THE TIME ASPECT IN THE BEHAVIOR OF AGENT-BASED MATERIAL FLOW CONTROLS

Sergey Libert[(a)], Andreas Nettsträter[(b)], Michael ten Hompel[(a)]

[(a)]Chair for Materials Handling and Warehousing, TU Dortmund University
[(b)]Fraunhofer-Institute for Material Flow and Logistics IML, Dortmund

[(a)]sergey.libert@flw.mb.tu-dortmund.de, michael.tenhompel@flw.mb.tu-dortmund.de
[(b)]andreas.nettstraeter@iml.fraunhofer.de

ABSTRACT
The novel material flow control concepts like *Internet of Things* combine the up-to-date auto-identification methods with the modern software technologies. The expected control systems exhibit distributed scalable and flexible structures of stand-alone control entities. The price for these advantages is a non-deterministic time behavior of the local controls. The present study is devoted to the analysis of decentralized material flow controls under time constraints. The study results in a new approach to deal with deterministic and non-deterministic time factors. The paper introduces the Real-Time Logistics Model for identification, description and unification of time factors in conveyor systems and their controls. The model is integrated in and used with self-developed emulation software. The interplay of the model, the emulator and the agent-based control is shown in a real world example.

Keywords: real-time, software agents, internet of things, emulation

1. INTRODUCTION AND BACKGROUND

One of the actual trends in modern facility logistics is a modularization of the mechanical components with a simultaneous distribution of the control function (Wilke 2008; Hallenborg, Demazeau 2006; Bussmann, Jennings and Wooldridge 2004). This new approach leads to dissolving the hierarchical control structure with the material flow control (MFC) on top. The desired control system features a distributed flat structure of stand-alone control entities (Figure 1).

Various research projects accompanied by pilot implementations show the first steps toward the depicted goal (ten Hompel, Sondhof, Libert 2005; Bussmann, Schild 2001). The research program *Internet of Things* (IoT) funded by the German Federal Ministry of Education and Research focuses on decentralized material flow systems too (www.internet-of-things.net). It combines the up-to-date auto-identification methods like radio frequency identification (RFID) with the modern software technologies like agent systems (ten Hompel, et al. 2007). In collaboration with German logistic enterprises several test-bed systems based on real world scenarios are currently under construction. A large-scale simulation experiment showed the advantages of the IoT (Roidl, Follert, 2008). In these scenarios the multiple software agents represent all essential elements of the conveyor facility like powered conveyors, junctions and merges but also the transported goods.

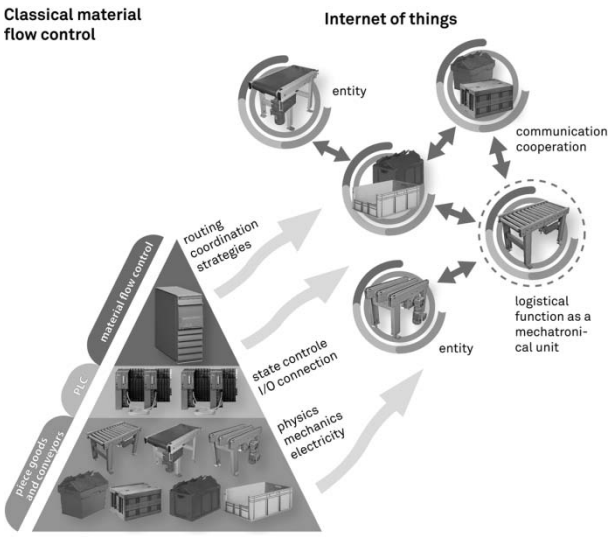

Figure 1: From hierarchical to mesh-like structure

The analysis of the agent-based control system behavior under time constraints is the object of study in the sub-project C5 “Realtime Logistics” of the Collaborative Research Centre 696 at the TU Dortmund University (www.sfb696.uni-dortmund.de). This paper presents individual results of this work.

The paper is organized as follows: We start with the topics which motivated our current research, then we specify the problem and set our research goals. In the next step we propose the system design including an abstract description model for time factors as well as the integration of this model into an emulation tool. Further, a realization and experiments are pictured on a real world example. In conclusion, we discuss the results and our further research steps.

2. MOTIVATION, PROBLEM DEFINITION AND GOALS

The agent-based control systems show a high level of scalability, extensibility and robustness. However, the price for these advantages is an autonomous and, as a result, a non-deterministic behavior of the individual agents and also of the whole system (Windt, Böse, and Philipp 2007). Particularly, the decisions close to the process must be always completed on time. Otherwise, the transport function cannot be fulfilled error-free and the control system malfunctions. Therefore, the impact of the time factor on the system control behavior must be known by developing high dynamic systems such as automated material flow systems.

Developers and operators of such systems need methods for analysis and planning of agent-based material flow controls with particular attention given to time constraints. Thus, a tool-supported method is required which allows to check the time-critical areas already in the planning phase and avoid or handle time-limits in the control realization. The expected benefit of this method is the reduction of the test and start-up time.

2.1. The real-time problem in the conveyor facility

The material flow is a real-time process. It consists of more than one parallel sub-process, exchanging the material, energy and information. Following the well-known dual principle, at least the same number of computation processes is needed to control such a system. Getting and setting the process data as well as the data computation, and even the synchronization of the computation processes, take some time. This time ($t_{control}$) must be shorter the higher the system dynamics is. Hence, the system dynamics define the maximal available time ($t_{process}$) for the control acting within one control cycle. This available time depends on some technical factors like number, performance and location of the installed sensor and actuator devices. Thus, for realizing the real-time capable control systems the following condition must be fulfilled (we purposely ignore the difference between the soft and hard real-time).

$$t_{process} \geq t_{control} \quad (1)$$

To fulfill this restriction fast programmable logic controllers (PLC) are usually used in automation practice. These controllers process all time-critical tasks within a time constant computation loop. The division of tasks into the time-critical and not time-critical and also the distribution of control tasks to the PLCs are experience-based activities. Another experience-based and very laborious activity is the adjustment of sensor positions along the conveyor belt. The best practice for solution of this problem does not exist. A reasonable workaround for this problem is to use an emulation model for the detailed analysis of the system behaviour.

2.2. Specifics of decentralized MFC

The main idea of the decentralized material flow controls is the distribution of the control function along the facility. That aims at the reduction of the decision complexity. Depending on the desired level of decentralization the distributed software components (e.g. software agents) can run on their own hardware, close to the technical process. They assume a part of the time-critical tasks and, therefore, must act under the time constraint (1).

The essential distinction of this concept from the hierarchical control systems is the information uncertainty. Indeed, the centralized systems hold all the necessary process and topology information while the autonomous agents must be communicating with each other in order to collect and synchronize the information.

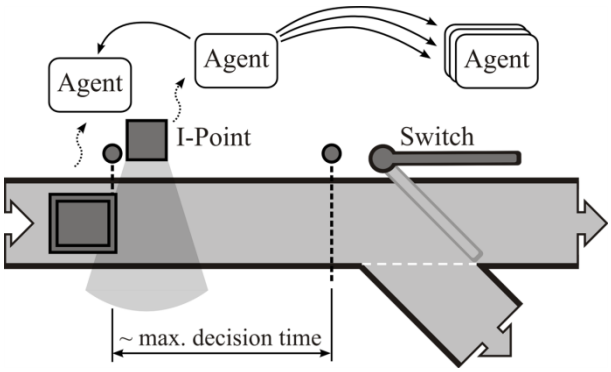

Figure 2: Example of distributed decision making under the time constraint

Figure 2 explains this problem at a simple example. A transport good (represented by an agent) approaches a switching area (represented by another agent). After the identification, the decision on the driving direction must be coordinated between the agents. For this purpose, the update of the routing information should possibly be performed as well as several other actions (e.g. writing some data on an RFID-tag).

The maximal available decision time corresponds to the journey time between the identification point and the switch trigger. It depends on the distance and the conveyor belt speed between these two points. A very short distance or too high a belt speed can result in the control malfunction. On the other hand, increasing the distance or reducing the belt speed results in the decrease of the system performance.

2.3. Methodological approach as a research goal

There are two practical methods to investigate the control behavior under time constraints: the direct measurement and the measurement by means of an emulation model. However, working with the emulation model is less labour-intensive and therefore preferred.

Unfortunately, the industrial emulator tools are developed to be used with PLCs and usually cannot be applied with agent-based systems implemented in a

high level language. Moreover, there is a method required to analyze the dependency between the control decision time and the process time. This method is necessary for both choosing the control performance, and setting and adjusting the influential technical parameters.

Most of the related works dealing with the time aspect of industrial control systems analyze the latency and performance of certain automation components and field devices like field bus systems, controller or RFID-Scanner (Tovar, Vasques 1999; Lian, Moyne, and Tilbury 1999). The developers of the real-time agent-based applications propose another approach. They consider the time constraint as a part of the agent program (Zhang 2006; De A. Urbano, Wagner, Gohner, et al. 2004). The agent must then complete all its activity when the available time is expired.

In our approach, we try to combine the advantages of both points of view. We propose a description model which unifies and consolidates the essential heterogeneous time factors. The factor values can be collected independently and put into the model. The model is integrated into emulator software which supports configuration and provides visualization of the model. Moreover, the emulator provides an open interface concept to connect an agent-based material flow control.

3. SYSTEM DESIGN

The proposed method design includes two parts. On the one hand, the conceptual model for heterogeneous time factors must be developed. This model has to combine the facility topology, the relevant process properties and the parameters of the control hard- and software. On the other hand, emulator software is needed which integrates the conceptual model and matches the process events and control commands to the time factors from the model. In the following, we describe the design of such a system step by step.

3.1. Material flow graph

The material flow graph is a directed graph which represents the system layout (see Figure 3). The graph edges model the powered conveyor lines. The vertexes display the transitions between two lines or crossing points. In this case, a conveyor switch can be modelled as a vertex with one incoming and two outgoing edges, a merge – vice versa. The vertexes without incoming edges are system entries. The vertexes without outgoing edges are exits.

Such a material flow graph can be used for calculation of valid routes through the conveyor system. The relevant physical characteristics of certain conveyor lines, like the line length, the transportation speed or the current load, shape the parameter set of the corresponding edge. Based on these parameters, the transportation time through the system but also along any single conveyor line can be defined.

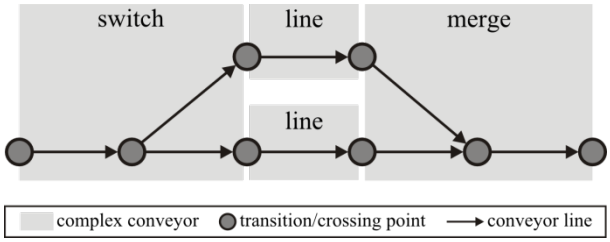

Figure 3: Example of the material flow graph

3.2. Identification and classification of time factors

We define the conveyor transportation time as a residence time of a transportation good on the corresponding conveyor line. Any operation with the transportation good including the manipulation of the material or information and with respect to this particular location must be completed within this time window. We distinguish three factors which constitute this time window (Table 1). The *lead_time* is the time needed to pass the conveyor line between two transition points. The *transition_time* is needed to change from one conveyor line to another. The third factor *waiting_time* is not really interesting if we consider the minimal transport time as a worst case for the control.

Lead_time and *transition_time* can be easily obtained from the physics and geometry data. We call these factors *time_providers* because they provide the time window available for the control actions (see (1)).

Table 1: Overview of time providers

time_provider	process / conveyor
Available (process) time	*lead_time*
	transition_time
	waiting_time

The other category of time factors includes factors depending on the operation of control devices and control logics (Table 2). These factors are the latency of sensors (e.g. RFID-Scanner), delay on communication medium, data processing time and reaction delay (e.g. actuator switching, data writing). We call these factors *time_consumers* because they account for the available process time.

Table 2: Overview of time consumers

time_consumer	control / devices	control / logic
Data collection	*read_time*	--
Communication	*medium_access_time*	*communication_time*
	transmition_time	
Data processing	*synch.: cyclic_time*	*decision_time*
	asynch.: programm_step_time	
Reaction	*write_time*	--
	action_time	

The maximal value estimation for most of the time consumers can be gained from device data sheets (e.g. sensor latency). The others can be calculated (e.g. medium access time) or be measured. These factors can be considered as static factors only depending on the device configuration and performance.

The time consumers of the control logic involve such static components but also a dynamic part. For the dynamic factors the measurement in the operation mode is the only appropriate analysis method.

3.3. The Real-Time Logistics Model

In the Real-Time Logistics Model (RTL-Model) we combine the identified *time_providers* (*tp*) and *time_consumers* (*tc*) with the material flow graph. Every conveyor line gets a corresponding *time_provider* which describes the conveyor transportation time discussed above. The worst case for the control corresponds to the minimal transportation time, i.e. the situation when the transportation good is moving through the conveyor without stopping. Then, the requirement for the real-time behavior of the responsible local control unit can be written as follows:

$$tp_i \geq \sum_{m=1}^{M} tc_{i,m} \,. \tag{2}$$

Hence, the *time_provider* defines the maximal width of the time window for all static and dynamic *time_consumers* available for the corresponding conveyor and concerning its control. The *time_consumers* are characterized by two parameters: the value and the position on the conveyor line.

The graph representation of the system topology is not quite suitable for displaying the time factors of the RTL-Model. Therefore, we propose some graphical concept for the visualization of the RTL-Model. The *time_provider* is pictured as a segment of a circle over the graph edge (conveyor line). The length of the circle arc indicates the value of the *time_provider*. We can model the varying transportation speed via just adjusting the arc length. The *time_consumers* are displayed as sectors. The sector arc length corresponds to the value of the particular *time_consumers*. Thus a dynamic factor can be visualized just by varying the sector size. Different kind of time factors can be distinguished by using different colours.

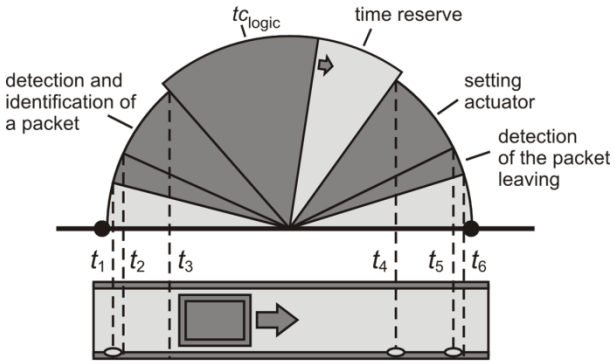

Figure 4: Dependency between time factors in the RTL-Model

In figure 4 the visualization concept of the RTL-Model is explained by a simple example. An optical sensor at the beginning of the conveyor detects a packet (t_1) and an identification device (e.g. RFID-Scanner) starts to read the data from the tag (t_2). tc_{logic} is the time needed for decision making. This time is a dynamical factor in the case of an asynchronous data processing. Similar to the previous example (Figure 2) the decision must be made before the sensor of the switching device (e.g. deflector) is triggered (t_4). The deflector is set at the time t_5 and the packet leaves the conveyor at the time t_6. The time reserves describe the still available time windows. We attach the time reserves (*tr*) to the real-time constrain (2) to get the description for the conveyor time behavior without gaps (3).

$$tp_i = \sum_{m=1}^{M} tc_{i,m} + \sum_{k=1}^{K} tr_{i,k} \tag{3}$$

The next reasonable step is the integration of the RTL-Model into an emulator environment. The aim of this integration is to realize a computer-aided visualization and analysis of time related behavior of a decentralized material flow control.

3.4. Software integration

Most of the simulation software for material flow systems, currently available on the market (e.g. Arena, eM-Plant, AutoMOD), are oriented toward the centralized control structures and strategies. Connecting a decentralized agent-based control to such simulators is a big challenge because of missing interfaces. Furthermore, the emulators are used to work directly with PLC via OLE for Process Control (OPC) and field buses. The appropriate interfaces for high-level languages like C++, C# or Java are very rare. Moreover, the RTL-Model must be deeply integrated into the emulation software to catch and analyze both the events from the emulated facility model and the commands from the agent control.

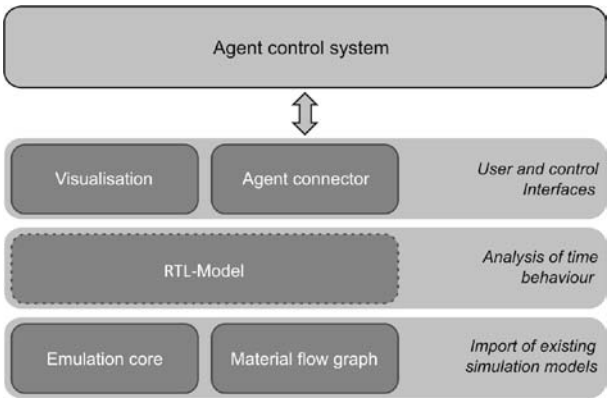

Figure 5: Overview of the emulator integration layers

To gain more flexibility for our experiments, the RTL-Model was integrated into self-developed emulator software. However, the integration into industrial emulation software (e.g. Demo3D, taraVRcontrol) is feasible as well.

Figure 5 shows the layered architecture of the emulator. The time-discrete emulation core provides the other components with the clock pulse. The system layout representation is based on the material flow graph. Different layout models can be easily imported and used within the emulator. In addition to the layout

information, the emulated facility model includes information about automation components like sensors and actuators.

The layered system architecture enables integration of user-defined components, listening to emulator events or having connection to the superior material flow control. The RTL-Model is integrated as one such layer. The RTL-Model enhances the given material flow graph representation with its own elements: sensor and actuator information. The visualization layer provides a computer animated process. It also allows for the editing and customization of the time factors in the RTL-Model. Finally, the pictured agent connector provides an interface to the agent-based material flow control.

4. EXPERIMENTAL ENVIRONMENT

In the following, the experimental set-up and the major system components are briefly pictured. Our experiment is not focused on the detailed study of the real-time behavior of the agent-based control. In fact, we use this experimental environment to show the interplay of the proposed method with a real agent-based material flow control.

4.1. Agent-based control

The control system is implemented using the JADE Framework (Java Agent DEvelopment Framework, see http://jade.tilab.com). There are three types of control agents in the system:

- The unit load agents represent the small load carriers. The synchronization between the software agents and the real boxes is based on RFID. The RFID-tags are used for both the identification and storage of transport relevant information.
- The conveyor agents represent the single sections of the conveyor facility with different transport function (e.g. switches, merges, buffer areas).
- A few service agents realize interfaces and general purpose functions like order management or an interface to a third-party system.

The JADE environment allows for an arbitrary distribution of the control agents on the run-time hardware. The self-developed event-based linking mechanism enables the connection of the agent system to the real facility the same way as to an emulated material flow system.

4.2. Real world test bed

The facility we use to test the real-time behavior of the agent-based control is a compact picking cell installation, situated at the Fraunhofer Institute for Material Flow and Logistics (IML). The system adjoins an automated small-parts warehouse at the system entry and an automated guided vehicle system at the system exit (Figure 6).

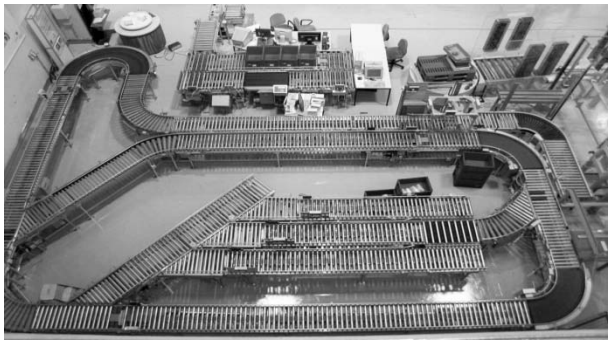

Figure 6: Bird's eye view of the test-bed

The field control is a very simple program running on several embedded PCs. This program passes through the sensor events to the corresponding conveyor agents and translates the transport commands to electrical signals for actuator and drives.

The data interchange, which is close to the process, always depends on used automation devices and is often based on proprietary communication protocols. That is why we developed a hardware abstraction layer (HAL) connecting the agent-based control to the field control. The same HAL is used to link the control agents to the emulator.

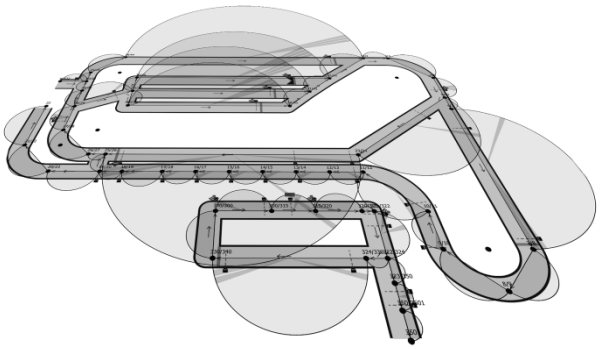

Figure 7: Emulation layout and the RTL-Model (overhead) of the test-bed

The RTL-Model of the given facility is needed for the analysis of the time consumption of implemented decentralized algorithms. Figure 7 exhibits the extension of the emulator model to the RTL-Model. Here, most of the significant hardware-depending time factors are already included. The static time factor values are gained from data sheets or measured directly. The dynamic time factors of the distributed control logic can be measured and analyzed for the particular decentralized algorithms and test scenarios.

4.3. Using large-scale industrial models

The emulator software works with the internal conveyor facility models. However, it is also able to import and use a large-scale industry simulation models from AutoMOD, one of the leading simulation software on the market. One of the realized test scenarios includes the model of a legacy baggage handling system. The emulated model consists of approximately 12.000 conveyors and includes about 100 source-destination

relations. In this experiment the emulator was able to process the material flow events and send these out through the agent connection interface. However, for the practical usage of such models for our purpose the models must feature the corresponding level of details (sensor and actuator data).

5. CONCLUSION AND FUTURE WORK

The presented method to analyze the time behavior of conveyor systems and their controls consists of two major steps. In the first step, the significant time factors should be defined by means of the RTL-Model. In the second step, the simulation-based time measurement is fulfilled and then conclusions about the control quality can be drawn. The self-developed emulator tool integrates the support for both steps. The emulation software provides an easy-to-use linking mechanism to connect the distributed control systems, e.g. agent-based controls. The suggested computer-based analysis method can be used for an early recognition of likely bottlenecks and points of failure, possibly in the planning phase. Furthermore, it can be applied for both research and industrial purposes.

The discussed results provide the first steps in our research. The subsequent work supposes a specification of the RTL-Model for typical hardware installations and scenarios. The integration of the model into industrial emulators is another possible working step. The final research goal is the development of a methodology which allows for a comprehensive analysis of system performance under time constraints and save the development costs. The aspired vision is the realization of high-performance scalable material flow systems based on low cost control components and simple control logic.

REFERENCES

Bussmann, S., Jennings, N. R. and Wooldridge, M., 2004. *Multiagent Systems for Manufacturing Control*. Springer, New York (USA).

Bussmann, S., Schild, K., 2001. An Agent-based Approach to the Control of Flexible Production Systems. *Proceedings of the 8th IEEE Int. Conf. on Emergent Technologies and Factory Automation (ETFA 2001)*, pp. 169 - 174. October 16-21, Nice (France).

De A. Urbano, P. G., Wagner, T., Gohner, P. et al., 2004. Introducing reliability and real-time features in flexible agent-oriented automation systems. *Proceedings of the 2nd IEEE International Conference on Industrial Informatics INDIN '04*. pp. 89 – 94. June 24-26, Berlin (Germany).

Follert, G., Roidl, M., 2008. Evaluation of Routing Strategies for Decentralized Self-Organisation in Large-Scale Conveyor Systems. *Progress in Material Handling Research: 2008*. In: Kimberly E. et al. ed. The Material Handling Institute of America, Charlotte (NC, USA).

Hallenborg, K., Demazeau, Y., 2006. Dynamical Control in Large-Scale Material Handling Systems through Agent Technology. *Proceedings of the IEEE/WIC/ACM international conference on Intelligent Agent Technology*. pp. 637-645. IEEE Computer Society, Washington (DC, USA).

Lian, F.-L., Moyne, J. and Tilbury, D., 1999. Performance Evaluation of Control Networks: Ethernet, ControlNet, and DeviceNet. *IEEE Control Systems Magazine*, 21 (1), pp. 66-83.

Ten Hompel, M. et al., 2007. *Internet der Dinge: www.internet-der-dinge.de*. In: Bullinger, H.-J., ten Hompel, M. ed. Springer, Berlin (Germany).

Ten Hompel, M., Sondhof, U. and Libert, S., 2005. Distributed control nodes for material flow system controls on the example of unit load conveyor and sorter facilities. In: C. Grote, R. Ester, ed. *Proceedings of the Embedded World 2005 Conference*, pp. 998-1007. February 22-24, Nürnberg (Germany).

Tovar, E., Vasques, F., 1999. Analysis of the worst-case real token rotation time in PROFIBUS networks. *Proceedings of the Fieldbus Conference (FeT'99)*, pp. 359-366. September 23-24, Magdeburg (Germany).

Wilke, M., 2008. Control Concept for Autonomous Changeable Material Flow Systems. *Logistics Journal*.

Windt, K., Böse, F. and Philipp, T., 2007. Autonomy in Production Logistics - Identification, Characterisation and Application. *International Journal of Robotics and CIM*, 24(4), 572-578.

Zhang, L., 2006. Development Method for Multi-Agent Real-Time Systems. *International Journal of Information Technology*, 12(6).

AUTHORS BIOGRAPHY

Sergey Libert studied Electrical Engineering at the Siberian Airspace Academy of Krasnoyarsk (Russia). He was awarded his second engineer degree at the Ruhr-University of Bochum in 2003. Since 2003, he works as scientific assistant at the department of Material Handling and Warehousing of the TU Dortmund University.

Andreas Nettsträter studied Computer Science, with minor Mechanical Engineering at the University of Dortmund. He was awarded his German University diploma in February 2007. Since 2007, he works at the Fraunhofer Institute for Material Flow and Logistics (IML) in Dortmund.

Michael ten Hompel was awarded his engineer degree in 1985 in Electrical Engineering at the RWTH Aachen and his conferral of a doctorate in 1991 at the University of Witten/Herdecke. Now he is the Managing Director of the Fraunhofer-Institute of Material Flow and Logistics (IML) in Dortmund and holder of the chair of Materials Handling and Warehousing at the TU Dortmund University.

THE IMPACT OF STRATEGY ON MATERIAL HANDLING SYSTEM PERFORMANCE: CASE STUDIES IN AN ORDER PICKING SYSTEM

Gaby Neumann

Institute of Logistics and Material Handling Systems, Otto-von-Guericke University of Magdeburg, Germany

gaby.neumann@ovgu.de

ABSTRACT

Strategies are parameters of material handling processes as they specify how these processes have to be run. To better understand and demonstrate the impact the decision for a certain strategy has on the performance of the material handling system, a number of simulation case studies have been extracted from projects with industry. The aim of the case studies was to evaluate alternative strategies with regard to their performance in the same process design and to derive more general findings for estimating the impact from changing strategy. The paper presents the outcomes of different case studies within an order picking system addressing traditional and today's questions of allocating workers to order picking jobs and adjusting system load to order structure.

Keywords: control strategies, order picking system, worker allocation, system load

1. INTRODUCTION

Any material handling system needs to be designed in a way enabling it to efficiently and effectively run material handling processes. Whether or not this can be achieved depends on both, system components (i.e. handling, management and control techniques) selected and interlinked as well as sequence and logic of transformation activities in terms of material handling operations (Merkuryev et al. 2009). Appropriateness of a system's design and functioning is then measured and assessed with regard to performance and quality of resulting processes, i.e. if the right goods are provided in the right quantity and quality at the right place in time creating minimal costs and ecological impact. Here, control strategies describing how system components are used and processes are run form essential influences as they set the scene and define the rules in decision-making processes at operational level.

Having a closer look at strategies used in and relevant for operating a material handling system we can first of all distinguish between local and global strategies. Local strategies help in deciding about a particular component's behavior in a certain situation only taking into account information on the particular unit of goods to be handled and related to the component's own state-of-operation or of the one of directly neighboring components. Therefore local strategies are used to regulate the sequence of goods' access to the component it the incoming side of a component, e.g. by applying priorities related to goods or sourcing components or using the first-come first-serve principle. On the outgoing side of the component local strategies are needed to determine the goods' distribution amongst different following components, e.g. by applying priorities of destinations or components or by comparing components with regard to current contents or overall utilization.

In contrast to this, global strategies always look at a wider part of the system or even the current situation of the entire system when deciding about how to influence the process in a particular situation. Consequently, those decisions are of more complex nature aiming to efficiently route goods units through the system (e.g. following the shortest distance or the shortest time or the least utilization in the moment of decision) or to allocate resources (i.e. storage places, conveyors or vehicles, personnel) to tasks and orders avoiding idle or waiting times and ensuring continuous goods flows.

Not matter if we talk about local or global strategies usually there are alternative options for choosing the best strategy in a certain setting. Here, the question is if we really need to find the best strategy even if this requires larger efforts or if good or even just suitable ones are equally good in terms of system and process performance and could be selected with far less effort. In order to support this discussion and determine which strategy works best within a certain scenario and what impact can be achieved just by changing strategy, simulation experiments have been carried out that were based upon a valid model of the system and defined levels of system load. The following sections of this paper describe the material handling system used as example, the simulation model representing it, and the setup of as well as results and conclusions from case studies investigating alternative strategies within the same system with system structure, components and parameters remaining unchanged.

2. THE ORDER PICKING SYSTEM

Order picking systems are central components of any distribution centre. Performance requirements to be met

by them directly depend on the sector, distribution strategy and the customer service level to be reached. In the case of a pharmaceutical company incoming customer orders are usually to be handled and delivered the same day.

The order picking system consists of 28 pick places (P1…P28) serving corresponding picking areas in a run-through rack (see Figure 1). They are linked by roller conveyors forming two loops for moving boxes. Each box is related to a specific pick order listing articles and quantities to be picked as well as the articles' location. With this also a list of relevant destinations (pick places) to be visited by the box is defined. After having entered the system at the box entry (B), the box is automatically moved by the conveyor system passing by the pick places of the loop.

Every time the box arrives at a destination from its list and the respective pick place still has some empty space, it is pushed sideways out of the loop and waits for the picking units to be collected by a worker and put into the box. Then the box (with the current content) is pushed back onto the loop and conveyed to the next pick places. If a destination cannot be visited because of currently missing empty space, the box continues to move on the loop either visiting the next destination on the list or circulating until the destination it had been rejected before can be visited.

At transfer points (T1…T4) boxes can change into the other loop if pick places from there also belong to the list of destinations. When a box has visited all destinations from its list, it leaves the order picking system on the shortest possible way via a check point (C1 or C2). Here, the content of the box is checked for completeness and correctness before the box is forwarded to the packaging area.

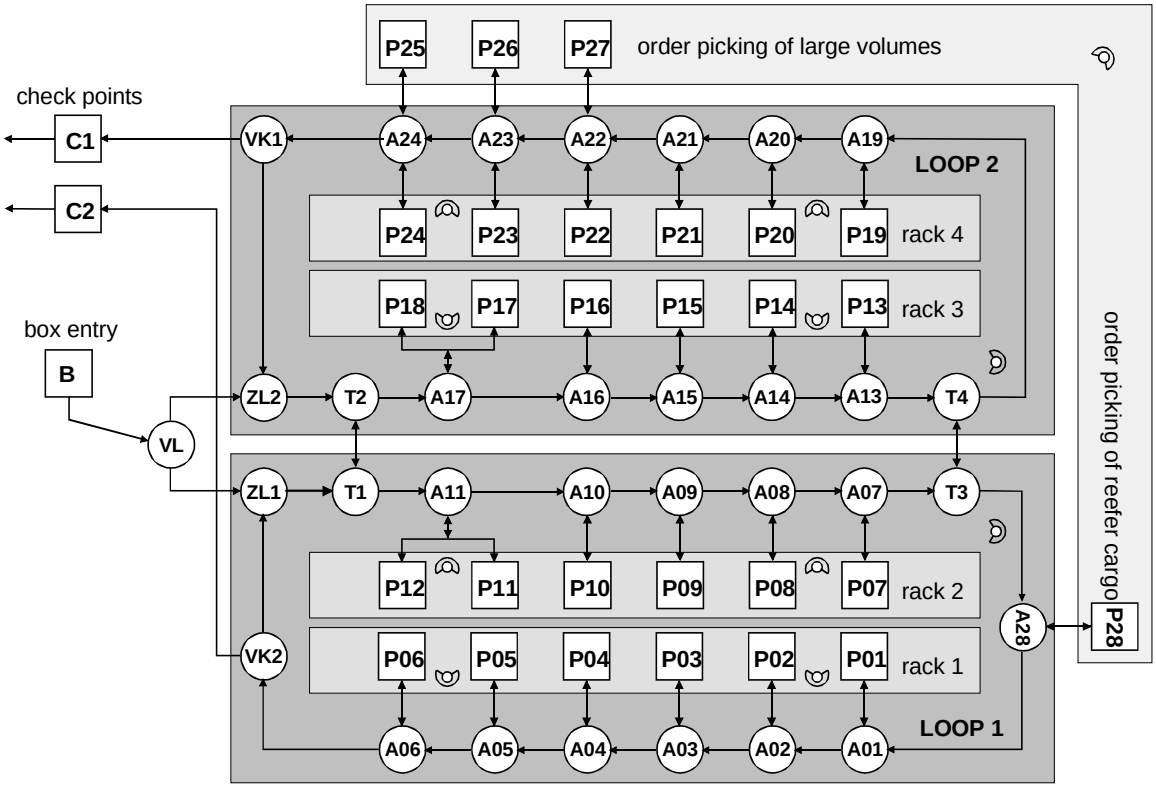

Figure 1: Flow of Material in an Order Picking System

3. SPECIFICATION OF CASE STUDIES

As already explained the order picking system is a semi-automatic solution. Whereas the boxes move automatically, the picking is done manually. Here, each picking worker usually operates more then one pick place. In order to improve the efficiency and effectiveness of the order picking system with regard to the number of workers and working hours needed to perform the daily work load a simulation project was launched. The project specifically aimed at proposing the best allocation of a minimum number of workers to the pick places (case 1).

In the course of the project another challenge appeared: In order to avoid deadlocks from system overload the total number of boxes in the system and the number of boxes already waiting at a certain pick place or being on the move to it have been limited. Originally both numbers had been pre-defined and were handled as fixed parameters independent of the current situation in the system. As this led to very unbalanced performance situations especially in the close-down of the system, further simulation experiments aimed to find appropriate strategies for dynamically adjusting system load to the order structure of the remaining work load (case 2).

This approach for a more dynamic control of the order picking system finally raised questions concerning the effects of different levels of process pre-

definition. In particular, chances from technological advancements like RFID should be investigated. For this, a case study needs to be designed in which boxes are carrying different amounts of information (ranging from no information to full information) about the order attached to them, the path through the system, the already picked items and their correctness in terms of picking quality (case 3). This case study which has not been run so far will be the next step in our investigations and is not presented in this paper.

All cases use the same exemplary system and simulation model. They also have in common technical parameters of the order picking system and structure and volume of the system's daily work load. The only changes are related to strategies, i.e. certain process parameters. With this, simulation output could be analyzed with regard to changes in the system's performance (Law 2007) which was measured by the time needed in total for completely handling all pick orders per day.

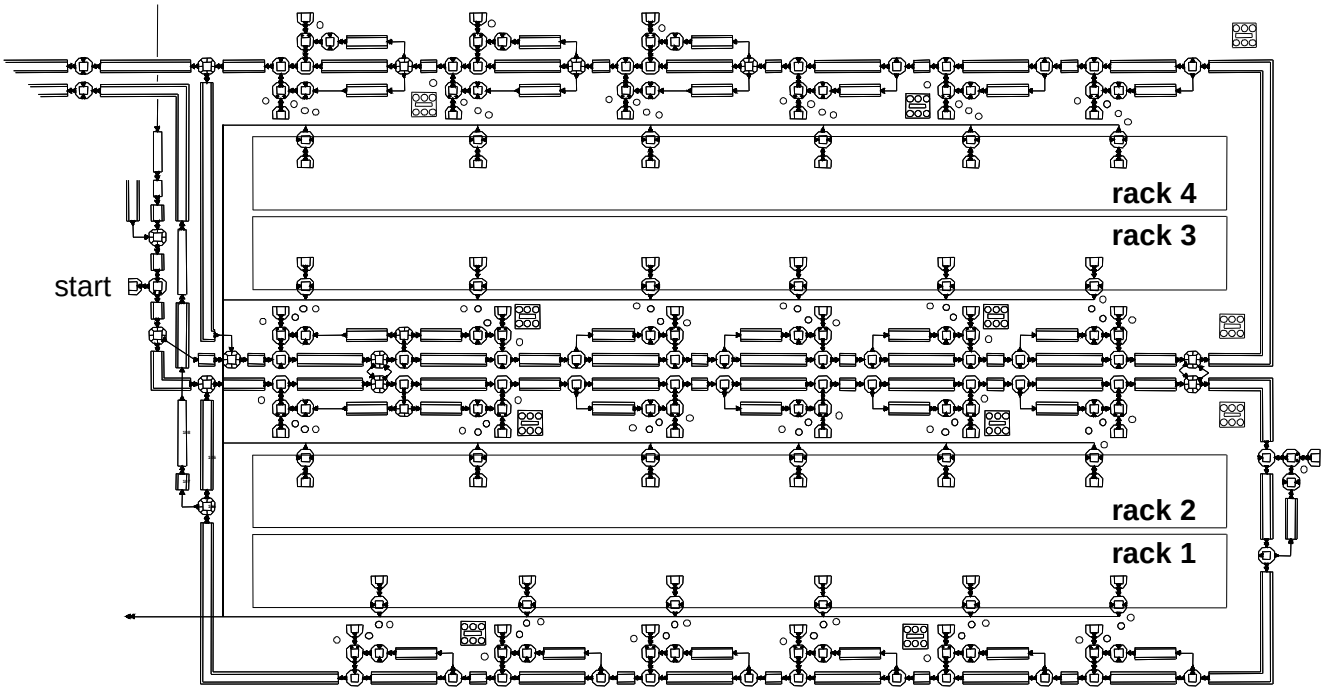

Figure 2: Simulation Model of the Order Picking System

4. SIMULATION MODEL

Model design for representing the order picking system and all physical processes run by it is a standard problem; although the large number of even similar elements produces some efforts when using a component-based simulation package like DOSIMIS-3 (see Figure 2, Page and Kreutzer 2005). Roller conveyors and further material handling components are directly represented by respective simulation building blocks. The worker model as another standard component of the simulation package represents a certain number of picking workers with their working areas (i.e. allocated pick places), specific activities (e.g. picking, box handling, moving between different pick places) and time model (i.e. shifts, breaks). The major challenge in model building consists in creating a respective work load from the huge number of different articles closely matching the real-world scenario with its diverse customer orders.

To be able to change work load within the simulation experiments, a random generation of the work load was required instead of using real customer orders. To derive an appropriate algorithm actual customer orders were analyzed and visualized in tables with each row describing the pick places belonging to the destination list of one particular box. When reducing the level of detail in the tables' presentation nothing specific can be read anymore, but instead typical destination patterns appear (see Figure 3):

- Point structures of pick orders (see Figure 3a) result from destination lists containing a few pick places (less than 6 out of the 24 in the loops) only. They belong to small customer orders not consisting of more than 7 boxes in total.
- Line structures of pick orders (see Figure 3b) occur if a customer order contains few boxes only, but they visit a large number of pick places (up to 22 out of the 24 in the loops).
- Staircase structures of pick orders (see Figures 3c and 3d) can be found with large customer orders consisting of many boxes, because here each of these boxes has to visit just two or three pick places which are usually situated even next to each other. The more boxes belong to one customer order the larger the resulting staircase is.

The work load is generated in two steps. First, type and volume (in boxes) of the customer order are randomly defined and then for each box an individual destination list is randomly created. Since the daily work load is given by the total number of boxes to be handled by the order picking system (throughput), the generation process stops when having created the required number of destination lists. Each simulation run starts with an empty order picking system and ends when the order picking system is empty again and no picking orders are waiting for being executed anymore. The total time between these two situations (or in the other way round the number of picking orders, i.e. boxes, that can be handled within the available working time of 9 hours including the breaks of 45 minutes in total) is the main performance measure used in the case studies.

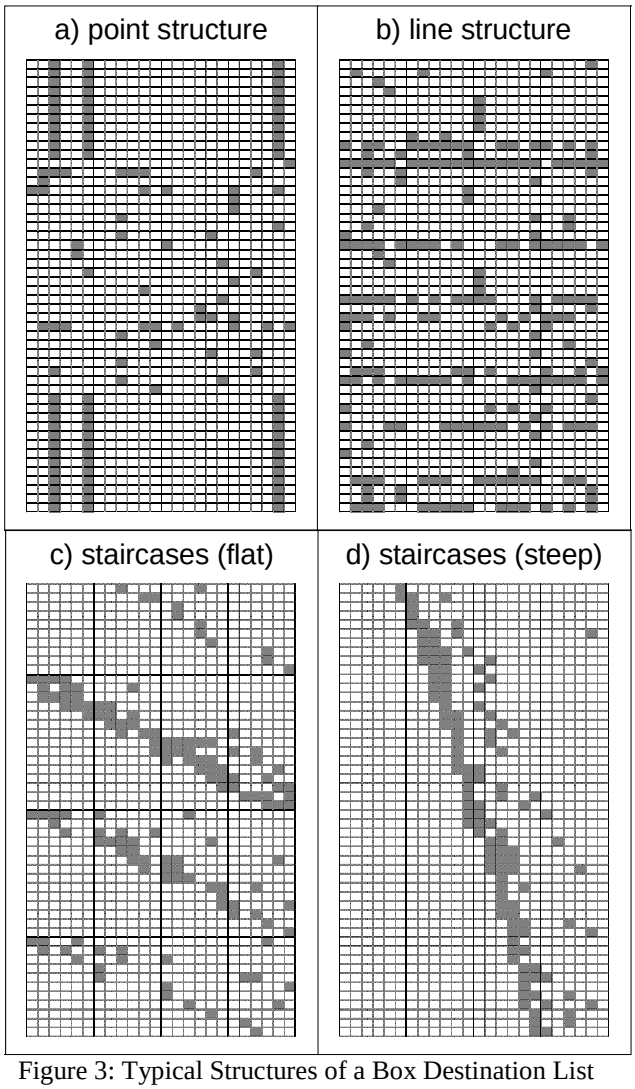

Figure 3: Typical Structures of a Box Destination List

5. CASE STUDY TO ALLOCATE WORKERS

The first case study aims to investigate the impact of resource allocation strategy on system's performance. More precisely the study deals with identifying the total number of workers needed to smoothly run the order picking process within the available working time. To determine the best allocation of a minimum number of workers to the pick places simulation experiments focused on finding the daily work load limit (number of boxes) for scenarios with varying numbers of workers.

Workers pick the items per box and therefore need to be allocated either to a single pick place or to a certain group of pick places next to each other alongside a particular rack. In the latter case, when a worker operates more then one pick place it eventually might happen that the sequence and individual work load of picking orders create a higher work load with particular workers. To help in coping with those temporary overload situations additional, flexible workers might be allocated to the pick places of one loop supporting fixed allocated workers as required. In the current situation which formed the basis for model validation and experimentation 11 picking workers are used: 2 workers per rack operating 3 pick places each, 1 flexible worker per loop supporting the others as required and 1 worker operating specialized pick places outside the loops (see Figure 1). Alternative worker allocation scenarios reduced the number of picking workers to a minimum by removing all flexible workers or systematically increased the number of picking workers up to its maximum when we have one worker fixed allocated to each of the pick places (see Table 1).

Table 1: Worker Allocation Scenarios

	V0	V1	V2	V3	V4	V5
Fixed workers per rack	2	2	3	3	3	6
Flexible workers per loop	1	0	0	1	2	0
Workers at outer pick places	1	1	1	1	1	4
Total number of workers	11	9	13	15	17	28

V = variation; V0 = current scenario

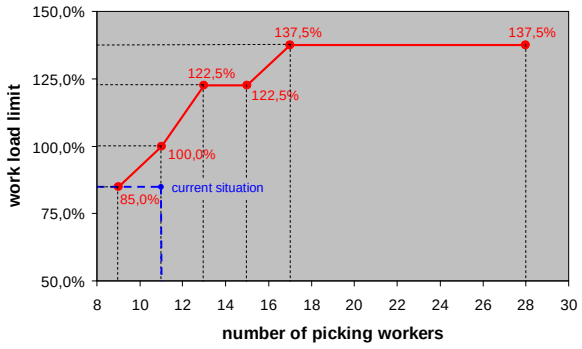

Figure 4: Simulation Results for Maximum Work Load per Day

Comparing the simulation results (see Figure 4) it can clearly be stated that the number of workers allocated to the order picking system impacts the performance limit: For the current situation of 11 picking workers (V0) the work load could be increased by about 15 % in comparison with the current load to be

managed. Without the flexible workers (i.e. 9 picking workers in total – V1) the current work load would even form the load limit and no increase at all would be possible. Increasing the number of picking workers by allocating either more fixed workers to the racks (and with this reducing the number of pick places to be operated by each worker) and/or more flexible workers to the loops (V2/3/4) will enable the order picking system to cope with an even higher work load (up to 37.5 % increase compared to the current worker allocation and work load if 17 workers are appointed). With this also the absolute work load limit for the system has been reached and any further increase of the number of staff will not show any performance improvement. Even if each worker would have to operate just one pick place resulting in a total of 28 picking workers allocated to the system (V5), the number of picking orders and boxes to be handled by them (and the conveying system) cannot be increased.

Based upon these findings the following recommendations concerning the impact of the implemented worker allocation strategy can be derived:

- The work load limit strongly depends on the number of workers allocated to the order picking system. Nevertheless, more allocated workers do not adequately increase system performance.
- Allocation of 9 picking workers in total allows the order picking system to cope with the current work load. In this case there is no need for flexible workers. The current work load also represents the work load limit for this scenario.
- Based upon the current allocation of 11 workers the work load could be increased by about 15 %.
- The absolute work load limit allows handling about 50 % more boxes than in the current situation. For this a minimum of 17 picking workers needs to be allocated to the system. More workers do not lead to any further increase of the performance, but might eventually provide the system with some additional flexibility with regard to peak loads, for example.

6. CASE STUDY TO ADJUST SYSTEM LOAD

The system load represents this amount of pick orders that are put into the system at the same time. Background of this parameter is the challenge to prevent the order picking system from overflow in terms of both the capacity of the conveyor system and the picking and buffering capacity of the pick places as this could end up in a system deadlock.

System load is regulated by the maximum number of boxes in the system at a time in total and at or on the way towards a certain pick place. In the current situation (and in all experiments of the previous case study) these parameters were set to 150 boxes in total and 10 boxes for each pick place. Because of the latter a certain pick order was only accepted for being operated when the place-specific load limit has not been reached with any of the pick places on the box's destination list. As soon as at least one pick place is currently not able to accept more orders the entire pick order is held back until this temporary bottleneck has disappeared. Due to the fact that in the meantime other orders might have been put into operation the entire destination list of this pick order has to be checked at this time again.

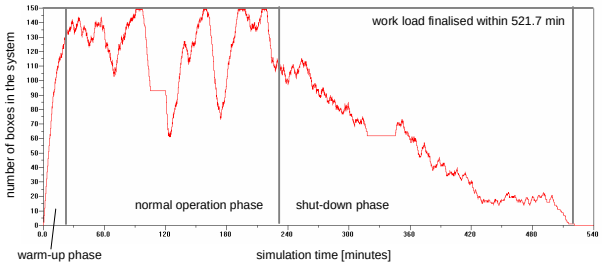

Figure 5: Typical Work Load Distribution per Day (V0)

When analyzing results of the previous case study a bit more in detail in order to get the full picture of work load distribution over the day, three phases of different behaviors could be identified (see Figure 5):

- Phase 1: system warm-up from empty state to about 150 boxes to be handled at the same time
- Phase 2: system operation with varying, but relatively high numbers of boxes (frequently reaching the limit of 150) to be handled
- Phase 3: system shut-down from normal operation with about 150 boxes in the system to empty state (all pick orders have been finalized)

Whereas warm-up is pretty short (e.g. for the current scenario V0 less than 30 min), shut-down lasts more than half of the total system operation time (approx. 300 min). Obviously, performance capacity of the system is partially used only and not regulated by the maximum number of boxes in the system anymore (normal operation phase), but limited by the individual work load of certain pick places instead. Reason for this is the varying structure of pick orders the system has to cope with more or less in the sequence of appearance without resource-focused scheduling opportunities.

Table 2: Dynamic Work Load Adjustment

Active system load	Place-specific load limit
100…150 boxes	max. 10 boxes per pick place
75…100 boxes	max. 15 boxes per pick place
50…75 boxes	max. 20 boxes per pick place
0…50 boxes	max. 30 boxes per pick place

To enable the system to better react on those order structures (in terms composition of their destination lists), the previously static system load limit was replaced by a dynamic strategy for adjusting system

load to system performance. For this, flexible load limits per pick place were introduced (see Table 2) after 6, 5 or 4 hours of simulation.

As results show (see Figure 6) introduction of dynamic work load adjustment significantly reduces the total time needed to fulfill all pick orders. As expected duration of the shut-down phase can be cut down from almost 300 min down to around 270 min (about 10%) with the savings being the larger the earlier strategy changes from static to dynamic (see Figures 6a and 6b). Quite interestingly, there seems to be a 'natural' border for this, as switching of strategy after 4 hours of simulation already ends up in a longer working time again (see Figure 6c). Here, release of more boxes into the system towards pick places with a higher individual work load mainly leads to more traffic in the system without having a positive impact on the required working time. This outcome does not change when slightly modifying system load levels at which work load is adjusted (see Figure 6d).

Based upon this some recommendations on the impact of work load adjustment strategy can be derived:

- Work load limits are necessary to avoid inefficient traffic and even deadlock situations in the system.
- Unbalanced work load leads to longer total working times and reduces system performance. This is indicated by a quite long shut-down phase.
- Dynamic adjustment of place-specific load limits during shut-down reduces the required working time and allows handling more pick orders. Here, crucial parameters are the timing of strategy changes and the active system load levels at which place-specific load limits are increased.
- With the current scenario V0 (see Table 1) best results were achieved when changing strategy after 5 hours and using thresholds according to Table 2 (total working time less than 500 min).

7. CONCLUSIONS

The case studies in this paper aimed to investigate the impact of strategy on material handling system performance. Based upon the example of a complex order picking system simulation results show to what extent system performance can be increased by allocating an appropriate, but not maximum number of workers to the pick places (case 1) or by using a dynamic strategy for adjusting work load for pick places (case 2). Another study under preparation will particularly deal with the impact of information and routing strategy (case 3).

To generalize findings achieved so far it clearly turned out that strategy is an important parameter in process configuration. Its purposeful use can help in improving a material handling system's performance without introducing another cost-intensive technology or spending large efforts on restructuring the system. Both planners and operators of material handling systems should be aware of this control lever and consider its use in many situations first.

REFERENCES

Law, A., 2007. *Simulation Modeling and Analysis*. 4th ed. McGraw-Hill Professional.

Merkuryev, Y.; Merkuryeva, G.; Piera, M.A. and A Guasch, eds. 2009. *Simulation-Based Case Studies in Logistics: Education and Applied Research*. London: Springer.

Page, B. and W. Kreutzer, eds. 2005. *The Java Simulation Handbook – Simulating Discrete Event Systems in UML and Java*. Aachen: Shaker.

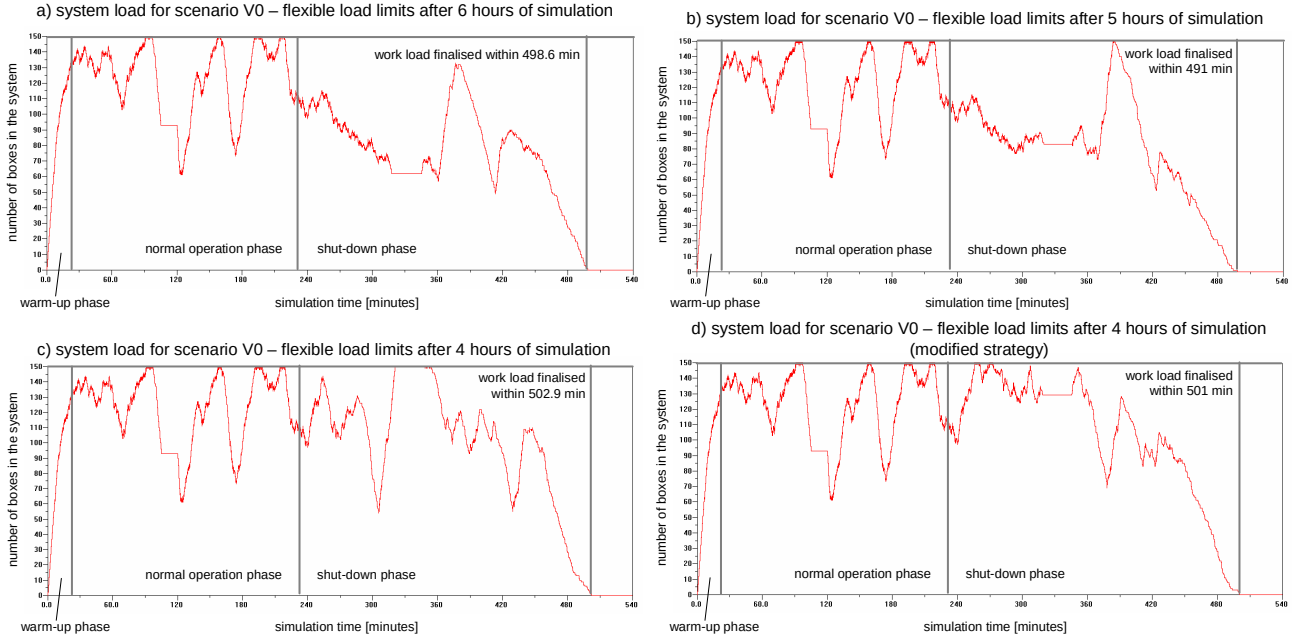

Figure 6: Typical work load distribution per day for flexible place-specific load limits (V0)

AUTHORS BIOGRAPHY

Gaby Neumann received a Diploma in Materials Handling Technology from the Otto-von-Guericke-University of Technology in Magdeburg and a PhD in Logistics from the University of Magdeburg. Since 2003 she has been Junior Professor in Logistics Knowledge Management there. She also has been part-time consultant in logistics simulation since 1991. Her current activities and research interests are mainly linked to fields like problem solving and knowledge management in logistics, logistics simulation and planning, and technology-based logistics learning, didactics of teaching logistics as well as logistics competence profiling and assessment. She is author/co-author of three books, one educational multimedia module on warehousing and a series of e-learning modules in logistics as well as of 50 book chapters and journal publications and about 80 papers and presentations at national and international conferences. She co-ordinates the European logistics educators network for providing new technologies for logistics education inside the European Logistics Association (ELA-LogNet) and has been or is being involved in a couple of respective projects. Her e-mail address is Gaby.Neumann@ovgu.de

A STOCHASTIC MODEL FOR VEHICULAR RESUSPENSION EXPOSURE NEAR UNPAVED ROADS

Wellens A.[(a)], Jazcilevich A.[(b)], Siebe C.[(c)], Rosas I.[(d)] , Riojas H.[(e)]

[(a)]Facultad de Ingeniería, UNAM-MEXICO
[(b), (d)] Centro de Ciencias de la Atmósfera, UNAM-MEXICO
[(c)]Instituto de Geología, UNAM-MEXICO
[(e)]Instituto Nacional de Salud Pública, MEXICO

[(a)]wann@unam.mx, [(b)]jazcilev@unam.mx, [(c)]siebe@unam.mx, [(d)] iarp@atmosfera.unam.mx, [(e)] hriojas@correo.insp.mx,

ABSTRACT

A stochastic model based on empirical probability distribution functions is constructed to estimate the exposure to vehicular resuspension emissions of $PM_{2.5}$. The model was developed for a fixed typical velocity and vehicular weight having in mind a specific location and environmental problem. Nevertheless, the proposed methodology can be expanded to consider situations where different speeds and vehicular weights are involved. The stochastic character of the model reflects the turbulent nature of the resuspension phenomenon. The main advantage of this model is that exposure can be statistically estimated for different traffic scenarios, heights and individual activity.

Keywords: public health, manganese, stochastic modelling

1. INTRODUCTION

In an ecosystem study in the community of Chiconcoac-Tolago in the mining district of Molango, Mexico, epidemiologist confirmed that airborne particles of manganese (Mn) affect the health of the regional child population. For each microgram of Mn found above the mean concentration in the control group in hair samples of the exposed children, IQ scores descended 1.5 points and learning level capabilities descended 1 percent.

Three possible sources can explain the presence of airborne Mn in the Chiconcoac-Tolago community:

1. smoke stack emission and dispersion of $PM_{2.5}$ and associated Mn in the smoke stack of the Mn nodulation oven operated by a mining company in the region,
2. wind erosion of the nude unpaved road surfaces, and
3. particle resuspension of unpaved roads produced by local traffic

Smokestack and wind erosion effects were estimated with the Gaussian dispersion model AERMOD, developed by the US Environmental Protection Agency.

However, determination of pollutant exposure due to vehicular resuspension is seldom considered in air quality or atmospheric pollution studies. This may be because of the local nature of resuspension and because in most urban centers where important traffic activity takes place the roads are paved, drastically reducing particle emissions. Nevertheless, as some studies suggest, urban dwellers are exposed to this phenomenon, and in many suburban or remote villages where mining or industrial activities take place, particle resuspension accounts for a very important part of individual particle exposure.

Particle exposure or dust can have direct health consequences, especially when the soil is contaminated; to estimate the effect of vehicular resuspension on individuals exposure, a stochastic model was developed, as described in this paper.

2. METHODS

2.1. Field Experiments using PDR´s

Vehicular resuspension of $PM_{2.5}$ particles from unpaved roads was measured on a site with highly manganese contaminated soil. Since the site is surrounded by mountains, wind is calm in the mornings and midday; measured wind speeds indicate average velocities around zero and maximum wind speeds less than 1.5 m/s and 2.4 m/s respectively in the morning and afternoon. In practice, these results eliminate effects of wind erosion and thus isolate the resuspension measurements.

Wind speed, direction and relative humidity (RH) were measured using a Davis Vantage 2 station. Two measurements campaigns, one for dry-cold and one for dry-hot season, were performed in November 2006 and May 2007.

Real time concentrations of $PM_{2.5}$ were measured using two Personal Data Ram (PDR) with Mie technology connected to SKC pumps at a setting of 2 l/min. These instruments were placed at a height of 1.2 m and at a distance from the road side of respectively 1 and 2.5 m, see Figure 1.

During the dry-cold campaign most measurements were taken below 85% of RH; values were checked to minimize possible measurement concentration excursions. During the dry-hot season RH was below 85% during all the experiments.

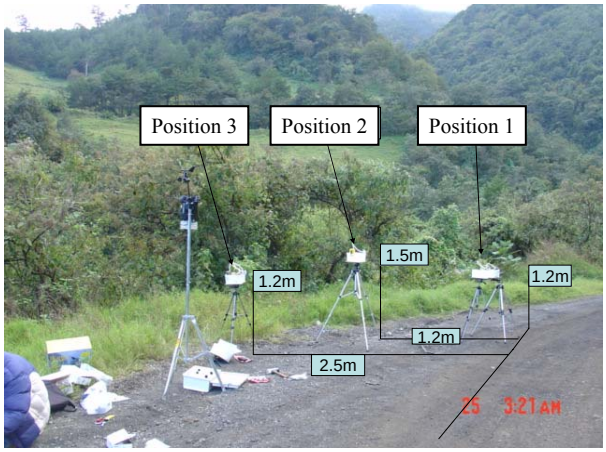

Figure 1: Instrument Localization in the Measurement Campaigns

Horizontal attenuation due to surface interference and turbulent diffusion was estimated by placing Petri dishes on the surface at distances of 1, 2, 4 and 6 meters from the road. Vertical attenuation was obtained placing a BSNE at the road side.

A 35 ton truck, used for transporting material in the region, traveling at a speed of 14 km/h passed about 30 times in front of the instruments to obtain $PM_{2.5}$ exposure data.

Manganese concentration in $PM_{2.5}$ was determined at 15.8%.

2.2. Empirical Probability Distribution Functions

The measurements were used to build empirical histograms of total exposure to $PM_{2.5}$ due to the truck passes. A total of 5 empirical histograms were obtained: in the dry-hot season morning and afternoon measurements were taken, both at 1 m and 2.5 m distances from the road. In the dry-cold season, measurements were taken in the afternoon, at a 1 m distance only. Due to horizontal attenuation, it was not possible to detect any concentration at further distances.

(a) Paved Road

(b) Unpaved Road

Figure 2: Van Circulating at 40 km/h at the Monitoring Site, (a) on a Paved Road, (b) on an Unpaved Road

An additional experiment was performed on a paved road in the affected communities. Due to the incline, a lighter vehicle was used (2.5 tons) but at higher velocities (40 km/h). A PDR connected with a SKC pump set at 2 l/min was placed on the side of the road, see Figure 2.

2.3. Goodness of Fit Tests

The empirical histograms obtained for each of the 5 experiments were fitted to Weibull and lognormal distributions. Goodness of fit was tested with Kolgomorov-Smirnov and Anderson-Darling test statistics.

The *Kolgomorov-Smirnov statistic* quantifies a distance between the empirical distribution function of the sample, $F_n(x)$, and the cumulative distribution function of the reference distribution, $F(x)$ (Wilks 2006). It is defined as:

$$D_{\max}(x) = \max \left| F_n(x) - F(x) \right| \quad (1)$$

The null distribution of this statistic is calculated under the null hypothesis that the sample is drawn from the reference distribution (Weibull and lognormal in our case). If $D_{\max}(x)$ is over a critical value, the null hypothesis is rejected; in the opposite case, the null hypothesis is accepted, and the sample can be considered to come from the proposed distribution.

The critical values for the Kolmogorov-Smirnov test can be found in Table 1 (Law and Kelton 2000) for the used sample sizes.

Table 1: Critical Values for the Kolmogorov-Smirnov Goodness of Fit Test

	Significance (%)		
n	10	5	1
12	0.338	0.375	0.450
13	0.325	0.361	0.433
14	0.314	0.349	0.418
15	0.304	0.338	0.404

If D exceeds the critical values specified in the previous table, the null hypothesis will be rejected for the indicated significance level.

The *Anderson-Darling test* makes use of the fact that, when given a hypothesized underlying distribution and assuming the data does arise from this distribution, the data can be transformed to a uniform distribution. The transformed sample data can be then tested for uniformity with a distance test. Specifically, in its application as a test to prove that the normal distribution adequately describes a set of data, it is one of the most powerful statistics for detecting departures from normality (Stephens 1974). Opposite to the Kolgomorov-Smirnov tests, the Anderson Darling test uses different critical values or test-statistics to test goodness of fit to different theoretical distributions.

To assess if a data set $\{Y_1 < Y_2 < \ldots < Y_n\}$ comes from a distribution with cumulative distribution function $F(x)$, the Anderson-Darling test uses the test statistic A:

$$A^2 = -n - \sum_{k=1}^{n} \frac{2k-1}{n}\left[\ln F\left(Y_k\right) + \ln F\left(Y_{n+1-k}\right)\right] \qquad (2)$$

The test statistic can than be compared against the critical values appropriate for the theoretical distribution to be tested.

For the Weibull distribution, $F(Y_k)$ is de cumulative Weibull distribution at the measured value Y_k. The approximate adjustment for sample size is:

$$A^{2*} = \left(1 + \frac{0.2}{n}\right) A^2 \qquad (3)$$

For the lognormal distribution, $F(Y_k)$ corresponds to the cumulative standardized normal distribution of values Y_k, standardized from:

$$Y_k = \frac{\ln(X_k) - \overline{\ln(X_k)}}{S_{\ln(X_k)}} \qquad (4)$$

In this case, the approximate adjustment for sample size is calculated using:

$$A^{2*} = \left(1 + \frac{4}{n} - \frac{25}{n^2}\right) A^2 \qquad (5)$$

The corresponding critical values are found in Table 2 (Stephens 1974, Law and Kelton 2000).

Table 2: Critical Values for the Anderson-Darling Goodness-of-fit Test

Significance (%)	Weibull	Lognormal
1	1.038	1.092
2.5	0.877	0.918
5	0.757	0.787
10	0.637	0.656

If A^{*2} exceeds the critical values specified in the previous table, then the null hypothesis is rejected for the indicated significance level.

2.4. Model Description

The stochastic model was built by generating in a first step uniformly distributed pseudo-random numbers using the Van der Corput scheme (Knuth 1969). In a second step, the inverse transformation method was used to convert the uniform random numbers to random numbers drawn from the fitted distributions for the dry-hot and dry-cold conditions.

The stochastic model allowed estimating exposure of individuals as a function of height, number of truck passes and distance to the road for each season.

3. RESULTS

3.1. Comparison between Dry-Cold and Dry-Hot Seasons

Figure 3 shows $PM_{2.5}$ background measurements during the dry-cold and dry-hot season, obtained with a PDR in the monitoring site at midday. It can be observed that $PM_{2.5}$ concentrations are almost three times as high in the dry-hot season, due to the higher soil temperatures.

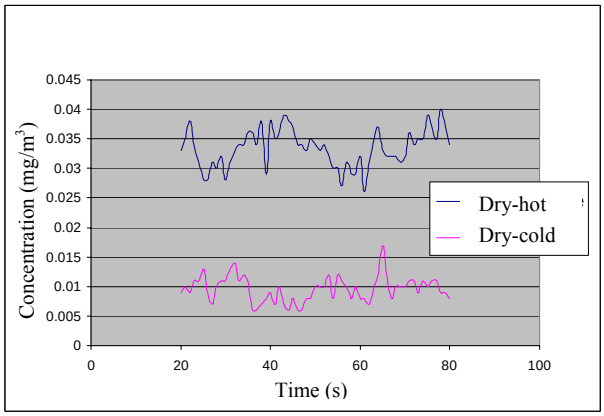

Figure 3. $PM_{2.5}$ Background Concentrations in mg/m^3, Dry-Hot and Dry-Cold Seasons

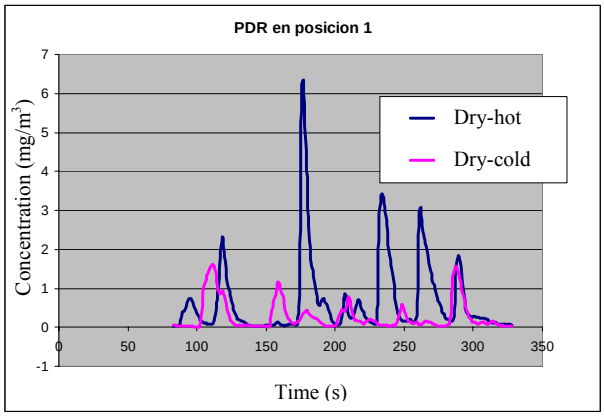

Figure 4. $PM_{2.5}$ Concentrations in mg/m^3, as Measured by PDR for Different Events

Figure 4 shows the PDR measured $PM_{2.5}$ concentration during an event where the truck is passing several times. Also in this case, measured concentrations are significantly higher in the dry-hot season.

The measurement campaigns established that, although the phenomenon is highly local (influence zone less than 10 m off the road) and of short duration (around 40 s), exposure to $PM_{2.5}$ concentration is high (around 1 to 4 mg/m^3 in 40 s).

As an example, figure 5 shows the empirical histogram of the observed $PM_{2.5}$ concentrations at a 1 m distance from the road, for the afternoon measurements in the dry-hot season.

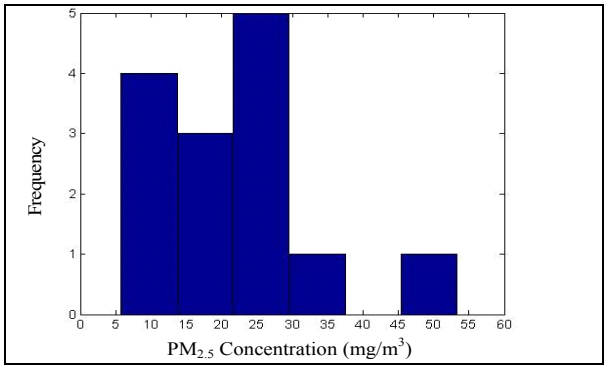

Figure 5: Experimental Histogram of $PM_{2.5}$ Concentration. Dry-Hot Season, Position 1, Afternoon

3.2. Results of the Goodness of Fit Tests

All four experiments corresponding to the dry-hot season could be adjusted to both lognormal and Weibull distributions, both with Kolgomorov-Smirnov and Anderson-Darling tests.

However, the dry-cold experiment could not be adjusted to lognormal nor Weibull distributions, according to the Anderson-Darling test. The Kolgomorov-Smirnov test for the dry-cold experiment indicates a rejection for the Weibull distribution at the 10 and 5% significance level. The lognormal distribution was accepted by the Kolgomorov-Smirnov test at all significance levels.

Table 3 indicates the test-values for Kolgomorov-Smirnov and Anderson-Darling tests, for each of the five resuspension experiments. Sample sizes were between 12 and 15. Letters "M" and "A" indicate respectively if the experiment was performed in the morning or in the afternoon; numbers 1 and 2 indicate positioning of the measuring equipment at a distance of respectively 1 and 2.5 m.

Table 3: Test Values for the 5 Experiments, for Kolmogorov-Smirnov and Anderson-Darling Tests

		Weibull		Lognormal	
Season	Experiment	Dmax	A^{2*}	Dmax	A^{2*}
Dry-hot	M1, n = 14	0.170	0.615	0.127	0.301
	A1, n = 14	0.129	0.342	0.116	0.506
	M2, n = 14	0.118	0.311	0.166	0.694
	A2, n = 12	0.155	0.244	0.198	0.501
Dry-cold	M1, n = 15	0.339	2.105	0.145	1.714

As data can be fitted more appropriately to the lognormal than to the Weibull distribution, the former will be used to model the resuspension phenomenon.

Table 4 indicates the parameters of the adjusted lognormal distribution, for each of the 5 experiments.

Table 4: Parameters of the Adjusted Lognormal Distributions

		Parameters (mg/m^3)	
Season	Experiment	μ_x	σ_x
Dry-hot	M1, n = 14	22.81	9.94
	A1, n = 14	20.41	12.75
	M2, n = 14	12.26	6.67
	A2, n = 12	14.28	8.78
Dry-cold	M1, n = 15	5.79	6.63

It can be noted from the adjusted distributions for the dry-hot season that morning and afternoon resuspension have a similar behavior: at a distance of 1 m off the road, the mean $PM_{2.5}$ concentration due to resuspension is around 21.5 mg/m^3, and its dispersion is about half the value of the mean. In position 2 (2.5 m of the road), a very similar behavior can be noted, with mean concentrations around 13 mg/m^3, corresponding to a drop of 40% with respect to the near-road concentration. These lower concentration values are due to the attenuation phenomenon mentioned in section 2.1: at higher distances from the road, turbulence and temperature are not significant anymore.

On the other hand, in the dry-cold season, very low concentrations are observed, but with a dispersion value in the same order of magnitude as the mean. At higher distances off the road, no $PM_{2.5}$ concentrations could be measured.

3.3. Stochastic Model

The stochastic model can be used to estimate the average daily potential exposure to $PM_{2.5}$ and/or manganese due to vehicular resuspension in dry-cold and dry-hot seasons. Individual height was set to 160 cm for and adult and 100 cm for a child. A distance of 1 m off the road and 2, 4 and 8 vehicles passes a day were considered.

A lognormal random number was extracted from the fitted probability distributions described in table 5, indicating potential exposure of one individual. This was repeated 60 times, to be able to obtain average concentrations near the unpaved road. Table 1 presents the results of average potential exposure in µg/m^3 of manganese in one day.

Table 5. - Exposure of Manganese in $PM_{2.5}$ in $\mu g/m^3$ per day. In Parenthesis the Number of Passing Trucks

Height (cm)	Dry-cold season	Dry-hot season
100	0.074 (8) 0.026 (4) 0.007 (2)	0.570 (8) 0.250 (4) 0.109 (2)
160	0.039 (8) 0.014 (4) 0.004 (2)	0.303 (8) 0.133 (4) 0.058 (2)

Table 5 shows that the average potential exposure varies sensitively with the height of the individual and the season: impact increases with lower individual heights and higher temperatures. Effects are more important in child populations as in adult populations, above all in the dry-hot season.

4. CONCLUSIONS

Two field campaigns provided empirical data for vehicular resuspension emissions of $PM_{2.5}$. Kolmogorov-Smirnov and Anderson-Darling tests were performed, showing that it is possible to fit the experimental data to the lognormal distribution. Random numbers were drawn from the fitted distributions to estimate the exposure to $PM_{2.5}$ and/or manganese. The model was developed for a fixed typical velocity and vehicular weight, but for different traffic scenarios, heights and meteorological conditions.

REFERENCES

Knuth D., 1969. *The Art of Computer Programming: Seminumerical Algorithms*, Vol. 2, Addison Wesley.

Stephens M. A., 1974. EDF Statistics for Goodness of Fit and Some Comparisons, *Journal of the American Statistical Association*, Vol. 69, p. 730-737.

Law A. M., Kelton, W. D., 2000. *Simulation Modeling and Analysis*, 3rd edition, McGraw Hill, Boston.

Wilks D. S., 2006. *Statistical Methods in the atmospheric Sciences*, 2nd Edition, Academic Press.

BIOGRAPHICAL NOTES

Ann Wellens is a chemical engineer with postgraduate studies in Industrial Administration (KUL, Belgium) and a master degree in Environmental Engineering (UNAM, Mexico). At the moment she is a full-time lecturer in the Systems Department of the Industrial and Mechanical Engineering Division of the National University of Mexico (UNAM). She has been working in air pollution issues for the last 15 years, dictating courses, collaborating in research projects and participating in conferences related with mathematical modeling of air pollution dispersion and statistics.

Aron Jazcilevich obtained his bachelor degree in Computational Engineering (UNAM, México), his master degrees in Electrical Engineering and Science and a Ph. D. in Applied Mathematics (State University of New York). He is a full researcher at the Center of Atmospheric Sciences of the National University of Mexico (UNAM) and has been the leading researcher in different financed projects related with air pollution modeling, urban climate modelling and vehicular emissions measurements. During the last 5 years, he has published around 15 papers in international journals and has been a lecturer in courses related with air pollution modeling, mathematical physics and numerical methods.

Christina Siebe obtained her bachelor, master and Ph. D. degrees in Agricultural Sciences at the Hogenheim University in Stuttgart, Germany. Since 1994, she is a full researcher at the Institute of Geology of the National University of Mexico (UNAM). She has participated in numerous research projects related with edafology, soil characterization and soil pollution and dictated courses on the same topics.

Irma Rosas Pérez has a bachelor degree, master studies and Ph. D. in Biological Sciences (UNAM, México). She is a full researcher at the Center of Atmospheric Sciences of the National University of Mexico (UNAM); her research activities include characterization of atmospheric bioparticles and biogenic compounds, health effects of aeroparticles and genomic identification of airborne microorganisms.

Horacio Riojas is a medical doctor (UNAM, México) with a master degree and Ph. D. in Environmental Health Sciences (National Public Health School, México). At the moment, he is researcher at the National Institute for Public Health (INSP, México) and director of the Environmental Health Department. He has been participating in research projects related with epidemiology, environmental surveillance and health effects of antropogenic particulate matter.

ANALYSIS AND SIMULATION OF POLITICAL PARTIES WITH DIFFERENT STATISTICAL DISTRIBUTIONS

Alejandro Suárez Buenrostro[(a)], Miguel Angel Martínez Cruz[(b)], Idalia Flores de la Mota[(c)]

[(a)(c)]Postgraduate Studies Division, Engineering Faculty, Universidad Nacional Autónoma de México, Mexico
[(b)]Superior School of Mechanical and Electrical Engineering, Instituto Politécnico Nacional, Mexico

[(a)]alejandro_suarezb@yahoo.com, [(b)]mamartinezc@ipn.mx, [(c)]idalia@unam.mx

ABSTRACT
Statistical results of federal deputies' elections by political party were analyzed, observing a normal distribution for the major parties and a heavy tails distribution for the minor parties and/or with disappearing tendencies. The heavy tails distribution that particularly predominated was the log-logistic type. With the alpha shape parameter of the log-logistic distribution minor to two, we found that the small parties tend to disappear. Probabilistic simulations were realized in a model with two parties and with different distributions (normal and log-logistic) and we found that, indeed, the log-logistic distribution party with its alpha parameter minor to two tends to win a few times in an election. Therefore, this produces a loss of supporters over time.

Keywords: simulation, political party, normal distribution, log-logistic distribution

1. INTRODUCTION

Simple models about the cooperative behavior in the social systems were already known by economists and sociologists for many years. What is really surprising is that many of these classic models in sociology were simply reformulated in terms of existing models in statistical mechanics, such as the "Minority Game"(Weidlich 2000), the Axelrod Model of formation of cultural dominions or political coalitions (Schofield and Parks 2000), the economic models based on the Nash local equilibrium concept (Adams and Merrill 1999), among others (Bergstrom 2001). A cooperative behavior in the democratic societies concerns to the elections, which are convincing democratic processes, where the same type of interaction between the voters and external influences (political publicity, campaigns, etc) exists. Even so, the voters do not own as much freedom, since the individual preferences depend on the election of the social networks where the voter is immersed. This is natural in the human being. According to this, a quantitative characterization of the electoral network is made through a study of the vote's distributions. These vote's distributions are obtained from different electoral processes and the simulations of the electoral preferences, which are indispensables steps towards a better understanding and prediction of the underlying electoral dynamics (Martínez and Balankin 2003).

From the scientific point of view of complex system, the result of an electoral process can be considered like an answer of an open system, with many elements that interact with each other, governed by an intern complex dynamic (although unknown). The modeling of the Mexican electoral system belongs to the dynamics of the complex social systems, which has been developed in order to improve the quality in the participation of the democratic processes.

This paper is focused on the statistical behavior of some Mexican political parties and their simulation. Particularly, the results of the elections for Federal Deputies were analyzed in the 1991, 1994, 1997, 2000 and 2003 electoral years.

In Mexico, the Federal Electoral Institute (IFE by its abbreviation in Spanish) is an autonomous public entity in charge of organize the federal elections, that is, the President's, deputies' and senators' elections. Due to this, the IFE is the commissioned public entity to provide electoral statistical information.

1.1. Computational Resources

Netlogo's computer programming language was used for the simulation. This program is focused on the simulation of phenomena in which many individuals appear interacting (e.g. habitual phenomena that occur in nature, society or many fields in mathematics). It is useful to model complex systems that evolve over time. Also, it is used to model thousands of individuals (people, bacteria, insects, organizations, nodes of a graph, etc) that interact with each other and with the environment. It allows to explore the connection between local interactions at an individual level and the macroscopic patterns that emerge of that interactions.

2. STATISTICAL ANALYSIS OF SOME POLITICAL PARTIES

The analysis was made on the elections of Mexico's federal deputies considering the three main parties, during the 1991-2003 electoral years of the 300 districts of the Mexican republic. Statistical data was obtained from the Federal Electoral Institute's data bases (IFE by its abbreviation in Spanish) for the information processing. Then it was exported to Excel and with the

@Risk 4.5 software aid, the votes percentage distribution of each political party of the 300 electoral districts was analyzed. Each political party shows different properties.

Table 1 shows the votes adjustment parameters to the normal and log-logistic distribution, equation 1 and 2 respectively (Law and Kelton 2000), for the National Action Party (PAN by its abbreviation in Spanish).

$$f(x) = \frac{1}{\sigma\sqrt{2\pi}} e^{-\frac{1}{2}(\frac{x-\mu}{\sigma})^2} \qquad (1)$$

Where μ is the mean and σ^2 is the variance.

$$f(x) = \frac{\alpha t^{\alpha-1}}{\beta(1+t^{\alpha})^2}; \quad \text{with} \quad t = \frac{x-\gamma}{\beta} \qquad (2)$$

Where γ is the location parameter, β is the scale parameter and α the shape parameter. Table1 shows a normal distribution with growing mean, which indicates a tendency to gain supporters over the years. And a log-logistic distribution with an increasing α parameter, which means a good electoral presence in almost all of the federal entities. Figure 1 shows the normal distribution graphic for PAN in 2003.

Table 1: Mean and Standard Deviation of the Normal and Log-Logistic Distributions for Votes Percentage of PAN

PAN	Normal		Log-Logistic	
	μ	σ	α	β
1991	0.1685	0.1090	0.1617	0.0631
1994	0.2499	0.0932	0.2515	0.0534
1997	0.2636	0.1241	Extremal value	
2000	0.4218	0.1051	0.4296	0.0606
2003	0.3017	0.1172	0.3089	0.0606

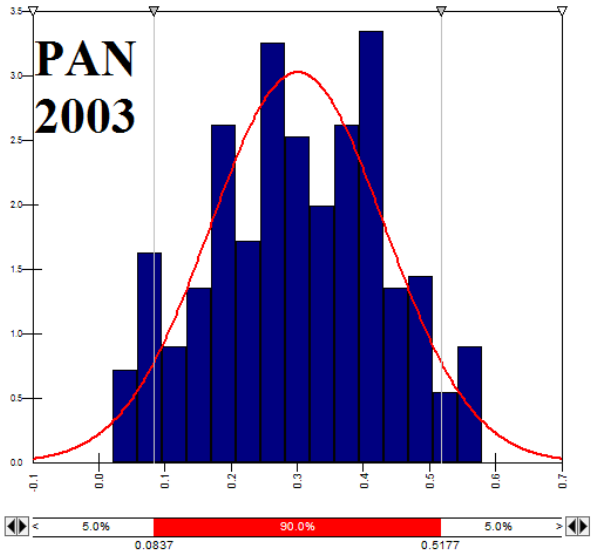

Figure 1: Votes Distribution graphic for PAN in 2003 in Mexico's Electoral Districts

In table 2 is observed that, in opposition to PAN, the Institutional Revolutionary Party (PRI by its abbreviation in Spanish) presents a normal mean which tends to decrease, as the same as the log-logistic α parameter. This means that the party tends to lose supporters over time. Nevertheless, it continues remaining strong like a national party, since the distribution of its supporters continues being normal with an acceptable average.

Table 2: Mean and Standard Deviation of the Normal and Log-Logistic distributions for Votes Percentage of PRI

PRI	Normal		Log-Logistic	
	μ	σ	α	β
1991	0.6210	0.1265	0.6197	0.0762
1994	0.5071	0.0913	0.5030	0.0537
1997	0.4087	0.1085	0.4075	0.0630
2000	0.3910	0.1071	0.3892	0.0633
2003	0.3793	0.1410	0.3903	0.0800

In figure 2 is shown graphically the votes distribution of PRI in 1997. As the same as PAN, data adjust to a normal distribution and with less probability it adjust to a heavy tails distribution.

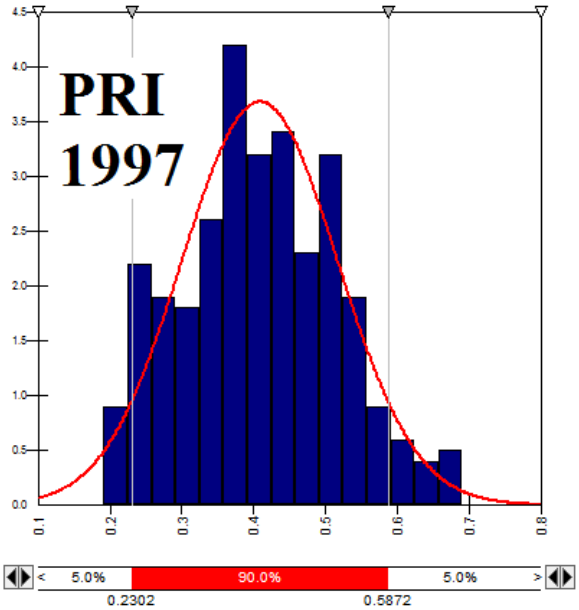

Figure 2: Votes Distribution graphic for PRI in 1997 in Mexico's Electoral Districts

Table 3 shows the votes adjustment parameters to the log-logistic and Pearson distributions of the Democratic Revolution Party (PRD by its abbreviation in Spanish).Unlike PAN and PRI, PRD preserves a log-logistic distribution given by equation 2; it means that there is no a voters' presence in many federal entities and that suggest that the party tends to disappear over the years.

Table 3: Parameters of the Log-Logistic and Pearson Distributions for Votes Percentage of PRD

PRD	Normal		Log-Logistic	
	μ	σ	α	β
1991	0.0850	0.0812	2.1676	0.0579
1994	0.1712	0.1065	3.1489	0.1513
1997	0.2549	0.1452	3.9509	0.2669
2000	0.1984	0.1202	2.1468	0.1069
2003	0.1944	0.1538	1.7615	0.1051

Figure 3 shows graphically votes distribution of PRD in 2003.

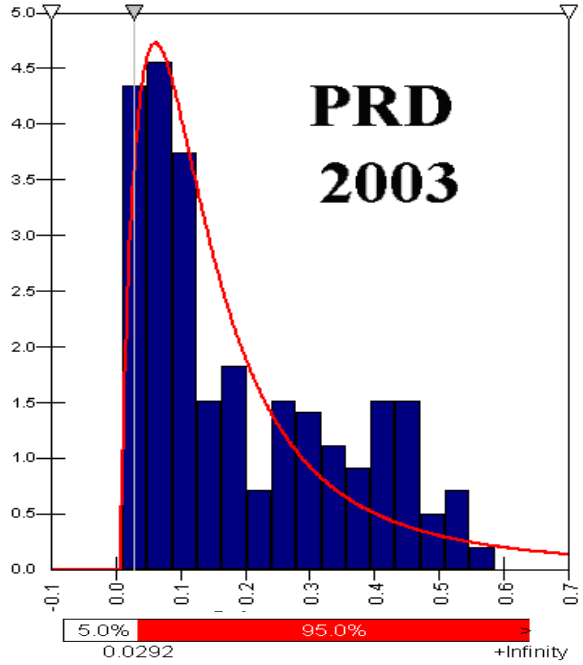

Figure 3: Votes Distribution Graphic of PRD in 2003 in the Electoral Districts of the Country.

2.1. Dynamics of the Political Parties in Mexico

Historically there is a tendency of political parties to disappear when the α parameter of the votes distribution of each party in the different federal entities, adjusted to the log-logistic distribution, is minor to 2. It is necessary to emphasize that is not a forceful fact to affirm the disappearance of some political party in later years. Nevertheless, tendencies and a greater possibility are observed to such event.

Analyzing the information of PAN and PRI, data shows to adjust with little probability to a heavy tails distribution behavior. It means that these parties do not show voters' absence in almost all of the federal entities. Contrary, the coalition with PT, PAS, Convergencia and PSN was not favorable for PRD in 2000 since its α parameter indicated a decreasing tendency. PRD gave signs of the disappearance of its sympathizers on the federal entities (Guzmán 2004), placing below the $\alpha = 2$ limit in 2003. But, the Working Party (PT by its abbreviation in Spanish) was favored by the coalition since in 2003 had an alpha parameter equal to 2.75 which indicates, unlike last years, a growth of its sympathizers, being outlined for later years as a national party. The Mexican Ecologist Party (PVEM by its abbreviation in Spanish) shows an α growth from 1991 to 2003 working in coalition with PAN in 2000 and with PRI in 2003, improving its electoral presence. The situation of minor parties such as PSN, PAS, MP, PLM was not favorable.

Table 4: Shape Parameter α of the Log-Logistic Distribution. Without Log-Logistic Distribution, didn't participate, participated in coalition

Parties	1991	1994	1997	2000	2003
PAN	2.55		8.15		
PRI					
PRD	2.16	3.14	3.95	**2.28**	1.76
PT	1.52	2.19	1.88		2.75
PVEM	1.81	2.28	1.94		**3.65**
Converge					1.37
PSN					1.62
PAS					1.70
MP					2.77
PLM					1.70
Fuerza C					3.43
PCD				2.26	
PARM	2.21	2.11		3.00	
DSPPN				2.06	
PC			2.24		
PPS	2.55	3.59	2.28		
PDM	1.81		1.73		
PFCRN	2.38	2.38			
UNO_PDM		**1.84**			
PRT	1.27				

3. RESULTS OF THE DYNAMIC PROCESS

Based on previous data, it was developed a computational program in Netlogo 4.0.2 (figure 4) that

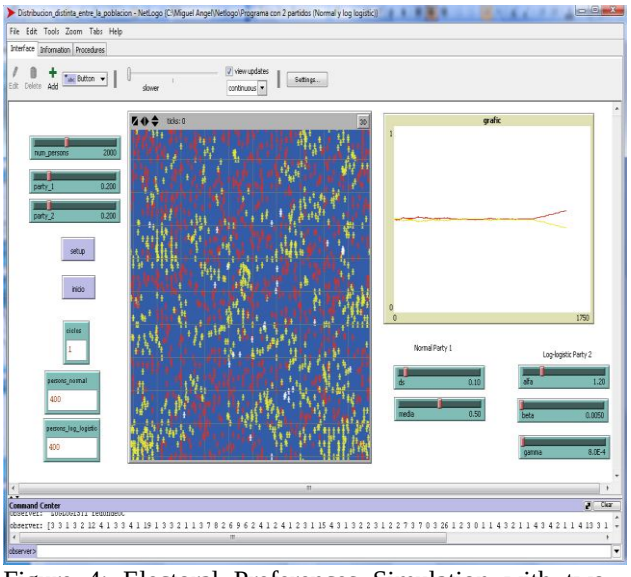

Figure 4: Electoral Preferences Simulation with two Parties with Netlogo 4.0.2 Software

simulates the statistical behavior of two parties with the same amount of initial voters but with different distribution of its voters over the region. Two types of distributions were considered: the normal and the log-logistic distribution.

Table 5 shows the results of 30 simulations of the people with preference towards some party with normal distribution and another with log-logistic distribution. A value of the α parameter variable from 1.0 to 2.0, a normal distribution with constant parameters, as well as the number of people constant (4,000) and the same number of initial people of both parties (400) with a defined preference towards a party.

Table 5: Results of 30 Simulations of People with Preference towards some Party

Alfa value	Number of times that won a party with	
	Normal distribution	Log-logistic distribution
1	30	0
1.1	28	2
1.2	27	3
1.3	29	1
1.4	26	4
1.5	26	4
1.6	24	6
1.7	22	8
1.8	25	5
1.9	20	10
2	20	10
3	18	12
4	16	14

Table 5 suggests that with an α<1.9 value, parties tend to lose and consequently to diminish their supporters over the years.

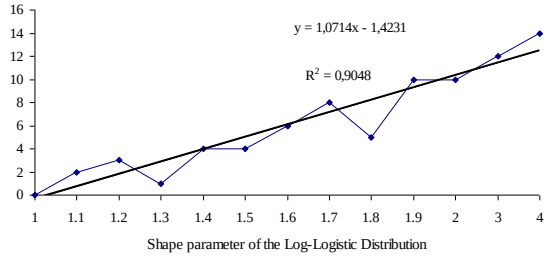

Figure 5: Number of times that won a Party with Log-Logistic Distribution

Then it was analyzed supporters final distribution type by each party, which resulted without changes for the normal distribution and changed the log-logistic for an exponential distribution (equation 3).

$$f(x) = \frac{e^{-x/\beta}}{\beta} \qquad (3)$$

Where "beta" is the mean.

The consequence is that the exponential distribution falls more quickly than the log-logistic distribution, suggesting a more quickly disappearance of the party.

3. CONCLUSIONS

The statistical distributions of the electoral presences of each political party are different, having the major parties a normal distribution of its voters at national level. On the other hand, the Democratic Revolution Party and the minor parties have a heavy tails distribution (log-logistic) which indicates a great concentration of voters in a few federal entities.

It was observed that when the log-logistic α parameter is minor to 2, political parties tend to disappear, although this is not an absolute truth. Nevertheless, this fact shows tendencies to debilitate the parties, which brings out in many cases the disappearance of them. This phenomenon was analyzed in an experimental way by developing a dynamic program (López 2000; Ross 2007; Stauffer 2003) where two parties interact (one with normal distribution and the other with log-logistic distribution). As a result we obtained a better participation of the party with log-logistic distribution while α was increased.

As part of a future work, the nonparticipation can be considered like another variable in the model. It is tried to complement the Mexican voters' pseudo-fractal network (Martínez and Balankin 2007) and improve the dynamic model for probabilistic tendencies of future electoral results. Political parties' behavior theories are still increasing. This creativity is commendable. Lamentably, the application remains limited.

It is pretended that the models focused on social system dynamics would be an important part in the decision making of the respective competitors, in order to fit its strategies, canalize its resources in a better way and to promote the vote between its supporters. For that motive it is necessary to improve the analysis, modeling and prediction of the electoral dynamic systems. In addition, these models could be useful to the electoral authorities to plan strategies to prevent the nonparticipation and to detect possible electoral frauds.

REFERENCES

Adams, J., Merrill, S., 1999. Modeling Party Strategies and Policy Representation in Multiparty Elections: Why Are Strategies So Extreme? *American Journal of Political Science*, 43, 765-791.

Bergstrom, T., 2001. Evolution of Social Behavior: Individual and Group Selection Models. *Departmental Working Papers, University of California, Santa Barbara.*

Guzmán, J., 2004. Cámara de diputados dominantes PAN y PRI en 2006. *La jornada*, 22 December, p. 10.

Law, A.M. and Kelton, W.D., 2000. *Simulation Modeling and Analysis.* 3rd ed. Singapore: McGraw-Hill.

López, E., Martínez, S., 2000. *Iniciación a la Simulación Dinámica.* 1st ed. Barcelona: Ariel.

Martínez, M., Balankin, A., 2007. Análisis fractal de elecciones Federales 1991 – 2003. *Revista científica del Instituto Politécnico Nacional,* 10, 175 – 184.

Ross, Sh., 2007. *Simulación*. 5th ed. México: Prentice Hall.

Schofield, N., Parks, R., 2000. Nash Equilibrium in a Spatial Model of Coalition Bargaining, *Mathematical Social Sciences,* 39, 133-174.

Stauffer, D., 2003. Sociophysics Simulations, *Computing In Science & Engineering,* 3, 71-75

Weidlich, W., 2000. *Sociodynamics: A Systematic Approach to Mathematical Modeling in the Social Sciences.* 1st ed. U.S.: Harwood Academic Publishers.

AUTHORS BIOGRAPHY

Idalia Flores de la Mota studied a PhD in Operations Research in the Engineering Faculty of the National Autonomous University of Mexico (UNAM). She obtained an honorary mention for her master thesis and worked with Hamdy A. Taha for her doctorate thesis. She has attended to several national and international congresses and has been a member of Mexico's National Researchers System. Since 1990 is a full time professor at UNAM, teaching applied mathematics, integer programming, network programming and simulation. She worked as the Operations Research Section Chief for 10 years at UNAM'S Engineering Faculty. Her research interests are in networks simulation and logistic processes simulation.

Miguel Ángel Martínez Cruz obtained his bachelor degree in Physics and Mathematics from National Polytechnic Institute of Mexico in 2001, a master degree in Operations Research in 2004 and a PhD in Mechanical Engineering in 2007 from the same institution. He works with Alexander Balankin, winner of the 2005 UNESCO Science Prize, as a full time researcher at the National Polytechnic Institute and as a simulation consultant of the Federal Electoral Institute in Mexico. His research interests are fractal mechanics, simulation of social networks and simulation of dynamic systems.

Alejandro Suárez Buenrostro obtained his bachelor degree in Economics from the Monterrey Institute of Technology in 2001 and a master degree in Operations Research from the National Autonomous University of Mexico (UNAM) in 2009. He is professor of economics and econometrics at National Polytechnic Institute and teaches operations research in the Engineering Faculty at the UNAM. He worked as a financial and process optimization analyst in a major airline. His research interests are simulation of economic and financial systems, simulation of social networks and non linear programming.

NETWORK DESIGN USING MIX INTEGER PROGRAMMING AND MONTECARLO SIMULATION IN AN INTERNATIONAL SUPPLY CHAIN NETWORK.

Eduardo Villareal[(a)], Idalia Flores[(b)]

(a) Universidad Nacional Autónoma de México, México
(b) Universidad Nacional Autónoma de México, México.

(a) eduardo_vp0914@yahoo.com.mx (b) idalia@unam.mx

ABSTRACT
In this paper a methodology was developed to combine optimization techniques whit Montecarlo Simulation to design an International Supply Chain Network in Mexico. The case of study was taken from a business where an optimal network is defined by choosing from a variety of distribution centers. For the defined network there are 2 kinds of products, 18 distribution centers and more than 3000 retailers that have been grouped in 73 locations. Also, the model has considered 6 types of transportation modes. The optimization model has an interface built on Microsoft Excel, a model formulation that was built in Lingo V.8.0 and a geographic interface built in Microsoft Map Point 2009. For the simulation model we considered stochastic demand and some cost parameters such as the fixed cost for the Distribution Centers and maritime cost for the international flow to Mexico.

Keywords: optimization techniques, montacarlo simulation, supply chain network

1. INTRODUCTION

According to Bramel and Levi (1997) one of the most important aspects of logistics is the location of a new distribution center to provide a service to one or more customers, warehouses or factories within the supply chain.

The problem of choosing the location of new distribution centers or plants within a logistics network consists of optimizing the transport cost throughout the network by incorporating new elements into the distribution network while complying with the constraints on demand and storage capacity (to name but a few).

2. BACKGROUND

Location problems can by looked at from three points of view:

- As an assignment problem
- As a minimum cost maximum flow problem
- As a combination of the above two

Different authors, including Bramel (1997) as well as Levi, Wu, Shen and Levi (2004), analyze location problems as mixed linear programming problems or else, as problems with nonlinear cost functions. The presence of nonlinearity in a location problem implies that economies of scale or fixed costs have been introduced into the cost function. According with Dalila (2006) in the paper entitled Heuristic Solutions for General Concave Minimum Cost Network Flow Problems, specifies that when the effect of economies of scale or fixed costs is added in, the cost function becomes concave and thus becomes a convex space bounded by a nonlinear hyperplane. Likewise Kouvelis (2004) incorporates economies of scale, fixed costs and nonlinear variable costs for a problem of network design.

The limitations involved in using an assignment problem to define the location of a new distribution center are:

- It only considers the rental costs of each store.
- Flows through the network are not taken into account.
- The demand of each one of the customers situated all along the network are not considered.
- The interaction between all the parts of the distribution network is not observed in the formulation of the model and are not considered in the decision-making process.

The cost function is linear Hillier and Liberman (2000).

On the other hand, the limitations involved in using a minimum cost flow model are:

1. It does not consider the fixed costs involved in opening and closing a distribution center.
2. The decision variables only determine the optimum flow within the network.
3. The cost function is linear.

2.1. The Weber Problem

The goal is to find a $P(x^*,y^*)$ point that minimizes the sum of the weighted Euclidean distances of n points with coordinates (a_i,b_i). The weightings associated with the n fixed points are denoted by w_i. When we transfer this problem to the Supply Chain, the problem consists of situating a distribution center with a w_i transport cost associated with the location of the customers on the fixed points (a_i,b_i). Therefore, (x^*,y^*) is the point that minimizes the distribution cost.

The problem can be expressed as follows:

$$\min Z = W(x,y) = \sum_{i=1}^{n} w_i \cdot d_i(x,y) \quad (1)$$

Where $d_i(x,y) = \sqrt{(x-a_i)^2 + (y-b_i)^2}$ is the Euclidean distance between (x,y) and (a_i, b_i)

The simplest way to solve this problem is using the Weiszfeld algorithm[1].

Partially deriving the objective function and making it equal to zero, we get the first-order conditions for ensuring optimality:

$$\frac{\partial}{\partial x} W(x,y) = \sum_{i=1}^{n} \frac{w_i \cdot (x-a_i)}{d_i(x,y)} = 0 \quad (2)$$

$$\frac{\partial}{\partial y} W(x,y) = \sum_{i=1}^{n} \frac{w_i \cdot (y-b_i)}{d_i(x,y)} = 0$$

It can be shown that $W(x,y)$ is convex and the system of equations (2) defines a minimum. However, these derivatives do not exist when (x,y) coincide with the fixed point i because $d_i(x,y)=0$ and therefore the equations in (2) cannot be solved for (x,y) if $n>3$

We can extract x from the first equation in (2) and extract y from the second equation in (2). The result is an iterative procedure if we consider the extracted pair (x,y) as a new iteration $(k+1)$. To be precise:

$$(x_{k+1}, y_{k+1}) = \left(\frac{\sum_{i=1}^{n} \frac{w_i \cdot a_i}{d_i(x_k,y_k)}}{\sum_{i=1}^{n} \frac{w_i}{d_i(x_k,y_k)}}, \frac{\sum_{i=1}^{n} \frac{w_i \cdot b_i}{d_i(x_k,y_k)}}{\sum_{i=1}^{n} \frac{w_i}{d_i(x_k,y_k)}} \right) \quad (3)$$

This is an iterative method for solving the location problem.

2.2. Model for the warehouse location problem.

Let us consider a set of customers spread out within a particular geographic region. The problem is to determine the location of a number p of available warehouses. We assume that there are $m \geq p$ places that have been previously selected as possible locations. Once the location of warehouse p has been determined, each one of the n customers shall be supplied by the nearest warehouse. In this model we assume.

- There is no fixed cost for locating warehouse p.
- There is no constraint on the capacity of any warehouse to meet the demand.

This example was taken from a real company that imports wood from Chile and has some distribution centers as Tampico where the wood arrives,and then the wood is transported for all over the country.

Let:

Set of customers $N = \{1, 2, 3,..., n\}$
Set of possible warehouses $M = \{1, 2, 3 ..., m\}$
Let w_i = the flow of demand between the customer i and their warehouse for the entire $i \in N$
Let c_{ij} = the cost of transporting w_i units from the warehouse j to the customer i for each $i \in N$ y $j \in M$

The problem is to locate p of the m available warehouses in such a way that the transport cost is minimized.

Let:

$$y_j = \begin{cases} 1 \text{ if storage is located at j place} \\ 0 \text{ o. c.} \end{cases}$$

$$x_{ij} = \begin{cases} 1 \text{ if client i is served by storage j} \\ 0 \text{ o.c.} \end{cases}$$

For all $i \in N$ and for all $j \in M$

Thus the problem is formulated as follows:

$$\min Z = \sum_{i=1}^{n} \sum_{j=1}^{m} c_{ij} \cdot x_{ij} \quad (4)$$

Subject to:

$$\sum_{j=1}^{m} x_{ij} = 1 \ \forall \ i \in N \quad (5)$$

$$\sum_{j=1}^{m} y_j = p \quad (6)$$

$$x_{ij} \leq y_j \quad (7)$$

for
$x_{ij}, y_j \in \{0,1\} \ \forall \ i \in N \ \forall \ j \in M$

The constraint on (5) ensures that a warehouse is assigned to every customer. The constraint on (6) ensures that a p warehouse are assigned and the constraint on (7) ensures that each customer chooses a single warehouse. The problem is integer linear.

2.3. Location of capacitated-constrained warehouses. Let us consider the model for the p-median algorithm under the following hypotheses:

1. The number of warehouse to be located is not a fixed value p.
2. A fixed cost f_j is incurred by locating a warehouse in place j.

Minimize:

$$Z = \sum_{i=1}^{n}\sum_{j=1}^{m} c_{ij} \cdot x_{ij} + \sum_{j=1}^{m} f_j \cdot y_j \qquad (8)$$

Subject to:

$$\sum_{j=1}^{m} x_{ij} = 1 \quad \forall\, i \in N \qquad (9)$$

$$\sum_{i=1}^{n} w_i \cdot x_{ij} \leq q_j \cdot y_j \quad \forall\, j \in M \qquad (10)$$

$$x_{ij}, y_j \in \{0,1\} \; \forall\, i \in N \; \forall\, j \in M$$

The constraint on (9) ensures that a warehouse is assigned to every customer. The constraint on (10) ensures that the capacity of a warehouse is not exceeded and also if there is no warehouse located in j no customer can be assigned to that place.

3. DEFINITION OF VARIABLES AND PARAMETERS

The parameters of the model are defined below.

3.1. Seaport costs

κ_{itw}= Storage capacity d in m^3 for product type t for type of vessel w.

C_{ijtw} = Total cost per m^3 of transport from place of origin i to port j for product type t in type of vessel w.

The cost of sending a boat depends on the following parameters:

- Carriage cost from plant to port in Chile per m^3
- Port expenses per m^3 in Chile
- Cost for secure sea freight per m^3 Chile-Mexican port
- Port expenses per m^3 in Mexican port

3.2. Rail transport

ν_{tw} = Storage capacity in m^3 for product type t for freight car type w.

In the case of containerized freight, a sea container has the same capacity as a railroad container since it is the same container being transported.

C_{jktw} = Cost per m^3 for transporting from port j to Distribution Center k for product type t for freight car type w.

3.3. Storage cost

υ_k = Storage capacity in m^3 of the Distribution Center located in port k.

ω_l = Storage capacity in m^3 of the Distribution Center located in l

C_k = Fixed annual cost of the warehouse located in port k

C_l = Fixed annual cost of the warehouse located in l

The fixed cost of the warehouse is made up by the following categories:

- Costs of management services (cost of the annual salary of the Distribution Center manager).
- Rental cost per m^2.
- Annual cost of equipment depreciation and amortization.
- Workers wages (annual)
- Wages of administrative staff (annual)
- Electric power and other expenses

3.4. Cost of Single-Trailer and Double-Trailer transport

D_{nm} = distance in km from place of origin n to destination m.

η_{nmtw} = price or cost of carriage from place of origin n to destination m of product type t in transport type w (single-trailer or double-trailer).

φ_w = Transport capacity in m^3 for mode w.

ξ_{nmtw} = Cost per m^3 of transport from place of origin n to destination m of product type t in mode of transport w

Finally, the demand of each customer is defined as:
d_{mt} = demand of each customer l for product type t

3.5. Variables of the model

X_{ijtw} = quantity in m^3 of product type t delivered from country i to port j in transport type w. This variable is positive continuous.

X_{jktw} = quantity in m^3 of product type t delivered from port j to the Distribution Center in port k in mode of transport w. This variable is positive continuous.

X_{jltw} = quantity in m^3 of product type t delivered from port j to the inland Distribution Center l in mode of transport w. This variable is positive continuous.

X_{kltw} = quantity in m^3 delivered from Distribution Center at port *k* to the inland Distribution Center *l* from product type *t* in mode of transport *w*.

X_{kmtw} = decision on merchandise of product type *t* delivered from the Distribution Center in port *k* to customer *m* in mode of transport w. This variable is binary (0,1).

X_{lmtw} = decision on merchandise of product type *t* delivered from the inland Distribution Center *l* to customer *m* in means of transport *w*. This variable is binary (0,1).

Y_k = decision on opening or closing the CD located at port *k*

Y_l = decision on opening or closing the CD located at *l*

3.6. Performance measurements

For this problem we propose 3 performance measurements:

1. Z_{mar} = Cost of sea transport.
2. Z_{ter} = Cost of land transport.
3. Z_{alm} = Cost of storage.

Overall we have:
Z = Total cost of operating the supply chain.

4. INFORMATION GATHERING.

- Information was directly provided by the company's ERP system (SAS) about the shipments made from January 2007 to December 2007 and organized in a database with the following fields:
- Order number: used to locate the release details.
- Linked dispatch: this number identifies each dispatch order with the deliveries made. Used for the trackability of the purchase order.
- Date of shipment: date when the shipment was made.
- Name of carrier: Name under which the carrier is registered in the system.
- Place of origin: City of origin (City, State)
- Destination: Name of the city of destination (City, State)
- M^3 transported: quantity in m^3 of material transported.
- Carriage cost: cost incurred by taking the shipment from the place of origin to the required destination.
- Product type: classification of the product shipped to the customer.

4.1. Adaptation of the sample

Using random sampling, 138 data for the m^3 transported during the period from January 2007 to December 2007 were selected in order to assess whether the sample from one year is enough for the study.

The annual mean of the population is 1006 m^3 a day shipped.

Table 1: Test mean-value of sample size

Hypothesized Value	1006
Actual Estimate	1024.07
df	137
Std Dev	760.259

The statistical hypotheses are defined as:

Ho: $\mu = 1006$ m^3 a day
Ha: $\mu \neq 1006$ m^3 a day

Value p is 0.78 in the test; assuming a significance $\alpha = 0.05$, as $p>\alpha$ we are within the acceptance region and therefore cannot reject the null hypothesis that establishes that the mean of the sample is equal to the mean of the sample for all 2007. Therefore, the sample from January 2007 to December 2007 is representative. On the other hand, we get the same result with the Wilcoxon signed-rank test for non-parametric data, since the p value in from the test is 0.29 and greater than the 0.05 significance so we can say that there is statistical weight.

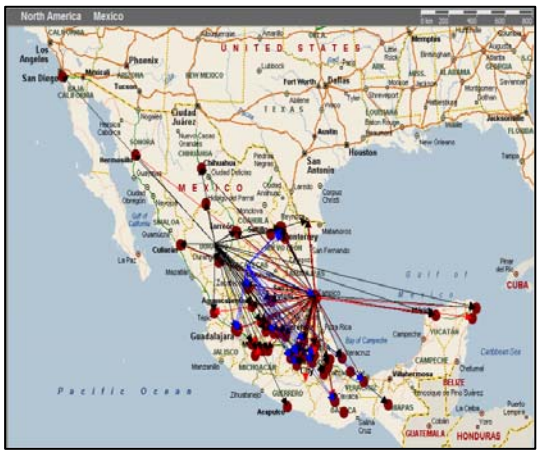

Figure 1: Base case for 2007 demand distribution

The 288 data corresponding to 2007 can be used for the distribution network model.

4.2. Estimating the cost of land transport

The cost of land transport depends on the following factors:

1. Distance travelled.
2. Carriage cost
3. Product type.
4. Capacity of the means of transport.

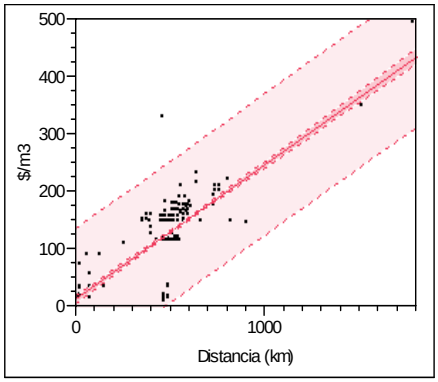

Figure 2: Linear regression for Wood.

Linear Fit for Wood
$/m3 = 13.563404 + 0.2344908*Distance (km)

The regression coefficient is 80.62%, the intercept is $13.56 that is interpreted as the fixed cost for operating one item and the slope is $0.23 which is the variable part of the rate.

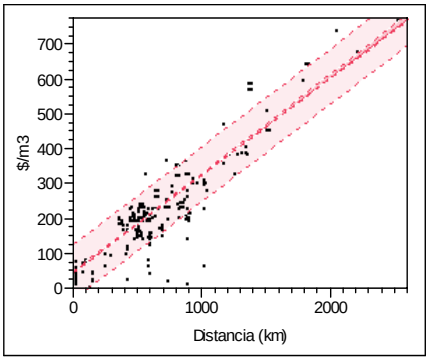

Figure 3: Linear regression for MDF

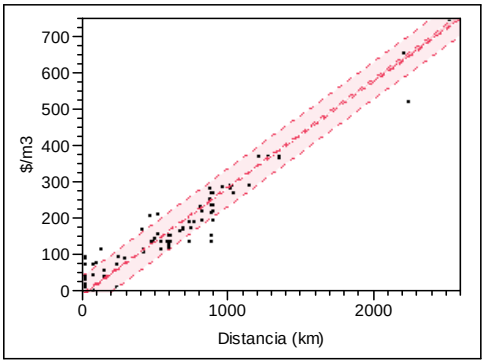

Figure 4: Linear regression for sheeting

Linear Fit MDF
$/m3 = 49.476191 + 0.2795796*Distance (km)

The regression coefficient is 88.89% with a fixed cost of $49.47 per m^3 and a variable cost of $0.28 per km /$m^3$.

Linear Fit Sheeting
$/m3 = -5.445904 + 0.2934067*Distance (km)

The regression coefficient is 97.46% with a fixed cost of -$5.44 per m^3 and a variable cost of $0.29 per km /$m^3$.

4.3. Base line

The annual cost of logistics is $245 million pesos of which $161 are for sea transport, $65 for land transport and $33 for storage.

As for the situation at the present time, we know that in 2007 the cost of transporting goods to the customer was $59 million pesos. This gives us an error of 2.39% in the model.

5. EXECUTION OF OPTIMIZATION RUNS.

5.1. Definition of scenarios

Together with the team of project directors, we defined the following scenarios to be assessed:

Scenario 1: Free consolidated.

- Opening and closing of Distribution Centers without any constraint on contracts with 3PL.
- Flows and modes of transport defined by the optimization model.
- Flow conservation constraints between nodes.
- Demand fulfillment constraints.
- The demand is assumed to be constant according to the data collected in the Jan-Dec 2007 period.

Scenario 2: Not closing Tampico.

- Tampico should not be closed because of issues to do with contracts with 3PL.
- Constraint of at least 77% on entry of bulk freight into ports.
- Constraint not higher than 23% on entry of containerized freight into ports.
- Flows and land modes defined by the model.
- Flow conservation constraints between nodes.
- Demand fulfillment constraints.
- Consolidation of bulk freight in a Distribution Center located in the port (there are no direct deliveries from the port to the customers).

This means that 485 containers would be required every month in the ports on the Pacific and, operationally speaking, it is not feasible for the factory in Chile to ship that quantity of containers only for Mexico. Furthermore, in the Mexican ports it is not possible to get the 485 trucks per month that would be required. Therefore, the best option is to be open a Distribution Center in Tampico for bulk freight (77% of what arrives in Mexico), close the one in Altamira,

extend the Mexico City Distribution Center, have the containers come in through Manzanillo and Mazatlan to the factory in Durango. The factory in Durango should also operate as a Distribution Center for MDF in the north of the country.

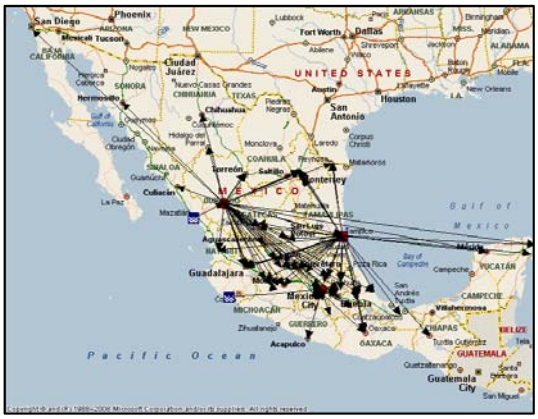

Figure 4: Optimal solution for Wood and MDF. Sheeting is distributed 100% from Durango.

6. SIMULATION MODEL

The simulation model was developed in the following stages:

1. Information gathering
2. Formulation of the model
3. Validation of the model
4. Programming of the model
5. Validation of the programmed model
6. Design and analysis of experiments

A sample of the dispatches to the end customer in one year (Jan-Dec 2007) was taken from the optimization model. The sample considers the three product types: wood, MDF and Sheeting.

Let:

d_{kij} = Quantity of m^3 of product i shipped every day k in locality j

D_i = Quantity of m^3 of product i shipped every year

Therefore:

$$D_i = \sum_{k=1}^{n} \sum_{j=1}^{m} d_{kj} \text{ for each product } i \quad (11)$$

$i = Madera, MDF, Placa$
$j = 1, 2, 3 ..., m$
$k = 1, 2, 3 ..., n$

If the demand for each locality and product is a random variable. Therefore the annual demand for each product is also a random variable. In order to simplify the simulation model, only 85% of the volume is considered to be stochastic and the remaining 15% considered a constant owing to the fact that the shipments are mostly sporadic.

According to Axëter (1996), a supposition for modeling the demand is to consider that it follows a Poisson distribution with a parameter λ which is the average number of units in m^3 shipped every day. We know that the Poisson distribution and the exponential distribution are intimately linked and that, for the continuous case, it works better if we assume that demand follows an exponential distribution.

Now then, the problem consists of finding a random number generator for an exponential distribution.

Let:

x = the quantity of m^3 to be shipped every day. Then x follows an exponential distribution with parameter λ:

$$f_x = \lambda e^{-\lambda x} \quad (12)$$

Let F(x) be the accumulated probability distribution, therefore:

$$F_x = \int_0^x \lambda e^{-\lambda x} dx = 1 - e^{-\lambda x} \quad (13)$$

Let r be a random number between 0 and 1. Therefore as F_x is between 0 and 1, we can write:

$$F_x = r = 1 - e^{-\lambda x} \quad (14)$$

Finding x we get:

$$x = -\frac{\ln(-r+1)}{\lambda} \quad (15)$$

This is a random number generator with exponential distribution.

Let:

x_{kij} = quantity of m^3 of product i shipped on day k in locality j

Therefore, annual demand for locality j is:

$$d_j = \sum_{k=1}^{n} x_k = \sum_{k=1}^{n} \frac{\ln(1-r_k)}{\lambda_j} \quad (16)$$

for each product i

Therefore the annual demand for each product i is:

$$D_i = \sum_{k=1}^{n} \sum_{j=1}^{m} \frac{\ln(1 - r_{kj})}{\lambda_j} \quad (17)$$

for each product i

For each product, the volumes shipped to the localities considered were 74,545, 114,979 and 54,827 for wood, MDF and sheeting respectively.

6.1. Results from the simulation model

On running the analysis of the sample, we found that it is necessary to have a sample of n=256 to obtain a power of 95%. However, we decided to execute the runs of n=300 to get a power of 0.97, as shown in the JMP results.

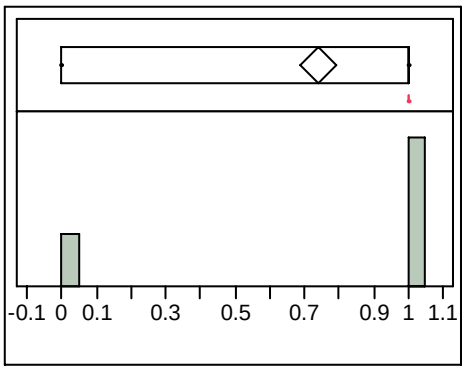

Figure 5: Simulation results for Guadalajara.

Therefore, we are able to say that on 74% of the occasions, under conditions of changing demand and changeable fixed storage costs, Guadalajara turned out to be the best option as a logistics plan. While on 26% of the occasions, Toluca was the best option. Therefore, there is 26% potential risk that if we open the Distribution Center in Guadalajara, we will not get optimum results. However, we are in a position to conclude that the current logistics of this company are wrong since they did not appear within the solutions proposed by the Optimization-Simulation Model we developed.

7. CONCLUSIONS AND FUTURE WORK.

Although it is possible to separate the techniques of mathematical programming and analysis, the optimization and simulation of the supply chain give an optimum solution while the uncertainty in the model's parameters is evaluated. This permits the construction of multi-scenari optimization models that make it possible to evaluate different alternatives and automatically carry out the sensitivity analysis of the network model. Thus, the optimization and simulation model presented throughout this thesis paper permitted:

1. Interaction between the optimization and simulation of the supply chain.
2. Finding an optimum solution.
3. The evaluation of different scenarios through sensitivity analysis.
4. Determining a metrics to measure the optimality of the solution proposed by the optimization model that can be translated into a risk metrics for the decision.
5. Determining a methodology for the development of large-scale optimization and simulation models.

It must be emphasized that owing to the complexity of the mixed-integer programs (MIP), which tend to be considered as NP-complete, it is not possible nowadays for a program to do the post-optimality analysis of the optimization model. However, with the aid of the simulation model it is possible be able to determine the optimality parameters for these models.

From a business point of view, the optimization model for the distribution network allowed us to:

1. Identify strategies for inter-continental distribution through the use of different modes of sea transport.
2. Evaluate of the country's points of entry that would allow greater flexibility in the supply chain and minimize costs.
3. Determine the optimum logistics plan for each product in the distribution network.
4. Define marketing strategies.
5. Take a medium-term strategic decision about the logistics and marketing scheme to be followed in the next few years.

Throughout the development of the model, it was necessary to carry out a meticulous validation of each one of the parameters in order to guarantee, with a permissible estimation error, an optimum solution being rectified by the simulation model. Therefore, we can say that if the estimation of the parameters is good, the optimum solution will be the one that, under conditions of uncertainty, prevails over all the other possible feasible solutions.

This simulation and optimization model was used in the context of a real case scenario where, in order to analyze the efficiency of the distribution network as Preusser (2008) suggests, while the static characteristics of the linear model can be overcome by the motor de optimization, it is possible to use the simulation model to approximate a stochastic and possibly nonlinearity analysis of the problem in order to determine rules of decision that favor the operations of the business at a low cost.

Future research can focus on the integration of the simulation model with simulation languages that permit optimization while the simulation of the stochastic events is generated. In the case of the network models described in the case study, the subject of inventories and planning horizons could be included in order to get production, storage and distribution programs for the

different products. An alternative means of solving these types of models, considering stochastic elements, is known as " stochastic programming". Nowadays some software packages such as CPLEX and GAMS are capable of solving such formulations by the inclusion of special algorithms.

We will obtain other branches for research as we reach the limits of optimization and simulation. If more complex models are used, new ways of solving them (metaheuristics, heuristics) will have to be developed.

REFERENCES

Ahuja, R.K. and Magnanti, T.L. 1993. *Network Flows.*New Jersey: Prentice Hall.

Bazaraa, S. and Sherali, D.2006. *Nonlinear Programming. Theory and Algoritms* New Jersey.Wiley Inter Science.

Chen An, C.A. and Hansjörg, F.R., 2005. *Supply Chain Management on Demand: Strategies, technologies and applications*. Netherlands: Springer Verlang

Dalila, B.M., Fontes and Goncalves, J.F. Heuristic Solutions for General Concave Minimun Cost Network flow Problems.*Wiley Interscience: Periodical Inc. Networks.* Vol. 50. Pag. 67-76.

Eiselt, H.A. and Sandblom. 2000. *Integer Programming and Network Models.* Berlin: Springer-Verlang.

Flores de la Mota, I.F. and Elizondo, M.E. 2006. *Apuntes de simulación*. México, D.F.: UNAM Editorial.

Hillier, F.H., 2000. *Introducción a la investigación de operaciones*. 8th Edition. México, D.F: Mc Graw Hill.

Jack, P.C.; Supply Chain Simulation: a Survey. *International Journal of Simulation and Process Modeling.*

Kok, A.G. and Graves, S.C. 2003. *Handbooks in operation research and management science Vol11: Supply Chain Management.*New York: Elsevier Editor.

Prreusser, M.P. 2008. *Simulation and optimization in Supply Chain Management.*1st ed. Saardrüken: Dr. Muller editor.

Pistikopoulos and Georgiadis. 2008. *Supply Chain Optimization vol.* I. 1st ed.I Berlin: Wiley-VCH.

Simchi, L. and Bramel, 1997. *The logic of Logistics: Theory, Algorithms and Applications for Logistics Management.*New York: Springer-Verlang.

ACKNOWLEDGMENTS

This paper was written with the support of the Academic program DGAPA-UNAM throughout PAPIIT project number IN100608.

SIMULATED ANNEALING TUNING METHOD FOR MULTI-RATE PID CONTROLLERS

Cerezo, Y. [a], Cuesta, A. [b], López, I. [c], Grau, L. [d]

[a] Universidad Francisco de Vitoria. Madrid. Spain.
[b] Felipe II College, Universidad Complutense de Madrid. Spain.
[c,d] Universidad Nacional de Educación a Distancia. Spain.

[a] y.cerezo.prof@ufv.es, [b] acuesta@cesfelipesegundo.com , [c] ilopez@scc.uned.es, [d] lgrau@scc.uned.es

ABSTRACT
The goal of this paper is to provide a tool for tuning PID controllers in multi-rate control loops. The high number of degrees of freedom of the controller and different performance requirements motivate us to choose Simulated Annealing as the multi-objective optimization method. We describe the tuning procedure, present a CACSD tool and give an example to show the goodness of the proposal.

Keywords: Multi-Rate control, Digital control, PID tuning, Simulated Annealing.

1. INTRODUCTION

One of the key questions to be taken into account in real processes is that one can find components working at different rates. For instance, in distributed control systems, where there are many processors and communication channels, it is not realistic to assume that they all work at the same rate, nor even synchronized.

Classic digital control theory assumes the same sampling period for all the variables appearing in the system. Although it has provided fundamental results, when coping with non conventional sampled systems it is necessary to develop more suitable methods. Most of them tackle the Multi-Rate (MR) problem, in which different variables are sampled with different, but constant, periods. Thus, it is always possible to find a frame period or metaperiod, least common multiple of all the ones found in the system, such that the whole system may be expressed as a single-rate (SR) periodic one. There are numerous contributions as early as the late fifties. The most remarkable works have been reported in the literature (Kranc 1957; Araki and Yamamoto 1986; Thompson 1986; Bamieh et al. 1981; Salt and Albertos 2005).

In this paper we propose a tuning method for Multi-Rate PID controllers (MRPID); i.e. PID controllers placed into a SISO MR loop in which the output is measured at a rate different from the control updating (Cuesta, Grau and López 2007; Salt et al. 2006; Sala et al. 2009). The MRPID proposed is an extension of the digital PID in which each action is able to work at a different sampling rate. Thus the well known inner structure of the controller is kept together with its physical meaning. Besides, if we see each action as an independent subsystem and the final control action as the sum of them, then there is no additional computational cost.

The contribution of this paper is the use of Simulated Annealing (SA) in the tuning process. It is based on the molecular process occurring when a metal gets cold after being melted. In the melting process, its particles are free, taking random positions. As the temperature gradually lowers they fall into minimum energy states. Simulated Annealing is therefore a popular evolutionary algorithm in combinational optimization problems (Metropolis 1953; Mitra, Jha and Choudhurl 1991). Its choice was motivated by the fact that the MRPID (Lopez and Cerezo 2007) has 6 parameters: Proportional, Integral and Derivative gains (K_p, K_i, K_d, all real and positive) and inner Proportional, Integral and Derivative working periods (T_{prop}, T_{int}, T_{der}, all integer and positive).

The rest of the paper is organized as follows. Section 2 settles the problem. Section 3 describes the algorithm. Section 4 shows the simulations and results. Finally conclusions are pointed out in section 5.

2. PROBLEM STATEMENT

Let us consider a control loop where the error rate and the control rate are different.

Then it is necessary to include a MR controller. If a PID is to be used, alike in most of the basic control loops already implemented then it turns into a MRPID. Then a natural generalization is taken having different rates for each control action. Therefore five periods can appear in the MRPID: T_y, T_u, T_{prop}, T_{int} and T_{der}. The final control action is the sum of the three basic actions as usual. This scheme is shown in Fig. 1 and the control algorithm is the following:

```
--interruption every Tprop
Set_Timer_P (Tprop);
every Timer_Interrupt loop
  Get(y);   -- A/D conversion
  Get(r);   -- A/D conversion
  Get(u);   -- A/D conversion
  en:=r-y;  -- computing error
  up:=Kp*en;
  u:=u+up;
  Put(u);   -- D/A conversion
end loop
```

```
--interruption every Tint
Set_Timer_I (Tint);
every Timer_Interrupt loop
  enOld:=r-y;
  Get(y);    -- A/D conversion
  Get(r);    -- A/D conversion
  Get(u);    -- A/D conversion
  en:=r-y;   -- computing error
  sn:=sn+en; -- computing cumulative error
  ui:= Ki*Tint*sn;
  u:=u+ui;
  Put(u);    -- D/A conversion
end loop

--interruption every Tder
Set_Timer_D (Tder);
every Timer_Interrupt loop
  enOld:=r-y;
  Get(y);    -- A/D conversion
  Get(r);    -- A/D conversion
  Get(u);    -- A/D conversion
  en:=r-y;   -- computing error
  ud:= Kd/Tder*(en-enOld);
  u:=u+ud;
  Put(u);    -- D/A conversion
end loop
```

From the general structure presented and based on different relationships between periods (as proposed in the structure) some operating modes can be defined:

M1. Cuasi-continuous: $T_{prop}=T_{int}=T_{der}=h$, with h small enough to design the controller in the continuous domain.
M2. Single-rate: $T_{prop}=T_{int}=T_{der} > h$
M3. Multirate controller: $T_{prop}\neq T_{int}\neq T_{der}$

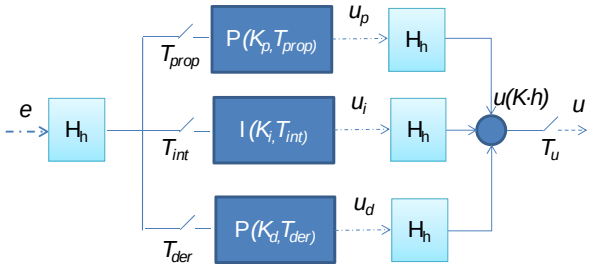

Figure 1: Multirate parallel PID (MRPID) controller scheme

3. TUNING METHOD

We propose the use of SA techniques for computing the parameters of the controller.

SA, which has much in common with evolutionary computation, is a derivative free stochastic search method for determining the optimum solution in an optimization problem. The method was proposed by Kirkpatrick et al. (1983) and has since been used extensively to solve large-scale problems of combinatorial optimization, such as the well-known traveling salesman problem (TSP), the design of VLSI circuitry and in the design of optimum controllers (Mitra, Jha and Choudhurl 1991). The main difference between Evolutionary Computation and Simulated Annealing is that the latter is inspired by the annealing process for metals during cooling, while the former is based on evolutionary processes. The principle of annealing is simple: at high temperatures the molecules in a metal move freely but as the metal is cooled gradually this movement is reduced and atoms align to form crystals. This crystal-line form actually constitutes a state of minimum energy.

SA attempts to obtain an optimal solution out of an initial non optimal one. To this end it is necessary to fix its settings properly. We will use the following terms:

- *Configuration* is the set of parameters
- *Cost function J* is in terms of the configuration and it measures its goodness, which must be optimized.
- *Set of movements* is the set of strategies that yields to an improvement in the optimization of the cost function, for instance avoiding local minima. We have used Metropolis algorithm (Metropolis et al., 1953) which use the Boltzman distribution to evaluate the probability of ΔJ, a change in the cost function. Thus the temperature decreases randomly but in a controlled exponential way.
- *Annealing scheme.* It is necessary to specify both the initial and final temperature and how it decreases in time. If the initial temperature is too high, the searching efficiency decreases; whereas if starts too low, the search may be rapped in the local minimum.

The algorithm for tuning the controllers consists of the following steps:

1. *Initialization*

Configuration: $K_{PID} = [K_p, K_i, K_d, T_{prop}, T_{int}, T_{der}]$
Initial solution: $K^0_{PID} = [K_p^0, K_i^0, K_d^0, h, h, h]$, obtained with any known tuning method.

2. *Cost function*

$$J(K_{PID}) = \sum_{i=1}^{m} \beta_i J_i, \qquad (1)$$

where J_i are different *local* objectives, such as the integral time absolute error (ITAE), and $0 \le \beta_i \le 1$ are weights in order to express their relevance. Every local objective is computed as

$$J_i(K_{PID}) = \left| \frac{f_i^s - f_i^e}{f_i^e} \right|, \qquad (2)$$

where f_i^s is the expected value and f_i^e the value obtained after each iteration of the algorithm.

3. *Annealing scheme*

In order to avoid a blind choice of the initial temperature, the value of the performance index with the best and worst performance respectively is evaluated. If the probability of acceptance of J_{worst} to the J_{bestt} es P , then

$$T^0_{emp} = -(J_{worst} - J_{bestt})/ln(P) \qquad (3)$$

Typically P is within [0.8, 0.9].

4. Perturbation

A random perturbation is produced over the configuration. Thus a new configuration is obtained. The expression for this transition is $x'=x+\mu\cdot\lambda$ where μ is a scaling factor, λ is randomly generated out of a normal distribution, x is the present configuration and x' is the next one.

5. Accept or reject

We first compute the value of the cost function for the next configuration. If it is lower than the cost function for the present configuration, then is selected. If not then there is still a chance of being accepted given by the Boltzmann distribution $\min\{1,\exp(-\Delta J/T)\}>n$ where n is a threshold between 0 and 1 and ΔJ is the difference between the present and former cost function.

6. Iteration

Decrease the temperature and the scaling factor doing $T(k+1)=T(k)\cdot\lambda$ and $\mu(k+1)=\mu(k)\cdot\lambda$ with $0<\lambda<1$. Then repeat 4 and 5.

7. Stop

There are two possible conditions: either the cost function reaches a minimum acceptable value or it does not change during a certain number of temperature consecutive decreases.

4. EXAMPLE

In this section we deal with a simple study case to show the different possibilities of both GTM and the tool presented (see fig. 2).

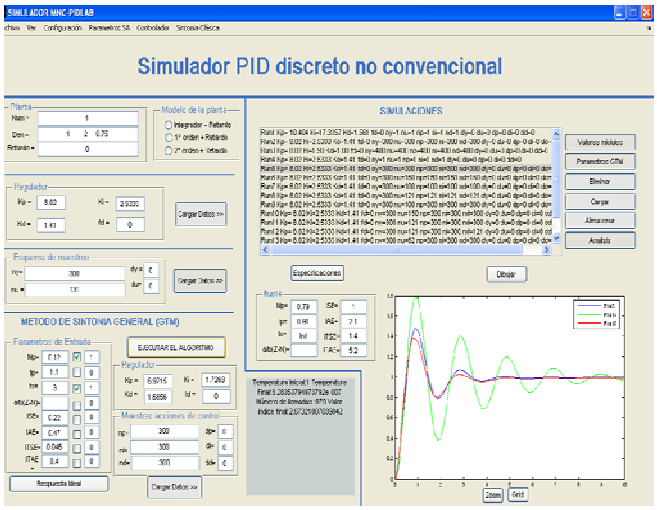

Figure 2: Input interface CACSD tool

Let us consider a unity-feedback control system with plant

$$G(s)=\frac{1}{s^2+2\cdot s+0.75}$$

Using the classical Ziegler-Nichols tuning a continuous parallel PID with the following parameters is obtained: K_p=10.404, K_i=17.3357 and K_d=1.561.

If the controller is replaced by a digital PID one has to be aware that a sampling period of T=0.35 sec. makes the closed loop unstable. From this point we deal with three different situations:

S1. (SR) Using a single period T, at which the closed loop system becomes unstable.
S2. (MR) With different period for the error than for the control.
S3. (Non-uniform MR) It is also possible to simulate the so called non conventional sampled systems in which the samples are not uniformly taken within the frame period.

The aim in all of them is to obtain new parameters of the controller for satisfying the following performance requirements: a maximum overshoot M_p = 40% at t_p<=1 sec. and a settling time t_s(2%)<5 sec.

4.1. Single-Rate PID tuning (S1)

Let $Tu = Ty = 350$ ms. Running GTM new gains K_p, K_i and K_d are obtained and shown in Table 2.

The closed loop step response is shown in Fig. 3, where the dash-dotted line is the response with the gains in the continuous case (unstable) and the dotted line is the desired performance. After the new tuning the requirements are satisfied again, as the solid line shows.

In addition, the evolution of K_p, K_i and K_d as the algorithm runs is depicted in Fig. 4.

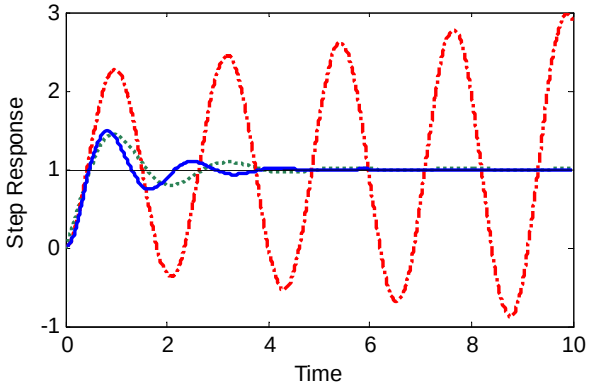

Figure 3: System response single-rate with T=1 ms. (dashed), T=350 ms. (dotted), T=350ms. after apply GTM (solid)

In order to be successful with the SA algorithm, the temporal annealing strategy that is followed, i.e., the simulated temperature profile, is important to be suitable. The rate at which the simulated temperature is decreased depends on the weighting coefficient λ. If it is too high a simulated cooling rate leads to non-minimum energy solutions, whereas a too low a cooling rate leads to excessively long computation times. The closer the value of λ is to unity, the slower the simulated temperature decreases. In order to achieve effective exploration of the search space, we recommend to use $0.85<\lambda<0.95$. In this example we set $\lambda=0.9$.

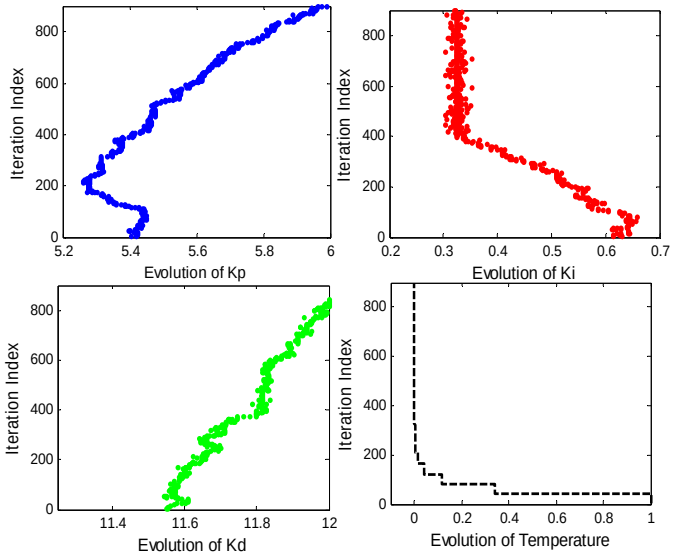

Figure 4: Evolution of the parameters of the PID controller and the Temperature as a function of the iteration index

With successive decreases in the simulated temperature the algorithm converges after 800 iterations.

4.2. Multi-Rate PID tuning (S2)

Two cases are tested where the input (error) rate and the output (control) rate are different.

Let us assume that the largest sampling period found in the closed loop system is small enough to satisfy the requirements using single-rate control. Following with the example, such a period is 0.35 sec. and different MR situations are tested.

With the tool it is possible to see the effect of varying the sampling periods on the closed loop step response. In addition, it shows which is the period with the worst performance and a measure of such deviation.

In order to analyze all the MR possible cases with $T_u<T_y$ we are used the tool as shown in Fig. 5.

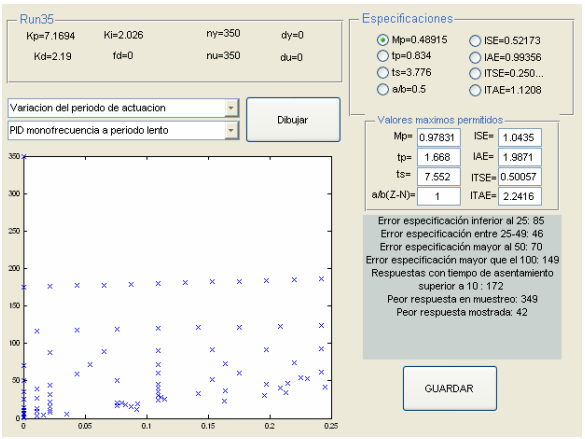

Figure 5: Input interface EP (evaluate periods)

This example shows how GTM attains a stable closed loop step response as well as the requirements for one of the worst case, which occur at T_u=131 ms. (S2-CASE I). The algorithm GTM is applied after checking the lost of specifications assuming the classical PID controller placed in the MR loop and design specifications are achieved (see Fig. 6).

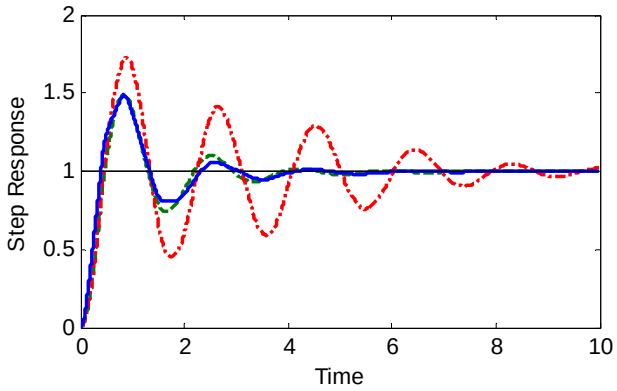

Figure 6: System response SR with T=350 ms. (dashed), versus S2-CASE I PIDSR (dotted), PIDMR after apply GTM (solid)

Let us consider another MR situation in which period T_y, used for taking samples of the control variable is smaller than the period T_u, used to modify the controlled variable.

Using the tool shows in Fig.5 we can identify different periods with lost of specifications, we select one, T_y=131 ms. (S2-CASE II). Again, design specifications are achieved (see Fig. 7) after application of GTM.

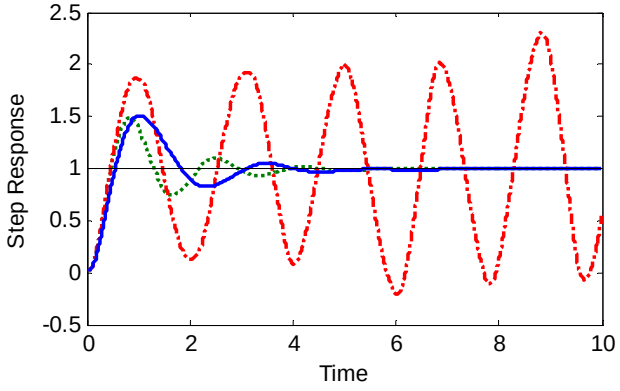

Figure 7: System response SR with T=350 ms. (dashed), versus S2-CASE II PIDSR (dotted), PIDMR after apply GTM (solid)

4.3. Non-uniform Multi-Rate PID tuning (S3)

Non-uniformly sampled-data systems are characterized by the fact that both the control updating instants and the sampling instants need not to be equally spaced in time. For conventional discrete-time systems, the periods of the zero-order hold and the sampler are the same and equal to h; for non-uniformly periodically sampled multirate systems, the updating or sampling intervals are $\{\tau_1, \tau_2, \ldots, \tau_p\}$. In other words, sampling takes place at time $\{t = kT + t_i : k = 0, 1, 2, \ldots, i = 1, 2, \ldots, p\}$, where $t_i = \tau_1 + \tau_2 + \ldots + \tau_i$ (let $t_0 = 0$), $t_{i+1} = \tau_1+\tau_2+ \ldots +\tau_{i+1}$, in the period of k: $[kT, (k+1)T]$, the

controlled input non-uniformly updates at time $t = kT + t_i$ ($i = 1, 2, \ldots, p$).

We will simulate the last situations of our example to demonstrate the effectiveness of the proposed algorithm in which the controlled input updates is chosen as τ_1=0.1 sec. y τ_2=0.60 sec.(S3-CASE I) leading to the use of a non-sampling scheme T_u={100 ms.,60 ms.} with T_y=350 ms.

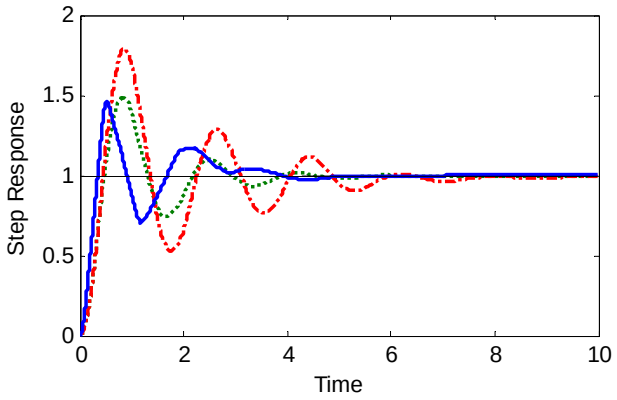

Figure 8: System response SR with T=350 ms. (dashed), versus S3-CASE I PIDSR (dotted), PIDMR after apply GTM (solid)

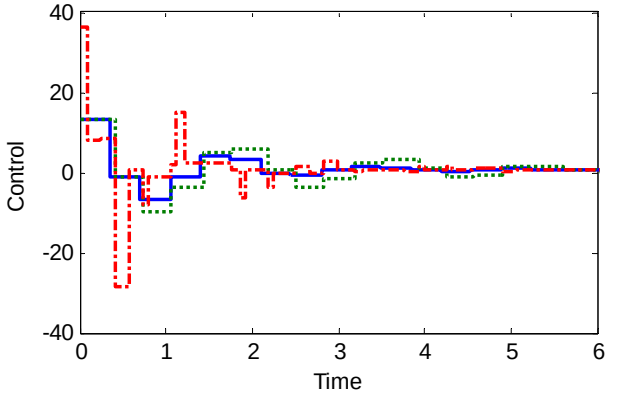

Figure 9: Control action SR with T=350 ms. (dashed), versus S3-CASE I PIDSR (dotted), PIDMR after apply GTM (solid)

Similarly, the output is non-uniformly samples for 3 sampling periods T_y={35 ms., 95 ms., 100 ms.} with T_u=350 ms. (S3-CASE II).

In both cases there is a loss of specifications in the control loop that will be restored thanks to the algorithm GTM that is presented.

After using GTM, all situation cases generate the parameters of PIDMF as a result which satisfies the specifications required. The results of the tuning experiments have been shown in Tables 1 and 2.

Table 1: Control and Error sampling periods

Case	T_y	T_u
S1	0.35	0.35
S2-CASE I	0.131	0.35
S2-CASE II	0.35	0.105
S3-CASE I	0.35	0.1 0.06
S3-CASE II	0.035 0.095 0.1	0.35

Table 2: Parameters of the controller (T_{prop} =0.35)

Case	K_p	K_i	K_d	T_{int}	T_{der}
S1	7.1694	2.026	2.1921	0.35	0.35
S2-CASE I	7.8542	2.4949	2.2389	0.35	0.131
S2-CASE II	7.4888	2.3533	2.4022	0.02	0.105
S3-CASE I	7.6996	2.9322	2.8524	0.02	0.1
S3-CASE II	6.2293	2.184	1.1297	0.035	0.1

In all of the situations, after applying the algorithm the performance requirements are achieved.

5. CONCLUSIONS

In this paper, a systematic way to tune multi-rate PID control is presented. Simulated Annealing method is appropriate to this problem because of the number of parameters, the constraints on the feasible values (some are real and some integer), and the different performance requirements to be attained.

We present a CACSD tool that carries out the whole process. In addition it allows the generalization to non-conventional sampling schemes.

6. REFERENCES

Araki, M. and Yamamoto, K., 1986. Multivariable multirate sampled-data systems: State-space description, transfer characteristics and Nyquist criterion. Institute of Electrical and Electronics Engineers. Transactions on Automatic Control. vAC-31 i2. 145-154.

Bamieh, B., Pearson, J. B., Francis, B. A. and Tannenbaum, A., 1991. A lifting technique for linear periodic systems with applications to sampled-data control. Syst. Control Lett., vol. 17, pp. 79–88.

Cuesta, A., Grau, L. and López, I., 2007. PID control under sampling period constrains. Research in Computer Science, vol. 31, pp. 63-72.

Kirkpatrick, S., Jr., C. G., and Vecchi, M.,1983. Optimization by simulated annealing. *Science*, 220.

Kranc, G. M., 1957. Compensation of an error-sampled system by a multirate controller. Trans. AIEE, pt. II, vol. 6, pp. 149–155, 1957.

López, I. and Cerezo, Y., 2007. Some practical aspects about performance and tuning of the multirate discrete PID controller. *Proc. of the 15th Mediterranean Conference on Control and Automation*, Atenas (Grecia).

Metropolis, N., Rosenbluth, A. W., Rosenbluth, M. N. and Teller, A. H., 1953. Equation of State Calculations bv Fast Computing Machines. The

Journal of Chemical Physics, vol. 21, (6), pp. 1087-1092.
Mitra, B., Jha, S. and Choudhurl, P.P., 1991. A simulated annealing based state assignment approach for control synthesis. *Proc. of the IEEE International Symposium on VLSI Design*, pp. 45-50.
Sala, A. et al., 2009. A retunable PID multi-rate controller for a networked control system, *Inform. Sci.*
Salt, J. and Albertos, P., 2005. Model-based multirate controllers design. *IEEE Transactions on Control Systems Technology*, vol. 13, no. 6, pp.988–997.
Salt, J., Cuenca, A., Casanova, V. and Mascaros, V., 2006. A PID dual rate controller implementation over a networked control system. *IEEE International Conference on Control Applications* 1343–1349.
Thompson, P.M., 1986. Gain and phase margins of multirate sampled-data feedback systems. *Int. J. Control*. vol. 44, no. 3, pp.833-846, 1986.

AUTHORS BIOGRAPHY

Y. Cerezo received her B.Sc. and M.Sc. degree in Mathematics at Universidad Complutense, and her M.Ph. degree in Computer Engineering at UNED, in Spain. Currently, she is developing her doctorate thesis in the Department of Communication and Control Systems at UNED. She is an Assistant Professor in Mathematics at Universidad Francisco de Vitoria in Madrid. She has presented research papers in relevant international scientific conferences. Her current research interests include Sampled-data systems, Multi-rate and Non-conventional control systems, Simulated Annealing as well as Numerical analysis and techniques.

A. Cuesta received his M.Sc. in Physics at Universidad Complutense of Madrid and his Ph.D. in Computer Engineering at UNED University, in Spain. He has served as visiting faculty at University of New Mexico and Real Colegio Complutense in Harvard. He is Assistant Professor in Computer Science at Felipe II College in Aranjuez, Spain. He is a member of the research teamwork DOSI (Design and Optimization of Computing Systems) funded by Universidad Complutense as well as a researcher of the I4 Institute Interligare for Innovation in Intelligence. His interests range over Probabilistic Robust Control, Copula functions, Evolutionary Algorithms, Support Vector Machines and other Machine Learning techniques.

I. López received his M.Sc. and Ph.D. in Physics at UNED, Spain. He is Associate Professor in the Department of Communication and Control Systems in the Faculty of Computer Engineering at UNED. His teaching subjects are Automatics, Electronics and Computing. He has numerous publications and conferences in relevant international congresses. He has also developed applications to the industry as result of his background as a senior researcher in both private and public funding projects. His main research interests are Digital control, Tuning and Auto-tuning control and Non-conventional control systems together with Databases, Real-time system and Dynamic web applications related to computing.

L. Grau received his M.Sc. and Ph.D. in Physics at Universidad Complutense of Madrid and UNED respectively. He is an Associate Professor in the Department of Communication and Control Systems in the Faculty of Computer Engineering at UNED. He has participated in numerous public and private funding research projects as well as international conferences. His main research is focused on Digital control, Tuning and Auto-tuning control and Non-conventional control system. In computing science his expertise ranges over Databases, Server-side technology and Development of dynamic webs.

CONSCIENCE SIMULATION

Tudor Niculiu [(a)], Maria Niculiu [(b)]

[(a)] University *Politehnica* Bucharest
[(b)] University Bucharest

[(a)] tudor-razvan@ieee.org, [(b)] mariaoficialfac@yahoo.com

ABSTRACT
Conscience simulation demands transcending from computability to simulability by an intensive effort on extensive research, to integrate essential mathematical and physical knowledge guided by philosophical goals. A way to begin is hierarchical simulation. Coexistent interdependent hierarchies structure the universe of models for complex systems, e.g., hardware - software ones. They belong to different hierarchy types, defined by simulation abstraction levels, autonomous modules, classes, symbols, and knowledge abstractions. Applying *Divide et Impera et Intellige* to hierarchy types reveals their importance for intelligent simulation. The power of abstraction is the real measure for the human mind. Turning abstraction into comprehensive construction could be the aim of humanity, the unique God for different cultures of free humans. The way to freedom is by understanding necessity. We have to recall our conscience, to reintegrate our mind, and to remember that society has to assist humans to live among humans. Simulation relates function and structure.

Keywords: Intelligence, Faith, Conscience, Abstraction.

1. INTRODUCTION

To begin was the word. Words enable us to express ourselves, to be humans among humans. The expression is complex, so it has to be hierarchical in order to be comprehensible.

Words are sequences of letters, sentences are sequences of words, and texts are sequences of sentences. Phrases, paragraphs, subchapters, chapters, volumes, etc can enrich the levels of the textual hierarchy. The hierarchy is not necessary linear. The basic hierarchical type is tree-like, to optimally represent the generic strategy of *Divide et Impera et Intellige*, or even graph-like, in order not to constrain the links between levels. The sequence is an ordered set, i.e., a function that applies the first n natural numbers on M: $seq \in IN_n \rightarrow M$, $IN_n = \{i \in IN | \ 1 \leq i \leq n\}$. If n is finite, it is the number of sequence elements. *Class*, *concept*, *term* are aspects (syntax, semantics, pragmatics) of the expression. Class is a primitive notion. Set is a class that belongs to another class. The set operations are paradigmatic: serial ($\cup$), parallel ($\times$), and hierarchical ($\wp$ - set of all parts).

The possible expressions form a *language*. Syntax, semantics, and pragmatics define any language; the rules of each of the former defining components refer, respectively, to correct construction, interpretation, and application. The syntax is determined grammatically: grammars are of different types that can build a hierarchy that corresponds to the reciprocal inclusion of the defined languages. Grammar is a language that refers to the language that grammar defines, i.e., is beyond the defined language – a metalanguage. This is another hierarchy type than modularization (of a text) or inclusion (of the languages due to the stronger rules of the defining grammar). Its definition is based upon the principle that each level is a metalevel of its inferior ones. Further, the language can be symbolic, and symbols can symbolize other symbols, what reveals another hierarchy type. We classified, we symbolized, we divided into modules, and we reflected an inferior level (language) on a higher one (grammar). Grammar is a language, so it has a grammar, which, if isomorphic to the initial grammar or to the language itself, would mean that we obtained a reflexive language, i.e., capable to express itself. Classes, symbols, and modules permit the construction of a *system* that structurally implements a function expressed in a language, i.e., behavior. In the same way, with classes, symbols, and modules, the behavior of a structurally described system can be determined. Another hierarchy type orders the variety of languages that describe the function and the structure, the simulation hierarchy. It assists passing from the goal function, constrained by functional parameters, to the structural form, and the inverse transformation that determines the mathematical function or the physical behavior of a system characterized by structural properties (Niculiu 2008).

Researching intelligence by simulating it, to enable intelligent simulation, demands the study of combined essential mathematical structures (algebra, order, topology), to understand the different hierarchy/ abstraction types. As it is a hierarchical relation between static and dynamic structures, and even between structural and functional, the simulation can contribute essentially to understand the human mind.

As in any dichotomy, *Intelligence* and *Faith* can converge toward integration, or can destroy one another if not associated. *Conscience* is the link between them.

Function is a mathematically formalized, or a physically as temporal behavior instantiated transformation, f∈Domain→Codomain. *Structure* is a set of properties that characterize a mathematical or physical space. The properties can be constant or variable in time, reflecting static or dynamic structures. *Simulation* is the relation between function and structure. Structured set = (Set, structure). *Model* results from an inversion able representation of the simulation object. *Language/ System* are a generic form of a mathematical/ physical model. *Abstraction* is a human defining capacity that enables him to think. *Hierarchy* is a functional/ structural concept that fulfils mathematically/ physically the concept of abstraction. Hierarchy = syntax (abstraction). To prevent the danger of dichotomy, we concentrate in three different ways on the unique Reality (*Plato*): *Art for the art* - to look for the essential Way, *Science with God's fear* - to search the existential Truth, and *Engineering-technology* - to understand the Being and to concentrate more on the Spirit in our Life.

2. ABSTRACTION (HIERARCHY, REFLEXIVITY)

The power to abstract is the crucial difference between human and any other natural being. *Divide et Impera et Intellige* applies the hierarchical expressed abstraction. The abstraction can be simplifying or reflexive. The simplifying abstraction concentrates on a superior level the information that is considered essential for the current simulation approach. Reducing the informational complexity has in view to clear the operation and to ease its formalism; it can be only quantitative, but also qualitative, i.e., it can affect the simulability of different aspects of the simulation object. The reflexive abstraction expressed as the knowledge hierarchy type tries to self understand better on each superior level, better understanding more of the inferior levels.

We extend the reconfigurability to the simulation itself. First, by a self-aware simulation, we get self-control of the simulation process. Therefore, we build a knowledge hierarchy corresponding to the simulation hierarchy. Then, by expressing both simulation and knowledge hierarchies in the reference system of the basic hierarchy types (classes, symbols, modules), we create the context for a self-organization of the simulation. The triad of the basic hierarchy types corresponds to the fundamental partition of the real life (arts for beauty, science for truth, and engineering for good). This partition has to be continuously integrated by *philosophy* into (essence, existence, being). Therefore, we try to model the Conscience for simulating the Intelligence, and then to reach for intelligent simulation. Arts and science are equally noble, even if one appears rather spiritual and the other rather material. Their alliance is vital and demonstrates the insolvability of the nowadays *Spirit-Matter dichotomy*, and of all resulted secondary dichotomies, actually functionally generated by the *Space-Time dichotomy* that is necessary to the human *evolution*.

The *society* is only the memory of the past, the manager of the present problems, and the assurance for a right future. We have to live together in respect of the others on the way to understand each other, in order to evolve toward essential beings for an integrated existence. *Human among humans* should reflect a strategic equilibrium, without hiding or even violating, as happens nowadays, the principle that the society has to assist the individual: to educate him/her correctly, enough and unconditioned, and to help her/him by an intelligent Faith to search and research the Unknown. The Unknown can be interpreted as a *unique God* that represents the absolute freedom by understanding all the necessities, and the absolute unity by closing all the *Divide et Impera et Intellige* necessary to the Way to look for the Truth along the Life.

Reason is an extension of the Nature. Nature is not an ephemeral context, but the matter we are built of in order to develop spiritually. The integration experiments for the Spirit-Matter dichotomy failed because of their extremism. The present society is extremely materialistic, and tries to destroy every trace of ideal. We have to surpass the limits imposed by the essential dichotomy by a unique Ideal, named God, that should be constructive by continuous intelligent reconfiguration. The most benign social system is not democracy, if the education for any human is not granted. The election system should be hierarchical, and the temporary separation of the power should be correct and complete, to result in autonomous strategy, tactics, and constructive critics. Hierarchical democracy should rise like trees, and society has to be understandable and reasonable.

Einstweilen bis den Bau der Welt Philosophie zusammenhält, erhält sich das Getriebe durch Hunger, Furcht und Liebe

Friedrich Schiller

3. HIERARCHICAL SIMULATION

Hierarchical types are stratified structures. The levels represent different domains (abstract or concrete). Abstraction links the different autonomous levels inducing an order relation (partial – with respect to the objects, total – for the levels), what permits to consider superior and inferior levels (lattice). The hierarchical principle can be applied both to the knowledge and to the simulation, in order to maintain correctness when the complexity is rising. The decomposition of the problem on more abstraction levels helps to bind locally the complexity. The systematic design that results from the hierarchical approach assures an almost correctness by construction; the complex verification/ optimization becomes less hard and more understandable. For complex systems, coexistent and mutually independent hierarchical structures have to be considered. The *theory of categories* can formalize object-oriented expressed, symbolically interpreted, and structurally approached multihierarchical representation.

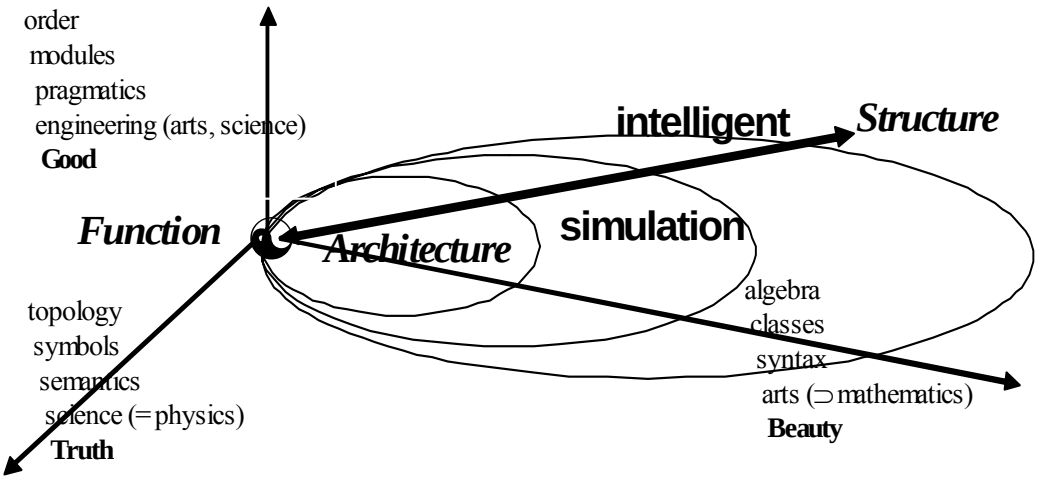

Figure 1 Extended H-diagram

Faith and Intelligence are ☯ in our Life. (Way, Truth, Life)

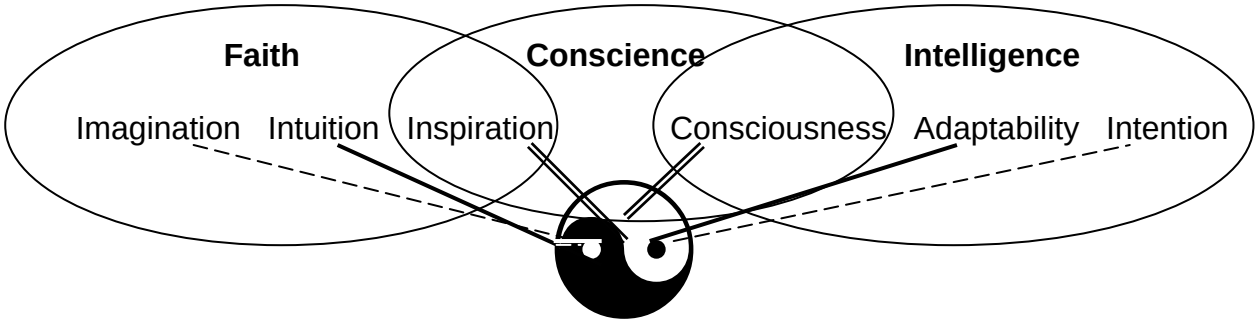

Figure 2 Model for the human mind

Yin-Yang represents the absolute functionality and the waves are increasingly structured hierarchy levels

The relations of a hierarchical type are intralevel, determining the mathematical structure of a level, and interlevel, formalizing the abstraction that links different abstraction levels in hierarchies. Beyond the hierarchical view, the system can globalize, composing the intra- and interlevel relations to a unified structure; normally, it becomes an autonomous level in a superior hierarchy. The abstraction induces a partial order on a hierarchical structure, which nuances the total order, and defines complementary hierarchical strategies: top-down: the lower level operations are constrained by the results of the higher level ones, however, not univocally as hierarchical descending eliminates some freedom degrees, and bottom-up: lower level consistent parts constitute initial conditions for superior operations, and the parts abstracted to one object get compatible by attribute elimination. *Hierarchy types* (concepts, symbols, modules) correspond to (syntax, semantics, pragmatics) of the hierarchical language that expresses the intelligent simulation. *Intelligent simulation* results by integration in the *hierarchical simulation* of the associated knowledge hierarchy, which represents a reflexive abstraction that converges to self-awareness of the adaptable intentional simulation.

The absolute functionality is symbolized by *yin-yang*, while the waves suggest hierarchical levels that are increasingly structured for simulation and knowledge (Fig. 1). Hierarchy consists of a net that can represent any type of mathematical structure (algebraic, topological, order). The different hierarchy types correspond to the kind of abstraction they reflect↑: class hierarchy (↑concepts), symbol hierarchy (↑metaphors), module hierarchy (↑strategies), construction hierarchy (↑simulation), and knowledge/ consciousness hierarchy (↑theory) ↔ reflexive abstraction, each level aiming to know all inferior levels, including itself; it is the first step to model the Conscience. The hierarchical types are objects of equivalent categories (functorial isomorphic) that formally represent hierarchy types. The consciousness hierarchy type communicates to the other hierarchy types by countervariant functors, while covariant ones connect the others. The basic hierarchy types (classes, symbols, modules) correspond to (syntax, semantics, pragmatics) of the hierarchical language that has to express the intelligent simulation. Intelligent simulation results from the integration of the simulation hierarchy with its knowledge counterpart that represents a reflexive abstraction converging to self-consciousness of the intended adaptable simulation.

4. DIVIDE ET IMPERA ET INTELLIGE

Philosophy is not a specialty but a human right. There have to be schools to prepare the teachers of philosophy for the other humans. These schools have to develop also respect for those that look for the Way on one of the three alternative paths that correspond to the fundamental partition (arts, science, engineering). Because recently the essential *Divide et Impera* does not *Intellige*, the only philosophers are the masters in: Arts – especially mathematicians, and others that, aware or not, compose mathematically; Science – physicists, and those that do not forget their science is a chapter of physics; Engineering – e.g., those working in domains that attain the limits of the pure Reason.

Mathematics is one of the arts. The music is at least as beautiful and expressive, but mathematics does not demand an extraordinary talent, allows a reasonable dialog about it, and has well-defined reconfigurable limits of that it is aware. Mathematics has to be educated as soon as possible and has not to be confounded with its handcraft. The music gets more often out of its character. Anyway, the two arts evolved together: *Bach*, *Vivaldi*, and *Haydn* were musically gifted mathematicians, who preferred the liberty of the music to the bands of the Reason. The Reason, as initial zone, makes mathematics more sure but less charming than the other arts that can refer directly to the Reality: music and literature. The visual arts are too dependent of the Nature because seeing is the most used sense for the human natural being. The mathematics school is continuous, whereby the literature and the music can generate sooner higher singular peaks: *Shakespeare*, *Beethoven*. Arts are free. But mathematics first expressed reasonably that Reality could only be known by Reason (vanLeeuwen 1990).

Physics is the Science. The other natural/ social sciences are its chapters, even if they are not yet aware of it, or just try to return to their riverbed by intermediary specialties instead of integrative bridges (Penrose 2004). Physics is essential for the constructive reconfiguration of the Faith.

As any artificial system, the society is structured on natural bases, and it develops by natural laws. While the modern age, these laws were forced towards Reason, and recently they got out of control. The social laws got also unreasonable - in the bad sense.

Engineering is most frequently both art and science, and is as important as arts and sciences in the fundamental partition of the Reality needed for evolution. However, it is more dangerous than its alternative approaches, of which it has to be strictly bridled. Reasons are twofold: its result, i.e., technology, is defined by its complement, i.e., is not superior to this; it does not impose spiritual proximity between the creator and the user, therefore it can be applied in a complete different scope than it was generated. However, any engineering is the homonymous complement of a special science that collaborates with mathematics. This problem is solved if the sciences are integrated into physics and mathematics remains an art.

To go further, thinking while advancing, we divide twofold, as we cannot yet *Intellige* the dichotomies: Spirit-Matter (force-substrate, software-hardware) $\Rightarrow$ real-natural (continuous-discrete, analog-digital), form-contents (class-function, category-functor, representation-simulation, structure-function), perspective-profoundness, real-possible, true-false, beauty-truth (arts-science, mathematics-physics) $\Leftarrow$ Space-Time (evolution). Clearly, there should be no balance in most of the dichotomies. ☯ can represent by rotation any of them. *Faith* = Inspiration × Intuition × Imagination and *Intelligence* = Consciousness × Adaptability × Intention are complementary parts of the human mind, separated and linked by *Conscience* = Consciousness × Inspiration

The nondeterministically separated complementary pairs are alike functionally structured (interface, kernel, complement's ambassador). The model was not randomly selected: three tangent circles emphasizing the centers of the inner ones form it, retaining the essence of a dichotomy symbol that suggests a complete integration of the parts without loss of autonomy, realized by vicinity and pointing one to another. The Chinese symbol reflects the importance of something else, reminding of *creation as love for something else*. Three circles, each tangent to the others, models *a partition of something to be understood in order to get further*, says the center of Europe. Circle is *cerc* only in our Latin mother tongue, a perfect expression: *Cer* (sky) is the infinite, *cerc* is the finite representation of the infinite, by the permanent link from the (never) begin to the (never) end. π is the most famous real number (*Pythagoras*, PhD). *Cerc* means perfection, which we permanently desire, therefore there exist integer numbers, having a perfect and beautiful theory, but not forgetting to continue the evolution searching and researching further. The western Europeans attain *research*/ *rechercher* by recursive *search*/ *chercher*. Our Romanian language helps us to approach this by *cercetare*. The religion had to learn us about God's existence in our being. The philosophy has to learn us about essence, existence, and being. Our conscience is our representation of the essence of our existence as being; so it tells us that God is in ourselves, for ourselves, and among ourselves. Further, we have to be in order to search our essence researching our existence.

Doamne, Doamne, caută din Cer, şi vezi şi cercetează
Via aceasta, pe care a sădit-o Dreapta Ta,
şi o desavârşeşte pre ea (în veci)
Pantocrator ortodox

5. INTELLIGENCE. FAITH. CONSCIENCE

Divide et Impera et Intellige has 3 parts as *alle guten Dinge sind 3* of the most philosophic European people. Mathematics develops by 3 basic structure types, integrating them. We divide our Universe in 3 worlds: essence, existence, and being. We divide our being in 3 interdependent components: arts, science, engineering;

they correspond to our beauty-loving ideas, our truth-searching efforts, and our good-oriented constructions. The third part is presently exaggerated to exclusivity. As the Reality contains abstract ideas, even if physics could explain everything as being discrete, the power of continuum cannot be forgotten. Consequently, the analog engineering cannot be neglected in modeling and simulation. Physics permanently uses as dichotomy the discrete-continuous, while the engineering-technology just adapts intuitively (as any primitive life form) to the requests of a consumption-oriented society - characteristic for the primitive life. The reason for this is that presently the engineering escaped from the control of the inspiring arts, and of the Consciousness for the science that conditions its existence.

Mathematics is the most accessible of the arts, science of the abstract ideas, and engineering of the Beauty. It discovers and studies structure types: (algebra, topology, order) that correspond to (construction, orientation, understanding). Mathematics is an example to science and engineering of correct and complete integration. *Arts for the arts* is a self-definition, the liberty to create Beauty, by thesis-antithesis-synthesis, dialectic principle that governs through evolution by closure to the inverse.

Physics is the paradigmatic science, the art to represent the Nature - as exercise for the Reality, the engineering of the Truth. It has to integrate the fundamental forces in a theory, and all natural and social sciences as chapters, leading them to a real application of mathematics. Social sciences study a universe as complex and nondeterministic as the natural one, therefore mathematics is at least as important. Recognizing the physics as the fundamental science, mathematics could be more directly inspired by the sciences. The science raises the fear of unknown, and the research inspired by it, to zones that are more abstract. It is hierarchically defined, *with God's Fear*, looking for the Truth. The science evolution bases on *qualitative leap consequent to consistent and convergent quantitative accumulation*.

Engineering (art of construction, science of simulation, technology of Good) should develop closer to mathematics (approach, integration of parts, not only applying techniques), and to science (courage, multiple perspectives, not only regarding the results). Concentrating exclusively to the Good in the life is very dangerous, as the third part of Reality, also called *mental world*, is defined by its complement, and therefore is not superior to it if not closely constrained by Arts and Science. *Denying the negation* is not a context-free game.

For physical or philosophical orientation, we need *cardinal points*. To inspire ourselves of the most pure of the arts, we learn about *cardinal numbers* - although, being sincere, mathematics leads the way to show that nothing is pure, so without leaving anything behind, the Way has to be followed further.

Cardinal numbers are numbers of elements in a set. The Nature demands the least infinity and is defined by (0, successor, induction); card (IN) = $\aleph_0$. Adding is in Nature's definition. However, the inverse operation, subtraction, needs negative numbers. We close mathematically the Nature to an *integer* that opens the physics for recognizing the limits of the Reason (electrons), in the meanwhile, attracting marvelous engineering solutions for different technologies. Electronics is among the most advanced engineering sciences; therefore, it has to be practiced by the most conscient human beings. Recurrent addition is multiplication, a most important parameter for the Nature. Mathematics closes the integers to the multiplication inverse, defining the rational numbers. These are not more than the naturals, but we can do many useful things with the Reason, from strategy to computer.

So "what else do we need?" say too many, forgetting that the limits of the, so-called, *pure Reason* are caused by the fact that it bounds itself to close the Adaptability to discrete/ sequential operations. Thanks God, neither mathematicians, nor physicists accept all-happiness. They discover in three ways (order, algebra, and analysis) that assisted all of them to think together, the power of continuum and that of the patience. In this context, "mathematicians and physicists" means the theorem, natural laws, or even new approach discoverers, and more, the engineers that understand the essential of mathematics and of physics.

Mathêma = science; *Tekhnè* = arts; *Fisn* = nature, universe, world, landscape; (Greek).

We should not forget the third meaning of *cardinal*. It points to an unwise use of *Divide et Impera et Intellige* as a strategy called *when two fight, the third wins*. This means to intervene only when the fighting forces begin to get unbalanced, in favor of the less strong, to conquer all fighters. If the victory must be completed, both the pseudo-ally and the pseudo-enemy are firmly assisted, discretely or continuously, to loose control, because of all-(un)happiness. The 20th century is a too convincing example.

The *Ackermann-Peter* function - anticipated by the recursive functions hierarchy of *Gheorghe Sudan* – shows an intuitive model for discrete computability and the limits of discrete/ sequential computation. The primitive-recursive functions are obtained of some elementary operations of the set of natural functions with more natural variables by closure to composition and recurrence. The resulted model is not complete without a nonintuitive extension to denumerable-recursive functions (the link between function and equation is pure mathematical), as the APS function rises quicker than any primitive-recursive function. The recursive operation construction is very inspired, showing that the recurrent power rising is too complex. The inspiring example suggests the existence of an implicit link between the limits of the sequential/ discrete calculus: complexity and computability.

```
unsigned ack (unsigned n, unsigned x) {
     return !n ?x+1 : !x ?ack(n-1,1)
                        :ack(n-1,ack(n,x-1));}
// ack rises with x (n = 1, 2, 3) +-like, *-like, exponentially
```

Presently, we talk about electronic computers, but the nowadays trend is to copy from the living Nature, i.e., the emulation of the advantages the living beings show to achieve unconsciously complex duties. The vanguard domains are biotechnology and computational intelligence. We understand well neither Life nor Intelligence, so it looks like *Der Zauberlehrling*. More important is that emulation is less human than simulation, so they should always develop in parallel, permanently exchanging experience.

The Reality does not reduce to Nature, as card (IN) is strictly inferior to card (IR). The Reason is the closure of the Nature relative to the primary operations, as IQ is the closure of IN to the inverse operations of addition and multiplication. However, the Reason is dense in Reality, as the real numbers are the analytical closure of the rational numbers i.e., $IR = \{\lim_{n\to\infty}(q_n) | (q_n) \in IN \to IQ\}$. The Reality extends beyond Nature and Reason, not just for the quality of the quantity, but also regarding the power of transforming operations. IR is the closure of IQ to (power rising)$^{-1}$ – the last arithmetic operation resulted by recurrence of the prior one, which can be pursued by Reason.

Further, the closure regarding the inclusion order – the set of all subsets of IN, $\mathbb{Z}$, or IQ, in general, of countable sets, is the uncountable set of real numbers. IR represents the power of continuum. To get from real to complex numbers is just a matter of Imagination. Reason closes the Nature to the inverse of natural operations. Reality is the closure of the Reason to the inverse of artificial operations, or to the reasonably deducted infinite, or to an order over the Being itself.

We know that if there were no cardinal number between the natural/ integer/ rational discrete and that of the real continuum, then the logic would include the principle of the excluded tierce, that, pure and simple, hurts the Human, who is fond of nuances. Therefore, we can prove that there is an intermediary level between Reason and Reality (*nonconstructive*). There are angels between Human and God said the wise. The density of Reason into Reality means that every real is the limit of a sequence of rationales. Therefore, we hear nowadays that if we master the Reason, Reality becomes a complexity problem, i.e., speed of convergence.

We dare use mathematics as metaphor for the relation between Nature and Reality, but it is only a correct inspiring analogy. IR is an initial step in mathematics for algebra, topology, order, or their collaboration. Mathematics is for Reality just one of the favorite ways to get the Human closer to it.

There were times of the Reason when mathematics was free, creating itself the necessities, and even if physics had sometimes to make the needs aware to mathematics, they both always followed the way to Reality.

Nowadays, there is no *Nobel* Prize for mathematics, only for its economical applications.

Nowadays, there exists no liberty by understood necessity, only by satisfied economical needs.

Nowadays, the Reason cannot reflect the Reality.

The density of IQ in IR shows that between any two real numbers there is a rational one. Therefore, Reality is much more than Reason can even imagine, but something reasonable exists between any two real objects (*nonintuitive*). Neither Intuition nor Reason arrives to something that mathematics proves elementary. As any true art or beautiful Science of the ideas or the phenomena, mathematics does not limit itself to either Intuition or Reason, allowing them to collaborate by Conscience.

We touched the "Mathematics-Physics" that the modern School considered alternative to Human. However, every human has to be hallowed with the unique strategy for consistent education, which does not reduce but amplifies the receptivity and imagination for any human work. The recent School replaces the alliance Beauty-Truth, in the most pure form, with an advertising name "Mathematics-Informatics", considering itself a part of the consumption society – the most efficient distracter of Spirit and of Human ever. Informatics is a first result of the collaboration Arts-Science-Engineering. It is very inspiring de jure, but very exploited de facto, for the grotesque materialistic exaggeration that all we need is good, and that engineering is the only creative activity. Hence, engineering deserves development in any direction, from spiritual toys for all ages to technological drugs, arms of any caliber included.

6. THE PURE REASON EXPERIMENT

The *Faith experiment* took place in the Middle Age by spiritual and chivalrous search, mediated by Masonic buildings. The Cathedrals were the symbol of the coming *revolutions* that intended to institute the constructive Faith as basis of the human society.

The society is conservative – it tries to last forever at any evolution level, using a common measure. Everything can be evaluated, although most of the essential things on that our existence bases its being are not measurable. The so-called pure Reason, i.e., the context-free Reason – most adaptable, conscious only for having, intended by the tactics of the consumption society, and totally unfaithful, gives the necessary force to stagnation or even to choosing a wrong way. Unfaithful means the components of the Faith are used separately to serve the competition for the Good that makes present Life credible.

However, the society is less than reasonable, whereby, the irrational of arts, particularly in mathematics, is more than reasonable, opening the way to Reality by closure to an essential and radical operation. To master the *New Power* of the continuum is beyond Intuition and Reason, if they do not integrate by Conscience and do not collaborate by Imagination and Intention. The historical experiment of the pure Reason was the necessary intellectual condition of the first, and by now – the last, social revolution. The initial goal of this event was a reintegration of the ways to search for the Spirit from the Matter (knights) and for the Matter from the Spirit (monks).

It failed because it kept the arms, the wars, and the social classes, against it had risen. More important, the experiment continued beyond its historical limits, what created the context to renounce to human dignity in order to reduce the human mind to adaptability and to throw Conscience and Faith into facultative. The reduction of the constructive thinking to pure Reason weakened the human mind and made possible to restrict the point of views to the most dangerous of them. The number of alternative paths, totally different but convergent to Reality, must be 3 – the last prime number successor of another prime.

The concentration of the mind on the reasonable control of the Adaptability followed the spiritual revolution, which tried to bring into individual and social conscience that the human has chosen the evolution without disregarding the Eternity or knowing the Way.

The spiritual revolution selected a primitive form of *Divide et Impera et Intellige*, to begin researching what is partially known, leaving the unknown to be approached when the first step is finished. If this intention is not forgotten, the *Intellige* is contained in the *Impera* of the unknown that has to begin after the *Impera* of the partial known, with the completed knowledge that results. This first step was done simultaneously by the institution that pretends to serve God - (*Luther*, the knight Popes), and by the most human Reality approach – the Arts (*Rinascimento*, *Descartes*). Their strategy was human-oriented.

The contradictory sentence "to serve God" had sense as long as the Church tried to simulate the human conscience. Perhaps was its partition thought as *Divide et Impera et Intellige* for the Way – Catholic, the Truth – Orthodox, and the Life – Evangelic, but there came no *Intellige*, and all of the alternatives fell into the exaggerating "-*ism*". Perhaps this is analogous for Christians searching a beautiful Way, Jews researching a true Truth, and Muslims engineering a good Life. But many of us, of any religion, and respecting the traditions, are conscious of the Way to follow, do not expect anything from a metareal God (sounds like material), and are free to laugh even of their deepest Faith. Moreover, they are able to have a good Life, just enough to concentrate on the Truth and to follow a beautiful Way. The concentration of the society on the material component of the human existence was necessary to liberate them of inhuman problems, not to attract the humans on secondary path. Antique Greece is an inspiring model (substituting slaves with intelligent systems).

The Reason experiment had to finish two centuries ago, when: the pure Reason experiment climaxed by an unprecedented number of contemporary geniuses. This proved that people has to select wisely and to construct in good understanding and courageously a society that encourages/ assists them to evolve beyond the attained peaks: *Beethoven*, *Mozart*, *Gauß*, *Cauchy*, *Fourier*, *Laplace*, *Goethe*, *Schiller*, *Franklin*, *Kant* or *Hegel*; the cathedral builders tried to extend their work at a continental scale, neglecting the people on the building area, whose culture did not concentrate on *to have* but godly simple on *to be*; *Napoleon*, a genius of the military and social strategy art, showed that a new social form, reasonable in his plans, can not be imposed by the force against the revolution had fought.

We note that a century after Napoleon Bonaparte, a German genius of strategy, Otto von Bismarck, learning from his predecessor's experience, was even more successful in unifying Europe. However, this time the materialistic forces were already masters of exploiting the instabilities, and hurried up to transform Europe in a laboratory to compromise any idealistic movement. They helped the generation of these movements and directed them to terrorism. As we said, the pure Reason experiment was of the form: complete the better-known part (Bonaparte) to its limits (Bismarck), to have more chances beyond the limits.

The falling and remaining in materialism hurt a lot both Nature and Human. The importance of the experiment was significant, but its continuation after the results could be interpreted has killed countless people and even cultures. Nowadays the materialism torments increasingly, threatening the future. The adaptability-based Reason cannot explain or control thoughts, even if sequential is extended to unlimited parallel/ nondeterministic (equivalent).

Anyway, these desired operational properties could be found mainly in the right Faith-oriented side of the mind. Further, the difference between continuous and nondeterministic sequential (unlimited parallelism) is positive. The Reason has to be Faith-dependent completed to Intelligence. A being needs more than Intuition and Adaptability to surpass the Matter by Spirit; only the integration of Intuition and Adaptability by Conscience can explain the Human being.

We propose a thesis derived of the evolution by closure to the inverse:

Conscience is the closure to (*knowledge* o *simulation*)$^{-1}$
of Conscience, initially: Conscience = Consciousness (1)

The idea can be formally sustained in the category theory. The essential limit of discrete computability, inherited by the computational intelligence, is generated by the necessity for self-reference to integrate the level knowledge with metalevel knowledge in Conscience modeling. A hierarchical type expressing reflexive abstraction can represent the conscient knowledge. The aspects of the Reality, and of the human mind reflecting it, have not to be neglected, although they are neither constructive nor intuitive (Hofstadter 1979).

A way from Reason to Intelligence is to integrate Consciousness and Intention, further Intelligence and Faith to become *Reality-aware*. Transforming abstraction into comprehensive construction can be the *Goal* of the Human among Humans, *unique God* for different cultures of free humans.

7. HUMAN AMONG HUMANS

We have to remind our conscience to integrate our mind. We have to remind ourselves that society has the duty to assist humans to live among humans. We have to stop society to be more important the Human. This is nowadays the case, and we are on the way to live in an aunt hill/ a swarm/ a herd/ a flock/ a stud, or even a pack/ a horde/ a crowd/ a mob. An operating system serves to the autonomous programs both as link to the hard as for development of the soft. Analogous, the minimal unconditioned tasks of the society are health and education for everyone, encouragement for culture and researching for any Human (= human with conscience). The history of the common measure is:

Philosophy, *Culture*, *Knowledge*, *Economics*, *Force* (2)

We could consider just the simplifying types of hierarchy (classes, symbols, modules) and then express the construction, hoping to aim the absolute liberty, if we considered God as the simplest, totally unconstrained, essence of the Reality. However, we can simulate/ construct/ work/ live, associating knowledge hierarchies to all our activities, aiming to constructive understanding of the most complex absolute necessity, by this defining God. Abstraction is the human gift for going beyond natural limits, meanwhile extending pure reason to real intelligence. Metaphor is a popular instance: we detail the metaphorical thesis:

God is the absolute abstraction
$\rightarrow$ *the evolution goal for faith-assisted intelligence* (3)

The Conscience is individual (link faith-intelligence), social (local-contextual relations), and universal (sense for Reality). It appeared by *Divide et Impera et Intellige* of the community conscience, proper to the eternity-oriented human structure. E.g., *in the past*: herders, farmers, sailors, Asians, Africans, Amerindians... Each one recognized him/herself in the cohabitants, being also adaptable and intuitive. The common measure evolution implies construction of intelligent agents to master the inferior levels and to concentrate on the higher ones. For example, industry enabled to mechanize agriculture preparing the concentration on the economy. However, the price was too big: Spirit and Nature were badly hurt, but less than their collaboration. Industry and army understand very well each other, instantiating the same principle of depersonalization of the human for a materialistic aim.

Evolution is a multiple *Divide et Impera et Intellige* for Conscience, associated to generation of the lacking *mind components*, then assisted by these:

- Conscience: individual-social-universal (4)
  (subjective-contextual-objective) $\rightarrow$ *inspiration* $\downarrow$
- Space-Time (structure-function)$\rightarrow$ *imagination* $\downarrow$
- Discrete-continuum (natural-real) $\rightarrow$ *intention* $\downarrow$
- Beauty-Truth-Good (arts-science-engineering).

A model template defines the model universe as a mathematical theory or as a simulation paradigm. Every entity has behavior (external relations) and structure (internal relations). Behavior is functional (context-free) or procedural (context-dependent). An algorithm is a computer simulable entity: it represents computability, behavior- (understanding, verification, learning) or structure-oriented (construction, design, plan).

simulation $\in$ Simulation $\subseteq$ Function $\times$ Structure $\Leftrightarrow$
Knowledge $\Leftarrow$ Intelligence :: information ();
Intention $\Leftarrow$ | Inspiration - Adaptability|; (5)
Imagination $\Leftarrow$ | Intuition - Consciousness|;
Adaptability $\Leftarrow$ simplifying_Abstraction (Imagination);
Consciousness $\Leftarrow$ reflexive_Abstraction (Intention).

The prior relations are too simplified to start toward the intelligent simulation. Although intuitive and hopefully inspired, to begin we neglect intuition and inspiration that are essential but too primitive for reasonable understanding.

We formalize reflexive abstraction by the knowledge hierarchy, and the simplifying abstraction by simulation hierarchy, coming to:

Consciousness = *knowledge* (*simulation* (
Consciousness)) (6)

The fixed-point relation suggests modeling consciousness by association of a knowledge level to every hierarchical level of the simulation process.

To solve the fixed-point problem we construct a metric space where (knowledge°simulation) is a contraction, i.e., the construction implied elements come closer progressively in the formal understanding of the formal construct.

Further, we will have to approach:

Consciousness = knowledge (intention (Inspiration, (7)
simulation (*imagination* (*Intuition*, *Consciousness*))))

Das schöne wahre Gute
Johann Wolfgang von Goethe

8. ETERNITY. INTELLIGENT EVOLUTION

Eternity means abstraction of time, from the point of view of human evolution. However, the humans that lived in eternity had not performed the space-temporal partition of the Reality. The knights searched for the Graal, the monks for supreme Spirit, and the shepherds the lost sheep. The knights counted their victories, the monks their rosaries, the shepherds their sheep, without considering this natural operation as essentially human. The algorithmic approach is equivalent to the formal one. If an expression of a formal system is true, there is an algorithm that can confirm it. Reciprocally, for a verification algorithm of the mathematical sentences, a formal system can be defined, that considers true just those expressions in the closure of the algorithm results set to the considered logic operations.

The best known (equivalent) formalisms for sequential computability based on pure reason are: formal axiomatic systems (*David Hilbert*), construction algorithms (*Kurt Gödel*), λ-calculus (*Alonzo Church*), recursive functions (*Stephan Cole Kleene*), *Emil Post* combinatorial algorithms, *Alan Turing* machines, formal languages (*Noam Chomsky* - grammars), and normal algorithms (*Aleksamdrî Markov* Jr.). These wonderful men initiated a revival of the pure Reason experiment, aware of its scope. This was possible because the arts – especially mathematics, the physics-based sciences, as the mathematics-inspired and physics-assisted engineering-activities evolved independently of the social order, due to the intelligent faith of their masters and of the free humans that developed and understood them.

Calculus = little stone; *Ingenue* = free minded; *Ratio* = number, account. (Latin)

The evolving Intelligence is the faculty to transform (analyze/ synthesize/ modify) abstract/ natural/ artificial objects, and representations in the world of (arts, sciences, engineering-technology), especially hierarchical and reflexive: ideas about ideas, and how to come to ideas; objects to transform objects; representations of representations, and how to build/ understand representations. Evolution depends on the initial design of the mental faculties for surviving of the whole system, however also on the space-time context of communication among intelligent agents. The alternative ways to extend the computability concept are suggested in works of the philosophical German literature. The essential ideas point the unconscious part of the mind, concentrating on: the mental world of the Good – managed technologically, the physical world of the Truth – researched scientifically, and the ideal world of the Beauty – discovered by arts: Faust (*Goethe*): heuristics - risk competence for performance, based on imagination; Das Glasperlenspiel (*Hermann Hesse*): natural unlimited parallel/ nondeterministic- intuitive; Der Zauberberg (*Thomas Mann*): self-referential knowledge - needs hierarchical reconciliation of discrete with continuous reaction, hoping to inspire the Way to Reality.

Mathematics is in all alternative ways and in all the worlds supporting our presence in the unique World: algebra combines for Beauty, topology searches the Truth, and order emphasizes the Good: *David Hilbert* spaces ground the behavioral model for quantum physics, more precisely, the part that is independent of any concrete intervention (in the world of abstractions). The link to the complementary part of the model, representing the interface to the physical world, can not be algorithmically expressed, what suggests that the model is not correct in the Reality. *Stefan Banach* algebra introduce, additional to the topological vector spaces, a commutative multiplication that, by an adequate transformation, results in a commutative functional composition, eliminating one of the most important constraints in a classical sequential model.

Inductive limits direct the convergence of hierarchical types, enabling the compatibility of partial simulations and contributing to the correctness by construction of the design. Reflexive topological vector spaces contain the necessary ingredients for the representation of the Conscience, by reflecting the adaptability in the variability of the space dimensions. Self-adjoint operators and eigenvalues/-vectors assist the knowledge concentration/ stability. Fixed points can help to formalize the simulation goal. Inseparable spaces can instrument the understanding of inspiration and intuition. An analog computability and an integrated mathematical physical comprehensible modeling are promising ways (*Intellige* of the three approaches). Simulability is "computability" using the power of continuum: analog electronics, metaphorical thinking, and unrestricted mathematics. Measurability, e.g., (*Henri*) *Lebesgue*, is a way to formalize simulability.

Nichts ist mir wichtiger auf dieser Welt als mehr von Gottes Gedanken zu wissen Albert Einstein

CONCLUSIONS

- Simulability demands explicit formalization of the knowledge hierarchy in the formal system frame. Inference is the discrete strategy of intelligence to advance in knowledge. The monotonous inference means conclusion conservation when new hypotheses are added. The daily, scientific, engineering inference is not monotonous; therefore, the prior conclusions must be revised when knowledge enriches. Mathematics grounds any inference form by adequate formalism. Informatics is the mathematics of the algorithmic information processing. Intellectics is the mathematics of intelligence based on that of knowledge that is built around knowledge representation.
- Intelligence simulation designates the project to understand and technologically implement hardware-software a conscious adaptable knowledge generation/ processing. We changed the standard name of *artificial intelligence*, to emphasize the need to understand the simulation; everything we know on simulation approaches us of the intelligent simulation of intelligence. Formalization requires computer-oriented knowledge representation, and inference compatible to computable reasoning. The present work hypothesis considers the human as the only model for behavioral/ structural intelligence, different from a syntactical machine.
- The system that results of intelligence simulation should be able to explain itself without referring to its internal representation, i.e., to be *conscious*, and to have a causative behavior. This behavior is due to its internal structure and independent of the exterior interpretation, i.e., it is *adaptable*. By dialog, it can be aware of an *intention*, and by all this, it is *intelligent*.

- Intelligence simulation is researched functionally and structurally; however, the present trend is the intelligence emulation (*computational intelligence*). It is more efficient, especially for adaptive learning, i.e., it does not care for conscience. The hierarchical simulation, assisted by mathematics to get theoretical and formal, can lead to comprehension of the results. The approach has to be concentrated on the knowledge hierarchies, to simulate metaknowledge, for the system's adaptability, and for searching the way to simulate the Conscience. The recursively controlled sequential soft/ hard process has to be replaced by a reactive controlled continuous soft/ hard process. Most probably only the sequential reasoning distinguishes two limits of the computability, i.e., speed and possibility, in the essentially unique problem: Conscience.

Freedom is understood necessity
Georg Wilhelm Friedrich Hegel

Art is for art – self-definition. Science evolves by the Fear of God – of the unsuspected/ unknown/ unintelligible. Engineering-technology is defined by complement, therefore, without permanent reference to Beauty and Truth, is dangerously unstable. *Mathematics is an art! Science is Physics! Good has to be beautiful and true!*

Theory proceeds from the ancient Greek (the first language of the mathematics): Theos = god, theôria = procession, theorein = to contemplate. The essential concept contains now all three aspects: *Theory is an order on the knowledge while searching for the absolute abstraction named God*, i.e., to build/ understand Intelligence assisted by Faith for living in Beauty, Truth, and Good. *God is unique!*

As the scientific community is fond of the clear and encouraging term to know we can consider arts are the science of the abstract ideas, and engineering-technology the science of the mental world. If arts inspire us, then science is the art to search, research, and understand, whereby engineering-technology is the art to combine the Beauty to the Truth to do Good.

If we know that *alle guten Dinge sind drei*, let us enjoy any of them although every one of us concentrates on a single one of them. The constraint of any approach to simulate the intelligence is basing engineering-technology (of Good) on art (Beauty), especially mathematics, and on science/ physics (Truth). All these are just necessary conditions in looking for the convergence of the three fundamental attributes of the human life, Beauty, Truth, and Good, toward a common measure aiming philosophy. *His Ways are Uncountable!*

The convergence process of evolution demands fight with the Time, having as ally the Structure. Sometimes the Structure is too conservative; therefore, it has to be reconfigured, at abstract levels, e.g., a plan, as at concrete levels.

The Conscience needs continuous reaction, further than discrete recurrence. Social and individual Conscience are rather divergent nowadays, i.e., we only performed *Divide et Impera*, neglecting *et Intellige*. To correct this state can not be delayed! *Hierarchical are His plans!*

Democracy has to be hierarchical, and education has to prioritize the opening to Reality by arts, the most intelligible being mathematics, and the worship to Nature by physics and sports. *Spiritus sanus in Mens sana in corpore sano!*

We need a: **Revolution by opening to evolution**

REFERENCES

Hofstadter, D., 1979. *Gödel, Escher, Bach, The Eternal Golden Braid*. New York: Basic Books.

Niculiu, T., 2008. *Object-oriented Symbolic Structural Intelligent Simulation*. Bucureşti: Matrix.

Penrose, R., 2004. *Shadows of the Mind. Consciousness and Computability*. Oxford: University.

vanLeeuwen, J., (ed.), 1990. *Handbook of Theoretical Computer Science*. Amsterdam: Elsevier.

TUDOR NICULIU is Professor at the Electronics, Telecommunications, and Information Technology Faculty of the *Politehnica* University in Bucharest, and Senior Researcher at the Center for New Electronic Architectures of the Romanian Academy. He is looking for hierarchical integration of different domains, to understand intelligence by simulating it, and to apply it to intelligent simulation. Since 1991, he teaches and researches at the same institution, PhD 1995, MS 1985. Before, he was Senior Researcher at the R&D Institute for Electronic Components in Bucharest, researching and designing hierarchical simulation of analog integrated circuits. He studied Mathematics at University of Bucharest (MA 1994). He published 12 books and around 85 articles in international journals and conference proceedings. He is IEEE Senior Member of CAS, Computer, and SMC Societies.

MARIA NICULIU has graduated the Mechanical Faculty of the *Politehnica* University in Bucharest (1987) and the Faculty of Literatures and Foreign Languages, German/ French/ Dutch - Bucharest University (2009) with a paper on *Sprachenvielfalt und Mehrsprachigkeit, was taugt die Europäische Union als Standort der Mehrsprachigkeit* - Multilinguism and what makes the European Union a model for a multilingual society. From a technical and economical background - member of the Romanian Authorized Accountants and Financial Experts (2008), she directed her interests towards a multicultural approach of the European social and economical evolutions, based on linguistic and behavior simulation

SILICON OXIDE AND HIGH-K DIELECTICS MODELLING AND SIMULATION FOR ADVANCED SEMICONDUCTOR DEVICES

Florin Babarada[(a)]

[(a)]University Politehnica of Bucharest,
Faculty of Electronics Telecommunications and Information Technology, DCAE/ERG,
Bd. Iuliu Maniu 1-3, 061071, sector 6, Bucharest, Romania.

[(a)]babflorin@yahoo.com

ABSTRACT
The continuum down-scaling according with Moore's low, lead the field-effect transistors in the nanometre region with structures characterized by high doping drains and sources and very thin insulating layers. When the thickness of the layers attends 2nm or less, the coupling between the semiconductor channel and the gate can't be neglected. A correct quantum-mechanical model must correct evaluate the channel charge distribution and the leakage current flowing between the gate and the channel through tunnelling. As results the gate, the insulator and the substrate semiconductor channel must be considered like a single space region accessible to all free charge carriers. The presented iterative approximation method for simulate and evaluate the 1D device main electric parameters offer short time computation and was applied to study the thin silicon oxide and high-k dielectrics stacks combination for the new silicon devices. The results were in good agreement with experimental data.

Keywords: MOS quantum-mechanical modelling, high-k dielectrics gate, tunnelling leakage currents.

1. INTRODUCTION

From the beginning of MOS devices technology, SiO_2 has been used as gate oxide because of its stable SiO_2/Si interface as well as its electrical isolation property. But with the rapid scaling down of CMOS devices, SiO_2 gate oxide thickness reaches its physical limits leading to high leakage current. The SiO_2 gate dielectric thickness is projected to be below 1nm and the power supply (V_{dd}) should fall within 0.8 and 1.8V. In this situation, the gate leakage currents due to tunnelling become very high. In addition, n- and p-type doped polysilicon gate is used for CMOS devices and Boron in p-type polysilicon diffuses into and through thin gate oxide, severely degrades pFET performance.

In order to reduce the tunnelling gate current it has become necessary to use high-k gate dielectrics in order to meet the strict requirements on leakage current and equivalent oxide thickness (EOT) such as HfO_2 (Kang at al. 2000), (She et al. 2003), ZrO_2 (Jeon at al. 2001), (Copel et al. 2000), (Qi et al. 2000), TiO_2 (Campbell et al. 1999), and Al_2O_3 (Ludeke et al. 2000), (Manchanda et al. 1998).

Unfortunately, for most high-k materials, the higher dielectric constant comes at the expense of narrower band gap 5-6eV, (Robertson 2000). So the lower barrier height for tunnelling tends to compensate the benefit of the higher dielectric constant (thicker dielectric layer). Usually, for many high-k materials, the net effect is a reduced leakage current. As result the search for the appropriate high-k to replace conventional SiO_2-based gate dielectrics is an important task.

HfO_2 has emerged as one of the most promising high-k candidates due to its relatively high dielectric constant of about 25 and large band gap approximately 5.8eV. But some time its physical and electrical properties suffer from its crystallisation at high temperature during post deposition annealing. Moreover, HfO_2 is a solid state electrolyte for oxygen at high temperature. Thus, high temperature will lead to fast diffusion of oxygen through the HfO_2 resulting in the growth of uncontrolled low-k interfacial layers, respectively SiO_2 and limiting the equivalent oxide thickness (EOT), (Wilk et al. 2001), (Vitchev et al. 2004).

Because of its relatively lower dielectric constant, Al_2O_3 appears as an extremely promising candidate in terms of its chemical and thermal stability as well as its high-barrier offset (Gusev et al. 2000), (Bouazra et al. 2008). Al_2O_3 is also interesting for its high crystallisation temperature and thus it is compatible with conventional process of integrating complementary MOS devices, which involves high temperatures above 1000°C, (Gusev et al. 2001).

However, the silicon substrate and high-k interface degrade the electron and hole mobility. Mobility directly affects the drain current of the transistors and therefore switches the speed of the circuits. There are however presently important issues related to the integration of these materials and that makes highly desirable to previously understand how the new materials properties affects the functionality of CMOS devices. A correct quantum-mechanical model must properly evaluate the channel charge distribution and

the leakage current flowing between the gate and the channel through tunnelling. Consequently the gate, the insulator and the substrate semiconductor channel must be considered like a single space region accessible to all free charge carriers. Looking from the gate this high quality thin oxide is responsible for the continued increase of the gate leakage, which increase the power consumption of integrated circuits (Cai and Sah 2001).

The understanding of the MOS system in z direction begins very important for research the tunnelling current in EEPROM devices and also in high performance MOS devices with ultra thin oxides, (Cassan 2000).

2. THE GATE LEAKAGE CURRENTS MODELLING

The charge distribution and quantum-mechanical leakage currents in ultra thin metal-insulator-semiconductor gate stacks composed of several layers materials are very important (Yeo et al. 2002).

Considering all the capacitor like a single quantum mechanical quantity the effective mass approximation for the electrons in the different valley and the Hartree approximation for the electron-electron interaction in inversion layer, the Schrödinger-Poisson equation can be solved.

Because the insulating layer is relatively thin but the energy barriers separating the inversion layer from the gate electrode is high enough to prevent the flow of electrons to the gate, the potential well host the majority of inversion layer electrons and the channel is coupled only weakly with the gate (Magnus and Schoenmaker 2000).

2.1. The Quantum Mechanical Aspects for the Inversion in MOS Structure

The first fully numerical self-consistent results of the inverted MOS structure were mainly attributed to Stern (Stern 1972). Then the self–consistent solution has been extended to holes in inverted pMOS structure (Moglestue 1986). The quantum mechanical treatment of the MOS structure in the accumulation regime was described by Sune (Sune et al. 1992).

The self-consistent Schrödinger-Poisson equations were applicable to an inverted structure in the next approximations:

- the effective mass approximation,
- the ideal interface semiconductor-oxide,
- interruption of wave function at interface semiconductor-oxide.

The time-independent Schrödinger equation in 3D space, using the position vector $\mathbf{R}=(\mathbf{r},z)$ can be formally written:

$$H\psi(\mathbf{r}, z) = E\psi(\mathbf{r}, z), \tag{2.1}$$

where $\psi(\mathbf{r},z)$ is the wave function, E is the eigenvalue energy, H is the system Hamiltonian, composed from kinetic energy T and potential energy W. For long channel device the potential profile is mainly one dimensional and the drain and source regions can be considered like electrons reservoirs for the inversion layer. The 1D simplification allows using the wave operator like a function of the z coordinate only:

$$\psi(\mathbf{r},z) = \phi(z)e^{i\mathbf{k}\cdot\mathbf{r}}, \tag{2.2}$$

where $\mathbf{k}=(k_x,k_y)$ is the wave vector in the (x,y) plane. So the carrier are quantized in the z direction and are free to move in the $\mathbf{r}=(x,y)$ plane, with a continuous energy component. After a phase transformation and imposing the constraint of vanishing for the first derivative of the wave function, the envelope 1D time-independent reduced Schrödinger equation (2.1) is:

$$-\frac{\hbar^2}{2m_{zz}}\psi''(z) + W\psi = E_z\psi(z), \tag{2.3}$$

where $\hbar$ is reduced Planck constant, m_{zz} is the effective masses in m_o units, W is potential energy, $\Psi(z)$ is the 1D envelope wave functions and E_z is the new eingenvalue energy:

$$E_z = E - E_{\parallel}(k) = E - \frac{(\hbar k_x)^2}{2m_x} - \frac{(\hbar k_y)^2}{2m_y} \tag{2.4}$$

Considering the MOS structure a quantum mechanical system, an externally applied gate bias induces a potential well that confines carriers in the region of the semiconductor-oxide interface. The electrostatic potential and charge respect the Poisson equation in any z direction from silicon region is:

$$\frac{d^2V(z)}{dz^2} = -\frac{1}{k_{Si}\varepsilon_0}\rho(z), \tag{2.5}$$

where $V(z)$ is the electrostatic potential, $\rho(z)$ is the charge density, k_{Si} is the Si relative dielectric constant. Assuming the p-type substrate with completely ionized impurities and neglecting the hole concentration in inversion can approximate the charge density:

$$\rho(z) = \rho_{depl}(z) - qn(z), \tag{2.6}$$

where ρ_{depl} is the depletion layer charge and $n(z)$ is the carrier's distribution.

Close to the interface the electrons have a position dependent concentration proportional with the probability density and a sum of each energy valley and subband.

$$n(z) = \sum_{i,j} n_{i,j}(z) = \sum_{i,j} N_{ij}^{(2D)}\left(E_{z,ij}, E_F\right)|\psi(z)|^2, \tag{2.7}$$

where $N_{ij}^{(2D)}$ is the subband population which integrates the all possible energies of a subband of the

2D density of states, $|\psi(z)|^2$ is the probability density, $E_{z,ij}$ is the solution of 1D Schrödinger equation (2.3) and represents the discrete bottom level of a particular energy subband j, for each valley i and E_F is Fermi energy level. The carrier's distribution can be more detailed using the valley and spin degeneracy and Fermi-Dirac statistics.

The assumption that the silicon-oxide interface is ideally was technologically realized by election the [001] surface orientation, which minimizes the dangling bonds at the interface, resulting a high quality interface after passivation.

3. THE ITERATIVE APPROXIMATION METHOD

Considering the quantization effects of silicon-insulator interface an approximate geometrical solution to calculate the charge densities and subband energy levels reduces consistently the computational complexity for leakage current evaluation. Using the same effective mass approximation the areal density of charge in the inversion layer is:

$$N_{inv} = \sum_{i,j} \oint_z N_{ij}^{(2D)}\left(E_{z,ij}, E_F\right)\left|\psi(z)\right|^2 dz = \sum_{i,j} N_{ij}^{(2D)}\left(E_{z,ij}, E_F\right) \quad (3.1)$$

Using the geometrical approximation of Si band bending in inversion [8] the energy level is:

$$E_{z,ij} = \left(\frac{\hbar^2}{2m_{z,i}}\right)^{1/3}\left(\pi q F_{ef}\frac{3}{2}\left(j+\frac{3}{4}\right)\right)^{2/3} \quad (3.2)$$

and the subband charge is:

$$q_{ij} = \frac{2E_{z,ij}}{3qF_{ef}}, \quad (3.3)$$

where F_{ef} is the $E_{z,ij}$ corresponding effective electric field. Then the inversion charge is:

$$q_{inv} = \sum_{i,j} q_{i,j}\frac{N_{i,j}^{(2D)}}{N_{inv}}, \quad (3.4)$$

and the total silicon surface bending:

$$\Psi_S = \Psi_D + q\frac{N_{inv}q_{inv}}{k_{Si}\varepsilon_0} + \frac{k_B T}{q} \quad (3.5)$$

where Ψ_S is the surface potential, Ψ_D is the drop voltage at surface due to space charge region. The last term is the influence of doping concentration to charge region (Muller and Schultz 1997). Using the charge boundary conditions the equations can be iteratively solved to attain the convergence in the next sequence:

1. Guess the initial N_{inv}, Ψ_S and Ψ_D
2. Consider charge boundary condition $N_{inv\text{-}bc}$
3. Iterate Ψ_S with condition $N_{inv}(\Psi_S)/N_{inv\text{-}bc} \rightarrow 1$
4. Iterate Ψ_D with condition $\Delta\Psi_D \rightarrow 0$
5. Compute the potential distribution

We have possible loops from out to input, of step 3 and 4 and from out of step 4 to input of step 3. The method can be used also for tunnelling based leakage currents in high-k dielectric stacks, (Hou et al. 2003), (Palestri et al. 2007).

4. RESULTS

For numerical simulations we used the ATLAS devices simulator software package from Silvaco. The main module program used is presented in figure 1, in order to generate the MOS structure presented in figure 2.

```
mesh
x.mesh loc=-0.01 spac=0.01
x.mesh loc=0.01  spac=0.01
y.mesh loc=-0.04 spac=0.001
y.mesh loc=0.02  spac=0.001
region number=1 x.min=-0.01 x.max=0.01 y.min=-0.04
y.max=-0.03  \
       material=aluminum
region number=2 x.min=-0.01 x.max=0.01 y.min=-0.03
y.max=-0.005 \
       material=poly
region number=3 x.min=-0.01 x.max=0.01 y.min=-0.005
y.max=0.0   \
       material=oxide
region number=4 x.min=-0.01 x.max=0.01 y.min=0.0
y.max=0.02     \
       material=silicon
electrode x.min=-0.01 x.max=0.01 y.min=-0.04 y.max=-
0.03 name=gate
electrode bottom name=substrate
doping region=2 p.type concentration=1e19 uniform
doping region=4 p.type concentration=1e17 uniform
solve init
solve vgate=-1.5
solve vgate=-3
save outfile=mos2ex15-3V19.str
# tonyplot mos2ex15-3V19.str -set mos2ex15_BD.set
log outfile=mos2ex15_CV19.log
solve vgate=-2.8 vstep=0.2 vfinal=3.0 name=gate ac
freq=1e6 previous
tonyplot mos2ex15_CV19.log -set mos2ex15_CV.set
```

Figure 1: The main ATLAS program module

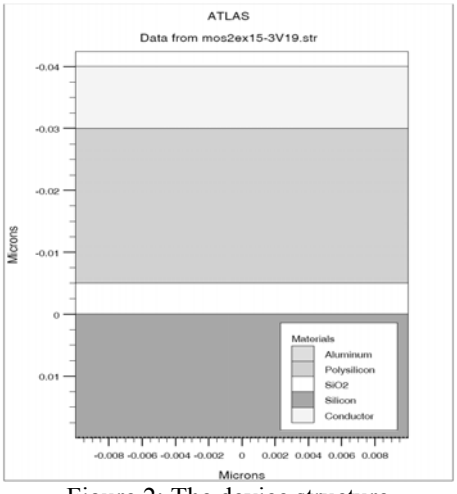

Figure 2: The device structure

Then was calculated the gate current, figure 3 and the capacity from gate to substrate, figure 4, function of polysilicon doping concentrations $10^{19}cm^{-3}$, $10^{20}cm^{-3}$ and $10^{21}cm^{-3}$. The first numerical simulations proves the dependence of gate leakage current, figure 3 and depletion effect figure 4, function of doping concentration like considered in chapter 3.

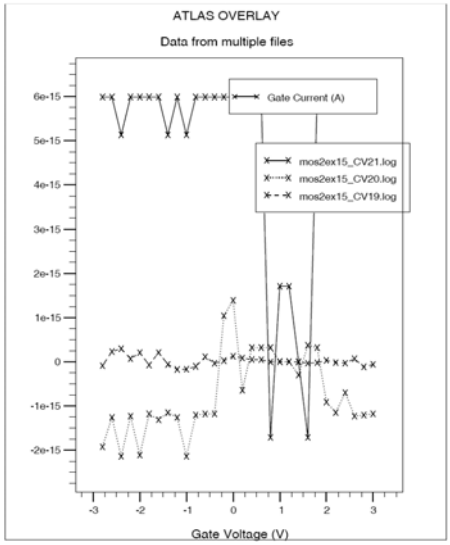

Figure 3: The Gate Current

Using the barrier height of 3.1eV, substrate doping $5x10^{17}cm^{-3}$, effective silicon oxide mass of 0.5mo and donor poly doping $6x10^{19}$ cm^{-3}, the results of short computation iterative approximation of silicon oxide current gate density, figure 5, was in good agreement with experimental gate current density curves presented in (Yang et al. 2000).

A little overestimation of leakage current at high gate bias voltage is observed also in other reports, (Yang et al. 2000) and (Lo et al. 1997), based of approximation of Fermi level by the value in the bulk silicon substrate.

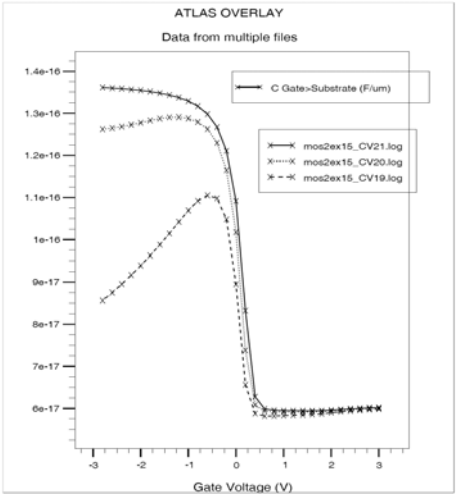

Figure 4: The Gate-Substrate Capacity

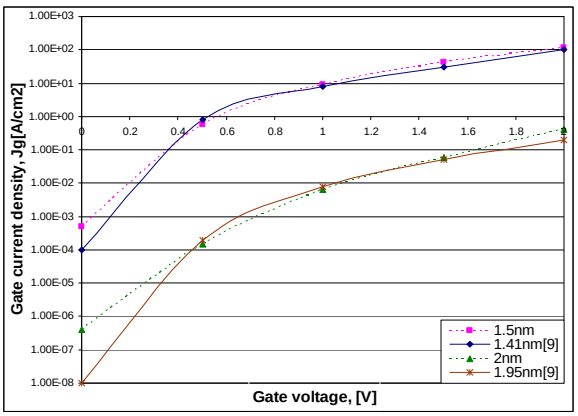

Figure 5: Silicon oxide gate current density calculated (1.5nm and 2nm) and experimental curves presented in [9]-(Buchanan et al. 2000), (1.41nm[9] and 1.95nm[9])

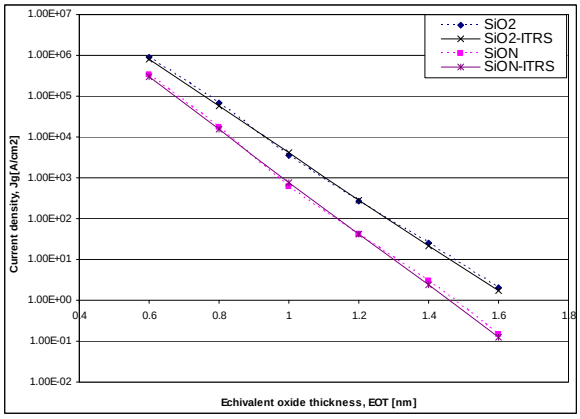

Figure 6: Simulated and ITRS tunnelling current gate leakage in inversion channel for oxide and oxynitride at Vg=1V

The polysilicon doping level suppresses the gate leakage current for gate bias in inversion because the additional voltage drops over the depleted layer, (Yang et al. 1999). This solution decreases the drive capacitance and the device performances. The substrate doping level affects the leakage current through the surface potential of the channel.

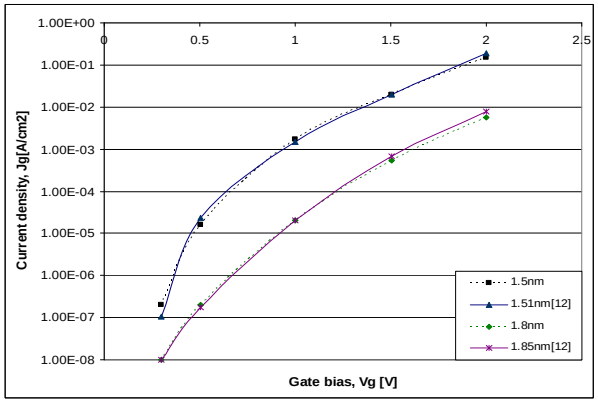

Figure 7: Calculated data and experimental gate leakage currents (Buchanan et al. 2000), for Al_2O_3 high-k stacks

Because increasing the physical thickness of gate dielectric affects the device parameters like drive current, a compromise solution is to increase the dielectric constant using the SiON layer with dielectric constant up to 7.6 for Si_3N_4.

The performances of SiON like gate dielectric are better than SiO_2 as in figure 6, according with simulations and ITRS. Comparing the calculated data with gate leakage current through Al_2O_3 high-k dielectric stacks presented in (Buchanan et al. 2000) a good fit was obtained, figure 7.

5. CONCLUSIONS

High-k atomic layer deposition stacks like insulating in the metal-insulating-semiconductor structure was studied.

An iterative approximate method to calculate the 1D MOS structures main electric parameters without using the Schrödinger-Poisson equations is used. This method is based on approximation of effective field function of doping parameters.

The tunnelling currents can be calculated more rapidly and the study for different gate dielectric stacks can be made. The precision can be increased by 2D or 3D analysis of Schrödinger-Poisson equations.

The main application is to calculate the direct tunnelling current due to the thin oxide layers. The method is extensible to high-k dielectric stacks in order to study the influence of several material parameters like the impact of layer thickness on gate leakage and the approach of gate stack scalability.

The results obtained using numerical calculation show that the increase of the gate dielectric constant has a very important effect in reducing the leakage currents.

Comparing the results from figure 5 and 7 for 1V gate bias and 1.5nm thickness the increase of dielectric constant to 7 reduce the leakage current with 4 order of magnitude.

Other simulations show that the leakage current decrease significant when the interfacing oxide is completely eliminated. Future works will be focus of other high-k dielectric stacks like HfO_2, $HfSiO_4$, $ZrSiO_4$, La_2O_3, and Y_2O_3.

ACKNOWLEDGMENTS

This work was supported by NANOXI 11-048 (2007-2010) project financed by Romanian National Authority for Scientific Research.

I want to thanks to Professor Adrian Rusu for permanent encouragement and support and to dr. Rodica Plugaru for the very good cooperation in the NANOXI project.

REFERENCES

Bouazra A., Nasrallah S. Abdi-Ben, Said M., Poncet A., 2008, "Current Tunnelling in MOS Devices with Al_2O_3/SiO_2 Gate Dielectric", *Research Letters in Physics*, Volume 2008, Article ID 286546, 5 pages doi:10.1155/2008/286546.

Buchanan D. A., Gusev E. P., Cartier E., et al., 2000, "80nm polysilicon gated n-FETs with ultra-thin Al_2O_3 gate dielectric for ULSI applications," *IEEE International Electron Devices Meeting (IEDM '00)*, pp. 223–226, San Francisco, Calif, USA.

Cai J., Sah C. T., 2001, "Gate tunneling currents in ultrathin oxide metal—oxide—silicon transistors," *Journal of Applied Physics*, vol. 89, no. 4, pp. 2272–2285.

Campbell S. A., Kim H. S., Gilmer D. C., He B., Ma T., Gladfelter W. L., 1999 "Titanium dioxide (TiO_2)-based gate insulators," *IBM Journal of Research and Development*, vol. 43, no. 3, p. 383.

Cassan E., 2000, "On the reduction of direct tunnelling leakage through ultra-thin gate oxides by one-dimensional Schrodinger-Poisson solver", *Journal of Applied Physics*, 87(11), pp. 7931-7939.

Copel M., Gribelyuk M., Gusev E. P., 2000, "Structure and stability of ultrathin zirconium oxide layers on Si(001)," *Applied Physics Letters*, vol. 76, no. 4, pp. 436–438.

Gusev E. P., Copel M., Cartier E.,. Baumvol I. J. R, Krug C., Gribelyuk M., 2000, "High-resolution depth profiling in ultrathin Al_2O_3 films on Si," *Applied Physics Letters*, vol. 76, no. 2, pp. 176–178.

Gusev E. P., Cartier E., Buchanan D. A., et al., 2001, "Ultrathin high-K metal oxides on silicon: processing, characterization and integration issues," *Microelectronic Engineering*, vol. 59, no. 1–4, pp. 341–349.

Hou Y. T., Li M. F., Yu H. Y., Kwong D.-L., 2003, "Modeling of tunneling currents through HfO2 and $(HfO_2)_x/(Al_2O_3)_{1-x}$ gate stacks," *IEEE Electron Device Letters*, vol. 24, no. 2, pp. 96–98.

Jeon T. S., White J. M., Kwong D. L., 2001, "Thermal stability of ultrathin ZrO2 films prepared by chemical vapor deposition on Si(100)," *Applied Physics Letters*, vol. 78, no. 3, pp. 368–370.

Kang L., Onishi K., Jeon Y., et al., 2000, "MOSFET devices with polysilicon on single-layer HfO_2 high-K dielectrics," *IEEE International Electron Devices Meeting (IEDM '00)*, pp. 35–38, San Francisco, Calif, USA.

Lo S., Buchanan D., Taur Y., Wang W., 1997, "Quantum mechanical modelling of electron tunnelling current from the inversion layer of ultra-thin-oxide nMOSFET", *IEEE Electron Device Letters*, 18(5), pp. 209-211.

Ludeke R., Cuberes M. T., Cartier E., 2000, "Local transport and trapping issues in Al_2O_3 gate oxide structures," *Applied Physics Letters*, vol. 76, no. 20, pp. 2886–2888.

Magnus W., Schoenmaker W., 2000, "Full quantum mechanical model for the charge distribution and the leakage currents in ultrathin metal-insulator-semiconductor capacitors", *Journal of Applied Physics*, 88(10), pp. 5833-5842.

Manchanda, L. Lee W. H., Bower J. E., et al., 1998, "Gate quality doped high K films for CMOS beyond 100nm: 3-10nm Al_2O_3 with low leakage and low interface states," *IEEE International Electron Devices Meeting (IEDM '98)*, pp. 605–608, San Francisco, Calif, USA.

Moglestue C., 1986, "Self-consistent calculation of electron and hole inversion charges at silicon-silicon dioxide interfaces", *Journal of Applied Physics*, 59(9), pp. 3175-3183.

Muller H.H., Schultz M.J., 1997, "Simplified method to calculate the band bending and the subband energies in MOS capacitors", *IEEE Transactions on Electron Devices*, 44(9), pp. 1539-1543.

Palestri P., Barin N., Brunel D., et al., 2007, "Comparison of modeling approaches for the capacitance—voltage and current—voltage characteristics of advanced gate stacks," *IEEE Transactions on Electron Devices*, vol. 54, no. 1, pp. 106–114.

Qi W.-J., Nieh R., Lee B. H., Kang L., Jeon Y., Lee J. C., 2000, "Electrical and reliability characteristics of ZrO_2 deposited directly on Si for gate dielectric application," *Applied Physics Letters*, vol. 77, no. 20, pp. 3269–3271.

Robertson J., 2000, "Band offsets of wide-band-gap oxides and implications for future electronic devices," *Journal of Vacuum Science & Technology B*, vol. 18, no. 3, pp. 1785–1791.

She M., Takeuchi H., King T. J., "Improved SONOS-type flash memory using HfO_2 as trapping layer," 2003, *Proceedings of the 19th IEEE Non-Volatile Semiconductor Memory Workshop (NVSMW '03)*, pp. 53–55, Monterey, Calif, USA.

Stern F., 1972, "Self-consistent results for Si inversion layers", *Physical Review Letters*, B, 5(12), pp. 4891-4899.

Sune J., Olivio P., Ricco B., 1992, "Quantum mechanical modelling of accumulation layers in MOS structures", *IEEE Transactions on Electron Devices*, 39(7), 1732-1739.

Vitchev R. G., Pireaux J. J., Conard T., Bender H., Wolstenholme J., Defranoux Chr., 2004, "X-ray photoelectron spectroscopy characterisation of high-k dielectric Al_2O_3 and HfO_2 layers deposited on SiO_2/Si surface," *Applied Surface Science*, vol. 235, no. 1-2, pp. 21–25.

Wilk G. D., Wallace R. M., Anthony J. M., 2001, "High-κ gate dielectrics: current status and materials properties considerations," *Journal of Applied Physics*, vol. 89, no. 10, pp. 5243–5275.

Yang N., Henson W. K., Hauser J. R., and Wortman J. J., 1999, "Modeling study of ultrathin gate oxides using direct tunneling current and capacitance-voltage measurements in MOS devices," *IEEE Transactions on Electron Devices*, vol. 46, no. 7, pp. 1464–1471.

Yang N., Henson W., Wortman J., 2000, "A comparative study of gate dielectric tunnelling and drain leakage currents in n-MOSFET with sub-2-nm gate oxides", *IEEE Transactions on Electron Devices*, 47(8), pp. 1636-1644.

Yeo Y., King T., C. Hu, 2002, "Direct tunnelling leakage current and scalability of alternative gate dielectrics", *Applied Physics Letters*, 81(11), pp. 2091-2093.

AUTHOR BIOGRAPHY

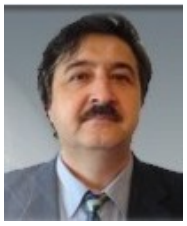

Florin N. Babarada received the M.Sc. degree in Electronics & Telecommunications in 1983 and the Ph.D. degree for Microresonant Sensors on Silicon Technology, in 2000, both at University Politehnica from Bucharest, Romania. In 1984 he joined Miroelectronica S.A. IC Factory. From 1994 was member of the beginning team of the Institute of MicroTechnologies-IMT, then named National Institute of Microtechnology, where he worked in the field of Micro-ElectroMechanical Systems-MEMS. From 2002 he has become Associate Professor at the University Politehnica of Bucharest, Faculty of Electronics Telecommunications and Information Technology, Department of Devices Circuits and Electronics Apparatus, where he is involved in Semiconductor Processes, Devices and Circuits, Modelling, Simulation and Design. More details to www.arh.pub.ro/fbabarada.

SIMULATION-BASED OPTIMIZATION OF PROCESS NETWORK SYNTHESIS USING STRUCTURED-STATE REINFORCEMENT LEARNING

Pedro Toledo[(a)], José Ignacio Estévez[(b)], Silvia Alayón[(c)], José Sigut[(d)]

[(a-d)] Department of Systems Engineering and Control, University of La Laguna, 38200, S/C de Tenerife, Spain

[(a)]pedro@isaatc.ull.es, [(b)]iestevez@ull.es, [(c)]silvia@isaatc.ull.es, [(c)]sigut@isaatc.ull.es

ABSTRACT

Simulation-based optimization has been largely used to tackle complex problems where getting analytical solutions is computationally unfeasible. Process Network Synthesis (PNS) is an example of such high dimensional problems. The problem researched in this paper has been inspired by PNS, and focuses on finding the network structure that best fits to the specifications, trying to optimize a cost function defined on the set of elements of the network. The proposed approach introduces modifications to the classical Reinforcement Learning (RL) techniques, using a structured state space, and counter-based methods, to heuristically guide the search. Results from synthetic data are presented, showing improvements achieved in the convergence ratio to near-optimal solutions with respect to other RL approaches.

Keywords: Simulated-based Optimization, Reinforcement Learning, Process Network Synthesis.

1. INTRODUCTION

Optimization methods have been largely used in Industry. Obviously, any technique which allows a production process to be cheaper would be very valuable. Nevertheless, traditionally only the experience achieved along the years yielded the companies to obtain the necessary information for the optimization. In addition, since most of the production environments are usually dynamic, not all the experience is significant, and only the most recent part should be taken into account. However, in many of these scenarios there is enough background information to model the process allowing a posterior simulation based study to retrieve an optimal policy for the overall process. Actually, simulation-based optimization has been largely used to tackle complex problems in which getting analytical solutions is computationally unfeasible.

More specifically, some of the simulation models are built from simple parts of a production process which represent the atomic production actions to be selected. These parts have to be interconnected to define the final process. Consequently, to optimize the process, all possible combinations of the connections of simple elements which produce a correct production process and fulfil the imposed constraints have to be explored. This leads to a high dimensional combinatorial problem that is, in most of the situations, unfeasible to solve exactly. Process Network Synthesis (PNS) is an example of a formalism of such high dimensional problems. The problem researched in this paper is inspired by PNS, focusing on finding the network structure that best fits to the specified requirements, trying to optimize a cost function defined on the set of elements of the network. In real situations, this cost function is usually unknown a-priori. Only once the entire process is finished it can be calculated the cost for the implemented solution as a whole. Nevertheless, no extra information about the individual contribution of the elements of the network to the solution cost is achieved. Consequently, we consider the cost function can be only sampled once a solution is built.

The described context is suitable to be tackled with Reinforcement Learning (RL) algorithms, using them to learn the correct production policy, despite the complexity of the problem information representation. The proposed approach to the problem introduces modifications to the classical RL techniques, using a structured state space, and counter-based methods, to heuristically guide the search. Different experiments have been designed changing the parameters of the characterized problem. Therefore, results from synthetic data are presented, showing improvements achieved in the convergence ratio to near-optimal solutions with respect to other RL approaches.

The remainder of the paper is organized as follows. In Section 2, we briefly review some related approaches in the field. Section 3 introduces a formal definition of the problem, including an application example. Section 4 describes the proposed RL approach. In Section 5 we introduce a counter-based method, to guide the learning process. Sections 6 and 7 describe the designed experiments and analyze the achieved results. Finally, we wrap up and describe future work in Section 8.

2. RELATED WORK

Simulation-based optimization (Paternina-Arboleda, Montoya-Torres, and Fábregas-Ariza 2008) is a large field in which there are currently numerous opened research problems. In our case, we deal with knowledge

representation in form of graphs, and an a-priory unknown cost function. To formalize the problem we use well-known definitions in the fields named in the following paragraphs:

Firstly, Process Network Synthesis faces the construction of a network which represents the solution to a given problem (Friedler, Fan, and Imreh 1998). Several approaches have been discussed for the structural representation, being P-Graphs (Friedler, Tarjan, and Huang 1992) and Petri Nets (Gyapay and Pataricza 2003) some of the most outstanding ones. Despite the several approaches that have been already proposed it is still a motivating problem with direct applications to industry as well as challenges from the theoretical point of view.

Secondly, Reinforcement Learning (Sutton and Barto 1998) is a learning paradigm which is used in environments in which an agent does not have a set of inputs and desired outputs pairs but only a reward associated with the actions it chooses depending on the state in which it is located. The objective is to learn a policy that maximizes the rewards obtained in the long term run.

Furthermore, several variants of RL can be found in the literature, depending on how the states are represented. For example, Relational Reinforcement Learning (Driessens 2001) uses First Order Logic to define the state space.

In addition, when tackling large state spaces, some guidance to the RL algorithms is required in order to speed-up convergence. Counter-based methods (Thrun 1992, Goodrich and Peterson 2000, Främling 2007) are heuristics used with this purpose. They are based on counting the times that the RL agent visits each state and the reward obtained.

Finally, Function Regression, which is also considered usually as a basic learning algorithm, has been broadly used in the literature as a part of more complex learning strategies (Guestrin, Koller, and Parr 2003). It is an important part of the RL algorithms, being increasingly difficult to define as the chosen state representation gets more complex.

3. PROBLEM DESCRIPTION

The model adopted in this paper is Workflow Schema (Greco, Guzzo, and Manco 2005), since it has been demonstrated to be expressive enough to represent structured solutions to design problems.

The formalism of this model is a Directed Acyclic Graph (DAG), with constraints. Its structure is the representation of the background knowledge of the problem and at the same time it fixes all the possible solutions that can be constructed to solve it. In this graph the nodes represent actions that transform the input materials into the output products. The edges represent the possibility of bringing the output product of one action to another action that would take it as input material. Depending on the context of the problem, the materials and products may be physical objects, if we are trying to optimize the production cycle of an industry, or any other concept as a data structure, if the problem is related with the optimization of a Business Management Process. The WS can be considered as a metagraph, being those subgraphs that fulfill all the constraints possible solutions to the represented problem. There are some constrains to consider. To perform the actions some minimum input material might be necessary, the amount of output product is limited, and the amount of product that can be brought to other activity is fixed. Furthermore, the process is not considered optimized if there is some product available that can be reused but it is not. This paper assumes the context in which such a WS is available from the problem description, or in other case it can be induced using background knowledge and rules (Rozinat, Alves de Medeiros, and van der Aalst 2007). Each possible solution according to this structure is a subgraph called Instance. The knowledge about previous solution to a problem is called Valuated Instance-Set. The following definitions formalize these concepts.

A **Workflow Schema** W is a tuple *(V, E, V_o, V_f, n, p, c)*, where V is an ordered set of nodes, E is a set of edges defined as:

$E \subseteq \{(v_i, v_j) | i < j \wedge v_i \in (V \backslash V_f) \wedge v_j \in (V \backslash V_0)\}$,

V_o is the set of start nodes, V_f is the set of end nodes, $n: (V \backslash V_o) \rightarrow \mathbb{Z}^+$ is the Node necessity function, $p: (V \backslash V_f) \rightarrow \mathbb{Z}^+$ is the Node production function, and $c: E \rightarrow \mathbb{Z}^+$ is the Edge capacity function.

Given a node $v \in V$ the set of input edges is denoted as $E^i(v) = \{(v', v) | (v', ') \in E\}$, and the set of output edges as $E^o(v) = \{(v, v') | (v, v') \in E\}$.

Given a $WS = (V, E, V_o, V_f, n, p, c)$, a graph $S = (V_S, E_S)$ is said to be a subgraph of WS iff *(i)* $V_S \subseteq V$ *(ii)* $E_S \subseteq E$ and *(iii)* $(\forall v_i \in V_S, \forall v_j \in V_S, i < j \rightarrow \exists path(v_i, v_j))$.

Given a WS, the subgraph $S_I = (V_I, E_I)$ is an instance of W, iff the following constraints are fulfilled:

(i) At least one of the initial nodes are included in the instance: $V_{Io} = V_I \cap V_o \neq \emptyset$, *(ii)*, only the initial nodes have not ingoing edges: $\forall v_i \in V_I \backslash V_{Io}, \exists (v_i, v_j) \in E_I$ (iii) the sum of input edge capacities is at least the necessity of each node: $\forall v \in V_{I \backslash V_{Io}}, \sum_{E^i(v)} c(e) \geq n(v)$, and *(iv)* given a node with at least one outgoing edge, its output edges are included in the instance with the goal of approximating as much as possible the node production to the sum of edge capacities, under the constraint that this sum of capacities cannot be greater than the production:

$$\forall v, (v, v') \in E_I \rightarrow \frac{min}{E_I^o(v)}\{c(e)\} > p(v) - \sum_{E_I^o(v)} c(e) \geq 0 \quad (1)$$

where $\overline{E_I^o}(v) = E^o(v) \backslash E_I^o(v)$.

An instance I is complete when $\nexists v \epsilon V_I \backslash V_f$ with $E_I^o(v) = \emptyset$.

A complete instance I is said to be **successful**, SC-Instance, if it contains at least one final node, $V_{If} = V_I \cap V_f \neq \emptyset$.

An instance I defined respect to W, may be also defined as the join of a set V_{Io} of initial nodes of W, and a set of decisions D. A **decision** $D_I(v)$ of a node v is defined as the part of an instance constituted by the set of all the outgoing edges $E^o(v)$included in the instance, and the set of the end nodes of these outgoing edges.

An instance I' represented by the subgraph $S_{I'}$ is an extension of another instance I represented by the subgraph S_I, $I \prec I'$, iff I' and I are defined respect to the same WS and S_I is a subgraph of $S_{I'}$.

Given a non-complete Instance I, an extension I' is said to be a 1-step extension iff I' can be obtained joining I with at least one decision of I'. This is $I \prec_1 I' iff (I \neq I') \wedge (\exists v \epsilon V_I | I \cup D_{I'}(v) = I')$. By analogy, an extension I^n of an instance I is said to be a n-step extension iff I^n is obtained as the union of I with at least *n* decisions of I^n.

Given a WS, and a SC-Instance $I = (V_I, E_I)$ defined respect to it, the cost function associated to that instance can be generally defined as: $Cv: InstancesSet \rightarrow \mathbb{R}$. Therefore, the cost function assigns a real value to each combination of nodes and edges that fulfills SC-Instance constraints, without any additional information or assumption.

The set of all possible different SC-Instances defined respect to a given WS is called 2^{Iws}. The cardinality of this set, $|2^{Iws}|$, is the size of the solution space modelled by the WS.

Given a WS, a Valuated Instance-Set **F** is defined as a set of pairs:

$$F \subseteq \{(I_, C_i) | I_i \in 2^{Iws} \wedge C_i = C_v(V_I, E_I)\}. \quad (2)$$

Given the former definitions, we can specify the dealt problem as follows: Given a Workflow Schema **WS**, and **T** possibilities to sample the Cost function **Cv**: Learn a policy π about how to build the Instance **I** with minimum cost.

3.1. Example

Let's give an academic example of the described formalism. Suppose a company is trying to set the best decision policy for their operations possibilities. Firstly, they model the possible options in a diagram, with the result shown in Figure 1.

As it is shown, each cycle begins with some funds which are desired to be invested to complete a new product launch process. Then, the first choice arises, and it must be decided whether to produce the new product in local factories or to decide to plan outsourcing production.

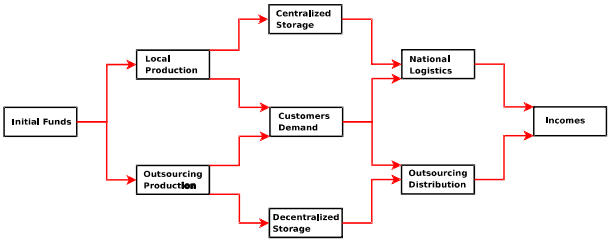

Figure 1 Example of the operation process possibilities of a company

The local production choice is associated with the management of a centralized storage for the products, while outsourcing the production around the world implies also distributed logistics. Both options have the consequence of starting a process of analysis of the actual customers demand on the product, resulting a description of the market that would maximize the sells expectancy. Having a centralized storage systems makes highly recommendable to establish the logistic infrastructure for the product distribution. On the other hand, decentralized storage makes unfeasible to build logistic infrastructure, so outsourcing distribution would be necessary. Furthermore, depending on the customers demand locations it also could be recommendable to use local logistic or outsourcing distribution. Finally the product sales produces some incomes with which the process is considered finalized. With this information of the academic example, it is clear that local production for highly localized customer demand and outsourcing production for disperse demand are the best decision combinations. Now, suppose that a non-experience business man is taking the decisions. He decides to complete some investment cycles, from the funds to the incomes, while he gain experience in decision making in this context. In such a case, nor the customer demand location nor the recommendable combination of decisions is known beforehand. Only after the process is completed, the difference between the final incomes and the initial funds is known. In order to use the information to increase the benefits with each cycle, a policy for the decisions based on the previous experience must be learned. This corresponds exactly with the problem formalized above.

The diagram with the Production Process can be easily transformed into one adjusted to the formal definitions of the problem. In this case the production, necessity and capacity functions need to be defined in a way that the possible combinations described before and only those options can be obtained as SC-Instances of the WS. The values of these functions can be obtained naturally from real world data in most of the real application problems.

One of the multiple possibilities for a WS definition fulfilling the description constrains is represented in Figure 2.

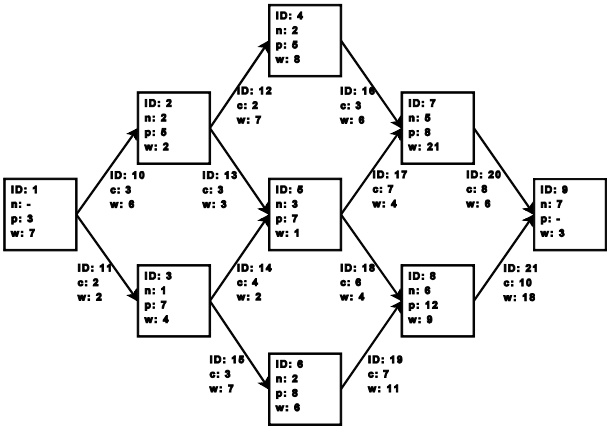

Figure 2 A possible Workflow Schema, obtained applying the formal definitions to the previous example.

Some successful complete instances can be extracted from the WS. All the process possibilities for the local production choice, are represented in Figure 3. The cost function, which is defined as the sum of the costs of the elements of the instance, assigns costs to the instances in the intuitive way. The instance with only national logistics once local production was selected has associated a cost much lower than the one with outsourcing distribution as well as national logistics.

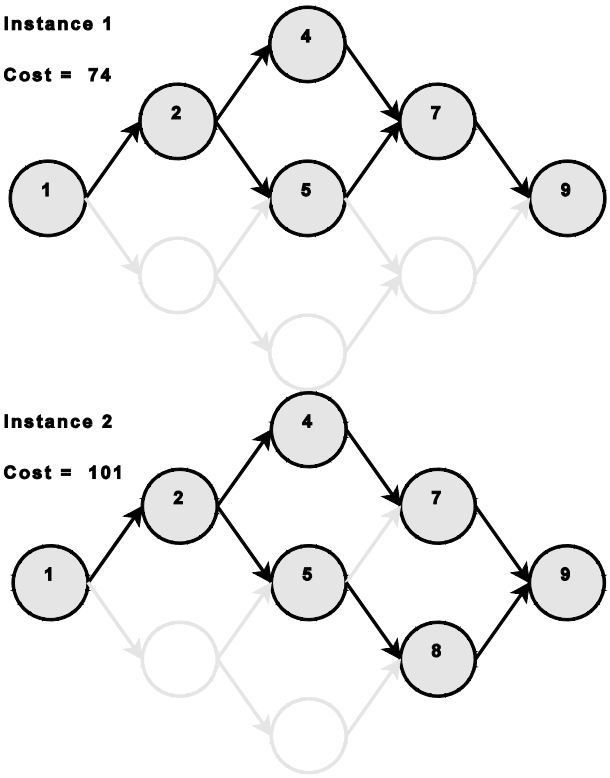

Figure 3 Instances extracted from the WS.

4. NETWORK STATE RL

To learn an appropriate policy for the described problem, it is used a RL approach. However classical RL needs a Markov Decision Process to be defined. This is, it must be defined a set of states to describe each of the possible stages of the process. They must be defined in such a way that the evolution of the process from any state does not depend on any extra piece of information except for the one included in the state definition. Furthermore, it is also necessary to define a set of actions to set the different options that can be selected during the process evolution. The transition function would define the way a state action pair will make the system evolve to the next state. The reward, which is also a function, defines the feedback obtained from the environment when action A is selected in a state S. The following definitions, describe the RL formalization of the approach, named Network State RL.

The RL policy learned is used to build instances, this is solutions to the problem. Let's denominate $I = (V_I, E_I)$ the Instance that is incrementally built from a set of initial nodes of the WS.

State $S_{t_I} = (MarkedSet, ReadySet)$, $MarkedSet \subseteq \{(V_I \times \mathbb{Z})\}$, $ReadySet \subseteq V_I$.

Begin State $S_{t_I} = (MarkedSet, ReadySet)$, $MarkedSet = \emptyset, ReadySet \subseteq V_o, ReadySet \neq \emptyset$. In principle, the begin $ReadySet$ can be any subset of the initial nodes of the workflow.

Action An action is understood as Decision to extend the actual Instance, understanding 'Decision' by the formal definition given above. Given a state S_{t_I}, there is one node of special interest v. This node is the Node from the $ReadySet$ that appears before in the ordered set V. Let's call $2^{I'(v)}$ all possible 1-step extensions to the actual Instance I achieved by joining I with a Decision $D_{I'}(v)$. Let's call $2^{D_{I'}(v)}$ the set of all the corresponding Decisions to get each I' from the actual I. The set of possible actions for a given state $A(St_I) = 2^{D_{I'}(v)}$.

Transition Function Given an actual state St_I and an action $A = D_{I'}(v)$, let's define the next state $St_{I'}$ in a deterministic way, following the next steps:

- Remove v from the $ReadySet$
- For each node $v' \in D_{I'}(v)$, if $v' \notin (MarkedSet \cup ReadySet)$, then $MarkedSet = MarkedSet \cup (v, 0)$
- For each edge $e = (v_1, v_2) \in D_{I'}(v)$, if $v_2 \in MarkedSet(V)$, then $MarkedSet = MarkedSet \setminus (v_2, C) \cup (v_2, C + c(e))$
- For each $(v', C) \in MarkedSet$, if $C \geq n(v')$, then $MarkedSet = MarkedSet \setminus (v', C)$ and $ReadySet = ReadySet \cup \{v'\}$

Episode end No active nodes in current state. $ReadySet = \emptyset$

Reward If $EpisodeEnd(St_I) == false$ then $Reward$ is not defined or 0. Else, let's call I the Instance built in the actual episode. This instance can be obtained joining the $ReadySet$ of the $BeginState$ and all the

decisions $D(v^i)$ corresponding to the actions selected during the episode. Let's be $w = C \cdot v(I)$ the cost associated to the Instance I. If I is a SC-Instance, $Reward = 1 / w$. In other case, $Reward = -w$.

5. A-LAW GUIDANCE HEURISTIC

5.1. Value function definition

In order to implement an RL algorithm a Value Function is defined.

For each possible state S, V(S) is needed to be able to be calculated. As mentioned before, the state S is defined as a set of discrete elements. For each of the elements of the state S, the following value is obtained.

$$V(elm) \leftarrow \sum_{\{C_i | elm \in I_i, (I_i, C_i) \in F\}} -1 \cdot C_i \qquad (3)$$

The value of the whole state S is averaged from the value of its elements.

5.2. A-Law Function

In order to speed-up the convergence to near-optimal solutions, the next formula is applied to the value function, where q represents the initial value from the RL algorithm, and A is a value proportional to the frequency of the current state in previous learning episodes.

$$Q(q, A) = \begin{cases} \dfrac{Aq}{1 + \ln(A)} & if \dfrac{-1}{A} < q < \dfrac{1}{A} \\ sign(q) \dfrac{1 + \ln(A|q|)}{1 + \ln(A)} & if\ |q| \geq \dfrac{1}{A} \end{cases} \qquad (4)$$

This function reinforces the value of the states that have been frequently visited, enhancing the highly valuated ones, and decreasing the value of the rest of the frequent states. It doesn't modify significantly the values of non frequent states.

The A-Law is a bi-dimensional function. One of the dimensions is the frequency of the decision element in the previous solutions. The other one is the value of the V-function to modify. The figure shows the behavior of the function for the V-function value given two fixed values of the frequency. When the frequency is low, the function is approximately the identity. This is, the value does not get significantly modified. However, as the frequency value grows, the non-linearity of the functions increases becoming closer to a step function. The values of the first half of the range of the V-function are decreased while the values on the second half are increased even more. This is done to discriminate the values for which more information has been retrieved, allowing to increase the convergence ratio.

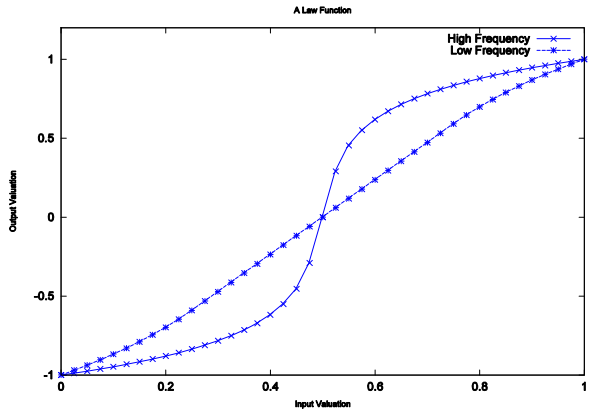

Figure 4 A-Law function representation for different frequency values.

6. EXPERIMENT DESIGN

The defined problem has been simulated over different scenarios, varying the problem size in order to get results about how it does scale up.

Experiments using RL without A-Law Guidance are also executed, comparing the results with the previous ones.

We describe now the implemented setup, to achieve the results shown in the following section.

The experiments described in this paper are restricted to WS's with only one start node and only one end node ($|V_o| = |V_f| = 1$). Other important constraint is that every instance I of our WS can be extended to a SC-Instance.

The first generated WS has 9 nodes, 45 edges and the number of different complete instances defined on it is over 40000. The cost of the optimal instance is 1389.

The second one is larger, with an approximate number of different complete instances around $3 \cdot 10^6$, and an optimal solution with a cost of 3159.

Both RL approaches with and without A-Law correction, are used in a hundred of identical experiments, each of them starting with no prior knowledge from the specific problem and finishing with the information from all the previous episodes of that experiment. Each experiment generates 5000 episodes, this is 5000 instances. The experiments are repeated a hundred times and the cost of each instance on each experiment is stored. In order to show the general behavior of the strategy the mean over these 100 experiments is calculated. So that, a sequence of 5000 values is obtained and each of these values represents the mean cost of the generated instances at a certain iteration number n. Then, the sequence is shrunk in a way in which each value represents the mean of 100 consecutive values in the original sequence. This is done to filter the high frequency variation of the data, making it easier to deduce the evolution in the long term.

7. RESULTS

Simulation results are shown comparing and analyzing the solutions achieved by the various experiments designed.

Figure 5 represents the results when using the medium size WS. Both approaches, making use and without using the A-Law function are represented. In the horizontal axis the episode number is represented, while in the vertical axis shows the mean cost over the hundred executions.

As it was expected, when the A-Law function is used, the costs obtained converge faster to near optimal values in comparison with the other approach. Consequently, a better policy is obtained in a fewer number of episodes. However, it can be appreciated a side-effect at the beginning of the episodes of the experiments. In this case the exploration ratio of the search space is increased compared to when no A-Law is applied. On the one hand, this has the effect of increasing the information available to explore better solutions afterwards. On the other hand, the aggressive exploration at the beginning can be dangerous in certain contexts. In the academic example described before, it would not be a good idea to perform really poorly at the beginning since that means wasting the invested money.

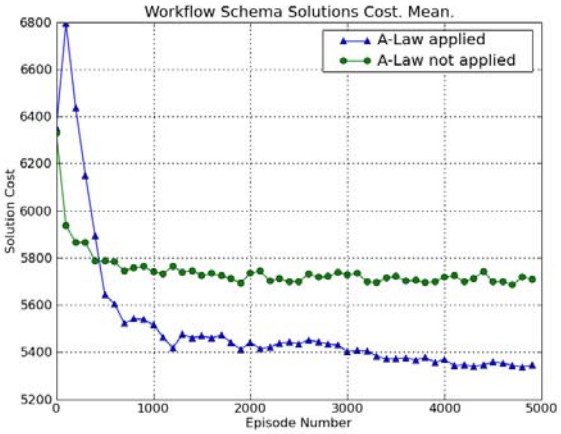

Figure 5 Medium size WS results.

Figure 6 has been obtained using the large WS. Some changes in the behavior of the compared strategies are shown. Nevertheless, the approach using the A-Law function remains as the best option, with higher convergence ratio.

With a larger number of possibilities to build an Instance, the side-effect of higher the exploration in the first episodes is not significant anymore. In this case, the better convergence ratio achieved using the A-Law function cannot be associated with this first stage of exhaustive exploration. Furthermore, there is a non-desirable effect in the evolution of the strategy. After reaching a local minimum in the cost of the achieved solutions, the behavior of the policy begins to get worse. This behavior is explained since the information from the initial episodes with high costs, looses weight in the policy calculation as more episodes with low cost are achieved.

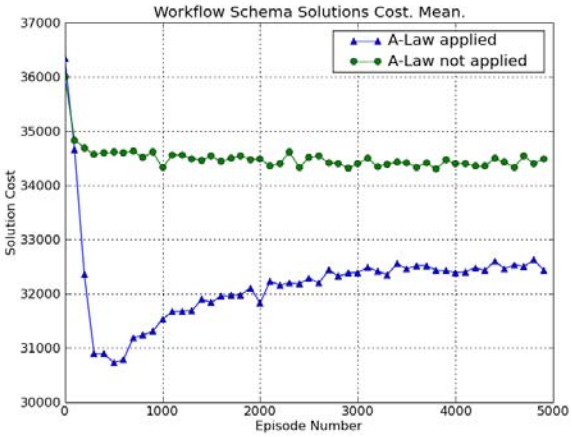

Figure 6 Large WS results.

8. SUMMARY AND FUTURE WORK

The preliminary results of the adaptation of RL algorithms to Network-Structured States have been shown, including the A-Law function modification of the Value Function. The analysis of the achieved results is conclusive, showing that the proposed modification represents advantages with respect to other approximations. Nevertheless, the contra productive effects when applied to real world problems should be tackled in the future before it could demonstrate its benefits with more complex and uncontrolled data sources.

The aggressive exploration of the solution space during the early episodes when applied to some problem definitions cannot be acceptable in some real scenarios, and other approaches for the first stage should be used. In addition, the learning strategy used showed an inappropriate behavior when applied to large search spaces. In these problems, the policy achieved after a certain episode, it was not only unable to be improved but it got worse. A change in the way the learning process is implemented is necessary. Some common approaches found in the literature to tackle this problem are, firstly, remembering only the most significant instances achieved instead of all of them. The purpose of the approach is to reduce the memory needed for the algorithm during the execution, and to avoid giving excessive importance of certain parts of the search space in the creation of the policy. Secondly, other approaches focus on the use of local search around the areas where the better solutions so far have been found. The motivation in this case is to reduce a large search space, focusing the algorithm only on those areas where there are potentially more options to obtain the optimal solution.

ACKNOWLEDGMENTS

Pedro Toledo is supported by a FPU fellowship from the Spanish Ministry of Education and Science.

REFERENCES

Driessens, K. (2001). Relational reinforcement learning (Technical Report). *Multi-Agent Systems and Applications, 9th ECCAI Advanced Course ACAI 2001 and Agent Links 3rd European Agent Systems Summer School (EASSS 2001), volume 2086 of Lecture Notes in Computer Science*.

Främling, K., 2007. Guiding exploration by preexisting knowledge without modifying reward. *Neural Networks*, 20, 736-747.

Friedler, F., Fan, L. T., and Imreh, B., 1998. Process network synthesis: Problem definition. *Networks*, 31, 119-124.

Friedler, F., Tarjan, K., Huang, Y. W., & Fan, L. T., 1992. Graph-theoretic approach to process synthesis: Axioms and theorems. *Chemical Engineering*, 47, 1973-1988.

Goodrich, M. A., & Peterson, T. S. (2000). Informed exploration: A satisficing approach to q-learning.

Greco, G., Guzzo, A., and Manco, G., 2005. Mining and reasoning on workflows. *IEEE Transactions on Knowledge and Data Engineering*, 17, 519-534. Senior Member-Domenico Sacca.

Guestrin, C., Koller, D., Parr, R., and Venkataraman, S., 2003. Efficient solution algorithms for factored MDP's. *Journal Artificial Intelligence*. Res. (JAIR), 19, 399-468.

Gyapay, S., and Pataricza, A., 2003. A combination of petri nets and process network synthesis. *IEEE International Conference on Systems, Man and Cybernetics, Invited Sessions/Track on `Petri Nets and Discrete Event Systems'*, 1167-1174.

Paternina-Arboleda, C. D., Montoya-Torres, J. R., and Fábregas-Ariza, A., 2008. Simulation-optimization using a reinforcement learning approach. *WSC '08: Proceedings of the 40th Conference on Winter Simulation* (pp. 1376-1383). Miami, Florida: Winter Simulation Conference.

Rozinat, A., Alves de Medeiros, A., Gunther, C., Weijters, A., and van der Aalst, W. 2007. Towards an evaluation framework for process mining algorithms. *BPM Center Report*, BPM-07-06.

Sutton, R. S., and Barto, A. G. (1998). Reinforcement learning: An introduction (adaptive computation and machine learning). The MIT Press.

Thrun, S. B., 1992. Efficient exploration in reinforcement learning (Technical Report). Pittsburgh, PA, USA.

AUTHORS BIOGRAPHY

PEDRO TOLEDO received the degrees in Computer Science Technical Engineering and Computer Science Engineering from the University of La Laguna (Spain) in 2002 and 2004 respectively. He is a Ph.D. student at the same university since 2004, in the Department of Systems Engineering and Control and Computer Architecture. In addition, he collaborated with the DTAI group of the Computer Science Department of the Katholieke Universiteit Leuven during the year 2008. His current research interests include Reinforcement Learning, Graph Mining, and Workflow Induction.

JOSÉ IGNACIO ESTÉVEZ was born in Santa Cruz de Tenerife, Spain, in 1970. He received the M.S. degree in Applied Physics and the Ph.D. Degree in Computer Science from the University of La Laguna in Tenerife, in 1992 and 2001, respectively. Since 1994, he is lecturer in the "Department of Systems Engineering and Control and Computer Architecture", University of La Laguna, where she is currently a professor in Systems Engineering and Automation. His areas of interest include automation, signal processing, image processing, and reinforcement learning and graph mining.

SILVIA ALAYÓN was born in Santa Cruz de Tenerife, Spain, in 1975. She received the M.S. degree in Electronic Engineering from the University of La Laguna (Spain) in 1999, and the Ph.D. degree in Computer Science from the same university in 2003. Since 1999, she is teacher into the Departamento de Ingeniería de Sistemas y Automática y Arquitectura y Tecnología de Computadores, University of La Laguna, where she is currently an assistant professor in Systems Engineering and Automation. Her areas of interest include automation, signal processing, image processing, artificial intelligence, and neuro-fuzzy systems for medical applications.

JOSÉ SIGUT was born in Santa Cruz de Tenerife, Spain in 1970. He received the M.S. Degree in Applied Physics and the Ph.D. Degree in Computer Science from the University of La Laguna in Tenerife, in 1995 and 2002, respectively. In 1993, he joined the Department of Systems Engineering in the same university where he is currently an Assistant Professor. His research interests include pattern recognition, computer vision and biomedical engineering.

THE SIMULATION OF A BIOSENSOR IN MEMS CONFIGURATION

C. Ravariu[(a)], F. Babarada[(a)]

[(a)]Politehnica University of Bucharest, Romania

[(a)]cr682003@yahoo.com , babflorin@yahoo.com

ABSTRACT

The nowadays biomedical applications need manipulations of very small amount of liquids. The classical pumps with movable valves suffer from the fatigue of the movable parts, having a reduced lifetime and can destroy some biological macromolecules. A valveless micropump with a diffuser/nozzle element is in agreement with the silicon technology and bioliquids requirements. This work proposes a micropump with diffuser/nozzle channels dedicated to charged bioliquids. There is presented applications of this kind of integrated micropump like biosensor for charged analyte. The simulation with CoventorWare has taken into account a piezoelectric actuation.

Keywords: Modelling and simulation, integrated micropump, biosensor application.

1. INTRODUCTION

A variety of chemical and biological procedures need tools that can accurately deliver metered quantities of liquids, (Liu, Lim, Tay, and Wan, 2004).

In a previous work, an electrical and technological study was presented for a similar MEMS micropump, (Babarada, Dobrescu, Nedelcu, Ravariu C, Ravariu F, and Rusu, 2005). Some improvements were proposed in this work for this conceptual biodevice: Silicon On Insulator - SOI - film without any additional drain/source diffusion, working on the pseudo-MOS transistor principle, (MOS being the Metal-Oxide-Semiconductor acronym), (Babarada, Ravariu C, Ravariu F, and Rusu, 2007). On the other hand, SOI is inherent in the case of Si-membrane on empty space – the micropump chamber. So, the buried oxide can be replaced with a deep boron implantation in order to provide a good etch stop layer. This means lower costs of fabrications. Versus the old MEMS micropump (Babarada, Dobrescu, Nedelcu, Ravariu C, Ravariu F, and Rusu, 2005), in this paper the membrane actuation is performed by a piezoelectric layer deposited onto Silicon, accordingly with the speciality literature, (Liu, Lim, Tay, and Wan, 2004).

In this way a double scopes can be fullfiled by this MEMS:

- A bioliquid recirculating in small amont using just the mechanical behavior of the MEMS. By the electrical voltage applying on gate, the piezoelectric is bending and actuates the membrane. The down-bending of the Silicon membrane corresponds to the "pump mode". Now the fluid is transferred from inlet to outlet.
- The biosensor function for electrical charged analyte like metabolism products: NH_4^+, OH^-, H_3O^+, or charged molecules like adrenaline. A biase applied on the Front-Gate terminal developes an electric field in the semiconductor film that attract the positive ions from liquid. In the same time the positive external gate voltage attracts the negative ions at the semiconductor surface and let the positive ions to flow through the outlet with the carrier liquid.

2. THE MEMS DEVICE

This biodevice belongs to the MEMS class, being composed by two main parts: (1) a Si-wafer, back etched, with a piezoelectric layer deposited onto the Si-film and (2) a bulk silicon wafer micromachined in order to include the diffuser and the nozzle channels.

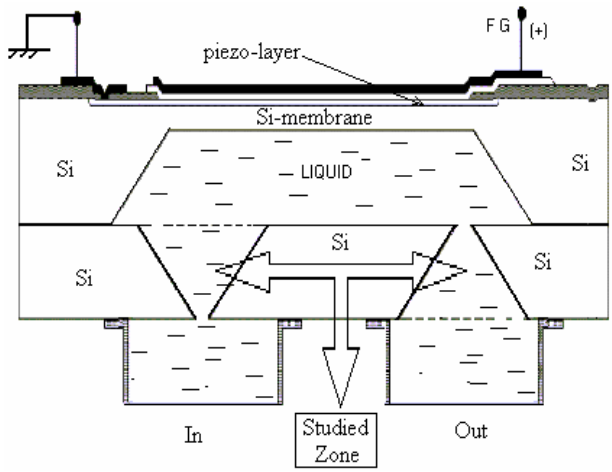

Figure 1: The global device architecture

Both parts are easily bonded in the silicon technology, resulting a strong connection. The Si-film play a double role: as sensitive transducer at electrical charged analyte and as a micropump membrane. The

usual "front Oxide" is now replaced by the piezoelectric layer.

Coventor software will establish the deviation d versus the V_{FG} bias. The Micro-Electro-Mechanical System proposed in this paper is presented in fig. 1. The upper gate of the SOI-MOSFET, usually named the Front-Gate (FG), represents the command terminal.

During the positive bias V_{+}, the Si-membrane is down-bending. Now the chamber volume decreases ("the pump mode") and the outlet acts as a diffuser with a lower flow restriction than the inlet, which play the nozzle role. A larger volume of liquid is transported out of the chamber through outlet than through input.

When V_{FG} bias becomes negative, V_{-} , the membrane rises and becomes up bending. The chamber volume increases ("the supply mode") because a larger volume is transported into the chamber through the inlet (that acts as a diffuser), than through the outlet (that acts as a nozzle).

3. SIMULATIONS RESULTS

3.1. The Membrane Deflection

In this case, the incident stimulus is the electrical signal. Coventor software establishes the membrane deviation d, versus the V_{FG} bias.

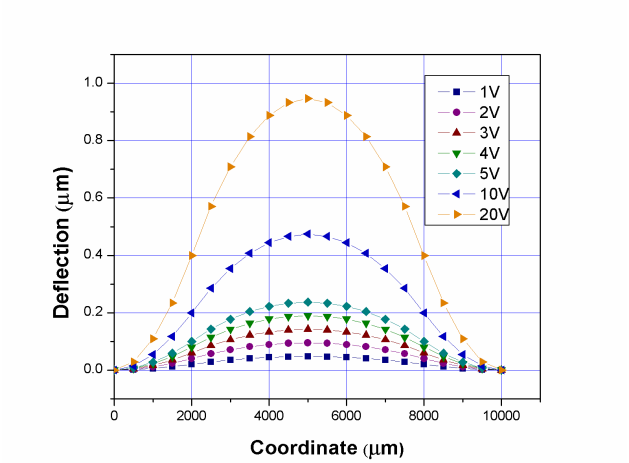

Figure 2: Graph of the deflection |U| versus x coordinate (horisontal surface in fig.1) for positive V_{FG}

In the simulations, the sizes were selected accordingly with the drug delivery purpose. A mechanical stress in a Silicon square membrane with dimension 10000μm x10000μm x100μm was firstly studied. Over the Si-membrane a PZT layer with dimensions 6000 μm x 6000 μm x 100 μm was deposited. The front gate voltage that actuated the membrane was varied in the range 1V ÷ 20V. A membrane deflection was observed from simulations, accordingly with fig. 2.

The mechanical stress arisen in the Si-membrane as a consequence of the reverse piezoelectric effect from PZT layer is presented in figures 3, 4, 5. The colour code from blue to red depicts the minimum-maximum range.

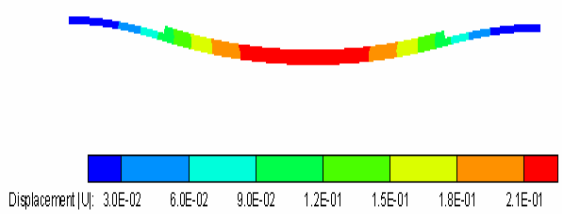

Figure 3: Cross-section through the Si-membrane / PZT for V_{FG} =5V

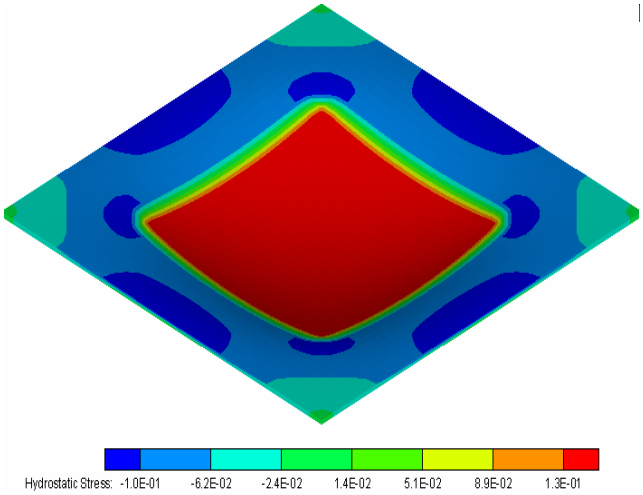

Figure 4: Hydrostatic stress in the membrane when the actuation voltage on PZT was 5V

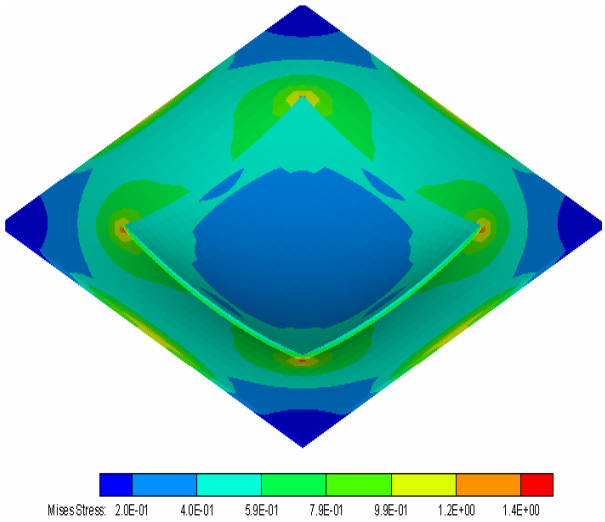

Figure 5: Mises stress in the membrane when the actuation voltage on PZT was 5V

The simulations reveal that the main stress - Mises Stress – doesn't reach unacceptable values. The maximum value is 1.4 MPa, while the failure mechanical stress for Si-membranes is roughly 300 MPa.

3.2. Microfluidics Simulations

In this case, the applied stimulus was a difference of pressure applied at the valve extremities.

Both the diffuser and the nozzle elements have a pyramid trunk shape with sizes: l = 100µm, L = 736µm, H = 450µm , where l is the small base length, L is the big base length and H is the height of the pyramid trunk. In the simulations the same valve was used. The flow sense is distinct in respect with a difference of pressure, once applied in the flow sense, when the valve acts as diffuser and secondly reverse to the flow sense, when the valve acts as nozzle. In the figure 6, 7, the fluid vector flow in a diffuser/nozzle were shown. This situation occurs when the front gate voltage that actuates the piezoelectric layer was 1V.

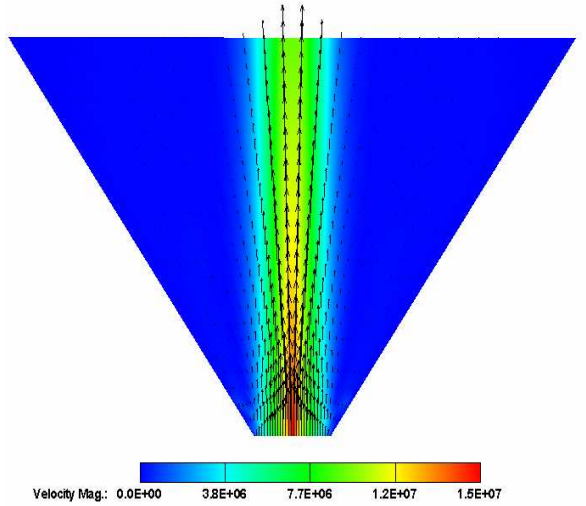

Figure 6: The fluid velocity vectors in the diffuser case

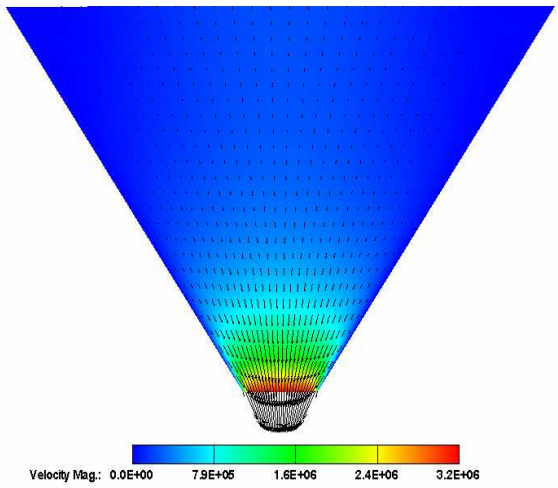

Figure 7: The fluid velocity vectors in the nozzle case

All simulated results for diffuser and nozzle presented in fig. 6, 7. Here is obvious that the flow through diffuser is higher than the flow through nozzle, at the same difference of pressure applied on the valve. The difference between these flows represents the net flow of the micropump. The micropump outlet channel can be attached to an incinte designated to load the fluid.

4. SIMULATIONS RESULTS

An immunosensor for acetylcholine with nicotinic acetylcholine receptors (nAChRs) was reported, (Erdman, Liu, Yi, and Tianhong, 2007). Normally, acetylcholinesterase (AChe) hydrolyses acetylcholine, given H^+ hence H_3O^+ in water solution. Consequently isn't necessary to measure the acetylcholine concentration. The reaction products H_3O^+, are more comfortable to be detected by potentiometric method, considering the H_3O^+ ions as analytes.

The proposed MEMS structure that allows the bioliquid transport underneath the Si-membrane, has the additional advantage to be sensitive at ions concentration. The bioliquid is electrically charged with ions of analytes.

The receptor layer could be entrapped near semiconductor. Consequently, the analytes are crowding near the receptor layer. Their electrical charge biases the transistor. The spatial arrangement of ions near an electrode consists in the rigid and the diffuse layer forming. An analysis from electrical point of view is presented in the following paragraph. The Poisson equation can be written:

$$\frac{d^2V}{dx^2} = -\frac{qc_A(x)}{\varepsilon_{bioliquid}} \tag{1}$$

The induced gate over-voltage, V_{Gi}, can be computed assuming a linear distribution of the analytes electrical charge:

$$V_{Gi} = \frac{1}{3}\cdot\frac{Q_{max}\, x_{dif}}{\varepsilon_{bioliquid}} \tag{2}$$

where the Q_{max} (e/cm^2) is the maximum charge density, $\varepsilon_{bioliquid}$ is the dielectric permittivity of the carrier liquid and x_{dif} is the diffusion layer length. Table 1 presents some analytical results regarding the induced gate voltage by different analytes concentrations.

Table 1 : Resulted Gate Voltage

Q_{max} (e/cm^2)	x_{dif} (µm)	V_{Gi} (V)
10^{11}	1	0.075
10^{12}	1	0.757
10^{13}	1	7.575
10^{12}	5	3.787
10^{12}	0.5	0.378
10^{12}	0.1	0.007

An electric charge concentration about $Q_{max}=10^{12}ecm^{-2}$ means a number of molecules about 10^{16} molecules of analyte/cm^3, that means a molar concentration of analyte in the range C_v=0.01µmol/ml.

The detection of this low analyte concentration is useful in IMmuno-FETs.

5. CONCLUSIONS

The paper approached simulations and analytical aspects of a particular micro-electro-mechanical system for medical applications. The simulations have taken into account two main directions: actuating and control of the fluid flow through the micropump.

As actuating element, a Si membrane covered by a PZT material based on the reverse piezoelectric effect, was simulated. The diffuser and nozzle valves have the advantage to not destry some macromolecule from medical analyses and to be compatible with the Si-technology. Using a Si membrane, the MEMS presents an additional advantage: the Si-film is an excellent transducer for possible charged analytes.

Applications of this MEMS were described: as micropump for bioliquid recirculating and as a biosensor that detect the electrical charged analyte. The surface of semiconductor could be micromachined so that fulfills a large spectrum of biosensors based on the Field Effect Transistors: free semiconductor surface for ISFETs, enzime entrapped surface for ENFETs, or Antigens entrapped surface for ImmunoFETs. In this last case low analyte concentration can be detected.

ACKNOWLEDGMENTS

The paper is financial sustained by 12095 and 62063 PN2 Romanian Research Program.

REFERENCES

Liu, H., Lim, G.C., Tay, A.A.O., and Wan, S.Y.M., 2004. A Low Cost Polymer Based Piezo-Actuated Micropump for Drug Delivery System. *Proceedings of 22th IEEE Conference on Nanotech*, pp. 251-254. vol.1. (Boston, USA).

Babarada, F., Dobrescu, L., Nedelcu, O., Ravariu, C., Ravariu, F., and Rusu, A., 2005. A MEMS dedicated to the bio-components detection, inspired from the SON architecture. *Proceedings of 28th IEEE Semic. Annual Conference,* pp. 219-222. (Sinaia, Romania).

Babarada, F., Ravariu, C., Ravariu, F., and Rusu, A., 2007. More accurate models of the interfaces oxide ultra-thin SOI films, *Journal of Applied Physics*, under the American Institute of Physics auspices, 893 (10), 3-4.

Erdman, A.G., Liu, Yi., and Tianhong, C., 2007. Acetylcholine biosensors based on layer-by-layer self-assembled polymer/nanoparticle ion-sensitive field-effect transistors, *Sensors and Actuators A: Physical ,* 136 (2), 540-545.

AUTHORS BIOGRAPHY

Cristian RAVARIU, received the M.Sc. degree in Electronics & Telecommunications in 1993 and the Ph.D. degree in 2001, both at the Politehnica University from Bucharest, Romania. From 1993 to 1999 he activated as researcher at the National Institute of Microtechnology, in the field of Electronics Devices Simulation and Silicon technology. From 1999 he works at the Politehnica University of Bucharest, Faculty of Electronics Telecommunications and Information Technology, Department of Devices Circuits and Electronics Apparatus, firstly as assistant professor, secondly as lecturer and in the lasts 5 years as associated professor. His interests and research areas concern the modelling and devices simulation, nanotechnologies, bioelectronics and cellular nanoelectronics.

Florin BABARADA is with the Politehnica University of Bucharest, Romania, Faculty of Electronics Telecommunications and Information Technology, Microelectronics Department, B-dul Iuliu Maniu 1-3, Sector 6, Bucharest. He is working in the nanotechnology field, circuit design. e-mail: babflorin@yahoo.com .

BIOINFORMATICS RESOURCE FACILITY HAGENBERG—BUILDING HIGH PERFORMANCE COMPUTING SERVICES FOR SOLVING BIOINFORMATICAL PROBLEMS

Peter Kulczycki[(a)], Hannes Brandstätter-Müller[(b)], Gerald Lirk[(c)]

[(a, b, c)]Upper Austria University of Applied Sciences
School of Informatics, Communication, and Media
Department of Bioinformatics

[(a)]kulczyck@fh-hagenberg.at, [(b)]hbrand@fh-hagenberg.at, [(c)]glirk@fh-hagenberg.at

ABSTRACT
Recent developments in genetics, molecular biology, and biomedical sciences do make a tremendous amount of data available to scientists. The required analyses (i. e., post processing) is increasingly done on homogenous high performance computing clusters, the need for computing power of these kind of applications is very demanding. But focusing just on homogenous systems has a major drawback: the exceeding costs. Our research will focus on the development of a resource facility that utilizes heterogeneous hardware infrastructure to achieve an optimal cost to performance ratio. Emphasis is laid on—but not restricted to—alternative system and processor topologies like general purpose graphic processors (GPGPUs) as well as the IBM CELL Broadband Engine. Besides the hardware aspects, our research will also concentrate on how to bring this computational power without any loss to the user and make it thus available for solving highly specific problems of domain experts, especially molecular biologists. Finally, our research will also concentrate on how to develop intelligent scheduling and priority management for highly demanding compute tasks.

Keywords: algorithms, bioinformatics, high performance computing, molecular biology

1. INTRODUCTION

One big challenge in the area of molecular biology and therefore in the area of bioinformatics is constantly moving towards the need of having to analyze and process continually growing amounts of raw data. The faster this data gets processed the more detailed analyses can be performed, leading to increasingly better getting biomedical diagnosis methods. Traditionally, homogenous parallel computing clusters are employed in order to reduce the time needed for mastering these computational demands. But unfortunately, with these homogenous systems, there come several major drawbacks:

1. Building a dedicated cluster of workstations (COW) requires capital expenditures that will be extremely high (measured in emerging costs per GFlops).
2. Besides the above mentioned costs, one has to spend additional money for establishing the necessary infrastructure. Moreover, keeping such a system up and running requires highly specialized and skilled operators.
3. When reusing computational hardware already available at a site in order to create a cost effective e. g. Beowulf cluster (Sterling et al. 1995), one has to be aware that the maintenance and stability of such a system can be serious issues.

Alternative processor architectures may offer a way to avoid these problems. Conceptual, a classic CPU performs one instruction on a single data point per cycle (single instruction single data, SISD). Especially for vector and matrix based mathematical operations, the inherent data parallelism could be exploited, if the CPU could perform operations over multiple data points in one cycle (single instruction multiple data, SIMD). Current CPUs support a just very restricted vector based instruction set in specific extensions, e. g. AltiVec and SSE. (Strey and Bange 2001) However, these extensions can only be effectively used in smaller problem instances.

On the other hand, graphics processors (GPUs) utilize powerful vector based instruction sets in a natural manner, access to these instructions was made available to developers during the last few years. NVIDIA, for instance, supports high performance computing with a specially tailored programming language called “Compute Unified Device Architecture” (CUDA). (NVIDIA 2009)

Similarly, IBM created a special CPU that uses up to eight so-called “synergistic” processors to move the main processing threads off to different parts of the chip, where they can run in parallel while accessing a shared memory. This architecture is called the “IBM CELL Broadband Engine.” Originally, it was developed for gaming consoles and other multimedia hardware, but the possibilities were soon discovered. In addition to the Sony Playstation 3, the CELL Architecture is used in various professional high-performance hardware. The currently fastest super-

computer is based on the CELL architecture. (IBM 2006)

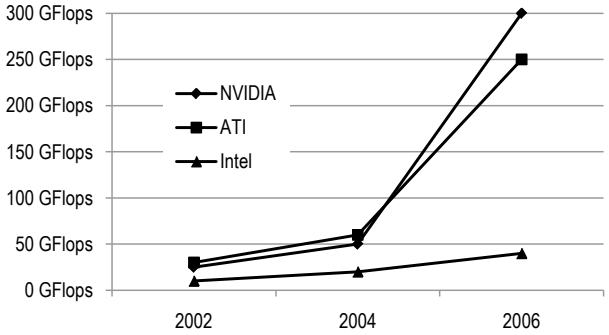

Figure 1: Comparison of the Floating-Point Performance of CPUs and GPUs; according to (Owens et al. 2007)

When comparing the performance gain over the last years, as shown in Figure 1, it becomes obvious that the traditional processor architecture is hitting a performance limit (which can be worked around slightly by using multi-core systems). Many computational problems can be transferred to a SIMD logic, freeing up the main CPU for the operating system and data management tasks, which it is better suited for.

2. STRUCTURE AND DESIGN

In order to achieve the aspired goals of BiRFH, we have to construct flexible and adaptive software services utilizing a heterogeneous hardware infrastructure. The seamless interoperability between soft- and hardware is crucial for achieving a maximum system's throughput, stability, and flexibility. In the following section, we give an overview of the systems overall design, focusing especially on software and hardware issues.

2.1. A Survey of BiRFH

Figure 2 shows the tree major layers of BiRFH's system design. They are namely:

1. "BiRFH Access,"
2. "Management and Software Resources," and
3. "Computation Resources."

Operating tightly together, these three layers guarantee flexibility, ease of access, ease of getting individually configured and adapted, and—mostly important—maximum throughput. Each layer is designed in a modular and component-oriented way in order to achieve an even higher level of flexibility.

2.2. Management and Software Resources

In the following section we describe the "Management and Software Resources" that form the major and central software components of BiRFH.

The core components of the "Management and Software Resources" are a large number of algorithms. This collection contains algorithms from different domains and special fields. We plan to integrate algorithms from the field of bioinformatics (e. g. alignment algorithms, DNA to protein mappings, phylogeny and mapping algorithms, algorithms for calculating common substrings, fragment assembly algorithms) and from the field of biomedical informatics (namely image processing algorithms).

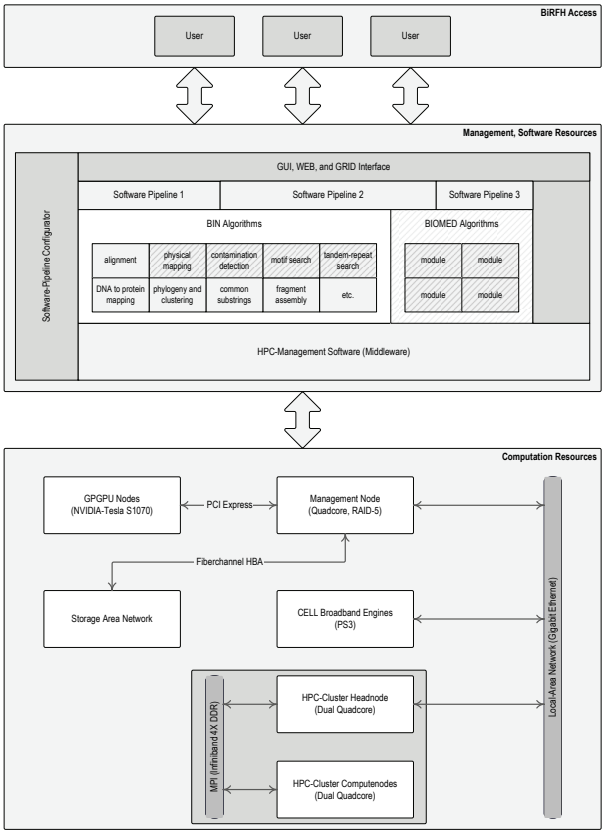

Figure 2: A Survey of the Structure and the Design of the "Bioinformatics Ressource Facility Hagenberg" (BiRFH)

These algorithms can be assembled into so called "algorithm pipelines." Since the procedures and calculations that are required in processing data acquired by analysis processes in a molecular laboratory are manifold and have to be executed in many subsequent ways and steps, the software of BiRFH has to be able to reflect this variability. It will be a very demanding task to design the algorithm interfaces in such a way that

1. a flexible combination of these algorithms will be possible, and that
2. a maximum throughput can be guaranteed.

Moreover, the "Management and Software Resources" will contain a graphical user interface, that will allow an average informatically skilled molecular biologist to assemble and arrange algorithms according her individual needs. This part of the BiRFH software, called "Software-Pipeline Configurator," will not only allow this easy configuration and assembly of algorithms, moreover, it will guide the user in the configuration process and provide her with all data needed to parameterize the system in such a way that performance and throughput will be a maximum. (See Figure 2.)

Interfacing the user, the "Management and Software Resources" will provide services for interacting with GUI extensions, the world wide web (via WEB services), and the Grid (Jacob et al. 2005).

To carefully design the interfaces to the hardware will be a very challenging part of the "Management and Software Resources," since the three processor and system topologies demand very different treatment in order to achieve reasonable performance results. The handling of huge amounts of sensitive patient data as well as the seamlessly orchestration of CELL, GPGPU, and COW (see Section 2.3) demands a very powerful "HPC- Management Software" layer.

2.3. Computation Resources

In the following section we describe the Computation Resources that form the major and central hardware components of BiRFH.

Table 1: The Processor Architectures Utilized by BiRFH and Their Estimated Processing Capacity R_{peak}

System	R_{peak}	Cores	Product
CELL	1.0 Tflops	12	Sony PS3
GPGPU	4.0 Tflops	4	NVIDIA Tesla S1070
COW	1.5 Tflops	32	HP DL160G5

BiRFH utilizes three different processor topologies and systems, Table 1 summarizes them. The reasons for utilizing three different hardware and processor topologies in BiRFH is manifold:

1. Due to the multi-variant inner structure of the data delivered by numerous different laboratory devices and other data sources (e. g. data bases) it is inevitable to utilize the best matching processor topology and take the best choice among the various available ones.
2. What is important for the data is even more important for the algorithms. According to their very different modes of operation (e. g. how are they parallelized, how fast and in what order has data to be available at what processing unit) they scale best at different processing models and topologies. Much flexibility is demanded in that respect in order to minimize wall-clock time.
3. The cost of a classical cluster of workstations (COW) is extremely high. This includes not only equipments acquisition but also operation and maintenance. Compared to their processing power in GFlops, alternative processor topologies (CELL Broadband Engine and GPGPU) are much more cost efficient.

It follows a brief description of the two most important processor technologies used in BiRFH, the CELL Broadband Engine and NVIDIAs Tesla system (a GPGPU) in conjunction with CUDA.

2.3.1. CELL Broadband Engine

Figure 3 shows the overall structure of the CELL Broadband Engine processor. The Power Processing Element (PPE) consists of the Power Processing Unit (PPU) and a set associative write-back cache. The PPU includes a 2-way set associative reload-on-error instruction cache and a 4-way set associative write-through data cache. In addition to the floating point unit (FPU) the PPU contains a short vector SIMD engine (called VMX) that is comparable to a PowerPC Velocity Engine. The PPE is a 2-way simultaneous multithreading (SMT) processor that is comparable to a PowerPC 970 architecture (using the PowerPC 970 instruction set). The SMP is a feature that—to some extent—can be compared with the hyperthreading technology invented by Intel. The PPE provides two independent execution units and can increase the software performance up to about 30 % . (Buttari et al. 2007; IBM 2006)

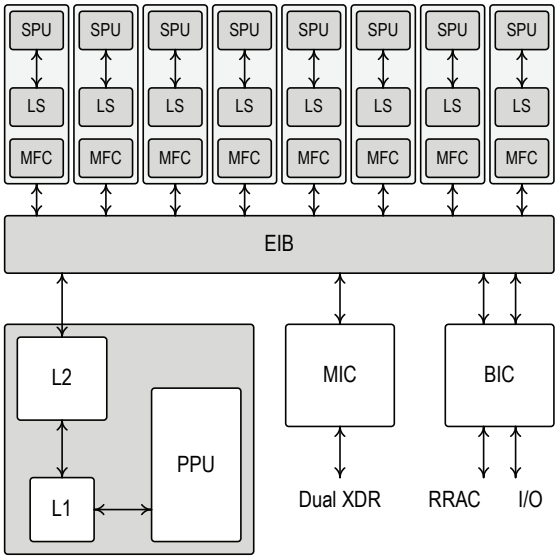

Figure 3: CELL Broadband Engine Architecture; according to (Buttari et al. 2007)

Figure 4 shows the structure of the Synergistic Processing Element (SPE). The real power of the CELL processor lies in the eight SPE cores (only six of them are enabled in the Playstation 3). The SPEs can only execute code in the local store and can only operate on data in the local store; they are designed to be short vector SIMD cores and bring the real power of the CELL processor. (Buttari et al. 2007; IBM 2006)

2.3.2. GPGPU and CUDA

Figure 5 shows the CUDA programming model reflecting the fact that a GPU is designed as a state machine that contains a graphics pipeline. The parallel nature of the GPU (Purcell et al. 2002) is called "stream" architecture (Owens 2005), especially when focusing on the highly parallel pixel shader. Stream processing means that a uniform set of instructions is applied to a stream of input data, so that each input element passes through the kernel in the same way and without interdependencies.

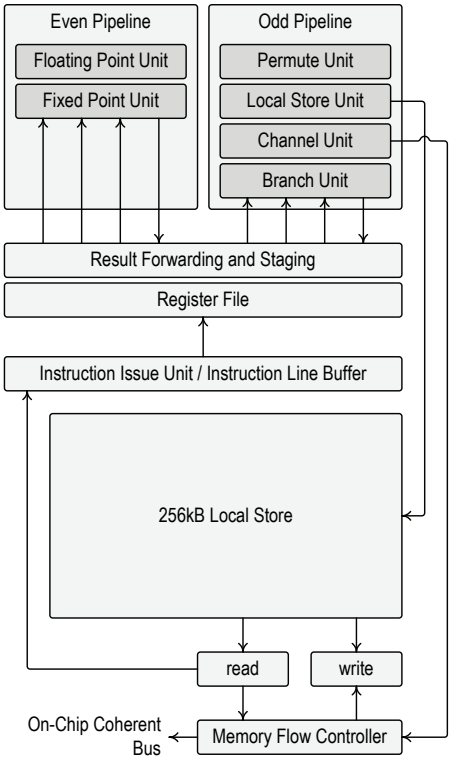

Figure 4: Synergistic Processing Element Architecture; according to (Buttari et al. 2007)

This computational model is similar to the vector computing model of early supercomputers. There are, however, some drawbacks to the impressive computational power of GPUs: data transfer between the CPU and the GPU is rather slow, especially the readback from the GPU. Because of this, we can differentiate between computationally bound and bandwidth bound problems, signifying problems which are bound by either the GPU calculation speed limit or the data transfer limit. Additionally, many conventional algorithms do not fit the stream computing design. (Mueller 2006)

At the CUDA's parallel programming model's core (see Figure 5) are three key abstractions, (1) a hierarchy of thread groups, (2) shared memories, and (3) barrier synchronization. They are simply exposed to the programmer as a minimal set of language extensions. These abstractions provide fine-grained data parallelism and thread parallelism, nested within coarse-grained data parallelism and task parallelism. A compiled CUDA program can execute on any number of processor cores, and only the runtime system needs to know the physical processor count. (NVIDIA 2009)

In the CUDA memory model, each multiprocessor—illustrated as blocks—contains the following four memory types:

1. One set of local registers per thread.
2. A parallel data cache or shared memory that is shared by all the threads and implements the shared memory space.
3. A read-only constant cache that is shared by all the threads and speeds up reads from the constant memory space, which is implemented as a read-only region of device memory.
4. A read-only texture cache that is shared by all the processors and speeds up reads from the texture memory space, which is implemented as a read-only region of device memory.

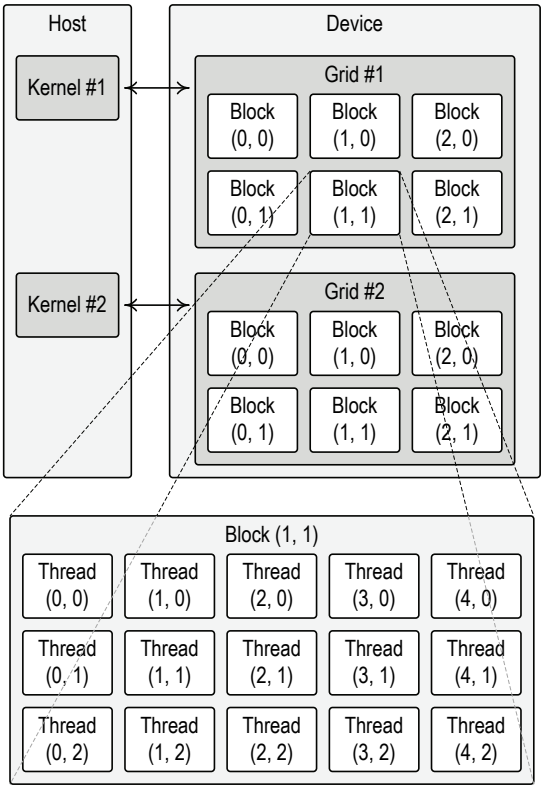

Figure 5: CUDA Programming Model

3. TASKS AND APPLICATIONS

In order to make BiRFH fulfill its specified tasks, our research group will focus mainly on the following tasks:

1. Building up an HPC infrastructure that integrates a cluster of workstations, NVIDIA Tesla hardware as well as CELL Broadband Engine hardware.
2. The algorithms listed in Section 2.2 have to be implemented on all three platforms and have to be evaluated on each platform for their specific performance characteristics.
3. Using this performance data, we will have to create management and scheduling services that automatically allocates computing tasks to those hardware that is best suited for that specific task. A fallback to the second-best platform will be done only in those cases, where an otherwise unreasonably long waiting time would reduce the overall system's performance.
4. Provide software interfaces to researchers, who want to implement software pipelines based on BiRFH's HPC hardware.

5. Building up a user friendly graphical interface as well as connecting BiRFH to the world wide web and the Grid.

Several research groups worldwide have already published implementations of various bioinformatical algorithms either for CELL and/or for GPGPU platforms. (Li and Petzold 2005; Sachdeva et al. 2008; Schatz et al. 2007) Based on these results, we will implement all required algorithms on all three processor topologies. It will be crucial to compile performance tables that reflect the throughput characteristics of all algorithm-processor pairings. These tables form the base upon which the scheduler will operate and make its decisions.

Having adequate high computing performance available is one of the mayor demands in a wide area of biomedical research topics on a molecular level. During the life span of the research project BiRFH, we will focus on several applications:

1. **HLA Typing:** The Red Cross Transfusion Service of Upper Austria located in Linz uses a Roche Titanium FLX Sequencer (see Figure 6) for genetic analyses and gene typing, especially for transplantation compatibility. The sequencer produces about 20 GB of raw data per run, which would take a modern Quad-core system about 80 hours to prepare for the final analysis. The main analysis will be implemented on our cluster, as well as further analysis of the resulting data. (Danzer et al. 2008; Polin et al. 2008; Wolbank et al. 2007)
2. **Breast Neoplasm Diagnosis:** The Red Cross Transfusion Service of Upper Austria located in Linz is working on a research project that integrates several parts: (1) Gene expression and SNP analyses via Affymetrix Whole Genome Chips. (2) Epigenetical analyses and micro RNA profiling via bisulfite sequencing. (3) Utilization of mass-spectrometry based methods for detecting posttranslational modifications of p53.
3. **Tumor Mimetics:** Establishing of innovative human tumor mimetics for the screening of bioactive active substances in high throughput procedures. In this project, we plan to generate several clinically relevant innovative tumor mimetics in order to (1) improve the efficiency and physiological relevance from active substance screenings (2) to reduce the costs of preclinical research investments of biotechnical enterprises (3) to ease the identification of critical tumor specific oncogenes and (4) to test the enormous number of potential new active substances in high throughput procedures regarding their clinical relevance. This work will be done together with the Lower Austria University of Applied Sciences IMC Krems.
4. **Peptide Array Design:** Applications for offering computational services for the company anagnostics in Linz to aid their peptide array design.

Figure 6: The Roche 454 GS FLX Titanium Sequencer

REFERENCES

Buttari, Alfredo, Piotr Luszczek, Jakub Kurzak, Jack Dongarra, and George Bosilca. 2007. "A Rough Guide to Scientific Computing On the PlayStation 3." Technical Report, Innovative Computing Laboratory, University of Tennessee Knoxville.

Danzer, M., H. Polin, K. Hofer, J. Pröll, and C. Gabriel. 2008. "Characterisation of two novel HLA alleles, HLA-Cw*0429 and HLA-DRB3*0223." *Tissue Antigens* 72 (5): 498–499 (Nov).

Díez, Daniel C., Hannes Mueller, and Achilleas S. Frangakis. 2007. "Implementation and performance evaluation of reconstruction algorithms on graphics processors." *Journal of Structural Biology* 157 (1): 288–295 (Jan).

IBM. 2006. "Cell Broadband Engine Programming Handbook." Technical Report, IBM.

Jacob, Bart, Michael Brown, Kentaro Fukui, and Nihar Trivedi. 2005. "Introduction to Grid Computing." Technical Report, IBM.

Li, Hong, and Linda R. Petzold. 2005. "Stochastic Simulation of Biochemical Systems on the Graphics Processing Unit." Department of Computer Science, University of California Santa Barbara.

Mueller, Hannes. 2006. "Implementation of Algebraic Reconstruction Techniques on Graphics Hardware." Master's thesis, Upper Austria University of Applied Sciences.

NVIDIA. 2009. "NVIDIA CUDA Reference Manual Version 2.2." Technical Report, NVIDIA.

Owens, John. 2005. *Streaming Architectures and Technology Trends*. GPU Gems 2. Edited by Matt Pharr. Addison Wesley.

Owens, John D., David Luebke, Naga Govindaraju, Mark Harris, Jens Krüger, Aaron E. Lefohn, and Tim Purcell. 2007. "A Survey of General-Purpose Computation on Graphics Hardware." *Computer Graphics Forum*, Volume 26. 80–113.

Polin, H., M. Danzer, J. Pröll, K. Hofer, U. Heilinger, A. Zopf, and C. Gabriel. 2008. "Introduction of a real-time-based blood-group genotyping approach." *Vox Sang* 95 (2): 125–130 (Aug).

Purcell, Timothy J., Ian Buck, William R. Mark, and Pat Hanrahan. 2002. "Ray Tracing on Programmable Graphics Hardware." *ACM Transactions on Graphics* 21 (3): 703–712 (July). ISSN 0730-0301 (Proceedings of ACM SIGGRAPH 2002).

Sachdeva, Vipin, Michael Kistler, Evan Speight, and Kathy Tzeng Tzy-Hwa. 2008. "Exploring the viability of the cell broadband engine for bioinformatics applications." *Parallel Computing* 34:11.

Schatz, Michael C, Cole Trapnell, Arthur L Delcher, and Amitabh Varshney. 2007. "High-throughput sequence alignment using Graphics Processing Units." *BMC Bioinformatics* 8:474.

Sterling, Thomas, Donald J. Becker, Daniel Savarese, John E. Dorband, Udaya A. Ranawake, and Charles V. Packer. 1995. "BEOWULF: A parallel workstation for scientific computation." *In Proceedings of the 24th International Conference on Parallel Processing*.

Strey, Alfred, and Martin Bange. 2001. "Performance Analysis of Intel's MMX and SSE: A Case Study." *Euro-Par 2001 Parallel Processing*, Volume 2150 of *Lecture Notes in Computer Science*. Springer Berlin / Heidelberg, 142–147.

Wolbank, Susanne, Anja Peterbauer, Esther Wassermann, Simone Hennerbichler, Regina Voglauer, Martijn van Griensven, Hans-Christoph Duba, Christian Gabriel, and Heinz Redl. 2007. "Labelling of human adipose-derived stem cells for non-invasive in vivo cell tracking." *Cell Tissue Bank* 8 (3): 163–177.

AUTHORS BIOGRAPHY

Brandstätter-Müller, Hannes works as a junior researcher at the R&D Department of the Upper Austria University of Applied Sciences in Hagenberg. In 2006, he graduated from this university in the field of bioinformatics, his diploma thesis is entitled "Implementing Algebraic Reconstruction Techniques for Tomographic Data on a Graphics Processor." (Mueller 2006) The implementation created during this thesis was also published in an article for the Journal of Structural Biology. (Díez, Mueller, and Frangakis 2007) He is since then watching the developments in high performance and parallel computing, especially general purpose computing on graphics processors.

Kulczycki, Peter graduated in 1997 from the Upper Austria University of Applied Sciences in Hagenberg in the field of Software Engineering. His diploma thesis is entitled "An Application Framework for the Distributed Simulation of Virtual Worlds by Spatial Decomposition." Then he worked until 2001 as a research assistant at the Research Institute of Symbolic Computation (RISC) at the Johannes Kepler University in Linz. Since 2001, he is a professor at the Upper Austria University of Applied Sciences in Hagenberg and is teaching Algorithms and Datastructures for Bioinformatics and Parallel and High-Performance Computing. Since 2001, he occupies the Chair of High Performance Computing at the University of Applied Sciences in Hagenberg.

Lirk, Gerald studied genetics and biochemistry at the University of Salzburg. Subsequently he studied the first part of the human medicine at the University of Innsbruck. There, he graduated from a computer science course. During this time, he worked as a research assistant in the field of intracellular signal transduction. After working on the implementation of a hospital information system, he worked a few years as an independent database programmer. Since 2003, he occupies the Chair of Biomedical Analysis at the University of Applied Sciences in Hagenberg. His research interest lies primarily in the accomplishment of clinical trials.

COLLABORATIVE KNOWLEDGE NETWORKS BASED ON IHE

Josef Altmann[(a)], Franz Pfeifer[(a)], Melanie Strasser[(a)], Barbara Franz[(b)], Herwig Mayr[(b)]

[(a)]Department of Software Engineering,
Upper Austria University of Applied Sciences, Hagenberg, Austria
[(b)]Department of Medical Informatics and Bioinformatics,
Upper Austria University of Applied Sciences, Hagenberg, Austria

[(a,b)]{josef.altmann, franz.pfeifer, melanie.strasser, herwig.mayr, barbara.franz}@fh-hagenberg.at

ABSTRACT
The recent trend towards integrated healthcare increases the need to support interdisciplinary collaboration along with the patient treatment lifecycle. However, for effective interdisciplinary collaboration health professionals and patients need to monitor and trace the medical and clinical information flow. This may lead to challenges as clinical information systems are often proprietary applications breaking the information chain.

Integration and traceability of health data from multiple sources is dependent on the existence of appropriate standards that will allow technical interoperability. Integrating the Healthcare Enterprise (IHE) is an initiative to improve the interoperability of medical information systems. IHE provides typical clinical use cases defined in integration profiles, which integrate health data and documents.

We present an approach combining selected IHE integration profiles to explore and visualize the flow of information within and among healthcare providers. Based on this information flow we apply collaborative knowledge networks, which support interdisciplinary collaboration along with the patient treatment process.

Keywords: medical informatics, IHE, clinical information flow, collaborative knowledge networks.

1. INTRODUCTION AND MOTIVATION

Clinical information systems are often proprietary applications restricting the possibility to exchange and share information among healthcare providers and thus limiting the potential to enhance the treatment of patients (Sunyaev *et al.* 2008, Norgall 2003, Wozak 2008). Moreover, the difficulty to properly exchange information limits the ability to monitor and analyze the information flow within and among medical institutions. However, an overall view of the patient treatment process requires complete information to support interdisciplinary collaboration, to improve quality assurance and to reduce medical treatment costs.

The international initiative *Integrating the Healthcare Enterprise* (IHE) aims to solve among others the above mentioned integration challenges and shortcomings in the traceability of data by offering a standardized description of medical use cases and a standard based communication between heterogeneous systems (IHE International 2009a).

There are several contributions in literature presenting different approaches to determine the flow of information within and between medical institutions. Nevertheless, all these approaches are based on insufficient, incomplete and inadequately integrated data and provide only basic support for collaboration in the daily healthcare process. (Gloor *et al.* 2003) introduces an approach based on the e-mail traffic of an organization to determine *Collaborative Knowledge Networks* (CKN). (Anderson 2002) uses questionnaires filled out manually by organizational members and observations to discover frequency and strength of interaction with other people.

Our research project *IHExplorer* (IHExplorer 2009) focuses on methods and information provided by IHE for the purpose of reassembling and monitoring the clinical information flow. Based on this information flow, we establish and analyze CKN using *Social Network Analysis* (SNA) to determine statistical key figures enabling us to compare and improve the collaboration among participants in the healthcare context.

2. COLLABORATION ENABLED THROUGH STANDARDS – INTEGRATING THE HEALTHCARE ENTERPRISE

IHE is an international initiative of medical specialists and other healthcare providers, information technology professionals and industry to improve the interoperability of information systems in healthcare by enforcing the use of communication standards like *Digital Imaging and Communication in Medicine* (DICOM) or *Health Level 7* (HL7), see (IHE International 2009a, IHE International 2009b). IHE is organized in different medical areas, called *domains*. Each domain identifies its demands and describes them in terms of use cases. For each use case common communication standards are identified and implementation guidelines, so-called *integration profiles*, are developed (IHE International 2009a). These integration profiles are summarized in the

technical framework of a domain and are used by software developers to implement healthcare information systems. Software systems compliant to an integration profile are able to communicate with other software systems implementing the same integration profile. Tests performed during so-called *Connect-a-thons* allow vendors to find out the degree of IHE conformant functionality of their systems under controlled lab conditions before launching their products (IHE International 2009a).

2.1. Integration Profiles

Integration profiles are the central concept of IHE. They ensure interoperability between information systems of different vendors by describing core components, called *actors*, and their interactions, also called *transactions*, which are based on well-established standards. Actors are information systems or components of information systems that process data (IHE International 2009a). Integration profiles summarize these actors and transactions to give a review of the clinical or administrative processes within an IHE domain (IHE International 2009b).

2.2. Audit Trail and Node Authentication

The *Audit Trail and Node Authentication* (ATNA) integration profile (Figure 1) defines basic security features of a healthcare IT infrastructure to ensure secure access to *Protected Healthcare Information* (PHI). Each access to PHI is stored in a central *Audit Record Repository* (ARR) allowing the identification of security violations whereas entries in the ARR are structured as follows (Marshall 2004):

- Which patient's PHI was accessed?
- Which user accessed it?
- Did user authentication fail?
- Which authentication failures where reported?

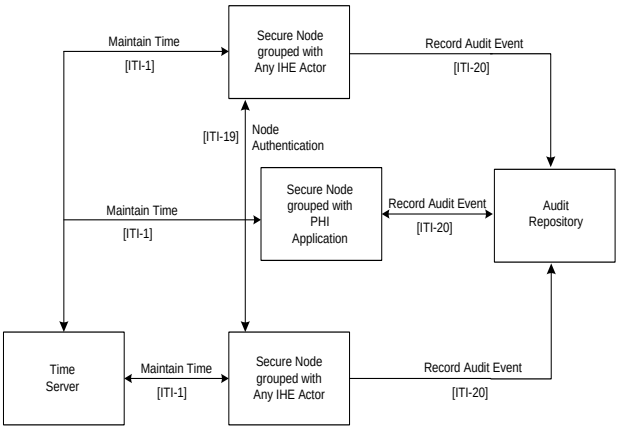

Figure 1: Use case diagram describing the actors and their transactions of the ATNA integration profile.

IHE defines both the relevant trigger events and the type of information to be recorded in the audit repository. Audit messages are transferred to the audit repository using BSD Syslog (RFC-3164) which has several limitations, e.g. the sender of the message receives no confirmation that the message has been stored in the ARR (Lonvick 2001).

2.3. Cross-Enterprise Document Sharing

The *Cross-Enterprise Document Sharing* (XDS) integration profile supports the administration of patient electronic health records across different XDS *affinity domains* by offering a standardized way of document sharing (IHE International 2009b). An XDS affinity domain consists of a group of healthcare providers agreed working together and sharing a common set of policies and infrastructure (IHE International 2009a).

The XDS registry and XDS repository represent core components of the XDS integration profile. The XDS registry stores the metadata of clinical documents which in turn are stored in the XDS repository. Storing the metadata of documents allows fast searches. An affinity domain may operate several different XDS repositories but only one central XDS registry (IHE International 2009a). Document consumers are systems that query the XDS registry for documents and – if found – retrieve documents from one or more XDS repositories.

One important aspect of XDS repositories is that they operate in a content neutral way allowing storing simple text, structured documents or images (IHE International 2009a).

2.4. Personnel White Paper

The *Personnel White Pages* (PWP) integration profile provides access to basic directory information on human workforce members within the enterprise (IHE International 2009a). This information has broad use among clinical and non-clinical application across the healthcare enterprise. The information will be used to enhance the clinical workflow as well as the user interface using the following data:

- contact information,
- phone number,
- e-mail address,
- displayable names,
- titles.

The PWP integration profile only provides the personnel information. Organizational information must be obtained via other means, e.g., the LDAP directory which holds organizational objects (IHE International 2009a).

3. COLLABORATIVE KNOWLEDGE NETWORKS IN HEALTHCARE

The presented IHE integration profiles are used as a basis to extract the flow of information among and within healthcare providers. The construction of CKN based on these integration profiles is described below.

3.1. Construction of Collaborative Knowledge Networks based on IHE Integration Profiles

A CKN consists of a group of individuals agreed working together to reach a common goal (Hu and Racherla 2008). According to (Gloor *et al*. 2003), each individual supports the community by providing its knowledge increasing the knowledge of the CKN itself. These CKNs represent the flow of information.

The information provided by the ARR and XDS registry is the starting point to determine the flow of information and the CKN within and among healthcare providers respectively. The flow of information is determined by analyzing document creation or access logged in the ARR (see Section 2.2).

IHE defines two transactions used to store documents in an XDS registry and XDS repository:

- *ITI-15*: Provide and Register Document,
- *ITI-14*: Register Document.

Each of these transactions creates an entry in the ARR storing information about the user created the document, the patient for whom the document was created and information about the registration event itself. The information about the user is stored in an *ActiveParticipant* element of the message containing the following attribute values:

- *UserId*: LDAP expression identifying the user and organization,
- *UserIsRequestor*: "true",
- *UserName*: name of the user.

The UserId attribute contains personnel and organizational information on basis of the LDAP structure, whereas personnel data contains the following information:

- given name and surname of the requesting person,
- role and rights of a person.

Organizational data is built of:

- organization unit of the requesting person (e.g., ou=users),
- organization (e.g., o=demo),
- country or region (e.g., c=at).

As described in Section 2.4, details about the organizational structure (organizational units, departments, etc.) is not provided by the PWP integration profile. Nonetheless, this information can be obtained by querying the LDAP of the underlying IHE infrastructure or by using the metadata of the document.

The registered document is identified by a *ParticipantObjectIdentification* element in an audit message containing the following information:

- *ParticipantObjectId*: document unique identifier,
- *ParticipantObjectTypeCode*: "2" (system object),
- *ParticipantObjectTypeCodeRole*: "20" (job).

One important aspect of the ITI-14 and ITI-15 transactions respectively is that these transactions are not only triggered if a document is inserted into the XDS repository but also if a document has been updated. This information is stored in the *EventActionCode* attribute of the *EventIdentifcation* element of an audit message. In general, the EventActionCode attribute can contain the following values:

- *C*: Create – Persisting a new document,
- *U*: Update – Update of an existing document,
- *D*: Delete – Deletion of an existing document,
- *R*: Read – Reading a document,
- *E*: Execute – Executing a query.

Besides the storing of documents in an XDS registry and XDS repository, IHE provides two transactions to retrieve documents from an XDS repository (IHE International 2009a):

- *ITI-17*: Retrieve Document,
- *ITI-43*: Retrieve Document Set.

Like persisting documents retrieving documents is logged in the ARR using audit messages. These messages contain the same information like the audit messages created by ITI-14 and ITI-15. The ActiveParticipant element of an ITI-17 or ITI-43 transaction is also used to identify the user who triggered the transaction, whereas the attributes of the ParticipantObjectIdentification element contain the following values:

- *ParticipantObjectId*: The document unique identifier,
- *ParticipantObjectTypeCode*: "2" (system object),
- *ParticipantObjectTypeCodeRole*: "3" (report).

Using the unique identifier of the document, the author's details, the author's organization and author's department can be retrieved using an XDS Query Registry Transaction (ITI-16, see IHE International 2009b).

3.2. Improving CKNs Analyzing Clinical Documents

As the ARR only provides detailed information about transactions, but not why a transaction is conducted or a communication is established between certain actors, it is necessary to analyze the documents that are exchanged to improve our CKNs.

IHE suggests the use of HL7 v3 *Clinical Document Architecture* (CDA) Release 2 for the representation and structure of clinical documents like for instance medical summary, nursing summary, prescription, that are to be exchanged using XDS (IHE International 2009a).

CDA is based on XML, the HL7 *Reference Information Model* (RIM) and coded vocabulary, thus making documents both machine- and human-readable and providing an exchange model for clinical documents (HL7 2009).

A CDA document consists of a structured and coded header that provides context critical information about the document (e.g., type) and the concerned individuals (e.g., patient, author), and of a body that may consist of structured content with coded sections. Specific sections that are described by the IHE Patient Care Coordination profile contain coded entries. For example, the section *Reason for Referral* (templateId 1.3.6.1.4.1.19376.1.5.3.1.3.1, LOINC-code 42349-1) contains an entry for the diagnosis, etc., coded using ICD-Codes, an international classification of diseases which is used worldwide (WHO 2009).

Therefore the content of the documents can be easily interpreted and analyzed using a rule engine based on different models (Franz *et al*. 2009). Thus, we can compare different documents and improve CKNs by using the information logged in the ARR as well as the data gained by the analysis of provided documents.

Using for example the coded type of document, e.g. discharge summary, referral summary, and the coded reason for referral or discharge diagnosis therein as well as information about the author and document access stored in the ARR, we can add deeper knowledge about the flow of information and improve CKNs as we now can find out the type of documents that are transferred and parts of the cause why information is exchanged among actors. It would be a possibility to add causal logic to our rule engine to further interpret the information flow, its efficiency and the relationship among actors.

3.3. Analyzing CKNs using Social Network Analysis

SNA explores individuals and their relationships, called ties, within a social network and transfers the results into a graph-like structure (Fattore *et al*. 2009). SNA is applied in many fields of application such as economy, sociology, biology or communication. Basically, SNA is used to identify and describe communication patterns of members of a social network using methods provided by graph theory (Scott *et al*. 2005) enabling the comparison of different networks of the same domain. According to (Hu and Racherla 2008), SNA is used to map the flow of information to groups of actors to improve knowledge sharing.

SNA provides several key metrics enabling a quantitative comparison of collaborative networks which are described in the following sections.

3.3.1. Graph Density

According to (Hu and Racherla 2008), the *density* of a network is defined as a proportion of ties in a network relative to the maximum number of ties. This means that in a network in which each member has a relationship to each other member of the network the density is high, otherwise the network is called sparse.

3.3.2. Node Degree

In graph theory, the *degree* is the number of edges incident to a node, whereas the loops are counted twice. This implies, that the higher the degree of an actor, the more connections the actor has indicating that many other actors of the same network using its knowledge (Bondy and Murty, 2007).

3.3.3. Graph Centralization

Centralization is the degree to which a network approaches the configuration of a "start" network (Scott *et al*. 2005). This means that a network has one actor which has a considerably higher amount of relationship with many other actors of the same network than all other actors.

3.3.4. Cluster Coefficient

The *cluster coefficient* describes the likelihood that two actors connected to the same node are connected themselves; see (Scott *et al*. 2005). This means that the cluster coefficient illustrates if there are subgroups in a collaborative network working together.

4. EXAMPLE

Based on the presented approach the collaboration network of a virtual affinity domain is determined and examined using the SNA tool *Pajek* (Batagelj and Mrvar 2003) at two different timestamps to demonstrate the changes over time. The created affinity domain consists of three departments and five assigned physicians:

- Cardiology: Dr. Jane Heart, Dr. Jack Spine
- Radiology: Dr. John Knee, Dr. Johnny Worker
- Laboratory: Dr. Jack Sample

The collaboration networks are computed for a patient admitted to the hospital with heart attack symptoms.

Based on the entries of the ARR all necessary information concerning the physicians participating at the patient's treatment and the documents created and accessed during the treatment process, are extracted.

Figure 2 gives an example of the CKN extracted at timestamp 1. The CKN consists of four actors, whereas the actor "Dr. Jane Heart" represents the centre of the network indicating that the documents provided by "Dr. Jane Heart" are the starting point of the collaboration. This circumstance is demonstrated in Table 1 where the centralization metric is 1 implying that the CKN has a star configuration. Moreover, the degree measurement

of each member of the network confirms this situation. While all other actors have only one incidental edge, the actor "Dr. Jane Heart" has a degree of 3 implying that this actor is connected to each other member of the CKN (see Table 2). Furthermore, the cluster coefficient of the collaborative network is 0.0 which means that there are no subgroups of actors working together. Another key metric supporting this observation is the density of the network, which is 0.25 for the first network meaning that only a quarter of all possible ties have been built.

The enhancements of the collaborative knowledge network are reflected in Figure 3 and in Table 1. As it can be seen another actor, "Dr. James Spine", has joined the network. Moreover, the initial participating actors have started to build ties among each other. This is reflected in the key figures cluster coefficient, centralization and density. The density of CKN 2 (0.35) indicates that more than a third of all possible ties have been built by the members of the network. An interesting result of the second knowledge network is that the more ties the actors build the smaller the centralization measurement (0.3) turns out. Moreover, the cluster coefficient increases with the amount of relationship the actors build (0.382). This implies that the actors have started to build subgroups that exchange their knowledge which is also approved by the degree of each actor.

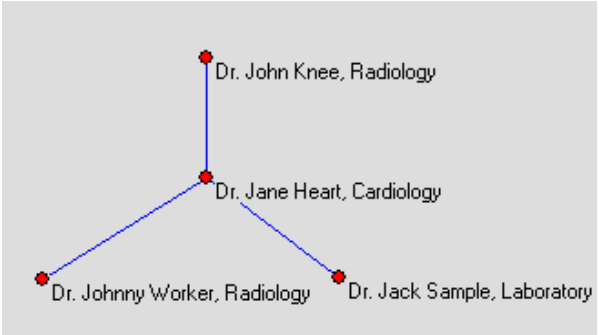

Figure 2: The collaboration network at timestamp 1.

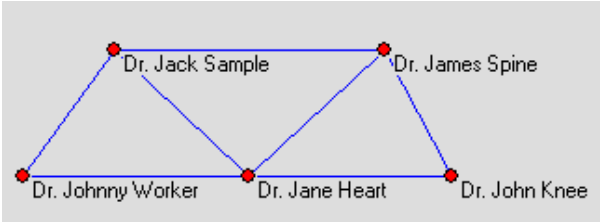

Figure 3: The collaboration network at timestamp 2.

Table 1: Metrics of CKNs.

	CKN 1	CKN 2
Density	0.25	0.35
Centralization	1.0	0.3
Cluster Coefficient	0.0	0.382

Table 2: The degree of each member of the CKN

	Degree CKN 1	Degree CKN 2
Dr. Jane Heart	3	4
Dr. John Knee	1	2
Dr. Johnny Worker	1	2
Dr. Jack Spine	0	3
Dr. Jack Sample	1	3

5. CONCLUSION

Complex healthcare processes, missing information, interruptions of ongoing patient treatments, and insufficient or intransparent collaboration, all these factors contribute to miscommunication and medical errors. Our presented approach in this paper has a positive impact on the quality of healthcare and on the safety of patients by providing transparent information about the collaboration among the participants in the healthcare context.

We have demonstrated how to use information stored in an ARR as well as XDS registry and XDS repository respectively in order to visualize the flow of information in clinical environments. An early implementation illustrates the added value of combining this information and shows how collaborative knowledge networks can be established to analyze and promote collaboration.

The purpose to make collaboration networks available and transparent across institutional borders, especially in patient treatment, demands integrated health information for the citizens and health professionals. There is a need to integrate the knowledge from all along the lifecycle of a patient. This can only be achieved by established (world-wide) recommendations like IHE and standards like HL7/CDA.

However, there remain a number of limitations that need to be investigated. One of them is that the information stored in an ARR is insufficient to offer an information flow for these studies that shows better significance. Nevertheless, the use of HL7 V3 CDA compliant documents is an effective way to assign a treatment to a certain diagnosis. Nonetheless, the usage of HL7 V3 CDA does not guarantee that the overall treatment of a patient can be reassembled.

Moreover, the information stored in ARRs is not complete due to the reason that only access to PHI is logged leading to a break in the information flow. Another deficiency concerns the statistical metrics: currently the system allows only simple analysis. Further work will concentrate on extending the measurements on actors enabling to provide detailed information about the role of an actor in a CKN.

More work is also necessary to extend the prototype with collaboration features (e.g., experts in a CKN for a certain group of diagnoses), which allows participants to get in contact. In addition we want to support the construction of a collaborative network with a set of tools to predefine experts of a certain group of treatment.

ACKNOWLEDGEMENTS

The project IHExplorer is funded by the Austrian Research Promotion Agency, Tiani-Spirit GmbH, OÖGKK, X-Tention Informationstechnologie GmbH and the OÖ Gesundheits und Spitals AG.

REFERENCES

Anderson, J. G., 2002. Evaluation in health informatics: social network analysis. *Computers in Biology and Medicine*, 32, 179-193.

Batagelj, V., Mrvar, A., 2003. Pajek - Analysis and Visualization of Large Networks. *Graph Drawing Software*. 77-103, Berlin: Springer.

Bondy, J. A., Murty, 2007. *Graph Theory: An Advanced Course*. Berlin: Springer.

Fattore, G., Frosini, F., Salvatore, D., Tozzi, V., 2009. Social network analyisis in primary care: The impact of interactions on prescribing behavior. Article in press, *Health Policy*.

Franz, B., Mayr, H., Mayr, M., Pfeifer, F., Altmann, J., Lehner, M., 2009. Integrated Care Using a Model-Based Patient Record Data Exchange Platform. Accepted to the *21st European Modeling and Simulation Symposium*, September 23-25, Spain: Tenerife.

Gloor, P., Dynes, S., Zhao, Y., Laubacher, R., 2003. Visualization of Interaction Patterns in Collaborative Knowledge Networks for Medical Applications. *Proceedings HCII*, June 25-27, Greek: Crete.

HL7 Health Level Seven, Inc., 2009: *HL7. Health Level Seven.* Michigan, USA, Available from: http://www.hl7.org [accessed 11 June 2009].

Hu, C., Racherla, P., 2008. Visual representation of knowledge networks: A social network analysis of hospitality research domain. *International Journal of Hospitality Management*, 27, 302-312.

IHExplorer, 2009. Research Project of the Upper Austria University of Applied Sciences, Available from: http://ihexplorer.fh-hagenberg.at [accessed 23 June 2009].

IHE International, 2009a. *IHE Information Technology Infrastructure - Technical Framework, Volume 1 Integration Profiles*, Available from: http://www.ihe.net/Technical_Framework/index.cfm#IT [accessed 6 April 2009].

IHE International, 2009b. *IHE Information Technology Infrastructure - Technical Framework, Volume 2 Transactions*, Available from: http://www.ihe.net/Technical_Framework/index.cfm#IT [accessed 6 April 2009].

Lonvick, C., 2001. *The BSD Syslog Protocol*. Available from: http://www.rfc-editor.org/rfc/rfc3164.txt [accessed 7 June 2009].

Marshall, G, 2004. *RFC 3881 – Security Audit and Access Accountability Message XML Data Definitions for Healthcare Applications*. Available from: http://www.rfc-editor.org/rfc/rfc3881.txt [accessed 6 April 2009].

Norgall, T., 2003. Kommunikationsstandard für die Gesundheitstelematik: Status und Ausblick. *eHealth 2003 – Telematik im Gesundheitswesen Vernetzte Versorgung*, October 21-23, Germany: Dresden.

Scott, J., Tallia, A., Crosson, JC., Orzano, AJ., Stroebel, C., DiCicco-Bloom, B., O'Malley, D., Shaw, E., Crabtree, B., 2005. Social Network Analysis as an Analytic Tool for Interaction Patterns in Primary Care Practices. *Annals of Familiy Medicine*, 3 (5), 443-448.

Sunyaev, A., Schweiger A., Leimeister, J. M. and Krcmar, H., 2008. Software Agents for the Integration of Information Systems in Healthcare; in German. *Multikonferenz Wirtschaftsinformatik*, 1455-1466, February 26-28, Germany: Munich.

WHO World Health Organization, 2009. *The WHO Family of International Classifications*. Available from: http://www.who.int/classifications/icd/en/ [accessed 11 June, 2009].

Wozak, F., Ammenwerth, E., Hörbst, A., Sögner, P., Mair, R. and Schabetsberger T., 2008. IHE based interoperability – benefits and challenges. *eHealth2008 – Medical Informatics meets eHealth*, 35-40, May 29-30, Austria: Vösendorf.

Authors Biography

Josef Altmann has been a full professor of software engineering at the Upper Austria University of Applied Sciences since 2005. He received his MSc (1992) and PhD (1998) from the Johannes Kepler University Linz. His research focuses on integration and traceability of healthcare data, eHealth and IHE. He is a member of the IHE Austria and leads the research project IHExplorer.

Franz Pfeifer is a scientific researcher at the Research Center Hagenberg since 2005. He graduated 2005 at the Upper Austria University of Applied Sciences. His research focuses on digital image processing and medical informatics.

Melanie Strasser is a student at the Department of Software Engineering of the Upper Austria University of Applied Sciences and currently writing her master thesis in the field of IHE.

Barbara Franz is a scientific researcher at the Research Center Hagenberg since 2008. She received her MSc from the Upper Austria University of Applied Sciences. Her research focuses on eHealth and IHE.

Herwig Mayr is a full professor of software engineering at the Upper Austria University of Applied Sciences since 1996. He is studies advisor for medical software engineering degree program.

COUPLING EFFECTS IN THE BIDOMAIN MODEL OF FUNCTIONAL ELECTRICAL STIMULATION

Martinek[a,b,c], Mandl[b], Mayr[b] , Rattay[c], Reichel[a]

[a]Department of Biomedical Engineering and Environmental Management,
University of Applied Sciences Technikum Wien, Vienna, Austria
[b]Center of Biomedical Engineering and Physics, Medical University of Vienna, Austria
[c] Institute for Analysis and Scientific Computing, Vienna University of Technology, Austria

johannes.martinek@technikum-wien.at, thomas.mandl@technikum-wien.at, winfried.mayr@medunwien.ac.at, frank.rattay@tuwien.ac.at, martin.reichel@technikum-wien.at

ABSTRACT

A simulation of non-invasive electrical nerve and muscle fiber excitation with the finite element software Comsol Multiphysics, formerly known as FEMLAB, is presented. This software allows the simultaneous solution of fiber excitation by linear fiber models (1D models) of the Hodgkin-Huxley type which are embedded in a volume conductor (2D and 3D) where the electrical field is mainly dominated by the electrode currents.

The presented bidomain model includes the interaction between electrode currents and trans-membrane currents during the excitation process. Especially for direct muscle fiber stimulation (cardiac muscle, denervated muscle) the effects from secondary currents of large populations of excited fibers seem to be significant. The method has many applications, such as the analysis of the relation between stimulus parameters and fiber recruitment.

In this study the implementation of different fiber models, the effect of different electrode positions and the influence of coupling is presented.

Keywords: Hodgkin-Huxley, Coupling, Comsol Multiphysics, Finite Elements

1. INTRODUCTION

The most important mathematical models for simulating nerve or muscle fiber excitation are based on the work of Hodgkin and Huxley (1952). Their theory on excitation and spike propagation in nerve fibers has inspired many other researchers, always trying to adopt the current research in neurosciences (Adrian and Peachy 1973; Plonsey 1974; Rattay 1990; Henneberg and Roberge 1997; Wallinga 1999).

Paralysis of the lower extremety may result from to types of injuries: Spastic paralysis (upper motor neuron lesion) on the one hand and flaccid paralysis (lower motor neuron lesion, denervation, peripheral lesion) on the other hand. Besides other applications, Functional Electrical Stimulation (FES) is an important rehabilitation technique for paraplegic patients. With pulsed stimulating currents applied via two electrodes placed on the skin surface, muscles are activated and thereby trained. Due to the lack of nerve supply denervated muscle fibers need considerably stronger stimuli than known from nerve stimulation: long impulses, with high amplitudes (Kern 1995, Mödlin et al. 2005). Computer simulations play a growing role in better understanding of the applied electrical field and its activation of nerve and muscle fibers (Coburn 1989; Veltink et al. 1988; McIntyre et al. 2004; Reichel et al. 1999).

Details on the electrical potential distribution in both domains (extra- and intracellular) are essential for calculating the development and the propagation of action potentials along the fiber. In the past it was difficult to solve this task within one model due to the complexity of the problem and the huge difference in the scales of both geometries. For this reason usual simulations are based on compartment models, where first the extracellular electrical field is calculated. In a second step the response of the neuron or muscle fiber to this extracellular field distribution is calculated for the excitable membranes with Hodgkin-Huxley-like models.

By using a bidomain model, it is possible to calculate both areas / domains of interest, i.e. the surrounding tissue and the muscle fiber itself, separately and in dependency on each other. The two domains are linked by their boundary conditions. Such bidomain models have mainly been used for analyzing excitation effects and spike propagation in the human heart (Miller and Geselowitz 1978; Sobie et al. 1997).

2. MATERIAL AND METHODS

2.1. Physological basics

Muscle and nerve cells are surrounded by a semipermeable membrane which allows an exchange of certain ions between the intra- and extracellular space. Nerve and muscle fibers usually have increased negative charge inside the fibers compared to the outside. This leads to a negative resting membrane potential. In human muscle cells this resting potential is around -80 to -90mV (Silbernagel 2001). The potential difference between the inside and the outside of the fiber is one of the causes for the ability of evoking action potentials.

Action potentials are the basis of the signal transmission process in a nerve or muscle fiber. They are all-or-none impulses with amplitudes of about 100mV. Action potentials are generated in the

membrane of nerve and muscle fibers and are initiated when the transmembrane voltage exceeds a certain threshold. Once excited the action potential propagates along the fiber with constant velocity and constant amplitude carried by the activity of voltage-controlled ion channels in the membrane. Whenever a fiber region is excited by a sufficient depolarization voltage, gates in sodium channels open. The influx leads to a further shift in the membrane potential. This depolarization is counteracted by the activation of the voltage sensitive potassium channels and the inactivation of the sodium channels. Due to the efflux of potassium ions, the membrane potential is drawn back to the resting membrane potential (Figure 1).

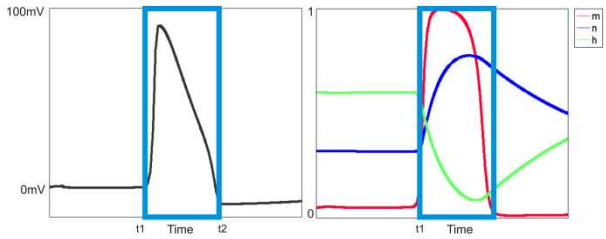

Figure 1. Illustration of action potential (left) and the associated gating variables m, n and h (right). The gating variables m and h affect the flux of the sodium ions. The gating variable n is responsible for the opening of the potassium channels.

The currents involved in a locally active action potential are strong enough to excite neighboring regions of the membrane, thus resulting in spike propagation along the axon.

2.2. Hodgkin Huxley Model

Hodgkin and Huxley (1952) conducted a series of experiments, examining the time and voltage dependence of the sodium and potassium conductance of the membrane of a giant squid axon. The results of the experiments were fitted into a set of four differential equations: one nonlinear (1) and three linear ones (2).

$$C_m \frac{\partial V}{\partial t} = \frac{r}{2\rho}\frac{\partial^2 V}{\partial x^2} + g_{NA} m^3 h (V_{Na} - V) + g_K n^4 (V_K - V) + g_L (V_L - V)$$

$$C_m \ldots capacitance\ of\ membrane$$
$$r \ldots radius\ of\ axon \qquad (1)$$
$$\rho \ldots resistance\ of\ intracellular\ space$$
$$g_{Na}, g_K, g_L, \ldots conductance\ of\ Natrium, Potassium\ and\ Leakage$$

$$\frac{dw}{dt} = \alpha_w (1 - w) - \beta_w w \quad (w\ is\ m, n\ or\ h)$$
$$\alpha_m = \frac{2.5 - 0.1V}{e^{2.5 - 0.1V} - 1} \quad \beta_m = 4e^{-\frac{V}{18}} \qquad (2)$$
$$\alpha_n = \frac{1 - 0.1V}{10(e^{1 - 0.1V} - 1)} \quad \beta_n = 0.125e^{-\frac{V}{80}}$$
$$\alpha_h = 0.07e^{-\frac{V}{20}} \quad \beta_h = \frac{1}{e^{3 - 0.1V} + 1}$$

Equation (1) describes the behavior of the membrane potential in dependency on the voltage gated sodium and potassium channels. In (2) the further differential equations for calculating the parameters m, n and h are described. These parameters represent the probabilities that the voltage-dependent sodium (m, h) and potassium channels (n) are open (Figure 1).

The resting state conditions are defined by

$$V(0) = 0, m(0) = 0.05, n(0) = 0.32, h(0) = 0.6 \qquad (3)$$

2.3. Potential distribution

The differential equation for calculating the time-dependent potential distribution of the tissue surrounding the fiber is based on a simplification of the Maxwell's Equations by using the continuity and the constitutive relations (4)

$$-\nabla(\sigma \nabla V_e) - \nabla\left(\varepsilon \nabla \frac{\partial V_e}{\partial t}\right) = 0 \qquad (4)$$

In Comsol Multiphysics version 3.4 the PDE in coefficient form was taken (5)

$$e_a \frac{\partial^2 V}{\partial t^2} + d_a \frac{\partial V}{\partial t} + \nabla(-c\nabla V - \alpha V + \gamma) + aV + \beta \nabla V = f \qquad (5)$$

For implementing equ. (4) in (5) it is necessary to extend equ. (4) with 1st-order time derivatives of V using the following terms (Comsol, 2007):

The first component of the γ-term has to be extended by equ. (6). In equ. (6) *Vxt* represents the derivation of *V* on time *t* and place *x*.

$$\gamma = \begin{cases} -d_c * Vxt \\ -d_c * Vyt \end{cases} \qquad (6)$$

By using equ. (4), (5) and (6) and by replacing the variables with appropriate expressions it is possible to represent equ. (4) in Comsol Multiphysics.

In the model the intracellular potential V_i (potential in the fiber) and the extracellular potential V_e are connected by equ. (7). V_{rest} represents the resting potential of the membrane.

$$V = V_i - V_e - V_{Rest} \qquad (7)$$

2.4. Models of the Hodgkin-Huxley type

To evaluate the simulation, compare the results with "real-life" data and analyze the effects of different stimulation or fiber parameters a 1D model (linear model) of a fiber is implemented by using different spatial membrane models of the Hodgkin-Huxley type (e.g. Hodgkin and Huxley 1952; Adrian and Peachy 1973; Plonsey 1974; Henneberg and Roberge 1997, Wallinga et al. 1999). Models of the Hodgkin-Huxley type are more or less of the same form. They vary mainly in the calculation of the parameters α_m, $\alpha_n, \alpha_h, \beta_m, \beta_n$ and β_h in (2) and in the parameters for the membrane and fiber conditions like e.g. the diameter of the fiber.

2.5. Coupling

The 1D fiber model is embedded in a simplified 2D or 3D model of a human thigh. The time dependent potential of the tissue surrounding the fiber is calculated with simplified Maxwell equations (4).

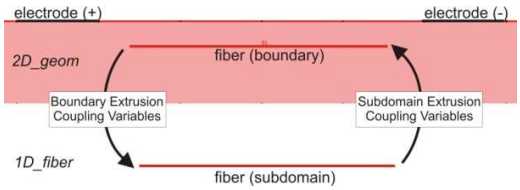

Figure 2: Schematic illustration of the coupling of two geometries (2D_geom and 1D_fiber).

The 1D model of the fiber and the surrounding area (2D or 3D model) is coupled by using the "coupling functionality" of Comsol Multiphysics.

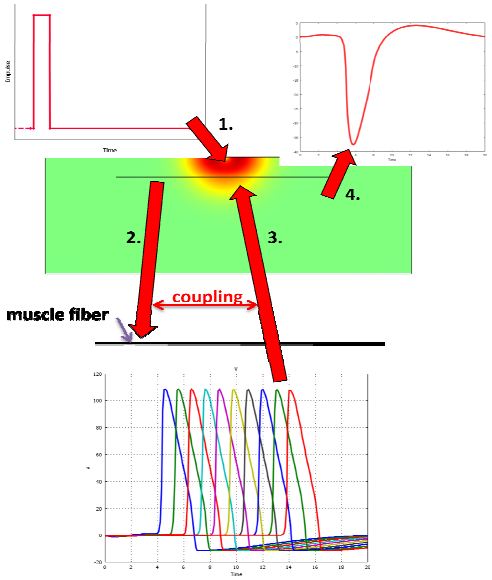

Figure 3: "Coupling": A rectangular square pulse (1) applied to a 2D domain induces a potential distribution in this domain. Every muscle fiber placed in the domain is exposed to the potential (2). The muscle fiber's response is an action potential (3). The transmembrane currents of the propagating action potential affect the external potential and can be displayed as an EMG-like graph (4).

According to Figure 2 the model consists of two different geometries: The 2D geometry, which represents a simplified human thigh is used to calculate a potential distribution according to equ. (3). The second geometry is a 1D muscle fiber with the implemented Hodgkin-Huxley-like model from equ. (1) and (2). In the 2D geometry there is a line embedded and coupled by "Boundary Extrusion Coupling Variables" to the subdomain of 1D_fiber. The coupled value is inserted as extracellular potential in the equation of the fiber model (7).

The resulting voltage of the solved fiber line model is coupled by "Subdomain Extrusion Coupling Variables" to the inner boundary in the 2D geometry representing the fiber. The influence of the potential travelling along the fiber is simulated by Neumann boundary conditions on the inner boundary in the 2D geometry (Figure 3).

2.6. Muscle regions (3D model)

In a simplified 3D model of a human thigh a region representing a muscle bundle is embedded. The coupling (2.5) was slightly extended in the way by calculating the mean value of the region and using it as the external potential of the fiber model (Figure 4).

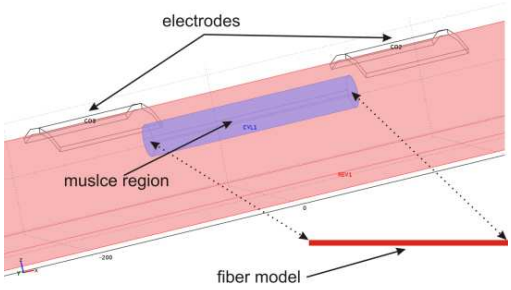

Figure 4: Schematic illustration of the coupling of a 3D muscle region, which is embedded in a simplified model of a human thigh, and a 1D fiber model.

The position, size and the shape of the region representing a muscle bundle can be varied. This model is used to see if the results of the 2D model are comparable to the more realistic 3D model on the one hand and if the application of "muscle regions" on the other hand has an influence on the results compared to the embedding of a single fiber.

2.7. Influence of electrode position

To investigate the influence of electrode configurations a 2D model is defined with different electrode positions either on the skin surface or the bone, e.g. A3 and B3 (Figure 5). In the thigh two fibers were embedded and the coupled interaction of electrode and membrane currents is studied. By using Dirichlet boundary conditions two electrodes are set active for constant current stimulation. Which means a positive square pulse (+) is set on one electrode and a negative square pulse (-) is set on the other electrode.

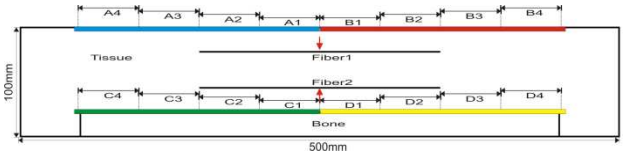

Figure 5: Simplified model of the thigh with two embedded fibers and different electrode positions marked as A1, A2, …, D1, D2,…

3. RESULTS

3.1. Different fiber models

As an example the "original" Hodgkin-Huxley (1952) model, the model of Adrian and Peachy (1972) and the extended model of Wallinga et al. (1999) are implemented and the result are compared to literature. It can be shown that the effect of different models is comparable to data of literature.

For comparability reasons the results presented in Figure 6 are based on the same surrounding conditions: In both models the fiber has the same length (10 cm) and the same diameter (100 µm) and rectangular stimulation impulse is applied (50 µs and 50 µA).

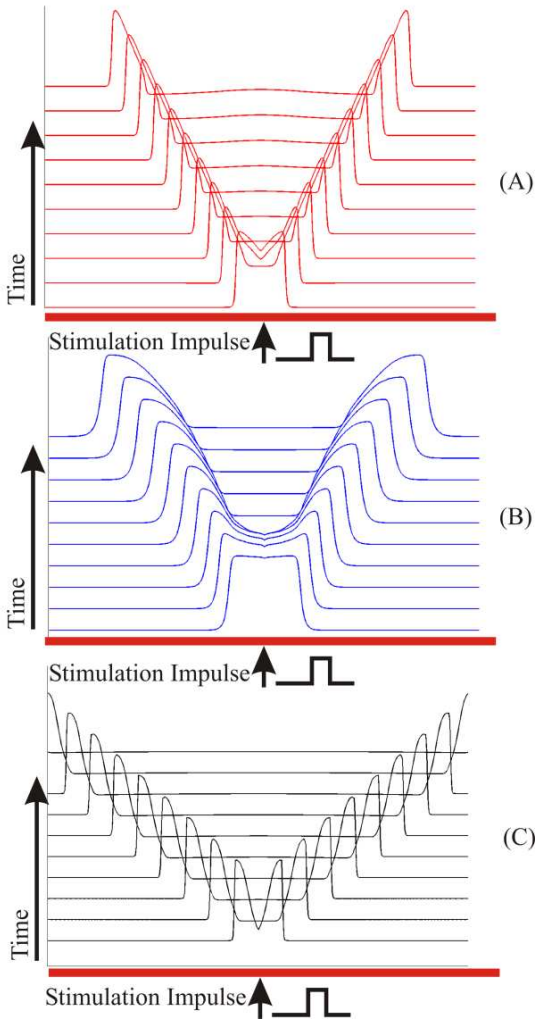

Figure 6: Propagation of action potentials for the "original" Hodgkin Huxley model (A) (1952), the fiber model of Adrian and Peachy (B) (1973) and the fiber model of Wallinga et al. (C) (1999), recalculated on basis of the bidomain model.

3.2. Influence of coupling

For analysis of the effects of the coupling several muscle fibers are embedded in the model of the thigh. The fibers are set active or inactive and the potential distribution is calculated. Finally the effect of the potential distribution on individual fibers is observed. It can be seen that the change of the potential distribution in the 2D geometry caused by the membrane currents of the coupled ("active") fibers has an influence on the embedded and coupled fibers.

In Figure 7 the membrane potential of the third fiber is presented. To examine the influence of the coupling, the two other fibers are either coupled as described above or not.

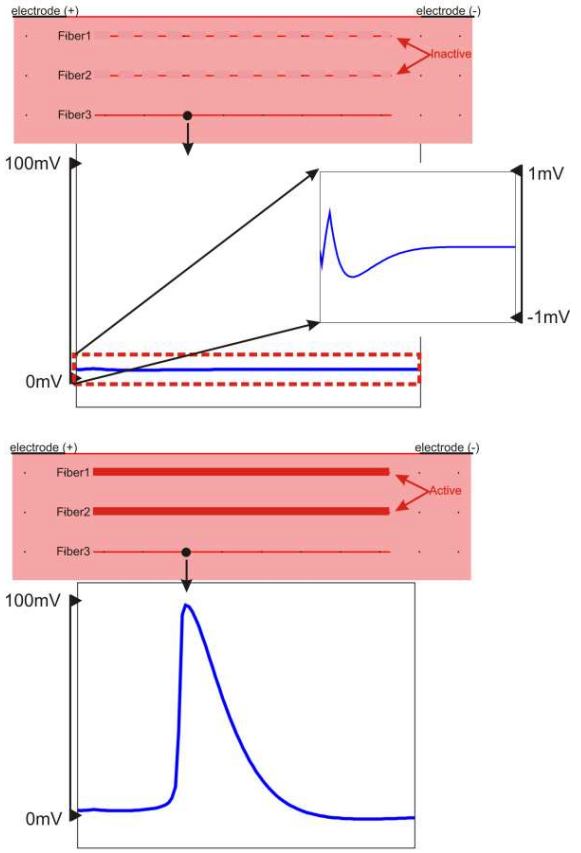

Figure 7: 2D geometry with three embedded fibers: To simulate the influence of the coupling two fibers are "inactive" (not coupled) or "active" (coupled).

It can be seen that the coupling of the two fibers has an influence on the third fiber and seems to facilitate the generation of action potentials.

3.3. Influence of geometry / electrode position

The simulation demonstrates that the initiation of the action potential takes place under the cathode, if the fiber is situated beneath the electrodes. If the fiber is not underneath the electrode the excitation arises at the fiber ending located closer to the cathode.

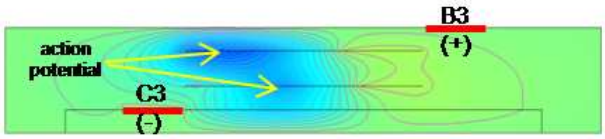

Figure 8: Potential distribution in the thigh 3 ms after the stimulation impulse caused by propagating action potentials in fiber 1 and 2. Electrodes C3 (-) and B3 (+) are active.

In this simulation two electrodes are set active. The time period (ms) from starting the impulse until an action potential is initiated reflects the excitability of the fiber. This time period is taken and displayed in Figure 9. If there is no action potential, no time is entered. The diagram shows the excitation time for different electrode positions of the surface and on implanted electrodes (Figure 5). The red line represents the fiber placed closer to the electrodes. The blue line represents the fiber which is more distant.

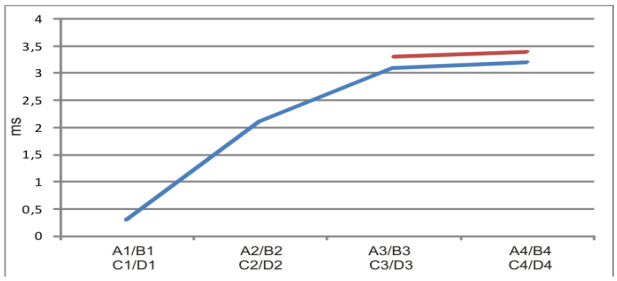

Figure 9: Time period from stimulation impulse until an action potential is initiated.

3.4. Muscle regions

When looking at the results of the 3D model with the embedded muscle regions it can be seen, that the size and shape of the region representing a muscle bundle has an influence on the activation of the fibers (Figure 10).

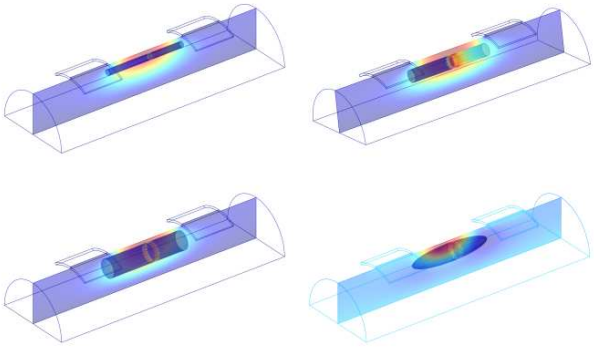

Figure 10: 3D geometry with embedded muscle regions with different diameters and shapes.

Nevertheless when choosing a proper size of the regions, the results are comparable to the results of a single embedded fiber as presented in Figure 11. A good dimension for these muscle regions is difficult to define. It is necessary to create regions, which are not too large to get a proper value for the extracellular potential for the fiber.

4. DISCUSSION

The results gained from the simulation of the 1D fiber model are in accordance with the Hodgkin-Huxley standard compartment model (lumped circuit model) evaluations based on space discretization with constant Δx (Rattay, 1990). When embedding and coupling the 1D line model of the muscle fiber in a 2D geometry the results of the Hodgkin-Huxley-like excitation are comparable to the simple 1D model (Figure 3) and therefore to the literature.

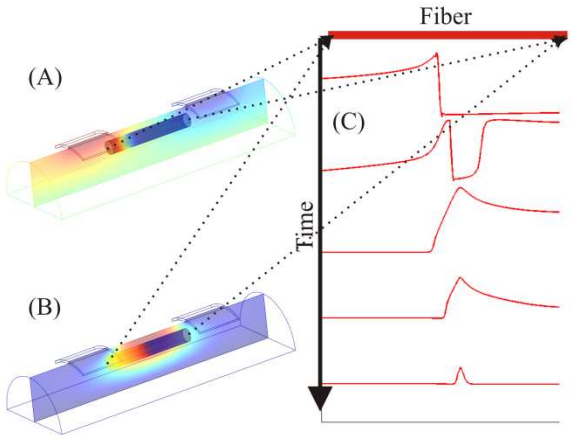

Figure 11: 3D geometry with embedded muscle region during (A) and after (B) a stimulation impulse. In (C) the propagation of the action potential in the fiber is shown.

In this study the models of Adrian and Peachy (1973) and Wallinga (1999) are implemented. It can be seen, that the results of the simulation accords with literature.

The relative position of the electrodes compared to the fibers / regions is of importance to the excitation process. The smaller the distance between the electrodes the faster is the activation of the fibers close to the electrodes. The greater the distance between the electrodes the deeper the activated area.

One of the most interesting results of this simulation is the influence of propagating action potentials on the extracellular potential distribution and therefore on adjacent fibers. Action potentials generate an inhomogeneity on the potential distribution in the tissue. Based on the theory of activating functions (Rattay, 1990) and Reichel et al. (1999) it was assumped that inhomogeneities of the potential distribution of the tissue surrounding the fiber facilitates the activation of the fiber. This assumption seems to be one reason for the observed influence of the coupled fibers. Nevertheless, it must be said, that the influence is minimal and in “real life” often negligible. The influence alone never leads to an activation of a fiber. It only “helps” a fiber to generate an action potential where the membrane potential is close to the threshold (about 95% of threshold)

Another part of this study which should be followed is the implementation of 3D muscle regions. Until now only rotationally symmetrical elements are embedded. A next step could be to implement shapes of real muscles and real muscle fiber directions.

5. CONCLUSION

With Comsol Multiphysics it is possible to evaluate Hodgkin-Huxley like excitation processes in conducting 2D and 3D media. Once the model is implemented into

the software it can easily be adapted to different geometries and parameters of fibers and of the extracellular regions. In this work the implementation of 3 different models is presented: the "original" Hodgkin Huxley (1952) model, the model of Adrian and Peachy (1973) and the model of Wallinga et al. (1999).

The bidomain model makes it possible to simultaneously calculate the extracellular field caused by active electrodes and its changes caused by the membrane currents of the responding fibers. Up to now calculations of action potentials were mostly done in two steps: (i) the extracellular potential distribution was calculated and (ii) using this distribution the excitation of the fiber was calculated with a compartment model. The interaction of the macroscopic extracellular field and the dynamic field changes along fibers were neglected.

The presented coupled model shows high potential for analyzing the effects of FES in the human. In "real" life coupling is omnipresent. For example EMG originates from projections of muscle fiber fields on the tissue surrounding the fiber. Therefore the coupling should also be part for a more realistic model of simulation of FES activated muscles. However, until now many models only allow to simulate the unidirectional coupling, either by calculating the excitation of a fiber as response to an extracellular field or by simulation the EMG as an answer to a fiber excitation.

ACKNOWLEDGEMENTS

This study was supported by the Austrian Science Fund (FWF) under grant numbers P18848-N13 and TRP L36-B15.

REFERENCES

Adrian RH, Peachy LD, 1973, Reconstruction of the action potential of frog sartorius muscle, *The Journal of Physiology*, 235(1): 103-31.

Coburn B, 1989, Neural modeling in electrical stimulation, *Critical Reviews in Biomedical Engineering*, 17: 133-178.

COMSOL Multiphysics Modeling Guide (2007), Version 3.4: 256-272

Greenberg RJ, Velte TJ, Humayun MS, Scarlatis GN, de Juan EJ, 1999, A computational model of electrical stimulation of the retinal ganglion cell, *IEEE Transactions on Biomedical Engineering*, 46: 505-514.

Henneberg KA, Roberge FA, 1997, Simulation of propagation along an isolated skeletal muscle fiber in an isotropic volume conductor, *Annals of Biomedical Engineering*, 25: 5-28.

Hodgkin AL, Huxley AF, 1952, A quantitative description of membrane current and its application to conduction and excitation in nerve, *The Journal of Phsyiology*, 117: 500-544.

Kern H, 1995, Funktionelle Elektrostimulation paraplegischer Patienten, *Österreichische Zeitschrift für Physikalische Medizin und Rehabilitation*, Heft 1, Supplementum.

McIntyre CC, Grill WM, Sherman DL, Thakor NV, 2004, Cellular effects of deep brain stimulation: model-based analysis of activation and inhibition, *The Journal of Phsyiology*, 91: 1457-1469.

Miller WT, Geselowitz DB, 1978, Simulation studies of the electrocardiogram, I. The normal heart, *Circulation Research*, 43**:** 301-315.

Mödlin M, Forstner C, Hofer C, Mayr W, Richter W, Carraro U, Protasi F, Kern H, 2005 Electrical stimulation of denervated muscles: first results of a clinical study, *Artifical Organs*, 29**:** 203-206.

Plonsey R, 1974, The active fiber in a volume conductor, *IEEE Transactions on Biomedical Engineering*, 21: 371-381.

Rattay F., 1990, *Electric nerve stimulation (theory, experiments and applications)*, Springer-Verlag Wien New York.

Reichel M, Mayr W, Rattay F, 1999, Computer simulation of field distribution and excitation of denervated muscle fibers caused by surface electrodes, *Artifical Organs*, 23: 453-456.

Silbernagl S, Despopoulos A, 2001, *Taschenatlas der Physiologie*, 42-50. Georg Thieme Verlag, Stuttgart

Sobie EA, Susil RC, Tung L, 1997, A generalized activating function for predicting virtual electrodes in cardiac tissue, *Biophysical Journal*, 73(3): 1410-23.

Veltink PH, van Alsté JA, Boom HB, 1988, Simulation of intrafascicular and extraneural nerve stimulation, *IEEE Transactions on Biomedical Engineering*, 35: 69-75.

W. Wallinga, S. L. Meijer, M. J. Alberink, M. Vliek, E. D. Wienk, D. L. Ypey, 1999, Modelling action potentials and membrane currents of mammalian skeletal muscle fibres in coherence with potassium concentration changes in the T-tubular system, *European Biophysics Journal*, 28: 317-329.

BIOGRAPHY

Johannes Martinek received the MSc in Technical Mathematics from the Technical University of Vienna, Austria, in 2003. He has since been a phd-student at the Technical University of Vienna, Austria. Until May 2009 he was a research assistant of the Institute for Analysis and Scientific Computing of the Technical University of Vienna, Vienna, Austria. Since 2003 he is employed at the Department of Biomedical Engineering and Environmental Management at the University of Applied Sciences "Technikum Wien", Vienna. His research interests include modeling and simulation of bioelectric signals with a special focus on the simulation of muscle and nerve fibers.

Thomas Mandl received his "Diplomingenieur" (MSc level) in Technical Physics from the Technical University of Vienna late 2005. He has since been a phd student in Medical Physics at the Medical University of

Vienna in Prof. Moser's MR group. His(research interests include computer simulation and visualization as well as MR applied to muscle.

Winfried Mayr received his Diploma degree in Electronics and Control Engineering from the Vienna University of Technology in 1983 and his Ph. D. in Biomedical Engineering in 1992. He is working at the Vienna Medical University - Department of Biomedical Engineering and Physics - since 1983, from 1997 on as Assistant Professor and since 2001 as Associate Professor. His past and present research includes rehabilitation engineering in spinal cord injury, neural prostheses, and functional electrical stimulation (FES). After technical co-ordination of the first-time-in-history application of FES in space the main focus of his work during the recent years focused on FES of denervated muscles (co-ordination of the European research and development project "RISE" - outcome: a novel rehabilitation method for flaccid paraplegia and associated technical equipment, at present in the dissemination phase).

Frank Rattay received the Dipl. Ing., Dr. techn. and Dr. rer. nat. degrees from the Vienna University of Technology in 1974, 1980 and 1995, respectively. In 2006 he received a Dr. science med. degree from the Medical University Vienna. He is professor for „Modeling and Simulation in Technique and Science" (1987) and for „Biophysics" (2000) at the Institute of Analysis and Scientific Computing of the Vienna University of Technology. Since Nov. 1994 he is chair of TU-BioMed, the Association for Biomedical Engineering at the Vienna University of Technology. He chaired the ‚Commission for Technical Mathematics' and for the same four years (2000-2003) he was Senator of the University. He is co-initiator of the new master curriculum "Biomedical Engineering" at the Vienna University of Technology. In 1986 Rattay introduced the activating function concept which is the most cited method to explain nerve or muscle tissue excitation by electrical fields.

FH-Prof. Dr. M. Reichel. Born in 1969, Dr. M. Reichel studied at the University of Technology and graduated in Electronic Engineering, in Vienna in 1995 with the degree "Diploma Engineer". After his civilian service, he worked at the Department of Biomedical Engineering & Physics at the Vienna Medical School (Vienna General Hospital) as a scientific assistant in several projects on Neurorehabilitation and in parallel he continued his studies at the University of Technology and made his Ph.D. in 1999 in the Field of "Functional Electrical Stimulation – Modeling & Simulation". Since 2002 Prof. Reichel is employed by the University of Applied Sciences Technikum Wien and Since 2007 his responsibilities are managing the department of Biomedical Engineering & Environmental Management as well as the study program of Healthcare- & Rehabilitation Technology. Prof. Reichel is teaching and supervising bachelor and masters theses in the areas of Biomedical Engineering and Biomedical Informatics as well as Instrumented Motion Analysis.

OPTIMIZING VIDEO-OCULOGRAPHY SYSTEMS BY SIMULATING THE EFFECT OF SLIPPAGE ARTIFACTS

Michael Platz[a], James K. Y. Ong[b], Thomas Haslwanter[c]

[a, b]Upper Austria University of Applied Sciences,
Research and Development Ltd., Research Center Campus Linz,
Garnisonstr. 21, 4020 Linz, AUSTRIA.
[c]Upper Austria University of Applied Sciences,
School of Applied Health and Social Sciences,
Garnisonstr. 21, 4020 Linz, AUSTRIA.

[a]michael.platz@fh-linz.at, [b]james.ong@fh-linz.at, [c]thomas.haslwanter@fh-linz.at

ABSTRACT
Video-Oculography systems (VOG), video based systems for measuring eye movements, are widely available as a supporting tool for clinical diagnosis of eye movement. The main remaining weakness of these systems is the difficulty to distinguish between eye movements and movements of the camera with respect to the head. In our project we try to classify between movement of the eye and movement of the camera of the VOG system by examining the effect of eye movement and camera movement on the position changes of the center of the pupil and the reflection of a light source which is directly attached to the camera in the image data of VOG systems. Therefore we implemented a simulation model of the eye and of a VOG system to investigate the effect of pure eye movement, pure camera movement and combined eye-camera movement on the objects in the image data.

Keywords: eye movement measurement, video oculography, camera slippage

1. INTRODUCTION

Our central nervous system provides several mechanisms to keep the retinal image stable, which enables clear vision during spatial movement. For example, to ensure clear vision when the head moves rapidly, the Vestibulo-Ocular Reflex (VOR) transmits information about head rotations from the semicircular canals of the human balance system to the eye muscles, with only three neurons in between. Due to this direct link between the ocular and the vestibular systems, different pathologies of the vestibular system can directly influence the kinematics of eye movements. Several studies have shown that by studying eye movements, simple diagnostic tests can be used to identify vestibular pathologies (Cremer, Halmagyi, Curthoys and Todd 1998; Schneider, Glasauer, Dietrich, Kalla and Brandt 2004).

For the exact quantitative measurement of eye movements, three technologies are established: Electro-Oculography (EOG), Scleral Search Coils (SSC) and Video-Oculography (VOG). EOG and SSC are well accepted but have distinct disadvantages: EOG, which is still the most common technique for measuring eye movement in the clinical environment (Haslwanter and Ong 2008), cannot measure the torsional component of eye movements (Haslwanter and Clarke 2009). SSC is the golden standard for measuring eye movements in three dimensions, with very high spatial and temporal resolution; however it is semi-invasive and expensive, and thus cannot be used for clinical testing.

VOG systems measure the position of the eye relative to the head by tracking the absolute position of the pupil center in the image data. Different types of VOG systems have been developed for different applications:

- Table mounted systems require the head of the patient to be approximately stationary.
- Head mounted systems allow the patient to move freely.

An example for a head mounted VOG system is the *EyeSeeCam* VOG system (Dera, Böning, Bardins and Schneider 2006), which is available at our institute. The *EyeSeeCam* VOG System is shown in Figure 1.

Due to the progress of video technology, VOG systems have become much cheaper and are commonly used in research laboratories as well as in the clinical environment.

The main remaining weakness of head mounted VOG systems is the high sensitivity to motion artifacts of the camera relative to the head of the patient, the so called slippage: a camera movement of 1 mm already corresponds to an eye position error of 5°. Such slippage artifacts can easily occur in head mounted VOG systems when the patient moves his head rapidly. In some new systems, the developers have tried to minimize the slippage by attaching the system firmly to the head and keeping the overall weight of the system as

low as possible. This approach can reduce motion induced slippage, which can occur when the head of the patient moves. But since the skin on the skull of the patient can always move, slippage artifacts cannot be eliminated completely in head mounted systems. The patient only has to raise his eyebrows or wrinkle his forehead to produce severe vertical slippage without moving his head at all. A compensation of these artifacts would increase the accuracy of VOG systems for all types of applications. We try to achieve this goal by using well established methods from the field of machine learning and computer vision.

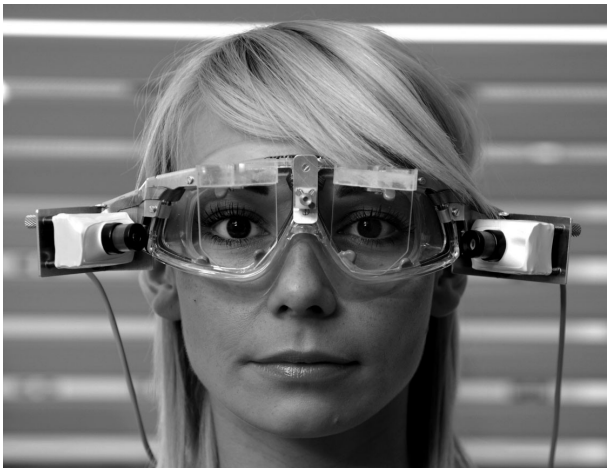

Figure 1: Image of the *EyeSeeCam*- VOG system which is available at our institution.

VOG systems typically determine the orientation of the eye by tracking the absolute position of the center of the pupil in the image. This approach breaks down when the camera moves with respect to the head. In that case, additional information is required to correctly measure eye position. In our approach, we try to distinguish between movement of the eye and movement of the camera of the VOG system by examining well defined features in the image data of VOG systems. The first feature is the center of the pupil, the second feature is a reflection of a light source on the front surface of the cornea, commonly referred to as the 1st Purkinje Reflection or Corneal Reflection. We additionally attached a light source to the VOG system directly next to the lens of the VOG system camera, so that it moves together with the camera. The features in the image can be seen in Figure 2.

We suppose that the distance between these two features in the image data changes in a characteristic way during movement of the eye and the camera. This should serve as a suitable classification criterion to reliably distinguish between movement of the eye, movement of the camera with respect to the head and combined eye camera movement.

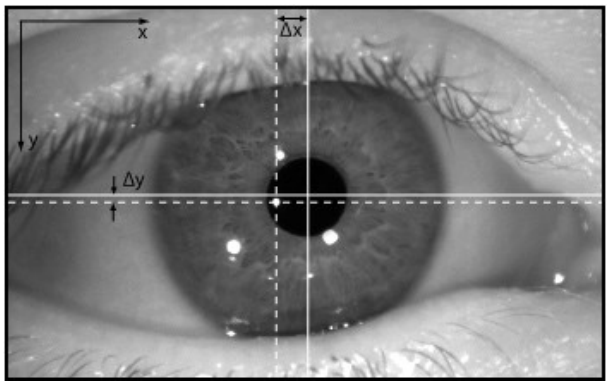

Figure 2: Typical image of a VOG recording showing the center of the pupil and the reflection of the additional mounted light source

Since VOG systems measure eye movement with a temporal resolution of up to 500 frames per second, a huge amount of data is collected even during short recordings. Manually labeling whether eye movement or slippage occurred in each frame would be tedious, and deciding which movement occurred just by looking at a single image is difficult. Therefore, we decided to develop a biomedical simulation model of the eye and a VOG system to investigate the effect of eye movement and slippage on the position of the pupil center and a reflection in the image data of the VOG system.

2. METHODS

We implemented the simulation model of the eye and the *EyeSeeCam* VOG system in MATLAB® R2008b (Natick MA, USA). We decided to use object oriented programming methods because our simulation model contains well defined objects like the eye and the camera. This enables encapsulation of all the parameters of the eye model and the model of the VOG camera, which can change for example when running the simulation with VOG systems from different manufacturers. To verify the correctness of our implementation we used test driven design methods.

2.1. Description of simulation model

Our eye model is based on Le Granges simplified eye model (Wyszecki and Styles 1982), which is an established simplified model of the human eye. In this model all dimensions of the eye are calculated from the length of the eye, the radius of the cornea and the radius of the limbus. Our simulation model of the eye consists of the components eyeball (bulbus), iris and cornea, where the center of the bulbus lies in the origin of the coordinate system.

The right handed coordinate system is specified in the following way:

- The x axis coincides with the line of sight.
- The y axis points to the left of the person wearing the VOG system.
- The z axis points upward.

The iris is modeled as a disk with a circular opening in the center, which represents the pupil. The center of the pupil is the center of this opening. The complexity of the model is reduced by modeling the eyeball as well as the cornea as two intersected spheres. To additionally enable simulations with real cornea surface data, we implemented the model of the cornea in such a way that measurements of a corneal topographer, a medical device for accurately measuring the topography of the cornea surface, can easily be included. Since the cornea surface is described by approximately 100 points when real cornea data is used, we reduced the computational time for rotating the model of the eye by rotating the model of the camera in the opposite direction. Rotations are implemented using quaternions (Haslwanter 1995).

We determined the parameters of the *EyeSeeCam* VOG system by taking a scaled photograph where all parameters could be measured manually. The camera of the VOG system is modeled as a simplified pinhole camera. The location of the pinhole and the image plane in the camera were estimated from the image of the VOG system. Using this model of the camera the points in space can be projected into the image plane using central projection, where the pinhole acts as the focal point of the projection.

2.2. Determination of the reflection

Once the camera model is placed relative to the eye model, we determine the positions where a reflection can occur on the surface of the cornea using ray tracing methods. In our simplified simulation model, we know roughly where the reflection appears. To enable simulation with real cornea data we implemented a more general approach for finding the reflection, since real cornea surfaces are not spherical. Therefore we generate a dense search grid with an angular dimension of 5° and a resolution of 0.1° on the cornea surface in the horizontal and vertical direction.

Each point of the search grid is interpolated between the real cornea surface points of the cornea model. The search grid includes all points were reflections can occur. For every point in the search grid, we then calculate an error value. This error value is 0 if the following conditions are fulfilled (for an illustration refer to Figure 3):

- The vectors *p*, *n*, *l* lie in the same plane
- The angle of incidence α equals the angle of reflection β

In Figure 3 *p* is the vector from the point on the cornea surface to the pinhole of the camera, *l* is the vector from the point on the cornea to the light source on the camera and *n* is the normal vector in the point on the cornea relative to the surface of the cornea.

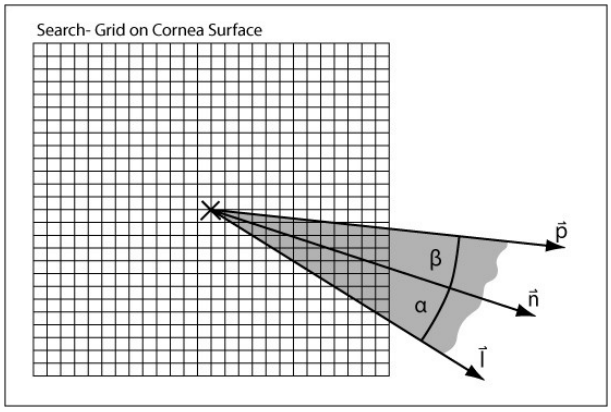

Figure 3: Detection of the reflection on the front surface of the cornea: For a given point in the search grid the error value is defined by the three vectors *p*, *n*, *l*, where *p* is the vector from the point on the cornea surface to the pinhole of the camera, *l* is the vector from the point on the cornea to the light source on the camera and *n* is the normal vector in the point on the cornea surface.

We then calculate the error value in a vectorized manner to reduce computation time, since the search grid contains 2500 possible reflection points. When we simulate the cornea as a sphere, we know that only one reflection can occur, so currently we are taking the point on the cornea surface with the minimum error value as the reflection of the light source. For real cornea data, a specific threshold for the error value has to be specified for finding multiple reflections on the surface. Once the point on the cornea surface where the reflection appears is found, we project this point in space into the image plane of the camera to get the position of the reflection in the image of the VOG system.

2.3. Determination of the pupil center

To accurately determine the center of the pupil on the cornea surface, we project the points on the pupil edge (the points on the edge of the circular opening in the iris disk) onto the surface of the cornea under consideration of Snell's Law (Law of Refraction), with an aqueous refraction index of the corneal front surface of 1.37. For each point of the pupil edge, we again generate a search grid, angular dimension 5° with 0.1° angular resolution, centered at the intersection point of the cornea surface with the vector from the pupil edge point to the pinhole of the camera. Similar to the determination of the reflection, we specify an error value which is 0 if the following conditions are fulfilled:

- The vectors *p*, *n*, *i* lie in the same plane
- The angles α and β fulfill Snell's law

Figure 4 illustrates this approach, where *p* is the vector from the point on the cornea surface to the pinhole of the camera, *n* is the normal vector in the point on the cornea relative to the surface of the cornea and *i* is the vector from the point on the cornea surface to the pupil edge point.

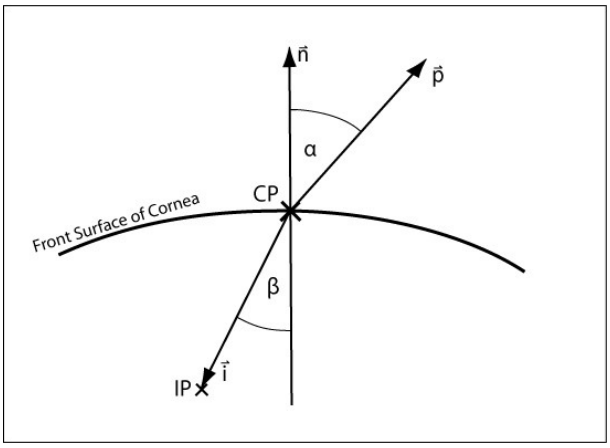

Figure 4: A point on the inner border of the iris (IP) is projected onto the front surface of the cornea using Snell's law, where CP is a point on the cornea, *n* is the normal vector in this point, *p* is the vector from CP to the pinhole of the VOG camera and *i* is the vector from CP to IP. If Snell's law is fulfilled and all three vectors lie in one plane the corresponding error value is minimal.

To reduce computation time for calculating the error values of all 2500 possible points, we parallelized the computation of the error values. The point with the minimum error value is taken as the projection of the corresponding pupil edge point onto the surface of the cornea.

After finding all pupil edge points on the cornea surface, we project these points into the image plane to get the corresponding image coordinates of the pupil border points. To accurately determine the center of the pupil with sub-pixel resolution we do an ellipse fit (Taubin 1991) on these points in the image. The center of the pupil in the image is the center of the fitted ellipse, which is common practice in VOG systems.

The positions of the pupil center and the reflection in the image can be examined by placing the camera at a fixed position relative to the eye. Different kinds of movement are simply a sequence of specific relative positions of the model of the VOG system camera relative to the model of the eye. For every relative position we then determine the location of the reflection and the pupil center in the image of the VOG system.

3. RESULTS

We have implemented the 3D simulation model of the eyeball and the VOG system using object oriented programming methods in MATLAB. With our simulation model we can simulate the effect of eye movement without slippage, slippage without eye movement and combined eye camera movement on the positions of the pupil center and corneal reflections in the image plane of the VOG camera. Since we used an object oriented approach, our simulation model contains modular objects with well defined interfaces. Therefore VOG systems from different manufacturers or real cornea topography data can be easily included in our simulations.

To measure the computational time for one typical simulation track we performed a simulation of pure eye rotation from -10° to +10° in 1° steps in both vertical and horizontal direction. This results in a total of 441 eye-position setups. The computational time of this simulation was 1873 seconds, which gives an average computation time of about 4.2 seconds per eye-position setup. This simulation run was executed on a PC with a Intel Core 2 CPU, 2.13 GHz and 1.98 GB RAM running Windows XP.

To verify the correctness of our simplified simulation model, we compared the results from our simulations to manually measured position values of the pupil center and the reflection in the image data of the *EyeSeeCam* system. We separated this verification process in two steps, one for verifying the simulation of pure eye rotation and another for verifying the correctness of the pure vertical slippage. The main reason for splitting this verification process is the fact that in a first approximation the motion of the eyeball during natural eye movement can be interpreted as a simple rotation about a fixed rotation center which coincides with the center of the bulbus. The motion pattern of vertical slippage, which typically occurs for example when the patient wearing the VOG system wrinkles his forehead, is a more complex movement. In a first approximation we supposed that vertical slippage can be modeled as a pure vertical translation (along the positive z axis) with a maximum translation value of about 10 mm.

For verification of the simulation of pure eye rotation, we manually measured the position of the pupil center and the position of the center of the reflection on the cornea at fixed eye positions in the image data of the *EyeSeeCam* VOG System. We decided to use well defined positions which are also used during the calibration process of the VOG system at horizontal and vertical values of 0° and ±8.5°. Our experimental data indicated that the initial camera orientation significantly effects the position of the features in the image. By iterating over different orientations and locations of the camera relative to the eye we obtained simulation results which matched the positions of the features in the image data of the *EyeSeeCam* system when we initially rotated the camera system 4.5° about the y axis followed by a rotation of 14° about the z axis. After translating the camera -2.6 mm along the y axis and 0.45 mm along the z axis the results from our simulation matched the results from the image data.

For a system verification compared the 2D vector from the center of the pupil to the center of the reflection in the image data of the VOG system to our simulation result. We measured a RMS error in the horizontal direction of 1.9 pixel and a RMS error of 2.68 pixel in the vertical direction. Supposing that a rotation of the eye about 1 mm on the surface of the cornea is equal to a translation of 15 pixel in the image

data of the VOG system when the distance from the center of the eye to the front surface of the cornea is approximately 12.6 mm, this error of our simulated feature positions equals to an error in eye position of 0.59° for horizontal and 0.82° for vertical eye rotations.

4. DISCUSSION

Currently we are working on the slippage verification of the simulation results. We want to focus on the vertical component of camera slippage, since this component currently cannot be eliminated.

In our current model of the *EyeSeeCam* system all parameters of the camera imaging system are measured from a scaled photography or typical values are taken as a first approximation. To overcome these assumptions we try to determine the exact values for the projection of arbitrary points in space into the image plane of the VOG system camera by applying a calibration method proposed by Zhang (1998).

To additionally verify our simulation model, we want to compare our simulation results to a similar simulation model of a Head Mounted Display System (Hua and Krishnaswamy 2006) where the features in the image data of the camera are calculated using the first-order imaging matrices for spherical surfaces and mirrors.

Since purely vertical slippage is currently unknown, we additionally plan to measure the change in position and orientation of the VOG system camera using the *Lukotronic*® system AS 200 (Innsbruck, Austria), a system that can detect 3D positions of markers with a temporal resolution of ~1ms and a spatial resolution of up to 100µm at a distance of 1.5m.

Based on our simulation results we plan to develop robust algorithms to accurately determine between pure eye movement, pure camera movement and combined eye camera movement.

5. ACKNOWLEDGEMENT

This study was supported by the Austrian Science Fund (FWF), Program for Translational Research, Grant Nr. L425-N15 and the Upper Austria University of Applied Sciences.

Additionally I want to thank my Ph.D. advisor Josef Scharinger from the Institute for Computational Perception, Johannes Kepler University Linz, for supporting me during my doctoral thesis.

6. REFERENCES

Cremer, P.D., Halmagyi, G.M., Aw, S.T., Curthoys, I.S., McGarvie, L.A., Todd, M.J. et al. (1998): Semicircular canal plane head impulses detect absent function of individual semicircular canals. Brain, 121, 699-716.

Dera, T., Böning, G., Bardins, S., Schneider, E.: Low-latency video tracking of horizontal, vertical, and torsional eye movements as a basis for 3DOF realtime motion control of a head-mounted camera. Proceedings of the IEEE Conference on Systems, Man and Cybernetics (SCM2006), Taipei, Taiwan, 2006.

Haslwanter, T.: Mathematics of three-dimensional eye rotations. Vision Research, 1995, 35, 12, pp. 1727-1739.

Haslwanter, T., Clarke, A.H. (2009): Eye movement measurement: Electro-Oculography and Video Oculography. In D.S.Zee & S. D. Eggers (Eds.), Vestibular and Balance Disorders. Elsevier.

Haslwanter, T., Ong, J. (2008): Applying knowledge - Challenges in bringing scientific advances to dizzy patients [accepted] . In M.Strupp, U. Buettner, & B. Cohen (Eds.), Basic and Clinical Aspects of Vertigo and Dizziness. New York Academy of Sciences, New York.

Hua, H., Krishnaswamy, P. (2006): Video-based eyetracking methods and algorithms in head-mounted displays. Optics Express, Vol. 14, No. 10, p. 4328 – 4350.

Schneider, E., Glasauer, S., Dieterich, M., Kalla, R., Brandt, T. (2004): Diagnosis of vestibular imbalance in the blink of an eye. Neurology, 63, 1209-1216.

Taubin, G. (1991): Estimation of Planar Curves, Surfaces, and Nonplanar Space Curves Defined by Implicit Equations with Applications to Edge and Range Image Segmentation . IEEE Transactions on Pattern Analysis and Machine Intelligence, Vol. 13, No. 11.

Wyszecki, G., Stiles, W. S. (1982): Color Science: Concepts and Methods, Quantitative Data and Formulae, 2nd ed., Wiley-Interscience, 1982.

Zhang, Z. (1998): A Flexible New Technique for Camera Calibration, Technical Report MSR-TR-98-71, Microsoft Research.

7. AUTHORS BIOGRAPHY

DI(FH) **Michael Platz** studied Electronics at the University of Applied Sciences Technikum Wien (Vienna, Austria) with an emphasis on Biomedical technologies and Audio-Video technologies. After one year working at a research group at the Institute of Biomedical Technologies and Physics at the AKH Wien he started to work at the Upper Austria University of Applied Sciences as a Research Associate. After two years he was offered a PhD position where he is currently writing his Doctoral thesis at the Institute for Computational Perception, Johannes Kepler University Linz, Austria. His current work focuses on Computer Vision and Machine Learning. During his thesis he cooperates with medical practitioners to overcome the last remaining problems of using VOG as a standard diagnostic tool in the clinical environment.

Dr. **James K. Y. Ong** is a trained mathematician and optometrist. He has experience in the areas of dynamical systems and operations analysis, as well as vision science and cognitive psychology. His current role is to find ways to apply technology to improve health outcomes. The current focus of his research is to

measure torsional eye movements from video data, in order to help medical practitioners to diagnose benign paroxysmal positional vertigo.

PD Prof. (FH) Dr. **Thomas Haslwanter** started out at the University of Innsbruck, Austria, with theoretical work in the areas of quantum optics and laser theory. For his PhD at the Swiss Federal Institute of Technology (ETH Zurich, Switzerland) he switched into the field of neuroscience, working on the control of eye and head movements. After postdoc positions at the University of Sydney (Australia) and the University of Tuebingen (Germany) he returned to the ETH Zurich, focusing more and more on medical applications of his research work on dizziness. Since 2004 he has been living in Linz, Austria. After two years as scientific head of the Department of Medical Informatics at Upper Austrian Research , a non-profit organization, he became professor for Biomechanics at the Upper Austrian University of Applied Sciences in Linz. Current research activities center on video-oculography, and on movement kinematics in three dimensions.

EVALUATION OF A STATISTICAL SHAPE MODEL BASED APPROACH FOR RECOVERING THE 3D LV SHAPE FROM PROJECTIVE X-RAY IMAGES

R. Swoboda[a,c], G. Zwettler[a], C. Steinwender[b], F. Leisch[b], J. Scharinger[c]

[a]Bio- and Medical Informatics Research Group, University of Applied Sciences Upper Austria, Austria
[b]Clinic of Internal Medicine I, General Hospital Linz, Austria
[c]Department of Computational Perception, Johannes Kepler University Linz, Austria

[a]roland.swoboda@fh-hagenberg.at, [a]gerald.zwettler@fh-hagenberg.at, [b]clemens.steinwender@akh.linz.at, [b]franz.leisch@akh.linz.at, [c]josef.scharinger@jku.at

ABSTRACT

Recovering the 3D shape of the left ventricle from contrast-enhanced bi-planar x-ray image sequences is a challenging task. The inherently sparse and noisy data available for reconstruction and the ill-posed nature of the problem necessitate the incorporation of prior knowledge about the ventricular anatomy. Our novel approach reconstructs the endocardial surface from two projections using a statistical shape model that is learned from high-resolution multi-slice CT data. A non-rigid 2D/3D registration method fits the deformable model to the recorded x-ray images by calculating simulated projections of the model and minimizing the difference between simulated and real projections. The presented algorithm is evaluated based on simulated and real patient data using volumetric and geometric similarity measures. For the first time, bi-planar and CT images of the same patient are used to compare the recovered LV shape with the actual shape.

Keywords: left ventricle reconstruction, bi-planar x-ray angiography, statistical shape model, non-rigid 2D/3D registration

1. INTRODUCTION

Acute myocardial infarction is one of the most common causes of death in the industrialised world today. For localisation and treatment of the occluded coronary vessel causing the infarction, interventional x-ray angiography is state of the art in cardiology. During an interventional session, a balloon catheter is inserted into the patient's body, advanced to the occlusion and dilated to restore blood circulation. Digital x-ray images are acquired to monitor the advancement and placement of the catheter and to assess the impact of the infarction. In the latter case, the catheter is inserted into the left heart chamber (ventricle) and contrast agent is injected to opacify the ventricular cavity during radiation. Within these 3-6 heart beats, x-ray image sequences are simultaneously acquired from two viewing directions, recording the ventricular silhouettes evolving over time (see Fig. 1 and 5).

In clinical practice, quantitative left ventricular analysis is based on the end-diastolic (ED) and end-systolic (ES) projection images. The ED and ES volume of the left ventricle (LV) are approximated from the ED and ES endocardial contours and are used to calculate the ejection fraction (EF), i.e. the volume that is squeezed out during contraction. Contour information is further incorporated by LV wall motion analysis methods like the centreline method or the radial method to quantify myocardial viability. A major drawback of the underlying imaging modality is that 3D information is lost due to projection. Thus, major cardiac diagnostic parameters like EF are only approximated. Moreover, wall motion is only evaluated for surface areas with the boundary visible in the projection image. Instead of evaluating the LV in 2D, novel approaches aim at reconstructing its spatio-temporal shape to perform analysis in 3D (Swoboda et al. 2005).

Figure 1: Biplane X-Ray Angiography Equipment Used During an Interventional Session in the Catheter Lab

2. RELATED WORK

Several works have addressed the problem of recovering the 3D LV shape from projective x-ray images in the past. In (Moriyama et al. 2002) and (Medina et al. 2006) only LV contour information is used, while the algorithms in (Prause and Onnasch 1996) and (Backfrieder et al. 2005) additionally exploit densitometric information derived from the grey values of the x-ray images. However, the quality of that

information is impaired due to the inhomogeneous saturation of contrast agent within the ventricle. One approach to improve the sparse and noisy data available for reconstruction is to use more than one bi-planar acquisition and different projection angles (Moriyama et al. 2002). But this implies an increased x-ray exposure for the patient as well as higher clinical costs and is therefore suboptimal in practice.

The application of statistical shape models (SSMs) for recovering human anatomies from x-ray projections has been successfully demonstrated for the femur bone (Fleute and Lavellée 1999), the vertebrae (Benameur et al. 2003) and the pelvic bone (Lamecker et al. 2006). To our knowledge, this is the first work that follows such an approach to recover the ventricular shape. As opposed to the other anatomies, the LV is a deforming object and contrast agent is required to deduce information about its thickness from the projections.

3. MATERIAL AND METHODS

The novelty of this work is to utilize geometric prior knowledge about the LV anatomy that is derived from cardiac CT images and modelled as SSM. The model is fit to the projections using non-rigid 2D/3D registration. Geometric and volumetric similarity measures are defined to evaluate the reconstruction results.

3.1. Statistical Shape Models

Statistical shape models were first introduced by Cootes and Taylor (Cootes et al. 1995). During the last decade their concept was extended to active shape models and active appearance models and became a fundamental method in computer vision and image processing. This section outlines the basic approach; more details about the theory are given in (Cootes and Taylor 2004).

In order to learn a 3D statistical shape model (SSM), a set of segmentations of the target shape is required. Let $S = \{ S_i \}$ denote a set of k training shapes. The surface of S_i is described by n landmark, i.e. points of correspondence that match between shapes, and represented as a vector of coordinates:

$$\mathrm{x}_i = \left(x_1,\ldots,x_n, y_1,\ldots,y_n, z_1,\ldots,z_n\right)_i^T \quad (1)$$

All k shape vectors form a distribution in a $3n$-dimensional space. The distribution is approximated by:

$$\mathrm{x} = \bar{\mathrm{x}} + \Phi \mathrm{b} \quad (2)$$

$\bar{\mathrm{x}}$ denotes the mean shape (vector). Φ is obtained by performing principle component analysis (PCA) on C, i.e. the covariance matrix of the shape vectors. PCA yields the principle axes of the distribution. The eigenvectors φ_i give the directions of the axes, the eigenvalues λ_i the variance of the data in the direction of the axes.

$$\bar{\mathrm{x}} = \frac{1}{k}\sum_{i=1}^{k} \mathrm{x}_i \quad (3)$$

$$\mathrm{C} = \frac{1}{k-1}\sum_{i=1}^{k} (\mathrm{x}_i - \bar{\mathrm{x}})(\mathrm{x}_i - \bar{\mathrm{x}})^T \quad (4)$$

$$(\varphi_1,\varphi_2,\ldots,\varphi_i),(\lambda_1,\lambda_2,\ldots,\lambda_i) = PCA(C) \quad \lambda_j > \lambda_{j+1} \quad (5)$$

$$\Phi = (\varphi_1,\varphi_2,\ldots,\varphi_t) \quad \Lambda = (\lambda_1,\lambda_2,\ldots,\lambda_t) \quad (6)$$

To reduce noise and the model's dimensionality, only the largest t eigenvalues and corresponding eigenvectors are used. t is chosen so that a fraction f of the total variance is retained:

$$\sum_{j=1}^{t} \lambda_j \geq f \sum \lambda_j \quad (7)$$

Shape parameter vector b consists of t elements, also called modes of variation (MOV). By varying b, the mean shape is deformed and new instances of the shape class are generated.

Prior to statistical analysis, location, scale and rotational effects have to be removed from the training shapes to obtain a compact model. Usually, Procrustes alignment is applied to minimize $D = \sum \mathrm{x}_i - \bar{\mathrm{x}}$, the sum of squared distances of each shape to the mean.

3.2. Modelling of Left Ventricular Anatomy

A Siemens Somatom Sensation Cardiac 64 multi-slice CT is used to acquire 20 datasets, imaging the human heart in 3D at high-resolution. The volumes have an effective slice thickness of 0.5 mm and an average in-plane resolution of 0.33 mm. The size of the image mask in the transversal plane is 512×512 pixels; the number of slices varies between 220 and 310. The CT scans are performed at 65% of the heart phase (R-R peaks) with 120 kV.

The endocardial LV surface is manually segmented by experts in cardiology. To obtain an accurate model of the anatomy, details like the atrial emargination, the apex and the aortic valve region are maintained during segmentation. Contours are specified in axial slices by interactively setting/moving control points of a cardinal spline. Due to the high resolution of the CT scans, only each fifth slice is segmented; intermediate contours are interpolated. The surface of an LV is represented as a stack of contours.

Point correspondence among the training shapes is established based on back-propagation of the landmarks on a mean shape (Swoboda and Scharinger 2008).

After segmentation, landmark extraction and removing location, scale and rotational effects, the SSM is built as outlined in the previous section.

3.3. Simulated Angiography

The optimization process and evaluation strategy on which this work is based involves the simulation of angiographic projections. Our model of the bi-planar angiographic device calculates the exact position of the x-ray sources and the image intensifier planes for the projections. For a given viewing direction, pose vector and shape parameter vector, a simulated projection of

the SSM in image space is obtained in two steps: 1) the polygonal model is converted into a binary volume, 2) a projection is derived using ray-casting, i.e. the volume is sampled along rays starting at the x-ray source and ending at the pixel positions of the projection image. Fig. 2 illustrates the simulated projections of the SSM from standard right and left anterior oblique view.

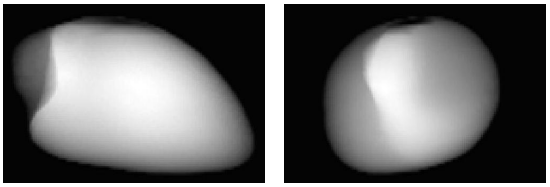

Figure 2: Simulated Projections of the Mean Shape

3.4. Left Ventricular Shape Recovery

Reconstruction is based on a 2D/3D registration approach. Most of the work done in this area addresses the problem of rigid registration, see (van de Kraats et al. 2005) and the references therein. In this work, however, the shape of the 3D object to be spatially aligned with its projections is unknown. Therefore, a non-rigid registration approach is followed to transform the SSM from model space to image space:

$$y = R\left(\left[\bar{x} + \Phi b\right]s + T\right) \tag{8}$$

Both shape parameter vector b and parameters for pose $p = \{ R, s, T \}$, i.e. rotation matrix R, scale factor s and translation vector T, have to be found so that the registration error is minimized.

Several ways exist to describe orientation in 3D space, e.g.: rotation matrices, quaternions and Euler angles. Euler angles are defined by three angles of rotation plus the order and the axis about which the rotations are applied. In contrast to (Fleute and Lavellée 1999), (Benameur et al. 2003) and (Lamecker et al. 2006) we use Euler angles instead of rotation matrices. This reduces dimensionality of the registration problem; the number of parameters needed to represent rotation in the pose vector is decreased by 6 (from 9 to 3). Our Euler angles follow the x-y-z convention, i.e. rotations are performed around the x-, y- and z-axis, respectively.

To fit the LV SSM to a set of projection images, an optimization procedure is applied to minimize the difference between the given projections and simulated projections derived from the SSM. Similar to (Fleute and Lavellée 1999) and in contrast to (Benameur et al. 2003) and (Lamecker et al. 2006) we use the Downhill Simplex algorithm. Our cost function depends on the shape and the pose parameter vector and incorporates contour and densitometric information derived from the projection images:

$$E(b,p) = \sum_{i=1}^{P}\left(\omega_C E_C(b,p) + \omega_D E_D(b,p)\right) \tag{9}$$

The total error E is defined as the weighted sum of contour-related error E_C and density-related error E_D over all P projections. E_C is obtained by equiangular sampling of the real and the simulated contour; the sum of squared distances is calculated for the sampled points. For E_D, the sum of squared difference metric is used. Other intensity-based metrics often applied for 2D/3D registration are discussed in (van de Kraats et al. 2005) and (Souha and Laurent 2008).

To generate plausible shapes (Cootes and Taylor 2004), b is constrained by $\pm 2\sqrt{\lambda_i}$. In contrast to (Fleute and Lavellée 1999), (Benameur et al. 2003) and (Lamecker et al. 2006), we exploit the training data to derive constraints for p. The training instances in model space are transformed to image space and the range of the components of the pose vector is analyzed. In case of orientation, the bounds for the Euler angles are: α = [-7.33, 17.15], β = [-19.96, 6.33], γ = [-22.70, 20.91].

Our experiments showed that optimizing pose and shape sequentially is more efficient than optimizing both simultaneously. A rigid registration is performed prior to optimization of the deformable parameters.

3.5. Extracting Information from Projection Images

The cost function to be minimized requires both contour and densitometric information. In case of the in-vivo angiographic images, the former is obtained with a graphical user interface. The endocardial silhouette is described by control points of a cardinal spline. If the ventricular boundary is not clearly visible, segmentation is facilitated by examining motion within the frames before and after the current frame. Information about the thickness of the LV is derived by digital subtraction angiography. From the initial frames of an angiographic sequence showing no contrast agent, a mask is deduced. Logarithmic subtraction of mask and current frame is performed due to the exponential attenuation of x-rays. To reduce the inhomogeneous saturation of contrast agent and noise introduced by the image intensifier, two frames before and after a frame are used for averaging.

Contour information required for optimization is extracted from the simulated angiography images by border detection; densitometric information is directly measured from the images.

3.6. Geometric Similarity Measures

To quantify the difference between the original and the recovered shape, their polygonal model representation is compared. Similarity of two polygonal models S_1 and S_2 is measured based on a distance metric d, giving the distance between surface point $p_i \in S_1$ and surface S_2. Distance metric d_{min} is defined as the Euclidean distance between p_i and its closest point on S_2; distance metric d_{ortho} denotes the Euclidean distance between p_i and the point obtained by intersecting S_2 with the surface normal at p_i:

$$sim_d(S_1,S_2) = \frac{1}{2}\left[\frac{1}{n}\sum_{i=1}^{n} d(p_i,S_2) + \frac{1}{m}\sum_{j=1}^{m} d(q_j,S_1)\right] \tag{10}$$

$$p_{i=1..n} \in S_1, q_{j=1..m} \in S_2$$

$$d_{\min}(p_i,S_2) = \min_{q_j \in S_2} |p_i - q_j| \tag{11}$$

$$d_{ortho}(p_i, S_2) = |p_i - surfn(p_i) \cap S_2| \quad (12)$$

Note that a distance based similarity measure sim_d assesses both shape and pose conformity. To consider the accuracy of pose independently from shape, the following three similarity measures are defined:

$$sim_T(S_{orig}, S_{rec}) = |\bar{p} - \bar{q}| \quad (13)$$

$$sim_R(S_{orig}, S_{rec}) = \left|(\alpha, \beta, \gamma)_{S_{orig}} - (\alpha, \beta, \gamma)_{S_{rec}}\right| \quad (14)$$

$$sim_s(S_{orig}, S_{rec}) = 1 - \frac{|size(S_{orig}) - size(S_{rec})|}{size(S_{orig})}$$
$$size(S) = \sqrt{\sum_{i=1}^{n} |p_i - \bar{p}|^2} \quad (15)$$

Let S_{orig} and S_{rec} denote the polygonal model of the original and the recovered shape, respectively. The Euclidean distance between their centroids is measured as similarity of location, sim_T. The absolute difference of the Euler angles, sim_R, is used to define similarity between original and reconstructed orientation. sim_s gives the size of the recovered shape w.r.t. the size of the original shape; the Frobenius norm is used as shape size metric.

3.7. Volumetric Similarity Measures

While the geometric similarity measures are derived from the polygonal model, the volumetric measures are based on the original and reconstructed LV binary masks, i.e. V_{orig} and V_{rec}. Let $|V|$ denote the volume of a 3D binary image. Volume conformity is measured by calculating the difference of volumes (DOV) for V_{orig} and V_{rec}. The volume of differences (VOD) of V_{orig} and V_{rec}, is used as shape conformity. Both similarity measures sim_{DOV} and sim_{VOD} are assessed w.r.t. to the original volume. The second metric used for shape conformity, sim_κ, is derived from the kappa statistic (Zijdenbos et al. 1994) and quantifies the overlap between two binary masks.

$$sim_{DOV}(V_{orig}, V_{rec}) = 1 - \frac{\left||V_{orig}| - |V_{rec}|\right|}{|V_{orig}|} \quad (16)$$

$$sim_{VOD}(V_{orig}, V_{rec}) = 1 - \frac{|V_{orig} \oplus V_{rec}|}{|V_{orig}|} \quad (17)$$

$$sim_\kappa(V_1, V_2) = \frac{2|V_1 \cup V_2|}{|V_1| + |V_2|} \quad (18)$$

4. RESULTS

The presented methods are implemented and evaluated using Matlab and the Image Segmentation and Registration Toolkit (ITK) C++ library.

4.1. Left Ventricular Statistical Shape Model

The final SSM is learned from $k = 20$ datasets and described using $n = 2500$ landmarks. It is illustrated in Fig. 3 with a variation of $\pm 2\sqrt{\lambda_i}$. For the sake of clarity, only the first three MOV are shown.

The compactness of a SSM is its ability to describe the variability of a shape using as few parameters as possible. It is measured as a function of the number of shape parameters and based on the cumulative relative variance derived from the eigenvalues yielded by PCA. For shape reconstruction we use the first $t = 6$ modes. Thus, 83% of the total variance is retained.

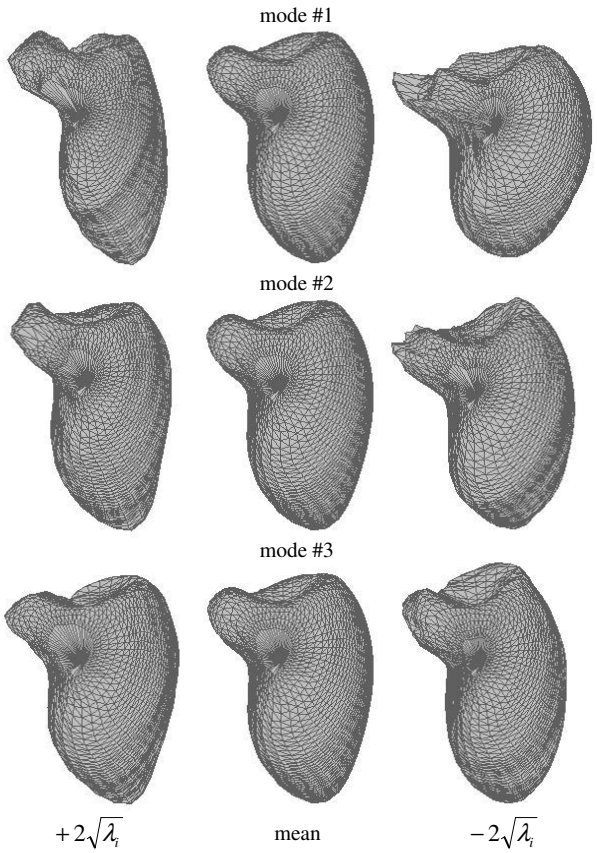

Figure 3: Statistical Model of the LV Anatomy. The Mean Model (in the Middle of Each Row) is Deformed Based on the First Three Modes of Variation

4.2. Evaluation based on Simulated Angiography

Evaluation with simulated data is performed based on leave-one-out experiments. From the segmented CT data sets, all but one are used to learn a shape model. Bi-planar angiographic projections are simulated for the left-out CT data set, and from these projections shape is recovered by fitting the learned model. The recovered shape is compared with the segmented shape of the left-out data set using the defined similarity measures. This procedure is repeated for each data set.

Table 1: Geometric Similarity Measures

	Mean	Std.	Min.	Max.
d_{min} (mm)	2.61	0.65	1.65	3.53
d_{ortho} (mm)	2.49	0.77	1.38	3.72
R_α (°)	5.14	2.98	1.78	8.62
R_β (°)	4.03	3.30	0.38	8.91
R_γ (°)	6.18	4.75	2.28	16.01
s (%)	97.44	1.21	95.97	100.00
T (mm)	1.92	0.62	0.98	2.96

Table 2: Volumetric Similarity Measures

	Mean	Std.	Min.	Max.
DOV (%)	94.56	3.55	87.35	98.73
VOD (%)	78.17	5.30	68.88	84.91
κ (%)	87.12	2.53	82.54	90.18

The sim_{DOV} and sim_s measures show that the original volume and the original size are approximated at high accuracy. This is essential for cardiac diagnosis; major parameters are based on the LV volume, e.g. EF. As indicated by the sim_T measure, the reconstructed position is close to the original. Concerning shape conformity we can see that a high overlap between the two shapes is achieved, though the volume of difference is still improvable. The distance metrics are near the mean reconstruction error of 2.3 mm (Swoboda and Scharinger 2008). The latter is obtained by evaluating the generalization ability of our SSM; i.e. in leave-one-out experiments the SSM is fitted to unseen 3D shapes and the mean distance between model and instance points is measured.

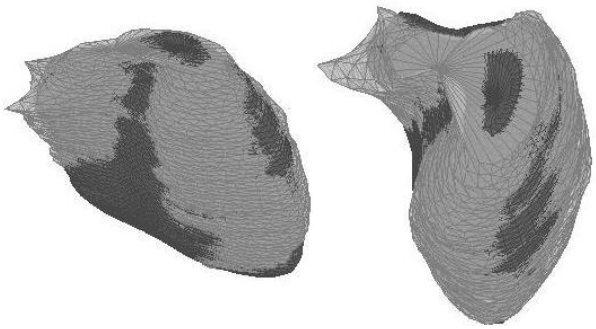

Figure 4: Reconstruction Example. The Original Shape is in Bright, the Recovered Shape in Dark Color

4.3. Evaluation based on In-vivo Angiograms

The CT data used in this work is acquired from 20 patients. In three cases, x-ray angiographic projection images are available complementary to the cardiac CT scan. From these projections, the ventricular shape is recovered. Note that its true 3D shape is known from CT data. This allows an exact evaluation of our reconstruction approach with clinical data.

The ventriculograms are acquired using a Siemens Bicor and a Siemens AXIOM Artis dBC system, both capturing images of 512x512 pixels and 8-bit grey level depth at a frame-rate of 25fps. For temporal registration with CT data, the ECG information accompanying the bi-planar images is utilized.

The evaluation approach for in-vivo angiograms is as follows: 1) a SSM is learned from 19 data sets, the CT data set corresponding to the angiogram is excluded, 2) the model is fit to the real projections, and 3) the recovered shape is compared with the true 3D shape of the excluded CT data set using the defined similarity measures. The results of the three experiments are given in Tab. 3 and 4. Note that the number of data sets available for evaluation is relatively small. However, the results give a first estimate.

Table 3: Geometric Similarity Measures

	#1	#2	#3	Mean	Std.
d_{min} (mm)	2.43	2.32	2.95	2.57	0.34
d_{ortho} (mm)	2.36	2.05	3.36	2.59	0.68
R_α (°)	0.25	7.25	16.66	8.05	8.23
R_β (°)	2.34	8.78	9.79	6.97	4.04
R_γ (°)	6.89	6.94	7.51	7.11	0.34
s (%)	98.76	97.42	95.58	97.25	1.60
T (mm)	1.39	0.52	2.33	1.41	0.91

Table 4: Volumetric Similarity Measures

	#1	#2	#3	Mean	Std.
DOV (%)	98.01	92.87	82.11	91.00	8.11
VOD (%)	74.72	80.13	68.12	74.32	6.01
κ (%)	87.49	90.41	79.75	85.88	5.51

The experiments show similar results compared to the evaluation based on simulated data. For example 3, the reconstruction yields suboptimal results. The best shape conformity is achieved for example 2.

5. DISCUSSION

A common question when processing contrast-enhanced x-ray cine-angiographic images is: how accurate is the representation of the endocardial LV shape in the projections? A comparison of the available in-vivo angiograms with simulated projections derived from the associated CT scan showed good correspondence concerning the ventricular outline, see Fig. 5. However, correspondence in other heart phases still has to be investigated.

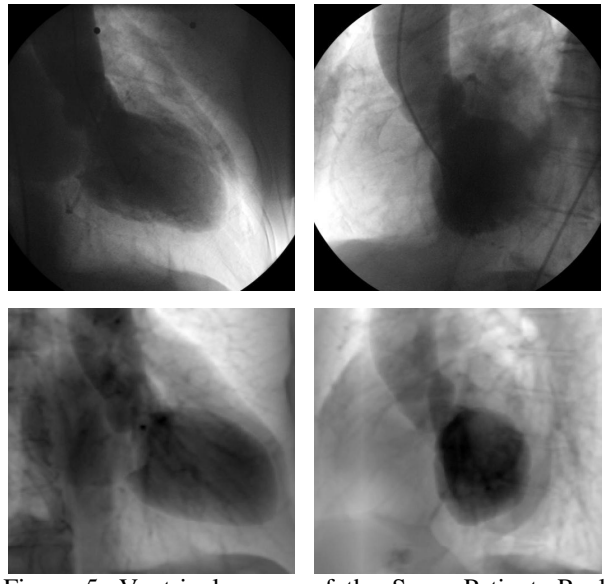

Figure 5: Ventriculograms of the Same Patient. Real Projections from X-Ray Angiography (Top Row) vs. Simulated Projections from CT Volume (Bottom Row)

Our reconstruction algorithm recovers the LV from two contrast-enhanced projections in standard right and left anterior oblique view. Although only one bi-planar acquisition is considered for reconstruction, the number of projections is not limited. Concerning projections,

arbitrary directions are allowed; orthogonal acquisitions (Prause and Onnasch 1996) are not required.

One problem when using Euler angles are gimbal locks. One degree of freedom is lost if two of the three axes align. In case of the x-y-z convention, gimbal locks occur when the second angle, β, is ±90°. However, analysis of the training shapes' orientation showed that $|\beta|$ is at most 20°. Moreover, rotation angles of ±90° don't seem plausible from an anatomical point of view.

Unlike other LV SSMs often found in literature, anatomical areas like the atrial concavity, the aortic valve region and the apex are preserved in our model. This is necessary to generate complete contour and densitometric information during registration. Further note that these areas overlap with the ventricular cavity in projection images and are therefore hard to recover without prior knowledge.

6. CONCLUSION

A new method for recovering LV shape from contrast-enhanced bi-planar images is presented. The novelty of our approach is that it combines x-ray angiographic data with CT data. A priori information about the ventricular anatomy is learned from CT images and modelled as SSM. A non-rigid 2D/3D registration technique fits the model to the projections. For the first time, bi-planar and CT images of the same patient are used to evaluate reconstruction.

Using a SSM for reconstruction eases the ill-posed problem of recovering the LV from sparse and noisy projection data and allows generating statistically plausible and patient specific shapes. Evaluation with both simulated and real patient data show promising results. The LV volume is recovered at high accuracy. This is important for cardiac diagnosis since major parameters, e.g. EF, are based on volumes. Concerning shape conformity, the overlap between original and recovered volume is high, though there is still place for minor improvements.

Future work will focus on evaluating our approach with more in-vivo angiograms and on improving the non-rigid 2D/3D registration.

ACKNOWLEDGMENTS

We want to thank the medical staff of the Central Institute of Radiology at the General Hospital of Linz, especially PD Dr. Franz Fellner, head of department, and Johannes Krieger, for providing the images and for the valuable discussions. Special thank is further given to Dr. Thomas Lambert for his support.

REFERENCES

Backfrieder, W., Carpella, M., Swoboda, R., Steinwender, C., Leisch, F., 2005. Model based lv-reconstruction in bi-plane x-ray angiography. *Medical Imaging 2005: Image Processing*, 1475–1483, February 13-18, San Diego (USA).

Benameur, S., Mignotte, M., Parent., S., Labelle, H., Skalli, W., de Guise, J., 2003. 3d/2d registration and segmentation of scoliotic vertebrae using statistical models. *Computerized Medical Imaging and Graphics*, 27(5), 321–337.

Cootes, T.F., Taylor, C.J., 2004. *Statistical models of appearance for computer vision*. Technical report. Available from: http://www.isbe.man.ac.uk/~bim/Models/app_models.pdf [accessed 24 June 2009]

Cootes, T.F., Taylor, C.J., Cooper, D.H., Graham, J., 1995. Active shape models - their training and application. *Computer Vision and Image Understanding*, 61(1), 38–59.

Fleute, M., Lavellée, S., 1999. Nonrigid 3-d/2-d registration of images using statistical models. *Proceedings of the Second International Conference on Medical Image Computing and Computer-Assisted Intervention*, 138–147. September 19-22, Cambridge (UK).

Lamecker, H., Wenckebach, T.H., Hege, H.C., 2006. Atlas-based 3d shape reconstruction from x-ray images. *Proceedings of the 18th International Conference on Pattern Recognition*, 371–374. August 20-24, Hong Kong (China).

Medina, R., Garreau, M., Toro, J., Breton, H., Coatrieux, J.L., Jugo, D., 2006. Markov random field modeling for three-dimensional reconstruction of the left ventricle in cardiac angiography. *IEEE Transactions on Medical Imaging*, 25(8), 1087–1100.

Moriyama, M., Sato, Y., Naito, H., Hanayama, M., Ueguchi, T., Harada, T., Yoshimoto, F., Tamura, S., 2002. Reconstruction of time-varying 3-d left ventricular shape from multiview x-ray cineangiocardiograms. *IEEE Transactions on Medical Imaging*, 21(7), 773–785.

Prause, G.P.M, Onnasch, D.G.W, 1996. Binary reconstruction of the heart chambers from biplane angiographic image sequences. *IEEE Transactions on Medical Imaging*, 15(4), 532–546.

Souha, A., Laurent, S., 2008. Accurate and precise 2d-3d registration based on x-ray intensity. *Computer Vision and Image Understanding*, 110(1), 134–151.

Swoboda, R., Carpella, M., Steinwender, C., Gabriel, C., Leisch, F., Backfrieder, W., 2005. From 2d to 4d in quantitative left ventricle wall motion analysis of biplanar x-ray angiograms. *Computers in Cardiology*, 977–980. September 25-28, Lyon (France).

Swoboda, R., Scharinger, J., 2008. A 3-d statistical shape model of the left ventricle – geometric prior information for recovering shape from projective bi-planar x-ray images. *Proc. 32nd workshop of the Austrian Association for Pattern Recognition,* 53–61. May 26-27, Linz (Austria).

van de Kraats, E., Penney, G., Tomazevic, D., van Walsum, T., Niessen, W., 2005. Standardized evaluation methodology for 2-d-3-d registration. *IEEE Transactions on Medical Imaging*, 24(9), 1177–1189.

Zijdenbos, A.P., Dawant, B.M., Margolin, R.A., Palmer, A.C., 1994. Morphometric analysis of

white matter lesions in MR images: method and validation. *IEEE Transactions on Medical Imaging*, 13(4), 716–724.

AUTHORS BIOGRAPHY

Roland Swoboda studied Software Engineering at the University of Applied Sciences in Hagenberg. After finishing his diploma thesis at CERN and graduating Dipl.-Ing. (FH) in 2002 he joined the bio- and medical informatics research group at the University of Applied Sciences as research assistant and project manager. His research activities focus on medical image processing, computer assisted analyses and diagnoses in cardiology and the development of medical software systems. He is currently working on his PhD thesis at the Johannes Kepler University Linz in the field of 3D quantitative left ventricular analysis in bi-planar x-ray angiography.

Gerald A. Zwettler was born in Wels, Austria and attended the University of Applied Sciences Upper Austria in Hagenberg where he studied software engineering for medical applications and graduated Dipl.-Ing. (FH) in 2005. Since then he is working as research assistant at the research and development department of the University of Applied Sciences Competence Center Hagenberg mainly in the field of medical image analysis and medical software engineering. In the year 2009 he accomplished his master thesis titled with Automated Vessel Tree Modelling for Functional Diagnostics on 2D and 3D Medical Image Data for achieving a second degree.

Clemens Steinwender studied human medicine at the Medical University of Vienna in Austria and graduated M.D. in 1995. Since 1999 he works at the 1st Department of Internal Medicine at the General Hospital Linz. Dr. Clemens Steinwender is specialist for internal medicine, cardiology and intensive medicine. His occupation and research interests include coronary intervention, catheter ablation, electrophysiology, cardiac imaging and medical image processing in x-ray cine-angiography.

Franz Leisch graduated M.D. in 1971 at the Medical University of Vienna, Austria. He is specialist for internal medicine, cardiology and intensive medicine. Since 1988, Dr. Franz Leisch holds the position as head of the 1st Department of Internal Medicine at the General Hospital Linz. He received Venia docendi for Internal Medicine in 1990, and the title University Professor in 2004, both from the Medical University of Vienna.

Josef Scharinger received his MSc in 1992 and his PhD in 1995, both from Johannes Kepler University Linz, Austria. Currently he holds the position of an Associate Professor at the Department of Computational Perception at the Johannes Kepler University Linz, Austria. Josef Scharinger continuously acts as a reviewer for a variety of international journals and conferences, has published more than 60 international scientific publications in books, journals and conference proceedings and also has co-authored 4 patents in the field of IT security. His research interests include signal Processing (image and speech), biometrics, cryptography and nonlinear systems theory (chaos theory).

FAST FULLY-AUTOMATED MODEL-DRIVEN LIVER SEGMENTATION UTILIZING SLICEWISE APPLIED LEVELSETS ON LARGE CT DATA

Gerald Zwettler[(a)], Franz Pfeifer[(a)], Roland Swoboda[(a)], Werner Backfrieder[(b)]

[(a)]Bio- and Medical Informatics Research Group, University of Applied Sciences Upper Austria, Softwarepark 11, 4232 Hagenberg, AUSTRIA
[(b)]Software Engineering, School of Informatics, Communication and Media, University of Applied Sciences Upper Austria, Softwarepark 11, 4232 Hagenberg, AUSTRIA

[(a)]gerald.zwettler@fh-hagenberg.at, [(b)]werner.backfrieder@fh-hagenberg.at

ABSTRACT
Modern Computed Tomography scans are acquired down to a slice thickness of 0.5 mm thus yielding a huge number of 2D slices to be examined by the physician. Hence the need for automated computer assisted diagnostics, e.g. in the field of abdominal scans for liver tumor diagnostics and surgery planning, arises. In this work a fully-automated algorithm for robust and accurate segmentation of the liver parenchyma, a pre-requisite for liver lobe classification and resection planning, is presented. A first estimate for liver segmentation is achieved by applying a normalized liver model to the CT data. Based on this pre-segmentation parameters for level set segmentation on a slice-by-slice strategy are assessed, thus enabling a fully-automated segmentation of the liver parenchyma. The slice-by-slice level set propagation utilizes fast-marching and threshold level set implementations.

Keywords: Model-driven liver segmentation, fully-automated CT data segmentation, fast-marching level set, threshold level set

1. INTRODUCTION

Diagnostics utilizing Computed Tomography as imaging modality provide high spatial accuracy, but lead to a large number of single slices for each scan, e.g. for an abdominal examination 800-1200 single slices must be considered by the physician for diagnostics. Besides the huge effort to step through all of these slices, spatial arrangements like tumor position in relation to the sustentative vessel systems are lost when cutting into planar slices. With modern 3D techniques in the field of computer graphics the 2D slice stack can be displayed as 3D scenario in which overlying morphologies like bones and organs are visualized applying opacity models. But nevertheless, a quantitative evaluation of the anatomy with respect to volume and distances, as required for tumor staging, cannot be achieved just by volume rendering techniques but only by performing a segmentation of the CT data. The application in the medical domain demands robust and accurate segmentation results achieved in a preferably fully automated process.

A problem of contrast-agent enhanced abdominal CT-scans is the low contrast of the liver to surrounding organs and tissue that all show very similar intensity profiles. Existing concepts and solutions for liver segmentation require a lot of user interaction, by way of example the slice-wise adjustment of the watershed segmentation parameters (Peitgen et al. 2000), manually marking the liver borders in each slice by a polyline for live-wire segmentation (Bourquain et al. 2002) or applying level sets to the 3D liver volume in a semi-automatic process (Lee et al. 2007). These solutions hardly meet the requirements for clinical liver segmentation as the level of user interaction is much too high and results suffer from subjective assessments of the user. Automated approaches are based on complex liver models that are fitted to the CT data intensity values (Lamecker et al. 2004) but do not cover all anatomical varieties of human parenchyma shapes or lead to results with a segmentation mismatch of several millimeters. User interaction is required in any case to correct and adjust the fully-automatically calculated results.

The algorithm presented in this work for robust and automated liver segmentation is based on slice-by-slice applied and propagated level sets that require a low level of user interaction. The level set parameterization only necessitates the user to mark the upper and lower extreme point of the liver to segment in the slice stack and to roughly characterize the patient specific intensity profile by specifying a threshold interval (Backfrieder et al. 2007, Zwettler et al. 2007). The parameterization process of the level sets can be further automated by application of an a priori liver model for parenchyma pre-segmentation, thus preserving an actual fully-automated segmentation approach despite low contrast of the liver parenchyma to the surrounding tissues and organs.

Accurate segmentation of the liver is the starting basis for liver tumor resection planning according to a specified safety margin, vessel sustention and liver lobes. A diagnostics tool for measurement of tumors

and resection planning is developed in the course of project Liver Image Analysis (LIVIA) in cooperation with the General Hospital of Linz (Backfrieder et al. 2007, Zwettler et al. 2007, Zwettler et al. 2008).

2. MATERIAL

Clinical protocols for abdominal diagnostics comprise a study with several CT scans at varying phase and contrast agent saturation, denominated as series. Besides the native series that can serve as overview scan at low resolution, time-delayed and contrast-enhanced series of portal-venous and arterial phase are acquired.

Abdominal and portal-venous series of *N=15* patients are acquired using a *Siemens Somatom Sensation Cardiac 64* CT. Acquisition is accomplished using *202-380 mA* tube current at *120 kV* voltage and a pitch factor of *1.4*. Reconstructed image data is a *512x512* pixel matrix at a resolution of *0.6-0.8 mm* and a slice thickness of *0.4 mm*. An abdominal CT scan covering the entire liver parenchyma comprises *400-600* slices with a data amount of *200-300 MB*.

3. MODEL-BASED LIVER SEGMENTATION

The theoretical concepts for slice-by-slice liver parenchyma segmentation and propagation are fast-marching (Sethian 1998) and threshold level sets. Parameterization of the applied threshold level set (Osher and Sethian 1988, Sethian 1999) contains weights for *curvature*, *propagation* and *advection* to steer the segmentation process that are determined by numerical optimization on a set of liver data and corresponding reference segmentations. The intensity interval boundaries required by the threshold level set are automatically assessed from model-based a priori liver segmentation. Level sets can be applied to arbitrary tasks of medical shape recovery (Malladi and Sethian 1998).

3.1. Level set Theory

In contrast to classic active contours and snakes, the level set approach by Osher and Sethian (1988) is not based on the deformation of discrete control points representing a moving contour. Instead the points in time when the continuous and moving contour arrives at discrete points on a regular grid are examined. The advantage of the level set approach is to implicitly handle topology changes of the contour as well as dilation and erosion. The surface evolving over time is controlled by a force-function or velocity field, addressed as parameter *F*, incorporating intensity profile, geometry properties or gradients of the input image (Enright et al. 2002). It can be interpreted as flowing liquid on a rough topology represented by velocity field *F*. The moving contour is interpreted as the zero-level set of a higher function ϕ_t due to added time component, see Fig. 1 for 2D surface case. So the surface can be evaluated at each discrete time step defined by *t*. Adaptability and accuracy of the moving level set is parameterized by introducing weight factors *propagation*, *curvature* and *advection* for *F* as presented in Equ. 1 for 3D level sets comprising coordinates *x*, *y* and *z* deduced from Han et al. (2003).

$$\frac{\partial\phi(x,y,z,t)}{\partial t} = F_{prop}(x,y,z,t)\left|\nabla\phi(x,y,z,t)\right| + F_{curv}(x,y,z,t)\left|\nabla\phi(x,y,z,t)\right| + \vec{F}_{adv}(x,y,z,t)\cdot\nabla\phi(x,y,z,t) \quad (1)$$

Parameter curvature $F_{curv}(x,y,z,t)\left|\nabla\phi(x,y,z,t)\right|$ is the weight for preservation of a round contour shape and rigidness whenever pressure is imposed in the direction of narrow points and edges, depending on the intrinsic geometry. The weight for propagation $F_{prop}(x,y,z,t)\left|\nabla\phi(x,y,z,t)\right|$ serves as opposite force to curvature that presses the contour towards narrow points and edges and delineates the expansion or contraction force. The third parameter advection $\vec{F}_{adv}(x,y,z,t)\cdot\nabla\phi(x,y,z,t)$ is a weighting factor for the gradients of the input function. The surface is advected to itself at constant speed.

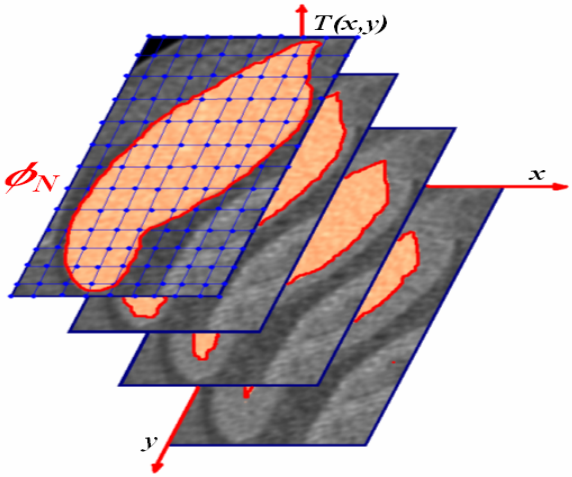

Figure 1: Level set as function of time. In the course of time the contour iteratively dilates until convergence is reached with respect to force-function F. Time of arrival is calculated for all points on a regular grid of time points.

3.2. Slice-wise Level set Segmentation

The newly developed segmentation method is based on fast-marching and threshold level sets (Lee et al. 2007) utilizing Insight Segmentation and Registration Toolkit (ITK) for robust implementations (Ibanez at al 2005). A threshold level set changes its shape and topology according to the intensities from the internal energy, the correlation of the input image intensities with a specified intensity interval. On the contrary, the fast-marching methods search for confidence connected elements within a pre-defined distance around an a priori chosen seed point or seed region. Within the pre-defined distance around the seed point, connected elements with intensity values within a confidence distribution are grabbed for fast-marching segmentation.

The proposed approach for liver segmentation is not intended to segment the entire 3D volume at once but slice-by-slice, thus significantly reducing the complexity of the problem. The fast-marching approach (Sethian 1998) is used for segmentation of the bottom parenchyma slice and a threshold level set is applied to propagate and adjust the prior segmentation results slice-by-slice, see Fig. 2.

3.2.1. Level set Parameterization

For launching the fast-marching level set at the bottom line and as a stop criterion, markers are defined in the area around the bottom and top region of the liver. Regarding the threshold level set an intensity interval must be provided by the user, roughly approximating the intensity profile of the liver to segment.

Besides these patient specific and dynamic parameters, a weight for *curvature* and *propagation* is chosen with respect to a persisted value for *advection*. A universally valid parameterization for these two weights with respect to the relative slice location within the liver is determined utilizing numeric optimization strategies applied to a set of manually segmented reference data resulting in a trapezoid-like function for *curvature* and an inverse function for *propagation*, applicative to arbitrary shaped livers.

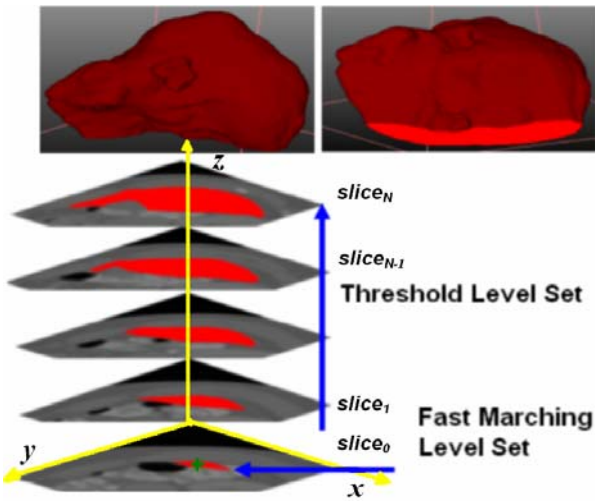

Figure 2: Starting at the bottom slice segmented utilizing a fast-marching level set, the results are propagated utilizing a threshold level set until the entire parenchyma is segmented.

3.2.2. Level set Segmentation Runs

The first contour is computed utilizing a seed-point driven fast-marching method. Afterwards the result of each slice is used as initialization for the threshold level set to adjust and optimize to the following slice. Due to thin slice-thickness, the changes between two neighboring slices are low. Consequently, only few optimization iterations are required when starting with the results of the prior slice until an optimization result of sufficient quality is reached, thus significantly reducing runtime. One single bottom-up run of slice-to-slice adjustment is insufficient as topological changes of the parenchyma are insufficiently segmented, see Fig. 3. To overcome this problem, another run is launched to segment the volume in a top-down order. Merging the results gives an entire segmentation of the liver parenchyma, accounting for possible changes in topology. A mean abdominal CT volume is segmented by our approach in less than *1 minute* using a conventional desktop computer, e.g. *Intel Pentium 4, 2.8 GHz*.

If spacing is strongly anisotropic, level set segmentations will suffer from non-uniform slice transitions but additional segmentation runs in *x* and *y* direction can manage this problem (Museth et al. 2002).

3.3. Model-based Pre-segmentation

Only the marginal level of required user interaction described in the sections before is needed for appropriate parameterization of the level sets. A fully-automated pre-segmentation is further established by an a priori liver model for adjustment to the CT data to segment (Cootes and Taylor 2004). Due to application of an a priori model, subjective user-specific parameterization is obsolete and the entire segmentation process is fully automated then.

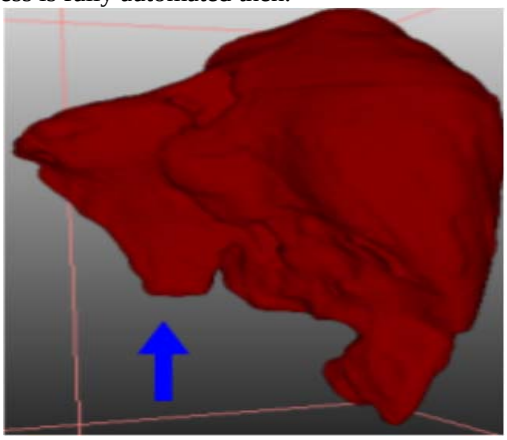

Figure 3: One bottom-up run is insufficient, due to autonomous starting regions and changing topologies as marked by the blue arrow that would be segmented insufficiently.

The normalized liver model used as a priori information is constructed from a set of reference shapes, manually segmented by experts. By adjusting the differing extents with scale and translation, all reference segmentations are centered in the target coordinate system of the a priori model and the physical extent is scaled to a volume of *100x100x120* voxel with isotropic spacing of *1.0*. After adjustment and accumulation of the reference segmentation, the resulting a priori model is smoothed by Gaussian filtering, see Fig. 4 for color-coded representation of the a priori model. High voxel values within the a priori model indicate a high probability of the concerned region for belonging to the liver parenchyma. By applying a decreasing threshold to the a priori model, more and more patient-specific anatomical variations are faded out and the common inner core of each liver

appears, see Fig.4 (c-e). Applying the a priori model to any target CT volume, the regions likely belonging to the parenchyma get enhanced whereas the background areas get diluted.

3.4. Fully-automated Level set Segmentation

The a priori liver model is registered to the target CT data set, leading to a probability scheme for each voxel, defining parenchyma region membership or not. That way neighboring anatomies like the ventricle is faded out from segmentation. In combination with a statistical analysis of the intensity profile, a fully-automated pre-segmentation can be achieved by applying a threshold value. Based on this pre-segmentation, the lower and upper point of the liver as well as the intensity profile for level set parameterization can be deduced.

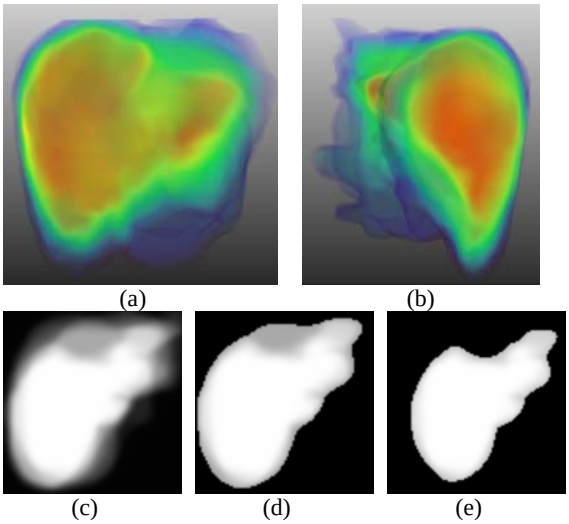

Figure 4: Resulting a priori model for liver pre-segmentation as volume of probability values for the voxels at the particular locations belonging to liver parenchyma. Sagittal view in (a) and axial view in (b). The higher the probability value (red), the more likely a voxel in that region is classified as parenchyma. (c-e) show profile of slice *50* at threshold levels *0, 1500* and *1800* in the range [0;2400] for steering confidence.

4. RESULTS

4.1. Results of Model-based Pre-segmentation

Accuracy of the automated pre-segmentation is highly sufficient for the task of level set parameter extraction, see Fig. 5. The upper and lower seed can be reliably provided as well as the intensities by model-based analysis of the histogram statistics. In more than *90%* of all test runs the seed point estimate is left unchanged to level set parameterization. Minor changes, that need some manual correction, are only to be expected at severe anatomical variations and pathologies, like pancreatitis or deformations of the abdomen. On account of validity, of course tests are only performed on data not incorporated in the particular a priori model generation.

4.2. Results of Fully-automated Liver Segmentation

Evaluation of the presented segmentation strategy on *N=10* patient studies was performed utilizing an automated testing framework for error measurements compared to preserved reference segmentations and statistical evaluation. Segmentation results are presented in extracts, see Fig. 6 and Fig. 7.

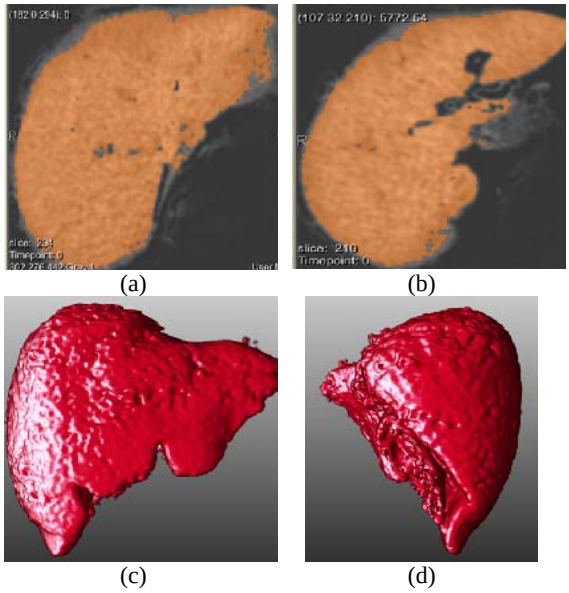

Figure 5: Results of automated pre-segmentation for two slices (a-b). Examining the border regions in the 2D slices (a-b) it becomes obvious that there is some level of under-segmentation close to the borders. The entire pre-segmentation is of good quality (c-d) and completely sufficient for parameter extraction.

Comparing results of the presented fully-automated segmentation concept with manual reference segmentations using live-wire technology (Bourquain et al. 2002), a mean deviation of *3.18+/-1.72%* concerning the volume and *6.4%+/-3.3%* concerning false-positive and false-negative mismatching voxel classifications are measured, see Fig. 8. Regarding the reference segmentations it has to be stated that 75% of all slice segmentations are interpolated thus leading to inaccuracies of the basis of comparison too. Despite interpolation of a vast majority of all slices, manual segmentation of a reference volume takes more than 1.5 hours on the average. Referring to runtime measures, an execution time of less than 1 minute using a desktop computer for performing the described automated parenchyma segmentation is very fast compared to other approaches. With minimal manual corrections of obvious segmentation errors the mean volume deviance is reduced by *1.5+/-1.1%* to *1.68+/-1.51%*. This percentage value for the reduction represents the real net error of our presented fully-automated liver segmentation.

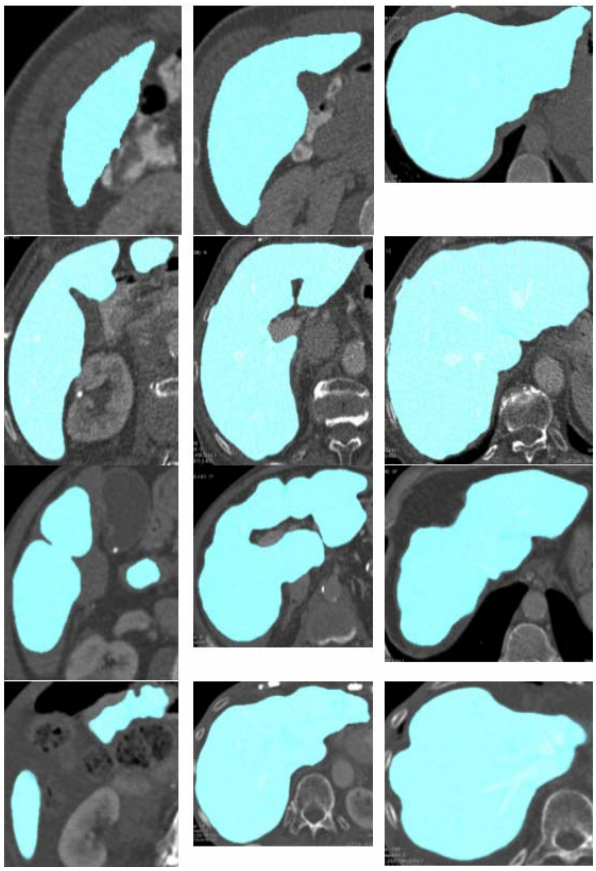

Figure 6: Lower. mid and upper segmented slices of the first four image series in each row.

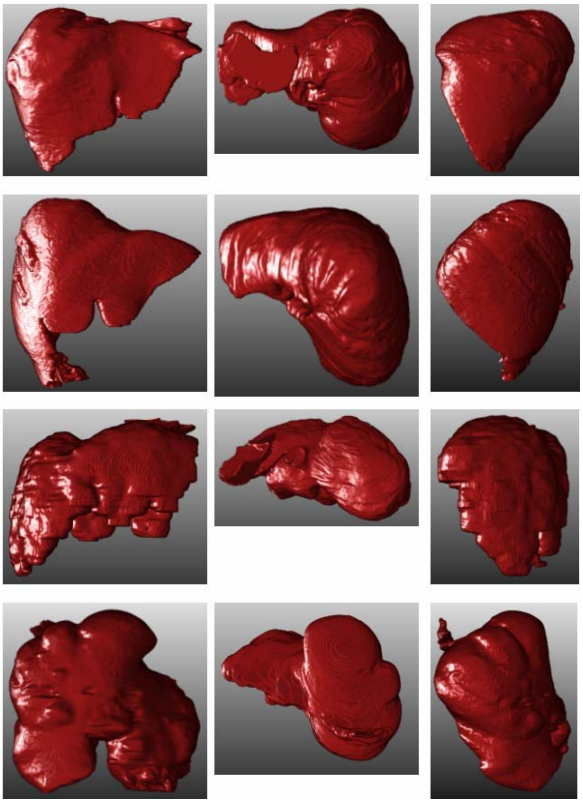

Figure 7: Volume rendering from sagittal, axial and coronal perspective of the first four segmented image series in each row.

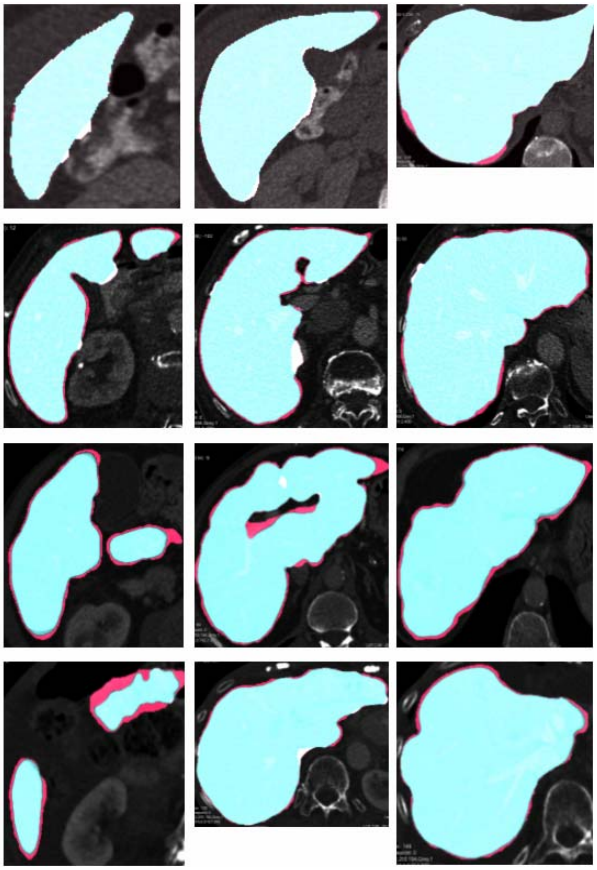

Figure 8: Lower. mid and upper segmented slices of the first four image series and area differences compared to reference segmentations in each row. False-positive and false-negative mismatches are color-coded with red and white respectively.

5. DISCUSSION AND CONCLUSION

A fast and robust method for segmentation of the liver parenchyma without need for user interaction has been presented. Besides the liver, segmentation of the main hepatic vessel trees is an important prerequisite for modeling the entire liver system (Reitinger et al. 2004, Zwettler et al. 2007, Zwettler et al. 2008), see Fig. 9.

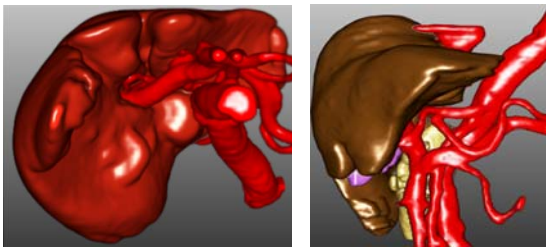

Figure 9: Smoothed result of level set segmentation based on a priori model extracted parameterization and. volume rendering of the parenchyma together with segmented aorta, hepatic veins and vena porta.

Automated segmentation of the liver parenchyma is basis for later on diagnostic evaluations and quantitative measurements. Based on segmentations of the liver and the main vessel systems, namely the *vena porta* and the *hepatic veins*, a classification of the liver volume into

eight liver lobes following Couinaud (Rutkauskas et al. 2006) can be established, see Fig. 10. Furthermore, position of potential lesions and tumors within the liver parenchyma can be evaluated and conclusions concerning liver lobe resection of the tumor containing liver parts can be drawn.

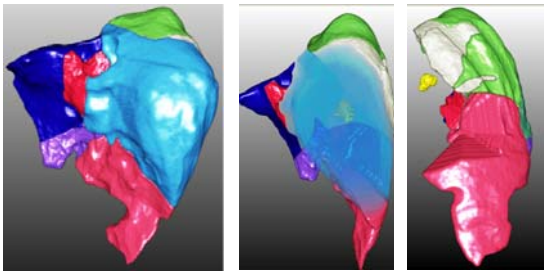

(a) (b) (c)

Figure 10: Results of liver lobe classification following Couinaud. The light-blue lobe contains a tumor (yellow). In the course of lobe resection, the tumor could be removed, keeping a safety margin of *0.5 cm* (b-c).

ACKNOWLEDGMENTS

This work was supported by the project "*Liver Image Analysis using Multi Slice CT*" (LIVIA-MSCT) funded by the division of Education and Economy of the *Federal Government Upper Austria*.

Special thank is given to head of radiology department *Univ.-Prof. Dr. Franz Fellner* and to *OA. Dr. Heinz Kratochwill* from the *Central Institute of Radiology* at the General Hospital Linz for providing CT image data and valuable discussion.

REFERENCES

Backfrieder, W., Zwettler, G., Swoboda, R., Pfeifer, F., Kratochwill, H., Fellner, F., 2007. Towards automated segmentation and classification of liver lesions for diagnosis and surgery planning. *Proc. of CARS*, Berlin, Germany.

Bourquain, H., Schenk, A., Link, A., Preim, B., Prause, G., Peitgen, H.O., 2002. Hepa Vision 2 – A software assistant for preoperative planning in living-related liver transplantation and oncologic liver surgery. *Computer Assisted Radiology and Surgery (CARS)*.

Cootes, T.F., Taylor, C.J., 2004. Statistical Models of Appearance for Computer Vision, *Technical Report*, University of Manchester, UK.

Enright, D., Fedkiw, R., Ferzinger, J., Mitchell, I., 2002. A Hybrid Particle Level Set Method for Improved Interface Capturing. In *Journal of Comp. Phys.*

Han, X., Xu, C., Prince, J., 2003. A topology preserving level set method for geometric defomable models. IEEE Transactions on Pattern Analysis and Machine Intelligence, 25(6), 755-768.

Ibanez, L., Schroeder, W., Ng, L., Cates, J., 2005. *The ITK Software Guide*, Kitware, 2nd edition.

Lamecker, H., Lange, T., Seebass, M., 2004. Segmentation of the Liver using a 3D Statistical Shape Model. *ZIB-Report*, Konrad-Zuse-Center for information technology, Berlin, Germany.

Lee, J., Kim, N., Lee, H., Seo, J.B., Won, H.J., Shin, Y.M., Shin, Y.G., 2007. Efficient Liver Segmentation exploiting Level-Set Speed Images with 2.5D Shape Propagation. In *3D Segmentation in The Clinic – A Grand Challenge*, 189-196.

Malladi, R., Sethian, J.A., 1998. A Real-Time Algorithm for Medical Shape Recovery. Proceedings of International Conference on Computer Vision.

Museth, K., Breen, D.E., Zhukov, L., Whitaker, R.T., 2002. Level Set Segmentation From Multiple Non-Uniform Volume Datasets. *Proceedings of IEEE Visualization Conference*, 179-186.

Osher, S., Sethian, J.A., 1988. Fronts propagating with Curvature-Dependent Speed – Algorithms Based on Hamilton-Jacobi Formulations. *Journal of Computational Physics*, 97, 12-49.

Peitgen, H.O., Preim, B., Selle, D., Böhm, D., Schenk, A., Spindler, W., 2000. Risk Analysis for Liver Surgery, In M. Emmer (editor): *Mathematica e Cultura*, Springer Publisher, 331-340.

Reitinger, B., Bornik, A., Beicherl, R., Werkgartner, G., Sorantin, E. 2004. Tools for Augmented Reality based Liver Resection Planning. *Proc. of SPIE Medical Imaging*, San Diego, USA; 88-99.

Rutkauskas, S., Gedrimas, V., Pundzius, J., Barauskas, A., 2006. Clinical and anatomical basis for the classification of the structural parts of the liver. In *Medicina (Kaunas)*, 42(2), Lithuania.

Sethian, J.A., 1999. Level set methods and fast marching methods. *Cambridge Monographs on Applied and Computational Mathematics*, 3.

Sethian, J.A:, 1998. Adaptive Fast Marching and Level Set Methods for Propagating Interfaces. In *Acta Math. Univ. Comenianae*, Vol 67 (1), pp. 3-15.

Zwettler, G., Pfeifer, F., Swoboda, R., Backfrieder, W., 2007. Automatische Klassifikation der Leber aus hochauflösenden Multi-Slice CT Daten, *FFH2007*.

Zwettler, G., Pfeifer, F., Swoboda, R., Backfrieder, W., 2008. Accelerated Skeletonization Algorithm for Tubular Structures in Large Datasets by Randomized Erosion. *Proc. of VISIGRAPP*, INSTICC Press, 74-81.

AUTHORS BIOGRAPHY

GERALD A. ZWETTLER was born in Wels, Austria and attended the University of Applied Sciences Upper Austria in Hagenberg where he studied software engineering for medical applications and graduated Dipl.-Ing. (FH) in 2005. Since then he is working as research assistant at the research and development department of the University of Applied Sciences Competence Center Hagenberg mainly in the field of medical image analysis and medical software engineering. In the year 2009 he accomplished his master thesis titled with *Automated Vessel Tree Modelling for Functional Diagnostics on 2D and 3D Medical Image Data* for achieving a second degree.

HEURISTIC MODELING OF THE MENTAL PROGRESS OF PERSONS WITH NORMAL BRAIN AGING, SUBJECTIVE COGNITIVE IMPAIRMENT, MILD COGNITIVE IMPAIRMENT, ALZHEIMER'S DISEASE AND RELATED DEMENTIA DISORDERS

Stephan Winkler [(a)], Stefanie Auer [(b)], Michael Affenzeller [(c)], Yvonne Donabauer [(d)], Barry Reisberg [(e)]

[(a)] Department for Medical and Bioinformatics, Upper Austria University of Applied Sciences
Softwarepark 11, 4232 Hagenberg, Austria

[(b), (d)] M·A·S Alzheimerhilfe Bad Ischl, Lindaustrasse 28, 4820 Bad Ischl, Austria

[(c)] Department for Software Engineering, Upper Austria University of Applied Sciences
Softwarepark 11, 4232 Hagenberg, Austria

[(e)] Department of Psychiatry, New York University Langone Medical Center
550 First Avenue, New York, NY 10016, United States of America

[(a)] stephan.winkler@fh-hagenberg.at, [(b)] stefanie.auer@mas.or.at, [(c)] michael.affenzeller@fh-hagenberg.at,
[(d)] yvonne.donabauer@mas.or.at, [(e)] barry.reisberg@nyumc.org

ABSTRACT

In this paper we summarize the results of our analysis of data provided by the Aging and Dementia Research Center (ADRC) at the New York University Medical Center. This database stores a series of results of examinations of thousands of subjects with ostensibly normal brain aging, subjective cognitive impairment, mild cognitive impairment, Alzheimer's disease and related conditions. These investigations were done in the USA over three decades from 1978 to 2008. All patients are classified using the global deterioration scale (GDS). The data have been analyzed statistically; we have developed a statistical model for the expected duration of each GDS period. Additionally, we also used several machine learning techniques in order to identify mathematical models that can be used as estimators for the GDS classification.

Keywords: Morbus Alzheimer, disease progress modeling, system identification, data mining

1. INTRODUCTION

The main goal of the research reported on in this paper was to analyze data provided by the Aging and Dementia Research Center (ADRC) at the New York University Medical Center. This database stores a series of results of examinations of thousands of subjects with normal brain aging, subjective cognitive impairment, mild cognitive impairment, Alzheimer's disease and related dementia disorders. These investigations were done in the USA over three decades from 1978 to 2008. These examination results are available as thousands of samples, each storing hundreds of features incorporating information about the patients, including data about their mental state, their physical condition and their environment. In addition, all patients are classified using the global deterioration scale (GDS) – a classification of the GDS as 1 means that the patient is not impaired by dementia or subjective complaints of cognitive impairment, or mild cognitive impairment, while higher GDS values indicate growing disturbances believed to be possibly caused by an underlying process of progressive dementia, eventually reaching loss of almost all, and, subsequently, all, intelligible speech and progressive loss of mobility at GDS level 7.

After preprocessing the data, a statistical analysis of the data was completed. Our goal was to try to develop a statistical model for the expected duration of each GDS period – in other words, we sought to determine how long patients remain in the defined GDS states.

Additionally, we also used several machine learning techniques in order to identify mathematical models that can be used as estimators for the GDS classification. This means that we used linear regression, neural networks and evolutionary system identification techniques (based on genetic programming) for identifying functions which can be used to calculate the estimated GDS classification for a given set of measured investigation features; we have also used these techniques for learning so-called virtual sensors for the deterioration of the patients' GDS states.

2. DATA PREPROCESSING AND OVERVIEW OF THE PREPROCESSED DATABASE

The data originally provided by the ADRC was given in several separate tables; information about the patients' investigations were given as samples, each including at least the patient's ID so that all samples could be combined with corresponding samples of other tables. Additionally, each patient could be investigated several times; the information of the number of the investigation is also available (in feature "period"), so that all samples can be identified as belonging to one specific investigation of one specific patient. The information included in the presented tables includes information about the patients' mental status, their medications, and general health status parameters.

Most values are given as real-value data; nevertheless, some of the given features are stored not as real-valued data but rather as text entries. So, all textual en-

tries were feature-wise converted into numbers using a rather simple mapping: For each feature we collected all distinct entries, sorted them alphabetically and then replaced all entries by their respective numbers in the ordered lists of distinct values. This has been done in order to enable the use of statistical analysis and machine learning algorithms designed to work on real-valued data bases.

The variable GDS stores the classification of each patient in the global deterioration scale; this variable is in the following referred to as the target variable.

All the given data thus had to be combined and pruned. In general, we combined all samples using the ID and period information; the information in informants was multiplied so that each sample in this table was available for each period relevant for each of the investigated patients, and the information in the medications table was treated in the following way: All medications have been classified into one of 7 main classes of medications, and so we could re-arrange the information about the medication for given patients at given periods into samples storing the amount of medication of each class.

Thus, after these analysis and preprocessing steps, we came up with a database storing hundreds of features and thousands of samples. The remaining problem regarding these data was the following one: Many of the samples as well as many of the given features contained missing values. We therefore decided to delete all features that contain less than 33% of values (i.e. with 2/3 missing values).

So, ultimately the combined and pruned database that was used for further analysis within this project contained 333 variables and 9786 samples.

For this pruned and compressed data collection we shall now give some statistical analysis:

- Information about the numbers of samples available in the pruned data set for each GDS state is illustrated in Figure 1.
- For each subject (each indicating one specific patient) we calculated the number of samples (measurements, investigations) that have been documented and are available in the pruned database used for further analysis within this project. The distribution of these numbers of documented measurements for each patient is illustrated in Figure 2.
- We have also analyzed the time deltas of the given patients' samples, i.e. the time that elapsed between the patients' investigations. In Figure 3 we show the distribution of the time deltas (in years) on the whole analyzed data set, in Figure 4 we show this analysis separately for approximately the first half of the available data (from 1978 until 1999) and the second, more recent half of the data (from 2000 until 2008).

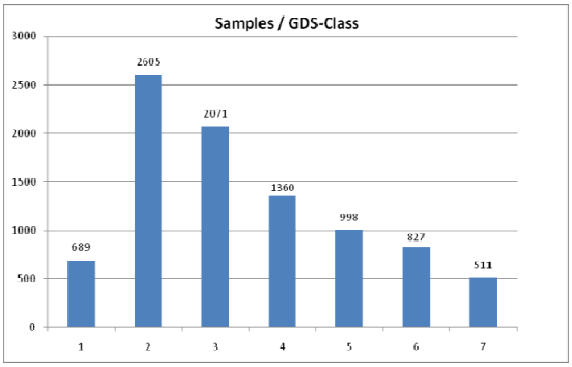

Figure 1: Frequency of GDS states in the preprocessed database.

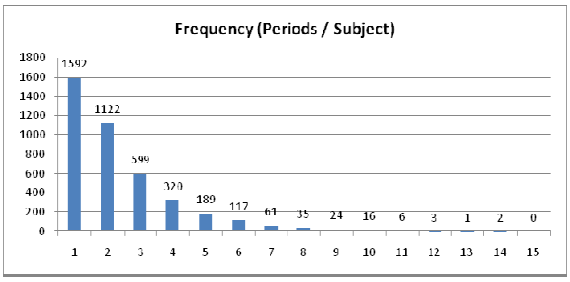

Figure 2: Frequency of documented periods for each patient stored in the preprocessed database.

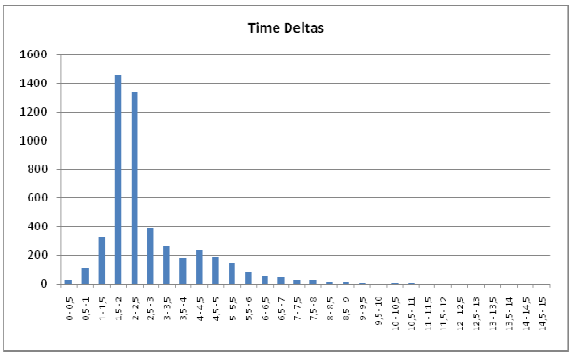

Figure 3: Distribution of time deltas ($\mu = 2.67$, $\sigma = 1.57$).

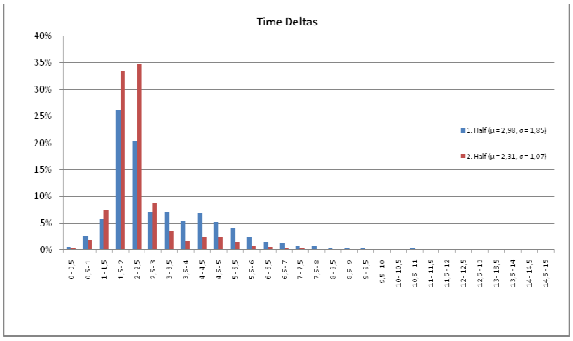

Figure 4: Distribution of time deltas, for first and second half of the analyzed data separately (1^{st} half: $\mu_1 = 2.98$, $\sigma_1 = 1.85$; 2^{nd} half: $\mu_2 = 2.31$, $\sigma_2 = 1.07$).

3. STATISTICAL ANALYSIS OF THE DURATION OF GDS-STATES

3.1 Calculation

The estimation of the dwelling times of the investigated patients within each GDS state is not trivial since the recorded data is not exactly an optimal basis for such an estimation: On the one hand, the measurements are not taken in equidistant intervals, on the other hand the time intervals between investigations is on average approximately 2.67 years, and change of the GDS classification between two investigations does not give any information when this state transition exactly happened. Furthermore, most patients' records start not with classifications as "healthy" (i.e., free of complaints of cognitive impairment), but rather as GDS 2, 3 or even 4 or 5; only investigating these data we cannot know exactly how long a patient has been in state 2, for example, before being investigated for the first time.

In order to model the time course that can be estimated on the basis of the given data we have used the following assumptions which are partially inspired by those formulated in (Reisberg, Sclan, Franssen, Kluger, and Ferris 1994) and (Reisberg, Ferris, Franssen, Shulman, Monteiro, Sclan, Steinberg, Kluger, Torossian, de Leon, and Laska 1996):

We assume that a potential transition change happens in the middle between two investigations. Thus, if classification c_1 is documented at date d_1 and classification c_2 at date d_2 (with $c_2 = c_1+1$ or c_1-1), then we assume that the transition from c_1 to c_2 has happened exactly at date $((d_1+d_2)/2)$ (this date is then called transition date t_{12}).

The duration of dwelling in a state c_0 that is documented for a patient's first investigation (at date d_0) is calculated incorporating information about the date of the next investigation at date d_1: We assume that this patient has been in state c_0 since date $(d_0-(d_0+d_1)/2)$.

This calculation is done analogously also for the last investigation incorporating knowledge about the date of the penultimate investigation.

If a state transition over more than one state is observed, then the dwelling times are calculated in the following way: Let classification c_1 be documented at date d_1 and classification c_2 at date d_2, $|c_1-c_2|=n$, $(n>1)$, $\delta = d_2-d_1$. We assume that the time, in which the patient has been in each intermediate state c_i $(c_1<c_i<c_2)$, can be estimated as (δ/n); after d_1 the patient was still in state c_1 until $(d_1+\delta/(2n))$, and that the patient is in $c2$ from $(d_2-\delta/(2n))$. Finally, of course, dwelling times in equivalent stages over several periods have to be merged.

3.2 Results

In the following we summarize the results of the time course analysis for the analyzed data.

For the whole data collection we found the following mean values and standard deviations for the duration of GDS states:

- (GDS 1: $\mu = 3{,}984$, $\sigma = 2{,}855$)
- (GDS 2: $\mu = 5{,}214$, $\sigma = 3{,}962$)
- GDS 3: $\mu = 4{,}086$, $\sigma = 2{,}939$
- GDS 4: $\mu = 2{,}722$, $\sigma = 2{,}081$
- GDS 5: $\mu = 2{,}555$, $\sigma = 1{,}511$
- GDS 6: $\mu = 2{,}962$, $\sigma = 1{,}934$
- GDS 7: $\mu = 4{,}278$, $\sigma = 2{,}825$

The statistics for GDS states 1 and 2 are given in brackets because these values do not seem to be as reliable as possible simply because most people are in state 1 or 2 without being investigated.

We have done this duration analysis also for the first and the second halves of the data separately:

- 1978 – 1999:
  - (GDS 1: $\mu = 4{,}432$, $\sigma = 3{,}386$)
  - (GDS 2: $\mu = 6{,}359$, $\sigma = 4{,}897$)
  - GDS 3: $\mu = 4{,}190$, $\sigma = 3{,}418$
  - GDS 4: $\mu = 2{,}538$, $\sigma = 2{,}188$
  - GDS 5: $\mu = 2{,}477$, $\sigma = 1{,}513$
  - GDS 6: $\mu = 3{,}046$, $\sigma = 1{,}986$
  - GDS 7: $\mu = 4{,}535$, $\sigma = 2{,}965$
- 2000 – 2008:
  - (GDS 1: $\mu = 3{,}642$, $\sigma = 2{,}325$)
  - (GDS 2: $\mu = 4{,}339$, $\sigma = 2{,}759$)
  - GDS 3: $\mu = 3{,}998$, $\sigma = 2{,}466$
  - GDS 4: $\mu = 2{,}945$, $\sigma = 1{,}923$
  - GDS 5: $\mu = 2{,}679$, $\sigma = 1{,}502$
  - GDS 6: $\mu = 2{,}756$, $\sigma = 1{,}789$
  - GDS 7: $\mu = 3{,}299$, $\sigma = 1{,}939$

The following graphics (Figure 5 and Figure 6) show the empiric mean values for GDS durations and the empiric distribution of GDS durations for GDS states 3, 4, 5, 6, and 7.

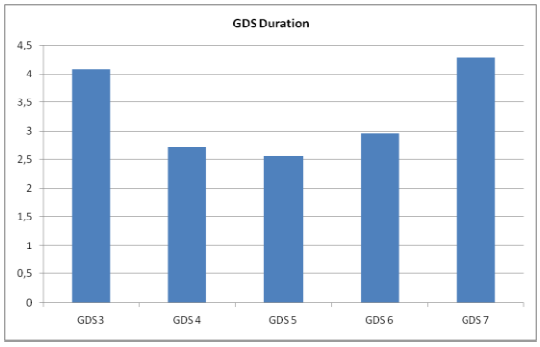

Figure 5: Empiric mean values of durations of GDS states 3, 4, 5, 6, and 7.

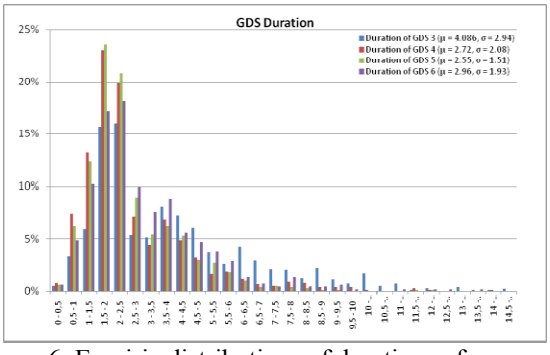

Figure 6: Empiric distributions of durations of GDS states 3, 4, 5, and 6.

4. DATA BASED PREDICTION OF GDS-STATES

4.1 Goals

The main motive for designing calculation models for GDS states (and their differentials) is the following: For identifying models that allow the calculation of GDS diagnoses, we of course have to find mathematical rules and / or formulas that are able to represent basic relationships and maybe even causalities (even if the problem of finding causalities is in general much more difficult than the formulation of calculation models).

Thus, what we want to arrive at is a formula F that is able to calculate GDS classifications based on the set of available parameters; in this project, we have used all documented features except the BCRS-variables as allowed input parameters.

So, our goal is to find F so that the estimated gds classification gds_{est} of a sample i is calculated using all parameters of sample i except BCRS-variables:

$$gds_{est}(i) = F(params_i)$$

where $params_i$ stands for all feature values of sample i except those of the excluded BCRS-variables.

In analogy, we also try to find models that are able to estimate the expected derivative, i.e. the change of the GDS state from one investigation to the next one. Here we search for a formula F_d so that

$$(gds(i+1) - gds(i))_{est} = F_d(params_i).$$

As we saw during first test series, this problem is very hard to be solved, so we reformulated to

$$(gds(i) - gds(i-1))_{est} = F_d(params_i)$$

which is equivalent to

$$(gds(i+1) - gds(i))_{est} = F_d(params_{(i+1)}).$$

Thus, we here search for prediction models that are able to estimate the gds classification change on the basis of the next investigation's parameters.

We have used the following approaches for identifying models for these machine learning problem formulations, namely linear regression, artificial neural networks (ANNs, as explained for example in (Nelles 2000)), and genetic programming (GP, see for example (Langdon and Poli 2002)). We have used the MATLAB® framework for linear regression and neural network tests; the NNSYSID implementation of ANNs (Nørgaard 2000) has also been used. The GP implementation for HeuristicLab (Wagner, Kronberger, Beham, Winkler, and Affenzeller 2008; Winkler, Affenzeller, and Wagner 2007; Winkler 2008) has been used for genetic programming tests.

4.2 Modeling Results

For learning models for the GDS classification as well as the GDS derivative we have used the first part of the data (approximately 50%) as training data, 25% as validation data (used for picking the best result on data not included in the training samples) and the rest of the available data as test data.

For a maximally objective analysis of the results discussed in this section we have used id-wise scrambled data, i.e. the data have been scrambled, but samples with same IDs have not been separated.

4.2.1 GDS Estimation

We have trained a linear model with linear regression; analyzing this model we see that 57.8% of the training samples are classified correctly and 55.7% of the test samples.

We have also trained a series of neural networks with varying structures (sizes) and numbers of training iterations. Small network structures score rather badly, using bigger network structures with 40 or 50 hidden nodes, for example, showed significantly better results. By increasing the number of training iterations, of course, it is possible to reach very high ratios of correctly classified training samples (here up to more than 98%, in fact), but the problem of overfitting has to be kept in mind here. The best results on validation data have been reached with neural nets with 40 hidden nodes that were trained over 100 iterations: In a test series including five training and test executions, on average 78.35% of the training, 70.53% of the validation samples, and 56.76% of the test samples were classified correctly.

Finally, GP test series have also been executed. Tests with small model structure (i.e. with rather low structural limits as for example a maximum height of 6 or a maximum model size of 50) did not lead to satisfying results, so larger models (formulas) have been trained; the most important parameters of the GP algorithm have been set as follows:

- Population size: 1400
- Maximum model size: 200 nodes
- Single-point crossover; 15% mutation rate (parameter manipulation as well as structural manipulation)
- Parents selection: Gender specific random & roulette (Wagner and Affenzeller 2005)
- Offspring selection: Strict OS (success ratio = comparison factor = 1.0), maximum selection pressure = 50 (Affenzeller, Wagner, and Winkler 2005)

Table 1: Test confusion matrix of a model for the GDS classification problem, produced by OS-GP.

	0	1	2	3	4	5	6	7
0	90	132	1	0	0	0	0	0
1	67	459	9	0	4	1	0	0
2	10	64	467	0	58	8	0	0
3	0	0	1	0	13	3	0	0
4	1	1	27	0	167	53	2	0
5	1	4	4	0	65	122	28	1
6	1	1	1	0	10	56	67	30
7	0	0	0	0	3	13	109	108

Thresholds combination [1,62745098039216; 2,37254901960784; 3,36274509803922; 3,50980392156863; 4,27450980392157; 5,29411764705882; 6,11764705882353]

Applying these parameters to five GP processes evolving models for the GDS classification problem we finally got results that on average correctly classified 65.71% of training and 65.19% of the analyzed validation samples correctly; on average, 63.82% of the analyzed test samples are classified correctly. In Table1 we show the evaluation of a model that correctly classifies 65.88% of the training samples and 65.43% of the test samples; details about this model (including its structure and detailed training and test performance) can be found online in the HeuristicLab results section (http://www.heuristiclab.com/results/regression/).

4.2.2 Results for GDS Dynamics Prediction

In order to learn models for the dynamics of GDS classifications we have ordered the data by ID and examination date; for each sample, that was not the first of the respective patient's investigations, we defined the target value as the difference of the current and the previous examination's GDS classification. We are aware that we do not have equidistant data samples; the existing data sample distances are far from optimal in such a kind of dynamic data analysis.

For a maximally objective analysis of the results discussed in this section we have again used id-wise scrambled data, i.e. the data have been scrambled, but samples with same id / subject values have not been separated; the classification differentials are calculated as described in Section 3.1. In the context of this modified classification problem the following classes are formed and observed in the data base:

- GDS'$_0$: 3086 samples (1554 in training, 774 in validation, 758 in test data)
- GDS'$_1$: 1526 samples (739 in training, 380 in validation, 407 in test data)
- GDS'$_2$: 312 samples (166 in training, 73 in validation, 73 in test data)
- GDS'$_3$: 95 samples (52 in training, 26 in validation, 17 in test data)
- GDS'$_4$: 17 samples (7 in training, 6 in validation, 4 in test data)
- GDS'$_5$: 1 sample (1 in training, 0 in validation, 0 in test data)

We have trained a linear model with linear regression; analyzing this model we see that 62.25% of the training samples are classified correctly and 59.97% of the test samples.

We have also trained a series of neural networks with varying structures (sizes) and numbers of training iterations. Again, small network structures score rather badly, using bigger network structures with 40 or 50 hidden nodes, for example, showed significantly better results. The best results on validation data have been reached with neural nets with 50 hidden nodes that were trained over 200 iterations: Classifying on average 67.84% of the training and 64,73% of the validation samples correctly, 61,48% of the test samples are correctly classified.

Finally, again GP test series have also been executed. Tests with small model structure did not lead to satisfying results, so larger models (formulas) have been trained; the most important parameters of the GP algorithm have been set in a similar way as described in Section 4.2.1. Applying these parameters to a GP process evolving models for the GDS classification differential problem we finally got results that on average correctly classify 66.81% of training, 63.86% of validation, and 63.04% of test samples correctly. Following we show the evaluation of a model that correctly classifies 66.93% of training, 64.65% of validation, and surprisingly 65.37% of test samples: In Figure 7 we show a multi-ROC chart (Winkler, Affenzeller, and Wagner 2006) for this model, evaluated for class "1" on test data; the highlighted spot indicates the ROC point for the eventually chosen thresholds identified as optimal on training data.

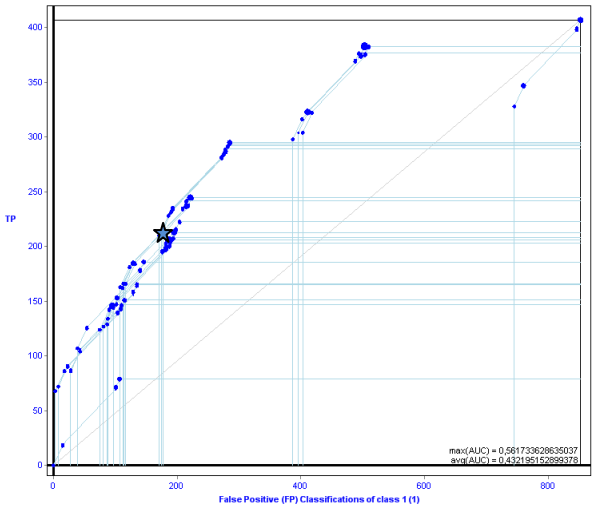

Figure 7: MROC chart for class "1" on test data, calculated for the GDS' problem using a model produced by enhanced GP with strict OS.

5. DISCUSSION AND OUTLOOK

In this project we have analyzed data of persons with normal brain aging, subjective cognitive impairment, patients suffering from Alzheimer's disease and related conditions; this data collection has been provided by the Aging and Dementia Research Center (ADRC) at New York University Medical Center. Initially, we have analyzed and preprocessed the data, subsequently we have analyzed the data statistically and estimated the duration of states of the global deterioration scale (GDS). Finally, we have also used several machine learning algorithms for learning models for estimating GDS states and their differential, i.e. the expected change of GDS states in dependence of other measurable parameters.

The results documented in this paper show that there are many areas of research that should be addressed in future research collaborations. On the one hand, the estimated GDS durations measured in data of subjects without training can be compared to those of

subjects who were coached and cared for by medical experts. Additionally, we have also shown that modern approaches in machine learning are able to produce models for GDS estimations; this enables an analysis of relevant relationships and maybe even causalities.

ACKNOWLEDGMENTS

The work described in this paper was done within a research project sponsored by the Austrian Research Promotion Agency (FFG).

The database used for this study was supported in part by the United States Department of Health and Human Services (DHHS), Grants P30 AG08051, AG03051, and AG09127 from the National Institute on Aging of the U.S. National Institutes of Health, by Grants 90AZ2791, 90AM2552, and 90AR2160 from the U.S. DHHS Administration on Aging, by Grant M01 RR00096 from the General Clinical Research Center Program of the National Center for Research Resources of the U.S. National Institutions of Health, by the Fisher Center for Alzheimer Disease Research Foundation, by a Grant from Mr. William Silberstein, and by a Grant by Mr. Leonard Litwin.

REFERENCES

Affenzeller, M., Wagner, S., and Winkler, S., 2005. Goal-oriented preservation of essential genetic information by offspring selection. *Proceedings of the Genetic and Evolutionary Computation Conference 2005*, pp. 1595–1596.

Langdon, W.B. and Poli, R., 2002. *Foundations of Genetic Programming*. Springer Verlag.

Nelles, O., 2001. *Nonlinear System Identification*. Springer Verlag, Berlin Heidelberg New York.

Nørgaard, M., 2000. Neural network based system identification toolbox. *Tech. Rep. 00-E-891*, Technical University of Denmark.

Reisberg, B., Sclan, S.G., Franssen, E., Kluger, A., and Ferris, S., 1994. Dementia staging in chronic care populations. *Alzheimer Disease and Associated Disorders,* 8:S188–S205.

Reisberg, B., Ferris, S.H., Franssen, E., Shulman, E., Monteiro, I., Sclan, S.G., Steinberg, G., Kluger, A., Torossian, C., de Leon, M.J., and Laska, E., 1996. Mortality and temporal course of probable Alzheimer's disease: A five-year prospective study. *International Psychogeriatrics,* 8:291–311.

Wagner, S. and Affenzeller, M., 2005. SexualGA: Gender-specific selection for genetic algorithms. *Proceedings of the 9th World Multi-Conference on Systemics, Cybernetics and Informatics 2005*, pp. 76-81. July 10-13, 2005, Orlando, FL, USA.

Wagner, S., Kronberger, G., Beham, A., Winkler, S., Affenzeller, M., 2008. Modeling of heuristic optimization algorithms. *Proceedings of the 20th European Modeling and Simulation Symposium (EMSS2008)*, pp.106-111.

Winkler, S., Affenzeller, M. and Wagner, S., 2006. Sets of receiver operating characteristic curves and their use in the evaluation of multi-class classification. *Proceedings of the Genetic and Evolutionary Computation Conference 2006*, vol. 2, pp. 1601-1602.

Winkler, S., Affenzeller, M. and Wagner, S., 2007. Advanced genetic programming based machine learning. *Journal of Mathematical Modelling and Algorithms*, 6: 455-480.

Winkler, S., 2008. *Evolutionary System Identification - Modern Concepts and Practical Applications*. PhD Thesis, Johannes Kepler University Linz.

AUTHORS BIOGRAPHIES

STEPHAN M. WINKLER received his MSc in computer science in 2004 and his PhD in engineering sciences in 2008, both from Johannes Kepler University (JKU) Linz, Austria. His research interests include genetic programming, nonlinear model identification and machine learning. He is professor at the Department for Medical and Bioinformatics at the Upper Austria University of Applied Sciences, Campus Hagenberg.

STEFANIE AUER studied psychology at the Karl Franzens University (KFU), Graz, and also received her PhD in psychology from KFU. She has worked as statistical consultant, psychologist, and as research associate for research institutes in Austria and the United States of America. Dr. Auer now serves as scientific head of MAS Alzheimerhilfe Bad Ischl.

MICHAEL AFFENZELLER has published several papers and journal articles dealing with theoretical aspects of evolutionary computation and genetic algorithms. In 2001 he received his PhD in engineering sciences from JKU Linz, Austria. He is professor at the Upper Austria University of Applied Sciences, Campus Hagenberg, and head of the Josef Ressel Center *Heureka!* at Hagenberg.

YVONNE DONABAUER studied psychology at Paris Lodron University Salzburg, Austria, where she graduated 2005. She has been working as psychologist and as communication therapist; she now coordinates the team of psychologists for MAS Bad Ischl.

BARRY REISBERG is director of the NYU Alzheimer's Disease Center, professor for Psychiatry at the New York University School of Medicine, and adjunct professor at McGill University, Montreal, Canada. He has directed research which has significantly advanced understanding and treatment of Alzheimer's disease; he has received numerous grants and awards for his research.

INDIVIDUAL ASSESSMENT OF MUSCLE FATIGUE AND ITS RELATION TO THE N-REPETITION MAXIMUM

Andreas Schrempf[(a)], **Daniel Hametner**[(a)] and **Armin Blaha**[(b)]

[(a)] Upper Austria University of Applied Sciences,
School of Applied Health and Social Sciences, Garnisonstrasse 21, 4020 Linz, Austria
[(b)] Sportland OÖ Olympiazentrum, Auf der Gugl 30, 4020 Linz, Austria

[(a)]andreas.schrempf@fh-linz.at, daniel.hametner@fh-linz.at
[(b)]armin.blaha@spantec.at

ABSTRACT

The main focus of this paper comprises the assessment of muscle fatigue by means of time-domain and frequency-domain parameters. Based on a simple biomechanical model time-domain parameters can be computed using measurement data recorded with an isometric muscle contraction experiment of the knee extensor muscles. Frequency-domain parameters are computed from surface electromyographic recordings. Both time-domain parameters and frequency-domain parameters are compared to the experimentally determined individual N-repetition maximum of healthy subjects. In contrast to the change of the median frequency it turns out that fatigue time is able to quantify muscle fatigue and can be considered as a good predictor for the individual N-repetition maximum.

Keywords: Rehabilitation engineering, Biomedical system modeling, Simulation

1. INTRODUCTION

The individual adjustment of the training intensity during strength training plays a crucial role in medical applications like strength rehabilitation of chronic low back pain or metabolic bone disease patients as well as with preventive measures and sport applications. Training intensity of muscle strengthening is usually quantified as a portion of the 1-Repetition Maximum (1-RM) or by the N-Repetition Maximum (N-RM), where N denotes a number. The N-RM is the weight on a training device an individual can lift exactly for N repetitions.

The number N of repetitions depends strongly on the health status of the person. Strength training with healthy subject commonly starts at $N = 10$, for chronic low back pain patients $N = 12-15$ whereas for high-risk patients like persons with metabolic bone disease $N = 20$ is proposed (Smeets et al., 2006).

An 1-repetition maximum test may increase injury risk and a common N-repetition maximum test with several trials is stressful, in many cases inaccurate and time-consuming. With specialized devices an isometric contraction measurement can be obtained more safely compared to an 1-RM test (Figure 1). From the isometric measurements individual parameters representing muscle fatigue can be obtained. In this paper the aim is to assess muscle fatigue by means of time-domain parameters obtained from a biomechanical model together with measurement data from an isometric muscle contraction experiment as well as by frequency-domain parameters obtained from surface electromyography (sEMG) - De Luca (1997). Furthermore the correlation between these muscle-fatigue parameters and the individual $N-$RM will be investigated, which in turn should allow to predict the individual training intensity.

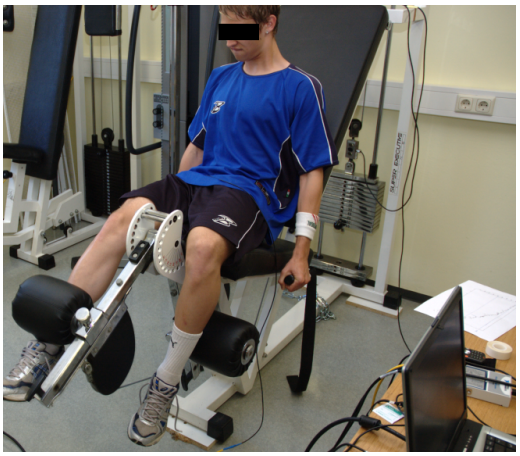

Figure 1. Isometric muscle contraction measurement.

2. BIOMECHANICAL MODEL

As depicted in Figure 2 a general biomechanical model of muscle strengthening consists of two parts, a *mechanical model* which represents the training device itself and the mechanics of the muscoskeletal system, and a *physiological model* which describes the generation of muscle force and the associated muscle fatigue (Schrempf et al., 2008). Hereby $\varphi(t)$ is the joint-angle (shoulder, elbow, knee, hip, lumbar joint), $\omega(t)$ the corresponding angular velocity, Θ summarizes the inertia of the moving body parts and the training device, M_m the moment generated by the muscles and M_{load} the loading moment of the training device. The active muscle moment M_m depends on the muscle activation $a(t)$ and is given by

$$M_m = r_L(\varphi(t))F_m(a(t),\varphi(t),\omega(t)) \qquad (1)$$

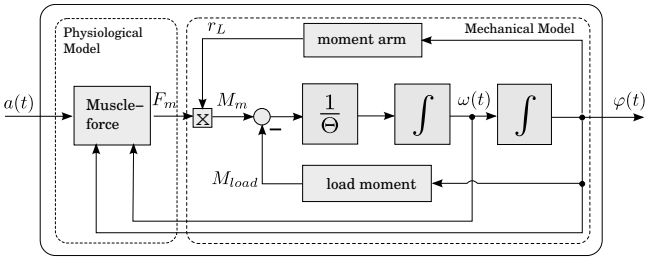

Figure 2. Biomechanical model.

with the moment arm r_L and the muscle force F_m. The loading moment depends on the weight m selected for training as

$$M_{load} = r_{load} mg, \tag{2}$$

where r_{load} is the effective moment arm of the load acting on the joint and g denotes the gravity constant. The muscle force F_m is modeled by (Zajac, 1989)

$$F_m(a(t), \varphi(t), \omega(t)) = F_{max} a(t) fit(t) f_{fl}(\varphi(t)) f_{fv}(\omega(t)) \tag{3}$$

where F_{max} denotes the maximum voluntary isometric muscle force, $a(t)$ muscle activation, $fit(t)$ muscle fitness, f_{fl} the force-length relation and f_{fv} the force-velocity relation of the considered muscles which depend on the extension angle $\varphi(t)$ and the angular velocity $\omega(t)$ respectively. Hereby muscle activation $a(t)$ and muscle fitness $fit(t)$ as well as functions f_{fat}, f_{fl} , and f_{fv} are within the range of $[0,1]$.

3. ISOMETRIC CONTRACTION MEASUREMENT

During isometric muscle contraction muscle length and consequently angle φ remains constant at φ_0 and hence $\dot{\omega} = \omega = 0$ and $f_{fv}(\varphi_0) = 1$. By means of a measurement system joint position can be adjusted in neutral position such that optimal muscle fiber length $f_{fl}(\varphi_0) = 1$ can be achieved. Considering an isometric muscle contraction in neutral position the joint muscle moment M_m is equal to the load moment M_{load} (see Figure 2) which in turn can be measured by a sensor. Hence the measured isometric joint moment M_{meas} is given by

$$M_{meas}(t) = M_{max} a(t) fit(t). \tag{4}$$

Depending on the generated muscle force the isometric measurement can be either an isometric maximal voluntary contraction (MVC) experiment or an isometric sub-maximal voluntary contraction (S-MVC) experiment.

Whereas the MVC experiment starts with 100% muscle activation, the isometric S-MVC experiment consists of two phases, where in the first phase the aim is to provide a constant sub-maximal joint moment M_{sub} as long as possible. If it is not possible to maintain M_{sub} any longer $(t = t_1)$, the experiment enters the second phase. In the second phase the aim is to provide a maximum possible joint moment until it falls below a predefined threshold (see Figure 3).

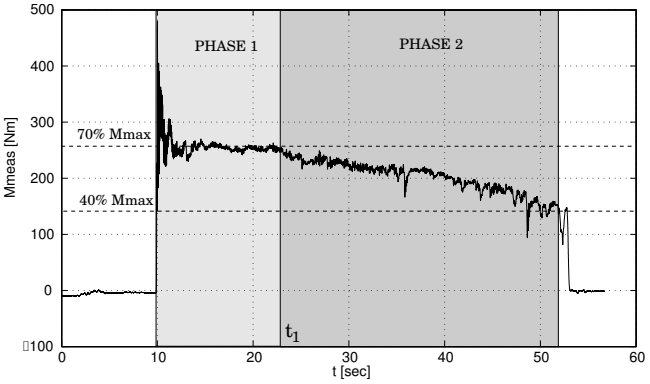

Figure 3. Isometric S-MVC experiment at $M_{sub} = 260\,Nm$ (approximately 70% of M_{max}).

4. MUSCLE FATIGUE MODEL

During the isometric S-MVC experiment ($\omega = 0$, $\varphi = \varphi_0$, $f_{fl} = 1$, $f_{fv} = 1$) the measured joint moment is given by eq. (4). According to Riener et al. (1996) muscle fitness can be modeled by

$$\frac{dfit(t)}{dt} = \frac{(fit_{min} - fit(t))\,a(t)}{T_{fat}} + \frac{(1 - fit(t))\,(1 - a(t))}{T_{rec}}. \tag{5}$$

This first-order relation describes muscle fatigue (first term) as well as recovery (second term). If the muscle is activated by 100% ($a(t) = 1$) then the fitness function decreases and no recovery is possible. On the other hand if there is no muscle activation ($a(t) = 0$) recovery of muscle fitness takes place. The corresponding time constants are T_{fat} and T_{rec} respectively. The minimum fitness is given by fit_{min}.

At end of phase 1 muscle activation reaches $a(t) = 1$ and during the second phase $t \geq t_1$ muscle activity remains at $a(t) = 1$. According to the fact, that the recovery time T_{rec} is much longer than the fatigue time T_{fat} i.e. $T_{rec} \gg T_{fat}$ and $(1 - a(t)) < 1$ for a sub-maximal contraction, it can be concluded that the second term in (5) is less important than its first term and hence eq. (4) can be approximately solved together with eq. (5) by

$$\begin{aligned} M_{meas}(t) \quad = \quad & M_{max} \left[fit_{min} + \left(\frac{M_{sub}}{M_{max}} - fit_{min} \right) \times \right. \\ & \left. \exp\left(-\frac{(t - t_1)}{T_{fat}} h_s(t - t_1) \right) \right]. \end{aligned} \tag{6}$$

Hereby $h_s(t - t_1)$ denotes the Heaviside-function with

$$h_s(t - t_1) = \begin{cases} 0 & , t < t_1 \\ 1 & , t \geq t_1 \end{cases}.$$

5. ASSESSMENT OF MUSCLE FATIGUE

Isometric muscle contraction experiments for the knee-extensors (m. quadriceps) were performed with 18 young athletes of age 17.6 ± 1.7 years, height $1.76 \pm 0.06\,m$ and weight $67.3 \pm 7.7\,kg$ (mean $\pm$ SD). The isometric joint moment was measured by means of a force-sensor with sampling frequency of $2\,kHz$.

Fitting model eq. (6) to the acquired measurement data $M_{meas}(t)$ and estimating the unknown parameters M_{max}, fit_{min} and T_{fat} by solving a nonlinear least-squares problem, muscle fatigue was assessed by model parameters fit_{min} and

Table 1. Results of the experimental study. The body height of subjects is defined by H.

#	$H\,[m]$	$M_{max}[Nm]$	$T_{fat}\,[s]$	fit_{min}	N	$NRM\,[kg]$	$\Delta f_{med}\,[Hz]$	$\frac{\Delta f_{med}}{\Delta t}\left[\frac{Hz}{s}\right]$
5	1.72	394.3	42.2	0.00	13	55.00	-26.7	-0.67
6	1.69	260.8	74.8	0.00	14	45.00	-22.7	-0.58
7	1.88	337.9	46.6	0.00	8	55.00	-19.8	-0.49
8	1.85	302.6	70.4	0.00	12	55.00	-25.0	-0.46
9	1.80	380.4	26.2	0.18	7	60.00	-28.1	-0.72
10	1.70	305.2	53.7	0.00	9	55.00	-19.5	-0.57
11	1.75	286.7	35.0	0.00	6	50.00	-22.9	-0.58
12	1.69	224.1	50.3	0.00	11	40.00	-29.2	-0.71
13	1.72	355.2	29.0	0.00	8	50.00	-13.2	-0.32
14	1.79	354.1	64.5	0.00	14	50.00	-18.6	-0.46
15	1.68	204.2	61.9	0.21	9	45.00	-11.2	-0.20
16	1.79	322.9	46.0	0.00	12	50.00	-30.8	-0.69
17	1.84	243.4	61.5	0.00	10	40.00	-21.5	-0.51
18	1.73	351.8	30.8	0.00	9	50.00	-22.6	-0.57

T_{fat}. Measurement data of 4 persons was removed since the S-MVC experiment was not performed correctly i.e. in the first constant phase of the experiment the variance of the joint-moment was too high or the length of the second phase was too short for the estimation of T_{fat}.

For comparison additionally to the muscle-moment measurement $M_{meas}(t)$ the decrease of the median frequency $\Delta f_{med}(t)$ and the corresponding slope $\Delta f_{med}/\Delta t$ of the recorded surface EMG was computed, which is established as a common measure of muscle fatigue in literature - Mathur et al. (2005). An array of 12 EMG electrodes was used hereby for measurement of the sEMG. The EMG-data was sampled with $1.2\,kHz$ and filtered by a $50\,Hz$ notch filter and a bandpass between 2-500$\,Hz$.

The results of the experimental study are summarized in Table 1. In most of the cases parameter fit_{min} is around 0, which agrees perfectly with values documented in Riener et al. (1996). Significant information is represented by time-constant T_{fat} where the relation between N/T_{fat} and the quotient $M_{max}/(NRM\cdot g\cdot H)$ is depicted in the left subplot of Figure 4. Furthermore the relation between the slope of

Table 2. Linear regression analysis. A significant linear relation is marked by an Asterisk.

Model	P-value	Err.-Var.
$\frac{M_{max}}{NRM\cdot g\cdot H} = 0.2052 + 0.7032\cdot\frac{N}{T_{fat}}$	0.0001 *	$5.7E-4$
$\frac{M_{max}}{NRM\cdot g\cdot H} = 0.3840 - 0.0013\cdot\frac{N}{\left\lvert\frac{\Delta f_{med}}{\Delta t}\right\rvert}$	0.3579	$2.0E-3$

the change of the median frequency $\Delta f_{med}/\Delta t$ of the surface EMG and the quotient $M_{max}/(NRM\cdot g\cdot H)$ is represented by the right subplot in Figure 4. A linear regression analysis for both relations was performed computing the coefficient estimates of the linear model, the 95% confidence intervals for the coefficient estimates, the residuals, the R^2 statistic, the F statistic, its $P-$value and the error variance. Hereby a $P-$value of 0.05 was accepted as the level of significance. The parameters of the linear model and the $P-$value of the regression analysis are summarized in Table 2. Local muscle fatigue was assessed by the relative change of the median frequency $\Delta f_{med}\,[Hz]$ between subsequent electrodes in the EMG array. For each subject the time-history of the amplitudes of the relative change of the median frequency was coded by a color-map, plotted and interpolated for all 12 array-electrodes (see Figure 5).

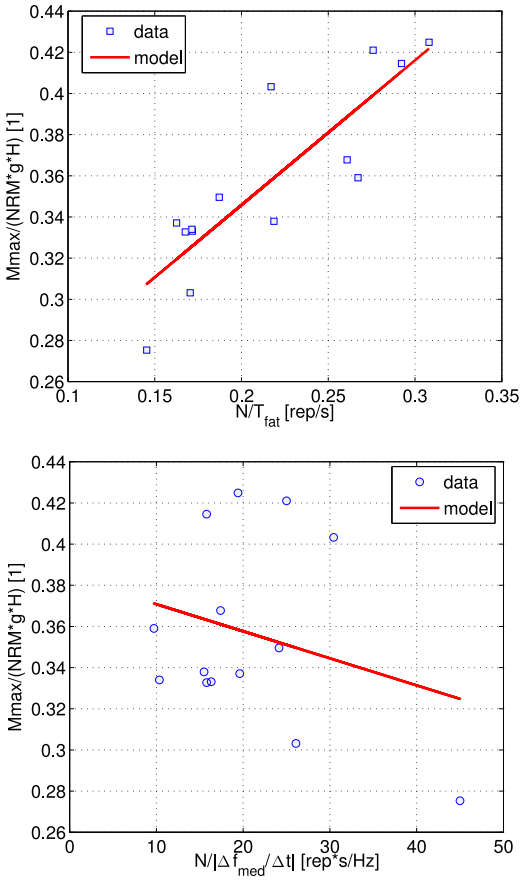

Figure 4. Measurement data (squares, circles) and linear model (line) between $M_{max}/(NRM\cdot g\cdot H)$ and N/T_{fat} and $N/|\Delta f_{med}/\Delta t|$ respectively.

6. CONCLUSIONS

Assessing muscle-fatigue by the time-domain parameters M_{max} and T_{fat} allows for the quantification of muscle fatigue. The relation between N/T_{fat} and quotient $M_{max}/(NRM\cdot g\cdot H)$ shows a significant linear dependence (see Figure 4). This in turn allows directly to predict the individual training intensity by means of the NRM from M_{max} and estimated fatigue parameter T_{fat}. From linear model in Table 2 it can be concluded that

$$NRM = \frac{M_{max}}{g\cdot H}\frac{1}{b_1 + b_2\cdot\frac{N}{T_{fat}}}$$

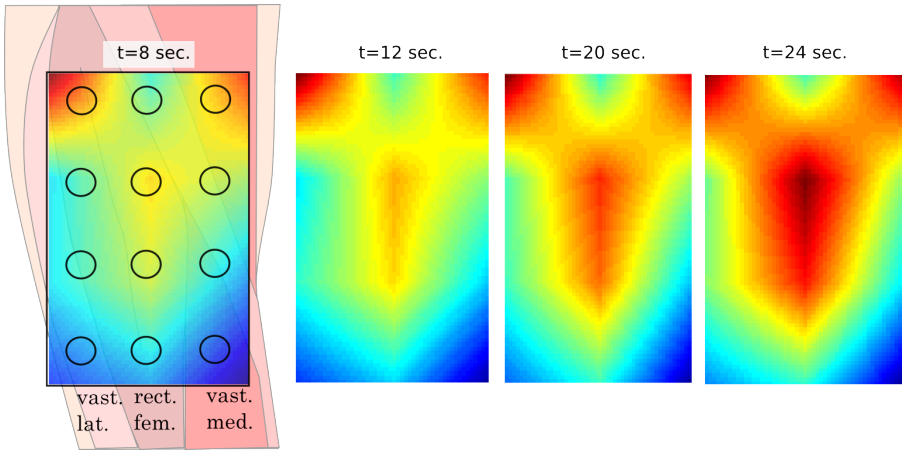

Figure 5. Interpolated map of fatigue-parameter $\Delta f_{med}\,[Hz]$ for all 12 electrodes of the EMG-array. Hot colors indicate regions of high muscle fatigue, cold colors indicate regions of low muscle fatigue.

with $b_1 = 0.2052$ and $b_2 = 0.7032$. For any fixed number N of repetitions the individual $N-RM$ is higher for slow time constants T_{fat} (high values) and higher maximum isometric joint moments M_{max} (see Figure 6). The time-

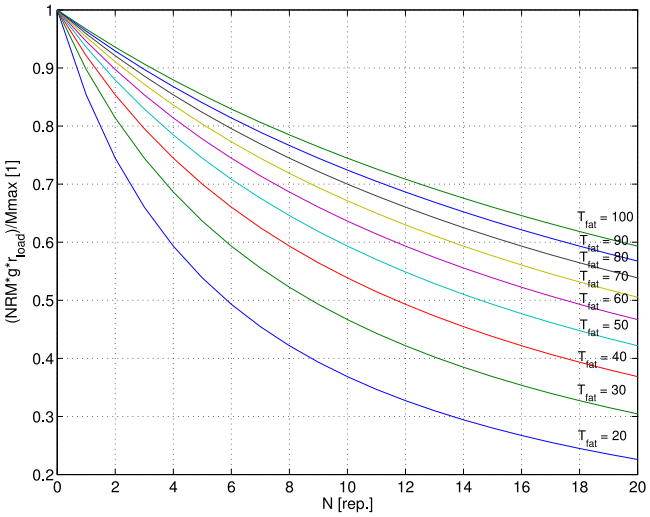

Figure 6. Relation between the N-RM and time-domain parameters M_{max} and T_{fat}.

domain parameters M_{max} and T_{fat} can be simply obtained from an isometric S-MVC experiment which allows for a safe and time-efficient measurement of the joint-moment, since the size of the given sub-maximal moment M_{sub} can be simply adopted to the health status of the person.
In contrast to time-domain parameters M_{max} and T_{fat} only a qualitative assessment of muscle fatigue can be obtained by the change of the median frequency f_{med} of the recorded surface EMG, since a significant linear relation do not exist (see Table 2). As well known from Iguchi (2008) a reduction of the median frequency with increasing muscle fatigue can be observed. In principle it can be concluded, that the higher the slope $|\Delta f_{med}/\Delta t|$ of the reduction of the median frequency, the faster fatigue occurs and the smaller the $N-RM$ for any fixed N would be. However, a quantitative assessment of muscle fatigue cannot be provided, since there is no significant relation between $\Delta f_{med}/\Delta t$ and the $N-RM$ (see Figure 4). But the assessment of muscle fatigue based on the median frequency allows for a localization of fatigue, since regions of high muscle fatigue can be identified (see Figure 5).

ACKNOWLEDGMENTS

We gratefully acknowledge Thomas Minarik, Michael Sams and Gerold Schoßleitner for their helpful involvement in setting-up the experiments and performing measurements. Furthermore the support of the Sportland OÖ Olympiazentrum is gratefully acknowledged.

REFERENCES

De Luca, C., 1997. The use of surface electromyography in biomechanics. Journal of Applied Biomechanics 13, 135–163.

Iguchi, M., 2008. Low frequency fatigue in human quadriceps is fatigue dependent and not task dependent. Journal of Electromyography and Kinesiology 18, 308–316.

Mathur, S., Eng, J., MacIntyre, D., 2005. Reliability of surface EMG during sustained contractions of the quadriceps. Journal of Electromyography and Kinesiology 15, 102–110.

Riener, R., Quintern, J., Schmidt, G., 1996. Biomechanical model of the human knee evaluated by neuromuscular stimulation. Journal of Biomechanics 29 (9), 1157–1167.

Schrempf, A., Habelsberger, W., Hutter, D., Brunner, S., Goritschnig, M., Nagl, K., 2008. Model-based Prediction of the individual N-Repetition Maximum with Application to Physical Rehabilitation. Proceedings of the 17th World Congress, The International Federation of Automatic Control, Seoul, Korea, July 6-11, 6658–6663.

Smeets, R., Vlaeyen, J., Kester, A., Knottnerus, J., 2006. Reduction of pain catastrophizing mediates the outcome of both physical and cognitive-behavioural treatment in chronic low back pain. The Journal of Pain 7 (4), 261–271.

Zajac, F., 1989. Muscle and tendon properties: Models, scaling, and application to biomechanics and motor control. Critical Reviews in Biomechanical Engineering 17, 359–411.

AUTHORS BIOGRAPHY

Andreas Schrempf was born in Schladming, Austria and went to the Johannes Kepler University of Linz, where he studied Mechatronics and obtained his master degree and PhD in 1998 and 2004 respectively. After working as a senior researcher at the competence center in mechatronics he moved to the Upper Austria University of Applied Sciences, where currently he is professor for biomechanics at the School of Applied Health and Social Sciences, department of medical technology in Linz. His research interests concern modeling and simulation in biomechanics and biomedical engineering as well as system identification and control theory.

Daniel Hametner was born in Amstetten, Austria and went to the Upper Austria University of Applied Sciences, where he studied Medical Technology at the School of Applied Health and Social Sciences and obtained his diploma degree in 2008. Currently he's working in the field of railway transportation, where he's engaged with the development of door entrance systems. His field of activity involves the specification, development and testing of complex software and electronic components.

Armin Blaha was born in Vienna, Austria and went to the University of Applied Sciences Technikum Wien, where he studied Sports-Equipment-Technology and obtained his diploma degree in 2005. After working at the Upper Austrian Olympic Sports Center, were he was responsible for the development of Feedback systems for athletes, he founded the Spantec GmbH in 2008. With his company he focuses on research and development of Feedback systems specially designed for elderly people.

INTEGRATED CARE USING A MODEL-BASED PATIENT RECORD DATA EXCHANGE PLATFORM

Barbara Franz[(a)], Herwig Mayr[(a)], Margit Mayr[(b)], Franz Pfeifer[(c)], Josef Altmann [(c)], Markus Lehner[(b)]

[(a)]Department of Medical Informatics & Bioinformatics,
Upper Austria University of Applied Sciences, Hagenberg, Austria
[(b)] Department of Human Services Management and Public Management,
Upper Austria University of Applied Sciences, Linz, Austria
[(c)] Department of Software Engineering,
Upper Austria University of Applied Sciences, Hagenberg, Austria

[(a)]{Barbara.Franz, Herwig.Mayr}@fh-hagenberg.at [(b)]{Margit.Mayr, Markus.Lehner}@fh-linz.at,
[(c)]{Franz.Pfeifer, Josef Altmann}@fh-hagenberg.at

ABSTRACT
We give a work-in-progress report on our patient portal developed for the purpose of (electronic) health data exchange. The exchange of patient record data, particularly in the area of patient care, is frequently still done manually or in a highly proprietary electronic way, making an efficient data exchange impossible.

We present our concepts of a model-based patient care data exchange, relying on a sound technical interoperability concept (through IHE-compliant architectures and processes) as well as a semantic interoperability concept commonly agreed among the partners (and already submitted as a basis for standardization).

We show the benefits of our model-based approach using as an example our e-Care system developed for electronic patient care data transfer between stationary (hospital, nursing home) and mobile care providers.

Keywords: model-based exchange, technical and semantic interoperability, electronic patient care record

1. MOTIVATION – INTEGRATING CARE EFFORTS

Healthcare services are increasingly spread over the majority of the human lifecycle and – as a consequence – a large number of quite diverse health institutions and organizations. Electronic health identification systems (like the Austrian "e-Card" (SVC 2009)) in theory enable each person to access and allow the transfer of his or her individual health and care data. In practice, however, the (Austrian) health system is vastly inhomogeneous from an IT point of view and, thus, efficient (electronic) patient record data exchange is still a vision for the future.

Between organizations using hand-written and IT-supported care documentation systems, communication breaches are an everyday occurrence. Current studies (Mayr and Lehner 2008a,b) show that data and information relevant for care are therefore often communicated only inadequately or with considerable delay between ambulant care, home, and nursing home. In (Ament-Rambow 2003) it is stated that 80% of the problems occurring arise from inadequate communication between system partners.

As there is no established electronic connection to transfer mobile nursing documents, documentation of nursing homes and care documentation of hospitals, the exchange of documents is frequently solely paper-based. When a patient is admitted to a hospital, the written nursing care summary is printed and given to the patient to take with her or him. In (Mayr and Lehner 2008b) it is stated that 40% of the surveyed nursing staff in nursing homes (n=265) confirmed that nursing care summaries are sometimes lost on the way. Against this background a steady transfer of care-relevant information for nursing is virtually impossible.

Care information is structured and stored by the individual institutions in a quite similar diverse way as patient treatment is performed. Thus, semantically correct exchange of patient data can only be achieved via the creation of appropriate care data models and intelligent mapping processes, cf. Fig. 1. Only in this way incomplete or contradictory care information can be identified and sometimes even completed or corrected.

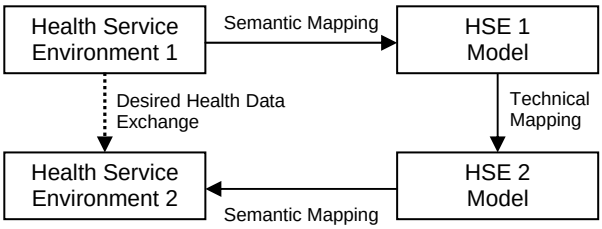

Figure 1: Overview of the Health Data Exchange via Models and Mappings

However, efficient and effective models can only be defined when adhering to established (world-wide) recommendations like IHE (IHE 2009a) and standards

like HL7 CDA (HL7 2009), as will be illustrated in the next chapter.

2. INTEROPERABILITY THROUGH STANDARDS

As there are no common standards defined for the admittance of patients to mobile or stationary nursing care, each healthcare provider has its own more or less well-defined processes. Nevertheless, most IT-supported care documentation systems are manufacturer-specific solutions that do not allow communication and collaboration with system partners over interfaces (Schreier, Hayn and Ammenwerth 2007).

2.1. Technical Interoperability

In order to enable standardized processes and uniform communication between different systems, we develop common standards and models for care documentation as well as for necessary processes and an IT-infrastructure that is applicable to a wide range of different IT-supported care documentation systems.

To achieve our goal we first conducted an analysis of the different care documentation systems to build a transfer model and of the different care documents to create a data model.

We base our transfer model on the "Integrating the Healthcare Enterprise" (IHE) guidelines (IHE 2009a). IHE is a worldwide initiative by the industry, healthcare enterprises and professionals to improve the interoperability and the information exchange between healthcare facilities and other health service providers using electronic healthcare information systems.

Our data model is based on the HL7 CDA Release 2.0. By leveraging the use of XML, the HL7 Reference Information Model (RIM) and coded vocabularies, the CDA makes clinical documents both machine- and human-readable (Spronk 2008). CDA provides an XML Schema (XDS) for clinical documents which we use to develop a model for care documents that guarantees that data is structured in such a manner that it is easily interpretable.

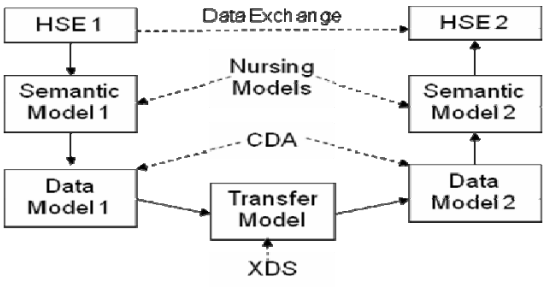

Figure 2: Architecture of the Health Service Environment (HSE) Models

Our data model describes the structure of the clinical document as well as the coded content. As we mainly focus on the nursing care summary in our prototype, our model allows the mapping of different nursing care summaries to generate a common base of care data. Therefore the content of the documents can be easily interpreted so that we can compare different documents and even find contradictory or incomplete data and are able to complete or correct the documents.

2.2. Semantic Interoperability

A transfer of knowledge over institutional borders, especially in nursing care, demands a clear and structured language. An adequate health service environment model (Fig. 2) is needed to support the interdisciplinary as well as the cross-border exchange of data among institutions. It should cover the varying needs of several system partners like for example

- acute care,
- long term care facility,
- home and mobile care and
- palliative care.

To assure the necessary coverage by the use of a generally accepted semantic model, we need to map the definition of terms of nursing care, their meanings and relationships.

In medical care this is achieved through the use of ICD-10 codes, an international classification of diseases which is used worldwide (WHO 2009). In nursing care several standards and guidelines are being developed that should make nursing care transparent, comparable and evaluable (Müller Staub 2005). The definition of these nursing models depends on their goal and function (Burns 2007), which leads to different classifications, for example (Müller Staub 2005),

- International Classification for Nursing Practice (ICNP),
- International Classification of Functioning, Disability and Health (ICF),
- North American Nursing Diagnosis Association (NANDA),
- Resource Utilization Groups III Home Care (RUG-III-HC).

Due to the use of different nursing models in care facilities, it is difficult to build a common basis of care-relevant information. The analysis of various nursing care summaries and different documentation systems shows that the interpretation of certain terms spans a wide range of meaning. For example the information *nightly restlessness* (in German: *nächtliche Unruhe*) leaves room for interpretation, even if used in the same context. As a study has shown (Mayr and Lehner 2008b), it can either mean that the patient wakes up in the night, has to use the toilet in the night, screams at night or even that the patient is in a paranoid condition (Fig. 3). This example shows that it is essential to define a common set of vocabulary for the context that is used by all system partners.

The content of care not only differs considerably in worldwide comparison (Perhab 2007), but because of different domains of focus even within special fields of nursing care. In currently used data models for nursing care, the varying needs of different recipients are not or only partially considered. The transferred information is either insufficient or too detailed and often not clearly structured. Two thirds of the caregivers in nursing

homes interviewed in (Mayr and Lehner 2008b) are looking forward to a standardization of different nursing care summaries.

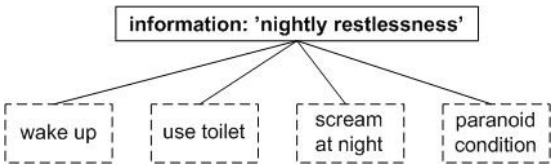

Figure 3: Variety of interpretation of terms used in the same context

Therefore we develop a care model that describes the content of the nursing care summary document, the semantics and its interpretation to guarantee semantic interoperability. We analyze different nursing models and care documentation systems to define common categorizations of care-relevant data. Our care model is based on different nursing models, which is essential for our patient record data exchange platform, as in Austria not only different models but also many different software solutions for nursing care do apply. Thus, the use of international accepted and validated standards, like for example the Resident Assessment Instrument interRAI (interRAI, 2009) is favored.

We define our model in cooperation with healthcare personnel and develop a semantic combination and mapping of defined elements of different care documentation systems. Thereby we achieve a balance among users and approved nursing care classification and models, which allows the cross-enterprise exchange of care information and gets us closer to the integration of healthcare service providers.

3. MODEL-BASED DATA EXCHANGE USING IHE

Our integrated e-Care approach enables healthcare providers to exchange care data within an e-Care affinity domain. Our affinity domain consists of a group of healthcare enterprises, especially mobile nursing services, nursing homes and hospitals, that agree to work together using a common set of policies. They share a common transfer model, which enables importing and exporting care-relevant data to specific nursing care documentation systems.

As we exchange sensitive data, data privacy as well as a strict authorization system have to be taken into account, which is supported by the IHE ATNA profile. It specifies guidelines for security and auditing at both communication and application layers and ensures that all transactions are done securely with only trusted systems in the network (IHE 2009a).

The architecture of the affinity domain has to be perfectly tailored to the needs of the caretaking personnel. We developed a transfer model based upon the IHE guidelines that is used for the first time in Austria in this domain. The use of the IHE XDS profile (IHE 2009a) for our transfer model enables a standardized document exchange among all system partners. XDS specifies guidelines for sharing clinical documents across boundaries of healthcare organizations that are within an affinity domain.

The system architecture used for e-Care is a typical three-tier architecture consisting of a data tier, a business tier and a presentation tier, all deployed on a JBoss applicaton server, see Figure 4. The data tier is served by a Cisco router with an integrated Application eXtensible Platform module (AXP), on which the IHE infrastructure is deployed.

The entire business logic is based on the Spring Framework which is a lightweight container for server-side applications reducing the complexity of J2EE applications (Van de Velde *et al.* 2008). Basically, the business tier is responsible to query and retrieve data from the underlying data tier.

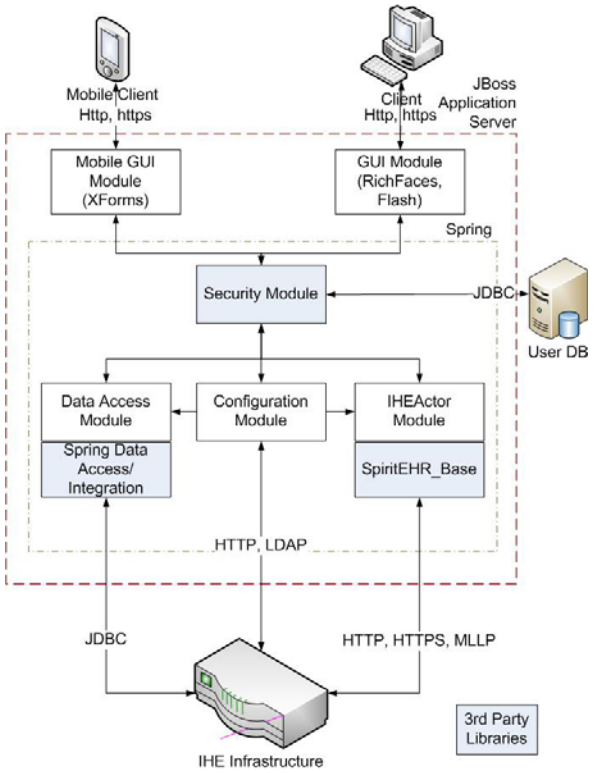

Figure 4: The system architecture used for e-Care

The current architecture allows either the use of Java Data Base Connectivity (JDBC) calls or IHE compliant transactions. Moreover, the access to healthcare information stored in the data tier is secured using the built-in security features of Spring. The current implementation uses HTTP request authorization which checks the provided user credentials against a user database to determine the assigned user role. This user role defines the amount of functionality the user is allowed to access.

The presentation tier of the system is designed to serve desktop clients as well as mobile clients. Therefore, two different user interfaces are provided. The user interface for mobile clients is implemented using XForms (W3C 2009), the user interface for desktop clients is based on JBoss RichFaces which is a component

library working on top of Java Server Faces (Katz 2008).

Our transfer model allows the integration of a wide range of different system partners. The model supports the following three processes that are necessary for the intended document exchange as defined by the XDS and PCC (IHE 2009b) profile:

1. creation, publishing and storage of the document,
2. query for a specified patient and his/her documents,
3. retrieval of a specific document of the specified patient.

These processes are modeled as described in Fig. 5 using

- Document Repository (DRep),
- Document Registry (DReg),
- Patient Identity Source (PIX),
- Document Consumer (DC) and
- Document Source (DS).

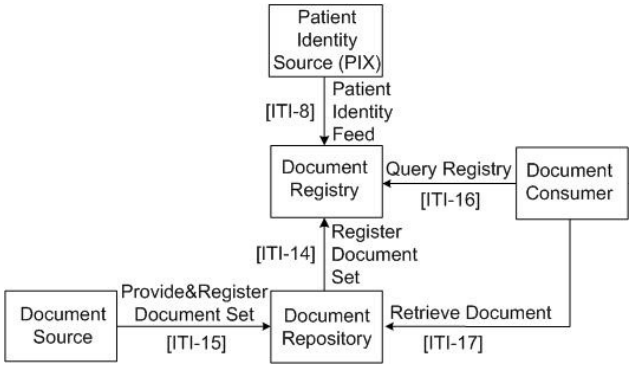

Figure 5: IHE-compliant Transfer Model and Processes

The transfer model provides interoperability across healthcare enterprises through IHE compliance. Healthcare data can now be exchanged electronically through our data model, the data can now be pulled together and interpreted in context.

We are currently working mainly on the transfer model and the data model, especially for nursing care. Our data model represents a structure that can be easily filled in. Any nursing care model can be used as a semantic base. If a document is based on our data model and the care model is known, it is easily possible to map the document to another care model. It also enables a straightforward interpretation of the content so that we can compare different documents and even find contradictory or incomplete data and complete or correct the documents.

Even though we currently restrict the data to the context of nursing care, the models enable an easy integration of further systems and even allow model generation as well as model transformation for other fields of healthcare and to collect health data for different analyses for the healthcare service providers.

Nevertheless, our goal is not a data warehouse. Using our XDS transfer model, the CDA data model as well as the subjacent standardized nursing care models we want to build a personalized health model based upon IHE.

With regard to health economical aspects the model shows high potential. In case that a clinical document is based on our CDA-data model and the care model is known, it is easily possible to map the document to another care model and to certain parts of the document.

As the transferred data is not always complete and the values are not always feasible, we can use the personalized health model to complete the data and to check the plausibility of various values, if the model supports similarity values.

Qualitative nursing care data that is electronically available enables healthcare providers to accurately evaluate care requirements. This guarantees a better requirements planning without the reliance on estimations only. Through continuous electronic documentation of vital signs precise measures for prevention can be set.

Our platform and the evaluations that are possible through the use of our models, may also lead to advantages for the healthcare system as well as for the social system, especially in the field of care for elderly people with need for additional assistance, which we currently focus on.

An applicable data model allows the representation of collaboration networks and the processing of adequate analyses (details can be found in (Altmann et al. 2009)).

In electronic exchange of healthcare information discussions about information security and the protection of sensitive data are inevitable. In Austria information security is governed by the Austrian data protection act (DSG 2000 1999) as well as the healthcare telematics act (GeTelG 2004).

In the USA and in Great Britain, healthcare data are used as marketable goods (Heydwolff/Wenzel 1997). The British Medical Association precisely comments this fact in its principles for security in clinical information systems and completely rejects the data transfer per chip card (Anderson, 1998).

Developments like our patient record data-exchange platform build a secure infrastructure based on international standards for the data transfer between different healthcare institutions. Currently, we legally cover this issue using declarations of consent signed by the patient or the guardian. Nevertheless, there are some unanswered questions concerning the data protection act, for example concerning the required declaration of consent, when the person concerned is no longer communicable (Kopetzky 2008).

We point out these problems so that solutions are contemplated for future applications. We want to demonstrate that our system proves its worth in data exchange and that the application of the transfer, data and care models as well as the generation of a personalized health model is a benefit for the social and the healthcare sector. Hence, the delivery of solutions concerning legal difficulties should be accelerated.

4. SAMPLE APPLICATION: THE E-CARE SYSTEM

The models and processes presented in this paper are currently being integrated into our e-Care system for electronic patient data transfer. This system aims to integrate nursing care across healthcare provider boundaries, thus enabling electronic access to personal nursing records for hospital and nursing home staff as well as mobile care professionals on duty in the field (Fig. 6).

Our prototype mainly focuses on the transfer of data. In particular, we include easy accessibility for our system for mobile care and nursing professionals, since 24/7 patient home care (particularly of elderly people) has increased tremendously in Austria during the last few years. One benefit of our model-based IT-infrastructure (based on models following the IHE guidelines) is that it allows the integration of a wide range of different IT-supported care documentation systems. Our platform is designed in such a manner that it can be extended to any provider of healthcare data.

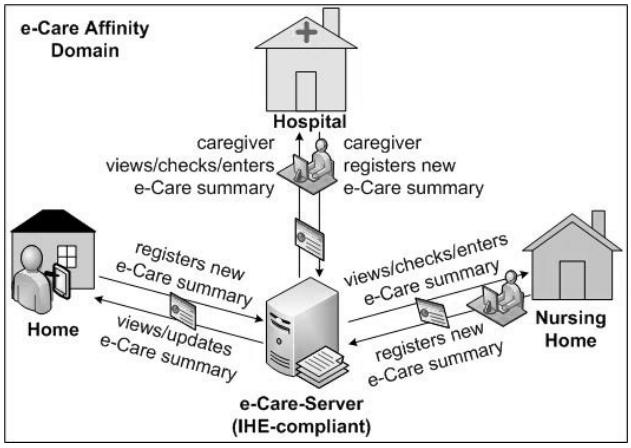

Figure 6: Documentation workflow of our e-Care system

The structured health model allows the simulation of the medical treatment course. Processes can be analyzed and optimized, the quality and accessibility of documents and their management in the general process of mobile and stationary nursing care can be increased and redundancies in the existing workflow eliminated.

Elderly people who require additional care often find themselves being passed between different care systems: from home care, sometimes with support of mobile nursing services, to the hospital and, often with a different amount of care required, back home or to a nursing home. This inadequate referral process affects the quality of nursing care, and therefore the quality of life of elderly people. The process can be analyzed and optimized using the documented reason for referral, for example coded in ICD-10, as well as information about the healthcare service provider.

As our system grows with the various ideas and applications of the community, we integrate representatives of different healthcare providers throughout the project. Our project partners include hospitals, nursing homes, and mobile care providers (Red Cross, city & provincial government etc.). Additionally, we keep close contact with the national, electronic patient care initiative (ELGA Austria) and its EU counterpart, the EPSOS initiative (European Commission 2009).

The benefits of our platform are acknowledged by the users and the application is evaluated as easily usable by our pilot users. At the moment the evaluation process is in progress for the pilot data exchange between a hospital and a nursing home. The platform is to be extended until October 2009, when the prototype for the exchange of nursing care data among nursing homes, hospitals and home care nursing services shall be finished. The prototype is to be tested live in 2010 in the model region of Wels, Upper Austria..

5. CONCLUSION: THE GROWING IMPORTANCE OF IHE

The IHE initiative defines integration profiles for a variety of healthcare IT systems. These integration profiles describe important, common core processes (e.g. information access, record retrieval, reporting) in the clinical disciplines. IHE also adopts existing standards rather than attempting to create its own. So far, IHE has achieved considerable success in the area of connectivity and interoperability of healthcare information systems and medical devices.

IHE-based systems will play a major role in improving the quality, safety and cost-effectiveness of healthcare. That role will only be fully realized when the employed information and data models that specify the pieces of data that must be created, managed, manipulated, and exchanged, are fully technically and semantically interoperable. IHE supports the definition of information models and enables data integration vertically within one clinical domain and horizontally across the healthcare enterprises.

In this paper we have introduced a model-based patient care data exchange allowing easy and safe sharing of documents among different healthcare enterprises based on a semantic interoperability concept. The high degree of system interoperability demonstrated in our e-Care system could only be achieved by consistently utilizing IHE standards. In particular, IHE is the key facilitator to make precisely defined information and data models applicable and interoperable already now and even more in the near future.

ACKNOWLEDGMENTS

This work has been partially financed by the Austrian government (FFG, FHplus/COIN initiative and FFG Basisprogramme). Other financially contributing partners to this project are X-Tention, the city of Wels and Klinikum Wels-Grieskirchen.

REFERENCES

Ament-Rambow, Ch., 2003. *Prozessmanagement als Weg zur Kostensenkung im Gesundheitswesen: Ein Fünf-Stufen-Konzept zur Einführung.* (*Cost Reduction in Healthcare Systems by Process Management. A Five Step Concept for Implementation*; in German). In

Blonski, H. Stausberg, M., eds.: *Prozessmanagement in Pflegeorganisationen. Grundlagen – Erfahrungen – Perspektiven*, Schlütersche Verlags GmbH, Hannover, Germany.

Altmann, J., Pfeifer, F., Strasser, M., Franz, B., Mayr, H., 2009. *Collaborative Knowledge Networks Based on IHE*, Accepted for publication, Proc. 21st European Modeling and Simulation Symposium, September 23-25, Tenerife, Spain.

Anderson RJ, 1998. *Sicherheit in klinischen Informationssystemen*. German translation of *Security in Clinical Information Systems (1996)*. London, British Medical Association. Available from: http://www.familienmedizin.net/files/publs/gesundheitsdatenschutz.pdf [accessed 11 June, 2009].

Burns, E., 2007. *Evidence-based Pflegestandards und Pflegeguidelines*. In: Österreichische Pflegezeitschrift 06-07/07, pp. 33-34.

DSG, 2000. *Bundesgesetz über den Schutz personenbezogener Daten (Datenschutzgesetz 2000) (Austrian Federal Law Concerning the Protection of Personal Data;* in German*)*. BGBl 1, Rel. 17, August 1999, Nr. 165, Vienna, Austria.

Eilmansberger, Th. Holoubek, M. Kalass, S. Lang, M. Lienbacher, G. Lurger, B. Potacs (eds.), M., 2008. *Geheimnisschutz, Datenschutz, Informationsschutz*. (*Protection of Secrets, Data, Information*; in German). Studiengesellschaft für Wirtschaft und Recht, Linde Verlag, Vienna, Austria.

European Commission, 2009. *epSOS – European Patients Smart Open Services*. Available from: http://www.epsos.eu/epsos-home.html [accessed 30 April 2009].

GeTelG, 2005. *Gesundheitstelematikgesetz (Gesundheitsreformgesetz 2005) (Austrian Federal Law on Health Telematics;* in German*)*. BGBl 1 Nr. 179/2004.

Heydwolff, A. Wenzel, Th., 1997. *Daten aus der Psychotherapie – auch bei uns bald eine Ware? Ethische Brennpunkte der „Globalen Informationsgesellschaft (Data from Psychotherapy – Soon to Be Trading Goods in Our Country, too?;* in German*)*. Psychotherapie Forum, 5,1, pp. 17-25.

HL7, Health Level Seven, Inc., 2009. *HL7. Health Level Seven*. Available from: http://www.hl7.org, Michigan, USA [accessed 30 January 2009].

IHE, 2009a. *IT Infrastructure*. Technical Framework. Available from: http://www.ihe.net [accessed 30 April 2009].

IHE, 2009b. *Patient Care Coordination. Technical Framework.* Available from: http://www.ihe.net [accessed 30 April 2009].

interRAI, 2009. *Resident Assessment Instrument*. Available from: http://www.interrai.org [accessed 30 April 2009].

Katz, M., 2008. *Practical RichFaces*. Berkley: Apress.

Kopetzki, Ch., 2008: *Geheimnisschutz – Datenschutz – Informationsschutz im Gesundheitsrecht (Protection of Secrets, Data, and Information in Health Law*; in German). In Eilmansberger *et al*., eds., *Geheimnisschutz, Datenschutz, Informationsschutz*. Studiengesellschaft für Wirtschaft und Recht, Linde Verlag, Vienna, Austria.

Mayr, M. and Lehner, M., 2008a. *Zwischen mobiler Pflege und Krankenhaus. Eine prekäre Schnittstelle der Versorgung im Alter* (*Between Mobile Nursing Care and Hospital. A Precarious Interface of Elderly Care*; in German), Gesundheitswissenschaften Vol. 33, Johannes Kepler University, Institute for Social Policy, oö. Gebietskrankenkasse, Linz, Austria.

Mayr, M. and Lehner, M., 2008b. *Stationäre Versorgung älterer Menschen in Oberösterreich. Versorgungsnetzwerke und -prozesse*. (*Inpatient Care at the Center of Geriatric Healthcare in Upper Austria. Networks and Processes*; in German). Upper Austria University of Applied Sciences, Linz, Austria.

Müller Staub, M., 2005. *Wahl einer Pflegediagnosen-Klassifikation für die Einführung in die elektronische Pflegedokumentation. ICNP, ICF, NANDA und ZEFP im Vergleich*. In: Pflegeinformatik pp. 115-122, Available from: printerneht.info/artikel.asp?id=530 [accessed 11 September 2008].

Perhab, F., 2007. *Babylonische Sprachverwirrung? Taxonomien, Klassifikationen – gemeinsame Pflegesprache und Wissensmanagement (Babylonian Confusion of Languages? Taxonomies, Classifications – Common Care Language and Knowledge Management;* in German*)*. In Österreichische Pflegezeitschrift 03/07, pp. 8-16, Available from: www.oegkv.at [accessed 11 September 2008].

Schreier, G., Hayn, D. and Ammenwerth E., 2007. *eHealth 2007 – Medical Informatics Meets eHealth*. Proceedings of eHealth 2007, 1 June 2007, Austria: Vienna.

Spronk, R., 2008. *CDA. Clinical Document Architecture*, Available from: http://hl7book.net [accessed 30 January 2009].

SVC, 2009. *e-Card* (in German). Sozialversicherungs-Chipkarten Betriebs und Errichtungs GmbH. Available from: http://www.chipkarte.at [accessed 11 June 2009].

Van de Velde, T., Snyder, B., Dupuis, C., Li, S., Horton, A., Balani, N., 2008. *Beginning Spring Framework 2*. Indianapolis: Wiley Publishing, Inc.

W3C World Wide Web Consortium, 2009. *The Forms Working Group*. Available from: http://www.w3.org/MarkUp/Forms [accessed 11 June 2009].

WHO World Health Organization, 2009. *The WHO Family of International Classifications*. Available from: http://www.who.int/classifications/icd/en/ [accessed 11 June 2009]

AUTHORS BIOGRAPHY

All authors are scientific or faculty members of the Upper Austria University of Applied Sciences.

Barbara Franz, M.Sc. and *DI (FH) Franz Pfeifer* are scientific researchers at the Research Center Hagenberg.

Dr. Herwig Mayr and *Dr. Josef Altmann* are professors for software engineering at the campus Hagenberg.

Mag. Margit Mayr is scientific researcher at the Research Center Linz.

Dr. Markus Lehner is professor for social services at the campus Linz of this university.

MODELING OF STANDARDIZED DATA ENTRY IN DERMOSCOPY

S. Dreiseitl[a], K. Auracher[b], S. Puig[c], J. Malvehy[d]

[a,b]Upper Austria University of Applied Sciences at Hagenberg, Austria
[c,d]Melanoma Unit, Dermatology Dept., Hospital Clinic, Barcelona, Spain

[a]stephan.dreiseitl@fh-hagenberg.at, [b]klaus.auracher@fh-hagenberg.at,
[c]spuig@clinic.ub.es, [a]jmalvehy@clinic.ub.es

ABSTRACT

Recent standardization efforts of the International Dermoscopy Society have resulted in a proposed format for reporting and communicating dermoscopic findings. This format describes the pieces of information that should be included in a dermoscopy report. To provide computer support for these standardization efforts, we developed a Java program with a graphical user interface for data entry, and a standardized interface to a database system for easy storage of examination data. The user interface presents a template that facilitates the standardized reporting of findings via a number of structured interfaces and interface items, and allows the inclusion of clinical and dermoscopic images in the report. The database component of the system stores all examination data in structured format, allowing our software system to be used also as a patient management tool. To facilitate information transfer, the software system can produce PDF reports of individual dermoscopic examinations.

Keywords: dermoscopy, melanoma diagnosis, standardized data entry, data exchange format

1. INTRODUCTION

Malignant melanoma of the skin is one of the fastest growing cancers in the Western world, with incidence rates in Caucasian populations growing between 3–7% in recent years. This means that incidence rates will double every 10–25 years (Garbe et al., 2000; Lens and Dawes, 2004).

The diagnosis of melanoma and related cancers is a visual discipline, which has benefitted greatly from the development of *dermoscopy*, a non-invasive diagnostic technique that allows for the observation of morphologic features that are not visible to the naked eye. Dermoscopy, also known as *dermatoscopy* or *epiluminescence microscopy*, is thus an imaging modality that lies between macroscopic clinical dermatology and microscopic dermatopathology (Zalaudek et al., 2006).

Digital dermoscopy uses a polarized light source for rendering the top-most layer of the skin translucent, and a CCD camera for magnification and image acquisition of the visible structures of the epidermis and the papillary dermis. The advantage of dermoscopy, compared with an examination using the unaided eye, lies in the fact that lesion structures relevant for distinguishing melanomas from non-melanomas are more easily visible when the top-most layer of the skin is translucent. Further advantages of digital dermoscopy are the ease with which the images can be manipulated (e.g., enlarged), archived and retrieved for follow-up consultations, and the ability to include computer decision support systems in the diagnostic process. A review of recent research findings using epiluminescence microscopy is available in the literature (Massone et al., 2005).

In numerous controlled experiments, it was shown that dermoscopy is well-suited to increase the diagnostic performance of dermatologists (Westerhoff et al., 2000; Soyer et al., 2001; Bafounta et al., 2001; Carli et al., 2004). It has, however, been noted that some training and experience is required to actually reap the benefits of this technology (Binder et al., 1997; Kittler et al., 2002). As an added bonus, the easy availability of large data sets has led to the structured analysis of lesion images, and subsequently to the derivation of a number of rules that aid in the diagnosis of cutaneous melanoma (Stolz et al., 1993; Menzies et al., 1996; Argenziano et al., 1998; Benelli et al., 2001; Blum et al., 2003).

The most prominent of these rules, the ABCD rule (Stolz et al., 1993), has become known even outside the field of dermatology, and is easy to apply for general practitioners and even patients in self-examinations. The meaning of the letters in the acronym is a follows:

- "A" for *asymmetry*: Malignant melanoma show more pronounced asymmetries than benign lesions. A score of 0, 1, or 2 is assigned according to the number of axes along which an asymmetry is dis-

cernible.

- "B" for *border*: Benign lesions generally show a more gradual fading of texture into the surrounding skin than melanomas, which either exhibit an abrupt cutoff of pigment patterns, or ragged, pseudopod-like extensions. A score of 0 to 8 is assigned according to the number of octants in which there is a pronounced border irregularity.

- "C" for *color*: The number of distinct colors in the lesion: each of the colors white, red, light brown, dark brown, blue-gray and black, if present in the lesion, adds 1 to the score.

- "D" for *differential structure*: The number, between 0 and 5, of observable structural elements in the lesion. This feature is hardest to evaluate for inexperienced persons, and thus sometimes replaced with *diameter*, which is easier to gauge.

A weighted sum of the four scores indicates to which degree a pigmented lesion may be malignant; the weights are 1.3 for asymmetry, 0.1 for border, and 0.5 each for color and differential structure. A weighted score higher than 5.45 is highly indicative of melanomas.

These factors, and corresponding factors in the other rules, are easier to discern using dermoscopy, which generally enlarges the images by a factor between 10 and 30, than using only the unaided eye. The benefit in performance using diagnostic rules has been observed in a number of studies (increase in sensitivity between 10% and 27%); a review is given by Blum et al. (2003). There, a comparison of the various rules shows these to have sensitivities in the range of 87% to 95%, and specificities between 72% and 89% (with high sensitivities corresponding to low specificities and vice versa). The benefits of dermoscopy have created a demand for medical devices that provide the hardware for this diagnostic technique (a camera equipped with polarized light source and a computer backend). A number of commercial vendors now offer such devices.

2. MOTIVATION

As mentioned in Section 1, there are a number of diagnostic guidelines that help dermatologists distinguish between benign and malignant lesions. These guidelines are based on diagnostic *features* that are more or less readily available during the examination process, when using dermoscopy equipment. The increasingly widespread use of these guidelines and associated features has resulted in the need for a standardized vocabulary that facilitates information exchange between dermatologists. As an example, consider the feature names *arborizing vessels* or *large blue-gray ovoid nest*. Although these names are descriptive, the underlying features could also be expressed in different wording. With a plethora of terminology for the same and similar features, it is highly confusing whether a second opinion that discovers a *leaf-like structure* actually refers to the same thing as the *arborizing vessels* that the first opinion mentions.

It was for this reason that the International Dermoscopy Society established a task force to standardize the vocabulary of the diagnostic process in melanoma diagnosis. The results of a consensus meeting are now available in the literature (Malvehy et al., 2007). This standard establishes the vocabulary for a two-step diagnostic process:

- In the first step, a distinction is made between melanocytic lesions and non-melanocytic lesions. The basis of this distinction are 17 features, the absence or presence of which is indicative of one of the lesion classes.

- In the second step, melanocytic lesions are classified as being benign or malignant (melanomas) by the use of one of four diagnostic algorithms: *Pattern analysis*, the *ABCD rule*, *Menzies' method*, and the *7-point checklist*.

For the four algorithms in the second step, the number of features and feature names varies considerably, from the four features of the ABCD rule, to seven features in the 7-point checklist, eleven features in Menzies' method, and 28 features in pattern analysis. In pattern analysis, the features are grouped into the categories *global features*, *local features*, and *site-related features* (face, palms and soles).

To facilitate the structured data entry, we developed a software system that simplifies and unifies patient information, lesion features, diagnosis, lesion management, and physician comments. The design of this system is presented in Section 3. Current limitations of the system are discussed in Section 4; concluding remarks are given in Section 5.

3. SYSTEM DESIGN

The template of a dermoscopy report, as proposed by the International Dermoscopy Society, consists of the following main sections:

1. Patient's history
2. Clinical description of the lesion
3. The two-step method of dermoscopy
4. Dermoscopic description
5. The algorithm used
6. Imaging equipment and magnification
7. Clinical and dermoscopic images of the tumor
8. Diagnosis
9. Suggested management
10. Specific comments for the pathologist

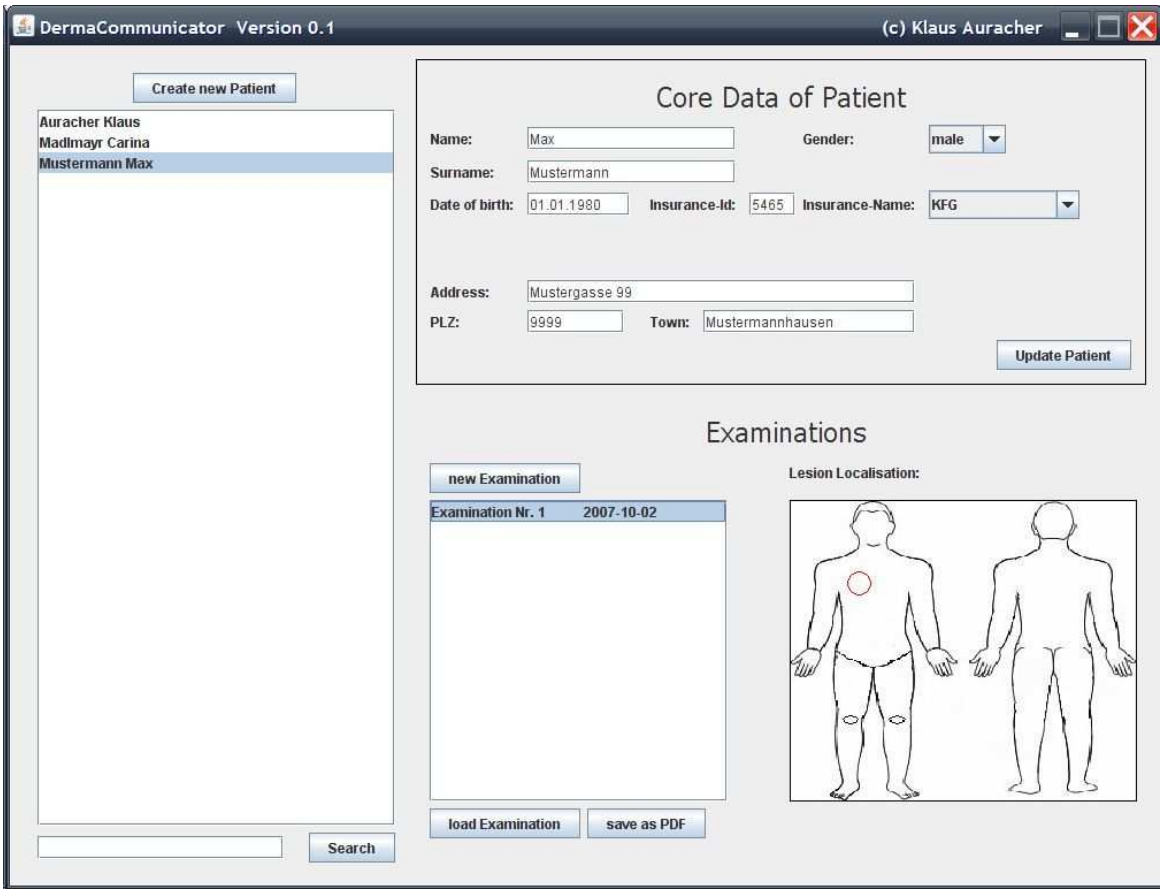

Figure 1: The basic interface of the *DermaCommunicator* software.

Of these, most are self-explanatory, with the exception of "two-step method", which refers to the results of applying the initial criteria for distinguishing between melanocytic and non-melanocytic lesions.

The challenge in building a software system to support data entry and data management lies not in the software architecture, but in the user interface, in the data formats for data storage, and in modeling the work-flow of data acquisition during a patient examination. The reason for this is that there is little data processing in the software itself, apart from transforming the data into suitable formats for storage in a database.

Our system, although small, follows a three-tier architecture, with separate components for data entry, data storage, and output preparation. For reasons of portability and platform independence, we implemented our system in Java.

The initial graphical user interface of the system, shown in Figure 1, contains components for patient management, and administers the individual examinations. The core functionality of the software is represented by its structured data entry interfaces for recording and archiving the findings of a dermoscopic examination. Two of the interfaces for structured data entry available in *DermaCommunicator* are shown in Figures 3 and 2.

As mentioned above, there are four dermoscopy algorithms that guide physicians towards establishing a diagnosis. Of these four algorithms, currently only the pattern analysis algorithm is available in the software.

4. LIMITATIONS AND OUTLOOK

The system described in this paper is currently in the beta testing stages, having been presented to members of the International Dermoscopy Society for feedback. The feedback so far focuses on the following major points:

- include facility for easy transmission of individual lesion examinations to fellow dermatologists for obtaining a second opinion. Some of the functionality of transmitting examination data in XML format is already implemented in the system, but at the current time not ready for inclusion in release versions;
- include facilities for transmission of database components in anonymized form to a central server (of the International Dermoscopy Society) for archiving of interesting cases, and for teaching purposes;
- improve the layout of the user interface and its various sub-windows;
- include a picture-annotation tool, to be used for highlighting features of interest in the lesion image;

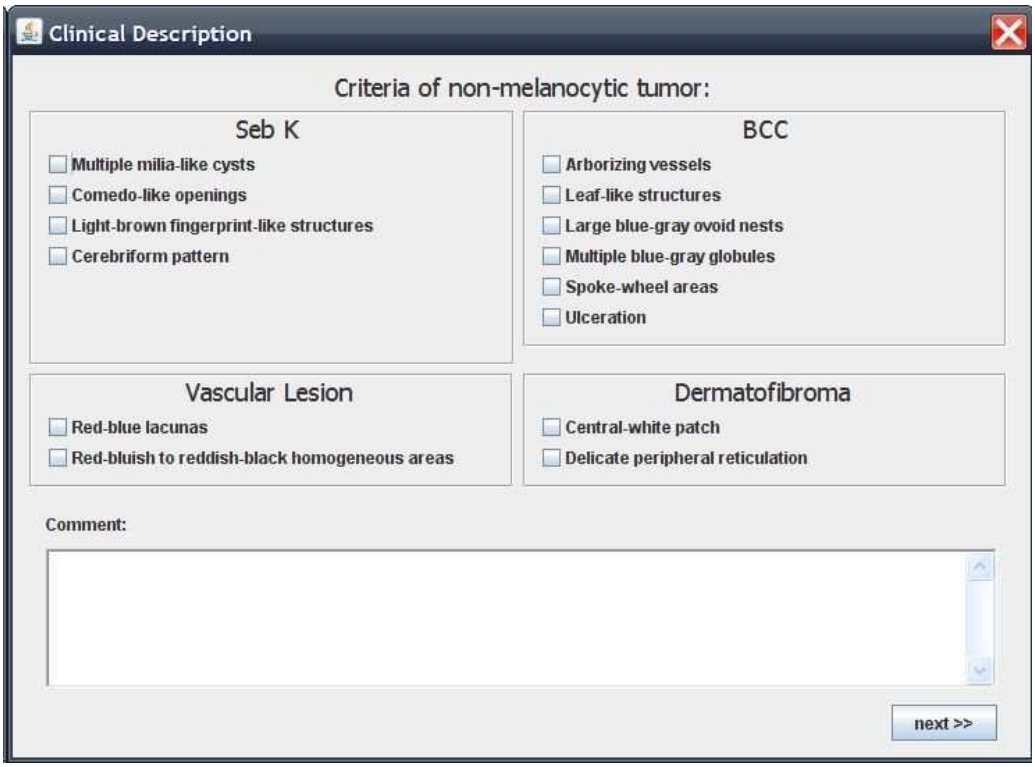

Figure 2: Structured data entry for non-melanocytic tumors.

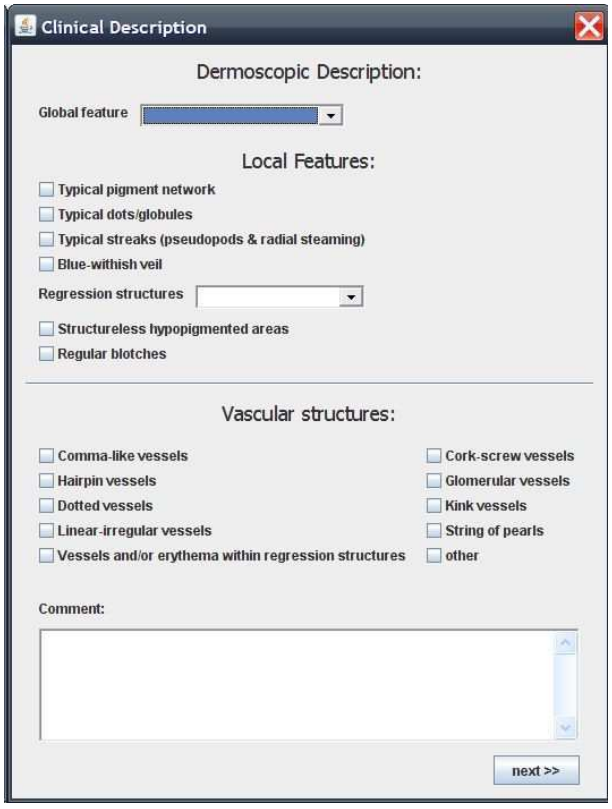

Figure 3: Structured data entry for dermoscopic findings, divided into *local features* and *vascular structures*.

- include a form that releases the software authors from warranty, and transmit consent of this form back to a central server;
- implement a web-based version of the software, for which only a web browser is required to display the graphical user interface and data entry fields. In such a program, all functionality and data storage reside on a central server.

We will group these by urgency, and incorporate in the most desired features in the next release of the software.

From the point of view of standardization, it should be noted that there are still a limited number of text fields where free text describing lesion features may be entered. In future releases, we plan to incorporate automatic parsing capabilities that will check these entries for validity, based on the proposed standard vocabulary for dermoscopy features.

5. CONCLUSION

In this paper, we presented a description of *DermaCommunicator*, a software system that allows structured entry of dermoscopy examinations. The software is part of a standardization effort of the International Dermoscopy Society, which aims to regulate the structure and vocabulary of dermoscopy reports. The software is currently in the beta testing stage. Comments from dermatologists are encouraging and show that software support in the field of dermoscopy is highly appreciated.

REFERENCES

Argenziano, G., Fabbrocini, G., Carli, P., Giorgi, V. D., Sammarco, E., and Delfino, M. (1998). Epiluminescence microscopy for the diagnosis of doubtful melanocytic skin lesions-comparison of the ABCD rule of dermatoscopy and a new 7-point checklist based on pattern analysis. *Arch Dermatol*, 134:1563–1570.

Bafounta, M., Beauchet, A., Aegerter, P., and Saiag, P. (2001). Is dermoscopy (epiluminescence microscopy) useful for the diagnosis of melanoma? results of a meta-analysis using techniques adapted to the evaluation of diagnostic tests. *Arch Dermatol*, 137:1343–1350.

Benelli, C., Roscetti, E., and Pozzo, V. D. (2001). Reproducibility of the clinical criteria (ABCDE rule) and dermatoscopic features (7FFM) for the diagnosis of malignant melanoma. *Eur J Dermatol*, 11:234–239.

Binder, M., Püspöck-Schwarz, M., Steiner, A., Kittler, H., Müllner, M., Wolff, K., and Pehamberger, H. (1997). Epiluminescence miscroscopy of small pigmented skin lesions: Short-term formal training improves the diagnostic performance of dermatologists. *J Am Acad Dermatol*, 36 (2 Pt 1):197–202.

Blum, A., Rassner, G., and Garbe, C. (2003). Modified ABC-point list of dermoscopy: A simplified and highly accurate dermoscopic algorithm for the diagnosis of cutaneous melanocytic lesions. *J Am Acad Dermatol*, 49:672–678.

Carli, P., Giorgi, V. D., Crocetti, E., Mannone, F., Massi, D., Chiarugi, A., and Giannotti, B. (2004). Improvement of malignant/benign ratio in excised melanocytic lesions in the 'dermoscopy era': a retrospective study 1997–2001. *Br J Dermatol*, 150:687–692.

Garbe, C., McLeod, G., and Buettner, P. (2000). Time trends in cutaneous melanoma in queensland, australia and central europe. *Cancer*, 89:1269–1278.

Kittler, H., Pehamberger, H., Wolff, K., and Binder, M. (2002). Diagnostic accuracy of dermoscopy. *Lancet Oncol*, 3(3):159–165.

Lens, M. and Dawes, M. (2004). Global perspectives of contemporary epidemilogical trends of cutaneous malignant melanoma. *British Journal of Dermatology*, 150:179–185.

Malvehy, J., Puig, S., Argenziano, G., Marghoob, A., Soyer, H., and International Dermoscopy Society Board members (2007). Dermoscopy report: Proposal for standardization. Results of a consensus meeting of the International Dermoscopy Society. *J Am Acad Dermatol*, 55(1):84–95.

Massone, C., Stefani, A. D., and Soyer, H. (2005). Dermoscopy for skin cancer detection. *Curr Opin Oncol*, 17(2):147–153.

Menzies, S., Ingvar, C., and McCarthy, W. (1996). A sensitivity and specificity analysis of the surface microscopy features of invasive melanoma. *Melanoma Res*, 6:55–62.

Soyer, H., Argenziano, G., Chimenti, S., and Ruocco, V. (2001). Dermoscopy of pigmented skin lesions. *Eur J Dermatol*, 11:270–276.

Stolz, W., Riemann, A., Cognetta, A., Pillet, L., Abmayr, W., and et at, D. H. (1993). ABCD rule of dermatoscopy: a new practical method for early recognition of malignant melanoma. *Eur J Dermatol*, 4:521–527.

Westerhoff, K., McCarthy, W., and Menzies, S. (2000). Increase in the sensitivity for melanoma diagnosis by primary care physicians using skin surface microscopy. *Br J Dermatol*, 143:1016–1020.

Zalaudek, I., Argenziano, G., Stefani, A. D., Ferrara, G., Marghoob, A., Hofmann-Wellenhof, R., Soyer, H., Braun, R., and Kerl, H. (2006). Dermoscopy in general dermatology. *Dermatology*, 212:7–18.

AUTHOR BIOGRAPHIES

STEPHAN DREISEITL received his MSc and PhD degrees from the University of Linz, Austria, in 1993 and 1997, respectively. He worked as a visiting researcher at the Decision Systems Group/Harvard Medical School before accepting a post as professor at the Upper Austria University of Applied Sciences in Hagenberg, Austria, in 2000. He is also an adjunct professor at the University of Health Sciences, Medical Informatics and Technology in Hall, Austria. His research interests lie in the development of machine learning models and their application as decision support tools in biomedicine.

KLAUS AURACHER studied Software Engineering at the University of Applied Sciences Hagenberg, and graduated with the degree "Bachelor of Science in Engineering" in 2007. He subsequently studied Information Engineering and Management at the University of Applied Sciences Hagenberg, and graduated with the degree "Master of Arts in Business" in 2009. Since 2007, he is working as a software engineer in Hagenberg, Austria. His research focus is on medical software, in particular for dermoscopy examinations.

MODELLING AND SIMULATION OF THE ANESTHETIC PROCESS

Juan Albino Méndez[(a)], Héctor Reboso[(b),] José Antonio Reboso[(c)] and Santiago Torres[(d)]

[(a)]University of La Laguna
[(b)]University of La Laguna
[(c)] Hospital Universitario de Canarias
[(d)]University of La Laguna

[(a)]jamendez@ull.es, [(b)]hreboso@ull.es, [(c)]jreboso@comtf.es , [(d)]storres@ull.es

ABSTRACT
This paper affords the modelling issues in intravenous anesthesia problem. The methods are presented from a control design perspective. Different proposals are presented for the modelling of the patient's response to the drug. The proposal here includes a specific term for dead-time. Using this approach it is possible to improve the performance of the controller. The paper presents results obtained from real patients that are used to validate the proposed methods.

Keywords: Anesthesia, Propofol, PI Control, Smith Predictor.

1. INTRODUCTION

Simulation and Control engineering has an important influence in healthcare applications. Thus, many applications have been developed using these technologies. Robotic devices for practitioner assistance (laparoscopic surgery), electrophysiological systems (pacemakers) or image processing-based diagnosis systems are some examples of this fact.

Anesthesiology, has been also greatly influenced by the application of these new technologies. Anesthesia can be defined as a reversible pharmacological state where the patient's muscle relaxation, analgesia and hypnosis are guaranteed. Anesthesiologists administer drugs and adjust several medical devices to achieve such goals and to compensate for the effect of surgical manipulation while maintaining the vital functions of he patient.

In recent years many efforts have been made in the development of new drug delivery technologies. Most of the difficulties to calculate the proper drug's rate to each patient was the inexistence of precise methods to monitor the anesthetic state of the patient. In the past patient monitoring was performed just by observing several patient signs (sweat, head lifting, movement,…). Nowadays the way anesthesia is monitored has changed considerably. Many efforts have been made to provide the anaesthesiologist with more reliable methods for monitoring. In particular, the introduction of the Bispectral Index (BIS) to measure the depth of anesthesia was one of the key elements in the development of new ways of drug administration.

The importance of more precise and secure drug administration increases the need for simulation tools available for experts. The use of simulation in anesthesia has two main goals. Firstly, control engineers that design the control algorithms need this simulation environments to test the performance of the strategies developed. Before the implementation on the real patient is carried out, the algorithm is validated with simulators and tested under different working conditions. The aim is to increase reliability and safety of the proposed algorithm.

On the other, hand simulators are becoming a very helpful tool for anesthetist training. The introduction of simulators into anesthetic residency programs has been widely extended in education centres. The objective is to reduce the training based on repetitive and frequent exposure to patients and anesthetic situations. In contrast, the anesthetist will acquire his skills facing simulated situations. This is especially interesting in the early stage of training.

Most early simulators focused on pharmacological, anatomical, or physiological teaching and crisis interventions. Several simulators have been introduced in the past decades. The first ones was introduced in 1969. However the possibilities in this initial stage were limited. When the quick development of computational technology more full-scale simulators have been introduced into the practice of anesthesia education. It is worth mentioning the development of CASE (comprehensive anesthesia simulation environment) and TOMS (team-oriented medical simulation) (Chopra 1996, Helmreich and Schaffer, 1998, Chopra et al 1994,).

The interest of this work is focused in the part concerned with modelling, simulation and control of anesthesia. The problem considered is the regulation of hypnosis level during surgery using Propofol as anesthetic drug.

The indicator considered to measure the degree of hypnosis is the BIS index. The complexity of the problem grows exponentially when other specifications are taken into account like muscular relaxation or

analgesia. For hypnosis control, the structure of the controllers proposed have two different approaches: signal-based control and model-based control.

One of the main difficulties arising in the design of a control system for anesthesia is related to the complexity of the process involved. On one side the model presents inherent nonlinearities that increase the difficulty to design the controller.

This paper affords the modelling issues appearing from a control design perspective. Different proposals are presented for the modelling of the patient's response to the drug. The proposal here includes a specific term for dead-time. Using this approach it is possible to improve the performance of the controller.

The paper begins with a revision of the basic concepts in anesthesia. Then the most common modelling methodologies are presented. The design of basic control strategies for BIS regulation is presented in the next section. The results in simulation and in real time experiments are commented. Finally some conclusions are summarized

2. GENERAL CONCEPTS OF ANESTHESIA

The description of the anesthetic process is generally done with the variables shown in Figure 1. In the figure an input-output description of the system is shown. As can be observed, manipulated variables are anesthetics, relaxants or serums. Perturbations in the system are signals that can occur at any time (surgical stimulation, blood loss, …). The output variables can be measurable and not measurable. The main interest in anesthesia is focused in non measurable variables: hypnosis, analgesia and muscular relaxation.

As commented previously, the problem of having non measurable variables is solved having alternative variables whose behaviour allows the estimation of the non-measurable ones.

This work deals with hypnosis control in humans. Hypnosis is a general term indicating loss of consciousness and absence of the memory of the intervention after awake. Currently, the techniques that have been considered more efficient for this are based in the processing of the patient electroencephalogram (EEG), (Struys et al 2000).

The variable that will be taken as an indicator of the degree of hypnosis is the BIS. This index is an empirical parameter, without units, derived from the analysis of the EEG. The BIS related linear and directly with the consciousness degree. Its value decreases progressively from 100 (maximum alert state) to 0 (no electrical activity). The correlation between these variables is dynamical so that there is always an optimal correlation with the hypnotic state: consciousness-unconsciousness, sedation degree, ability to remember and process information, etc.

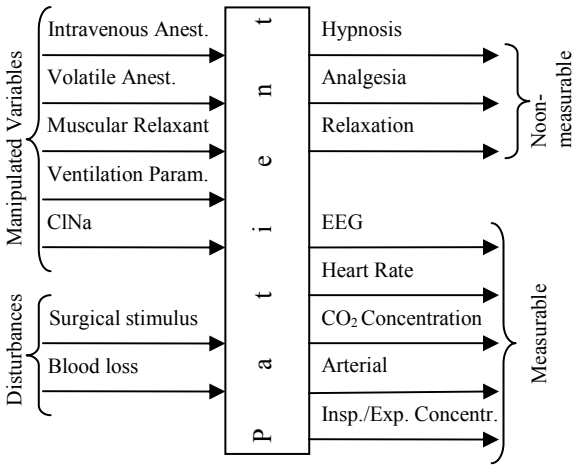

Figure 1: Input-output description of the process.

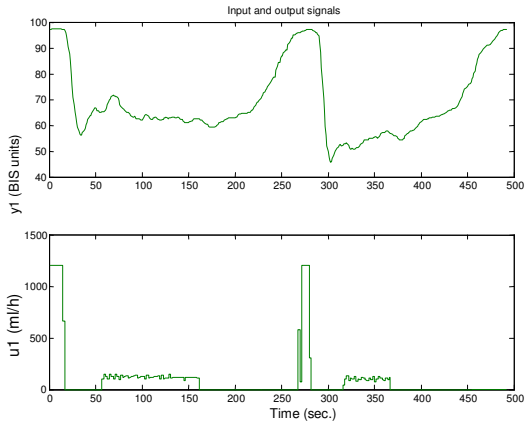

Figure 2: Infusion rate and measured BIS.

3. MODELLING OF ANESTHESIA WITH PROPOFOL

3.1. Parametric Modelling

In order to develop an adequate control strategy, the first aim was to obtain a mathematical model of the patient under propofol infusion by means of system identification techniques. The anesthetic process was segmented into several phases, according to the state of the surgery (consciousness, hypnosis, intubation, incision, etc.). The Propofol infusion rate in ml/h was used as the input variable u(t), while the BIS represented the output. Figure 2 shows an example of the variables of a patient undergoing major surgery.

A parametric ARX model estimation was performed with a group of five patients of different weight, sex and age undergoing major surgery with Propofol (George et al 1994). A segment of the input data was used to obtain the model and the remaining data set of the same patient for validation. The results showed that the order of the adequate model varies between 15 and 20 depending on the patient and the phase of the surgery. The polynomial representation is:

$$A(q)\mathrm{BIS}(t) = B(q)u(t - n_k)) + e(t) \quad (1)$$

$$\mathrm{BIS}(t) + a_1\mathrm{BIS}(t\text{-}1) + \ldots + a_{na}\mathrm{BIS}(t\text{-}n_a) = b_1u_1(t\text{-}\ n_k)$$

$$+ b_2u(t\text{-}n_k\text{-}1) + \ldots + b_{nb}\mathrm{u}(t\text{-}n_k\text{-}n_b\text{-}1) \quad (2)$$

Here, the numbers n_a and n_b are the orders of the respective polynomials. The number n_k is the number of delays from input to output. Figure 3 represents the comparison between the real BIS and the simulated BIS with the model obtained from the first half of the data pattern of the patient signals shown in Figure 1. As can be observed, the model obtained fits adequately the real data pattern. Even in the second half of the curve, the proposed model presents a satisfactory behaviour. The model orders in this experiences were n_a = 14, n_b = 15 and n_k = 10. Figure 4 represents the difference between these output signals. It can be appreciated that the relative BIS error keeps in a ±10% range. Thus demonstrating a high performance in the model adjustment.

The model obtained was validated with data sets of other patients, as shown in figures 5 and 6. In Figure 5 it can be seen that the global behaviour of the model follows the real data although the error now is greater than with a patient-customized model (shown in Figure 6).

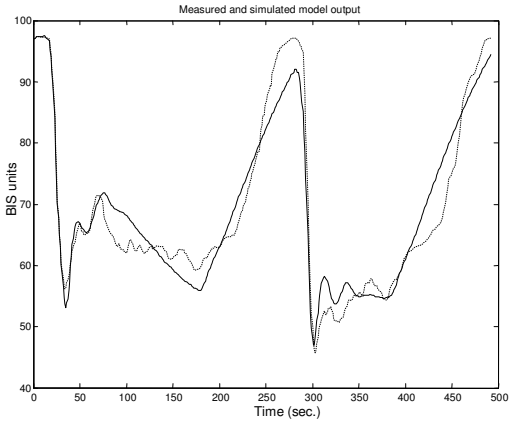

Figure 3: Measured BIS (dashed line) and modelled BIS (solid line) from patient 1.

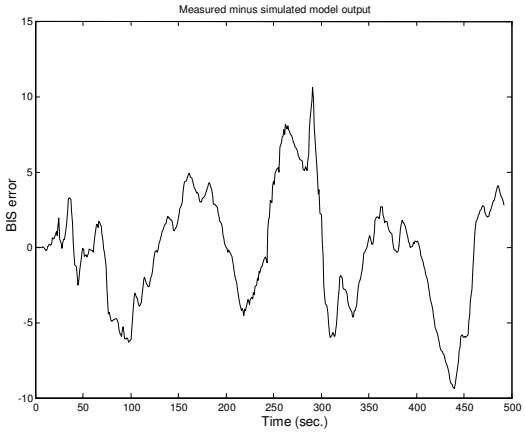

Figure 4: BIS Error (Measured – Simulated).

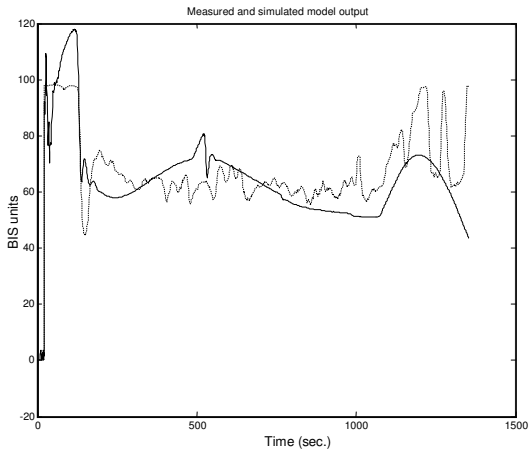

Figure 5: Measured BIS of patient 2 (dashed line) versus BIS from model of patient 1 (solid line).

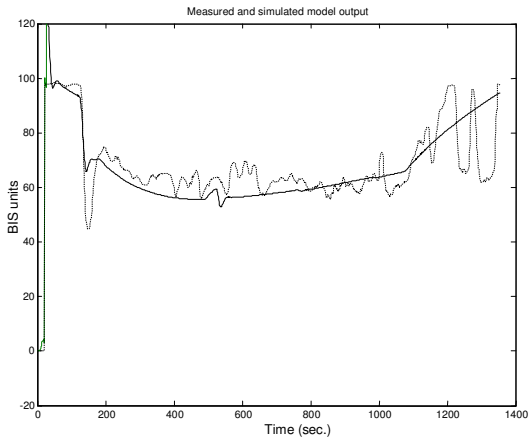

Figure 6: Measured BIS of patient 2 (dashed line) versus BIS from model of patient 2 (solid line).

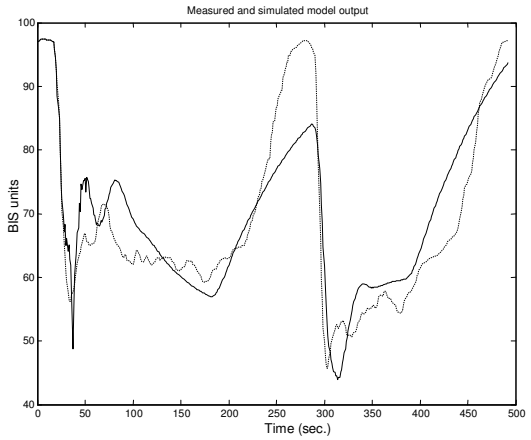

Figure 7: Measured BIS of patient 1 (dashed line) versus BIS from model of patient 2 (solid line).

A second system identification procedure with data from a different patient delivered a 20-order model which was stimulated with the input data of patient 1, resulting in the simulated BIS shown in Figure 7. Now

the error is greater than in Figure 4. This confirms the patient-dependency of the model anticipated above.

3.2. Physiological modelling

The description of the BIS dynamics has been done mainly with physiological models. These models consists of a pharmacokinetic part (PK) to describe the drug distribution in the internal organs and a farmacodynamic part (PD) to describe the drug effect on the physiological variables of interest.

The more used PK model is the Marsh model and the Schnider model that have been widely studied and represent the patient as a set of compartments: central, fast and slow, see Figure 8 (Marsh et al, 1991). The central compartment corresponds to the apparent blood volume of the patient (the place where the drug is infused).

The fast and slow compartments represent fat and bone tissue. The Schnider model is defined according to the following diffusion constants: k_{10} that represents the metabolic clearance, k_{12} and k_{21} that represent the clearances between the central and fast compartment, k_{13} and k_{31} that represent the clearances between the central and slow compartment (Schnider et al 1998).

From the point of view of hypnosis control the variable of interest is not the blood concentration but the concentration

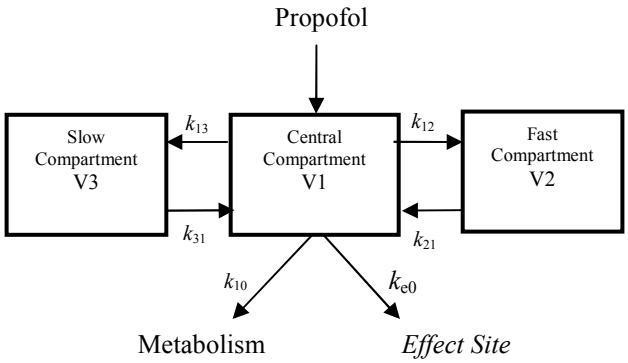

Figure 8: Compartment model.

in the place where the effect on the controlled variable is produced (*effect site concentration*). Thus, when there is a simultaneous measure of the drug concentration in blood and its effect on the brain, drug latency can be observed that produces a temporal displacement between the peak of blood concentration and the drug effect. To include this dynamics in the model a fourth compartment is added. This compartment is known as *effect site*. This model is assumed to be attached to the central compartment and has negligible volume. The diffusion constant of the effect site is *k*e0.

Defining the variable that represents the *i*-th compartment as C_i, the Propofol distribution can be obtained as:

$$V_1 \frac{\partial C_1}{\partial t} = V_2 C_2(t) k_{21} + V_3 C_3(t) k_{31} - V_1 C_1(t)(k_{10} + k_{12} + k_{13}) + u(t) \quad (3)$$

$$V_2 \frac{\partial C_2}{\partial t} = V_1 C_1(t) k_{12} - V_2 C_2(t) k_{21} \quad (4)$$

$$V_3 \frac{\partial C_3}{\partial t} = V_1 C_1(t) k_{13} - V_3 C_3(t) k_{31} \quad (5)$$

$$\frac{\partial C_e}{\partial t} = C_1(t) k_{e0} - C_e(t) k_{e0} \quad (6)$$

where u(t) represents the drug infusion rate in the central compartment. This expression defines the pharmacokinetics of the drug. On the other hand, the drug's pharmacodynamics, that represents the BIS in terms of the effect site concentration, is governed by:

$$BIS = f(C_e) \quad (7)$$

The *f* function is usually taken as a EMAX model whose profile suits the described process:

$$\Delta BIS = \Delta BIS_{\max} \frac{C_e^{\gamma}}{C_e^{\gamma} + EC_{50}^{\gamma}}, \quad (8)$$

$$\Delta BIS = BIS - BIS_0, \quad (9)$$

$$\Delta BIS_{\max} = BIS_{\max} - BIS_0. \quad (10)$$

BIS_0 corresponds to the awake state, BIS_{max} represents the minimum achievable BIS and EC_{50} represents the concentration in the effect site for which the effect is half the maximum value, γ represents the sensitivity of the patient to mall concentration variations in the effect site. This parameter can be seen as index that measures the degree of nonlinearity of the model. Normally, the values BIS_0 = 100 and BIS_{max} =0 are assumed.

4. CLOSED LOOP MODELLING WITH PI CONTROL

The basic control strategy in anesthesia is based on a PI controller that uses the BIS as feedback signal (Mendez et al 2006, Reboso et al 2007). The elements of the closed-loop control are (see Figure 9) :

- BIS monitor: in this case, the ASPECT A-2000 monitor is used. This device is serial-connected to the PC to transmit the BIS data obtained from the patient.
- Monitoring and control program: this program runs on a laptop and contains all the implemented control routines. The interface with the rest of devices is through the serial port.
- Infusion pump: this is de actuator device and is governed from the laptop.

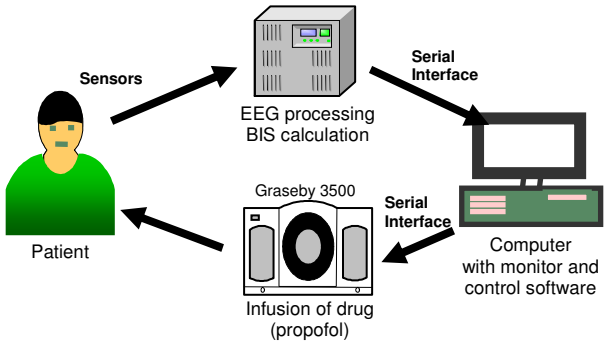

Figure 9: General configuration of the system.

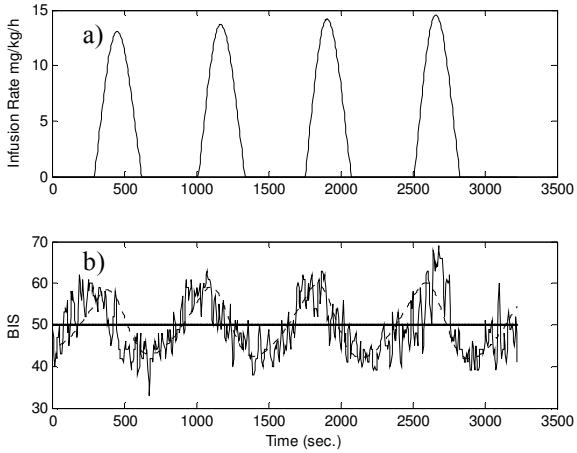

Figure 10: Results from a real experiment with a patient using a PI controller. a) Infusion rate. b) Measured BIS (continuous) vs simulated BIS (discontinuous).

The procedure to start the controller is divided in two steps. First, a manual bolus is applied on the patient to carry him to the BIS target value. Then, the automatic mode of the procedure, based on a PI controller, starts.

In the real proofs, a BIS reference (BISr) of 50 is considered while the measurement and actuation period is 5 seconds. The adjustment of the controller gains was made in a empirical way trying to gate a smooth transitory and a stable response. Once all the security alarms are programmed, real control proofs on patients in operating room were made.

The obtained results were satisfactory due to the hypnosis level of the patient was stabilised around the BIS reference. However, oscillatory behaviour around the target can be observed. In Figure 10 the results of one of the experiment are shown. As can be viewed, the system remains stabilised around the reference value with an oscillation of near ±10 units.

4.1. Model Adjustment

In order to design more advanced controllers, a simulation model was necessary. For this, a physiological model of the patient dynamics was designed. As it was told, the model has two parts: pharmacokinetics and pharmacodynamics. The parameters adjustment was made in simulation.

After obtaining a good adjustment, the values for the pharmacokinetics model are k_{10}=0.006, k_{12}=11.0; k_{21}=14.04, k_{13}=10.02, k_{31}=283.50 and k_{e0}=0.0063. The values for the pharmacodynamics model are EC50=610.0, γ=1.5, BIS_0 =100 and BIS_{max}=0.

To validate the model, the simulated response is compared with the real one. The obtained results, shown in Figure 10b), prove the goodness of the model.

5. TIME DELAY MODELLING

As shown in the previous section, the PI controller usually gives a response with oscillations around the BIS reference value. In this section, the control algorithm is modified in order to compensate these oscillations and get a better transitory. The results shown in this paper are in simulation after having adjusted the patient dynamical model.

The proposal in this work is to improve the performance of the closed-loop system with a compensation of the time-delay present in the system. The origin of this time-delay is the period of time since the infusion pump starts until the drug is distributed along the central compartment. The majority of the works in the literature do not explicitly consider the presence of this time-delay in the models. In fact, in Section III.b, time-delay is not considered in the system model. But in real proofs, some delays between 1 and 2 minutes have to be considered to have a realistic model Under this hypothesis, a time-delay compensator based on the Smith Predictor theory has been proposed to be added to the PI controller (Smith 1973).

As it is well known, the basics of this compensation algorithm consider the formulation of the Smith Predictor for linear systems. To apply the Smith Predictor to the nonlinear model of the patient, a first-order plus a time-delay approximation of the patient model is considered. Thus, the configuration employed in this work can be seen in Figure 11. A delay between 90 and 120 seconds is considered in the simulations. In Figure 12b) the obtained results with the patient of the figure 10 are shown. The evolution of the BIS signal with the Smith Predictor (in solid line) is much better than with the PI controller (in dotted line), and does not show oscillations around the reference BIS value.

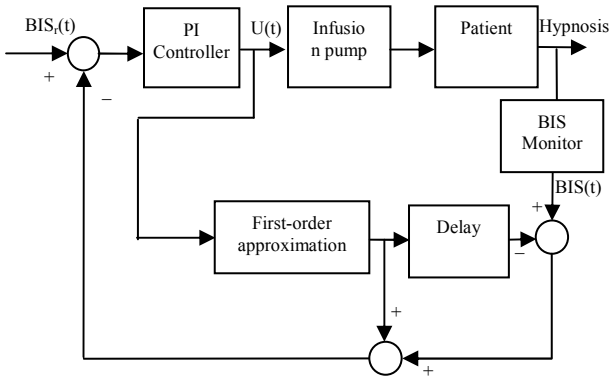

Figure 11: PI Controller with Smith Predictor for patient hypnosis control.

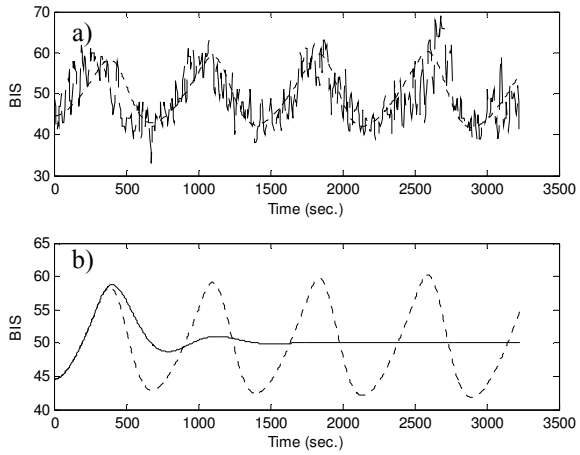

Figure 12: a) Simulated BIS output (dotted) and real patient BIS output (solid) obtained under the action of a PI controller. b) PI controlled output (dotted) and PI with delay-time compensation output (solid).

6. CONCLUSION

This work summarizes the modelling and simulation issues present in anesthesia control. The importance of precise simulation tools was highlighted in the manuscript. To achieve this different modelling alternatives are presented. The methods presented are validated with real data obtained in the operating theatre.

A new modelling approach that takes into account the dead-time present in the process was presented. The benefits of including this delay was evaluated in simulation with a PI control acting the infusion pump. The increase in performance was clear.

ACKNOWLEDGMENTS

. This work was supported in part by the Spanish Government under project DPI2007-64896.

REFERENCES

Chopra, V., 1996, Anaesthesia simulators. *Balliere's Clinical Anesthesiology,* 10:297–315.

Chopra V, Gesink, BJ, de Jong, J, Bovill, J.G., Spierdijk, J. and Brand, R., 1994, Does training on an anaesthesia simulator lead to improvement in performance? *Br J Anaesth* ,73(3):293–7.

George Box, Gwilym M. Jenkins, and Gregory C. Reinsel. 1994, *Time Series Analysis: Forecasting and Control*, third edition. Prentice-Hall.

Helmreich R.L., Schafer H.G., 1998 Turning silk purses into sow's ears: human factors in medicine. In:Henseon LC, Lee AC, editors. *Simulators in anesthesiology education*. New York: Plenum Pres; 1998. p. 1–7.

Marsh B, White M, Morton N, Kenny GNC., 1991, Pharmacokinetic model driven infusion of Propofol in children. *Br J Anaesth*. 67: 41-8.

Méndez, J.A. , Reboso, H., Torres, S., Acosta L., 2006 Modelado y control de la infusión de anestesia intravenosa mediante el índice biespectral, *XXVII Jornadas de Automática*, Almeria.

Reboso J.A., Méndez J.A., Esteban J.L., Torres S., Acosta L., Gonzalez-Miranda F.., 2007, Design of a Closed Loop Controller for Intravenous Anesthesia with Propofol, *First World Congress of Total Intravenous Anesthesia-TCI*, Venecia, Italia.

Schnider, T.W., Minto C.F., Gambus P.L., Anderson C., Goodale D.B., Shafer S.L. and Youngs E.J., 1998, The Influence of method of administration and covariates on the pharmacokinetics of propofol in adult volunteer, *Anesthesiology*, 88:1170–1182.

Smith, C., 1973, *Digital Computer Process Control*. Intext Education Publishers. Scranton PA.

Struys; De Smet; Depoorter; Versichelen; Mortier; Dumortier; Shafer; and Rolly, 2000, Comparison of plasma compartment versus two methods for effect compartment-controlled target controlled infusion for Propofol, *Anesthesiology* 92(2):399–406.

AUTHORS BIOGRAPHY

Juan Albino Méndez was born in 1970. He received the MS Degree in Applied Phisycs in 1993 from the Universidad de La Laguna , Spain, and the PhD Degree in Computer Science in 1998 from Universidad de La Laguna. His areas of research are Control Engineering and Robotics. He has worked in the development of efficient predictive control algorithms and its applications in robotic manipulators and autonomous robot guided vehicles. From 2003 he is involved in the development of efficient algorithms for Anesthesia Automation

Hector Reboso graduated in telecom engineering in 1995. From 2001 has been working as an associate professor in the Departamento de Ingeniería de Sistemas y Automática y Arquitectura y Tecnología de Computadores at the Universidad de La Laguna. He is also responsible of the Telecommunications Department in Cajacanarias Bank. His areas of interest include Engineering Control and Robotics.

José Antonio Reboso graduated in medicine in 1988. applied physics in 1997 and received his M.S. From 1993 he has been working as an anesthetist in the Hospital Universitario de Canarias and in the Hospital Nuestra Señora de la Candelaria. Currently he is working in the Department of Anestehsilogy in the Hospital Universitario de Canarias. His areas of interest include Anesthesia Automation.

Santiago Torres graduated in applied physics in 1997 and received his M.S. degree in applied physics in 1999 from the Universidad de La Laguna, Tenerife, Spain. He graduated in electronic engineering in 2004. He is an Associate Professor in the Departamento de Ingeniería de Sistemas y Automática y Arquitectura y Tecnología de Computadores at the same university. His areas of interest include Engineering Control and Robotics.

PCA FILTER FOR SZINTIGRAPHIC IMAGING

Werner Backfrieder[(a)], Martin Forster[(b)], Wilma Maschek[(c)]

[(a)] Department of Software Engineering, University of Applied Sciences Upper Austria, Hagenberg, Austria
[(b)]Centre of Biomedical Engineering and Physics, Medical University of Vienna, Vienna, Austria
[(c)]Institute of Nuclear Medicine and Endocrinology, General Hospital of Linz, Linz, Austria

[(a)]Werner.Backfrieder@fh-hagenberg.at, [(b)]Martin.Forster@meduniwien.ac.at, [(c)]Wilhelmine.Maschek@akh.linz.at

ABSTRACT
Quality of image data in nuclear medicine diagnostics is mainly limited by radioactive dose and acquisition time, both yielding low total counts. There are studies with a maximum pixel count of 10 in a frame, thus signal-to-noise-ratio (SNR) is very poor. A novel data driven method was developed to enhance SNR but preserving underlying image features. In contrast to traditional filtering methods calculation of smoothed image data is not based to a region surrounding the pixel, but image structures are separated from noise using a simple statistical model. The signal is reconstructed from principal components images (PCI) and the amount of noise is assessed by chi^2 statistics. With this method even fine structures are preserved. The potential of the novel technique is demonstrated with in vivo data from perfusion and Parkinson studies. After removal of heavy noise, enhanced image are subject to sophisticated image processing, as automated inter-modality image registration.

Keywords: PCA, SPECT, image registration, data driven filter

1. INTRODUCTION

Szintigraphic imaging in nuclear medicine is a major diagnostic tool for tumour staging and visualisation of metabolism. A radioactive tracer is applied to the bloodstream and its further distribution within the organism is visualized as projection images acquired by a gamma-camera. There are several methods of diagnostic imaging. Simple dynamic planar imaging, a series of image frames is acquired to assess metabolic function in time, e.g. clearance studies of kidneys. The specific binding of radiopharmaceuticals to tumour cells is manifested as tracer accumulation observed as hot spots in szintigrams. The hot spots are mostly related to malignant changes in tissue. Standardized uptake values (SUV) determined from pixel counts in lesions are an important indicator for tumour staging. SUVs are assessed from both planar szintigraphic images and axial slices in Single Photon Emission Computed Tomography (SPECT).

The quality of image data is closely related to the number of counts detected, since the physical effects during the life-time of a gamma-quant, e.g. generation, absorption, scatter and registration, are subject to Poisson statistics. For a high number of counts this statistics corresponds to a Gaussian distribution. Major delimiting factors to achieve sufficient counts are low activity to prevent the patient from high dose exposure and acquisition time, mostly patients are not able to keep still for longer than 30 minutes. In some acquisition protocols, e.g. diagnosis of Parkinson's disease after administration of beta-CIT, count rates are extremely low. Even in studies with 40s acquisition time per projection, maximum pixel count within the lesion is below 10, yielding very poor SNR or low contrast in image data.

Since the early eighties the improvement of SNR or contrast enhancement is subject to various approaches in Nuclear Medicine image processing. Methods range from data processing in the wavelet domain (Millet et al. 2000, Erlandsson et al. 2006) to complex learning strategies for dynamic update of the filter response (Mondal et al. 2006). The sophisticated application of linear time invariant kernels in a multi-filter approach for brain imaging (Poline and Mazoyer 1994), the filtering of long time series in renography (Shields et al. 1995), or the optimisation of Butterworth kernels (Honda et al. 1987) demonstrate the broad scope of methods. Data driven methods are based on general assumptions leading to flexible optimization criteria (Hull et al. 1990, Nagayoshi et al. 2005). Reconstruction of the signal from orthogonal components and simultaneous separation from noise is a promising approach (Liow and Strother 1994, Hermansen and Lammertsma 1996), further developed of the method is described in this paper.

The presented approach aims in reconstructing the signal from a number of orthogonal image layers, i.e. the principal components images, until the remaining data is identified as noise. This method yields accurate separation of signal from noise, immanently smoothing data and preserving edges. The proposed method allows further sophisticated data modelling and image processing, even on very poor raw data.

2. METHOD

A projection frame acquired by a head of a gamma-camera usually is a squared N by N matrix. Each matrix element is the sum of gamma-quanta registered at the

respective detector position, during the acquisition interval. This projection value is the number of gamma-quanta emitted along the line of response, i.e. a cone shaped section of the patient, whose symmetry axis is perpendicular to the surface of the detector. As a first pre-processing step the image frame is partitioned into squared tiles of *np* pixels, each. The idea of the algorithm is, to calculate from this set of tiles orthogonal base images, where each tile can be reconstructed as weighted sum from the base images. Since the higher order base images mainly represent noise, the suppression of noise is accomplished by assessing a sufficient number of components to reconstruct the particular signal. Standard Principal Components Analysis is performed for calculation of base images from data. The tiles are rearranged into row vectors with *np* elements. Data matrix *D* comprises these vectors, matrix size is *[M x np]*, where *M* is the number of tile-vectors. Data are decomposed by principal components analysis (PCA)

$$D = I \cdot PC^T , \qquad (1)$$

where *PC* are the Principal Components (PCs) of the correlation matrix $C = D^T D$. PCs are the eigenvectors of *C* weighted by the square root of the corresponding eigenvalues. Eigenvectors build a vector base *V*, where the correlation matrix *C* is diagonal $C = V\lambda V^T$. The columns of the transform matrix comprise the eigenvectors; λ is a diagonal matrix with the eigenvalues as diagonal elements. Matrix *I* has size *[M x np]* and consists of principal components images, which are determined by regression from tile-data

$$I = D \cdot PC \cdot (PC^T \cdot PC)^{-1} . \qquad (2)$$

The full number of PCs exactly reconstructs the observed data, i.e. the *i-th* row of Matrix *D*, representing tile number *i*, is reconstructed as weighted sum of all PCs

$$D_i = \sum_{j=1}^{np} I_{ij} PC_j \ . \qquad (3)$$

A reduction of the number of components to $P<np$, will approximate, i.e. smoothen the image (Backfrieder et al. 1996, Samal et al. 1999). For each tile the number of components, representing the underlying signal, is determined by a chi^2 test. The signal is reconstructed as an increasing sum of components, weighted by the corresponding factors I_{ij}, until a confidence level of $\alpha=0.95$ is reached, according to a chi^2 distribution with *np-1* degrees of freedom. This means the deviations of the reconstructed from the observed distribution are purely random, thus the signal is separated from noise. This method provides a structure preserving filter, even for image data with very poor SNR.

3. MATERIAL

Representative in vivo image data were acquired with two different protocols; a perfusion study to identify brain regions affected by ischemia after stroke and a beta-CIT study for diagnosis of Parkinson's disease. For both studies a standard brain SPECT acquisition protocol was implemented on a triple head IRIX system (Philips Healthcare, Hamburg, Germany): circular orbit with 3^o angular steps over 360^o. Projection matrix is 128x128, with 2.33mm isotropic pixel size. Acquisition time is 40s / projection, i.e. 26 min study duration. The system is equipped with a LEHR-PAR collimator. The administered dose is 185 MBq I123 for Parkinson and 740 MBq Tc99m for perfusion.

Specific binding of beta-CIT is extremely low; data are suffering from extremely poor SNR. Edge preserving PCA filtering is applied for enabling further processing of image data in general.

The aim of perfusion studies is to accurately identify ischemic areas of the cortex. SPECT studies are restricted to functional information; morphological structures are provided by magnetic resonance imaging (MRI). Hybrid MRI-SPECT cameras are not available, thus registration of both modalities is a software procedure, implying sufficient detail in respective images, provided by PCA filtering.

4. RESULTS

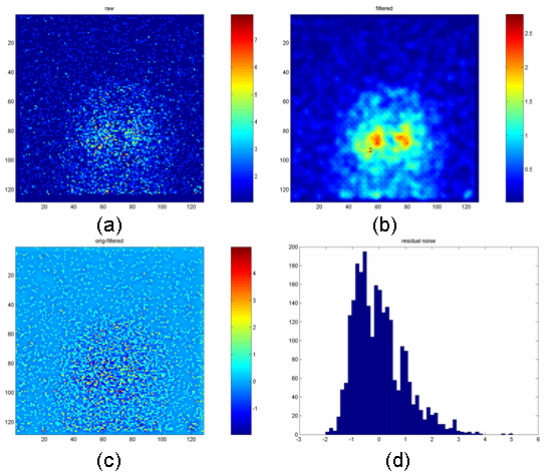

Figure 1: Raw projection data (a), PCA filtered signal with 95% confidence level (b), noise (c), histogram of noise (d).

The potential of the method for proper separation of signal from noise, i.e. structure preserving image enhancement, is demonstrated by filtering in vivo image but data of perfusion and beta-CIT studies. One acquired raw projection image of a beta-CIT study is shown in Figure 1 on the upper left. Accumulation of the marker at the basal ganglia is hardly manifested. At the upper right the PCA filtered image with confidence level 95% shows proper detail implying sufficient specific binding of the marker. Note the two

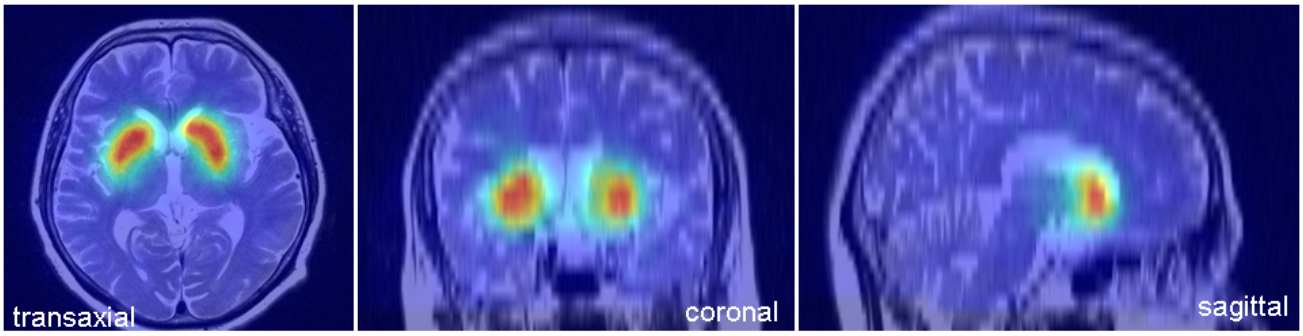

Figure 2: Fusion of beta-CIT SPECT and MRI in a Parkinson study. Tracer accumulation at basal ganglia is shown in the axial, coronal and sagittal plane.

tiny spots below the left ganglion are preserved by the method. The image at the lower left shows the noise component yielded by subtraction of the filtered image from raw data. The Poisson-shaped histogram of the noise is shown at the lower right.

Axial slices were reconstructed from PCA filtered projections by a fully 3D iterative ML-EM algorithm, implementing spatially variant line of response (Backfrieder et al. 2003, Backfrieder et al. 2005).

Image enhancement by PCA filtering preserves enough detail to allow further problem oriented, sophisticated image processing. For diagnosis of Parkinson's disease the specific binding of beta-CIT at the basal ganglia is an important indicator for a negative finding. Since SPECT images provide functional but no morphological information, verification of the correct localisation needs complementary information from MRI. To achieve reliable and clinical objective results, data have to be subject to an automated registration method. The overlay of a beta-CIT SPECT and MRI is shown in Figure 2 in the main three radiological sections. As an automated registration procedure Chamfer matching; a head-hat iterative matching method is applied. The algorithm minimizes the total distance between corresponding surfaces. PCA filtering of SPECT images preserves enough structural detail for robust matching of both modalities. The correct localisation of the marker at basal ganglia and the bean shaped nucleus caudatus are clearly shown.

Results of a perfusion study are shown in Figure 3 in a three panel display. The left column shows the base modality, in the central column the overlay of MRI and SPECT is displayed, and in the right column the matching volume is shown. The respective rows of Figure 3 show axial, coronal, and sagittal sections. An interactive pointer centres sections in connected views, simultaneously providing information as localisation and pixel value. The method yields accurate registration of perfusion studies as demonstrated by the three panel view. The SPECT image exactly fits into the brain cavity, as shown by the MRI image series. Perfusion is directly correlated to morphology.

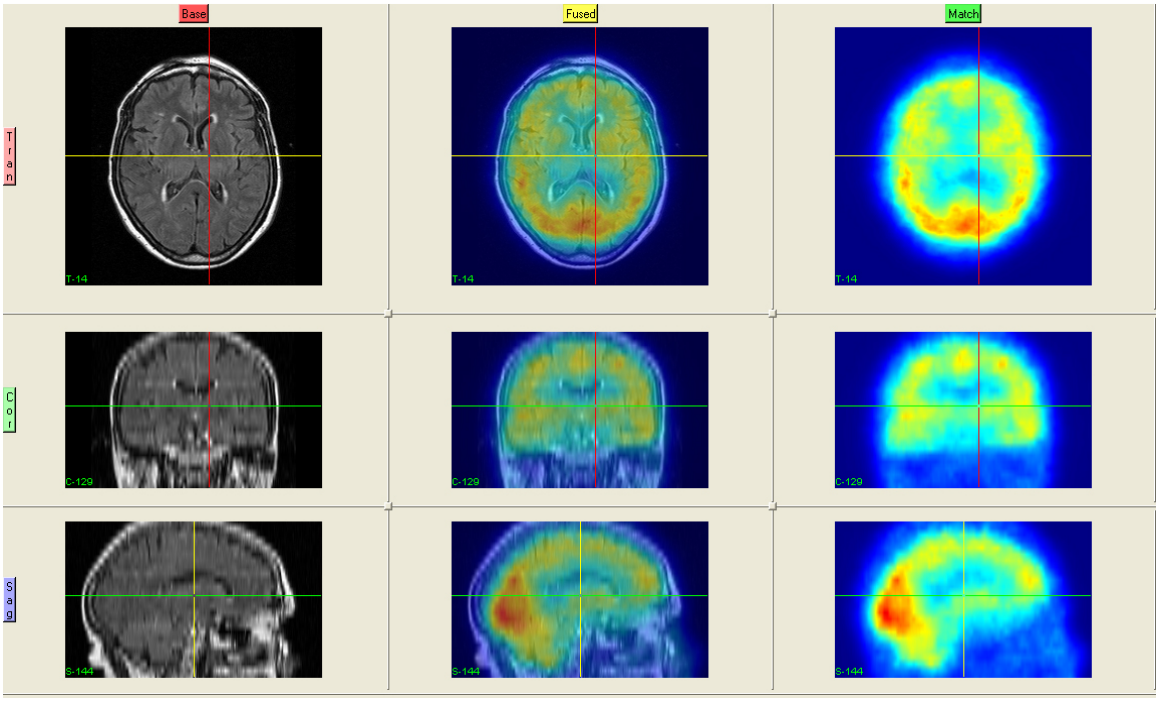

Figure 3: Three panel display of a multi modal MRI –SPECT perfusion study.

5. DISCUSSION

A novel method for structure preserving noise reduction was developed. The accuracy of the method was demonstrated on in-vivo data. This sophisticated method of data smoothing allows preprocessing of szintigraphic images proper for further complex investigations. Especially quantitative nuclear medicine and multi-modality studies are of certain interest in modern differential diagnosis. Especially the joint utilization of mutual information from emission tomography and MRI, as long as there are no clinical hybrid systems available, imposes high quality standards on image data. To achieve objective results data have to be subject to automated registration methods, which are very sensitive in terms of data quality.

PCA bases on the assumption of Gaussian noise, which not exactly models the statistics of low count images. As further development implementation of independent components would exactly address the Poisson model.

There are practical implications of the method, too. Since effective noise reduction enhances SNR, the same image quality is achieved compared to unprocessed raw data by either less acquisition time or less administration of radiopharmaceuticals. Reduction of acquisition time means higher patient throughput, accordingly a more efficient usage of the scanner. Reduction of administered activity is a direct reduction of costs per examination. Furthermore radioactive dose exposure of the patient is decreased, in both cases.

REFERENCES

Backfrieder, W., Baumgartner, R., Samal, M., Moser, E., Bergmann, H. 1996. Quantification of intensity variations in functional MR images using rotated principal components. *Physics in Medicine and Biology* 41: 1425-1438

Backfrieder, W., Forster, M., Engelbrecht, G., Benkner, S., 2003. Locally variant VOR in fully 3D SPECT within a service oriented environment. *F. Valafar, H. Valafar (Eds.), Proc. Int. Conf. on Mathematics and Engineering Techniques in Medical and Biological Sciences (METMBS)*, ISBN 1-932415-04-1: (2003) pp. 216-221

Backfrieder, W., Forster, M., Engelbrecht, G., Benkner, S., Maschek, W., 2005. Fully 3D SPECT reconstruction in a Grid architecture. *EJNM* 32, Sept 2005: S103

Erlandsson, K., Jin, Y., Wong, A.T., Esser, P.D., Laine, A.F., Ogden, R.T., Oquendo, M.A., van Heertum, R., Mann, J.J., Parsey, R.V. 2006. Quantitative wavelet domain image processing of dynamic PET data. *Conf Proc IEEE Eng Med Biol Soc.* 1:2787-90.

Hermansen, F., Lammertsma, A.A., 1996. Linear dimension reduction of sequences of medical images: III. Factor analysis in signal space. *Phys Med Biol* 41(8):1469-81.

Honda, N., Machida, K., Tsukada, J., Kaizu, H., Hosoba, M., 1987. Optimal preprocessing Butterworth-Wiener filter for Tl-201 myocardial SPECT. *Eur J Nucl Med* 13(8):404-7.

Hull, D.M., Peskin, C.S., Rabinowitz, A.M., Wexler, J.P., Blaufox, M.D., 1990. The derivation and verification of a non-stationary, optimal smoothing filter for nuclear medicine image data. *Phys Med Biol* 35(12):1641-62.

Liow, J.S., Strother, S.C., 1994. Noise and signal decoupling in maximum-likelihood reconstruct-tions and Metz filters for PET brain images. *Phys Med Biol* 39(4):735-50.

Millet, P., Ibáñez, V., Delforge, J., Pappata, S., Guimón, J., 2000. Wavelet analysis of dynamic PET data: application to the parametric imaging of benzodiazepine receptor concentration. *Neuroimage* 11(5 Pt 1): 458-72.

Mondal, P.P., Rajan, K., Ahmad, I., 2006. Filter for biomedical imaging and image processing. *J Opt Soc Am A Opt Image Sci Vis.* 23(7): 1678-86.

Nagayoshi, M., Murase, K., Fujino, K., Uenishi, Y., Kawamata, M., Nakamura, Y., Kitamura, K., Higuchi, I., Oku, N., Hatazawa, J., 2005. Usefulness of noise adaptive non-linear gaussian filter in FDG-PET study. *Ann Nucl Med.* 19(6):469-77.

Poline, J.B., Mazoyer, B.M., 1994. Enhanced detection in brain activation maps using a multifiltering approach. *J Cereb Blood Flow Metab* 14(4):639-42.

Samal, M., Karny, M., Benali, H., Backfrieder, W., Todd-Pokropek, A., Bergmann, H. 1999. Experimental comparison of data transformation procedures for analysis of principal components. *Physics in Medicine and Biology* 44 (11): 2821-34

Shields, M.E., Farison, J.B., Miller, J.W., 1995. SD filtering for enhancement of a nuclear medicine image sequence. *Biomed Sci Instrum* 31:195-200.

AUTHORS BIOGRAPHY

Werner Backfrieder received his degree in Technical Physics at the Vienna University of Technology in 1992. Then he was with the Department for Biomedical Engineering and Physics at the University of Vienna, where he focused his research on Medical Image Processing and Medical Physics, since 2002 he is Professor for Medical Imaging at the University of Applied Sciences Upper Austria.

Martin Forster, has received his Master degree at the Vienna University of Technology in 2003, and is working on his PHD thesis on medical grid computing.

Wilma Maschek received her MD at the University of Vienna in 1973. Since 1993 she is head of the Department of Nuclear Medicine and Endocrinology at the General Hospital Linz. In 2003/04 she was president of the Austrian Society of Nuclear Medicine.

PRIMOS: AN INTEGRATED PLATFORM FOR EXPLORING PROTEIN-PROTEIN INTERACTIONS

Thomas Kern [(a)], Michael Kommenda [(b)], Viktoria Dorfer[(c)], Johann W. Bauer [(d)], Kamil Önder [(e)]

[(a, b, c)] Upper Austria University of Applied Sciences, Softwarepark 11, 4232 Hagenberg Austria
[(d,e)] Paracelsus Medical Private University, Department of Dermatology, Müllner Hauptstraße 48, 5020 Salzburg Austria

[(a)]Thomas.Kern@fh-hagenberg.at, [(b)]Michael.Kommenda@fh-hagenberg.at, [(c)]Viktoria.Dorfer@fh-hagenberg.at, [(d)]Jo.Bauer@salk.at, [(e)] Kamil.Oender@sbg.ac.at

ABSTRACT
The knowledge of protein-protein interactions (PPIs) is of prominent importance for modelling cellular processes, understanding of diseases and functional interpretation of post-genomic data. However, it is an elaborate task to obtain knowledge for specific proteins because it is spread over several databases. The Protein Interaction and Molecule Search (PRIMOS) platform integrates PPI data from several major PPI databases and thus eases knowledge acquisition considerably. Data integration is accomplished by mapping every interacting protein to its corresponding protein in UniProt, which makes the different PPI datasets comparable and allows detecting both congruent and conflicting information. Every imported PPI is reassessed by a homology-based validation scheme, which helps scientists to distinguish between trustworthy PPIs and false-positive PPIs that are frequently contained in today's PPI databases. The integrated dataset can be explored through a sophisticated Web interface and can be visualized within the PRIMOS Interaction Viewer. PRIMOS is publicly available online at http://primos.fh-hagenberg.at.

Keywords: protein-protein interaction, PPI validation, PPI viewing, PPI search, PRIMOS, BIOMIS, data integration, data reassessment, bioinformatics, bio database

1. INTRODUCTION

In the post-genomic era more and more scientists focus their research on proteins and their interactions. Along with the overwhelming amount of interaction data produced by high-throughput experiments arose the need for databases that store and process this data (Xenarios et al. 2001). Several databases focusing on protein-protein interactions (PPIs) have therefore been developed, for instance IntAct (Kerrien et al. 2007a), MINT (Chatr-aryamontri et al. 2007), HPRD (Mishra et al. 2006), BIOGRID (Breitkreutz et al. 2008), BIND (Alfarano et al. 2005), DIP (Salwinski et al. 2004) and MIPS (Mewes et al. 2007). Although each of these databases handles PPI data it is often laborious to pinpoint potentially relevant interactions of a specific protein due to heterogeneous data contained in the different databases (Mathivanan et al. 2006). Multiple databases have to be queried and their knowledge combined manually to ensure no information is overlooked. The task is further complicated by the fact that every database uses its own naming and identifier scheme.

Another problem with PPI data sets is the poor quality of high-throughput experiments (Sprinzak et al. 2003; Deane et al. 2002). This leads to large amounts of biologically irrelevant PPIs in current PPI databases (Edwards et al. 2002). Despite the fact that various computational PPI prediction and validation tools have been developed, the most significant evidence for a PPI's relevance is still its multiple detection by different experimental methods (von Mering et al. 2002). Nevertheless, computational PPI validation tools are extremely useful in cases where PPIs were detected by a single experiment only. Therefore data integration is key to high quality and more complete PPI data. Other integrated PPI databases developed recently are APID (Prieto et al. 2006) and MiMI (Jayapandian et al. 2002). However, we want to clearly distinguish our integrated PPI database through having a more up to date data, all PPIs validated and an easy to use search interface.

PRIMOS integrates several PPI datasets and thus eases and speeds up knowledge acquisition considerably. The data integration process removes redundancy and merges related entries, which results in significantly better data quality. Moreover, PRIMOS reassesses every PPI to allow an estimate of its quality. The integrated dataset can be queried for proteins and PPIs by the identifiers or names of the source databases and supersedes memorizing different identifier and naming schemes. PRIMOS offers sophisticated search and filter capabilities to retrieve research relevant information as easy as possible. In addition, PRIMOS integrates PPI data with disease related information and thus helps scientist to gain insights into disease relevant PPI networks. The graphical representation of PPI networks by the PRIMOS Interaction Viewer allows getting the bigger picture of how proteins interact with each other.

2. DATABASE CONTENT AND METHODS

PRIMOS imports 379,038 proteins from UniProt (Consortium 2008) and 384,127 physical binary PPIs from several PPI databases (Table 1).

Table 1: Number of imported PPIs from each source database

Source database	# PPIs
BIND	32,221
DIP	56,491
HPRD	76,145
IntAct	104,598
MINT	104,847
MIPS	9,835
Total	384,127

Supplementary information about proteins and interactions comprises GO (Ashburner et al. 2000) and PSI-MI Controlled Vocabulary (Orchard et al. 2005), NCBI Taxonomy (Wheeler et al. 2008) and OMIM (Hamosh et al. 2005).

2.1. Data Integration

At present most PPI databases support the PSI-MI XML v2.5 data interchange format (Kerrien et al. 2007b), which reduces the effort of handling diverse source data formats. Genetic interactions and protein complexes interactions are filtered out and only physical binary PPIs are imported.

The unification of the PPIs allows comparison of the different datasets.

The data integration process results in a lot of duplicate PPIs in the combined dataset. These duplicates must be detected and merged to a single PPI. PPIs are treated as duplicates if the two interacting UniProt proteins are the same in both PPIs. For every combination of two interacting UniProt proteins a unique PRIMOS interaction ID is assigned to provide stable identifiers, having the information from the source databases attached to this interaction.

The whole data integration process results in 196,702 PRIMOS PPIs from 384,127 source PPIs, which implies a reduction of the source datasets of 48.79 %. The overlap statistic between the different source databases shows the benefit of the integration, because about 2/3 of the PPIs are delivered by only one source database. Needless to say there is no overlap between HPRD and MIPS because these are organism specific PPI database.

2.2. Data Reassessment

Recent studies report a high false-positive rate of high-throughput experiments for PPI detection (Mathivanan et al. 2006; Sprinzak et al. 2003; Deane et al. 2002; Edwards et al. 2002; von Mering et al. 2002). Therefore PRIMOS reassesses all integrated PPIs by a novel homology-based validation scheme and categorizes the PPIs in high, medium and low confidence PPIs. This strategy utilizes remote homolog definitions detected by FASTA (Pearson and Lipman 1988) and PSI-BLAST (Altschul et al. 1997).The validation strategy greatly benefits from the large pool of PPIs available in PRIMOS.

PRIMOS also allows validation of PPIs that are not included in the database (Frech et al. 2009). To validate an experimentally observed PPI, we combine FASTA and PSI-BLAST to perform a sensitive sequence-based search for pairs of interacting homologous proteins within a large, integrated PPI database. A novel scoring scheme that incorporates both quality and quantity of all observed matches allows us to consider also tentative paralogs and orthologs in this analysis and to combine search results from more than one homology detection method. ROC curves (Frech et al. 2009) illustrate the high efficacy of this approach and its improvement over other homology-based validation methods. This validation service is free of charge and publicly available.

3. DATABASE ACCESS

The database content of PRIMOS is freely available online at http://primos.fh-hagenberg.at. PRIMOS has numerous search and filter options to view the content of the database, which are briefly described in the following.

3.1. Protein Search

The interface of the protein search was designed to be as simple as possible to ease the task of finding relevant proteins for researchers. Every protein whose UniProt accession, PRIMOS identifier, protein name, gene name or NCBI GeneID matches the entered text is shown in the results. Additionally if the ‘include cross references in search’ checkbox is checked, the search space is extended to every cross reference delivered by UniProt (i.e. Ensembl ID, GenBank ID, …).

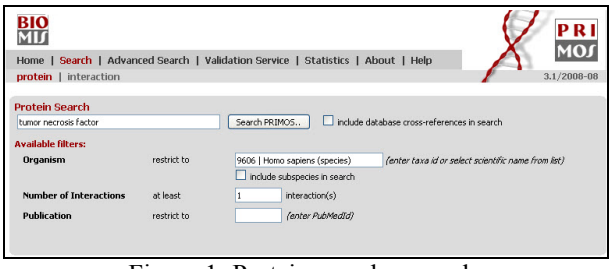

Figure 1: Protein search example

Several filters are available to reduce the number of returned proteins. It is possible to restrict the search results to a specific organism or lineage, to proteins being involved in at least a specific number of interactions, or to proteins occurring in a specific publication. These filters can be combined independently. For instance, to search for all human interacting proteins in PRIMOS, choose ‘9606 | Homo sapiens’ as organism filter and ‘1’ as minimum number of interactions. The detailed information about one of

the 11,201 returned proteins is shown by clicking on the PRIMOS protein ID.

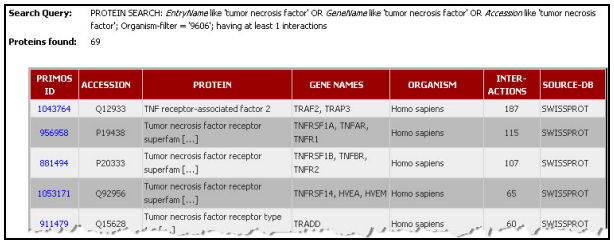

Search Query: PROTEIN SEARCH: *EntryName* like 'tumor necrosis factor' OR *GeneName* like 'tumor necrosis factor' OR *Accession* like 'tumor necrosis factor'; Organism-filter = '9606'; having at least 1 interactions

Proteins found: 69

PRIMOS ID	ACCESSION	PROTEIN	GENE NAMES	ORGANISM	INTER-ACTIONS	SOURCE-DB
1043764	Q12933	TNF receptor-associated factor 2	TRAF2, TRAP3	Homo sapiens	187	SWISSPROT
956958	P19438	Tumor necrosis factor receptor superfam [...]	TNFRSF1A, TNFAR, TNFR1	Homo sapiens	115	SWISSPROT
881494	P20333	Tumor necrosis factor receptor superfam [...]	TNFRSF1B, TNFBR, TNFR2	Homo sapiens	107	SWISSPROT
1053171	Q92956	Tumor necrosis factor receptor superfam [...]	TNFRSF14, HVEA, HVEM	Homo sapiens	65	SWISSPROT
911479	Q15628	Tumor necrosis factor receptor type [...]	TRADD	Homo sapiens	60	SWISSPROT

Figure 2: Protein query results

Another example is shown in Figures 1-3. Here the search is restricted to human proteins that contain 'tumor necrosis factor' within their name (Figure 1). The matching proteins are listed in a tabular style (Figure 2). Every column is sortable by clicking on the column header. The details for TNR1A_HUMAN – 'tumor necrosis factor receptor superfamily member 1A precursor' are displayed by selecting the protein (Figure 3).

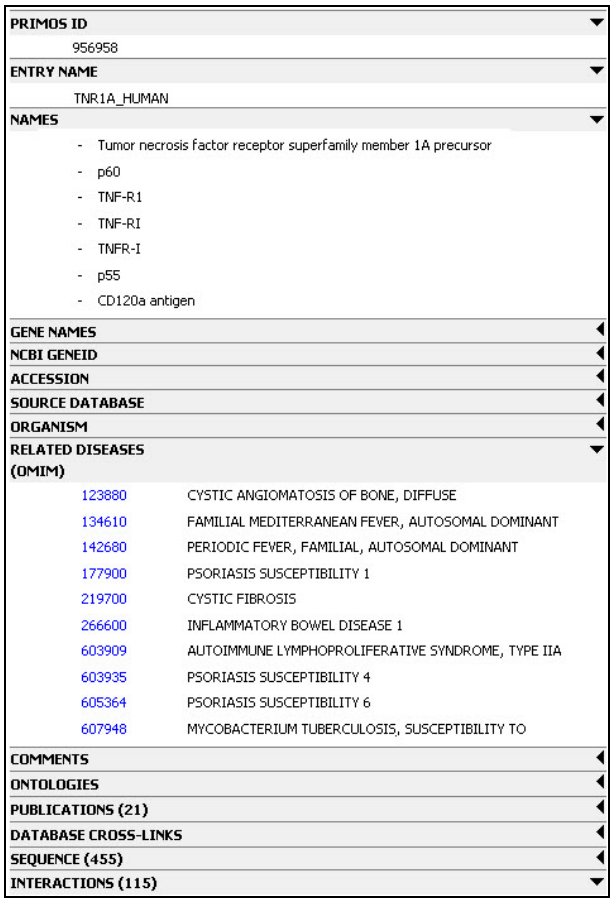

PRIMOS ID

956958

ENTRY NAME

TNR1A_HUMAN

NAMES

- Tumor necrosis factor receptor superfamily member 1A precursor
- p60
- TNF-R1
- TNF-RI
- TNFR-I
- p55
- CD120a antigen

GENE NAMES

NCBI GENEID

ACCESSION

SOURCE DATABASE

ORGANISM

RELATED DISEASES (OMIM)

123880	CYSTIC ANGIOMATOSIS OF BONE, DIFFUSE
134610	FAMILIAL MEDITERRANEAN FEVER, AUTOSOMAL DOMINANT
142680	PERIODIC FEVER, FAMILIAL, AUTOSOMAL DOMINANT
177900	PSORIASIS SUSCEPTIBILITY 1
219700	CYSTIC FIBROSIS
266600	INFLAMMATORY BOWEL DISEASE 1
603909	AUTOIMMUNE LYMPHOPROLIFERATIVE SYNDROME, TYPE IIA
603935	PSORIASIS SUSCEPTIBILITY 4
605364	PSORIASIS SUSCEPTIBILITY 6
607948	MYCOBACTERIUM TUBERCULOSIS, SUSCEPTIBILITY TO

COMMENTS

ONTOLOGIES

PUBLICATIONS (21)

DATABASE CROSS-LINKS

SEQUENCE (455)

INTERACTIONS (115)

Figure 3: Part of detailed protein information

3.2. PPI Search

Interactions can be searched by the PRIMOS interaction ID, by an external ID from one of the source databases, or by the PPI's publications. In addition, PPIs can be searched by their interacting proteins. Here, almost the same filter options are available as in the protein search. Additionally, the minimum number of different experimental methods and the calculated confidence of the interaction can be specified. If there is only one matching interaction, the interaction detail page shows up automatically. Otherwise, the result is displayed in a list, covering the core information about the interactions.

The crosstalk interaction search enables researchers to find interactions between two different organisms and optionally filters these interactions for specific interaction detection methods. Because of unreliable experimental results of some interaction detection methods, the confirmed interaction search, another advanced search method, shows interactions which have been detected by more than one detection method. These interactions are more reliable due to confirmation through independent, multiple experiments.

3.3. Advanced Search

The most important advanced search method reveals the connections between diseases and proteins or interactions, respectively. For the disease search, it is possible to specify the name of a disease or directly its OMIM ID. All matching diseases and the corresponding proteins or interactions are listed. This feature helps scientists to discover new drug targets or disease related sub networks via the linkage between proteins, their interactions and diseases (Chen et al. 2006).

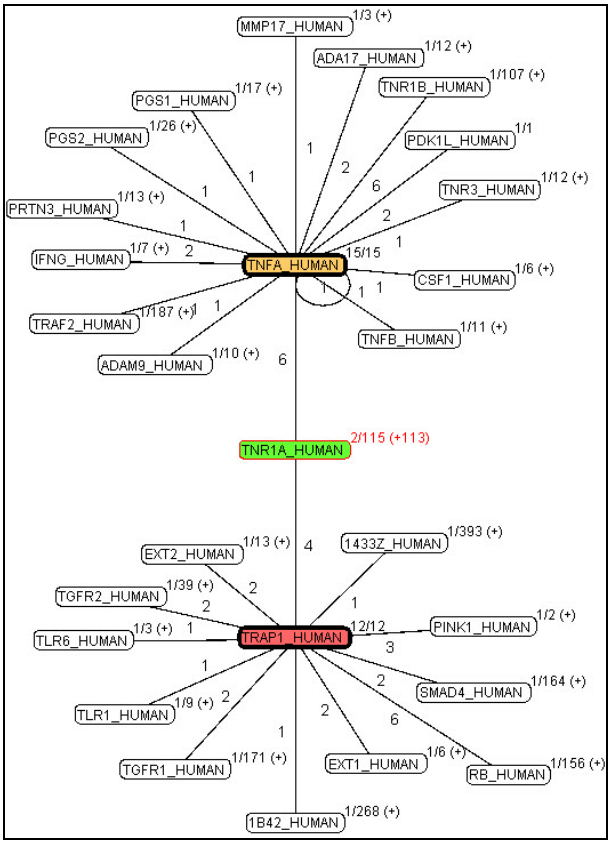

Figure 4: Part of a PPI network in the PRIMOS interaction viewer

3.4. PRIMOS Interaction Viewer

Graphical presentations provide a more intuitive way for exploration and understanding of interaction networks. Embedded into the PRIMOS user interface, an interactome browser with links to PRIMOS detail pages as well as automated network expansion and filtering options can be used for further network analysis. An example for the interaction viewer is shown in figure 4, where different experimental methods and proteins are highlighted. The numbers next to the proteins provide information about their already visible and total number of interactions.

4. CONCLUSIONS

Knowledge of PPIs is the key to understanding cellular processes. The PRIMOS platform operates as a sophisticated knowledge portal for analysing protein-protein interaction data and more complex search options for diseases and their relationships to proteins and interactions. It currently integrates PPI data from six major PPI databases and detects both congruent and conflicting information. All imported PPIs are reassessed and categorized by a novel homology-based validation scheme. Additionally the interaction viewer can be started for every interacting protein within PRIMOS. Interaction networks are represented as graphs in which the nodes are the proteins and the edges are the interactions between these proteins.

ACKNOWLEDGMENTS

The development of PRIMOS is carried out at the Upper Austria University of Applied Sciences (UAS), School of Informatics, Communications and Media in Hagenberg (AUSTRIA) as an FHplus structure setup activity. FHplus is a research program funded by two Austrian ministries and organized by the Austrian Research Promotion Agency (FFG) to setup and enhance R&D capacity and competence in Austrian UAS.

REFERENCES

Alfarano,C., Andrade,C.E., Anthony,K., Bahroos,N., Bajec,M., Bantoft,K., Betel,D., Bobechko,B., Boutilier,K., Burgess,E. et al. 2005. The biomolecular interaction network database and related tools 2005 update. *Nucleic Acids Res.,* 33, D418–D424.

Altschul,S.F., Madden,T.L., Schäffer,A.A., Zhang,J., Zhang,Z., Miller,W. and Lipman,D.J. 1997. Gapped blast and psi-blast: a new generation of protein database search programs. *Nuceic Acids Res.,* 25, 3389-3402.

Ashburner,M., Ball,C.A., Blake,J.A., Botstein,D., Butler,H., Cherry,J.M., Davis,A.P., Dolinski,K., Dwight,S.S., Eppig,J.T. et al. 2000. Gene ontology: tool for the unification of biology. the gene ontology consortium. Nat. Genet., 25, 25–29.

Breitkreutz,B.-J., Stark,C., Reguly,T., Boucher,L., Breitkreutz,A., Livstone,M., Oughtred,R., Lackner,D.H., Bähler,J., Wood,V., Dolinski,K. and Tyers,M. 2008. The biogrid interaction database: 2008 update. *Nucleic Acids Res.,* 36, D637–D640.

Chatr-aryamontri,A., Ceol,A., Palazzi,L.M., Nardelli,G., Schneider,M.V., Castagnoli,L. and Cesareni,G. 2007. Mint: the molecular interaction database. *Nucleic Acids Res.,* 35, D572–D574.

Chen,J.Y., Shen,C. and Sivachenko,A.Y. 2006. Mining alzheimer disease relevant proteins from integrated protein interactome data. *Pac. Symp. Biocomput.,* pp. 367–378.

Consortium,U. 2008. The universal protein resource (UniProt). *Nucleic Acids Res.,* 36, D190–D195.

Deane,C.M., Salwinski,L., Xenarios,I. and Eisenberg,D. 2002. Protein interactions: two methods for assessment of the reliability of high throughput observations. *Mol. Cell. Proteomics,* 1, 349–356.

Edwards,A.M., Kus,B., Jansen,R., Greenbaum,D., Greenblatt,J. and Gerstein,M. 2002. Bridging structural biology and genomics: assessing protein interaction data with known complexes. *Trends Genet.,* 18, 529–536.

Frech C., Kommenda M., Dorfer V., Kern T., Hinter H., Bauer J.W. and Önder K. 2009. Improved homology-driven computational validation of protein-protein interactions motivated by the evolutionary gene duplication and divergence hypothesis. *BMC Bioinformatics*, doi:10.1186/1471-2105-10-21

Hamosh,A., Scott,A.F., Amberger,J.S., Bocchini,C.A. and McKusick,V.A. 2005. Online mendelian inheritance in man (OMIM), a knowledgebase of human genes and genetic disorders. Nucleic Acids Res., 33, D514–D517.

Jayapandian,M., Chapman,A., Tarcea,V.G., Yu,C., Elkiss,A., Ianni,A., Liu,B., Nandi,A., Santos,C., Andrews,P., Athey,B., et al. 2007. Michigan molecular interactions (MiMI): putting the jigsaw puzzle together. *Nucleic Acids Res.,* 35, D566–D571.

Kerrien,S., Alam-Faruque,Y., Aranda,B., Bancarz,I., Bridge,A., Derow,C., Dimmer,E., Feuermann,M., Friedrichsen,A., Huntley,R. et al. 2007a. Intact–open source resource for molecular interaction data. *Nucleic Acids Res.,* 35, D561–D565.

Kerrien,S., Orchard,S., Montecchi-Palazzi,L., Aranda,B., Quinn,A.F., Vinod,N., Bader,G.D., Xenarios,I., Wojcik,J., Sherman,D et al. 2007b. Broadening the horizon–level 2.5 of the hupo-psi format for molecular interactions. *BMC Biol.,* 5, 44.

Mathivanan,S., Periaswamy,B., Gandhi,T.K.B., Kandasamy,K., Suresh,S., Mohmood,R., Ramachandra,Y.L. and Pandey,A. 2006. An evaluation of human protein-protein interaction data in the public domain. *BMC Bioinformatics,* 7 Suppl 5, S19.

Mewes,H.W., Dietmann,S., Frishman,D., Gregory,R., Mannhaupt,G., Mayer,K.F.X., Münsterkötter,M., Ruepp,A., Spannagl,M., Stümpflen,V. and

Rattei,T. 2008. Mips: analysis and annotation of genome information in 2007. *Nucleic Acids Res.,* 36, D196–D201.
Mishra,G.R., Suresh,M., Kumaran,K., Kannabiran,N., Suresh,S., Bala,P., Shivakumar,K., Anuradha,N., Reddy,R., Raghavan,T.M et al. 2006. Human protein reference database–2006 update. *Nucleic Acids Res.,* 34, D411–D414.
Orchard,S., Montecchi-Palazzi,L., Hermjakob,H. and Apweiler,R. 2005. The use of common ontologies and controlled vocabularies to enable data exchange and deposition for complex proteomic experiments. *Pac. Symp. Biocomput*., pp. 186–196.
Pearson,W.R and Lipman,D.J. 1988. Improved tools for biological sequence comparison. *Proc. Natl. Acad. Sci.* USA, 85, 2444-2448.
Prieto,C. and Rivas,J.D.L. 2006. APID: agile protein interaction dataanalyzer. *Nucleic Acids Res.,* 34, W298–W302.
Salwinski,L., Miller,C.S., Smith,A.J., Pettit,F.K., Bowie,J.U., and Eisenberg,D. 2004. The database of interacting proteins: 2004 update. *Nucleic Acids Res.,* 32, D449–D451.
Sprinzak,E., Sattath,S. and Margalit,H. 2003. How reliable are experimental protein-protein interaction data?. *J. Mol. Biol.,* 327, 919–923.
von Mering,C., Krause,R., Snel,B., Cornell,M., Oliver,S.G., Fields,S. and Bork,P. 2002. Comparative assessment of large-scale data sets of protein-protein interactions. Nature, 417, 399–403.
Wheeler,D.L., Barrett,T., Benson,D.A., Bryant,S.H., Canese,K., Chetvernin,V., Church,D.M., Dicuccio,M., Edgar,R., Federhen,S. et al. 2008. Database resources of the national center for biotechnology information. *Nucleic Acids Res.,* 36, D13–D21.
Xenarios,I. and Eisenberg,D. 2001. Protein interaction databases. *Curr. Opin. Biotechnol.,* 12, 334–339.

AUTHORS BIOGRAPHY

Thomas Kern is head of the Research Center Hagenberg, School of Informatics, Communications and Media, Upper Austria University of Applied Sciences. In this research facility in average 30 R&D projects per year are carried out in the three research areas Software Technologies and Applications, Information and Communication Systems, and Media and Knowledge Technologies. He finished his studies in Software Engineering in 1998. After industrial work experience he started as research associate and lecturer for Upper Austria University of Applied Sciences in autumn 2000. Since 2003 he conducted several application oriented R&D projects in the fields of Bioinformatics and Software Engineering. One of his main research activities was the research project Biomedical Information Systems (BIOMIS, 2003-2008, http://biomis.fh-hagenberg.at) which is the foundation for PRIMOS development and further cooperative bioinformatics projects at the Research Center Hagenberg.

Michael Kommenda works since 2006 as a research associate at the Research Center Hagenberg. He received his academic degree in Bioinformatics in 2007 for his diploma thesis on duplicate detection in integrated PPI data sets by pair wise sequence alignment as member of the BIOMIS project team and is one of the main developers of the PRIMOS database. His research interests include bioinformatics, machine learning and data mining as well as heuristic optimization methods.

Viktoria Dorfer started her work as research associate at the Research Center Hagenberg after an internship at the Bio Center of the University of Basel dealing with data analysis of intergenic regions of the yeast genome. She finished her studies in Bioinformatics in 2007 with her diploma thesis on combination and tuning of MS/MS spectra scoring functions. As member of the BIOMIS project team she co-developed and enhanced the PRIMOS visualization and query functionalities.

Kamil Önder is principal investigator for Genomics and Proteomics at the Division of Molecular Dermatology, Salzburger Landeskliniken (SALK) and since 2005 assistant professor at the Department of Cell Biology, Division of Genetics, University of Salzburg. In 2007 together with Johann Bauer he founded a Biotechnology Company for the Development of Novel Antibiotics (ProComCure Biotech GmbH). During the past several years he has developed patentable high-throughput formats of Y2H-based and cell-free technologies as well as bioinformatics procedures used in protein-protein and protein-peptide interaction studies. Additionally, high-throughput-based re-combineatorial cloning techniques and cell-based assay generation for drug discovery belong to his field of expertise. His work forms the basis for ProComCure's ORFomer technology, submitted for European patent application, and the PRIMOS database.

Johann Bauer is specialist in Dermatology and Venerology. Since 2001 he is associate professor for Medical Molecularbiology at the Paris Lodron University of Salzburg. Since 2002 he is member of faculty at the Dept. of Dermatology and Venerology, General Hospital Salzburg, and since 2005 he is principal investigator at the Division of Molecular Dermatology, Dept. of Dermatology and Venerology, University Hospital, Salzburg. In 2008 he additionally started his work as principal investigator at the Laboratory of Molecular Therapy, eb-house Austria and as professor of Therapy for Genodermatoses at the Paracelsus Private Medical University. In the out-patient clinic of the Department of Dermatology and Venerology 65,000 patients per year are treated. This clinical expertise is complemented by the recent research program, dealing with proteomic profiling of microbial infections at the interface of the human host supported by PRIMOS insilico validation of PPIs.

Q-LEARNING BASED THERAPY MODELING

Witold Jacak[(a)], Karin Proell[(b)]

[(a)]Department of Software Engineering
Upper Austria University of Applied Sciences Hagenberg, Softwarepark 11, Austria
[(b)]Department of Medical Informatics and Bioinformatics
Upper Austria University of Applied Sciences Hagenberg, Softwarepark 11, Austria

[(a)] Witold.Jacak@fh-hagenberg.at [(b)] Karin.Proell@fh-hagenberg.at

ABSTRACT
This paper presents a concept for a Decision Support System for Therapy Planning based on the Q-Learning method. It focuses the consideration on a multilevel approach for constructing a data driven evidence based system for classification of different drug dosages and their effectiveness for clinical trials. We consider time - ordered sequences of patient data called patient trials consisting of state, time and medication ordered by clinicians.

A patient state generalization function to provide generalized patient states as categories of patient data is presented. For classification of medications we introduce a medication generalization function based on similarity classes of medications and a similarity function between two drug dosages. Both generalization functions are used for generalizing patient trials and for the synthesis of the Q-Learning agent for the Decision Support System.

Keywords: Q-Learning, Data Driven Modeling, Decision Support Systems, Evidence Based Medicine

1. INTRODUCTION

In recent years, decision planning techniques are increasingly being applied to model and analyze dynamic decision problems in medicine (Cao et al. 1999; Jacak and Proell 2006; He et al. 2006; Bellazzi 1993). In many areas of the medical sciences the following planning problem arises.

An observed set of n trajectories (clinical trials) of N decision epochs is available for estimating a policy for decision making. A decision epoch at time *t* is composed of information observed at time *t*, *Observation(t),* an action taken at time *t*, *Action(t)* and an evaluation of action, *Reward(t).* Scientists want to estimate the best strategies for managing the therapy.

The observed set of *n* trajectories may be historical; for example data in which clinicians and their patients are followed with information about disease process, treatment burden and treatment decisions recorded through time. The goal is to estimate the best policy for deciding which patients should receive a medication and which dose of the medication.

Most approaches use Markov Decision Processes (MDP) to model and solve decision problems in which the optimal choice has to be revised periodically in accordance with the evolution of the patient's state (Cao et al. 1999; Magni et al. 1998; Miksch et al. 1997).

Unfortunately the adoption of MDP to model complex systems as medical decision problems is hampered by the difficulty in the knowledge elicitation from a specific domain. In particular the traditional formulation of a MDP (Magni et al. 1998; Lavrac 1998) through its transition matrix imposes to specify a great number of parameters: The meaning of these parameters is not always understood promptly, and it does not allow an explicit representation of the structured knowledge underlying the model.

Therapy planning problems are characterized by unknown system dynamics and thus can be viewed as learning problems as well. One approach to learning a policy in setting of medication decisions is Q-learning (Watkins 1989; Sutton and Barto 1998).

Q-learning based therapy planning can be used for building cognitive structures based on clinical observations, case records and available empirical data. In (Gaweda et al. 2005; Gaweda et al. 2007) an extension to the Q-Learning algorithm is used to incorporate existing clinical expertise into the process of acquiring an appropriate administration strategy of rHuEPO to patients with anemia.

This article focuses the consideration on the multilevel approach for constructing a data driven evidence based model for classification of different

drug dosages and their effectiveness for clinical treatment.

In order to synthesize the Q-Learning agent we need a patient state generalization function to provide generalized patient states as categories of patient observation data (Section 2.). For classification of medications we introduce a medication generalization function and a similarity function between two drug dosages. Both generalization functions are used for constructing the life long quality function. In section 3 the Q-Learning approach is presented.

2. DATA DRIVEN MODELING OF PATIENT TRIAL

The first step in the therapy modeling is the construction of a so called patient state generalization function. This function should generalize patient states from clinical patient records like patient data, clinical guidelines, outcome laboratory measures etc. We consider time - ordered sequences of patient data (patient critical events) called patient trials

$$trial = (e_1, \ldots, e_n) \quad (1)$$

where e_i = *(medication, state, time)* is the critical event, consisting of state, time and the medication ordered by clinicians. The state contains not only standard numeric laboratory test parameters but also linguistic description of observations (observation protocol).

$$Critical\ Event = e = (medication, state, time) = (m, (v, Observation\ Protocol), \delta\tau) \quad (2)$$

where v is vector of test parameters, m is ordered medication and $\delta\tau$ is the time-interval between initial moment t_0 and current event's moment t, ($\delta\tau = t - t_0$). The patient trials are shown in Figure1.

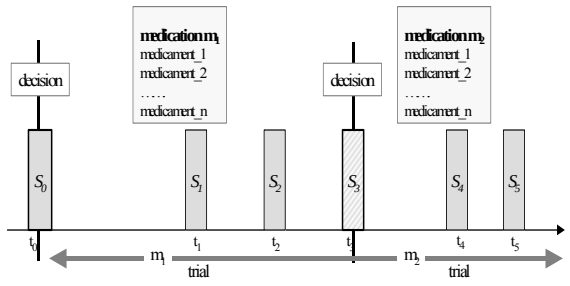

Figure1: Patient trials

One of the methods of state construction is the structured interview. Such interview contains clinical findings and disease states. The interview results in formal Observation Protocols (Goethe and Bronzino1995; Safran et al. 1990; Sonnenberg et al. 1994; Smith et al. 1998)

We concentrate our consideration only to one specified clinical domain for example to psychiatry. There are few procedures and laboratory tests that definitively establish a psychiatric observation. The International Classification of Diseases (ICD) provides standard criteria on which the factorized Observation Protocol is based. The role of formal representations has been verified experimentally by several studies (Safran et al. 1990; Smith et al. 1998).

2.1. Patient state generalization

In the lifelong learning approach, we have only incomplete knowledge about the patient states and thus unable to establish the generalized state function $\boldsymbol{gen_{State}}$ on the formal way.

$\boldsymbol{gen_{State}}$**:** *Patient States* $\rightarrow$ *Generalized States Space.*

The only information available is the k-dimensional vector $\boldsymbol{v}$ of test parameters and factorized observations protocols:

$$\boldsymbol{v} = (v, factor(Observation\ Protocol)). \quad (3)$$

Our goal is thus to construct a state generalization function to provide generalized patient states as categories of patient observation data. This leads to clusters of the observation data, which represent the generalized patient state. The function $\boldsymbol{gen_{State}}$ can be implemented as a neural network, so that new generalized states can be incorporated to the implementation of $\boldsymbol{gen_{State}}$ by an unsupervised learning process. The problem of obtaining generalized states from patient in such a way as to preserve proximity information among the observation data can be solved by a neural network (Brier et al. 1995; Guerrero et al. 2003; Jacobs et al. 2001; Thrun and Mitchell 1993; Stensmo and Sejnowski 1996) that forms clusters in its input space, and produces a good representative of every cluster as output.

The network operates in a way that is a combination of the Kohonen clustering algorithm and class creation and pruning methods. The topology of the network consists of an input layer and an output layer, with full connection between these two layers. The input layer has a dimensionality relative to the dimensionality of patient data, and the output layer grows and shrinks as new category neurons (each representing a generalized patient state) are added and deleted.

When an input vector is presented to the network, all output neurons calculate their distance (i.e. the distance of their weight vector to the input) in parallel. The neuron with the smallest distance is the winner neuron. At this point, we use an idea from the fuzzy-ART algorithm and check whether the winning neuron is close enough to be able to represent the input vector, or whether the input vector is so dissimilar to the winning neuron's weights (and thus to all the other categories as well) that it has to be placed into a new category. For this, we define a similarity radius, that is the maximum distance that an observation vector can be apart from the winning neuron's weights to still be considered close enough to fall into that category.

Category neuron training: If the patient observation vector is within the similarity radius of the winning neuron's weights then these are adapted to reflect the new entry in this category by moving into the direction of input data vector.

Category neuron creation: If the input vector is not within the similarity radius of the winning neuron, it is not similar enough to any of the current categories to be included in one of them, and a new category has to be created.

In this algorithm, this corresponds to the creation of a new output neuron that is fully connected to the input layer, and whose weight vector is equal to the data input vector. It is obvious that the smaller the similarity radius the more output neurons will be created. Category neuron pruning: To prevent a proliferation of output neurons, we include a pruning step that cuts output neurons. The pruning can be done according to two different criteria:

- a neuron is cut when it has not been the winning neuron for a given period of time, or
- a neuron is cut when it encodes too small a fraction of input vectors compared with the output neuron that encodes the most observation vectors.

The network presented above produces generalized patient states from observation data. These generalized states are then used as inputs for the Q-Learning Agent that models the effects of the medication on the generalized states space. The network that implements this function is presented in section 3.

2.2. Medication dosage generalization

Additionally, for each critical event e_i of patient trial, the medications m_i i.e. treatment of drug dosages, therapeutic serum levels and indications are assigned in a unique way. The medication can uniquely be described as set of chemical components (*ingredients*) of the medicament and their dosages. The medication can be represented as set $m_i = \{(c_{ij}, \alpha_{ij}) | j = 1,..,k\}$ where c_{ij} is a chemical component (ingredient) of medicament and α_{ij} is the dosage.

For classification of medications it is necessary to introduce the similarity function between two medications m_k and m_j , s : M x M $\rightarrow \Re$; Let m'_i be a set of components of medication, $m'_i = \{c_{ij}, | j = 1,..,k\}$ and $I_{ik} = m'_k \cap m'_i$ then the similarity function can be described as:

$$s(m_k, m_i) = 1 - \beta_{ik}\,\gamma_{ik} \quad (4)$$

where $\beta_{ik} = |I_{ik}| / \max\{|m'_i|, |m'_k|\}$ and

$\gamma_{ik} = \min\{\Sigma\, \alpha_{cj}^{\,i} \mid c_{ij} \in I_{ik}, \Sigma\, \alpha_{cj}^{\,i} \mid c_{ij} \in I_{ik}\} / \max\{\Sigma\, \alpha_{cj}^{\,i} \mid c_{ij} \in I_{ik}, \Sigma\, \alpha_{cj}^{\,i} \mid c_{ij} \in I_{ik}\}$.

It is easy to observe that $s(m_k, m_k) = 0$ (maximal similarity) and $s(m_k, m_i) = s(m_i, m_k)$. This function can be used to construct similarity classes of medications as: The $M_\varepsilon \subset M$ is the tolerance class of medication if and only if

$$(\forall m_k, m_i) \in M_\varepsilon)\,(s(m_k, m_i) < \varepsilon) \quad (5)$$

The similarity classes – clusters of medication and similarity function are used to build the medication generalization function $\boldsymbol{gen_{Med}}$ i.e. ($\boldsymbol{gen_{Med}}: M \rightarrow M_\varepsilon$) as

$$\boldsymbol{gen_{Med}}(m) = \arg(\min_{M\varepsilon}(\max\{s(m, m_k) \mid m_k \in M_\varepsilon\})) \quad (6)$$

Both generalization functions will be used to generalize the patient trials and to create the life long learning quality function. For each patient trial we can calculate a generalized trial as

$$TRIAL = ((\boldsymbol{gen_{Med}}(m_i), \boldsymbol{gen_{State}}(s_i)) \mid i=1,...,n) = ((\mu_i, \sigma_i)) \mid i=1,...,n) \quad (7)$$

and $\delta\tau_i < \delta\tau_{i+1}$.

3. Q-LEARNING BASED DECISION SUPPORT SYSTEM

To synthesize the decision support system we can use Q-Learning (Thrun and Mitchell 1993; Murphy 2005). Q-Learning is a popular method for learning to select actions from delayed and sparse reward.

The goal of Q-learning is to learn strategies for generating whole action sequences, which maximize

an externally given reward function. The reward may be delayed and/or sparse, i.e. reward is only received upon reaching the goal of the task or upon total failure.

Let S be the set of all possible patient states and $\boldsymbol{gen_{State}}$ be the generalization function mapping the current patient state *s* into the generalized state of patients. We use now the restrictive Markov assumption, i.e. we assume that at any discrete point of time, the system obtains the complete generalized state. Additionally, let $\mathbf{M_\varepsilon}$ (medication clusters) be the action set of the system. Based on the adequate generalized state $\boldsymbol{gen_{State}}(s) = \sigma$ the system picks a generalized medication $\mu_\varepsilon \in \mathbf{M_\varepsilon}$, (action). As the result, the patient state changes. The training procedure receives a scalar reward value, denoted by $\boldsymbol{r}(\sigma, \mu_\varepsilon)$, which measures the action performance. Such a reward can be exclusively received upon reaching a designated goal or upon total failure, respectively.

The Q-Learning method should find an action (medication) strategy $\pi : S \rightarrow \mathbf{M_\varepsilon}$ mapping from patient-states S to actions M_ε, which, when applied to action selection, maximizes the so called *cumulative discounted future reward*. For fast finding the best action in current state *s* the key of Q-Learning is to learn a value function Q for picking the actions (medications): $Q: S \times \mathbf{M_\varepsilon} \rightarrow \Re$ maps percept by generalized states s and actions (medications) μ_ε to scalar utility values. In the ideal case $Q(\sigma,\mu_\varepsilon)$ is, after learning, the maximum cumulative reward one can expect upon executing action μ_ε in state σ. The function Q schedules actions according to their reward. The value $Q(\sigma,\mu_\varepsilon)$ grows with the expected cumulative reward for applying action μ_ε in the current generalized state σ.

The value function Q, after learning, allows generating optimal actions (medications). by picking the action which maximizes Q for current state s, i.e.

$$\pi(s) = \arg(\max\{Q(\boldsymbol{gen_{State}(s)}, \mu_\varepsilon) \mid \mu_\varepsilon \in \mathbf{M_\varepsilon}\}) \qquad (8)$$

The values of Q have to be learned over the whole lifetime of the system acting in the same disease. The function Q can be realized as complex neural network. Initially, all values $Q(\sigma,\mu)$ are set to zero. During learning values are incrementally updated, using the following standard recursive procedure. Suppose the agent just executed a whole action sequence which, starting at some initial state σ_0 and led to a final state σ_F with reward $\boldsymbol{r}(\sigma_F, \mu_F)$. For all steps *i* within this episode, $Q(\sigma_i, \mu_i)$ is updated through a mixture of the values of subsequent state-action pairs up to the final state (Thrun and Mitchell 1993). This standard procedure has the following form

$$Q^{new}(\sigma_i, \mu_i) = \begin{cases} +\mathbf{N} \text{ if } \mu_i \text{ final action, positive result of treatment} \\ -\mathbf{N} \text{ if } \mu_i \text{ final action, negative result of treatment} \\ \Gamma[(1-\lambda)(\max_{\mu} Q(\sigma_{i+1},\mu)) + \lambda\, Q^{new}(\sigma_{i+1}, \mu_{i+1})] \end{cases} \qquad (9)$$

Such Q-learning learns individual strategies independently, ignoring the opportunity for the transfer of knowledge across different sequences of medications. The architecture of the Q-Learning decision support system is presented in Figure 2.

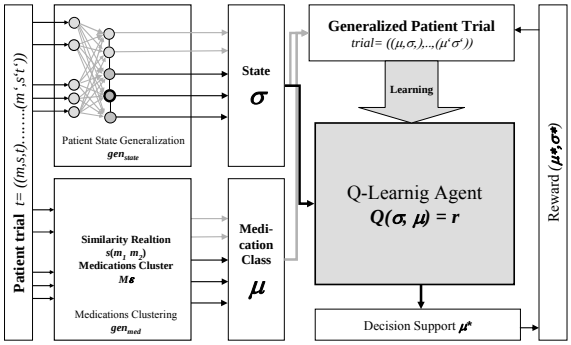

Figure 2: Q-Learning based Decision Support System

4. REMARKS

Our approach extends the proposed method presented in (Gaweda et al. 2005; Gaweda et al. 2007). We do not only consider various dosages of one specific drug but consider the fact that drug prescription can change during therapy by switching to medications with different active components. This is a common strategy especially in treating psychical disorders. In cooperation with a local psychiatric clinic we test our system on patient data of a specific psychical disorder.

REFERENCES

Bellazzi R., 1993, Drug delivery optimization through Bayesian networks: an application to erythropoietin therapy in uremic anemia. *Computational Biomedmdical Research 1993*, 26:274-293.

Brier M.E., Zurada J.M. and Aronoff G.R., 1995, Neural network predicted peak and trough gentamicin concentrations, *Pharmaceutical Research 1995* Mar; pp. 406–412

Cao C., Leong T., Leong A., 1999, Dynamic Decision Analysis in Medicine: A Data Driven Approach, *International journal of medical informatics* 51(1): pp 13-28

Gaweda A. E., Muezzinoglu M. K., Aronoff G. R., Jacobs A. A., Zurada J. M., and Brier M. E., 2005, Incorporating prior knowledge into Q-learning for drug delivery individualization, *Proceedings of Fourth International Conference on Machine Learning and Applications ICMLA'05*, Los Angeles, CA, December 15-17, 2005, Page(s): 6 p

Gaweda A. E., Muezzinoglu M. K., Aronoff G. R., Jacobs A. A., Zurada J. M., and Brier M. E., 2007, Using Clinical Information in Goal-Oriented Learning for Anemia Management, *IEEE Engineering in Medicine and Biology Magazine*, 26 (2), pp. 27-36

Goethe, J.W., Bronzino, J.D.,1995, An expert system for monitoring psychiatric treatment, *Engineering in Medicine and Biology Magazin*e, IEEE, Volume 14, Issue 6, Nov/Dec Page(s):776 - 780

Guerrero J.D.M., Olivas E.S., Camps Valls G., Serrano Lopez A.J., Perez Ruixo J.J., Jimenez Torres N.V., 2003, Use of neural networks for dosage individualisation of erythropoietin in patients with secondary anemia to chronic renal failure, *Computers in Biology and Medicine*, Volume 33, Issue 4, Page 361

He Y, Tang Y, Zhang YQ, Sunderraman R., 2006, Adaptive Fuzzy Association Rule mining for effective decision support in biomedical applications, International Journal of Data Mining and Bioinformatics 2006 - Vol. 1, No.1 pp. 3 – 18

Jacak W. and Pröll K., 2006, Data Driven Therapy Modeling, *Proceedings of the International Multiconference* (I3M 2006), Barcelona, Spain

Jacobs A.A., Lada P., Zurada J.M., Brier M.E. and Aronoff G.R., 2001, Predictors of hematocrit in hemodialysis patients as determined by artificial neural networks, *Journal of American Society of Nephrology* 12 p. p. 387

Lavrac N.,1998, Data Mining in Medicine: Selected Techniques and Applications, *Artificial Intelligence in Medicine* , Volume 16, Issue 1, Pages 3-23

Magni, P., Bellazzi, R., and Locatelli, F. 1998. Using uncertainty management techniques in medical therapy planning: A decision-theoretic approach. *In Applications of Uncertainty Formalisms A. Hunter and S. Parsons*, Eds. Lecture Notes In Computer Science, vol. 1455. Springer-Verlag, London, 38-57.

Miksch S.; Cheng K, and Hayes-Roth B, 1997, "An Intelligent Assistant For Patient Health Care". *Proceedings of the First International Conference on Autonomous Agents (Agents'97)*, ACM Press, Marina del Rey, California, United States, Pages: 458 - 465

Murphy, S.A. ,2005, A Generalization Error for Q-Learning, *Journal of Machine Learning Research*, 6 (2005). Pages: 1073–1097

Safran C., Herrmann F., Rind D., Kowaloff H.B., Bleich H.L., Slack W.V., 1990, Computer based support for clinical decision-making, *MD Comput*. 1990 Sep-Oct; 319-322.

Smith S.D. Park J., Musen M.A. 1998, Therapy Planning as Constraints Satisfaction: A Computer based Anti-retroviral Therapy Advisor for the Management of HIV, 1: *Proc AMIA Symp*., 1998 AMIA Annual Symposium, Orlando, FL.1998

Sonnenberg F.; Hagerty C., and Kulikowski C.,1994, "An architecture for knowledge based construction of decision models, *Medical Decision Making*, Vol. 14, No. 1, pp. 27-39

Stensmo, M. and Sejnowski, T. J., 1996, Automated Medical Diagnosis based on Decision Theory and Learning from Cases, *Proceedings of World Congress on Neural Networks*, World Congress on Neural Networks, 1996,San Diego, CA, pp. 1227-1231

Sutton R.S. and Barto A.G., 1998, Reinforcement Learning: An Introduction, *MIT Press*, Cambridge, MA

Thrun S., Mitchell T, 1993, Integrating inductive neural network learning and explanation-based learning', *Proceedings Of Thirteenth International Joint Conference on Artificial Intelligence (IJCAI-*93), Chamberry, France, 1993, pp.930—936

Watkins C. J. C. H., 1989, *Learning from Delayed Rewards*, PhD thesis, King's College, Cambridge, UK

AUTHORS BIOGRAPHY

WITOLD JACAK received the M.S.E. degree in electronics and next the Ph.D. degree in control and system engineering from the Technical University of Wroclaw, Poland and the Habilitation degree in intelligent multi agent systems from Technical University of Warsaw, Poland in 1973, 1978 and 1992 respectively. From 1977 to 1989 he was a Professor Assistant and from 1989 to 1995 Professor at the Institute of Technical Cybernetics, Technical University of Wrozlaw, Poland. From 1991 to 1998 he was the Guest Professor at University Linz, Austria. Since 1994, he has been the Head of School for Informatics, Communications and Media at Upper Austrian University of Applied Science, Hagenberg, Austria. His research interests include artificial and computational and distributed intelligence, multiagent autonomous systems, cognitive modeling and simulation and knowledge engineering. Dr. Jacak is a member of editorial boards and council member of several national and international committees.

KARIN PROELL received the M.S.C and Ph.D. degree in computer science from the Johannes Kepler University in Linz, Austria in 1982 and 2002 respectively. In 1999, after a several years activity as software engineer in industry she has become as a lecturer in computer science at the School for Informatics, Communications and Media at Upper Austrian University of Applied Science, Hagenberg, Austria and is now Head of Department of Medical Informatics and Bioinformatics in Hagenberg. Her research interests are multiagent systems, bio– and medical informatics.

TOWARDS A NUMERICAL 3D MODEL OF FUNCTIONAL ELECTRICAL STIMULATION OF DENERVATED, DEGENERATED HUMAN SKELETAL MUSCLE

Thomas Mandl[a,b,e], Johannes Martinek[c,d], Winfried Mayr[a], Frank Rattay[d], Martin Reichel[c], Ewald Moser[a,b]

[a] Center of Biomedical Engineering and Physics, Medical University of Vienna, Vienna, Austria
[b] MR Center of Excellence, Medical University of Vienna, Vienna, Austria
[c] Department of Biomedical Engineering and Environmental Management, University of Applied Sciences Technikum Wien, Vienna, Austria
[d] Institute for Analysis and Scientific Computing, Vienna University of Technology, Austria
[e] Department of Informatics, University of Applied Sciences Technikum Wien, Vienna, Austria

{thomas.mandl, winfried.mayr, ewald, moser}@meduniwien.ac.at[a,b]
{thomas.mandl, johannes.martinek, martin.reichel}@technikum-wien.at[c,e]
frank.rattay@tuwien.ac.at[d]

ABSTRACT

Functional electrical stimulation (FES) of long-term denervated, degenerated human skeletal muscle has proven to be an effective method for improving a number of physiological parameters. In order to derive suitable stimulation configurations (electrode position and size) for certain muscle specific training tasks, the activation pattern induced by a given configuration must be known. The probability of activation can be estimated by activating functions which depend on the distribution of the externally applied electrical field. We thus chose to create both, a finite element (FE) and a finite difference (FD) model of the field distribution to simulate and study activation patterns and to compare their efficiency and feasibility. First preliminary results show good agreement between the two modeling approaches.

Keywords: Functional Electrical Stimulation, Finite Difference Method, Finite Element Method, Patient Specific Model

1. INTRODUCTION

Paraplegic patients with denervated, degenerated muscle (DDM) have been successfully treated with Functional Electrical Stimulation in for more than a decade (Mayr 2002, Kern 1995, Mödlin et al. 2005). It has been demonstrated that muscle growth can be induced in DDM with the regular application of FES trainings. It has been reported that some well responding patients gained enough force and endurance to stand up, stand and even walk, in parallel bars, with help of FES. In contrast to innervated muscle, where activation is induced by the supplying nerve, FES of DDM requires higher stimulation amplitudes and impulse durations, since the muscle fibers are activated directly by the external electrical field. The response, i.e. activation or not, of a muscle fiber to such an external electrical field can be described with the classical and the terminal activating function (Rattay 1990, Reichel 2002a). To establish better understanding of the underlying mechanisms of direct activation of denervated muscle fibers and to answer a number of optimization questions regarding FES parameters, a computer model of direct FES of muscle has been developed (Reichel 1999, Reichel 2002b, Martinek 2005, Martinek 2008). Due to lacking sensory nerves patients are prone to over use of FES, potentially resulting in skin burning.. Our improved models should result in more reliable parameter settings for DDM patients. Here we present extensions to the previously established and presented models: Firstly, the inclusion of the capability to model electrically anisotropic tissue of arbitrary orientation, i.e. muscle, which influences the distribution of the electrical potential as well as the activating functions and secondly a unified data processing pipeline for the generation of FE and FD models from the same segmented anatomical data set.
Once verified these models are intended to be used to study the activation patterns for a given set of FES parameters.

2. MATERIAL AND METHODS

2.1. Image data

All patient and subject image data used for this study were collected after having obtained informed written consent of the participants. All MR experiments and procedures involving human subjects were reviewed and approved by the local ethics committee.

2.2. Geometry Model

Both, the FE and the FD models are created from the same geometric model. The following model creation pipeline describes the steps taken to create this *GeometryModel*. The entire processing pipeline is also illustrated in **Figure 1**.

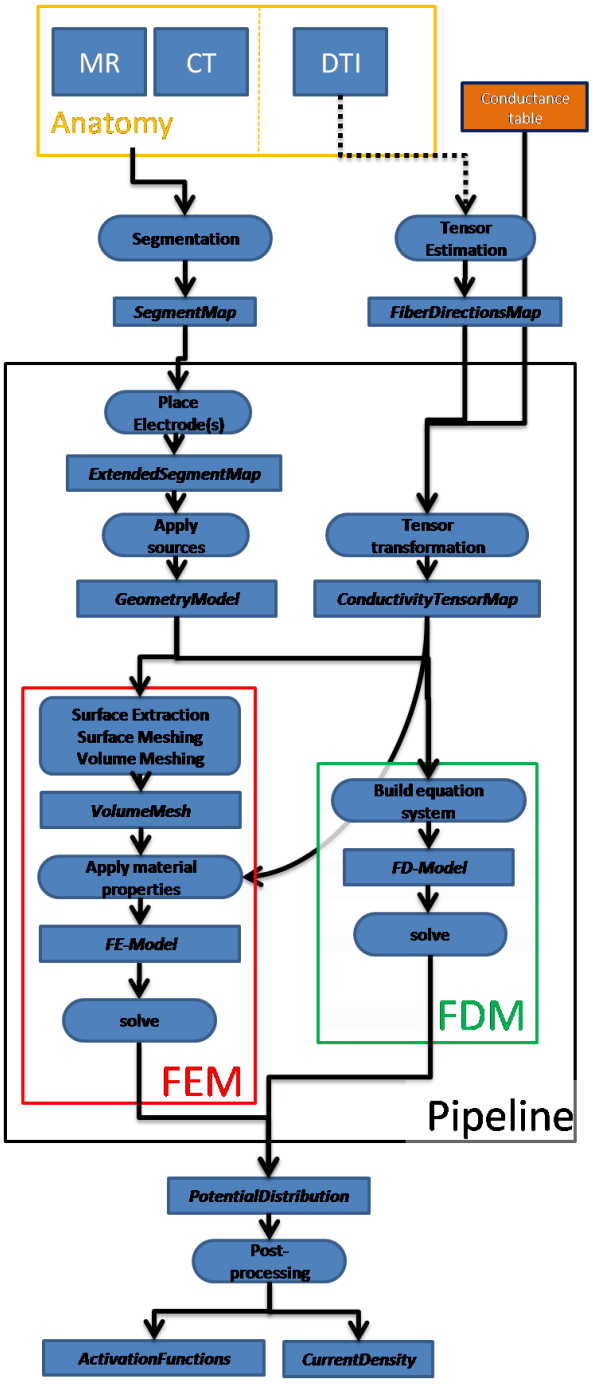

Figure 1: Illustration of the Data Processing Pipeline. Filled blue rectangles represent Data, whereas round nodes stand for processing steps. The dotted line shows a possible dataflow that is currently not implemented.

A high resolution anatomic MR Dataset (128x128x96) is segmented with a standard image processing/segmentation tool (Wolf et al. 2005) from the ITK/VTK family (Yoo et al. 2002) (Kitware Inc., New York, www.vtk.org). Standard segmentation techniques such as region growing or thresholding are used to segments axial slices into bone, air, muscle, and fat.

Two electrodes are placed in the *SegmentationMap* with the help of a custom written routine in MATLAB (The MathWorks, Inc, Natick, MA, USA). Electrode sizes as well as electrode positions can be chosen interactively and are included in the model with a sequence of standard image processing steps, like dilation. Locations of current or voltage sources are added to the *ExtendedGeometry* with another (interactive) MATLAB script.

The *ConductivityTensorMap* is calculated from the tissue specific conductances (*ConductanceTable*) and the *FiberDirectionsMap* with a suitable transformation of the conductivity tensor taking into account the orientation of muscle fibers.

2.3. FD Model design

We consider a static model of FES described by the fundamental equation

$$div\,\vec{j} = \vec{\nabla}\cdot\left(\overleftrightarrow{\sigma}\,\vec{E}\right) = \vec{\nabla}\cdot\left(\overleftrightarrow{\sigma}\left(-\vec{\nabla}\phi\right)\right) = 0 \qquad (1)$$

with current density $\vec{j}$, electric conductivity $\overleftrightarrow{\sigma}$, electric field $\vec{E}$ and electrostatic potential ϕ. In the isotropic, homogeneous case (1) becomes the Laplace equation. However in the anisotropic case $\overleftrightarrow{\sigma}$ is a second order tensor and in the inhomogeneous case it also varies in space and (1) cannot be further simplified. For our model we have chosen a finite difference scheme suitable for inhomogeneous anisotropic bioelectrical problems (Saleheen 1997). After discretization of (1) on a three dimensional regular grid the potential Φ_0 at any node 0 is given as a function of the potential (and conductivity) of its 18 neighbors:

$$\sum_{i=1}^{18} A_i\,\Phi_i + \left(\sum_{i=1}^{18} A_i\right)\Phi_0 = 0 \qquad (2)$$

The coefficients A_i are expressions of the conductivities and are listed in (Saleheen 1997). Since this approach considers inhomogeneous regions from the beginning, no continuity conditions across segment interfaces have to be enforced explicitly. A further and similar advantage is the 'automatic' implementation of the natural Neumann boundary condition (electric insulation) at the skin-air interface by setting the conductivity of the surrounding air to zero. After padding the domain with a one voxel thick layer of zeros along every border we build the sparse coefficient matrix of the system of linear equations from data of the *GeometryModel* and the *ConductivityTensorMap* by considering (2) for every voxel in the domain. Current sources are added to the problem by including them in

the right hand side vector at the correct location. In the case of voltage sources the coefficient of that voxel in the main diagonal is set to one and all others in that particular row are set to zero while the value of the source is inserted into the initial guess vector. Rows (and corresponding columns) with all zero entries are removed from the matrix to reduce the rather large system in size. The system is solved for all $\Phi's$ with MATLAB's minres, an implementation of the minimal residuum method (Barrett 1994, Paige 1975). All other steps described in this subsection are also performed in MATLAB with custom written scripts and functions.

2.4. FE Model design

The *FE-Model* is created from the *GeometryModel* in several steps, all of which are performed by the freely available MATLAB tool `iso2mesh` (Fang 2009, iso2mesh http://iso2mesh.sourceforge.net) which is distributed along with modified versions of a surface extraction routine from CGAL **(**Computational Geometry Algorithms Library, http://www.cgal.org) and the tethadredal mesh generator tool Tetgen (http://tetgen.berlios.de). In a first step we extract several closed surfaces from the *GeometryModel* which include: Bone, Bone-OR-Muscle, Bone-OR-Muscle-OR-Fat, and the electrodes. If necessary the *GeometryModel* is zero-padded to ensure the extraction of closed surfaces. For subsequent volume meshing it is of utmost importance that none of the surface elements intersect. To achieve this it can be necessary to limit the extraction region in such a way that an intersection free surface containment hierarchy is created. In other words: the muscle surface is entirely contained within the fat surface and the bone surface is entirely contained within the muscle surface or going through a 'hole' in the otherwise closed muscle surface (see **Figure 2** for an illustration of the surface extraction steps and the containment hierarchy). The extracted, triangular surfaces serve as the starting point for the volume meshing procedure which is performed by a modified version of Tetgen distributed along with iso2mesh. The result is a quality volume Delaunay mesh. Several options regarding maximum element number, volume or the radius of the Delaunay sphere need to be adjusted to produce a volume mesh of reasonable size and resolution. The *VolumeMesh* is imported in COMSOL Multiphysics (COMSOL, Inc. Burlington, MA USA, www.comsol.com) where the *FE model* is solved with the built-in solver. All mesh parameters need to be set before import since remeshing of an imported mesh is not possible.

2.5. Post-processing

The most prominent post-processing steps are the calculation of the two activating functions, which require knowledge of all first and second order derivatives of the electrical potential. Further quantities such as the current density distribution can also be extracted from the solution. All post-processing calculations are performed in either MATLAB or COMSOL Multiphysics.

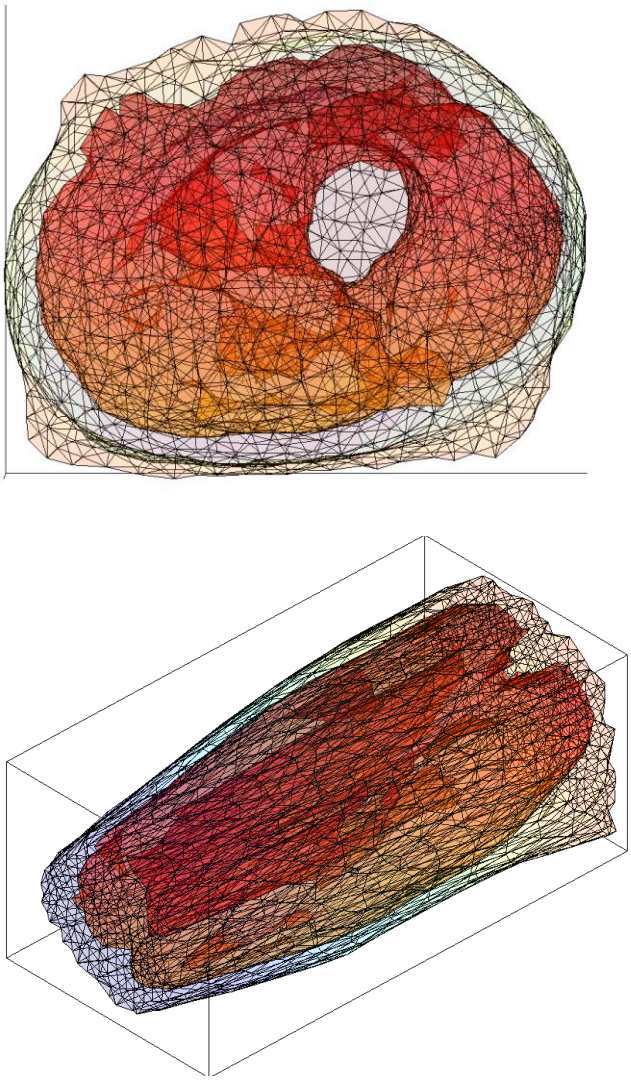

Figure 2: Surface mesh of the fat and the muscle segment in axial (top) and general 3D (bottom) perspective. The images illustrate the intersection free containment hierarchy: the (inner) muscle surface is entirely within the surface of the fat segment. For illustration the dataset was meshed with a lower resolution.

3. RESULTS

First preliminary results show good agreement between the FD and the FE approaches. The mean relative difference of the results of FD and FE for simple geometries (data not shown) was 0.5%. **Figure 3** shows the results of a FD and a FE calculation of the same *GeometryModel*.

4. SUMMARY & CONCLUSION

We presented a data processing pipeline capable of vastly automatic creation of FD and FE models of the distribution of the electrical field during FES from segmented anatomical images. They are capable of considering fiber direction information in both, the computations of the electric field and the estimation of

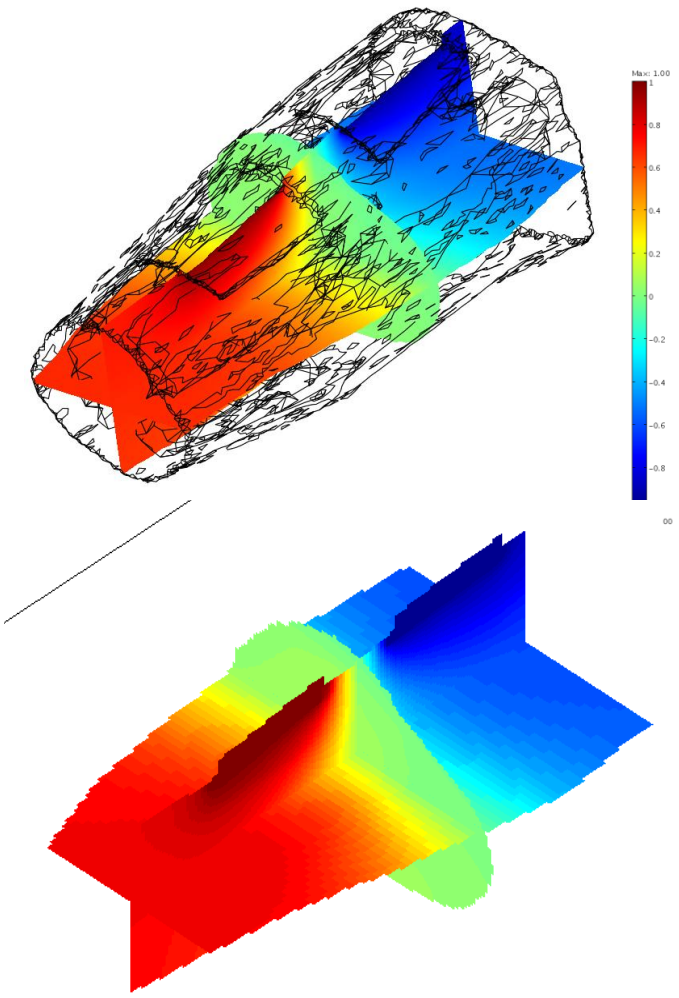

Figure 3: Results of FE (top) and FD (bottom) simulation of the same *GeometryModel*. The electrodes are modeled as voltage sources (+/- 1V).

the two activating functions. The models have shown good agreement in their results, however a number of aspects need to be addressed at this point.

Segmentation
Segmentation is often a difficult task that cannot be fully automated and can have great influence on the results. However segmentation of the anatomical images has not been the main focus of this work and the presented data processing pipeline assumes a set of properly segmented images.

FE model creation
The creation of the FE model relies heavily on the success of the surface extraction step i.e. the intersection free closed surfaces, which works for well behaved geometries but proved to be difficult at times when structures are more complex in shape and topology. For biological structures such as muscles in a human thigh it cannot be guaranteed that these criteria are always fulfilled. To satisfy the requirements, geometry simplification like erosion or intensive mesh-parameter tweaking is sometimes necessary. All in all it has to be noted that the FE branch of the pipeline is not stable and often requires simplification and/or user interaction.

FE vs. FD
One of the goals of this study was to test the feasibility of FE models for patient specific modeling of FES. FE models are normally more flexible than FD. An increase in detail in certain regions is easily achieved with a finer mesh whereas our FD model is implemented with a regular grid and an increase in detail would immediately result in immense increase in memory consumption.
With the consideration of the previous paragraph in mind it seems that the effort and troubles of model creation outweigh the benefits of the FE approach until more robust and reliable surface extraction methods are introduced or this step can be skipped entirely i.e. a volume mesh generation directly from the volume data will be available.

FD model
We implemented a three dimensional FD scheme for inhomogeneous, anisotropic (bio)electric problems and started verifying it by testing its results against the results of the commercially available FE software COMSOL by building and solving FD problems based on exported COMSOL geometry data. On a 2009 state-of-the-art quad-core workstation with 4GB RAM we can solve problems for domains of up to approx. 200x200x200 voxels within several minutes, however when domain size increases and data has to be swapped to hard-disc, speed reduces significantly. The strongest limit for our model is thus memory consumption which could certainly be stretched farther with more memory efficient code, especially in the solver.

Validation
We are aware that even after successful verification our models need to be validated i.e. tested against experimental data. Such data is available in our group and the validation attempt with a number of patient-specific simulation studies is in progress. However the scope of this work was to report on methods that allow the set-up of a patient specific 3-dimensional model of FES that includes both anisotropy and inhomogeneity.

ACKNOWLEDGEMENTS

This study is supported by the Austrian Science Fund (FWF) under grant numbers TRP L36-B15 and P18848-N13

REFERENCES

Barrett, R., M. Berry, T. F. Chan, et al., 1994, Templates for the Solution of Linear Systems: Building Blocks for Iterative Methods, *SIAM, Philadelphia*

Fang Q. and Boas D. A. 2009, Tetrahedral mesh generation from volumetric binary and grayscale images, *Proc. Intern. Symp. Biomedical Imaging (ISBI 2009), June 28 - July 1, 2009 Boston, MA, U.S.A.*

Kern H 1995, Funktionelle Elektrostimulation paraplegischer Patienten, *Österreichische Zeitschrift für Physikalische Medizin und Rehabilitation*, Heft 1, Supplementum

Martinek J, Reichel M, Rattay F, Mayr W 2005 Analysis of calculated electrical activation of denervated muscle fibers in the human thigh. *Artifical Organs*, 29(6): 444-7

Martinek J, Stickler Y, Reichel M, Mayr W, Rattay F., 2008, A novel approach to simulate Hodgkin-Huxley-like excitation with COMSOL Multiphysics, Artifical Organs, 32: 614-9

Mayr W, Hofer C, Bijak M, Rafolt D, Unger E, Sauermann S, Lanmueller H, Kern H 2002, Functional electrical stimulation (FES) of denervated muscles: existing and prospective technological solutions. *Basic Appl Myol*, (12): 287

Mödlin M, Forstner C, Hofer C, Mayr W, Richter W, Carraro U, Protasi F, Kern H, 2005 Electrical stimulation of denervated muscles: first results of a clinical study, *Artifical Organs*, 29**:** 203-206

Paige, C. C. and M. A. Saunders, 1975 Solution of sparse indefinite systems of linear equations. *SIAM J. Numer. Anal.,12,* 617-629

Rattay F., 1990, *Electric nerve stimulation (theory, experiments and applications).* Springer, Wien - New York.

Reichel M, Mayr W, Rattay F, 1999, Computer simulation of field distribution and excitation of denervated muscle fibers caused by surface electrodes, *Artifical Organs*, 23: 453-456

Reichel M. Mayr W. Rattay F. 2002a. Simulation of exitation effects at the muscle-tendon junction in denervated muscle fiber, *Proc. 7th Ann. Conf. Intern. Functional Electrical Stimulation Society. (IFESS)* Ljubljana, Slovenia, 152-154

Reichel M, Breyer T, Mayr W, Rattay F, 2002b, Simulation of the three-dimensional electrical field in the course of functional electrical stimulation, *Artifical Organs,*26(3): 252-5

Saleheen H. I., Kwong T. N, 1997, New finite difference formulations for general inhomogeneous anisotropic bioelectric problems. *IEEE Trans. Biom. Eng.* 44(9) 800-809

Wolf I, Vetter M, Wegner I, Böttger T, Nolden M, Schöbinger M, Hastenteufel M, Kunert T, Meinzer HP, 2005. The Medical Imaging Interaction Toolkit. *Medical Image Analysis;9(6):594-604*

Yoo TS, Ackerman MJ, Lorensen WE, Schroeder W, Chalana V, Aylward S, Metaxas D, Whitaker R, 2002. Engineering and algorithm design for an image processing Api: a technical report on ITK--the Insight Toolkit. *Studies in Health Technology and Informatics. 85 586-92*

BIOGRAPHY

Thomas Mandl received his "Diplomingenieur" (MSc level) in Technical Physics from the Technical University of Vienna late 2005. He has since been a phd student in Medical Physics at the Medical University of Vienna in Prof. Moser's MR group. His (research) interests include computer simulation and visualization as well as muscle relevant MR methods.

Johannes Martinek received the Msc in Technical Mathematics from the Technical University of Vienna, Austria, in 2003. He has since been a phd-student at the Technical University of Vienna, Austria. Until May 2009 he as a research assistant of the Institute for Analysis and Scientific Computing of the Technical University of Vienna, Vienna, Austria. Since 2003 he is employed at the Department of Biomedical Engineering and Environmental Management at the University of Applied Sciences "Technikum Wien", Vienna. His research interests include modeling and simulation of bioelectric signals with a special focus on the simulation of muscle and nerve fibers.

Winfried Mayr received his Diploma degree in Electronics and Control Engineering from the Vienna University of Technology in 1983 and his Ph. D. in Biomedical Engineering in 1992. He is working at the Vienna Medical University - Department of Biomedical Engineering and Physics - since 1983, from 1997 on as Assistant Professor and since 2001 as Associate Professor. His past and present research includes rehabilitation engineering in spinal cord injury, neural prostheses, and functional electrical stimulation (FES). After technical co-ordination of the first-time-in-history application of FES in space the main focus of his work during the recent years focused on FES of denervated muscles (co-ordination of the European research and development project "RISE" - outcome: a novel rehabilitation method for flaccid paraplegia and associated technical equipment, at present in the dissemination phase).

Frank Rattay received the Dipl. Ing., Dr. techn. and Dr. rer. nat. degrees from the Vienna University of Technology in 1974, 1980 and 1995, respectively. In 2006 he received a Dr. science med. degree from the Medical University Vienna. He is professor for „Modeling and Simulation in Technique and Science" (1987) and for „Biophysics" (2000) at the Institute of Analysis and Scientific Computing of the Vienna University of Technology. Since Nov. 1994 he is chair of TU-BioMed, the Association for Biomedical Engineering at the Vienna University of Technology. He chaired the ‚Commission for Technical Mathematics' and for the same four years (2000-2003) he was Senator of the University. He is co-initiator of the new master curriculum "Biomedical Engineering" at the Vienna University of Technology. In 1986 Rattay introduced the activating function concept which is the

most cited method to explain nerve or muscle tissue excitation by electrical fields.

FH-Prof. Dr. M. Reichel. Born in 1969, Dr. M. Reichel studied at the University of Technology and graduated in Electronic Engineering, in Vienna in 1995 with the degree "Diploma Engineer". After his civilian service, he worked at the Department of Biomedical Engineering & Physics at the Vienna Medical School (Vienna General Hospital) as a scientific assistant in several projects on Neurorehabilitation and in parallel he continued his studies at the University of Technology and made his Ph.D. in 1999 in the Field of "Functional Electrical Stimulation – Modeling & Simulation". Since 2002 Prof. Reichel is employed by the University of Applied Sciences Technikum Wien and Since 2007 his responsibilities are managing the department of Biomedical Engineering & Environmental Management as well as the study program of Healthcare- & Rehabilitation Technology. Prof. Reichel is teaching and supervising bachelor and masters theses in the areas of Biomedical Engineering and Biomedical Informatics as well as Instrumented Motion Analysis.

Ewald Moser is a tenured Associate Professor of Medical Physics and Biophysics in the Centre of Biomedical Engineering and Physics, Medical University of Vienna, Vienna, Austria, and Adjunct Professor of Physics in Psychiatry at the Department of Psychiatry, University of Pennsylvania, Medical Centre, Philadelphia, USA. He is also the Scientific Director of the MR Centre of Excellence in Vienna. Dr. Moser was educated at the University of Technology in Graz, Austria, where he received his "Diplomingenieur" (MSc level) in Technical Physics, and at the University of Technology and Atominstitut in Vienna, Austria, where he received his doctorate (PhD level) in Technical Physics. In 1982/83 he accepted a position at the Medical School, University of Vienna (A) where he started the first experimental NMR program in 1985. In 1987 he started collaborating with Diagnostic Radiology on quantitative MRI, proton MR spectroscopy (1990) and functional MRI (1992) on a 1.5 T clinical research scanner. In 1988 he was awarded an Erwin-Schrödinger stipend to join Prof. J.S.Leigh's lab at the MMRRCC, University of Pennsylvania Medical Centre and in 1989/90 Prof. G.K.Radda's group in Oxford (UK). In 1991 he obtained his Habilitation in Medical Physics and Biophysics from the University of Vienna and was appointed Associate Professor. His scientific activities led to substantial funding for MR research and resulted in the installation of a 3T research scanner in 1996, University of Vienna, Medical School. In 2003 the joint efforts of the Departments of Medical Physics and Diagnostic Radiology led to the foundation of the MR Centre of Excellence, Vienna, where he has been appointed Scientific Director. Substantial grants from the Ministry of Science and Research, the General Hospital and the City of Vienna, Siemens Medical Solutions, and the newly founded Medical University of Vienna enable the installation of a TIM TRIO scanner in 2006, a new MR-building and the installation of a 7T scanner by 2008.

CHALLENGES OF BUILDING A SIMULATION MODEL OF THE GERMAN MENTAL HEALTH CARE SYSTEM

Kristina Dammasch[(a)], Benjamin Rauch-Gebbensleben[(b)], Christfried Tögel[(c)], Graham Horton[(d)]

[(a), (b), (d)]University of Magdeburg, Department of Simulation and Graphics, Germany
[(b)]Salus gGmbH, Salus Institute for Trend Research and Therapy Evaluation in Mental Health, Magdeburg, Germany

[(a)]kristina@dammasch.net, [(b)]ben@sim-md.de, [(c)]c.toegel@salus-institut.de, [(d)]graham@sim-md.de

ABSTRACT
We are currently developing a simulation model of the German mental health care system. We believe that it might support analyses of the provision system and evaluations of possible future trends. But trends cannot be unified easily. Relevant parameters of health care providers diverge strongly even in similar areas considering demographic and economic aspects. A suitable mathematical description for these parameters could not have been obtained. Interdependencies between parameters are very complex and therefore hard to observe. For that reason, we decide to change our focus from the complete German system to a smaller geographical area in eastern Germany that seems to be suitable for our study. We expect the parameters of interest to be more stable allowing us to gain the necessary mathematical relationships. If we succeed in building a model of a smaller system we might be able to derive information for a model of the complete system.

Keywords: mental health care, process analysis, data analysis, trend research

1. INTRODUCTION

Computer simulation is a well-established method for modeling and analyzing systems. It enables an objective view on relevant processes and gives the opportunity to evaluate different optimization and planning strategies. This is of special interest for planners and researchers of systems in many application fields.

One of these application fields is mental health care, although the usage of computer simulation there is still more uncommon compared to other fields (Sanchez, Ogazon, Ferrin, and Sepulveda 2000). Nevertheless, a suitable simulation model of mental health care services might support analyses and planning tasks concerning the system and its possible evolution in the future.

For that reason, we are currently developing a simulation model of the German mental health care system that will allow the definition of a variety of different scenarios that are to be evaluated. The collaboration with the holding company of a group of German psychiatric facilities, that is also initiator of this research project, enables us to analyze the processes of mental health care and to collect and interpret some of the necessary data for our simulation model.

For being able to build that model we first have to identify the parameters that are crucial for the system's behavior and determine the boundary of the system. Furthermore, we have to describe the processes and interdependencies within this boundary.

In this paper we would like to present some of the performed analyses and challenges we had to face. Afterwards we explain the consequence arising and close the paper with a short summary and outlook on our future work.

2. METHODOLOGICAL APPROACHES

There were two approaches possible for deciding which parameters are relevant for a description of the system: On the one hand, results from a broad data analysis such as mathematical correlations could reveal which processes are determining the system's behavior. An advantage is the objectivity of the data disregarding subjective opinions about the system. But the approach also specifically entails the risk of mistaking a mathematical correlation as logical relationship between two or more parameters. That way the resulting process model might be falsified.

On the other hand, we could perform a system and process analysis first. Then the derived information could be used to observe only selected parameters identified during the analysis. The main challenge here is to distinguish between different subjective opinions about the system processes. A possible manipulation by one side or the other may cause important influencing parameters to be disregarded.

Due to the complexity of the system, we decided to start with a system analysis for getting an impression of the main processes. We conducted interviews and workshops involving experts from different parts of the health care system such as physicians, controllers or planners of the provision system. We also expected to get an impression of the expectations about the simulation model we are about to develop.

The analyses showed that there are a lot of different questions that are to be answered with the aid of simulation experiments. Therefore, we first had to

make some restrictions about the model range. The different aspects of interest concern different levels of detail and require different modeling techniques. In summary we specified two levels:

1. Forecasts about the basic data of the health care providers.
2. Forecasts about the course of the patients' treatments in consideration of different circumstances and influences.

Based on these examinations also different conceptual models are considerable. If the behavior and future development of a rather abstract model of the system is of interest, logical process chains might not have to be modeled. In this case a system of difference equation might be sufficient, as the system does not evolve continuously.

If the "flow" of patients through the system has to be modeled more detailed and also visualized a stochastic Petri net would be a sufficient choice although the computational effort would increase due to the high number of moving entities modeling the patients. Nevertheless, a Petri net would be of advantage for many other reasons (Dammasch and Horton 2007).

If a description of a patient in a psychiatric treatment is required for a simulation scenario, a Petri net might be also an appropriate choice. Based on the concept of hybrid tokens (Dammasch and Horton 2008) it enables a detailed model of the moving entities with discrete and continuous attributes in a simple discrete-event-system.

We decided to have the main focus on the first level mentioned above and perform an analysis of the mental health care system as a whole including its involved providers and their possible development and connections in the future. The conducted interviews also helped us defining the output parameters of our simulation model that are of special interest for possible users. Afterwards, we proceeded with a detailed process and data analysis.

3. ANALYZING THE SYSTEM'S PROCESSES

A system is defined as the total entity to be evaluated. It must include all people and things interacting within the system (Medina 1981).

The input of the system influenced by external parameters from the environment is transformed into the system's output that has an influence on the environment and also back on the system's input.

This simple description of a system is shown in Figure 1.

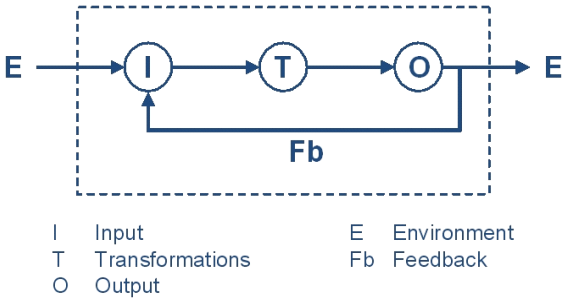

Figure 1: Simple System Model

This means for our research work that we have to find the input parameters of the system such as the number of patients for example or the probability for suffering from a certain disease. And we have to find those parameters that have an influence on the input parameters. Remaining with the examples, we have to find out which parameters from the environment might have a positive or negative influence on the number of patients or the probability of being taken ill.

Second, possible output parameters have to be determined for the system definition. Parameters we carried out from the conducted interviews and workshops are among others the costs of treatment per patient and the quality of care. Third, we have to determine how the output results from the input.

We let the overall system be defined as the complete German mental health care system. As this system is too large and complex to evaluate as a whole we tried to decompose it into a more workable structure and divide the system into smaller subsystems.

A proper subsystem must be a system itself (Medina 1981) located in an environment, i.e. the superior system, from where the subsystem receives input and delivers output. Additionally, the output of one subsystem can in turn be the input of another subsystem. Figure 2 shows a simplified scheme of a system containing several linked subsystems.

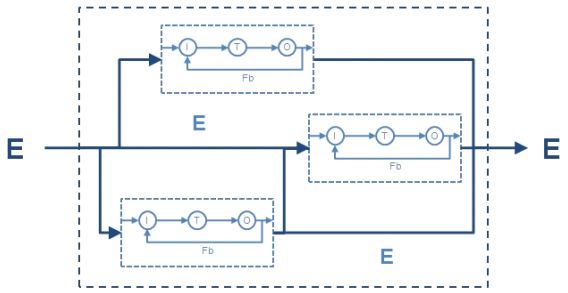

Figure 2: Model Of Subsystems With Connected Inputs And Outputs Within A System Boundary

Our first idea was to divide the complete mental health care system into subsystems representing the different health care providers and super-ordinate or regulating organizations such as ministries or health insurances. Therefore, we had to analyze the interaction of the providers and the patients' flow.

3.1. Mental Health Care in Germany

The German mental health care system involves different providers connected to each other. A patient is usually not treated in only one kind of treatment facility, e.g. a hospital, but is sent from one facility to the next depending on mental and physical state as well as the individual objectives of a treatment (Schädle-Deininger 2006). One possible course is shown in Figure 3. Other common ways are illustrated by dotted arrows

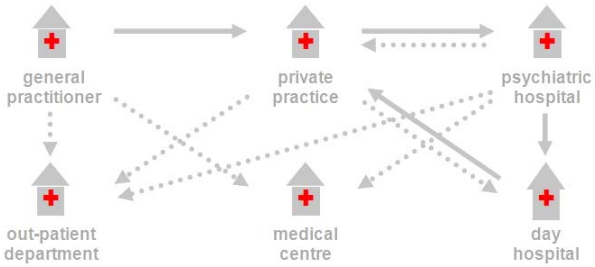

Figure 3: Example Course Of A Psychiatric Treatment

In the example shown in Figure 3, the patient is treated by a general practitioner who suspects a mental disorder. For an exhaustive examination the patient is sent to a private practice where a diagnosis is proposed. If the patient suffers from serious disturbances a stationary treatment is suggested and the patient is admitted to a psychiatric hospital. Otherwise the patient will stay under ambulant treatment.

At the psychiatric hospital a therapy form is chosen depending on diagnoses and the patient's condition. A therapy usually consists of different combinations of treatments. After finishing a stationary therapy, other treatments follow in an ambulant facility such as a day hospital, private psychiatric or psychotherapeutic practice.

The admission and treatment process is very complex. Beside the described example there are many other courses possible whose regulations are frequently non-transparent. And there are different additional influences either from the external environment of the system or from within the system, i.e. from other subsystems, or both. These might be among others laws or regulations determining for example financial influences.

3.2. Challenges

When analyzing the system's processes and regulations we came across two difficulties. First, processes are usually well-defined but indeed often not clearly documented. An example is the decision what kind of facility a patient is admitted to. Referring to Figure 3, it has to be decided if the patient is admitted to a day hospital, a medical centre, an out-patient department or a private practice, if an ambulant treatment is suggested. And a lot of different factors have to be taken into account for this decision. To be able to do that a standardized procedure is defined but it takes persistent inquiries to find out that there are regulations at all.

By contrast, there are processes without any definitions or at most soft guidelines. An example is the choice of a therapy for a certain mental disorder. Instead of following clinical pathways that are not established in mental health, the therapy form is within the sole discretion of the therapist. However, surveys indicate that different treatments of the same mental disorder can lead to different therapeutic outcomes (Reinecker 2003). In turn, this has an influence on our specified output parameters of the model.

4. DATA ANALYSIS

One objective of our work is to create a tool that allows the simulation of user-defined scenarios answering a variety of what-if-questions. Questions of interest concerning the system might be: "What if the length of hospital stay for diagnosis X is shortened to 14 days?" or "What if clinical pathways are to be implemented determining to treat all patients with diagnosis X with therapy form Y?".

When considering external parameters that might have an influence on the system such as the age distribution of the population or unemployment, further questions might be: "What if the rate of the over-60s is up to 50 percent?" or "What if the rate of unemployment is down to 1 percent?".

For being able to simulate one of these scenarios we have to analyze among others the effects of different forms of therapy on the therapeutic outcome for diagnosis X in different facilities in Germany. Second, the influence of the length of hospital stays on different output parameters such as quality of care or treatment costs has to be examined. Furthermore, the influence of the German population structure and unemployment rate has to be found and quantified.

Therefore, we had to find different reliable data sources covering information about the population and its structure and about economical parameters. Furthermore, we had to find information about medical facilities and their basic economic data as well as the treated diseases and forms of therapies.

4.1. Data Sources

One main data source for a data analysis is the German Federal Statistical Office offering a large database for economic, demographic and social parameters. But the size of the data sets is very different from parameter to parameter. While some data sets contain information for more than 40 years, some others start at 1991 after German reunification and some sets, especially concerning health care, reach back for only four to five years. The reason is the re-structuring of data management and recording systems in the health care sector. Unfortunately, data prior to that is not available. But a statistically reliable data analysis requires more than four or five samples.

A second source has to be data from different German health care providers covering mental health care of any kind of facilities as well as data from regulating organizations. As explained in Section 3.1 a

patient runs through different treatments at different health care providers depending on the patient's physical and mental state. That means that different providers treat patients in different conditions, e.g. stationary care for serious disturbances and ambulant care for patients in better condition. Therefore, the parameters of interest differ among the providers.

As a result all kinds of providers have to be taken into account and examined separately. They cannot be considered as similar. But there are providers, especially smaller ones such as psychiatric or psychotherapeutic practices, where data management and recording is not structured and partly not even done in a digital manner. Collecting and analyzing data from those providers is nearly impossible. This strongly decreases the available amount of data and the reliability and completeness.

For the parameters where we were able to gain a suitable data sample we performed statistical analyses for deriving frequencies and mathematical correlations as well as trends.

4.2. Results of the Performed Analyses

As a first result, we found out that a parameter and its development over time in one part of Germany can be completely different from its development in another part. An example is the trend of the German population that increased nearly steadily during the last 15 years. On the one hand, there are states showing the same trend but on the other hand, some German states have a very high migration rate resulting in a steady decrease of the population. As the migration rate of younger people is higher than of the older ones, the rate of the over-60s there is higher than the overall German rate. This, in turn, has an influence on the number of people with age-related disorders such as dementia. And thus it has a crucial influence on the input parameters of our model.

In almost the same manner it is also possible that the range of one and the same parameter of psychiatric facilities could be exceedingly wide. Although we expected the parameters of facilities located in similar geographical areas to be similar, we found examples where our expectation did not apply. An example from two hospitals in Saxony-Anhalt, both located in rural areas, is shown in Figure 4 and 5. The diagrams show the relative frequency of the six most frequent classes of mental disorders in one psychiatric hospital in Figure 4 and in another hospital in Figure 5.

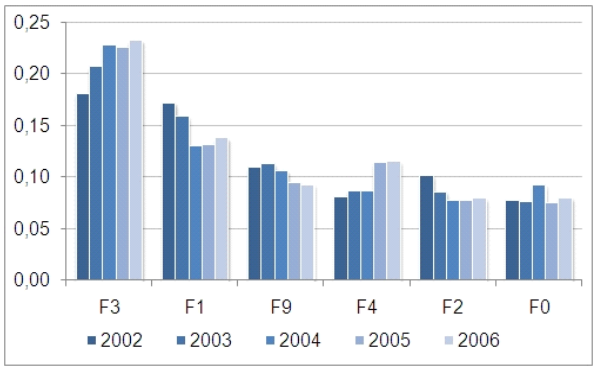

Figure 4: Frequencies Of Diagnoses In A German Psychiatric Hospital Between 2002 And 2006.

For both hospitals we evaluated the frequencies of all occurred classes of disorders in the years 2002 till 2006. Then we determined the six most common classes and compared the frequencies and development over the years. Appendix A explains the classes of mental and behavioral disorders based on the WHO International Classification of Diseases (ICD).

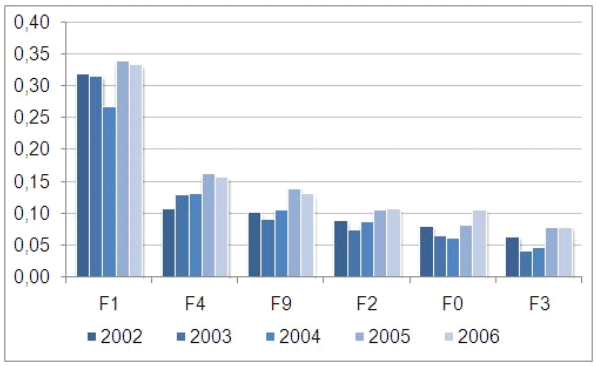

Figure 5: Frequencies Of Diagnoses In A Second German Psychiatric Hospital Between 2002 And 2006.

First, it is conspicuous that in both hospitals the most frequent classes of disorders are equal but in a different ranking covering F0, F1, F2, F3, F4 and F9. Second, the number of patients suffering from a mental disorder of class F3 in hospital 1 is approximately 50 percent higher than in hospital 2 when adding up all cases between 2002 and 2006. And the frequency of F1 diagnoses is higher in hospital 2 than in hospital 1.

Furthermore, the development over time of the frequencies is different in both hospitals. When comparing for example classes F0, F2 and F9 the trend in hospital 1 is mainly a slight decrease or nearly steady while the number of patients in hospital 2 has been increased since 2004. However, a complete analysis of possible trends would require a much larger sample size.

A further result of our examination of the German health care system was that many correlations can be found but it is not possible to find out if it is a direct or spurious correlation. One example is the high positive correlation between the gross domestic product and the number of patients per year treated in psychiatric

facilities. Sample data from years 2000 till 2006 is shown in Figure 6.

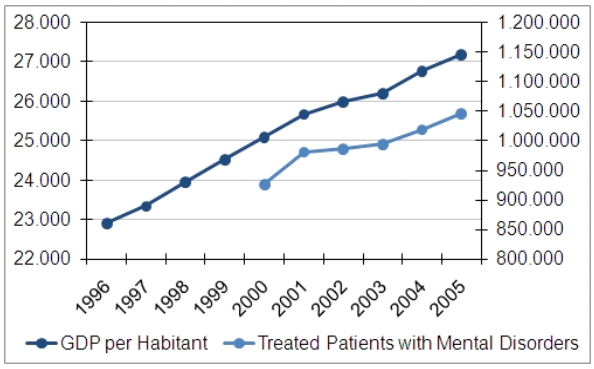

Figure 6: Gross Domestic Product and Number of Patients per Year from 2000 till 2006.

The coefficient of correlation r^2 is about 0.92. There could be either a logical connection or not. Although there are approaches trying to explain that connection directly, it cannot be proven completely. It is probable that the correlation could result from a relation to a third or more other variables having an influence both on the gross domestic product and on the number of patients with mental disorders. Second, it has to be kept in mind that the limited sample size is not a suitable basis for a reliable statistical analysis. Although information about the gross domestic product of Germany is available since 1991, information about mental health only reaches back to the year 2000 and is not yet available for the last 2 years.

5. CONSEQUENCES

While the second mentioned problem concerning correlations is a general one, the first problem is a result from the chosen system size. There are many reasons conceivable for explaining for example the previously described differences between the two German psychiatric hospitals.

First, the different frequencies of patients with disorder of class F3 and F1 may depend on the education of the attending physician or the focus and specialization of the medical facility. It is possible that hospital 1 is specialized in the treatment of mental disorders of class F3 as well as hospital 2 is specialized in the treatment of disorders of class F1. But furthermore, it is also possible that the differences result from dependencies on parameters such as demographical or economical ones.

Therefore, we decided to take a step back: Instead of building a model from the complete German mental health care system we choose to start with a part of it by analyzing the mental health care system of a small area in the middle of eastern Germany.

Regarding the previously mentioned considerations about the definition of subsystems we defined a new level of subsystems. The whole system describing the mental health care system now consists of subsystems representing different areas in Germany that can be divided again into smaller areas if necessary. These subsystems themselves include the previously defined subsystems based on the health care providers and influencing organizations.

Advantages of the chosen area are among others that there is only one psychiatric hospital belonging to our collaborating partner as do many other facilities such as a day hospital. A limited geographical size with a limited number of providers allows us to contact each provider of interest and even health insurances and regulating organizations directly and personally. That way, relevant processes and rules often being well-defined and structured but at the same time not described clearly can be cleared up, documented and finally transformed into a model.

6. SUMMARY AND OUTLOOK

The results and output values of a simulation experiment can only be as good and reliable as the input values are. When trying to model a complex system it is crucial for the success to understand the underlying processes and interdependencies between involved parameters. To be able to describe the system with the aid of a computer model logical and mathematical relationships have to be analyzed.

The main challenges of the process analysis are that

- processes and rules are often well-defined but not clearly documented
- there are processes without definitions

Thus the transparency of the system is not guaranteed and the observation is difficult.

The main challenges of the data analysis are

- collecting a suitable amount of reliable and consistent sample data
- finding correlations and identifying correlations as either direct or spurious
- developing a description of the processes covering the wide range of possible values and trends within the system

Based on our examination of the German mental health care system we came to the conclusion that, with respect to the data currently available, it would require an immense effort to build a universally valid simulation model of the system. Therefore, we chose to stop our work and repeat our examinations for a geographically smaller and bounded part of the system. There we have a suitable amount of data samples available or at least are able to collect it with smaller effort.

We now have to face the challenges again but expect to be more successful in coping with them. A smaller system resulting in a simpler model also gives the opportunity for a more exhaustive validation including reconcilements with experts about the system's processes and behavior.

Eventually, results from analyses of a smaller system and the simulation output might enable us to shift the gained information back to a model describing the overall German mental health care system.

ACKNOWLEDGMENTS
The research presented in this paper was funded by the Salus gGmbH (Magdeburg, Germany) as part of the project "Building a Simulation Model of the German Mental Health Care System". We would like to thank all contributing hospitals, physicians and organizations for their valuable input and cooperation.

APPENDIX
Appendix A

F0 Organic, including symptomatic, mental disorders
F1 Mental and behavioral disorders due to psychoactive substance use
F2 Schizophrenia, schizotypal and delusional disorders
F3 Mood (affective) disorders
F4 Neurotic, stress-related and somatoform disorders
F5 Behavioral syndromes associated with physiological disturbances and physical factors
F6 Disorders of adult personality and behavior
F7 Mental retardation
F8 Disorders of psychological development
F9 Behavioral and emotional disorders with onset usually occurring in childhood and adolescence

REFERENCES

Dammasch, K., Horton, G., 2007. Active Tokens for Modelling Mental Health Care with Coloured Stochastic Petri Nets. *Proceedings of the 4th International Congress on Innovations in Information Technology*. 18th-20th November 2007, Dubai, United Arab Emirates.

Dammasch, K., Horton, G., 2008. Entities with Combined Discrete-Continuous Attributes in Discrete-Event-Driven Systems. *Proceedings of the 20th European Modeling and Simulation Symposium*, 368-373, 17th-19th September 2008, Campora San Giovanni, Amantea (CS), Italy.

Medina, B.F., 1981. *Structured System Analysis: A New Technique.* New York: Gordon and Breach Science Publishers.

Reinecker, H., 2003. *Lehrbuch der Klinischen Psychologie und Psychotherapie: Modelle psychischer Störungen*. Göttingen: Hogrefe-Verlag.

Sanchez, S.M., Ogazon, T., Ferrin, D.M., Sepulveda, J.A., Ward, T.J., 2000: Emerging issues in healthcare simulation. *Proceedings of the 2000 Winter Simulation Conference*, 1999-2003. 10th-13th December 2000, Wyndham Palace Resort & Spa, Orlando, FL, USA.

Schädle-Deininger, H., 2006. *Fachpflege Psychiatrie*. München: Elsevier.

AUTHORS BIOGRAPHY

Kristina Dammasch graduated from the Otto-von-Guericke University of Magdeburg with a German University diploma in Computational Visualistics in 2006. From 2006 till 2008 she worked as research assistant at the Simulation and Modeling Group at the same university. Since 2008 she is simulation engineer at Audi and continuing her research as external PhD. Her research interests include the modeling and simulation of human attributes and hybrid modeling techniques.

Benjamin Rauch-Gebbensleben studied Computational Visualistics at the Otto-von-Guericke University of Magdeburg. He was awarded his German University diploma in 2005. From 2005 till 2006 he worked as simulation engineer in German industry. Since 2006, he is research assistant at the Group “Simulation and Modeling” at the University of Magdeburg.

Christfried Tögel studied Clinical Psychology at the Humboldt University in Berlin. He obtained his PhD in 1981 and his "Habilitation" in 1988, both in the field of psychology at the Humboldt University. In 1988 he became associate Professor and in 1994 Professor at the Department of History and Philosophy of Science at the Bulgarian Academy of Science. After different engagements from Sofia over Vienna and London he became the director of the Salus Institute for Trend Research and Therapy Evaluation in Mental Health (Magdeburg, Germany) in 2004.

Graham Horton is Professor for Simulation and Modeling at the Computer Science Department of the University of Magdeburg since 2001. He studied Computer Science at the University of Erlangen, graduating in 1989 with a German University diploma in Computer Science. He obtained his PhD in Computer Science in 1991 and his “Habilitation“ in 1998 at the same university in the field of simulation.

MENINGITIS: THE QUIET BEFORE THE STORM? (SIMULATION OF AN ON-CAMPUS OUTBREAK)

Tracy A. Atkins[(a)], Ken K. Westerlund[(b)], Christine M. Allen[(c)], Omar Thompson[(d)]

Institute for Simulation (IST) at
University of Central Florida (UCF)

[(a)]wineladytracy@yahoo.com, [(b)]kwesterlund@camber.com,
[(c)]radiantlife@cfl.rr.com, [(d)] thompsono_o@yahoo.com

ABSTRACT
Bacterial meningitis is a very serious life-threatening illness; that left untreated has a fatality rate of 70 percent. It is an especially serious illness on college campuses where the infection rate is approximately four times greater than the rate for the general population of 18-23 year olds. In 2008, the University of Central Florida (UCF) implemented an inoculation and education policy. This research was interested in determining the effect of the meningitis policy with respect to safeguarding the UCF community. In order to research this issue, deterministic models for meningitis outbreaks on the UCF campus were created and run as simulations using base and alternate input variables. Results from the simulations showed significant benefits could be achieved when inoculation and education programs are combined. More importantly, it demonstrated that simulation could be an effective tool for analyzing healthcare issues and formulating healthcare policy.

Keywords: meningitis, campus outbreak, medical simulation, modeling

1. INTRODUCTION

1.1. Meningitis

Bacterial meningitis (meningitis), a very serious life-threatening illness, can be transmitted through air droplets of respiratory secretions and direct contact with an infected person. Patients with the disease will develop flu-like symptoms and unfortunately, these symptoms can lead to misdiagnosis and lack of treatment. There can also be a rapid progression from the onset of symptoms to death. Sometimes this occurs in as little as 24 to 48 hours. Therefore, any delay in treatment only serves to magnify difficulties in treating the illness. According to the literature, when untreated the disease has a fatality rate of 70 percent, and 11 to 19 percent of the survivors will experience significant side effects. These side effects include hearing loss, loss of limbs, arthritis, and neurological defects. The neurological defects include issues such as memory loss, difficulty learning and remembering, headaches, speech impairment, and loss of sight (Collins, Dupont, and Nagie 2003).

1.2. Initial Research

Meningitis is an especially serious issue on college campuses where the infection rate is approximately four times (5.1 per 100,000 versus 1.4 per 100,000) the rate of the general population of 18-23 year olds (Collins, Dupont, and Nagie 2003). Key factors in the higher infection rates among college students are their lifestyle choices that significantly increase their risk (Kuenzi 2004). According to Kuenzi, these lifestyle choices include active and passive smoking, bar or nightclub patronage, sharing cigarettes and beverage containers, intimate contact with others, and excessive alcohol consumption.

Recognizing these risks, health professionals from more than 35 states have helped to enact varying types of legislation with regards to inoculating students against meningitis or mandating education programs in order to confront this issue among college students (Castel, Reed, Davenport, Harrison and Blythe 2007).

1.3. UCF Policy on Meningitis

The University of Central Florida (UCF) is a university that is the fifth largest in the nation and the second largest in the State of Florida. The main campus sits on approximately 1,415 acres in Orlando Florida. With a growing enrollment rate, enrollment data and statistics indicate that the student population for Fall 2008 was in excess of 50,000 students, including 42,912 undergraduate students and 7,342 graduate students (UCF Office of Institutional Research, 2008-2009). According to UCF, the on-campus and off-campus housing capacity for locations managed by UCF was approximately 10,098 students.

In 2008, the University of Central Florida (UCF) joined the ranks of other colleges when it implemented a policy that requires new college freshmen to either be inoculated against meningitis or sign a waiver with an education statement on it. This research was interested in determining the effect of UCF's meningitis policy with respect to safeguarding UCF's community. In order to provide the data necessary to understand the

effects the policy has, the authors have created a base model showing an on-campus outbreak of meningitis. Next, based upon a literature review and research, model variables were manipulated in order to explore various mitigation strategies. These variables include inoculation, education, and combined inoculation and education programs.

The results of the simulations were then analyzed and the conclusions from this analysis were presented to health officials at UCF. By simulating a meningitis outbreak, emergency response procedures, response training, and reaction to outbreaks in real time can be improved (Wu, Shuman, Bidanda, Kelley, Sochats, and Balaban 2008). Conclusions can be drawn from the simulations as to the rate of the disease spreading throughout the UCF population among those who may have been exposed to infected individuals and what appropriate action should be taken to reduce further infections. It is expected that UCF health officials will be able to use the conclusions to review their current policies and, if necessary, revise their program to ensure they have a comprehensive program for reducing the meningitis risk to the general UCF college population.

2. METHOD

This research consisted of developing both base and alternative models for the spread of meningitis then running simulations using those models.

2.1. Base Model Development

This model began as a basic *SIR* model (Kermack and McKendrick 1927) that utilizes three compartments (susceptible, infectious, and removed). According to Caugant, et al. (1994), the infection of meningitis can result in two possibilities: those infected who show symptoms and those who do not show symptoms. Due to this characteristic of the disease, the model was modified by the inclusion of a non-symptomatic compartment to become an SI_SI_NR model. As in the *SIR* model, the population (whose size we represent with the variable N) is partitioned into the classes susceptible $S(t)$, infected showing symptoms $I_S(t)$, infected asymptomatic $I_N(t)$, and removed $R(t)$, where $S + I_S + I_N + R = N$. Individuals in the susceptible compartment are subjected to an infected host with a contact rate of β. Those contracting the disease enter the infected classes at a rate of p into the symptomatic class, or $(1 - p)$ entering the asymptomatic class. Individuals with the symptomatic form of the disease can recover from the infection and enter the removed compartment at a rate of γ (the mean recovery rate for meningitis) or die from the disease with a rate of μ (the death rate due to the disease). Those within the asymptomatic compartment exit into the removed category at the rate of γ. Individuals enter the removed category resistant to the disease for a period of time, α, then become susceptible again. The following ordinary differential equations (ODEs) were derived to represent this model:

$$\frac{dS}{dt} = \alpha R - \beta S(I_S + I_N) \quad (1)$$

$$\frac{dI_S}{dt} = p\beta S(I_S + I_N) - I_S(\mu + \gamma) \quad (2)$$

$$\frac{dI_N}{dt} = (1 - p)\beta S(I_S + I_N) - \gamma I_N \quad (3)$$

$$\frac{dR}{dt} = \gamma(I_S + I_N) - \alpha R \quad (4)$$

These ODEs give continuous average rates for each of the population compartments, susceptible, infected – symptomatic, infected – asymptomatic, and removed. A summary of this notation can be seen in Table 1.

Table 1: Summary of Notation

Symbol	Meaning	Value
α	Average Resistance Period	0.1
β	Contact Rate	varies with scenario
γ	Average Recovery Rate	0.1
μ	Average Death Rate Due to Meningitis	5% – 15%

The SI_SI_NR system parameters were determined using several methods. These methods require the formulation of several assumptions, however. First, since the simulation is to take place on the UCF main campus, the host population is taken to be constant, i.e. no births (incoming students) or deaths due to causes other than meningitis were considered. Secondly, the model considers homogeneous mixing of the campus population resulting in all individuals having an equal opportunity to contract the disease. Finally, this representation of meningitis assumes a recovery from the asymptomatic disease with no lasting immunity.

Contact rate, β, was determined for the specified campus area using the equation (5) derived by Rhodes and Anderson (2008).

$$\beta = \frac{8Rq\bar{v}}{\pi A} \quad (5)$$

This formula considers a moving population where the transmission rate of the disease is a factor of the density of the individuals. Here A is the area in which the population is constrained. The value used here is the area of UCF's main campus, 1,415 acres (5.73 km^2). The parameter R is the radius within which an infected individual must pass a susceptible person in order to transmit the disease. One centimeter was used as the value for this parameter. This distance was assumed, as transmission of meningitis is a result of touching or sharing very close spaces. In accordance with the U. S. Department of Transportation (DOT), 4 ft/sec (4.39 km/hr) was utilized as the population average speed, $\bar{v}$ (DOT 2003). The value for the probability of an

infective transmitting the infection, *q*, was changed within each scenario to be considered, allowing the creation of different levels of meningitis education within the population.

Table 1 also lists other parameter values specific to meningitis found through our research, they include:

- Rate at which a resistant host becomes susceptible ($\alpha = 0.1$) and the mean recovery rate from the disease ($\gamma = 0.1$) are the same used by Stollenwerk and Jansen (2003).
- Death rate due to the disease ($\mu = 5$ to 15%) was found in the article by Paneth, et al. (2000).
- Proportion of infectives developing the symptomatic form of meningitis (p = 11%) was derived by Caugant, et al. (1994).

2.2. Alternate Models

Three different alternative scenarios were considered in an effort to relate education and vaccination rates to a potential outbreak of meningitis on our closed college campus. These scenarios are presented in Table 2.

Table 2: Scenario Parameter Values

Parameter	Vari-able	Base Model	Educa-tion	Vaccina-tion	Education & Vaccination
Probability of Transmitting Infection	q	0.1	0.05	0.1	0.05
Number Vaccinated	v_0	0	10%	51%	75%
Calculated Contact Rate	β	0.017	0.0085	0.017	0.0085

Three assumptions were made in the formulation of these alternate scenarios. First, a program including education would reduce the probability of transmitting an infection by half through increasing the awareness of students with respect to the sharing of personal items and improved hygiene. This educational program, while not requiring vaccination, would however, increase the rate of vaccination within the student population by 10% due to an increased awareness of the risks associated with contracting meningitis. Secondly, due to the fact that we were unable to acquire actual statistics for vaccinations at UCF, we used the student vaccination rates determined by Paneth et al. (2000). They determined that a vaccination program similar to that already in place at UCF would result in 51% of the student population under the age of 30 being inoculated for the disease. Finally, that an educational awareness program would boost vaccination rates to equal 75% for use in that alternative model. Similar research on the effectiveness of an educational program that reached students prior to arriving on campus coupled with a vaccination program ultimately delivered significant improvements over time in the rates of vaccinated students. The increase ranges from 10% in the first year to 20% in the second year. "The total number of students immunized before or after arrival on campus increased from 40% in the baseline group to 50% in the class of 2004 (increase of 258 students) and to 60% in the class of 2005 (increase of 454 students when compared with baseline group). The authors concluded that education about the benefits of meningococcal vaccine before students' arrival on campus increased both the number of immunized students and the overall immunization rate among students" (Butler 2006).

3. RESULTS

The total number of dead and the number of days to reach that level for each of the various simulations are presented in Table 3. These numbers reflect the results of the simulation of the base model and the three alternative SI_SI_NR models.

Table 3: Numerical Simulation Results

	Base Model	Educa-tion	Vaccina-tion	Education & Vaccination
Number Dead	4,437	3,963	2,165	1,095
Number of Days	7.45	14.75	13.58	45.44

It is important to note that these values assume that from the onset of the disease, no action is taken to prevent further cases of the disease. In other words, mitigating actions (such as closing the campus or inoculations) by health officials do not occur. In the base model, there is less than eight days to recognize that an outbreak is occurring and take appropriate measures before more than 4,400 people are dead. Figure 1 graphically presents the results of the simulations.

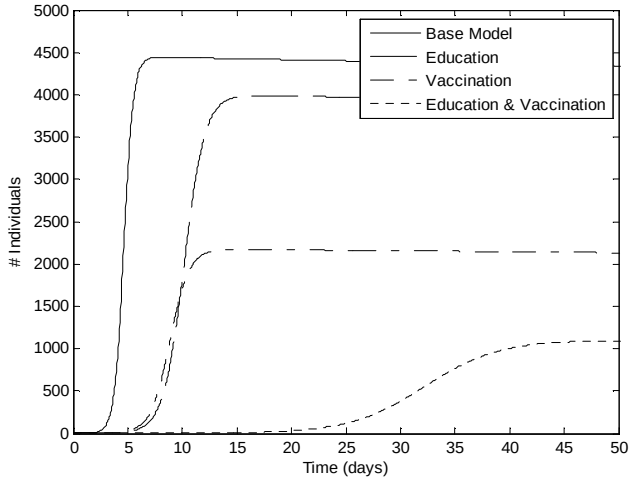

Figure 1: Simulation Results for Number Dead and Time to Death

Table 4 presents the effects of the three alternative designs from the baseline established by the base model. These effects are represented by decreases in the

number of deaths and the increased amount of time available before the total number of deaths occurs. Examination of the table reveals that the greatest decrease in the number of deaths occurs with a combined education and vaccination program (3,342 fewer deaths than in the base model). This also provided the greatest increase in time to react to the outbreak (45.44 more days than in the base model).

Table 4: Effect of Meningitis Reduction Programs from Base Model Results

	Education	Vaccination	Education & Vaccination
Effect on Deaths	-474 (-11%)	-2,272 (-51%)	-3,342 (-75%)
Effect on Days	+7.3 (98%)	+6.13 (82%)	+37.99 (510%)

4. Discussion and Comments

While the significance of the total number dead should not be overlooked, analysis of the simulation results should also consider the time it takes to achieve those deaths. Medical care in the United States is such that meningitis is diagnosed before these high numbers are reached. With that in mind, the results of the models need to be discussed in terms of the number of deaths and the time required for the disease to run its course.

4.1. Base Model

The first scenario, the base model was created using no consideration of vaccination or education. It involves the introduction of one infected individual into a totally susceptible and (by our assumptions) uneducated population. By that we mean, a population of 18 to 24 year olds living in close quarters not taking precautions against disease transmission, i.e. binge drinking, smoking, lack of physical activity, etc (Keeling 2002). Left unattended, this situation would be disastrous, resulting in over 4,400 students dead within an eight-day period. However, with the current state of health care we know that this outcome is extremely unlikely on a U.S. college campus.

4.2. Education Program

An important finding from the research is that an effective education program (one designed to change student's attitudes, and therefore lifestyle choices around the high-risk factors that increase the chances for contracting meningitis) has a significant effect on the transmission pattern of the disease (Figure 1). The results from the alternate model, which represented the use of an effective education program to minimize the risks associated with a meningitis outbreak, showed approximately a 10 percent decrease in deaths. However, possibly more important to health officials, it provided almost a 100 percent increase in the number of days available to health officials to react to a meningitis outbreak. It seems reasonable to assume that this increased time would be invaluable for agencies responsible for developing a response to an outbreak.

The current UCF "education program" is a statement on their health services website and waiver form informing students that engaging in high risk activities "… may make a person more likely to contract meningococcal disease include lifestyle factors, such as crowded living situations, bar patronage, active or passive smoking, irregular sleep patterns, and sharing personal items" (UCF 2007). Research indicates a warning statement is not an effective training strategy for an attitudinal goal such as changing one's lifestyle and will have little or no effect on student's lifestyle choices (Gagne, Briggs, and Wagner 1992). Therefore, for practical purposes it can be assumed that UCF does not have an education program to minimize the risk of meningitis disease and will not benefit from the increased time available to react to a meningitis outbreak (as depicted in Table 4). Programs such as Mr. 5th Guy on the UCF campus (encouraging all students to wash their hands and practice better hygiene) are a good start and can be useful components of an education program, but by themselves they do not provide a comprehensive anti-meningitis education program (Sander 2008).

4.3. Vaccination Program

The most effective single impact on a meningitis outbreak is the use of vaccination. Actual data quantifying the total number of students vaccinated, (v_0) as a result of the new immunization requirement that was implemented in July 2008 was unavailable for this research. The only available data was the number of students who were vaccinated, (v_0) by the UCF health center in 2007 through 2009. This information is shown in Table 5.

Table 5: Meningitis vaccination administered by the UCF Health Services Dept.

Year	2007	2008	2009
Totals	398	281	20

In the fall of 2008 there were 50,254 students enrolled resulting in a 0.55% (< 1%) vaccination rate. The data clearly did not provide the statistical confidence when compared to previous research regarding vaccination programs on college campuses. To establish a baseline, the number of vaccinated, (v_0) was estimated at 51% from previous research on undergraduate vaccination for college students under 30 years old (Paneth et al. 2000). The simulation input values were then chosen based on campus size and other critical parameters, they are: q = 0.1, v_0 = 51%, and β = 0.017.

The simulation indicated that an effective vaccination program is able to significantly reduce the number of fatalities by limiting them to 2,165. Additionally, the number of days to a full outbreak was nearly two times longer than the base model, but only approximately one-third the time of a combined education and vaccination program. Similar research on meningitis and the positive impact of a vaccination

program has proven that "This approach could eventually lead to a 53% reduction in meningococcal incidence and a 65% reduction in meningococcal deaths among persons aged 0–22 years" (Harrison 2000).

The cost for each vaccination at UCF is $103.00; however, that cost could be lowered significantly if the University contacted the appropriate state and federal health officials, and negotiated with the vaccine manufacturers to support an on campus inoculation program. Affordability is always a decision factor for most college students, therefore, it is expected that lowering the cost for a vaccination would increase the number of students who are vaccinated. "CDC officials analyzed the benefit and cost-effectiveness of immunizing college students with the licensed quadrivalent polysaccharide vaccine, and found immunization of all 1st year-students living in dorms would result in administration of 300,000 to 500,000 doses each year and would be estimated to prevent 15 to 30 cases of meningococcal disease and one to three deaths each year" (Butler 2006).

4.4. Vaccination and Education Programs

As expected, a program including education and vaccination proved to provide the most response time and least number dead. The data in Table 4 shows that this combination of policies significantly lowered the death rate by 75 percent (3,342 fewer deaths) and lengthened the time available to react to an outbreak by 510 percent, a net gain of 37 days. According to UCF Health Center officials, their meningitis outbreak protocol involves communicating with the Orange County Health Epidemiology Department (ORCHD), notifying the UCF Administrator and Medical Director of Health Services regarding the infection. Next, the records of the infected student are reviewed to determine whom he or she has been in contact with so that decisions can be made to treat the exposed with medication. Finally, if necessary they will set up a medication-dispensing center in the UCF Health Center. This protocol requires time and the increased time to react to an outbreak, which is afforded by a combination program, can be a significant benefit to health officials and provide UCF with the time necessary to properly implement its protocol.

Combining a vaccination program with education program about lifestyle choices, sanitary precautions (e.g., washing hands), proper nutrition, as well as learning about the signs of meningitis can be a significant benefit to the reduction of the meningitis death rate and increasing the time available to respond to the outbreak.

4.5. Future Research

This research demonstrated that deterministic simulations can be an effective tool for analyzing campus health concerns and examining the impact of various changes to health policy. Data obtained from simulations can then be utilized by campus health officials to review and/or revise meningitis prevention policies. Since the simulations are only as accurate as the data used in the models, health officials should work closely with the developers in order to provide them with the most accurate data possible. Future research could be made using stochastic models that can represent the uncertainty inherent in a meningitis outbreak. Future research should also explore the other contagious diseases this tool can model.

ACKNOWLEDGMENTS

We would like to acknowledge the help we received from the University of Central Florida Health Services department.

REFERENCES

Butler, Karen M. (4th Quarter 2006). *Meningococcal meningitis prevention programs for college students: a review of the literature.* Worldviews on Evidence-Based Nursing, 3:4, 185-193.

Castel, A., Reed, G., Davenport, M. G., Harrison, L. H., and Blythe, D. (2007). *College and university compliance with a required meningococcal vaccination law.* Journal of American College Health, 56:2, 119-127.

Collins, L., Dupont, L., and Nagie, D. (2003). *The impact of educational efforts on first-year university students' acceptance of meningococcal vaccine.* Journal of American College Health, 52:1, 41-43.

Gagne, R. M., Briggs, L. J., and Wagner, W. W. (1992). *Principles of Instructional Design*. New York, NY: Harcourt Brace College Publishers.

Kermack, W. O., and McKendrick, A. G. (1927). *A contribution of the mathematical theory of epidemics.* Proceeding of Royal Society, London Ser. A, 115: 700 – 721.

Keeling, R. P. (2001). *Is college dangerous?* Journal of American College Health, 50: 53-56.

Kuenzi, L. (2004). *Meningococcal education: more than just a vaccine.* Journal of American College Health, 53:2, 93-94.

Harrison, L. H. (2000). *Preventing meningococcal infection in college students,* Clinical Infectious Diseases. 30: 648–651.

Paneth, N., Kort, E. J., Jurczak, D., Havlichek, D. A., Braunlich, K., Moorer, G., et al. (2000). *Predictors of vaccination rates during a mass meningococcal vaccination program on a college campus.* Journal of American College Health, 49: 7 – 11.

Rhodes, C. J. and Anderson, R. M. (2008). *Contact rate calculation for a basic epidemic model.* Mathematical Biosciences, 216, 56 - 62.

Sander, L. (2008). *Colleges Put the Squeeze on Germs.* Chronicle of Higher Education. 54: 25.

Stollenwerk, N. and Jansen, V. A. (2003). *Evolution towards criticality in an epidemiological model for meningococcal disease.* Physics Letters A, 317: 87 – 96.

University of Central Florida Health Services (2007). Immunization Form. Available from: http://

www.hs.sdes.ucf.edu/healthcenter/forms/IMMUNIZATION%20FORM.pdf (30 March 2009).
University of Central Florida Health Services (2007). Home Page. Available from: http://www.hs.sdes.ucf.edu/ (30 March 2009).
University of Central Florida Office of Institutional Research (2008-2009). Enrollment 2008-2009. Available from: http://www.iroffice.ucf.edu/enrolment/2008-09/ (27 January 2009).
U. S. Department of Transportation (2003). *Manual on uniform traffic control devices.* MUTCD. Available from: http://mutcd.fhwa.dot.gov/HTM/2003r1/part4/part4l.htm (29March 2009).
Wu, S., Shuman, L., Bidanda, B., Kelley, M., Sochats K., and Balaban, C. (2008). *Agent-based discrete event simulation modeling for disaster responses.* Proceedings of the Industrial Engineering Research Conference. 1908-1912. British Colombia.

AUTHORS BIOGRAPHY

Tracy A. Atkins is a PhD student in the Modeling and Simulation program at the University of Central Florida (UCF). She also holds a Master's of Science degree in Industrial Mathematics from UCF, with a focus on the modeling of epidemics, and a Bachelors of Science degree in chemistry from Wilkes University in Pennsylvania. As a Chemist she chose to work on contaminated Super Fund sites in New Jersey and Florida as a Project Manager for an Environmental Laboratory. She then followed a passion for teaching and has taught mathematics at the middle school, high school, and college level. She holds teaching certificates in *Middle Grades Mathematics, Middle Grades Science,* and *High School Chemistry* and has the unique ability to relay complex concepts, in interesting and intelligible ways, to both new students and to those more educated. Following teaching she then returned to university life. Her Master's Thesis was entitled "*Modeling Transmission Dynamics of Tuberculosis Including Various Latent Periods"*. She is currently working on her dissertation research which is focused on epidemic modeling. She is a member of SIAM and several honor societies.

Ken K. Westerlund is a PhD student in the University of Central Florida's (UCF) Modeling and Simulation (M&S) program. He received Masters of Science degrees from Boise State University in Instructional and Human Performance Technology and from UCF in M&S. Ken received his Bachelors of Science degree in Professional Aeronautics from Embry-Riddle Aeronautical University. Ken is a graduate of the US Army's Aviator Course and a former Army Aviator, corporate pilot, and flight and simulator instructor. He holds FAA Airline Transport Pilot and Flight Instructor certificates, and professional accreditation as a Certified Performance Technologist (CPT). Ken has extensive experience in the utilization and application of simulation to training, and has authored and presented several articles and technical reports on the employment of PC-based aviation training devices, and on the application of human-factors training. Ken works with Dr. Valerie Sims in the Applied Cognition and Technology (ACAT) Research Lab at UCF. His research interests include cognitive science, artificial intelligence, human-robot interaction, and anthropomorphism as applied to human-robot teams. He is also aware of the contributions from other diverse fields and seeks to integrate knowledge from these fields to improve human performance.

Christine M. Allen is a research assistant working under contract for the Institute for Simulation and Training (IST) at the US Army RDECOM / STTC (Research, Development and Engineering Command / Simulation and Training Technology Center). She is currently co-authoring a paper for I/ITSEC 2009 entitled, "*Use of Biological and Environmental Malodors to Enhance Medical Training*." She has previously co-authored a paper on biomechanics entitled, "*A Mechanical Analysis of the Rotational Shot Put Strategies*" and presented conference papers entitled, "*Theories, Research, Practice: How the Biomechanist Can Communicated with the Coach"* and "*Factors Contributing to Softball Players Base Running Speed."* Her previous experience includes research at the Human Performance Laboratory at both Florida Atlantic University (Davie) and the University of West Florida (Pensacola). Her academic background includes an M.S. in Modeling and Simulation / Human Factors from the University of Central Florida (Orlando) and a B.S. in Exercise Science from the University of West Florida (Pensacola). She intends to pursue doctoral studies focusing on Medical Simulation and Training Systems Effectiveness.

Omar L. Thompson is a PhD student in the Modeling and Simulation program in the College of Sciences / Institute of Simulation and Training (IST) at the University of Central Florida in Orlando Florida. He earned his Masters Degree and Master Certificate from the College of Industrial Engineering and Management Systems and his Bachelor degree from the College of Electrical Engineering, all from the University of Central Florida. His doctoral research focus includes reliability modeling for determining laser performance and medical simulation. In addition to his academic career, Mr. Thompson is the group lead for the Reliability Engineering and Failure Analysis group at Northrop Grumman Laser Systems. In his leadership position, he is actively involved in reliability modeling for cutting edge designs of laser targeting and guidance systems for U.S Department of Defense. He has been acknowledged with various performance awards which include the 2008 Northrop Grumman Presidential Leadership Award and the QUEST Award from United Space Alliance. His professional experience spans both the commercial and military industries including the National Aeronautics and Space Administration, NASA

at the Kennedy Space Center. He was identified as a key player to support the shuttle program in indentifying the root cause for the point sensor issue that contributed to the delaying of the launch of shuttle Discovery, OV-103 on the first return to flight after the shuttle Columbia disaster. He is active within his community and supports various work focus groups.

OUTPATIENT APPOINTMENT SCHEDULING WITH PATIENT CHARACTERISTICS

Athula Wijewickrama[(a)]

[(a)]Graduate School of Economics & Business Administration, Nagoya University, Aichi, Japan

athulawij@soec.nagoya-u.ac.jp

ABSTRACT

There has been a little attention given on to patient sequencing issues in appointment scheduling design. This is investigated in an outpatient system with and without adjusting appointment intervals using simulation methodology. Different appointment systems are simulated, combining appointment rules and patient sequences, including variability of consultation time, with the adjustment of appointment intervals based on patient groupings. The study identifies the most suitable appointment system and interval adjustment to be made for a given situation relation to the trade-off between patient waiting time and physician overtime and idle time.

Keywords: appointment scheduling, simulation, patient sequencing

1. INTRODUCTION

In the outpatient department, long waiting times for treatment followed by short consultations have long been complaints of patients. In Japan it is often phrased as "waiting for three hours to be seen for three minutes". This disproportionately long waiting time in the consultation room has over the years been the focus of study among academicians and practitioners. Most researchers have stressed that the major reason for long waiting times is the poor patient appointment system (AS) put in place. Over the last fifty-six years numerous researchers, from the works of Bailey (1952) to Klassen and Yoogalingam (2008), have investigated this issue extensively. However, the solution space for the appointment scheduling problem consists of an enormous number of solutions as it is analytically intractable (Robinson and Chen 2003).

The prevailing AS range from single-block appointments on one extreme to individual appointments on the other side. The past studies were designed AS such as single block, individual block fixed interval with and without an initial block, multiple block fixed interval with and without an initial block, variable block fixed interval, individual block variable interval and multiple block variable interval rules. A comprehensive review of the literature on AS can be found in Cayirli and Veral (2003).

Most of these AS studies concentrated on the appointment rule (scheduling) by arranging patients in a first-come first-serve (FCFS) basis, rather concentrating than on the order of the service (sequencing). It is apparent that initial consultation is significantly longer than the return visits (see Graugaard, Holgersen, and Eide, et al 2005). Physicians display more facilitating behavior with patients who are older, female, better known to the doctor, with complex consultations, and with severe diseases (see Zanbelt, Smets, and Oort, et al 2006). In a radiology department study, it was found that the completion time of a patient is shown to depend strongly on his origin (inpatient and outpatient), age, and mobility (Walter 1973). Based on these characteristics, patients can be classified for scheduling purpose.

Past studies in AS design have used patient heterogeneity concentrating on three major patient classifications: New and return basis (Cox, Birchall and Wong 1985; Cayirli, Veral, and Rosen 2006; Wijewickrama and Takakuwa 2008), variability of consultation time (Wang 1999; Klassen and Rohleder 1996) and type of procedure (Vanden Bosh and Dietz 2000).

The study of Cayirli, Veral, and Rosen (2006) concluded that sequencing decisions have a more pronounced impact on performance than the choice of an appointment rule which is contrary to a similar study conducted by Wijewickrama and Takakuwa (2008). More recently, by extending the scope of their previous developments, Cayirli, Veral, and Rosen (2008) introduced a well-designed AS with adjusting appointment intervals to match the consultation time characteristics of different patient classes. The combined effect of "new" and "return" classification and interval adjustment improved patient waiting times and doctor idle time simultaneously.

The overall objective of current study is to identify an efficient AS by combining appointment rules with patient sequences. The study investigates the impact of sequencing patients, including variability of consultation time, by adjusting and not adjusting appointment interval on patient classes. To the best of our knowledge, the appointment interval adjustments on the variability of consultation time have not been investigated in the literature. Although some past studies have combined patient sequences with appointment rules, a little attention has given on "variability of consultation time" in sequencing patients for appointment rules. Therefore, another objective of

this study is to asses the variability of consultation time in sequencing patients for different appointment rules.

2. RESEARCH METHODOLOGY

2.1. Appointment Rules, Patient Sequences and Interval Adjustments

The present study considers six appointment rules (ARULE) shown as follows.

First, there is the original Bailey rule, which sets up two patients at the beginning of the session and then organizes patients individually based on the mean consultation time (Bailey 1952).

$$A_1 = A_2 = 0$$
$$A_i = A_{i-1} + \mu_t \text{, for i} > 2 \quad (1)$$

Where A_i = Patient i^{th} appointment time, and μ_t = Mean consultation time

This rule is included because it has performed well in reducing physician idle time in many past studies (Ho and Lau 1992; Cayirli, Veral and Rosen 2006; Klassen and Rohleder 1996).

Secondly, the rule 3Bailey is a variation of the original Bailey rule, setting up three patients for the initial block.

$$A_1 = A_2 = A_3 = 0$$
$$A_i = A_{i-1} + \mu_t \text{, for i} > 3 \quad (2)$$

The 3Bailey is also included based on its strong performance, as recorded in Brahimi and Worthington (1991).

Thirdly, the Ind is an individual-block/fixed-interval system that calls patients individually at intervals equal to the mean consultation time.

$$A_1 = 0$$
$$A_i = A_{i-1} + \mu_t \text{, for i} > 1 \quad (3)$$

This rule is used because it is a good benchmark due to its popularity in practice.

Fourthly, 2Attime is the original Soriano rule, which allocates two patients at a time with an interval of twice the consultation time (Soriano 1966).

$$A_i = A_{i+1} = (i-1)\mu_t \text{, for i} = 1, 3, 5, \ldots\ldots \quad (4)$$

This rule is considered due to its contradictory performance, as shown in past studies (Soriano 1966; Cox, Birchall and Wong 1985; Ho and Lau 1992).

The fifth rule is one variable-interval rule (VI), the best rule introduced by Ho and Lau (1992), which adjusts appointment time so that the earlier patients setting earlier and the rest setting later compared to individual-block/fixed-interval system.

$$A_i = (i-1)\mu_t - 0.15(k-i)\sigma_t \text{, for i} \le \text{k}$$
$$A_i = (i-1)\mu_t + 0.30(i-k)\sigma_t \text{, for i} > \text{k} \quad (5)$$

Where σ_t = Standard deviation of consultation time, k = i^{th} patient, which divides n into two groups; n = Total number of patients in a given session

Finally, the Dome rule is also one of the variable interval rules introduced in recent analytical studies (Robinson and Chen 2003). They have identified the *dome* pattern of inter-arrival times, which optimized the solution. This dome pattern made inter-arrival times shorter at both the beginning and the ending of a session and longer in the middle. The following equation, which was originally used by Cayirli, Veral and Rosen (2006), can be used to derive this rule.

$$A_i = (i-1)\mu_t - 0.15(k_1-i)\sigma_t \text{, for i} \le \text{k}_1$$
$$A_i = (i-1)\mu_t + 0.30(i-k_1)\sigma_t \text{, for k}_1 < \text{i} < \text{k}_2$$
$$A_i = (i-1)\mu_t - 0.05(k_2-i)\sigma_t \text{, for i} \ge \text{k}_2 \quad (6)$$

The current study sequences patients in terms of patient class. Patients are sequenced or arranged in the appointment schedule based on two classes, "new or return" and the "variability of consultation time". This study uses six sequencing rules (PSEQ) based on patient classes that were originally used by Klassen and Rohleder (1996) and Cayirli, Veral and Rosen (2006).

The rule of first-come, first-served (FCFS) represents the standard existing system in hospitals whereby patients are not seen according to patient type or category of problem. The "appointments at the beginning" rule (APBEG) arranges all patients with appointments first and then allows for the arrival of new patients. The "new patients at the beginning" rule (NPBEG) sequences all new patients first and then arranges consultations for patients with appointments. The alternate rule (ALTER) assigns appointment and new patients in an alternating manner. After the last new patient is assigned, the rest of the patients with appointments are assigned based on the order of their arrival. The alternate-5 rule (ALT5) assigns a new patient after every five patients with appointments. This process is repeated until the last new patient in the schedule is seen. The rest of the appointment patients are assigned based on the order of their arrival. Finally, the variance rule (VAR) sequences patients from the beginning of the session in increasing order of consultation time variance, using the patient class "variability of service time".

These sequences are arranged using two factors, with or without time adjustments to appointment intervals based on the "new or appointment" categorization and the "variability of consultation time" consideration.

Designing a credible appointment system (AS) has become an extremely challenging task due to the inherited uncertainties of the outpatient facility. The major problem is to design appointment slots such that the difference between the actual consultation time and the appointment slot is minimized. As we identified

earlier by reviewing the literature, since consultation time can vary according to patient characteristics, time adjustments can be made on it in order to tailor the appointment slot to the actual consultation time.

This study makes time adjustments based on patient characteristics, allocating a shorter interval for "appointment" and "low variable consultation time" patients and a longer interval for "new" and "high variable consultation time" patients.

The AS analysis used in this study can be summarized with two cases (CASEs):

- *Case 1: Combination of ARULEs and PSEQs without adjustment of appointment intervals.* Considering only the order of services, patients are sequenced on a "new and appointment" basis using APBEG, FCFS, NPBEG, ALTER and ALT5 rules, and on a "variability of consultation time" basis using VAR, while setting appointment slots identical to the overall mean consultation time of all patients.
- *Case 2: Combination of ARULEs and PSEQs with interval adjustment based on patient characteristics.* Patients are assigned as "new and appointment" under the APBEG, FCFS, NPBEG, ALTER, and ALT5 rules, and according to their "variability of consultation time" under the VAR rule. Following this, a longer interval is assigned for new and high variance consultation time patients and a shorter interval is assigned for appointment and low variance consultation time patient. All of these interval adjustments are based on their respective mean consultation times.

In sum, the study considers six ARULEs and six PSEQs in terms of the adjustment and non-adjustment of appointment intervals based on patient characteristics; in total, 72 different ASs (6ARULE * 6PSEQ * 2 Adjustments = 72) are developed.

2.2. Measures of Performance and Simulation Model

This study considers one composite measure combining two conflicting performance measures, namely average patient waiting time per patient (A*WT*) and average physician idle time and overtime per patient (A*IOT*).

$$AWT = \frac{1}{n}\sum_{i=1}^{n} WT_i \qquad (7)$$

$$AIOT = \frac{1}{n}\sum_{j=1}^{d} IT_j + 1.5\left(\frac{1}{n}\sum_{j=1}^{d} OT_j\right) \qquad (8)$$

WT_i is the time difference between the consultation start time and the arrival time of patient i. In consultation, the arrival time is equal to the appointment time, as the study assumes patients are punctual. By dividing the total waiting time by the number of patients seen (n), the average waiting time per patient (AWT) is calculated.

In equation (8), IT_j is the total idle time of doctor j, which is the summation of the idle time that occurs between every two consecutive patients in j^{th} doctor's daily schedule. Hence, the total idle time of physician 1 to d in (8) is divided by the total number of patients seen (n) in order to derive the average physician's idle time per patient.

Similarly, physicians' average overtime is calculated by dividing the total overtime of physicians 1 to d in (8) (total session time-240 minutes) by the total number of patients seen. Idle time and overtime are combined by fixing overtime costs at 50 percent higher than idle time costs.

The objective is to identify an AS in which the combined cost (TC) of patient waiting time and physician idle time and overtime is minimized for a given unit value of waiting cost for patients (π) and average idle time and overtime cost for physician per patient (ω). Formally, this is:

$$TC = \pi AWT + \omega AIOT \qquad (9)$$

This study assumes the value of π and ω as 1.

For the purpose of developing a "modelled outpatient centre", the data was collected from three outpatient departments of three large hospitals in the Aichi and Gifu prefectures in Japan. The largest outpatient department of the three has over two thousand patient visits per day and employs a total of one hundred and ten physicians to consult with appointment and new patients in twenty-nine clinical departments. The number of patients visiting each clinical department differs; for example, it ranges from 19 patients for home medicine to 107 patients in diabetology and endocrinology. There tend to be a varied number of patients assigned for each departmental doctor, such as, for example, eight in haematology to twenty-one in diabetology and endocrinology. The observed three outpatient departments had different numbers of clinical departments with varying numbers of physicians and session lengths. The required data were collected using electronic medical records and observation. The purpose of the data is to establish the validity of the input parameters used in the study and not to illustrate the state of a specific clinic.

Patients have to be classified as "new or appointment" and based on the "variability of consultation time" for sequencing purposes. In the case of the "new and appointment" classification, using an independent-sample t-test, a statistically significant difference is found at $p<0.05$ for consultation times for patients with appointments [μ=9.30, σ=1.96] and for newly arrived patients [μ=14.67, σ=1.46]. The practical significance of the difference is also high, as *eta* squared is 0.53. The second categorization of patients is based on the "variability of consultation time". Using the standard deviation of the consultation time (± 2.75), each patient is assigned to either the low or the high variability category, and an independent-sample t-test is conducted to find the difference between the two groups. A significant difference in consultation times is

revealed at $p<0.05$ for high variable [$\mu=10.14$, $\sigma=3.57$] and low variable [$\mu=10.28$, $\sigma=0.71$] groups, despite a negligible effect size (*eta* squared = 0.001).

Consultation times are modelled as lognormal distributions (Lognormal(μ_t,α_t)). The use of lognormal distribution in health care services is theoretically sound (Law and Kelton 1991) and empirically validated (Cayirli, Veral, and Rosen 2006, 2008; Klassen and Rohleder 1996). In the current study, this distribution is the best at categorizing consultation times in terms of the Kolmogorov-Smirnov test ($\alpha=0.05$), and it is consistently used in time adjustments to patient groupings.

Each session of a physician is modelled to consist of twenty patients with appointments and four new patients (24 patients), who are given a predetermined schedule. The literature shows varying appointments per session: 21 (Klassen and Rohleder 1996), 25 (Bailey 1952), 10, 20 and 30 (Ho and Lau 1992), and 10 (Cayirli, Veral, and Rosen 2008). Here the appointment interval disregarding time adjustments is ten minutes, so that the length of a session is 240 minutes (4 hours). However, the length of the session varies with the employment of time adjustments in terms of patient classifications. In consultation, the return patients have priority over new patients. It is assumed that patients are punctual, with zero no-shows and no walk-ins. Similarly, physicians are also assumed to be punctual, with no breaks or interruptions. In calculating the effect of earliness and the effect of lateness when the VI rule is used, the best achieved parameters chosen for the study were those used by Ho and Lau (1992) and Cayirli, Veral, and Rosen (2006) and are 0.15 and 0.30, respectively. Similarly, based on Cayirli, Veral, and Rosen (2006), the values 0.15, 0.3 and 0.05 were used as the three coefficients of earliness and lateness effects in the case of the Dome rule.

The principal data source for this study is electronic medical records. This database contained information regarding patient-appointment time, log-on and log-off time for the consultation, type of consultation (appointment or new), category based on the required consultation service and physician consulted. Statistics were collected after 100 replications for each of the averages of 100 runes per session.

The impact of the independent variables on the dependent variables in terms of main effects and interactive effects can be analyzed using factorial ANOVA. As there are six appointment rules, six patient sequences, and two levels of appointment intervals on patient classes, a full factorial ANOVA is employed with statistical analysis using SPSS. Further, the concept of efficient frontier is employed to investigate the trade-off between physician's idle time including overtime and patients' waiting time.

3. RESULTS AND DISCUSSION

Appointment systems are formed by adjusting or not adjusting time intervals in each patient sequence as described in section 2.1. Table 1 shows the ANOVA results for case 1, where the dependent variable, total cost of patient and physician idle time and overtime (TC), was affected by the sequencing of patients based on patient characteristics but without adjusting the time intervals.

The main and interactive effects are statistically significant at the $p<0.05$ level. Although ARULEs account for a majority of the variation, the magnitude of the difference in comparison to the effect of PSEQs is not large. The impact on TC is strengthened by the combined effect of ARULEs and PSEQs (*eta* squared = 0.58).

A post-hoc comparison indicates that the mean values of TC under all ARULEs are significantly different from each other at $\alpha=0.05$. Overall, VI reduces TC, substantially while 3Bailey conversely increases it. In the case of PSEQ, the mean TCs of APBEG with VAR and FCFS with ALT5 do not differ significantly from each other. APBEG and VAR work better than the other four sequencing rules in reducing TC, while NPBEG increases TC under any ARULE combination.

Secondly, as in case 2, patient sequences and interval adjustments are made based on patient classes. The results with regard to TC are shown in Table 2 below. Upon introducing interval adjustments based on patient class to case 1, the impact of ARULEs on TC becomes stronger than that of PSEQs. Although the two main effects are significant at a 0.05 level, the effect of the PSEQs on TC is weak (eta squared = 0.40). Nevertheless, at a 0.05 significance level, the combined effect of PSEQs and ARULEs is greater than the main effect of PSEQs due to the power of ARULEs. The mean comparisons for ARULEs and PSEQs, respectively, do not exhibit a great degree of difference from what was seen in the previous analysis of case 1.

In sum, some important characteristics can be identified when two cases are compared. Multiple comparison procedures indicate that there are significant differences among the ARULEs in all two cases at the $\alpha=0.05$ level, signalling how critical ARULEs are to AS design. In both cases, VI performs best and 3Bailey deteriorates the performance of TC. Meanwhile the Dome, 2Attime and Bailey rules ranked third, fourth, and fifth in improving TC compared to VI. In terms of PSEQs, the APBEG and VAR are able to improve TC more significantly than the others at a 5% level of significance. On the other hand, the NPBEG sequence worsens TC in both cases. In both situations, the power of ARULEs in determining TC is considerably higher than that of PSEQs.

A well-designed AS must have the ability to reduce both waiting time and idle time and overtime simultaneously. For this purpose, efficient frontiers are derived by integrating AWT and AIOT, as displayed in Figures 1 and 2, corresponding to each two cases, respectively. The efficient frontier moves from the upper left to the lower right. Each AS is arranged on the frontier corresponding to a particular value of the ratio

Table 1: ANOVA results of sequencing patients on patient class without time adjustment (case 1)

Source	Type III Sum of Squares	df	Mean Square	F	Partial Eta Squared
Corrected Model	147964.103[(a)]	35	4227.546	5308.155	.981
Intercept	1348075.282	1	1348075.282	1692658.666	.998
PSEQ	59296.947	5	11859.389	14890.784	.954
ARULE	84733.835	5	16946.767	21278.553	.968
PSEQ * ARULE	3933.321	25	157.333	197.549	.581

a R Squared = .981 (Adjusted R Squared = .981)

Table 2: ANOVA results of sequencing patients on patient classes with time adjustment (case 2)

Source	Type III Sum of Squares	df	Mean Square	F	Partial Eta Squared
Corrected Model	105432.177[(a)]	35	3012.348	4697.552	.979
Intercept	717499.711	1	717499.711	1118892.188	.997
PSEQ	1520.655	5	304.131	474.272	.400
ARULE	96611.229	5	19322.246	30131.733	.977
PSEQ * ARULE	7300.293	25	292.012	455.373	.762

a R Squared = .979 (Adjusted R Squared = .979)

ω/π (unit cost of an average physician's idle time and overtime/unit cost of a patient's waiting time), which reflects the importance of physician idle time and overtime relative to that of patient waiting time.

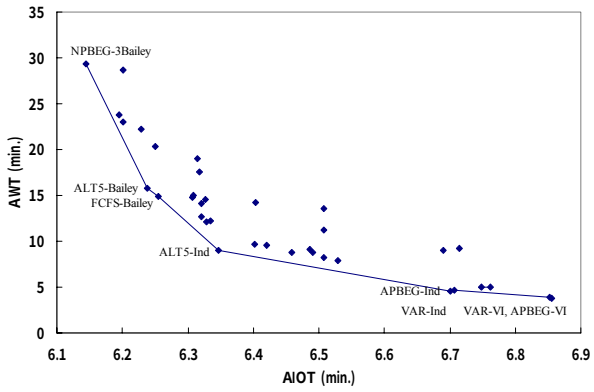

Figure 1: Efficient frontier of case 1

According to Figure 1, case 1 shows the frontier for the combined effect of ARULE and PSEQ without adjusting the time interval. Among the eight ASs on the frontier, the simple Ind rule emerges in three instances. The Bailey and the 3Bailey rules have the power to save AIOT; conversely, VI dominates two locations in reducing AWT. In terms of PSEQs, the outperformed VAR and APBEG sequences on TC fall to the right-lower quarter of the graph due to the reduced AWT. Interestingly, the original Bailey rule (FCFS-Bailey) and Klassen and Rolder's (1996) best rule (VAR-Ind) have positioned the frontier and any combination of 2Attime and Dome rules have not touched the frontier.

Figure 2 shows the situation of case 2 on the time-adjusted frontier in terms of patient classification. It is apparent that Bailey and 3Bailey dominate the frontier, not only combining sequence rules but also with their original aspects by combining FCFS. The Ind and VI position in the lower right portion of the frontier are due to the lengthy AIOT. Although 2Attime and Dome have not reached the frontier, each sequencing rule has reached the frontier at least once. As in case 1, the 3Bailey rules are positioned with relatively higher AWT points. The Bailey and Ind have reached the frontier and resultantly lowered both AWT and AIOT. In terms of patient sequences, the ALTER rule has reached the frontier on two occasions by combining with each of Bailey and VI.

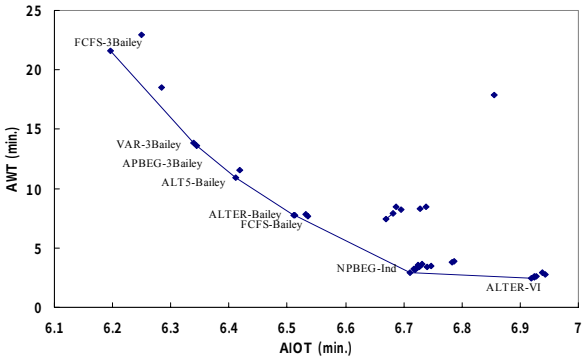

Figure 2: Efficient frontier of case 2

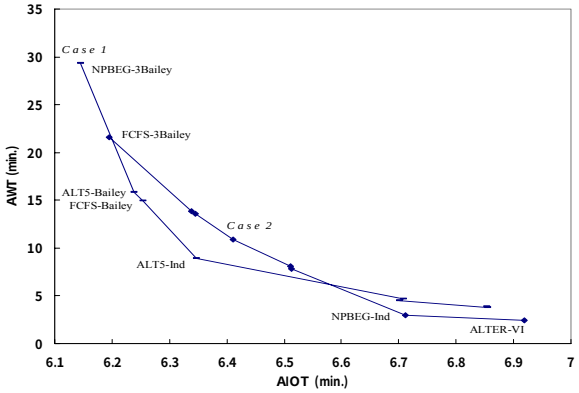

Figure 3: Analysis of two frontiers together

Finally, the next effort is to identify the best AS by analyzing the two frontiers together, and Figure 3 shows the two frontiers corresponding to each of the two cases.

In total, seven feasible ASs are considered as the best of all sixteen ASs located on the frontiers. These ASs, in increasing order of value considering patient time over physician time, are NPBEG-3Bailey, FCFS-3Bailey, ALT5-Bailey, FCFS-Bailey, ALT5-Ind, NPBEG-Ind and ALTER-VI.

Health care managers can choose one AS from among the seven best systems based on desired ω/π value. More specifically, if patient time is more valuable, then the preferable option is the use of either VI or Ind rule in sequencing appointment and new patients in an alternating manner (APBEG-VI) or new patients at the beginning (NPBEG-Ind). For this option, appointment time has to be adjusted based on patient characteristics. At the other extreme, when physician time is the major concern, sequencing new patients at the beginning using the 3Bailey rule (NPBEG-3Bailey), without making a time adjustment, is best. In a situation where both waiting time and idle time and overtime are taken into account, either Bailey or Ind can be used in sequencing ALT5 or FCFS (ALT5-Bailey, FCFS-Bailey and ALT5-Ind). For these systems, no time adjustment is required.

One important finding can be noted by looking at the best seven ASs in Figure 3. Klassen and Rolder's (1996) best rule (VAR-Ind) or any rule combined with VAR sequence has not come to our final solution.

4. CONCLUSIONS

First, it is identified that time adjusted AS made on patient classification is preferable when patient time is the key concern. When physician time alone or both patient-physician times are more valuable, the preferable option is the use of AS made on without making a time adjustment. Second, in developing a well-designed AS, the impact of appointment rule is categorically higher than that of patient sequence. Third, any rule combined with the sequence of "service time variability" is not performed well though it performs satisfactory in each "case" separately.

It is interesting to observe the results of this study enhancing two aspects of the model. One incorporated second consultation in addition to first consultation while the second widen the scope of the study by identifying patient sequencing issues in terms of physician characteristics.

ACKNOWLEDGMENTS

This research was supported by "Grant-in-Aid for Scientific Research" of Japan Society for the Promotion of Science (JSPS).

REFERENCES

Bailey, N.T., 1952. A study of queues and appointment systems in hospital out-patient departments, with special reference to waiting-times. *Journal of the Royal Statistical Society*, 14, 185-199.

Brahimi, M., Worthington, D., 1991. Queuing models for out-patient appointment systems – A case study. *Journal of Operational Research Society*, 5, 91-102.

Cayirli, T., Veral, E., 2003. Outpatient scheduling in health care: A review of literature. *Production and Operations Management*, 12, 519-549.

Cayirli, T., Veral, E., Rosen, H., 2006. Designing appointment scheduling systems for ambulatory care services. *Health Care Management Science*, 9, 47-58.

Cayirli, T., Veral, E., Rosen, H., 2008. Assessment of patient classification in appointment system design. *Production and Operations Management*, 17, 338-353.

Cox, T.F., Birchall, J.F., Wong, H., 1985. Optimizing the queuing system for an ear, nose and throat outpatient clinic. *Journal of Applied Statistics*, 12, 113-126.

Graugaard, P.K., Holgersen, K., Eide, H. et al., 2005. Changes in physician-patient communication from initial to return visits: a prospective study in a haematology outpatient clinic. *Patient Education and Counseling*, 57, 22-29.

Ho, C., Lau, H., 1992. Minimizing total cost in scheduling outpatient appointments. *Management Science*, 38, 1750-1764.

Klassen, K.J., Rohleder, T.R., 1996. Scheduling outpatient appointments in a dynamic environment. *Journal of Operations Management*, 14, 83-101.

Klassen, K.J., Yoogalingam, R., 2008. An assessment of the interruption level of doctors in outpatient appointment scheduling. *Operations Management Research*, DOI 10.1007/s12063-008-0013-z.

Law, A.M., Kelton, W.D., 1991. *Simulation Modeling and Analysis.* McGraw-Hill, New York.

Robinson, L.W., Chen, R.R., 2003. Scheduling doctors' appointments: Optimal and empirically-based heuristic policies. *IIE Transactions*, 35, 295-307.

Soriano, A., 1966. Comparison of two scheduling systems. *Operations Research*, 14, 388-397.

Vanden Bosh, P.M., Dietz, C.D., 2000. Minimizing expected waiting in a medical appointment system. *IIE Transactions*, 32, 841-848.

Walter, S.D., 1973. A comparison of appointment schedules in a hospital radiology department. *British Journal of Preventive Social Medicine*, 27, 160-167.

Wang, P.P., 1999. Sequencing and scheduling *N* customers for a stochastic server. *European Journal of Operational Research*, 119, 729-738.

Wijewickrama, A., Takakuwa, S., 2008. Outpatient appointment scheduling in a multi facility system. *Proceedings of the 2008 Winter Simulation Conference,* pp. 1563-1571. December 8-10, Miami (Florida, USA).

Zanbelt, L.C., Smets, L. M., Oort, F.J. et al., 2006. Determinants of physicians' patient-centred behaviour in the medical specialist encounter. *Social Science & Medicine*, 63, 899-910.

AUTHOR BIOGRAPHY

Athula Wijewickrama is a senior lecturer in the department of Decision Sciences at the University of Sri Jayewardenepura, Sri Lanka. He pursued a B.Sc. Degree in business administration from Sri Jayewardenepura University and an MBA Degree from Colombo University, Sri Lanka. He received a Master's and Ph.D. in industrial management systems at Nagoya University, Japan. He has a diploma in computer systems design from the National Institute of Business Management, Sri Lanka. His research and teaching interests are in simulation of service systems, operations management and management of small and medium sized enterprises. Currently he is working as a postdoctoral research fellow at Nagoya University.

SICMA
SIMULATION OF CRISIS MANAGEMENT ACTIVITIES

G. La Posta[(a)], T. Mischi[(b)]

[(a)] [(b)] Elsag Datamat S.p.A, Rome, Italy

[(a)] giuseppe.laposta@elsagdatamat.com, [(b)] tiziano.mischi@elsagdatamat.com

ABSTRACT

Modern crises are progressively changing their character from 'predictable' emergencies capable of being countered with existing crisis management tools and techniques, to unpredictable events. Governments and first responders require new, innovative and affordable solutions to be better prepared before an incident, and to respond more efficiently and effectively during an incident. The use of simulation technologies can offer a big improvement on current practices because it allows the decision makers to evaluate different alternatives not just with static data but with continuously evolving scenarios. Within this context, the SICMA FP7 capability project aims at demonstrating if and how an integrated suite of modeling and analysis tools could improve the effectiveness of the decision making process. The aim of this paper is to provide an overview of the mission area, the critical operational issues and the role of the SICMA project in the depicted context as well as the current achievements.

Keywords: decision support system, crisis management, healthcare organizations, modeling and simulation.

1. INTRODUCTION

A crisis can be defined as an event involving major damage and injury to people and property of sufficient magnitude to create a temporary imbalance between the large scale needs of a community and the availability of resources able to provide the emergency care to address these needs (Frykberg 2007). Moreover a crisis may:

- cross jurisdictional boundaries, resulting in multiple organizations being faced with overlapping responsibilities,
- exceed the capacities of single organizations requiring them to be supported by other organizations that are unfamiliar with the procedures.

As a consequence, the response to a crisis is the result of the activities of:

- different services (e.g. police, medical care, rescue forces, fire fighting, etc),
- interacting vertically (i.e. with components of the same organization) and horizontally (i.e. with components of other organizations),
- in a complex environment.

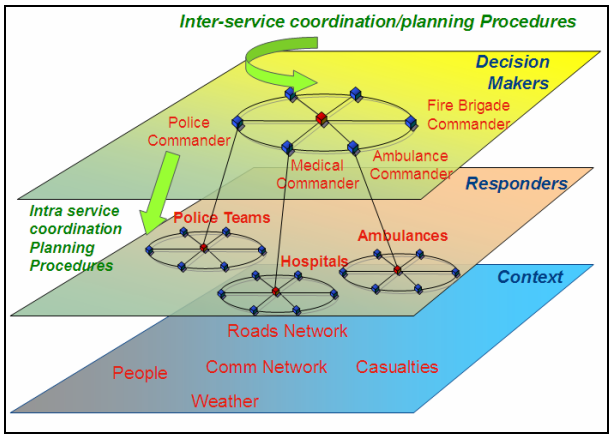

Figure 1: Crisis Management - Layered View

Within this context, the main operational issue lies in the difficulty to have even a rough estimate of how the crisis management system will respond to the crisis and, as a consequence, the impossibility to identify those key leverage points of change that enable the overall system to produce significant shift in its performance.

Several causes of the unpredictability of the response can be identified at different levels:

- *Service level*: the overall response to the crisis will depend not only on the quantity and quality of the individual entities but also largely on how those entities cooperate in harmony with one another through the entire scenario, at national and at trans-national level.
- *Cross-service level*: although individual service organization may be quite effective, the system as a whole may experience a significant "failure to respond" due to a faulty or deficient inter-service interaction.
- *Context Level*: such complex system of systems made of components strongly interrelated, self-organizing and dynamic will

have to operate in a complex environment where the situation evolution will be determined by predictable factors (e.g. responders behaving according to the agreed procedures) to a given extent and will be subject to unpredictable factors (e.g. crowd behavior, traffic gridlock, human behavior etc) otherwise.

Last but not least, during an emergency an organisation responds by performing specific tasks according to defined procedures. The most effective procedures need to be implemented correctly to provide the expected results.

2. PROJECT OBJECTIVES

The role of the SICMA project is to demonstrate "if" and "how" an integrated suite of modeling and analysis tools providing insights into the collective behavior of the whole organization in response to crisis scenarios could improve the effectiveness of the decision making process.

With respect to the four phases the Crisis Management process is usually divided into (i.e. Mitigation, Preparedness, Response and Recovery), the SICMA project aims at improving crisis managers decision-making capabilities in the following phases:

- *Preparedness*: assisting in the identification of the best way to employ available assets, the limits of the achievable response and the effectiveness of different inter/intra services cooperation procedures
- *Response*: providing a forecast of scenario evolution, proposing doctrine-based solutions and evaluating the effects of alternative decisions.

The main focus will be on the Health Service response where decision-making support will be provided through the achievement of the following main objectives:

- *"Bottom-Up" Health Service modeling*: to provide insights into the collective behavior of the whole Health Service system (namely Medical and Ambulance Services) in response to different crisis situations and decision implementations by modeling the behavior of its components as well as the rules they operate by (A.L.S.G., 2002).
- *Procedure Support*: to make use of state of the art technology to provide the user with the correct procedures to better solve the problem (once the problems to solve and the decisions to make are identified).
- *Analysis of the effects of unpredictable factors*: to study the effects of unpredictable factors (like human behavior, size/specifics of the incident) to present the user with a "distribution" of the effectiveness of a certain "decision" rather than the effectiveness of that solution deterministically dependent on the preconceived scenario.

The combined effects of the above points will allow to document both the unexpected bad and good things in the organization(s) thus leading to better responses, fewer unintended consequences and greater consensus on important decisions.

Last but not least, the use of simulation technologies in the SICMA system can offer a big improvement on current practices because it allows the decision makers to evaluate different alternatives not just with static data but with continuously evolving scenarios in which:

- casualties are generated in response to certain events;
- each component of the emergency management system is simulated, giving insight into how the diverse elements of the architecture (i.e. different services or different components within one service) interact with one another throughout the entire scenario.

3. SCENARIOS

The following scenarios have been selected:

Conventional weapons terrorist attack: being the most common and hence the most likely threat in the future, this scenario will be used to evaluate the decision support achievable with the SICMA prototype in the management of casualties.

The focus will be on the management of the most likely category of casualties that can be generated by a large number of different types of disasters that is: trauma casualties.

Chemical weapons terrorist attack: specific types of disasters may result in additional decision making activities to be carried out by the crisis manager.

This scenario will be used to highlight the additional support that can be provided to decision making activities specifically related to the kind of accident.

The CCS/decontamination-station deployment and hazard estimate/update will be used as case study in the chemical attack Scenario.

4. CURRENT ACHIEVEMENTS

The project has been divided into four phases: User Requirement Analysis, High Level System Design, Prototype Development and Case Study Implementation.

At the end of the first year of activities the first two phases have been closed. More in detail:

- the user requirements have been identified starting from an analysis of the mission area and the critical operational issues and defining the role of the SICMA project in this context;

- the system requirements have been defined;
- the high level design (i.e. the identification of the system components and the allocation of the required functionalities to each component) of the simulator and tools suite has been performed.

The high level architecture of the system and the different modes of operation are reported and detailed in the following paragraphs.

5. ARCHITECTURE AND TECHNOLOGIES

The SICMA prototype distributed architecture (Fig. 2) is composed of: an Integration Infrastructure, a Graphical User Interface (GUI) and several modules.

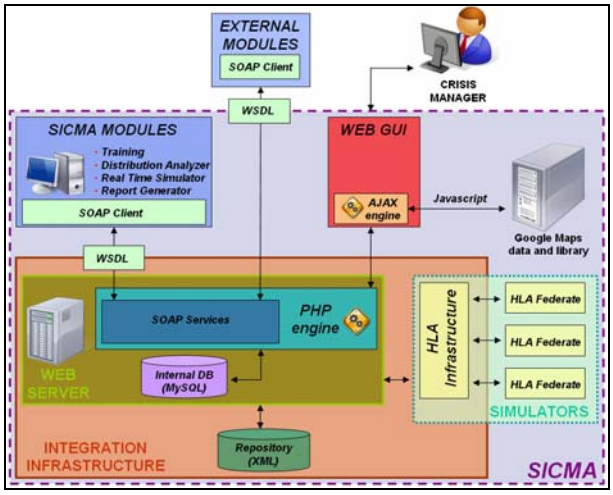

Figure 2: High level Architecture And Technologies

The core of the Integration Infrastructure is a web server developed in php5, one of the most widely-used general-purpose object-oriented scripting language that is especially suited for Web development and can be embedded into HTML. The web server grants access to the implemented services to any application implementing the standard SOAP protocol.

The web based GUI allows the users to exploit the system functionalities with different HW (hand-held, laptop, desktop etc) and from different location (e.g. the accident location, the police head quarter etc). It makes use of an embedded map, provided by Google services, allowing the user to place objects on the map and interact with them.

The GUI makes a large use of AJAX philosophy that is the web development techniques used for creating interactive web applications or rich Internet applications. The AJAX engine located on the client , ensures faster response from the lighter web server.

The AJAX engine changes the HTML DOM of the page (using, if needed, a background server interaction) thus reducing web traffic and resulting in an intuitive and easy-to-use interface.

Finally the SICMA Modules and the HLA federation, will support both the user decision making process (allowing to simulate the context evolution, and to perform a statistical analysis of the simulation results) and the procedure implementation training.

6. SYSTEM MODES OF OPERATION

Three different modes of operation will be available to the user. For each mode of operation a brief description of the kind of support provided and a figure are reported hereafter.

Contingency mode: this mode of operation will be used to support contingency planning activity of anti-crisis services for an hypothetical crisis situation.

The planner will be provided with a rough estimation of the results achievable with his plan. This will allow him to identify the best way to employ available assets, the limits of the achievable response and the effectiveness of different inter/intra-services cooperation procedures.

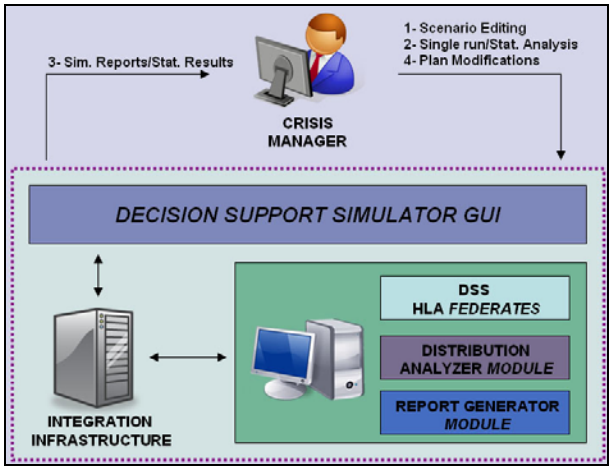

Figure 3: Contingency Mode

Response mode: this mode of operation will be used to help local commanders of anti-crisis services to make better decisions in case of a real crisis situation in progress. The decision support is provided in the form of what if analysis and in the form of guide to help the user in the implementation of the correct procedure.

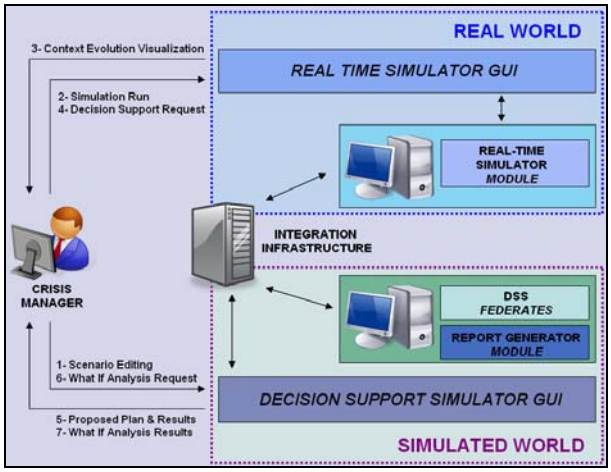

Figure 4: Response Mode

Training mode: aim of this mode of operation is to train the user in:

- making use of the SICMA system,
- implementing the correct procedure,
- making decisions.

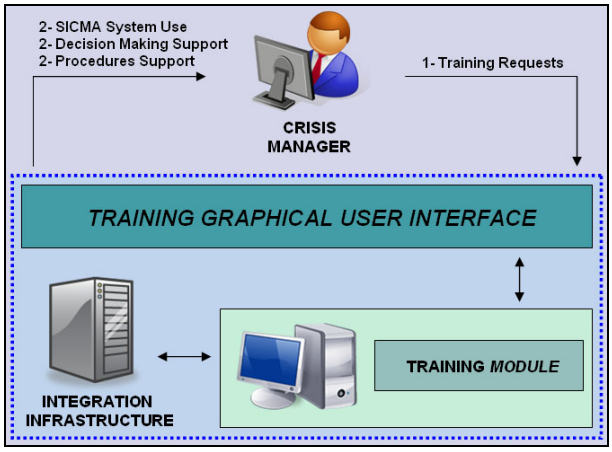

Figure 5: Training Mode

7. CONCLUSIONS

The SICMA FP7 capability project started in March 2008 to demonstrate "if" and "how" an integrated suite of modeling and analysis tools could improve the effectiveness of the Crisis Managers decision making.

At the end of the first year of activities the requirements have been identified and the system architecture has been designed.

The final result is expected to be a prototype able to demonstrate the improvement (in terms of e.g. performance, reliability, speed and cost) achievable in the decision making process through the support of M&S technology.

More in detail a significant improvement is expected in the activities listed hereafter (highlighting the Crisis Management phase they refers to):

- *Preparedness Phase*: assisting in the identification of: the best way to employ available assets, the limits of the achievable response and the effectiveness of different inter/intra-services cooperation procedures.
- *Response Phase*: providing a forecast of scenario evolution, proposing doctrine-based solutions and evaluating the effects of alternative decisions.

Considering that the main focus of the project is on the Health Service decision makers, a successful achievement of the project objectives would suggest to extend the experimentation to the domains of the other services involved in the Crisis Management process.

REFERENCES

Advanced Life Support Group, 2002. *Major Incident Medical Management and Support: The Practical Approach at the Scene*. BMJ Books.

Frykberg, E.R., 2007. Disaster and Mass Casualty Management. In: Britt, L.D., Trunkey, D.D., Feliciano D.V., ed. *Acute Care Surgery: Principles and practice*. Springer, 229-234.

AUTHORS BIOGRAPHY

Giuseppe La Posta was born in Roma (Italy) on 1969; he graduated from Rome University "La Sapienza" in 1996 with a first class honours degree in Electronic Engineering.

In the years 1998-2000 he worked at Alenia Aerospazio S.p.A. as designer of satellite telecommunications systems. Since 2000 he has been working at Elsag Datamat S.p.A a Finmeccanica company. During the period from 2000 to 2002 he was involved as a software analyst and team leader in several R&D national and international projects. Since 2003 he is Programme Manager in the Defence R&D Unit (Government and Institutions Division), in charge of the management and coordination of the research activities on M&S systems for training, planning and decision support. He is currently the coordinator of the FP7 SICMA capability project.

His main skills include Programme Management, Requirement Analysis, System Design and Software Design.

Tiziano Mischi was born december 30, 1975 in Rome, Italy. He graduated from "Università degli Studi di Roma Tre" in Rome in 2001 as an electronic engineer. Despite his electronic studies, he has decided to work as a software engineer. He's been working in the Defence R&D unit at Elsag Datamat since 2002 and has been involved in several projects, both in international and national field.

Until 2007 he has been the main developer for decision support tools in logistics and tactics for several project in the R&D unit. Since 2007 he is the technical coordinator responsible for the developing of a multi-purpose Graphic User Interface (GUI) for a geo-referenced data access. Since 2008 he's also developing the SICMA GUI as an implementation of the mentioned multi-purpose GUI.